Aalborg Universitet

AALBORG UNIVERSITY
DENMARK

Channelization, Link Adaptation and Multi-antenna Techniques for OFDM(A) Based Wireless Systems

Rahman, Muhammad Imadur

Publication date:
2007

Document Version
Publisher's PDF, also known as Version of record

Link to publication from Aalborg University

Citation for published version (APA):
Rahman, M. I. (2007). Channelization, Link Adaptation and Multi-antenna Techniques for OFDM(A) Based Wireless Systems. Institut for Elektroniske Systemer, Aalborg Universitet.

General rights
Copyright and moral rights for the publications made accessible in the public portal are retained by the authors and/or other copyright owners and it is a condition of accessing publications that users recognise and abide by the legal requirements associated with these rights.

? Users may download and print one copy of any publication from the public portal for the purpose of private study or research.
? You may not further distribute the material or use it for any profit-making activity or commercial gain
? You may freely distribute the URL identifying the publication in the public portal ?

Take down policy
If you believe that this document breaches copyright please contact us at vbn@aub.aau.dk providing details, and we will remove access to the work immediately and investigate your claim.

Downloaded from vbn.aau.dk on: May 01, 2017

Channelization, Link Adaptation and Multi-antenna Techniques for OFDM(A) Based Wireless Systems

by

Muhammad Imadur Rahman, MSc

Dissertation

Presented to the International Doctoral School of Technology and Science

in Partial Fulfillment of the Requirements for the Degree of

Doctor of Philosophy

Aalborg University

Defended on 21 September 2007

Supervisors:
Prof. Ramjee Prasad
Assoc. Prof. Elisabeth de Carvalho

The Assessment Committee:
Prof. Paul Walter Baier, University of Kaiserslautern, Germany
Prof. Preben Mogensen, Aalborg University, Denmark
Dr. Uma Jha, Director, Product Management, Qualcomm Inc., USA

Moderator:
Assoc. Prof. Flemming Bjerge Frederiksen, Aalborg University, Denmark

ISBN: 87-92078-06-0
ISSN: 0908-1224

Copyright © September, 2007 by
Muhammad Imadur Rahman
Center for TeleInFrastruktur (CTiF)
Aalborg University
Niels Jernes Vej 12
9220 Aalborg Øst
Denmark
e-mail: *imr@es.aau.dk*

All rights reserved by the author. No part of the material protected by this copyright notice may be reproduced or utilized in any form or by any means, electronics or mechanical, including photocopying, recording, or by any information storage and retrieval system, without written permission from the author.

Cover design by Maizura Ailin.
Printed in Aalborg, Denmark.

Dedicated to...

My late *father*; the best man that I have ever known.

Not forgetting my *mother*, the living encouragement for me

My wife *Ailin*, who is constantly very supportive to all my plans

Our little boy, *Akif*, the source of all our happiness

"What is Faith? When your good deed pleases you
and your evil deed grieves you, you are a believer.
What is Sin? When a thing disturbs (the peace of)
your heart, give it up."
- Prophet Muhammad (Peace be upon Him)

"When I despair, I remember that all through history
the way of truth and love has always won.
There have been tyrants and murderers and
for a time they seem invincible, but in the end,
they always fall - think of it, always."
- Mahatma Gandhi

"God helps those, who help themselves."

- Holy Quran, Holy Bible and Holy Talmud

Abstract

One of the main advantages that Orthogonal Frequency Division Multiplexing (OFDM)-based systems offer is the possibility to access narrowband time-frequency resource for increasing the system performance. The wireless channel conditions up to sub-carrier bandwidth level can be exploited to enhance the system performance. Utilizing this fact, we propose a non-Channel State Information (CSI) based channelization scheme in the first part of this thesis, namely Sub-Carrier and Band Hopped Orthogonal Frequency Division Multiple Access (SCBH-OFDMA). This channelization scheme is a flexible access technique by making use of sub-carrier and band hopping which can be adapted in different scenarios, thus creating an adaptive system in terms of heterogeneous channel conditions. SCBH-OFDMA improves the outage scenario via increased frequency diversity using combined sub-carrier and band hopping. When CSI and/or Channel Quality Information (CQI) is available at the transmitter, then possibilities for exploiting the time-frequency granularity provided by OFDM increase, one such technique is frequency domain Link Adaptation (LA). By using a less-complex and more spectrally efficient LA algorithm, we have performed an unified investigation of different channel and system related parameters under one framework. The impact of a number of implementation issues is also analyzed. Based on these results, a simplified implementation of LA is suggested, where parameters are adapted at different stages, but not necessarily simultaneously. The link adaptation studies are performed in WiMAX/UMTS-LTE context, but they should be applicable for any other OFDM based broadband wireless systems.

Multi-antenna techniques are another important component for development of future broadband wireless systems. In this thesis, the trade-off between diversity and array gain in terms of Transmit Diversity (TxDiv) and Transmit Beamforming (TxBF) systems is studied. In general, the trade-off is analyzed and studied in terms of outage capacity, outage probability and Bit Error Rate (BER). In the next step, the Cyclic Delay Diversity (CDD) property is used in OFDM receiver, where the diversity combining is performed prior to the Discrete Fourier Transform (DFT) operation. A new method has been studied to optimize the Pre-DFT diversity combining by selecting the cyclic shifts and weight factors based on known CSI at the receiver. We denote the scheme as Pre-DFT Maximal Average Ratio Combining (MARC). The proposed MARC scheme yields good

diversity gains although the performance of Maximal Ratio Combining (MRC) on sub-carrier level is not reached. On Ricean channels, the proposed scheme performs much better than CDD with fixed delays, while the gain in Rayleigh channels is surprisingly small. We have also studied Joint Diversity and Multiplexing (JDM) systems, where both diversity and multiplexing gains are available under the same Multiple Input Multiple Output (MIMO) signalling scheme. Due to diversity benefits obtained in JDM in collaboration to achieved Spatial Multiplexing (SM) gains, the studied schemes perform better compared to SM-only schemes. JDM systems are also more robust to spatial correlation caused by insufficient antenna spacing and Line of Sight (LOS) conditions, compared to original SM schemes, e.g. Vertical - Bell Labs LAyered Space-Time Architecture (VBLAST) schemes.

Performance of multi-antenna schemes, or MIMO schemes, in Orthogonal Frequency Division Multiple Access (OFDMA) systems without any interference are well-known. In the last part of this thesis, the impact of Co-Channel Interference (CCI) caused by one MIMO scheme to any other MIMO schemes is studied for cell-edge users in terms of Signal to Interference and Noise Ratio (SINR), probability density function (pdf) and BER. Depending on the receiver scheme, number of logical streams are more important than number of physical streams as interferers. When Space-Time Block Code (STBC) is an interferer, then a symbol-by-symbol processing receiver experiences multiple interfering streams. This makes the receiver unable to nullify the interfering signals. In this scenario, a more intelligent solution for interference cancelation needs to be found. We propose an interference cancelation receiver robust to different types of MIMO interferers at cell edge for the downlink of cellular OFDMA systems. The receiver systematically performs a multiple symbol processing which is the appropriate processing when an interferer using STBC is present. A module detecting the presence of a STBC interferer is proposed: when no STBC interferer is detected, the receiver switches to a single symbol processing. Using this knowledge and understanding, we also propose a frequency sharing for the downlink of a OFDMA based cellular system at cell edge. This frequency sharing among the main interfering Base Stations (BSs) ensures that the number of receive antennas for each Mobile Station (MS) is larger than or equal to the number of desired and interfering links. The proposed method uses the knowledge of the number of available receive antennas at the MS and ensures that the interference order is always kept under control so that the desired MS is not severely affected by CCI.

Dansk Resumé[1]

En af de hovedfordele som Orthogonal Frequency Division Multiplexing (OFDM) baserede systemer giver, er muligheden for at tilgå smalbåndet tidsfrekvens ressourcer for at øge system udnyttelsen. De trådløse kanal tilstande kan blive brugt helt ned til sub-carrier niveau for at forøge system udnyttelsen. Ved at bruge denne kendsgerning, tilbyder vi et ikke Channel Status Information (CSI) baseret kanaliseringsskema i den første del af denne tese, som vil blive kaldt: Sub-Carrier and Band Hopped Orhtogonal Frequency Division Multiple Access (SCBH-OFDMA). Dette kanaliseringsskema er en fleksibel access teknik, som ved at bruge sub-carriers og band hopping kan omstilles til forskellige scenarier og derved skabe et adaptivt system i heterogene kanal tilstande. SCBH-OFDMA forbedrer outage scenariet ved en forøget frekvens diversitet ved at bruge en kombineret sub-carrier og band hopping. Når CSI og/eller Channel Quality Information (CQI) er tilgængelige ved senderen, forøges mulighederne for at udnytte den tids-frekvens opløsning givet med OFDM. En af disse tekniker er frekvens domæne Link Adaptation (LA). Ved at bruge en mindre kompleks og mere spektrum effektiv LA algoritme, har vi udøvet en samlet undersøgelse af forskellige kanal og system relaterede parametre under en samlet WiMAX/UMTS-LTE ramme for link tilpasning. Vi har undersøgt flere parametres indvirkning. Fra disse resultater har vi forslået en simplificeret implementering, hvor parametrene er tilpasset til forskellige stadier og ikke samtidigt.

Multiple antenne teknikker er et andet vigtigt element for at udvikle fremtidige bredbåndede trådløse systemer. Vi studerer trade-off mellem diversitet og array gevinst i form a Transmit Diversity (TxDiv) og Transmit Beamforming (TxBF) systemer. Overordnet, er trade-offet analyseret og studeret ved brug af outage kapacitet, outage sandsynlighed og Bit Error Rate (BER). Bi har brugt Cylic Delay Diversity (CDD) egenskaber i vores OFDM modtager, hvor diversitets kombinering er udført før den Diskrete Fourier Transformation (DFT). En ny metode er blevet studeret for at optimere Pre-DFT diversitets kombination ved at vælge de cykliske skift og vægtningsfaktorer baseret på kendt channel state information. CDD giver god diversitets gevinster, selvom virkningen af Maximal Ratio Combining (MRC) ikke helt bliver opnået på subcarrier niveau. Ved brug

[1]Many thanks to Christian Rom, Lisbeth Schiønning Larsen and Maizura Ailin for their help in Danish translation.

af Ricean kanaler, er de optimerede skemaer meget bedre end CDD med statiske tidsforsinkelser, hvorimod med Rayleigh kanaler er gevinsten forbløffende lille. Vi har også studeret Joint Diversity and Multiplexing (JDM) systemer, hvor både diversitet og multiplexing gevinster kan opnås med det samme Multiple Input Multiple Output (MIMO) signaleringsskema. På grund af fordele opnået med JDM i samarbejde med Spatial Multiplexing (SM) gevinster, er de studerede skemaer bedre i forhold til SM skemaer alene. JDM systemer er også mere robuste overfor rumlig korrelation skabt ved en for lille antenne afstand og Line of Sight (LOS) tilstande.

Virkningen af multi-antenne skemaer, eller MIMO skemaer, for Orthogonal Frequency Division Multiple Access (OFDMA) systemer uden nogen interferens er almen kendte. I den sidste del af denne tese, har vi studeret effekten af Co-Channel Interference (CCI) skabt af et MIMO skema på hvilket som helst andet MIMO skema for celle grænse brugere i form af Signal to Interference and Noise Ratio (SINR) probability density function (pdf) og BER. Afhængig af modtager skemaet, er antal logiske strømme mere vigtige end det antal af fysiske strømme som interfererer. Når Space-Time Block Code (STBC) er en interferens, så oplever en symbol-per-symbol baseret modtager flere interferens strømme. Dette gør det umuligt for modtageren at ophæve de interfererende signaler. I dette scenario skal en mere intelligent løsning findes. Vi forslår en interferens ophæver modtager, som er robust overfor forskellige MIMO interferens typer ved celle kant til downlink i cellulære Orthogonal Frequency Division Multiplexing Access (OFDMA) systemer. Modtageren udfører systematisk en multi-symbol bearbejdelse, som er den hensigtsmæssige bearbejdelse, når en interferens kilde, der bruger STBC, er til stede. Et modul til at opdage tilstedeværelsen af en STBC interferens er forslået: Når igen STBC interferens er opdaget, skifter modtageren til enkel symbol bearbejdelse. Vi bruger denne viden og forståelse til at forslå en frekvens deling til downlink af en cellulær OFDMA ved celle kant. Denne frekvens deling iblandt de Base Stations (BSs) som skaber mest interferens garanterer, at antallet af modtager antenner for hver Mobile Station (MS) er større eller lig med det antal ønsket interfererende links. Den forslåede metode bruger viden omkring antallet af tilgængelige modtager antenner ved MS og sørger for, at interferens rækkefølgen altid er holdt under kontrol, således at den ønskede MS ikke er for hårdt ramt af CCI.

"Exchange gifts, and mutual love arises; shake hands, and enmity will fall away."

- Prophet Muhammad (Peace be upon Him)

Acknowledgments

First and foremost, all gratitude to God the Almighty, *Alhamdulillah*. It is my utmost belief in Him and His boundless blessings that allowed me to finish the PhD project.

I would like to express my heartiest gratitude to my main PhD Supervisor Prof. Ramjee Prasad. Since my first day in Aalborg University as a guest student pursuing my MSc thesis work, he has always been there for me. Whenever I have felt down, I could simply knock on his door and discuss different issues. He has always given me the courage to continue and see my work until the end. I have learnt many things from him, which will indeed be useful for my future career. Also, many thanks to Assoc. Prof. Elisabeth de Carvalho for her guidance and supervision in the last part of the thesis work.

In the beginning of my PhD studies, Assoc. Prof. Frank Fitzek and Assoc. Prof. Ole Olsen guided me to formulate the work area, without which I could not have completed this work. I should mention a special friend of mine, Suvra Sekhar Das, who I met in Aalborg in the very beginning of my PhD studies and with whom I have forged a strong relationship throughout the PhD studies. I will remember the countless discussions, debates and arguments we had together in the weekends and late evenings. It was a pleasant association that I will cherish. Nicola Marchetti and Daniel Figueiredo have been great friends for these few years. I have learnt many things from Nicola, and I will definitely remember all the cookies and cakes that his '*mamma*' used to send from Italy. Also, I would like to thank other fellow PhD students in the *JADE* project and in the former *WING* group for numerous stimulating discussions and exchange of ideas. I have supervised a number of students who have contributed enormously to my knowledge and experience. Special thanks go to Yuanye Wang, who has worked with me for at least 3 semesters, and I have really enjoyed my work with him. A number of friends have read part of my thesis and provided valuable comments and suggestions, many thanks to them also.

Besides the 'nerdy' academic environment at the university, I have formed great friendship and enjoyment from my friends in the Muslim Society @ Aalborg University (MS@AAU). The weekend activities, intense theological and geo-political discussions, football sessions, BBQs- all of those were great. I have also made many other friends in the Aalborg area who have always been

helpful to me. Thank you to all of you.

My mother, the living encouragement for me, is an amazing lady. She has always been with me with her prayers and well wishes. I come from a large family; we are six brothers and three sisters. I feel very privileged to be part of a big family, where all us siblings care for each other. We have always been there for each other and I must say that the encouragement and beautiful words that I have received from my siblings were simply great.

No expressions can express my gratitude and love for Ailin. Since we got married, she is always there for me, with suggestions, advices and cooperation. She sacrificed a lot for my PhD studies, and I will definitely remember this throughout my life. Our '*little*' boy, Akif, has been the love of our life. His smile and intelligent words kept me going for the last few years.

Last but not the least, my late father would have been the happiest person today, if he would have been alive. May God rest him in peace and place him in heaven!

Thank you.

MUHAMMAD IMADUR RAHMAN

Aalborg University
September 2007

Contents

Abstract v
Dansk Resumé vii
Acknowledgments ix
List of Figures xvii
List of Tables xxiii

Chapter 1 Introduction **1**
1.1 Forthcoming 4G Systems 2
1.2 Problem Statement 5
1.3 Thesis Overview and Organization 8

Chapter 2 Multi-carrier Modulation and MIMO Systems **11**
2.1 Channel Impairments and Multi-carrier Modulation 11
2.1.1 Physical Characteristics of Multipath Channels 12
2.1.2 The Benefit of Using Multi-carrier Transmission 16
2.2 OFDM Fundamentals 18
2.2.1 OFDM Transceiver Systems 19
2.2.2 Channel Coding and Interleaving 20
2.2.3 Combating ISI and Reducing ICI 22
2.2.4 Spectral Efficiency 23
2.3 Multi-User OFDM Systems 24
2.3.1 Orthogonal Frequency Division Multiple Access 25
2.3.2 OFDMA-based Standards 28
2.4 Multi-antenna OFDM Systems 31
2.4.1 Multi-antenna and Diversity 31
2.4.2 Multi-antenna and Spatial Multiplexing 34
2.4.3 Usability of Multi-antenna Techniques in OFDM Systems 35

Chapter 3 Sub-Carrier and Band Hopped OFDMA **41**
3.1 Background and Motivation 41
3.1.1 Why Sub-carrier Hopping? 43
3.1.2 Why Band Hopping? 43
3.2 Multiple Access (or Channelization) Approach 44

3.2.1 User Grouping . . . 44
3.2.2 Sub-Carrier and Band Hopping Strategy . . . 46
3.3 Analytical Model . . . 47
3.3.1 DL Transmitter . . . 49
3.3.2 Wireless Channel . . . 51
3.3.3 DL Receiver . . . 52
3.4 Numerical Evaluations . . . 55
3.4.1 Simulation Parameters . . . 55
3.4.2 System level Simulation . . . 57
3.4.3 Interference Calculation . . . 61
3.4.4 Outage SINR Analysis . . . 62
3.4.5 Goodput Simulations . . . 63
3.5 Chapter Summary . . . 67

Chapter 4 System Design Issues for SCBH-OFDMA Scheme **69**
4.1 Transceiver Structure . . . 69
4.2 Frame Format . . . 70
4.3 Pilot Sequence . . . 71
4.4 Estimation of Coherence Bandwidth and Time . . . 72
4.5 Grouping procedure . . . 72
4.6 System Complexity . . . 73
4.7 Hopping Sequence Design . . . 74
4.7.1 Facts in Downlink . . . 74
4.7.2 Design Goal . . . 74
4.7.3 Assumptions . . . 74
4.7.4 Physical Considerations . . . 75
4.7.5 Sequence Design Preliminaries . . . 76
4.7.6 Slow Band Hopping (SBH) . . . 77
4.7.7 Fast Band Hopping (FBH) . . . 79
4.7.8 Sub-Carrier Hopping (SCH) . . . 81
4.7.9 Implementation of Hopping Mechanism . . . 82
4.8 Chapter Summary . . . 90

Chapter 5 Frequency Domain Rate and Power Allocation **91**
5.1 Link Adaptation Preliminaries . . . 92
5.2 Link Adaptation Algorithms . . . 95
5.2.1 Simple Rate Adaptation (SRA) . . . 95
5.2.2 Adaptive Power Distribution (APD) . . . 96
5.2.3 The Proposed Link Adaptation Algorithm . . . 97
5.3 Spectral Efficiency and Complexity Analysis in Un-coded system . . . 100
5.3.1 Analysis in Terms of Spectral Efficiency . . . 101
5.3.2 Complexity Analysis in Terms of Number of Iterations . . . 101
5.3.3 Number of Loaded Sub-carriers . . . 101

5.3.4 Adaptive SNR Lookup Table Method . . . 103
5.3.5 Adaptive Sub-channel Size . . . 103
5.4 Link Adaptation Scenario . . . 105
5.4.1 Link Adaptation Process . . . 105
5.4.2 Different LA Mechanisms Used in This Study . . . 105
5.4.3 System Parameters . . . 107
5.4.4 Frame Structure . . . 108
5.4.5 Threshold Measurement . . . 109
5.5 Interaction between Spatial Diversity and Link Adaptation . . . 110
5.5.1 Multi-Antenna Diversity Schemes . . . 110
5.5.2 FER and Throughput Performance of Multi-Antenna assisted LA Systems . . . 114
5.5.3 Impact of LA Rates in Different Multi-Antenna Schemes . . . 116
5.6 Chapter Summary . . . 118

Chapter 6 Multi-Dimensional Link Adaptation Strategies 121
6.1 Role of Power Adaptation in Collaboration with Bit Adaptation . . . 121
6.1.1 AMC and Power Adaptation at Same Rate . . . 122
6.1.2 AMC and Power Adaptation at Different Rates . . . 125
6.1.3 Overhead Analysis . . . 130
6.2 Link Adaptation considering Several System Issues . . . 132
6.2.1 Strategies for Bit and Power Loading Algorithms . . . 133
6.2.2 Sub-Channelization . . . 134
6.2.3 Fixed Coding Rate . . . 135
6.2.4 AMC Rate . . . 137
6.3 Influence of Transmitter Non-linearities . . . 138
6.3.1 Interaction between PAPR and Link Adaptation . . . 139
6.3.2 Link Adaptation with HPA in Coded OFDM System . . . 144
6.3.3 Results for Fading Channel . . . 145
6.4 Chapter Summary . . . 147

Chapter 7 Transmit Diversity Vs Beamforming 151
7.1 Introduction . . . 151
7.2 A Brief Look at Diversity and Beamforming . . . 152
7.2.1 Beamforming . . . 152
7.2.2 Space-Time Block Coding (STBC) . . . 156
7.2.3 Receive Diversity System . . . 157
7.2.4 MIMO Diversity System . . . 158
7.2.5 SNR Statistics of Diversity and Beamforming Systems . . . 158
7.3 Downlink Capacity and Error Probability Analysis . . . 159
7.3.1 Ergodic Capacity . . . 159
7.3.2 Outage Capacity . . . 161
7.3.3 Error Probability . . . 164
7.4 Downlink Beamforming and Transmit Diversity in Multi-User OFDM Systems . . . 165

© Muhammad Imadur Rahman, 2007

7.4.1 Issues in OFDM-TDMA . . . 165
7.4.2 DL-BF in OFDMA . . . 166
7.4.3 DL-BF in Clustered OFDMA . . . 167
7.5 Performance Analysis and Comparison . . . 168
7.5.1 Channel Model . . . 168
7.5.2 Angular Spread and Spatial Correlation . . . 168
7.5.3 Simulation Parameters . . . 170
7.5.4 BER Results and Discussions . . . 171
7.5.5 Pilot Design Issue . . . 172
7.6 Chapter Summary . . . 175

Chapter 8 Exploiting Cyclic Delay Diversity in OFDM System 177
8.1 Introduction . . . 178
8.2 OFDM System Model . . . 180
8.3 Post-DFT Maximum Ratio Combining . . . 181
8.4 Benefitting from Cyclic Delay Property in OFDM System . . . 182
8.4.1 System Model with Cyclic Delay Diversity . . . 182
8.4.2 Capacity of CDD Based OFDM System . . . 185
8.5 Pre-DFT Maximum Average Ratio Combining . . . 187
8.5.1 Optimum SNR for the Combined Signal . . . 187
8.5.2 Optimum Diversity Weights . . . 189
8.5.3 System Analysis with Dual Antenna Receiver . . . 190
8.5.4 Numerical Analysis and Discussions . . . 193
8.6 Cyclic Delay Assisted Spatial Multiplexing . . . 198
8.6.1 Transmission Structure . . . 199
8.6.2 System Capacity of CDA-SM-OFDM . . . 202
8.6.3 Simulation Results and Discussions . . . 205
8.6.4 Performance Results and Discussions . . . 206
8.7 Chapter Summary . . . 208

Chapter 9 Joint Diversity and Multiplexing Systems 211
9.1 Introduction . . . 211
9.1.1 What are JDM Schemes? . . . 212
9.1.2 State-of-the-Art on JDM Schemes . . . 213
9.2 SM-OSFBC Transmission Scheme . . . 214
9.2.1 Transmitter . . . 214
9.2.2 Two-Stage Linear Receiver . . . 216
9.2.3 OSIC-based Non-Linear Receiver . . . 219
9.3 SM-QSFBC Transmission Scheme . . . 222
9.3.1 Transmitter . . . 222
9.3.2 OSIC Receiver . . . 223
9.4 Numerical Results . . . 225
9.4.1 System Parameters . . . 225

9.4.2 System Capacity Analysis . . . 226
9.4.3 FER Performance . . . 227
9.4.4 10% Outage Spectral Efficiency . . . 229
9.4.5 Effect of Spatial Correlation . . . 229
9.4.6 Performance in Presence of LOS . . . 232
9.5 Chapter Summary . . . 233

Chapter 10 Impact of MIMO Co-channel Interference **235**
10.1 Introduction . . . 235
10.2 Assumptions and Definitions . . . 237
10.2.1 Assumptions . . . 237
10.2.2 Link Definitions . . . 237
10.2.3 Scenario Definition . . . 238
10.3 Symbol by-Symbol Linear Receivers . . . 239
10.3.1 MRC Receiver . . . 239
10.3.2 MMSE Receiver . . . 239
10.4 SINR Expressions . . . 240
10.4.1 SIMO in Desired Link . . . 240
10.4.2 AS in the Desired Link . . . 242
10.4.3 TxBF in the Desired Link . . . 244
10.4.4 STBC in the Desired Link . . . 244
10.5 SINR Analysis . . . 246
10.5.1 Cellular Scenario . . . 246
10.5.2 Equal Power Scenario . . . 248
10.6 Probability of Error . . . 251
10.6.1 When Interferer is not STBC . . . 251
10.6.2 When Interferer is STBC . . . 252
10.7 BER Evaluations via Numerical Simulations . . . 253
10.7.1 Simulation Parameters . . . 253
10.7.2 Equal Power Scenario . . . 254
10.7.3 Cellular Scenario . . . 256
10.8 Chapter Summary . . . 256

Chapter 11 MIMO Systems at Cell Edge: Robust Receiver Design **259**
11.1 Introduction . . . 259
11.2 Multiple Symbol Processing . . . 260
11.2.1 Scenario and Assumptions . . . 260
11.2.2 Linear MMSE receiver: Multiple symbol processing . . . 261
11.2.3 Impact on System Level and Implementation Related Issues . . . 263
11.3 Numerical Evaluations . . . 267
11.3.1 Simulations Parameters . . . 267
11.3.2 SINR statistics . . . 267
11.3.3 Mean SINR . . . 269

© Muhammad Imadur Rahman, 2007

11.3.4 Initial Investigations in Time-Invariant Channel 270
11.3.5 Simulation with Different Type of MIMO Interferers 271
11.3.6 Time-Variant Case 272
11.3.7 STBC Detection Module 275
11.4 Fractional Frequency Reuse at Cell Edge 277
11.4.1 Motivation and Problem Definition 277
11.4.2 Prior Arts 277
11.4.3 The FFR method 278
11.4.4 Evaluation of proposed FFR method 280
11.5 Chapter Summary 280

Chapter 12 Conclusions and Future Outlook **283**
12.1 Overall Summary 283
12.2 Contribution of Thesis 285
12.3 Future Outlook 286

Chapter A List of IPRs, Publications and Technical Reports **289**

Chapter B List of Abbreviations **295**

Chapter C List of Symbols **303**

Chapter D Useful Definitions **307**

Bibliography **311**

Vita **323**

List of Figures

1.1 Time-Frequency OFDM granularity that can be exploited for increasing system spectral efficiency . . . 6
1.2 Cellular interference scenario . . . 7

2.1 Channel impulse responses and corresponding frequency response . . . 13
2.2 Single Carrier Vs Multi-carrier Approach . . . 17
2.3 OFDM Transceiver Model . . . 21
2.4 Role of Guard Interval and Cyclic Prefix in Combatting ISI and ICI . . . 22
2.5 Spectrum Efficiency of OFDM Compared to Conventional FDM . . . 23
2.6 Time-frequency diagram for the OFDMA scheme. . . . 25
2.7 Simplified block diagram of the OFDMA transmitter, receiver schemes. . . . 26
2.8 (a) Contiguous sub-carrier assignment. (b) Interleaved sub-carrier assignment. . . . 26
2.9 Examples of sub-channel conditions . . . 27
2.10 Classification of multi-antenna techniques . . . 32
2.11 Example of space diversity . . . 34
2.12 An example of MIMO Spatial Multiplexing system . . . 35
2.13 Qualitative representation of throughput versus distance from BS for SISO, SM and Spatial Diversity . . . 40

3.1 Different combinations of sub-carrier and band hopping in SCBH-OFDMA scheme. 45
3.2 Illustration of grouping strategies. . . . 46
3.3 OFDM System model - Downlink Transmitter . . . 48
3.4 OFDM System model - Downlink Receiver . . . 48
3.5 OFDM System model - Channel . . . 51
3.6 System level simulator flow . . . 58
3.7 Power Delay Profile Model . . . 60
3.8 cdf of 10% outage SNR for all users for different levels of CCI . . . 65
3.9 Aggregate cell goodput for different levels of CCI and different system bandwidth . 66

4.1 Downlink Transmitter. . . . 70
4.2 Downlink Receiver. . . . 70
4.3 DL user data channel format for SCBH-OFDMA. . . . 71

4.4 FFT complexity versus FFT size. 73
4.5 Two-tier cellular systems considered in the hopping sequence design. 75
4.6 Band allocations for SBH groups in a two tier cellular system 78
4.7 PRNG hopping 85
4.8 Number of interfering cells colliding with a group at a given time. 89
4.9 Probability of collision for different interfering cells. 89

5.1 Block Diagram of a system using link adaptation, i.e. adaptive modulation and power adaptation 93
5.2 Flow Diagram for the SRA 95
5.3 Flow Diagram for the Adaptive Power Distribution algorithm 97
5.4 Flow diagram of the proposed algorithm 98
5.5 Spectral efficiency achievement of the adaptation algorithms 102
5.6 Number of iterations required by different adaptation algorithms 102
5.7 Sub-carrier loading for different algorithms 103
5.8 Link Adaptation Model 106
5.9 Flowchart of *AMC fixP* and *AMC adaptP* mechanism 106
5.10 Link adaptation frame structure. 108
5.11 Non-adapted FER and throughput vs. Post-SNR for different modulation and coding combinations. 109
5.12 BER vs SNR curves for SISO, AS (time) and AS (frequency), with fd=50Hz 113
5.13 Performance results of *instantaneous link adaptation* in multi-antenna assisted OFDM systems 114
5.14 Performance results of *slower link adaptation* in multi-antenna assisted OFDM systems 114
5.15 Spectral efficiency results for different MIMO schemes for different LA rates at different levels of Pre-SNRs 117

6.1 Power savings of different link adaptation rate with and without power adaptation . 123
6.2 FER results of instantaneous link adaptation with different power adaptation 124
6.3 Spectral efficiency and power saving of instantaneous link adaptation with different power adaptation mechanisms 124
6.4 Examples of different power and bit allocations rates. 127
6.5 Flowchart of link adaptation mechanism when faster power control and slower AMC is used. 128
6.6 Spectral Efficiency for Different AMC and PC Rates 129
6.7 Throughput comparison (for subN = 8) and Power utilization of different Link adaptation algorithms at different RMS delay spread and Doppler conditions 134
6.8 Achievable spectral efficiency using different sub-channel sizes. 135
6.9 Spectral efficiency performance comparison for fixed coding with adaptive modulation vs adaptive modulation and coding. 136
6.10 Throughput comparison for different bit adaptation rates 138
6.11 Amplifier distortion with different power BO 140
6.12 SDNR plot for 64-QAM in AWGN channel. 141

6.13 Effect of HPA and BO on 16QAM constellation points 142
6.14 Effect of HPA and BO on uncoded system in AWGN channel 143
6.15 Effect of HPA and BO on coded system in AWGN channel 143
6.16 Total Degradation Plot for FER Threshold of 0.1 144
6.17 BLER Performance of Link Adapted System with and without HPA 144
6.18 Spectral Efficiency Comparison for different BO values 144
6.19 Spectral Efficiency for Link Adapted System in AWGN Channel 144
6.20 Effect of HPA and BO in Fading Channel 146
6.21 FER Performance of Link Adaptation with and without HPA 147
6.22 Spectral Efficiency Comparison for different BO values in Fading Channel 147
6.23 SDNR for 64QAM in fading channel 147
6.24 Total Degradation Plot for FER Threshold of 0.1 in fading channel 147
6.25 Summary of hybrid link adaptation approach 148

7.1 Beamforming and transmit diversity systems in OFDM system 153
7.2 Time- and Frequency-domain beamforming approach on an OFDMA system 155
7.3 Probability density function (pdf) of SNR for different combinations of diversity and beamforming systems. 159
7.4 Ergodic channel capacity for transmit diversity, receive diversity and beamforming techniques with 2, 4 and 8 antennas. 160
7.5 Outage capacity and outage probability for transmit diversity and beamforming with varying number of transmit antennas. 162
7.6 Theoretical average bit error probabilities for transmit diversity and beamforming systems. 165
7.7 Impact of antenna correlation corresponding to different angle spread on transmit diversity and beamforming. 169
7.8 BER performance for STBC/SFBC for different AS 173
7.9 BER performance for BF for different AS 173
7.10 BER comparison between BF and STBC for Indoor channel 174
7.11 BER comparison between BF and STBC for Outdoor channel 174

8.1 Multiple Antenna Receiver Diversity with MRC at sub-carrier level 179
8.2 CIR and CTF of two separate paths, their linear sum and the combined channel after applying cyclic delay principle 183
8.3 Transmitter Model for CDD based MISO-OFDM Transmission Scheme. 184
8.4 cdf of system capacity and 5% outage capacity for SISO and $P \times 1$ CDD systems. . . 186
8.5 OFDM receiver with Pre-DFT Combining CDD. The instantaneous channel is estimated from the received signals to determine the optimum cyclic shifts (and gain factors, if MARC combining is performed). 187
8.6 Diversity weight estimation method for Pre-DFT MARC with CDD receiver diversity scheme; for clarity, channel estimation procedure and COFDM part of the receiver is not shown in the Figure 190

© Muhammad Imadur Rahman, 2007

8.7 Average SNR with two-branch Pre-DFT MARC and Pre-DFT EGC with cyclic delays as a function of the delay parameter n (in samples). 192
8.8 Histogram of Cyclic Shifts obtained for Maximum Average SNR with 10000 samples. 193
8.9 Magnitudes of Channel Transfer Functions before and after diversity combining. Pre-DFT MARC, Post-DFT MRC, and Pre-DFT EGC are shown in the figure. 194
8.10 Uncoded BER with and without application of diversity, Rayleigh fading channels with various τ_{rms}. 195
8.11 Uncoded BER with and without application of diversity, Ricean channel with $K = 4$. 195
8.12 Performance results in terms of coded BER; Rayleigh channel, $\tau_{rms} = 1$ sample; rate $\frac{1}{2}$ convolutional coding with constraint length 5. 196
8.13 Relative Processing cost for Pre-DFT MARC and Post-DFT MRC in comparison to number of OFDM sub-carriers and number of OFDM symbols/packet. 198
8.14 Transceiver Architecture for CDA-SM-OFDM System 200
8.15 Comparison of normalized eigenvalue spread and mean eigenvalue for 4×2 CDA-SM-OFDM system with 2×2 and 4×2 SM-OFDM system 204
8.16 Comparison of system capacity and 5% outage capacity for 4×2 CDA-SM-OFDM system with 2×2 and 4×2 SM-OFDM system 205
8.17 Average FER and spectral efficiency in bps/Hz of different types of spatial multiplexing schemes. 206

9.1 Simplified System Model for SM-OSFBC/SM-QSFBC Transmission Scheme 215
9.2 Simplified data flow for OSIC receiver 220
9.3 10% channel outage capacity for reference systems 226
9.4 FER performance for the schemes 228
9.5 10% Outage spectral efficiency 228
9.6 FER with respect to increasing transmit correlation (i.e. decreasing antenna spacing) and fixed receive correlation at system SNR of 12dB 230
9.7 FER with respect to increasing receive correlation (i.e. decreasing antenna spacing) and fixed transmit correlation at system SNR of 12dB 230
9.8 Outage spectral efficiency with respect to decreasing transmit correlation (i.e. increasing antenna spacing) and fixed receive correlation at system SNR of 12dB . . . 231
9.9 Loss in average spectral efficiency with respect to increasingly strong LOS component 233

10.1 Cell Scenario for interference studies 238
10.2 *pdf* of SINR with SIMO as the desired link in cellular scenario 247
10.3 *pdf* of SINR with AS as the desired link in cellular scenario 247
10.4 *pdf* of SINR with STBC as the desired link in cellular scenario 247
10.5 *pdf* of SINR with TxMRC as the desired link in cellular scenario 247
10.6 *pdf* of SINR with SIMO as the desired link in equal power scenario 249
10.7 *pdf* of SINR with AS as the desired link in equal power scenario 249
10.8 *pdf* of SINR with STBC as the desired link in equal power scenario 249
10.9 *pdf* of SINR with TxMRC as the desired link in equal power scenario 249

10.10 Probability of error comparison for SIMO at desired link and other schemes at interfering link . . . 251
10.11 BER vs SNR with SIMO-SIMO combination and symbol-by-symbol based receiver in equal power scenario . . . 254
10.12 BER vs SNR with SIMO-STBC combination and symbol-by-symbol based receiver in equal power scenario . . . 254
10.13 BER vs SNR with AS-SIMO combination and symbol-by-symbol based receiver in equal power scenario . . . 254
10.14 BER vs SNR with AS-STBC combination and symbol-by-symbol based receiver in equal power scenario . . . 254
10.15 BER vs SNR with SIMO-XXX combination, Q=5, I=3, and symbol-by-symbol based receiver in equal power scenario . . . 255
10.16 BER vs SNR with AS-XXX combination, Q=5, I=3, and symbol-by-symbol based receiver in equal power scenario . . . 255
10.17 BER vs SNR with SIMO-SIMO combination and symbol-by-symbol based receiver in cellular scenario . . . 256
10.18 BER vs SNR with SIMO-STBC combination and symbol-by-symbol based receiver in cellular scenario . . . 256

11.1 Estimation of covariance matrix . . . 265
11.2 pdf of SINR with different combinations for 2-symbol processing when SINR definition of 'unbiased' MMSE is used . . . 268
11.3 $log_{10}(cdf)$ SINR with different combinations for 2-symbol processing when SINR definition of 'unbiased' MMSE is used . . . 268
11.4 Mean SINR for SIMO-XXX cases with 1- and 2-symbol processing. . . . 270
11.5 Mean SINR for different STBC-XXX cases. . . . 270
11.6 BER results for SIMO-SIMO with single-symbol and 2-symbol processing with linear MMSE receiver . . . 270
11.7 BER results for SIMO-STBC with single-symbol and 2-symbol processing with linear MMSE receiver . . . 271
11.8 BER results for SIMO-SIMO, SIMO-STBC and SIMO-Diff cases with 2-symbol processing in cellular scenario . . . 272
11.9 BER results for SIMO-SIMO-MMSE system, $\mathbf{R_{zz}}$ Window size =100, velocity = 0.6713kmph . . . 274
11.10 BER results for SIMO-SIMO case in time-variant channel scenario . . . 274
11.11 BER results for SIMO-STBC case in time-variant channel scenario . . . 274
11.12 BER results for different $\mathbf{R_{zz}}$ estimation method, at 5dB of E_s/N_0 . . . 275
11.13 Successful detection and false detection when STBC module is used . . . 276
11.14 BER results for SIMO-STBC case with and without the STBC detection module in time-variant channel scenario . . . 276
11.15 Scenario Description. Only 2 interfering BSs are considered. . . . 279
11.16 Example of frequency assignment between 3 neighboring cells as shown in Figure 11.15 279

© Muhammad Imadur Rahman, 2007

D.1 Spectrum definitions. 308

List of Tables

1.1 Evolution of Wireless Standards 3

2.1 Channel coherence bandwidth with respect to different RMS delay spread 14
2.2 Channel coherence time at 2.0GHz and 3.5GHz of carrier frequency with respect to receiver mobility 15
2.3 Value of parameters for urban terrain 16
2.4 Comparison of Single Carrier and Multi-carrier Approach in terms of Channel Frequency Selectivity 19
2.5 IEEE 802.11a OFDM PHY Modulation Techniques 20
2.6 General WiMAX Parameters 28
2.7 System parameters for OFDMA-FSCH scheme under development by IEEE 802.20 working group 29

3.1 Choice of hopping strategy depends on coherence bandwidth, B_c and coherence time, T_c. 47
3.2 Division of hopping strategies 47
3.4 Distribution of velocity and PDP length 59
3.5 10% and 20% outage SINR values for different schemes with different levels of SINRs 63

4.1 Construction of order 5, matrix $\{1\}$ 83
4.2 Matrix $\{2\}$ of order 5 83
4.3 Matrix $\{3\}$ of order 5 83
4.4 Matrix $\{4\}$ of order 5 83
4.5 General construction of order 4 matrix in GF(2) 83
4.6 Construction of matrix $\{1\}$ of order 4 in GF(2) 84
4.7 Construction of matrix $\{1\}$ of order 8 84
4.8 General Construction of order 8 matrix in GF(2) 86
4.9 Matrix $\{2\}$ of order 8 in GF(2) 87
4.10 Matrix $\{3\}$ of order 8 in GF(2) 87
4.11 Matrix $\{4\}$ of order 8 in GF(2) 87
4.12 Matrix $\{5\}$ of order 8 in GF(2) 87
4.13 Matrix $\{6\}$ of order 8 in GF(2) 87

4.14 Matrix {7} of order 8 in GF(2) 87

5.1 System parameters for evaluations of link adaptation algorithms 101
5.2 SNR margin for different sub-channelization size 104
5.3 SNR margin for adaptive sub-channelization with different threshold 104
5.4 SNR Lookup Table for a SISO system with frame-by-frame adaptation 110
5.5 Alamouti transmitter 112
5.6 Alamouti receiver 112
5.7 SNR Lookup Table for MIMO systems, LA is performed on frame-by-frame basis. . 115
5.8 SNR Lookup Table for MIMO systems, LA is performed on per 20 Frames 115

6.1 Parameters from UMTS-LTE Standard 126
6.2 Overhead in Mbps for Adapt Power LA 132
6.3 Average SNR thresholds (in dB) for switching coding rate for different RMS delay spread and Doppler condition 137
6.4 SNR Lookup Table for SISO with Different AMC Rates 137
6.5 Table for Calculation of Total Degradation in dB 143
6.6 LUT with basic and updated values for system with FEC= $\frac{1}{2}$ in AWGN Channel (Values in dB) 145
6.7 LUT with basic and updated values for system with FEC = $\frac{1}{2}$ in Fading Channel(Values in dB) 146

7.1 Tarokh's $\frac{1}{2}$ rate Space-Time Block Encoding Scheme 156
7.2 Parameters for comparison between diversity and beamforming 170

8.1 Comparison of channel coherence time with OFDM packet duration for IEEE 802.11a WLAN Standard 198
8.2 OFDM Simulation Parameters, taken similar to $IEEE$ 802.11a standard 206
8.3 Tags used in figures for corresponding schemes 207

9.1 Tags used in figures for corresponding schemes 226
9.2 Correlation for corresponding spatial separation among antennas. 229

10.1 An example of pathloss values from different interfering BSs and the desired BS . . 238
10.2 Receivers for CCI cancellation in frequency flat channels. 241
10.3 Parameters used in Semi-Analytical evaluations of SINR expressions 246
10.4 Mean SINR in dB with SIMO as the desired link in cellular scenario 248
10.5 Mean SINR in dB with AS as the desired link in cellular scenario 248
10.6 Mean SINR in dB with STBC as the desired link in cellular scenario 248
10.7 Mean SINR in dB with TxMRC as the desired link in cellular scenario 248
10.8 Mean SINR in dB with SIMO as the desired link in equal power scenario 250
10.9 Mean SINR in dB with AS as the desired link in equal power scenario 250
10.10 Mean SINR in dB with STBC as the desired link in equal power scenario 250
10.11 Mean SINR in dB with TxMRC as the desired link in equal power scenario 250

10.12Simulation parameters used in Simulations 253
10.13Power levels in Simulations 253
10.14Classification of MIMO schemes based on its interfering impact 257

11.1 Simulation parameters 267
11.2 Mean SINR for different cases with 7 Rx-antenna 269
11.3 Channel time-variance related parameters 273

© Muhammad Imadur Rahman, 2007

"The more you open your heart, the less you suffer."

Anonymous

1 Introduction

Wireless communication has gained a momentum in the last decade of 20th century with the success of 2nd Generation (2G) of digital cellular mobile services. Worldwide successes of GSM, IS-95, PDC, IS-54/137 etc, systems have shown new way of life for the new information and communication technology era. These systems were derived from a voice legacy, thus primary services were all voice transmission. 2G systems provided better quality of services at lower cost and a better connectivity compared to previous analog cellular systems. Numerous market researches show that there is a huge demand for high-speed mobile multimedia services all over the world. With the advent of 3rd Generation (3G) wireless systems, it is promised that higher mobility with reasonable data rate (up to 2Mbps) can be provided to meet the current user needs [1, 2]. But, 3G is not the end of the tunnel; ever increasing user demands have drawn the industry to search for better solutions to support data rates in the ranges of tens of Mbps. Naturally dealing with ever unpredictable wireless channel at high data rate communications is not an easy task. Hostile wireless channel has always been proved as a bottleneck for high speed wireless systems. This motivated the research towards finding a better solution for combating all the odds of wireless channels; thus, the idea of multi-carrier transmission has surfaced recently to be used for future generations of wireless systems.

3G promises wire line quality of services via wireless channel. For wide area coverage, further evolutions of 3G systems, such as High Speed Packet Access (HSPA) systems, are already being implemented in different parts of the world. Certainly the bit rate will be much higher than 2Mbps for such a system, up to tens of Mbps, to be exact 14.4Mbps for High Speed Downlink for Packet Access (HSDPA) and 5.76Mbps for High Speed Uplink for Packet Access (HSUPA) [3]. For

local area coverage, Wireless Local Area Networks (WLANs), such as IEEE 802.11a, HiperLAN/2 or MMAC[1] standards are capable of providing data rates up to 54Mbps. Along with these three, there are few other emerging short-range wireless applications available, such as Bluetooth, HomeRF, etc.

WLANs have potentially become an established tool in different user environments, namely home, corporate and public environment etc. They are used to connect wireless users to a fixed LAN in indoor environments. A major WLAN application is in public sectors, where WLAN can be used to connect users to the backbone network [4]. Airports, hotels, high-rise offices, city centers will be target areas for such public WLAN usage. A popular vision of future generations of telecommunications systems suggests that they will be an amalgamation of capabilities of high data-rate wireless wide area networks (such as UMTS) and newly standardized WLANs, i.e. the future networks will provide high rate at wide area in highly mobile scenario [5]. However, systems of the near future will be required to provide data rate of greater than 100 Mbps; hence there is a need to further improve the capacity of existing wireless systems. Although the term 4G is not yet clear to the industry, it is likely that they will enhance the 3G and beyond 3G networks in capacity, allowing greater range of applications and better universal access. Some of the visionaries term these systems as Mobile Broadband Systems (MBSs). Seamless and uninterrupted service quality for a user regardless of the system he/she is using will be one of the main goals of future systems. The expected systems will require an extensive amount of bandwidth per user.

1.1 Forthcoming 4G Systems

Several technologies are considered to be candidates for future applications. With the advent of Worldwide Interoperability for Microwave Access (WiMAX) and Universal Mobile Telecommunications Systems- Long Term Evolution (UMTS-LTE) activities under IEEE 802.16 and 3GPP respectively, there is a clear direction in the possible solutions for future 4th Generation (4G) systems. The research community agrees that high data rate at wider coverage area with suitable Quality of Service (QoS) mechanisms will be required for 4G systems [6].

Though some understanding of the future 4G systems is already achieved, yet, these research efforts have so far given rise to several distinctive features of the 4G technologies. So, an unified definition, characteristics and specifications of 4G systems is still subject to ongoing discussions [5]. We consider one of the major 4G features is to be reflected in the (co)existence of heterogeneous terminals. Namely, while 2G terminals were characterized by homogenous services and platforms, it is widely believed that different types of terminals will exist in 4G. The difference will be in terms of display size, energy consumption, complexity, etc. Each type of terminal fits a specific service or a subset of supported services. This sets the requirements for variable, but high data rates systems (in the order of tens of Mbps and more). Some services should also be available with high data rate under high mobility conditions.

Since 4G systems will be deployed in a wide range of environments and over heterogeneous terminals, it is of primary importance that the air interface should be adaptive. There is a

[1] IEEE802.11a is an USA-standard, HiperLAN/2 is a European standard and MMAC is developed in Japan. All three of the standards are almost similar in their PHY layers.

1G	2G	2.5G	3G	Beyond 3G	4G
Analog voice	Digital voice	Voice + data	Multimedia services	Broadband multimedia	Ubiquitous networks
NMT AMPS C-net	GSM PDC IS-95A IS-136	GPRS HSCSD EDGE IS-95B	WCDMA CDMA 2000 TD-SCDMA	HSPA WiMAX UMTS-LTE CDMA 2000 1xEV	IMT-A ??
FM modulation Analog switching Cellular concept Hard handover	Digital modulation Error control Data compression High quality voice	Voice + data Higher rate than 2G	'Any time, any where' Multimedia traffic Packet based data Dynamic RRM	High data rate High QoS support Broadband wide area	Heterogeneous networks Adaptive air interface Guaranteed QoS
FDMA	TDMA/ CDMA/ FDMA	TDMA/ CDMA/ FDMA	WCDMA	WCDMA/ OFDMA	OFDMA
very low rate	9.6-28.8kbps	57-115kbps	0.144∼2Mbps	∼10's of Mbps	∼100's of Mbps

Table 1.1: Evolution of Wireless Standards

© Muhammad Imadur Rahman, 2007

firm trend of service personalization, which imposes the tailoring of the content to the end-user device such as to enable adaptable service presentations, fitting the capabilities of the terminals in use regardless of network types. The user will have the services at disposal through soft-availability in terms of a flexible mapping of service to capabilities of the heterogeneous terminals taking the channel conditions and context into account. A single PHY layer technology cannot be optimal for all environments, terminal capabilities and user requirements, viz. short or long range, indoor or outdoor, low or high data rate, high or low mobility, multi-user capability, device processing power, weight and cost, service type, etc. A system capable of dynamically adapting one or more of the above parameters may offer superior performance. Hence, evaluation of different PHY technologies suited to various scenarios is necessary for selecting the optimal solution in each case. This presents the ground for implementing optimum adaptive PHY technology.

There are a number of generic PHY techniques that are expected to play major roles in the future wireless technologies:

1. Multi-carrier techniques will form the basis of PHY techniques [6], in which OFDM is the most widely recognized candidate. Multiple-access can be easily employed using OFDMA technique.

2. Multiple Input Multiple Output (MIMO) antenna techniques have been shown to offer large capacity gains under favorable environments compared to single antenna techniques. Besides, MIMO techniques can also be used to increase reliability of wireless links.

3. Advanced channel coding techniques, such as Turbo and Low Density Parity Check (LDPC) codes, through the suboptimal, but very efficient iterative decoding, have been shown to be the most efficient error-correction codes, getting closest to the Shannon limit.

4. Some forms of Code Division Multiple Access (CDMA) techniques, such as Frequency Hopping (FH) and Direct Sequence (DS), which will enable spectrum sharing in some specific multi-user and multi-cell systems.

With the emergence of mobile WiMAX and UMTS-LTE, which allows inter-operability and wide range of benefits compared to other technologies, it seems that these technologies are on tracks of their own towards the 4G goal. Thus, either working in complements or in competition, WiMAX and UMTS-LTE will be strong candidates to be the standard of next generation mobile technology [7]. These technologies propose solutions for many types of high-bandwidth and long distance applications and will enable service carriers to converge the all-IP-based network for triple-play services of data, voice, and video. With their QoS support, longer reach, and high data capacity, the envisioned 4G systems are positioned for broadband access applications in both rural and urban areas; and in both Fixed Wireless Access (FWA) and MBS scenario. Among other residential applications are high speed Internet, Voice Over IP telephony and streaming video/online gaming with additional applications for enterprises such as Video conference and Video surveillance, secured Virtual Private Network (with need for high security). The future technologies will also allow covering applications with media content requesting more bandwidth [5, 6].

1.2 Problem Statement

Orthogonal Frequency Division Multiplexing (OFDM) is a special form of multi-carrier transmission where all the sub-carriers are orthogonal to each other. It promises great resilience to severe signal fading effects of the wireless channel at a reasonable level of implementation complexity [8]. Judging the recent acceptance of OFDM technology for various different wireless systems, it can be seen that there is a strong possibility that next generation wireless era belongs to OFDM technology [5]. One of the main advantages that OFDM provides is the fine granularity in the time- and frequency-domains that can be exploited efficiently to optimize the system performance. Figure 1.1 shows the different time and frequency units in any OFDM system. One of the main challenges in designing any multi-user wireless system is to assign the available resources efficiently. Hence, it is an important question to utilize the time-frequency resources in an OFDM-based system so that the multiple access scheme is implemented according to the user requirement and the system scenario. Several techniques are proposed for implementing the multiple access in OFDM systems, namely OFDMA [9]; Orthogonal Frequency Division Multiplexing - Time Division Multiple Access (OFDM-TDMA) [10], which are basically pure Frequency Division Multiple Access (FDMA) and Time Division Multiple Access (TDMA) on top of an OFDM system. There are a number of proposals where the benefits of CDMA and OFDM are combined together, such as Multi-Carrier Code Division Multiple Access (MC-CDMA) [11], and Variable Spreading Factor - Orthogonal Frequency and Code Division Multiple Access (VSF-OFCDMA) [12], etc. These techniques are suitable for some specific scenarios, as they are designed according to the requirement of particular user environments [13]. It is well-known that when CSI is known at the transmitter, then time-frequency resources as seen in Figure 1.1 can be utilized optimally [14]. For wide area systems, users experience heterogeneous channel conditions in terms of delay spread and Doppler; also the scattering environment is very different for different users. Due to these reasons, it may become prohibitive to obtain the Channel State Information (CSI) at the transmitter side for designing the proper signalling scheme. With this motivation, we have proposed a channelization technique, namely Sub-Carrier and Band Hopped Orthogonal Frequency Division Multiple Access (SCBH-OFDMA), which improves the outage scenario, requiring only a single bit feedback on the statistical measure of the channel that the user is experiencing.

When full or partial CSI is available, a window of opportunity appears for improving the system performance. One of the techniques is Link Adaptation (LA), which exploits the known channel conditions to adapt the link parameters accordingly, so that the fading can be avoided and appropriate amount of bits can be transmitted across certain sub-carriers (or sub-channels). Several different techniques are proposed in literature [15, 16, 17, 18, 19]. Most of these algorithms are highly complex in terms of computational requirement, though high spectral efficiency is achieved. Based on these algorithms, we studied an algorithm, namely Simple Adaptive Modulation and Power Adaptation Algorithm (SAMPDA), which is a compromise between spectral efficiency and computational complexity. One of the very important issues in LA related studies is the rate at which we could adapt the bit and power level at specific sub-channels. Some theoretical studies are performed in this regard, such as [20]. In these studies, it is proposed that power and bit adaptation need not be done simultaneously, as it does not provide any additional gain compared to only bit-

© Muhammad Imadur Rahman, 2007

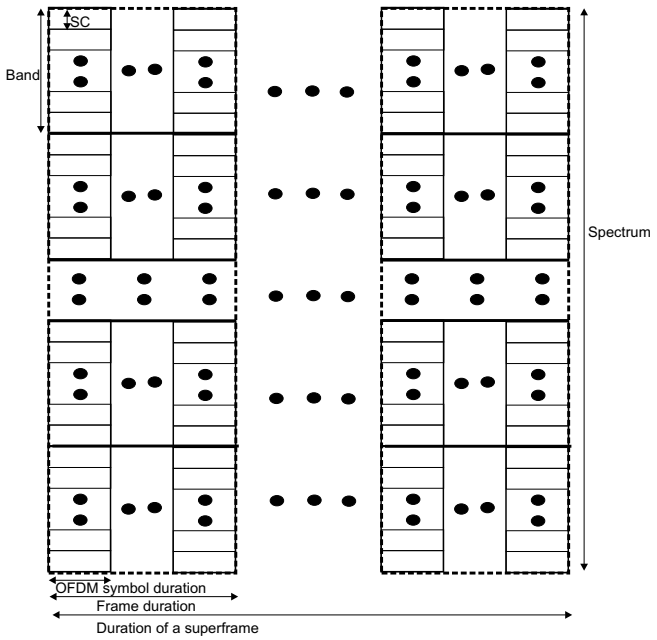

Figure 1.1: Time-Frequency OFDM granularity that can be exploited for increasing system spectral efficiency

adapted systems. In this work, we have shown in certain scenarios, bit and power adjustments can be done simultaneously and some gains in terms of power savings can be obtained. To the best of our knowledge, these studies are not conducted for WiMAX/UMTS-LTE type scenario so far. It is also an interesting problem to study the suitable size of time-frequency domain resources of any OFDM resources (as seen in Figure 1.1) that can be utilized in LA process. We also handle this issue in this thesis. So far, most of the available LA studies consider an idealized scenario, where system impairments in terms of transmitter non-linearities, frequency de-synchronization etc, are not considered. It is expected that these impairments would require revised threshold levels for bit and power adaptation purposes.

Besides the recent advancements of OFDM techniques, MIMO algorithms will also be an important element in all future wireless systems. Numerous MIMO diversity and multiplexing algorithms are studied in the available literature [21, 22, 23, 24, 25, 26]. In line with this research, there is a need to study advanced (and simplified) MIMO techniques for either decreasing the implementation complexity while preserving the MIMO benefits, or increasing the spectral efficiency by exploiting more spatial dimensions. In this light, we have studied a number of MIMO signalling techniques, where both diversity and multiplexing benefits can be obtained in the same structure. The combination is done in the space domain, in comparison to hybrid MIMO structures that combine diversity and multiplexing in the time-domain, such as [27]. We call such schemes as Joint Diversity and Multiplexing (JDM). Besides, we have also studied Cyclic Delay Diversity (CDD) based receive diversity system, where a novel Pre-DFT combining receiver is developed and a trade-off between required complexity and system performance is studied. All these studies are done on a pure link level, where no interference is considered.

In a cellular system, the performance of well-known MIMO techniques can become very

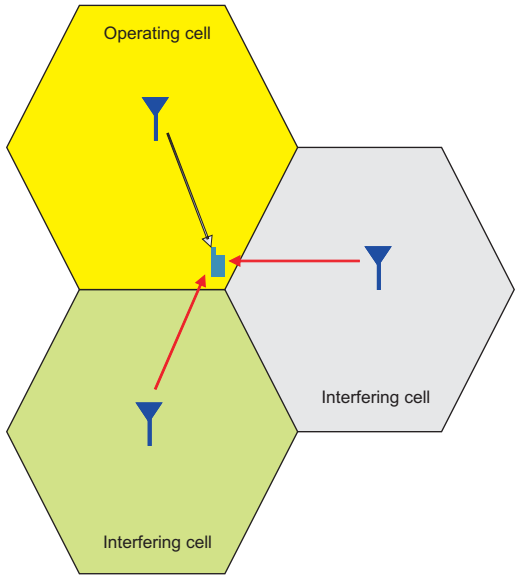

Only two interfering cells are shown for simplicity. In practice, there will be at least one full tier of interfering cells.

Figure 1.2: Cellular interference scenario

different than its performance in link level scenario. Due to the fact that users in neighboring cells may operate in co-channel, we may experience a scenario where the performance of any MIMO can be severely affected by Co-Channel Interference (CCI) caused by the same or other MIMO schemes. The interfering links in Figure 1.2 may use the same or any other MIMO schemes. This depends on the MIMO scheme assigned to any user based on its channel condition. In broadband systems, such as WiMAX and UMTS-LTE, aggressive frequency re-use factor will be pursued (i.e. reuse factors will be close to 1), thus, the possibility that the same or other MIMO schemes will collide in the same sub-channel will be very high. Recent studies of MIMO schemes in CCI scenario concentrate very much on theoretical capacity analysis, such as [28, 29, 30]. Besides these works, there is a number of works where some specific solutions for CCI cancelation or avoidance is studied when a MIMO link is interfered by the same MIMO link from interfering cells [31, 32]. Very little attention has been given so far about the impact on BER and/or system throughput when a MIMO link is interfered by the same or other MIMO schemes. It is well-known that the nature and number of interfering logical streams are important in interference cancelation schemes [33]. Besides, the number of logical streams has more impact on the desired link than the power of the interferers. Using this knowledge, we have studied the impact of different MIMO schemes on each other in terms of error rate. Then, we have proposed a robust receiver solution together with a frequency-reuse proposal at the cell-edge where the CCI is severe.

© Muhammad Imadur Rahman, 2007

1.3 Thesis Overview and Organization

This rest of this thesis is organized as follows:

Chapter 2: The basics about the wireless channel characteristics, OFDM fundamentals and preliminaries about multi-antenna techniques are presented in Chapter 2.

Chapter 3: This chapter describes our proposed channelization technique, Sub-Carrier and Band Hopped Orthogonal Frequency Division Multiple Access (SCBH-OFDMA). We present the basic idea behind SCBH-OFDMA and a system model of the access technique. Then we describe the system level performance of the proposed technique in cellular scenario, with varying amount of CCI. The performance of SCBH-OFDMA is compared with static sub-carrier allocation and random sub-carrier hopping based OFDMA system.

Chapter 4: Related to SCBH-OFDMA, Chapter 4 discusses several system design issues regarding the SCBH-OFDMA technique. This includes transceiver structure, user grouping procedure, frame formats, hopping sequence design, etc.

Chapter 5: Frequency domain Link Adaptation (LA) is studied in Chapter 5. In Section 5.2, we have described two of the LA techniques available from literature, and based on this, we study another algorithm, Simple Adaptive Modulation and Power Adaptation Algorithm (SAMPDA). A brief comparison of these three algorithms in uncoded scenario is presented afterwards. We study the interaction between spatial diversity and link adaptation in this chapter, where we have analyzed the impact of different rates of adaptations in collaboration with multi-antenna techniques.

Chapter 6: Based on the understanding and knowledge obtained in Chapter 5 about frequency domain link adaptation, we study the impact of different rates of bit and power allocations together with the possibilities of different LA mechanisms to be implemented, considering the impact of delay spread, Doppler conditions, possible LA rates etc. We also include the impact of transmitter non-linearities in LA-based system in Chapter 6.

Chapter 7: Issues related to the usage of Transmit Beamforming (TxBF) and transmit diversity schemes are studied in this chapter. Special attention is given to outage probability for certain outage capacity of the systems. From this point onwards, we have performed numerical evaluations to compare the usability of diversity and array gain in indoor and outdoor scenarios.

Chapter 8: We study the exploitation of Cyclic Delay Diversity (CDD) technique in OFDM system in Chapter 8. First, we have explained the CDD principle, followed by implementing CDD in OFDM receiver. A new technique, Pre-DFT Maximal Average Ratio Combining (MARC), is proposed that can be used in low delay spread environment to obtain receive diversity by utilizing Pre-DFT combining techniques. A performance comparison is presented in terms of BER with and

without coding, between MRC for receiver diversity and CDD for transmitter and receiver diversity in the context of IEEE 802.11a and/or HiperLAN/2 WLAN systems. We have also studied implementation of CDD on top of a Spatial Multiplexing (SM) system, and studied the so-called Cyclic Delay Assisted Spatial Multiplexing (CDA-SM) system in this chapter.

Chapter 9: In this chapter, we study Joint Diversity and Multiplexing (JDM) systems, where both the diversity and multiplexing benefits are obtained simultaneously at the same MIMO structure. Two types of JDM systems, namely Spatially-Multiplexed Orthogonal SFBC (SM-OSFBC) system and Spatially-Multiplexed Quasi-orthogonal SFBC (SM-QSFBC) systems are studied in the chapter.

Chapter 10: In this chapter, we have summarized our analysis and simulations related to cellular interference of some specific MIMO schemes on the same and other MIMO schemes. The goal is to study the impact of interference from MIMO schemes at a user located in the cell edge. Semi-Analytical evaluations of SINR is done to find out the SINR statistics of different combinations of desired and interfering links. We have studied linear combining receivers for all the link combinations.

Chapter 11: Based on the analysis in Chapter 10, we propose a robust receiver technique for interference cancelation and a suitable fractional frequency re-use for interference avoidance to be used at cell edge.

Chapter 12: Conclusions are drawn in Chapter 12. We have summarized the conclusions of the work conducted under this PhD project in this chapter, followed by the summary of the contribution and future outlook.

© Muhammad Imadur Rahman, 2007

2

Multi-carrier Modulation and MIMO Systems

In this chapter, we explain the preliminaries about the relevant issues under the work area of this PhD project. We have summarized the wireless channel characteristics and the motivation for using multi-carrier modulation in Section 2.1. OFDM fundamentals are briefly explained in Section 2.2. Basic multiple access over OFDM is discussed in Section 2.3, where the main concentration is OFDMA based techniques. We include a brief summary of two important wireless standards based on multi-carrier systems in Section 2.3.2. Finally, we have briefly presented some fundamental issues related to multi-antenna techniques in Section 2.4, where we have also included a short discussion about usability of different multi-antenna techniques in OFDM based systems.

2.1 Channel Impairments and Multi-carrier Modulation

Wireless channel is always very unpredictable with harsh and challenging propagation situations. Wireless channel differs from wire line channel in a lot of ways. One of the most unique characteristics of wireless channel is multipath reception. Together with multipath, there are other serious impairments present at the channel, namely propagation path loss, shadow fading, Doppler spread, time dispersion or delay spread, etc.

2.1.1 Physical Characteristics of Multipath Channels

2.1.1.1 Multipath Scenario

Multipath is the result of reflection of wireless signals by objects in the environment between the transmitter and receiver. The objects can be anything present on the signal traveling path, e.g. buildings, trees, vehicles, hills or even human beings. Thus, multipath scenario includes random number of received signal from the same transmission source; depending on the location of transmitter and receiver, a direct transmission path referred to as the *Line-Of-Sight* (LOS) path may be present or may not be present. When LOS component is present (or when one of the components is much stronger than others), then the environment is modeled as Ricean channel, and when no LOS signal is present, the environment is described as Rayleigh channel [34, 35].

Multipaths arrive at the receiver with random phase offsets, because each reflected wave follows a different path from transmitter to reach the receiver. The reflected waves interfere with direct LOS wave, and cause a severe degradation of network performance. This results in random signal fades as the reflections destructively (and/or constructively) superimpose one another, which effectively cancels part of signal energy for a brief period of time. The severity of fading will depend on delay spread of the reflected signal, as embodied by their relative phases and their relative power [34, 36, 37].

A common approach to represent the multipath channel is as the Channel Impulse Response (CIR). The channel baseband equivalent impulse response function, $\tilde{h}_u(t)$ is defined as

$$\tilde{h}_u(\tau, t) = \sum_{l=0}^{L} h_{u,l}(t)\delta_c(\tau - \tau_l) \tag{2.1}$$

where $h_{u,l}(t) = A_{t,l}\exp(-j\theta_{t,l})$ is the complex gain of the lth multipath component at time t. Here, $A_{t,l}$, $\theta_{t,l}$ and τ_l are the amplitude, phase and delay of the lth path. The CIR given by Eq.(2.1) is also called Power Delay Profile (PDP), which is shown in Figure 2.1.

Delay spread is the time spread between the arrival of the first and last multipath signal seen by receiver. The time dispersion in a channel is commonly measured by the Root Mean Square (RMS) delay spread τ_{rms}. It is the square root of the second central moment of the PDP as defined below [34, 36, 37, 38]:

$$\tau_{rms} = \left[\bar{\tau^2} - (\bar{\tau})^2\right]^{\frac{1}{2}} \tag{2.2}$$

where,

$$\bar{\tau^2} = \frac{\sum_{l=1}^{L} A_l^2\tau_l^2}{\sum_{l=1}^{L} A_l^2} = \frac{\sum_{l=1}^{L} P(\tau_l)\tau_l^2}{\sum_{l=1}^{L} P(\tau_l)} \tag{2.3}$$

$$\bar{\tau} = \frac{\sum_{l=1}^{L} A_l^2\tau_l}{\sum_{l=1}^{L} A_l^2} = \frac{\sum_{l=1}^{L} P(\tau_l)\tau_l}{\sum_{l=1}^{L} P(\tau_l)} \tag{2.4}$$

For clarity, we can remove the time index from the expressions related to CIR, as the CIR can be assumed to be time invariant, or at least to be wide sense stationary over a small-scale time or distance interval [38, Section 5.2]. $\bar{\tau}$ in Eq.(2.4) is the mean excess delay, defined as the

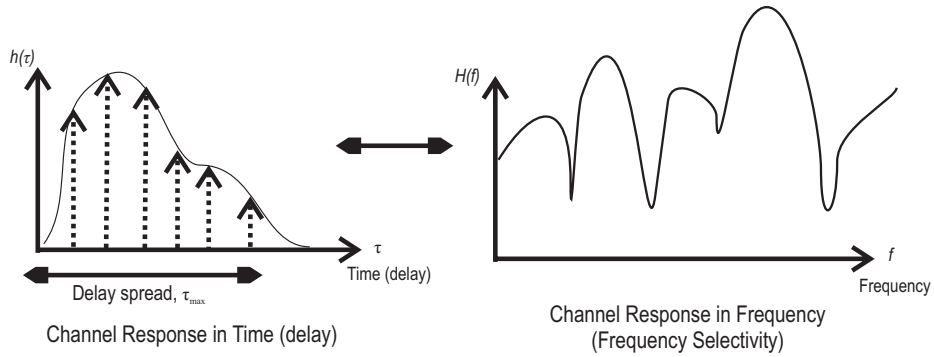

Figure 2.1: Channel impulse responses and corresponding frequency response

first moment of PDP; $\bar{\tau^2}$ is the excess delay spread, defined as the first moment of squared delays. Eqs.(2.2 - 2.4) do not depend on the absolute power level of $P(\tau_l)$, rather they only consider the relative amplitude between the first and later multipaths. In practice, values for τ_{rms}, $\bar{\tau^2}$ and $\bar{\tau}$ depend on the choice of noise threshold used to process $P(\tau_l)$ [38].

The corresponding frequency-domain Channel Transfer Function (CTF), $H_u(f,t)$, can then be found using Fourier transformation:

$$\begin{aligned} H_u(f,t) &= \mathcal{F}\left\{\tilde{h}_u(\tau,t)\right\} \\ &= \int_{-\infty}^{\infty} \tilde{h}_u(\tau,t) e^{-j2\pi f\tau} d\tau \end{aligned} \tag{2.5}$$

Related to delay spread is *Coherence Bandwidth*, which is used to define channel frequency selectivity level [34, 36]. If the coherence bandwidth is defined as the bandwidth over which the frequency correlation function is above 0.5, then the coherence bandwidth is approximately, $B_c = \frac{1}{5\tau_{rms}}$ [35]. Based on this, we can define the values for coherence bandwidth as shown in Table 2.1. If the system bandwidth is much smaller compared to the coherence bandwidth, then the channel is said to be frequency non selective. In this case, the correlation coefficient is almost 1 for the frequencies within the system bandwidth. Physically, the frequency response within the system bandwidth is almost flat, so this kind of fading is also called flat fading. On the other hand, if the system bandwidth is larger than the coherence bandwidth, then the channel is said to be frequency selective.

In a digital system, the delay spread can lead to Inter-Symbol Interference (ISI). In Figure 2.1, the delay spread amounts to τ_{max}. It is noted that delay spread is always measured with respect to the first arriving component. Let's assume a system transmitting in the time intervals T_{sym}. The longest path with respect to the earliest path arrives at the receiver with a delay of τ_{max}; in other words, the last path arrives τ_{max} seconds after the first path arrives. This means that a received symbol can theoretically be influenced by previous symbols, which is termed as ISI. With high data rate, T_{sym} can be very small; thus the number of symbols that are affected by ISI can be in multiple of tens or more. Combating the influence of such large ISI at the receiver is very challenging and sometimes may become unattainable at very severe channel conditions [39, 40, 41].

© Muhammad Imadur Rahman, 2007

RMS delay spread	Coherence bandwidth
τ_{rms}	B_c
50ns	4MHz
100ns	2MHz
0.5μs	400kHz
1.0μs	200kHz
2.0μs	100kHz
3.0μs	66.67kHz
5.0μs	40kHz

Table 2.1: Channel coherence bandwidth with respect to different RMS delay spread

2.1.1.2 Doppler Effect

The Doppler effect is caused by the relative motion of transmitter and receiver. For example, in an urban environment in the city center, the vehicles are always moving; the walking pedestrians are also changing their locations continuously, thus their movements affect the transmission medium. The Doppler effect is expressed with so called Doppler shift or Doppler frequency which happens when there is a relative movement between the transmitter and receiver with a velocity v. The Doppler shift can be defined as [38]:

$$f_d = \frac{1}{2\pi}\frac{\Delta\phi}{\Delta t} = \frac{v}{\lambda}cos\theta \tag{2.6}$$

where $\Delta\phi$ is the change of phase, defined as:

$$\Delta\phi = \frac{2\pi\Delta l}{\lambda} = \frac{2\pi v\Delta t}{\lambda}cos(\theta) \tag{2.7}$$

where, Δt is the time taken by the receiver to travel from one place to another and Δl is the difference in the pathlengths from the transmitter to these two locations of the mobile receiver. θ is the angle of arrival of the signal component. Although the receiver has moved from one place to another, the change in θ can be neglected assuming that the transmitter and receiver are located far away. It is obvious that the maximum Doppler shift is $f_m = \frac{v}{\lambda}$. Fourier transform of Doppler spread gives Doppler power spectral density.

Related to Doppler spread is a term, namely coherence time, which is inversely proportional to maximum Doppler frequency, thus, the time variance of the channel is directly related the relative motion of transmitter and receiver [38]. Coherence Time (T_c) is a measure of the time-variance of a channel. If it is defined as the time over which the time correlation function is 0.5, then the coherence time is approximately, $T_c = \sqrt{\frac{9}{16\pi f_d^2}} = \frac{0.4231}{f_d}$ [38, Section 4.4.3], when $f_d = \frac{v}{c}f_c$ is maximum Doppler shift. Here v, c and f_c are user velocity, speed of light and carrier frequency respectively. From Table 2.2, we can get an estimate of the largest allowable symbol duration for the channel to be quasi-static over one multi-carrier symbol duration.

A high Doppler can be experienced when a user is located in a fast moving car or in a speedy train, because the relative motion will be higher when either transmitter or receiver is moving very fast. This relative motion of transmitter and receiver changes the received signal from the

	2.0GHz		3.5GHz	
v, kmph	f_d, Hz	T_c, ms	f_d, Hz	T_c, ms
3	5.56	76.2	9.72	43.5
10	18.52	22.8	32.41	13.1
20	37.04	11.4	64.82	6.5
50	92.59	4.6	162.04	2.6
100	185.19	2.3	324.08	1.3
150	277.78	1.5	486.11	0.9
200	370.37	1.1	648.15	0.7
250	462.96	0.9	810.19	0.5

Table 2.2: Channel coherence time at 2.0GHz and 3.5GHz of carrier frequency with respect to receiver mobility

original transmitted signal. When they are moving towards each other, the frequency of the received signal is higher than the source and when they moving away from each other, the received frequency decreases. When the relative speed is higher, then Doppler shift can be very high, and thus the receiver may become unable to detect the transmitted signal frequency. Even at lower relative motion when the Doppler shift is usually very little, if the transmission and reception technique is very sensitive to carrier frequency offset, then the system may fail.

2.1.1.3 Shadow Fading or Shadowing

Shadow fading is another troublesome effect of wireless channel. Wireless signals are obstructed by large obstacles, like huge buildings, high hills, etc. These large objects cause reflections off their surface and attenuation of signals passing through them, resulting in shadowing, or shadow fading. The amount of shadowing depends on the size of the object, the structure of the material, and the frequency of the Radio Frequency (RF) signal. Large attenuations by huge obstacles can result in deep fading behind them. Under this condition, most of the received signal energy comes from reflected and diffracted paths of the original signal, because LOS is absent due to large objects between the transmitter and the receiver.

2.1.1.4 Propagation Path Loss

Together with the multipath effect, shadowing and Doppler spread, the propagation loss is also a very significant factor. The propagation loss increases by 2nd to 6th power of distance; typically fourth power of distance for usual wireless channels [34, 42, 43]. So, for higher distances, propagation loss becomes significant. Well defined situation specific path loss models are available to estimate the propagation pathloss. Many traditional models are popular for calculating the path loss such as the Hata-Okumura and the COST231-Hata model [38]. However both of these models are derived for frequency ranges up to 2000 MHz. An empirically derived model is proposed in [44] which can be used for other frequency ranges. Though this model is for FWA application, it is still valid for the system under study. For a given close in distance (or reference distance) d_0 of

© Muhammad Imadur Rahman, 2007

Parameters	Urban terrain	Unit
a	4.6	
b	0.0075	m^{-1}
c	12.6	m

Table 2.3: Value of parameters for urban terrain

100m, the median path loss (PL) in dB, is given by,

$$PL = A + 10n_p \log_{10}\frac{d}{d_o} + s, \qquad d > d_o, \tag{2.8}$$

where

$$A = 20\log_{10}(4\pi d_o/\lambda) \tag{2.9}$$

and n_p is the path loss exponent for each terrain category. It is given by,

$$n_p = a - bh_b + c/h_b, \quad 10m < h_b < 80m \tag{2.10}$$

The values of a, b and c are different for different terrain types. Values for urban area are given in Table 2.3 [45]. s is the shadowing factor and follows a log normal distribution with a typical shadowing variation of around 6 dB [44].

This model is proposed for a receiver antenna height of 2m and an operating frequency of 2GHz. Correction factors for other frequencies and antenna heights are proposed in [45]. The modified path loss expression can be written as,

$$PL_{mod} = PL + \Delta PL_f + \Delta PL_h \tag{2.11}$$

where,

- PL is path loss given by Eq.(2.8),
- ΔPL_f is frequency correction term given by $6\log_{10}(f/2000)$, f is the frequency in MHz, and
- ΔPL_h is receiver antenna height correction term given by $-10.8log_{10}(h/2)$, where h is the new receiver antenna height (in meter) such that $2 < h < 8$.

2.1.2 The Benefit of Using Multi-carrier Transmission

Time dispersion represents a distortion of the signal that is manifested by the spreading of the modulation symbols in the time domain. It is well-known that the coherence bandwidth of the channel is always smaller than the modulation bandwidth in case of broadband multimedia communications, so, ISI is unavoidable in such wireless channels. In many instances, fading by the multipath will be frequency selective. This frequency-selectivity effect has a random pattern at any given time. This fading occurs when the channel introduces time dispersion and the delay spread is larger than the symbol period. Frequency selective fading is difficult to compensate because the fading characteristics are random and sometimes may not be easily predictable. When

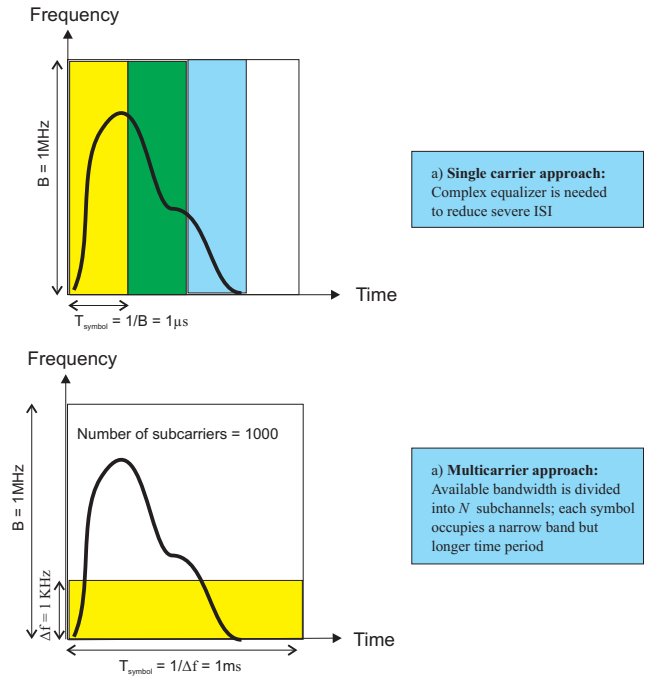

Figure 2.2: Single Carrier Vs Multi-carrier Approach

there is no dispersion and the delay spread is less than the symbol period, the fading will be flat, thereby affecting all frequencies in the signal equally. Practically flat fading is easily estimated and compensated with a simple equalization [34, 35].

A single carrier system suffers from ISI problem when the data rate is very high. According to previous discussions, we have seen that with a symbol duration T_{sym}, ISI occurs when $\tau_{max} > T_{sym}$. Multichannel transmission has surfaced to solve this problem. The idea is to increase the symbol duration and thus reduce the effect of ISI. Reducing the effect of ISI yields an easier equalization, which in turn means simpler reception techniques.

Wireless multimedia solutions require up to tens of Mbps for a reasonable QoS. If we consider single carrier high speed wireless data transmission, we see that the delay spread at such high data rates will definitely be greater than the symbol duration even considering the best case outdoor scenario. Now, if we divide the high data rate channel over a number of sub-carriers, then we have larger symbol duration in the sub-carriers and the delay spread is much smaller than the symbol duration.

Figure 2.2 describes this very issue. Assuming that we have available bandwidth B of 1MHz in a single carrier approach, we transmit the data at symbol duration of 1μs. Consider a typical outdoor scenario where the maximum delay spread can be as high as 10μs, so at the worst case scenario, at least 10 consecutive symbols will be affected by ISI due to the delay spread.

In a single carrier system, this situation is compensated by using equalization techniques. Using the estimates of channel impulse response, the equalizer multiplies complex conjugate of the estimated impulse response with the received data signal at the receiver. There are other well-known equalization algorithms available in the literature, such as adaptive equalization via Least

© Muhammad Imadur Rahman, 2007

Mean Square (LMS), Recursive Least Squares (RLS) algorithms [46], etc. However, there are some practical computational difficulties in performing these equalization techniques at tens of Mbps with compact and low cost hardware. It is worth mentioning here that compact and low cost hardware devices do not necessarily function at very high data speed. In fact, equalization procedures take bulk of receiver resources, costing high computation power and thus overall service and hardware cost becomes high.

One way to achieve reasonable quality and solve the problems described above for broadband mobile communication is to use parallel transmission. In a crude sense, someone can say in principle that parallel transmission is just the summation of a number of single carrier transmissions at the adjacent frequencies [8]. The difference is that the channels have lower data transmission rate than the original single carrier system and the low rate streams are orthogonal to each other. If we consider a multi-carrier approach where we have N number of sub-carriers, we can see that we can have $\frac{B}{N}$ Hz of bandwidth per sub-carrier. If N = 1000 and B = 1MHz, then we have a sub-carrier bandwidth Δf of 1kHz. Thus, the symbol duration in a sub-carrier will be increased to 1ms (= $\frac{1}{1kHz}$). Here each symbol occupies a narrow band but a longer time period. This clearly shows that the delay spread of 1ms will not have any ISI effect on the received symbols in the outdoor scenario mentioned above. So, we can say that the multi-carrier approach turns the channel to a flat fading channel and thus can easily be estimated.

Theoretically increasing the number of sub-carriers should be able to give better performance in a sense that we will be able to handle larger delay spreads. But several typical implementation problems arise with a large number of sub-carriers. When we have large numbers of sub-carriers, we have to assign the sub-carriers frequencies very close to each other, if the available bandwidth is not increased. We know that the receiver needs to synchronize itself to the carrier frequency very well, otherwise a comparatively small carrier frequency offset may cause a large frequency mismatch between neighboring sub-carrier. When the sub-carrier spacing is very small, the receiver synchronization components need to be very accurate, which is still not possible with low-cost RF hardware. Thus, a reasonable trade-off between the sub-carrier spacing and the number of sub-carriers must be achieved.

Table 2.4 describes how multi-carrier approach can convert the channel to flat fading channel from frequency selective fading channel. We have considered a multi-carrier system with respect to a single carrier system, where the system data rate requirement is 1Mbps. When we use 128 sub-carriers for multi-carrier system, we can see that the ISI problem is clearly solved. It is obvious that if we increase the number of sub-carriers, the system will theoretically provide even better performance.

2.2 OFDM Fundamentals

Orthogonal Frequency Division Multiplexing (OFDM) promises a higher user data rate transmission capability at a reasonable complexity and precision. At high data rates, the channel distortion to the data is very significant, and it may not be possible to recover the transmitted data with a simple receiver. A very complex receiver structure may be required which makes use of computationally extensive equalization and channel estimation algorithms to correctly estimate the channel,

Design Parameters for outdoor channel	Required data rate	1Mbps
	RMS delay spread, τ_{rms}	10μs
	Channel coherence bandwidth, $B_c = \frac{1}{5\tau_{rms}}$	20KHz
	Frequency selectivity condition	$\sigma > \frac{T_{sym}}{10}$
Single carrier approach	Symbol duration, T_{sym}	1μs
	Frequency selectivity	$10\mu s > \frac{1\mu s}{10} \Longrightarrow$ **YES**
	ISI occurs as the channel is frequency selective	
Multicarrier approach	Total number of sub-carriers	128
	Data rate per sub-carrier	7.8125kbps
	Symbol duration per sub-carrier	$T_{carr} = 128\mu s$
	Frequency selectivity	$10\mu s > \frac{128\mu s}{10} \Longrightarrow$ **NO**
	ISI is reduced as flat fading occurs. CP completely removes the remaining ISI; and also inter-block interference is removed	

Table 2.4: Comparison of Single Carrier and Multi-carrier Approach in terms of Channel Frequency Selectivity

so that the estimations can be used with the received data to recover the originally transmitted data. OFDM can drastically simplify the equalization problem by turning the frequency selective channel to a flat channel, as described in Section 2.1.2. A simple one-tap equalizer is needed recover the data. Besides, future telecommunication systems must be spectrally efficient to support a number of high data rate users. OFDM uses the available spectrum very efficiently which is very useful for multimedia communications.

2.2.1 OFDM Transceiver Systems

A complete OFDM transceiver system is described in Figure 2.3. In this model, Forward Error Correction (FEC) coding and interleaving are added in the system to obtain the robustness needed to protect against burst errors (see Section 2.2.2 for details). An OFDM system with addition of channel coding and interleaving is referred to as Coded Orthogonal Frequency Division Multiplexing (COFDM).

In a digital domain, binary input data is collected and FEC coded with schemes such as convolutional codes. The coded bit stream is interleaved to obtain diversity gain. Afterwards, a group of channel coded bits are gathered together (1 for Binary Phase Shift Keying (BPSK), 2 for Quadrature Phase Shift Keying (QPSK), 4 for 16-QAM, etc.) and mapped to corresponding constellation points. At this point, the data is represented in complex numbers and they are in serial. Known pilot symbols mapped with known mapping schemes can be inserted at this moment. A serial to parallel converter is applied and the IFFT operation is performed on the parallel complex data. The transformed data is grouped together again, as per the number of required transmission sub-carriers. Cyclic prefix is inserted in every block of data according to the system specification and the data is multiplexed to a serial fashion. At this point of time, the data is OFDM modulated and ready to be transmitted. A Digital to Analogue Converter (DAC) is used to transform the time domain digital data to time domain analog data. RF modulation is performed and the signal is up-converted to transmission frequency.

© Muhammad Imadur Rahman, 2007

After the transmission of OFDM signal from the transmitter antenna, the signal goes through all the anomaly and hostility of wireless channel. After receiving the signal, the receiver down-converts the signal to the baseband, and converts to digital domain using Analog-to-Digital Converter (ADC). At the time of down-conversion of received signal, carrier frequency synchronization is performed. After ADC conversion, symbol timing synchronization is achieved. An FFT block is used to demodulate the OFDM signal. After that, channel estimation is performed using the demodulated pilots. Using the estimations, complex received data is obtained which are de-mapped according to the transmission constellation diagram. At this moment, FEC decoding and de-interleaving are used to recover the originally transmitted bit stream.

2.2.2 Channel Coding and Interleaving

Since OFDM carriers are spread over a frequency range, there still may be some frequency selective attenuation on a time varying basis. A deep fade on a particular frequency may cause the loss of data on that frequency for that given time, thus some of the sub-carriers can be strongly attenuated which will cause burst errors. In these situations, FEC in COFDM can fix the errors [41]. An efficient FEC coding in flat fading situations leads to a very high coding gain, especially if soft decision decoding is applied. In a single-carrier modulation, if such a deep fade occurs, too many consecutive symbols may be lost and FEC may not be too effective in recovering the lost data [47].

Data rate (Mbps)	Modulation scheme	Coding rate	Coded bits per sub-carrier	Code bits per OFDM symbol	Data bits per OFDM symbol
6	BPSK	$\frac{1}{2}$	1	48	24
9	BPSK	$\frac{3}{4}$	1	48	36
12	QPSK	$\frac{1}{2}$	2	96	48
18	QPSK	$\frac{3}{4}$	2	96	72
24	16-QAM	$\frac{1}{2}$	4	192	96
36	16-QAM	$\frac{3}{4}$	4	192	144
48	64-QAM	$\frac{2}{3}$	6	288	192
54	64-QAM	$\frac{3}{4}$	6	288	216

Table 2.5: IEEE 802.11a OFDM PHY Modulation Techniques

Experience show that the BER performance of basic OFDM systems can be quite poor. Depending on the channel conditions, it may not even be possible to obtain a BER of 10^{-5} or 10^{-6} without channel coding. Thus, all OFDM systems nowadays are converted to COFDM. The benefits of COFDM are two-fold in terms of performance improvement. First, the benefit that the channel coding brings in, that is the robustness to burst errors. Second, interleaving brings frequency diversity. The interleaver ensures that adjacent outputs from channel encoder are placed far apart in the frequency domain. Specifically for a $\frac{1}{2}$-rate encoder, the channel encoder provides two output bits for one source bit. When they are placed far apart from each other (i.e. placed on sub-carriers that are far from each other in frequency domain), they experience unique gain (and/or unique fade), i.e. independent fading. It is very unlikely that both of the bits will face a

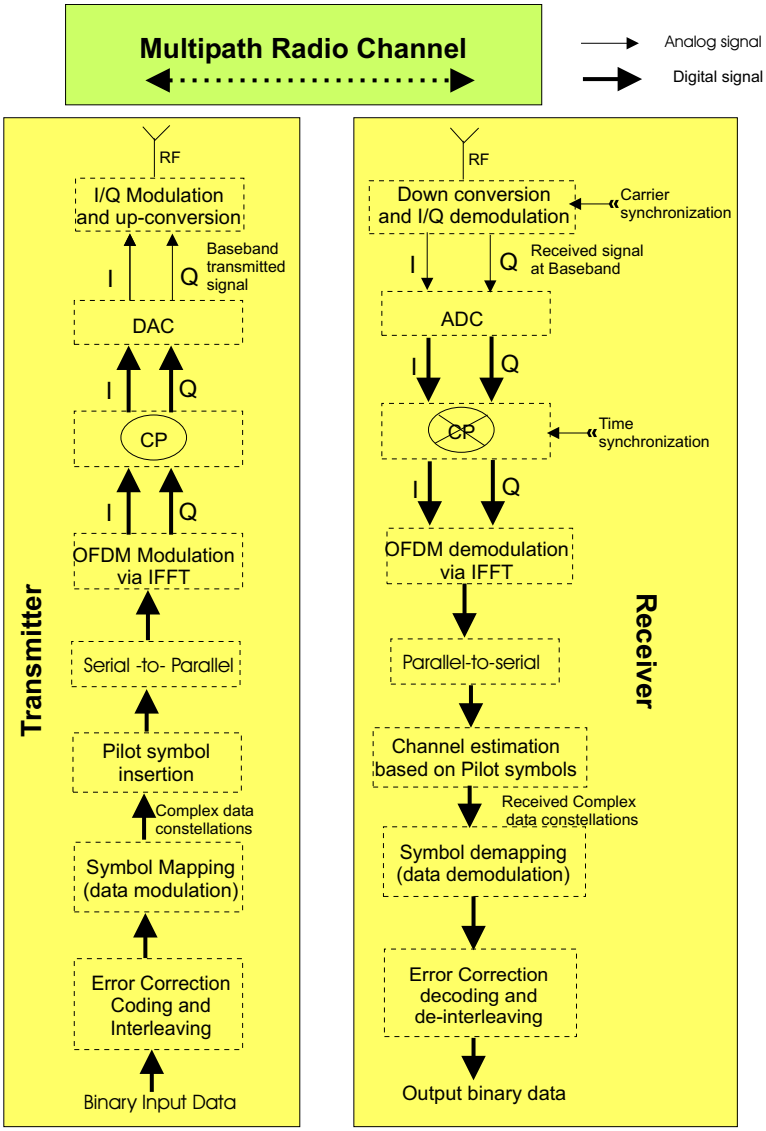

Figure 2.3: OFDM Transceiver Model

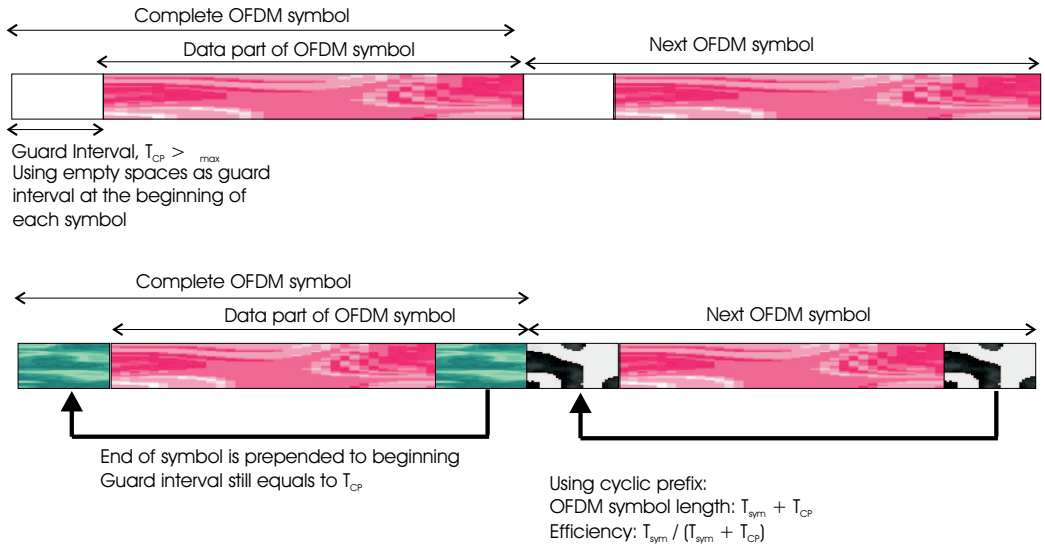

Figure 2.4: Role of Guard Interval and Cyclic Prefix in Combatting ISI and ICI

deep fade, and thus at least one of the bits will be received intact on the receiver side, and as a result, overall BER performance will be improved [48].

According to Table 2.5, the IEEE 802.11a standard enables several data rates by making use of different combinations of modulation and channel coding schemes. It is worth mentioning here that the standard demands all 802.11a compliant products to support all the data rates. Table 2.5 presents the different arrangement of modulation and coding scheme that are used to obtain the data rates [49].

2.2.3 Combating ISI and Reducing ICI

When a signal passes through a time-dispersive channel, the orthogonality of the signal can be jeopardized. The Cyclic Prefix (CP) helps to maintain orthogonality between the sub-carriers. Before the CP was invented, a guard interval was proposed as the solution. the Guard interval was defined by an empty space between two OFDM symbols, which serves as a buffer for the delay spread occurred due to multipath phenomenon. The interval must be chosen larger than the expected maximum delay spread, such that multi path reflection from one symbol would not interfere with another. In practice, the empty guard time introduces Inter-Carrier Interference (ICI). ICI is crosstalk between different sub-carriers, which means they are no longer orthogonal to each other [8]. A better solution was later found, that is cyclic extension of OFDM symbol or CP. CP is a copy of the last part of OFDM symbol which is appended to the front of the transmitted OFDM symbol.

The CP still occupies the same time interval as the guard period, but it ensures that the delayed replicas of the OFDM symbols will always have a complete symbol within the FFT interval (often referred as FFT window). This periodicity plays a very significant role as this helps maintaining the orthogonality. The concept of being able to do this, and what it means, comes from the nature of the IFFT/FFT process. When the IFFT is taken for a symbol period during the OFDM

modulation, the resulting time sample process is periodic. In a Fourier transform, all the resultant components of the original signal are orthogonal to each other. So, in short, by providing periodicity to the OFDM source signal, CP makes sure that subsequent sub-carriers are orthogonal to each other.

At the receiver side, CP is removed before any processing starts. As long as the length of CP interval is larger than the expected delay spread τ_{max}, all multipaths of previous symbols are removed and orthogonality is restored. The orthogonality is lost if the delay spread is larger than length of CP interval. Inserting the CP has its own cost, we loose a part of signal energy and transmission time since it carries no information. The loss is measured as

$$SNR_{loss_CP} = -10\log_{10}\left(1 - \frac{T_{CP}}{T_{sym}}\right) \tag{2.12}$$

Here, T_{CP} is the interval length of CP and T_{sym} is the OFDM symbol duration. It is understood that although we loose part of signal energy, the fact that zero ICI and ISI situation somehow pay off the loss, or at least satisfy a good trade-off.

To conclude, CP gives two-fold advantages, first occupying the guard interval, it removes the effect of ISI and by maintaining orthogonality it completely removes the ICI. The cost in terms of signal energy loss is not too significant provided that the CP duration is optimal corresponding to channel delay spread scenario.

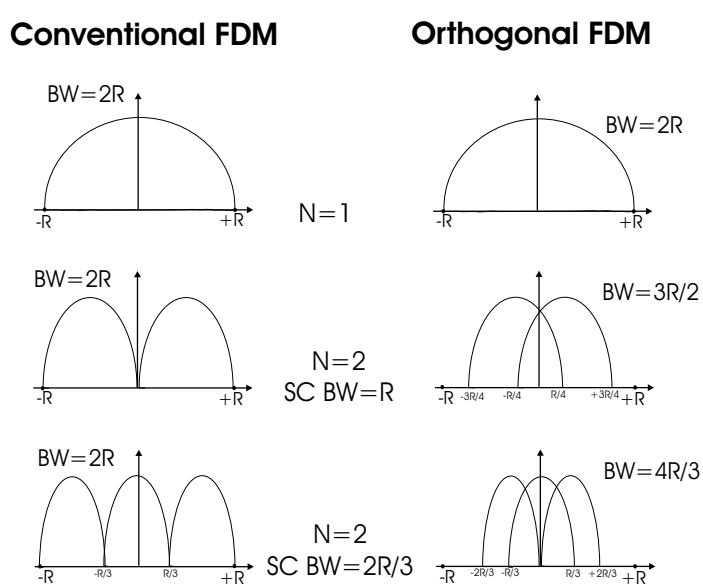

Figure 2.5: Spectrum Efficiency of OFDM Compared to Conventional FDM

2.2.4 Spectral Efficiency

Figure 2.5 illustrates the difference between conventional Frequency Division Multiplexing (FDM) and OFDM systems. In the case of OFDM, a higher spectral efficiency is achieved by maintaining orthogonality between the sub-carriers. When orthogonality is maintained between different sub-

© Muhammad Imadur Rahman, 2007

channels during transmission, it is possible to separate the signals very easily at the receiver side. Classical FDM ensures this by inserting guard bands between sub-channels. These guard bands keep the sub-channels far enough from each other so that separation of different sub-channels is possible. Naturally inserting guard bands result in inefficient use of spectral resources, like the insertion of the CP in OFDM systems.

Orthogonality makes it possible in OFDM to arrange the sub-carriers in such a way that the sidebands of the individual carriers overlap, but still the signals are received at the receiver without being interfered by ICI. The receiver acts as a bank of demodulators, translating each sub-carrier down to DC, with the resulting signal integrated over a symbol period to recover raw data. If the other sub-carriers all down converted to the frequencies that, in the time domain, have a whole number of cycles in a symbol period T_{sym}, then the integration process results in zero contribution from all other carriers. Thus, the sub-carriers are linearly independent (i.e., orthogonal) if the carrier spacing is a multiple of $\frac{1}{T_{sym}}$ [50].

2.3 Multi-User OFDM Systems

It is worth noting here that though OFDM provides an efficient transmission scheme at high data rate, it does not possess any inherent multi-user capability. Thus, an extra multiple access or channelization technique needs to be implemented on top of OFDM, such as TDMA, FDMA or CDMA. CDMA has been accepted as the multiple access technique for 3G mobile communications. But research shows that the use of conventional CDMA does not seem to be realistic when the data transmission rate is in the order of a hundred Mbps, due to severe inter-code interference and the difficulty to synchronize such a fast sequence [51].

Basically, orthogonal frequency resources (i.e. orthogonal sub-carriers) can be shared among users, which is the simplest multiple access technique based on OFDM modulation. Besides, there are a number of *hybrid* multiple access techniques that can be found in literature. Here *hybrid* means an amalgamation of OFDM and multiple access techniques (with the main accent to the spread spectrum) to provide an efficient multi-user scenario with very high data rate. The following are a number of the techniques that can be found in literature:

1. OFDMA (Orthogonal Frequency Division Multiple Access)
2. OFDMA-FSCH (OFDMA Fast Sub-Carrier Hopping, downlink of Flash-OFDM)
3. OFDMA-SSCH (OFDMA Slow Sub-Carrier Hopping, uplink of Flash-OFDM)
4. MC-CDMA (Multi-Carrier CDMA) [11]
5. OFDM-CDMA-SFH (OFDM-CDMA Slow Frequency Hopping) [52]
6. VSF-OFCDMA (Variable Spreading Factor - Orthogonal Frequency and Code Division Multiple Access) [12]

Although a number of access techniques are studied by researchers, it is more and more clear that OFDMA has emerged as the preferred technique for cellular Downlink (DL) as it is al-

ready approved as the suitable access technique in several standards. So, we will concentrate on OFDMA for further discussions.

2.3.1 Orthogonal Frequency Division Multiple Access

This section describes the basics about OFDMA scheme, also referred to OFDM-FDMA. In OFDMA, a fraction of OFDM sub-carriers are assigned to a sub-channel. Multiple access is realized by allocating different sub-channels to different users. The scheme was first proposed for CATV systems [53], and later adopted for wireless communication systems [9].

In principle, sub-carriers can be assigned arbitrarily among the sub-channels. This study assumes that they are equally distributed among the sub-channels. The sub-carrier assignment is made for the user lifetime, or at least for a considerable time frame, illustrated in Figure 2.6. In later sections, sub-carrier assignment schemes and assignment lifetime are examined in more detail.

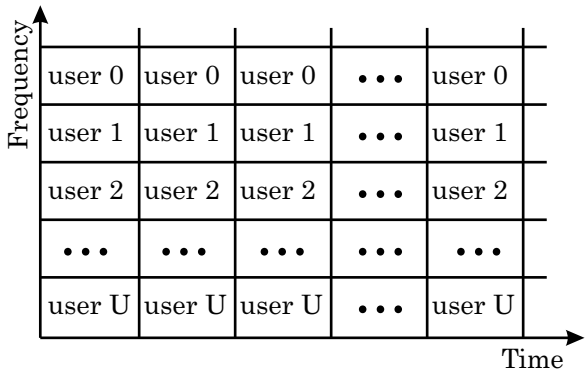

Figure 2.6: Time-frequency diagram for the OFDMA scheme. For simplicity, one sub-carrier is assigned to each user. The vertical blocks on the time axis represents OFDM symbols.

In Figure 2.7, a simplified block diagram of the OFDMA transmitter scheme is illustrated. User data is modulated using a baseband modulation scheme, e.g. 16-QAM, such that the user symbols match the number of allocated sub-carriers. The symbols are assigned to sub-carriers, using the assignment map defined by the sub-carrier assignment scheme. When all users are mapped into the OFDM symbol, the symbol is transmitted, incorporating all traditional features of OFDM, with the addition of multi-user capabilities. At the receiver side, data of the uth user can be received with the knowledge of the sub-carrier assignment.

OFDMA can support a number of identical down-streams, or different user data rates, (e.g. assigning a different number of sub-carriers to each user). Based on the sub-channel condition, different baseband modulation schemes can be used for the individual sub-channels, e.g. QPSK, 16-QAM and 64-QAM. This is investigated in numerous papers and referred to as adaptive sub-carrier, bit, and power allocation or QoS allocation [54, 55, 14, 56].

Static and Dynamic Sub-carrier Assignment There are basically two approaches for the sub-carrier assignment; static and dynamic. The sub-carriers are assigned into sub-channels in a contiguous or interleaved manner [57].

© Muhammad Imadur Rahman, 2007

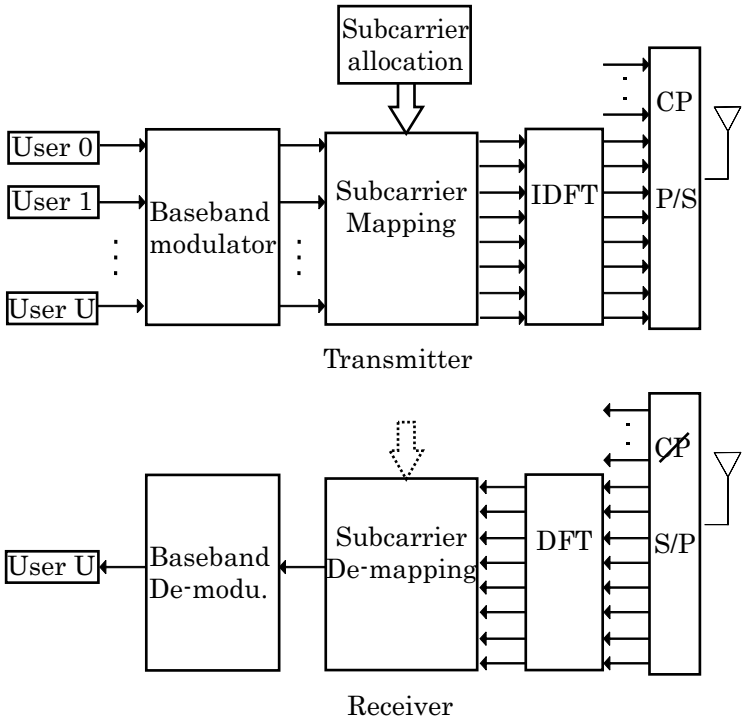

Figure 2.7: Simplified block diagram of the OFDMA transmitter, receiver schemes.

For contiguous assignment, the sub-carriers are divided into contiguous sub-channels, where one benefit is the simplicity, but a disadvantage is the possible throughput degradation due to channel fading. In the interleaved case, the sub-carriers are successively assigned to the different users and then interleaved over the total number of sub-carriers. One important advantage is that it has potential to reap more channel diversity gain. The disadvantage is that issues like synchronization for the entire OFDM symbol become crucial, as the user sub-channel is scattered over the OFDM symbol. In other words, sensitivity to synchronization errors is stronger for interleaved sub-carriers compared to contiguous sub-carriers. Furthermore, the required number of pilot tones for channel estimation, synchronization, etc may become higher in interleaved sub-carrier allocation. In Figure 2.8, examples of contiguous and interleaved assignment are illustrated.

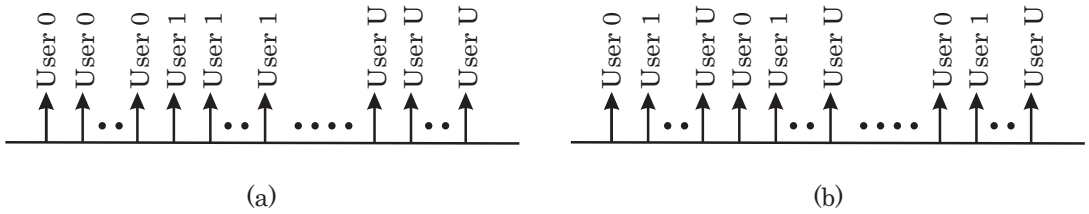

Figure 2.8: (a) Contiguous sub-carrier assignment. (b) Interleaved sub-carrier assignment.

In the dynamic sub-carrier assignment case, channel information is used to assign the sub-carriers best suited for each user. This is advantageous in the sense that users at different locations have different channel conditions, and most likely different optimal sub-carriers. The benefit is that

high throughput rate can be obtained, the disadvantages are that; channel information is needed, sub-carriers must be reassigned whenever conditions change, leading to additional signalling overhead whenever sub-carriers are reassigned [54].

Sub-carrier Hopping When CSI is not available to the transmitter, then dynamic sub-carrier allocation is not possible. Thus, a tradeoff in comparison to static sub-carrier allocation can be achieved by using sub-carrier hopping. In a sub-carrier hopping based OFDMA system, once sub-carriers are allocated to users, the index of the assigned sub-carrier is changed, i.e. hopped at every OFDMA symbol. Users are separated by non-overlapping sub-carrier hopping patterns [58]. These patterns constitute the hop-set available at the BS. The arrangement of the hop-set available at neighboring cells depends on the cellular structure of the system.

The benefit of sub-carrier hopping becomes available with channel coding impact. Using these sub-carrier recovery methods, data may be recovered fully even if one (or more) sub-carriers are faded. However, there is a limit to the amount of faded sub-carriers channel coding is able to handle. When this limit is exceeded, performance suffers.

Sub-carrier hopping reduces the probability of burst errors without *a priori* knowledge of the channel. By dividing faded sub-carriers among all users, sub-carrier hopping increases the effectiveness of channel coding and increases the overall performance of an OFDMA system.

Frequency of Sub-carrier Assignment The frequency with which the sub-carriers are reassigned generally corresponds to the lifetime of the user, or at least for a significant time frame. In Figure 2.9, different sub-channel conditions are illustrated, assuming contiguous sub-carrier assignment. For users 0 and 1 the OFDM symbols are permanently good and bad, respectively. User 2 has alternating good and bad OFDM symbols, and user 3 only has few bad OFDM symbols. In the following, it is discussed for which condition static and dynamic assignment is the most profitable choice.

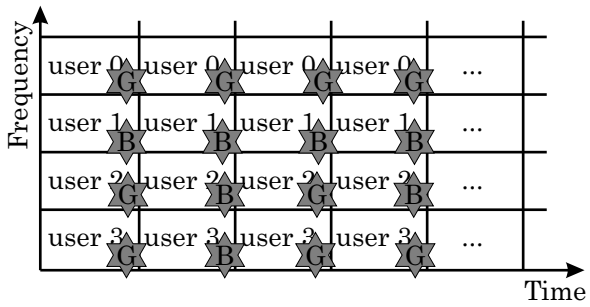

Figure 2.9: Examples of sub-channel conditions where users receive either good or bad OFDM symbols, different patterns are illustrated. (G = good OFDM symbol, B = bad OFDM symbol).

In the best (worst) case, the sub-channel is respectively good (bad), for static channel conditions. Static assignment is made without information of the channel, meaning that the sub-channel is either good (bad) for the assignment duration. For dynamic assignment, perfect channel information is assumed, and the user will always be assigned a good sub-channel.

© Muhammad Imadur Rahman, 2007

In cases with alternating good and bad sub-channels, assuming channel coherence time corresponding to a considerable number of OFDM symbols, the situation is somewhat different. In the static assignment, the sub-channel will be good for some time intervals and bad for the rest. Static sub-carrier assignment is in this case a poor solution, as the user sub-channel will be bad for a number of OFDM symbols. For dynamic assignment, it is favorable to make the assignment within a time period corresponding to the channel coherence time, thereby always assigning good sub-channels. For dynamic assignment, perfect channel information is normally assumed [56].

For a time-variant channel, i.e. when the channel coherence time is within the same range as the OFDM symbol time, the static assignment scheme could be a good solution. As the channel is time-variant, errors will have a burst-like pattern. Static assignment could be a solution, as some of the same properties from sub-carrier hopping are obtained; in sub-carrier hopping channel fading is combated by averaging the fading. The same condition is realized by having static assigned sub-carriers, as the time-variant channel is constantly changing; the difference from sub-carrier hopping is that the channel is "hopping". For dynamic assignment, the reassignment must be made at a rate corresponding to the channel coherence time, e.g. every OFDM symbol, introducing large overheads for signalling.

2.3.2 OFDMA-based Standards

2.3.2.1 WiMAX Group of Standards

The term Worldwide Interoperability for Microwave Access (WiMAX) is generally used to refer to IEEE 802.16 group of standards. This standardization group works towards defining a common standard for Broadband Wireless Access (BWA) or wireless MAN as commonly known. The Physical Layer (PHY) and Medium Access Control (MAC) Layer issues are addressed in this standardization, and the standard defines a common MAC layer and a number of different PHY options. The latest amendment, IEEE 802.16*e*, published in February 2006, covers *"Physical and Medium Access Control Layers for Combined Fixed and Mobile Operation in Licensed Bands"* [59]. The recent IEEE 802.16*e*, laying down the standard for mobile BWA, promises very high data rate while providing *Anytime, Anywhere, Anything* service.

A key advantage of WiMAX over other standards is that it offers a single standard approach as opposed to other technologies that rely on vendor specific proprietary solutions [60, 61]. This means manufacturers can take advantage of economies of scale, while operators will have a wider range of choice. The WiMAX forum is a body of WiMAX related industry members that take care of the standardization process.

Operating Frequency	2-11 GHz and 10-66 GHz
Coverage area	Maximum 50 km(FWA), 5 km (mobile)
Data rate	Up to 70 Mbps (Single Carrier, LOS), 15 Mbps (mobile)
Channel bandwidth	Variable. From 1.75 MHz to 28 MHz
Key technology	OFDM and scalable OFDMA (mobile)

Table 2.6: General WiMAX Parameters

Technical aspects: Unlike other wireless standards, WiMAX allows for channel bandwidth from 1.75 MHz to 28 MHz at almost any carrier, both licensed and unlicensed [62]. The PHY mode supported at 10-66GHz is only single-carrier while at sub 11GHz, both single-carrier and multi-carrier transmissions are supported, with various options for the multi-carrier mode, from OFDM (256 point FFT) to OFDMA (2048 point FFT). Modulation level of 64-QAM is supported by all PHY whereas the Selection Combining (SC) PHY mode supports 256-QAM.

Taskgroup "e" of the IEEE 802.16 workgroup laid out option for scalability at the PHY OFDMA. This enables optimum performance through scalable sub-channelization structure and variable Fast Fourier Transform (FFT) size.

Links between the BS and MS are identified by a unique connection ID in the MAC. This allows for different QoS, and hence providing support for wider range of applications, especially those requiring low latency and faster response, such as Voice over IP (VoIP) or video transmission. Number of different transport technologies, such as IPv4, IPv6, Asynchronous Transfer Mode (ATM), Ethernet etc are also supported at the MAC layer, giving it a greater flexibility [60, 7, 63, 64].

2.3.2.2 OFDMA-FSCH Based Standards

An OFDMA-FSCH based standard is called "Fast Low-Latency Access with Seamless Handoff (FLASH) OFDM" [65]. FLASH-OFDM operates below the 3.5 GHz range and is designed for Frequency Division Duplex (FDD) operation. It has a bandwidth of 1.25 or 5 MHz. Sub-carriers are separated by 12.5 kHz. This corresponds to a total of 400 sub-carriers for 5 MHz bandwidth and 100 for 1.25 MHz bandwidth. The sub-carriers are assigned to individual users when they have data to send. Each subcarrier is adaptively modulated [65].

OFDMA-FSCH scheme has been proposed to IEEE 802.20 working group [66] and is still under development by IEEE 802.20 working group. Similar to flash-OFDM, channel bandwidth is 1.25 MHz. The system parameters are listed in Table 2.7 [66]:

Basic System Description Parameter	Value
Carrier frequency	$\leqslant$ 3.5 GHz
Channel bandwidth	1.25 MHz
Subcarrier separation	11.25 kHz
Available sub-carriers	113
Symbol duration	0.1 ms
Cyclic prefix Duration	11.1 μs (16 samples)
Modulation	QPSK or 16-QAM
Peak rates	DL > 4 Mbps, UL > 800 Kbps
Slow subcarrier hopping in UL	tones hop every 7 OFDM symbols
Coding (Low-Density Parity-Check Codes) rates	1/6 to 5/6

Table 2.7: System parameters for OFDMA-FSCH scheme under development by IEEE 802.20 working group

The access intervals are separated from data intervals in the Uplink (UL). Access intervals have a duration of 0.8 ms, i.e. 8 symbols [66]. Like in flash-OFDM, Frequency Division Duplex (FDD) is used. Adaptive coding and modulation is supported by allowing users to report their channel conditions to the BS. For more details on the frame structures, the reader can refer to [66].

© Muhammad Imadur Rahman, 2007

One disadvantage of multi-carrier based access schemes is their susceptibility to frequency offset errors. As discussed in Section 2.1, the maximum Doppler frequency shift is less than 162 Hz for a vehicle speed of 50 km/h and for a carrier frequency below 3.5 GHz. At the maximum Doppler frequency shift, the sub-carrier separation of 12.5 kHz as standardized in flash-OFDM corresponds to a relative frequency offset error which is less than 1.3 % for a carrier frequency less than 3.5 GHz. This corresponds to an Signal to Noise Ratio (SNR) degradation less than 0.2 dB for the QPSK modulation scheme and approximately 1 dB for the 64-QAM modulation scheme [67]. The largest constellation in IEEE.802.11, i.e. 64-QAM, can not tolerate beyond 2 % of frequency error [67]. The problem of frequency offset errors can be solved by inserting pilot symbols. However, as the sub-carrier separation bandwidth decreases, more pilot symbols are needed to cope with doppler frequency shift effects.

2.3.2.3 OFDMA-SSCH Based-Standards

FLASH-OFDM technology considers OFDMA-SSCH for the UL. The sub-carrier hopping is performed once every 7 OFDM symbols [65], so this kind of sub-carrier hopping can be classified as *slow*. The 7 symbols mentioned before are called *dwell time* (among them, one is a reference symbol and the other 6 are data symbols). Since there are no shared UL pilots, data is modulated in each dwell time with the reference symbol.

In each *superslot* (11.3 ms long), there is an *access interval* of 8 symbols (i.e. 0.8 ms). The access intervals are separated from *data intervals* and they are used by access mobiles (which are not yet UL-synchronized) and by existing mobiles (for periodic timing tracking). Concerning signaling (a very important issue whenever it refers about sub-carrier hopping), an access signal is a multi-tone signal which provides diversity and timing resolution. The access signals can be detected with low processing complexity. Only this kind of signals are contention-based, after access all signaling is contention-free.

2.3.2.4 UMTS-LTE: 3GPP Standard

In order to prepare for future needs, 3GPP has initiated activities on the long term evolution of UTRAN (Universal Terrestrial Radio Access Network), which is clearly aiming for system performance beyond WCDMA, HSDPA and HSUPA. The UTRAN long-term evolution work is looking for the market introduction of Evolved UTRAN (EUTRAN) around 2010, with resulting specification availability planned toward end of 2007. The feasibility study is currently ongoing and key decisions on the multiple access as well as on the protocol architecture have been recently reached. Feasibility study is finalized for September 2006 time frame, after which actual specification development would start [68, 69].

Three basic concepts are proposed in Downlink (DL) [68, 70]:

- OFDMA (FDD /TDD)
- MC-WCDMA (FDD)
- MC-TD-SCDMA (TDD)

In the DL direction a suitable solution is OFDM, mainly due to the simplicity of the terminal receiver in case of large bandwidth in difficult environment. Also for the network side transmission Peak to Average Power Ratio (PAPR) was not considered such a key problem [69, 70].

For the DL, the adoption of OFDMA enables flexible support of different bandwidth options. The basic OFDM chain is illustrated in Figure 2.3 as used for the feasibility studies at least, though obviously several advanced techniques are being considered on top of the basic OFDMA operation. These technologies include advanced Automatic Repeat reQuest (ARQ) techniques, frequency domain scheduling, MIMO antenna technologies and variable coding and modulation [70, 6, 69, 71].

One of the key aspects for the air interface is a scalable solution to support the large number of different bandwidths, starting from 1.25 MHz up to 20 MHz. The single set of parameters for sub-carrier spacing etc. provides support for different bandwidths by only changing the number of sub-carriers while keeping the frame length as well as symbol length constant. The parameters defined during the feasibility study can be found in [68, 69].

The decision was made in 3GPP community to adopt the Single-Carrier FDMA (SC-FDMA) for the UL direction due to the good performance in general and superior properties in terms of UL signal PAPR when compared to OFDM in the UL [69, 72].

2.4 Multi-antenna OFDM Systems

Multi-antenna is one of the key technologies for mitigating the negative effects of the wireless channel, providing better link quality and/or higher data rate without consuming extra bandwidth or transmitting power. The usage of multiple antennas at either receiver, transmitter or at both locations provides different benefits, namely *array gain*, *interference reduction*, *diversity gain* and/or *multiplexing gain* [73]. The combination of multi-antenna techniques with OFDM can be very beneficial, due to the fact that OFDM greatly simplifies the multi-channel equalization problem in multi-antenna systems, thus making implementation of multi-antenna techniques practical in frequency-selective fading channels. Numerous research works are published on utilizing multiple antennas for OFDM-based 4G wireless systems, which can be broadly classified into three categories as illustrated in Figure 2.10:

- Smart array processing, such as Beamforming (BF), which aims at increasing receiving power and rejecting unwanted interference.
- Diversity combining, which is employed to mitigate fading and increase link reliability.
- Spatial multiplexing, which is used to increase data rate.

2.4.1 Multi-antenna and Diversity

In a multipath environment, the received signal is the sum of multiple scattering paths with random amplitudes and phases. The interaction between these paths causes channel gain variations in time and deep fades. These fades lead to degradation in the received signal, which might make it

© Muhammad Imadur Rahman, 2007

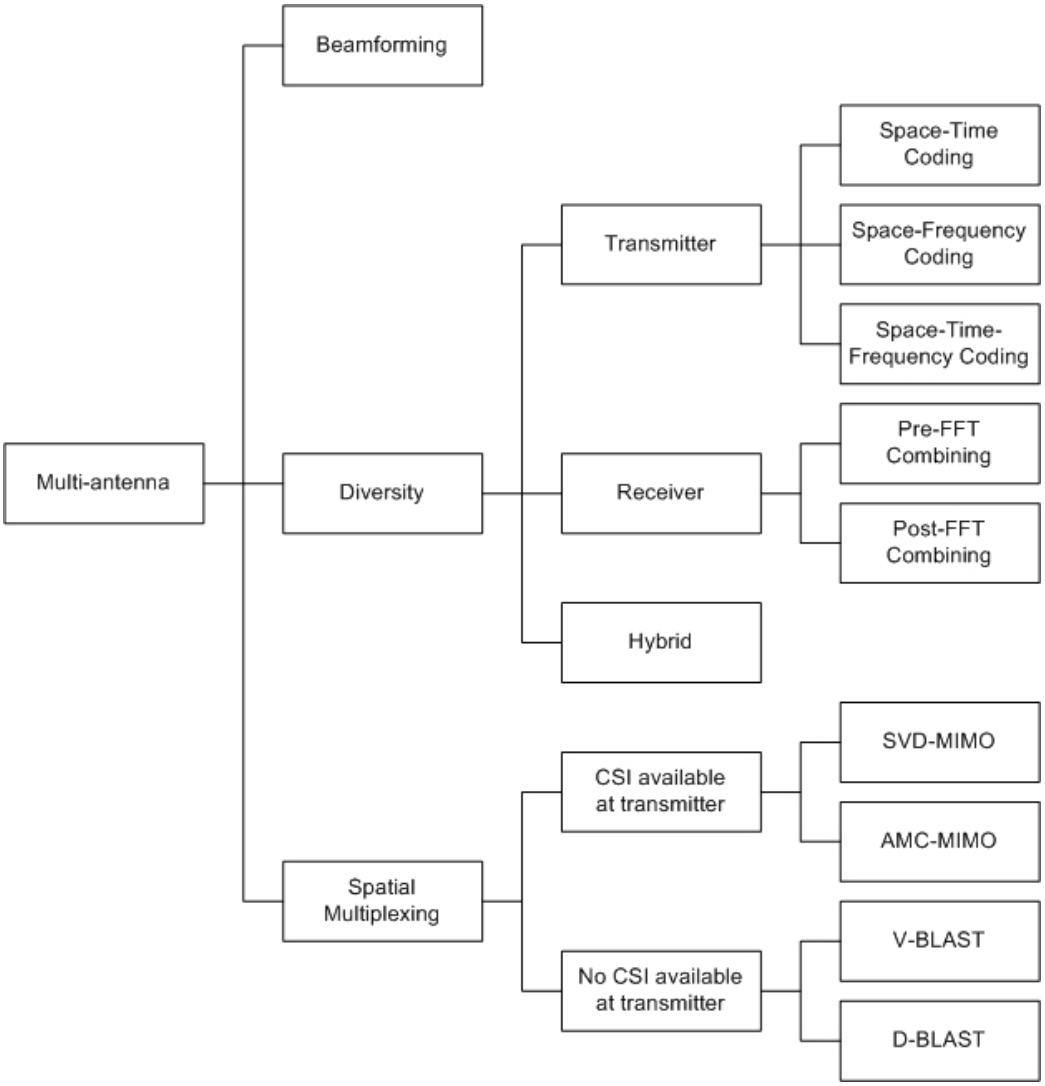

Figure 2.10: Classification of multi-antenna techniques

impossible for the receiver to correctly detect the transmitted signal. Diversity is one of the most effective techniques to combat fading in wireless communications.

The main idea behind diversity is to send multiple copies of the transmitted signal via multiple (presumably independent) channels to the receiver. When the channels have low, or ideally zero, cross-correlation, the probability that all of them fall into deep fading simultaneously is very low [39]. That means if one radio path undergoes a deep fade at a particular point in time and/or frequency and/or space, another uncorrelated path may have a strong signal at that point. By having more than one path to select from, both the instantaneous and average SNR at the receiver can be greatly improved.

There are different types of diversity techniques, which can be categorized by the methods from which multiple versions of the received signal are introduced at the receiver.

2.4.1.1 Time Diversity

In time (or temporal) diversity, the transmitted signal is repeated several times at different time frames. Thus, the receiver will receive more than one version of the transmitted message at different time. The only requirement for time diversity technique is that the time separation between two repetitions be greater than the channel coherence time, so as to ensure that the received signals are uncorrelated. If N_b diversity branches are needed, the reception delay is at least N_b times the repetition interval. As a result, time diversity system would observe large delay, especially when the number of branches N_b increases or when the channel coherence time is large. When the receiver is stationary and the fading is not time-selective, time diversity will not bring the desired gain [43].

2.4.1.2 Frequency Diversity

Another method to obtain multiple versions of the incoming signal at the receiver is frequency (or spectral) diversity. This method utilizes two or more frequency bands to transmit the same message. The receiver will listen to these frequency bands to get N_b diversity branches. The requirement for frequency diversity is that those frequency bands must be sufficiently separated in order to ensure that the fading in different frequency bands are uncorrelated. The coherence bandwidth of the channel is a convenient quantity to use in describing the degree of correlation existing between different frequencies. For frequency separation of more than several times the coherence bandwidth, the signal fading would be essentially uncorrelated. For example, if the channel coherence bandwidth is 500kHz for a certain mobile environment, the frequency separation should be more than 1-2MHz [43]. In mobile radio, where frequency is a precious resource, this diversity technique is not always a preferable choice. Frequency diversity also requires separate transmitter chain for each of the branches.

2.4.1.3 Space Diversity

Space (or spatial) diversity is a method in which two or more antennas physically separated from each other are used to obtain independent versions of the received signal. These antennas can be

© Muhammad Imadur Rahman, 2007

located at the receiver (receive diversity), at the transmitter (transmit diversity) or at both. Figure 2.11 illustrates a scenario where receiver diversity is employed at the BS to compensate for low transmitting power at the MS. This technique is now commonly used in the BS of the 2G wireless systems.

The level of cross-correlation between signals received by those antennas depends on the distance between antennas. In general, the minimum distance between antennas must be greater than the coherence distance of the channel so that the spatial fadings become uncorrelated [73]. Ideally, antenna separation of half of wavelength ($\lambda/2$) should be sufficient [43]. Space diversity is a convenient and attractive method of diversity for mobile radio. It is relatively simple to implement and it does not require additional frequency spectrum. If antenna separation is sufficient, spatial diversity can be employed to reduce fading, even if the channel is neither time- nor frequency-selective. The downside of space diversity is the cost, the size, the power consumption and the complexity of having additional antennas.

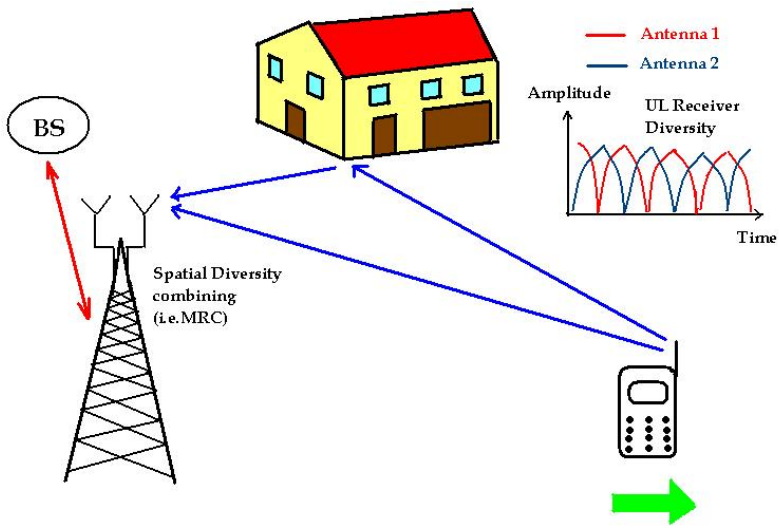

Figure 2.11: Example of space diversity

When multiple copies of the transmitted signal arrive at the receiver, they have to be pre-combined in a determined manner, in order to obtain the diversity gain. The diversity combining techniques for OFDM technique is studied in this thesis work and shall be discussed in greater details in Chapter 8.

2.4.2 Multi-antenna and Spatial Multiplexing

Parallel to diversity techniques, a recently new approach of multi-antenna transmission systems is spatial multiplexing. With respect to diversity technique, spatial multiplexing aims at increasing data rate of the system.

Spatial multiplexing techniques require that multiple antennas be present at both transmitter and receiver. Such antenna arrangement is often referred to as Multiple Input Multiple Output (MIMO), as illustrated in Figure 2.12. The number of transmitting and receiving antennas

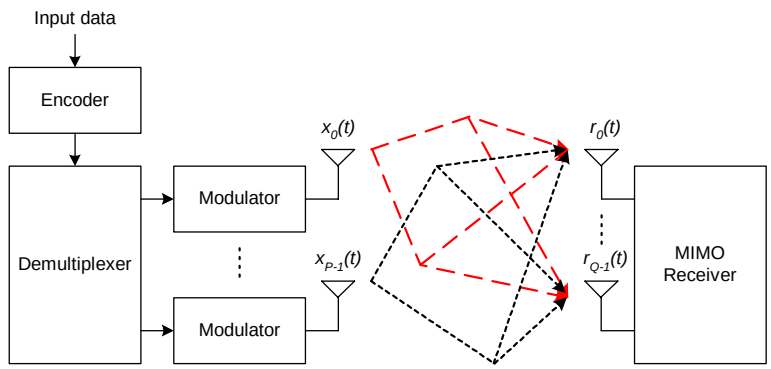

Figure 2.12: An example of MIMO Spatial Multiplexing system

are denoted by P and Q, respectively. At the transmitter, P independent data streams, $x_0(t)$, $x_1(t)$, $\ldots$, $x_{P-1}(t)$, are transmitted on different transmitting antennas simultaneously and in the same frequency band. For the sake of simplicity, flat fading channel is assumed between pairs of transmitting and receiving antennas. At the qth receiving antenna, the independent signals $\{x_0(t), x_1(t), \ldots, x_{P-1}(t)\}$ are linearly combined to produce the received signal $r_q(t)$, which is given by

$$r_q(t) = h_{q,0}x_0(t) + h_{q,1}x_1(t) + \cdots + h_{q,P-1}x_{P-1}(t) + \vartheta_q(t), \qquad q = 0, 1, \ldots, Q-1, \tag{2.13}$$

where $h_{q,p}$ is the envelop of flat fading channel between the pth transmitting antenna and the qth receiving antenna, and $\vartheta_q(t)$ is the thermal noise of the qth receiving antenna. Under a rich scattering environment, the channels between pairs of transmitting and receiving antennas undergo different multipaths and thus become independent from each other. The independence of the channels means that the receiver can estimate $\{x_0(t), x_1(t), \ldots, x_{P-1}(t)\}$ from $\{r_0(t), r_1(t), \ldots, r_{Q-1}(t)\}$ independently, provided that the channel responses are known [73]. The problem is equivalent to solving a set of Q linear equations with P unknown variables, and it can be solved if $Q \geq P$.

As a result, spatial multiplexing promises higher throughput without increasing system bandwidth or transmit power. It is shown in [74] that, under certain circumstances, system capacity increases linearly with the number of antennas used.

The main reason of using OFDM with MIMO is the fact that OFDM has the capability of turning a frequency-selective MIMO fading channel into multiple flat fading channels [75]. This renders the multi-channel equalization particularly simple, since for each OFDM subcarrier only a constant matrix needs to be inverted. In this thesis, different spatial multiplexing techniques are analyzed for OFDM-based systems in Chapter 9.

2.4.3 Usability of Multi-antenna Techniques in OFDM Systems

Together with other important parameters, sub-carrier bandwidth, Δf, and OFDM symbol duration, T_s, are closely related to the choice of multi-antenna techniques in OFDM systems. In general, when Δf is large enough, so that T_s is very small compared to channel coherence time, T_c, then a number of algorithms that are dependent on the channel information at the transmitter are easily

© Muhammad Imadur Rahman, 2007

and effectively implementable. In this case, the feedback can be used for several OFDM symbols, thus, the total amount of feedback to be transported can be reduced. In the other case, when T_s is large (and conversely Δf is small), the CSI feedback will be outdated quite fast and would require very frequent transmission of CSI between transmitter and receiver. This will cost in terms of spectral efficiency.

2.4.3.1 Considerations with Receive Diversity

In general, receive antenna diversity is practical, effective and hence, commonly-used technique for mitigating the effect of multipath fading. By employing multiple antennas at the receiver and having a suitable combining scheme, significant diversity gain can be achieved, which can be used to maximize the coverage and/or link reliability [76]. The diversity gain comes without having to increase the transmit power and/or to extend the frequency spectrum. It also does not generally introduce delay like time diversity technique. Receive diversity is relatively simple to implement, as compared to transmit antenna diversity and other MIMO techniques. Nevertheless, additional antenna(s) also means increasing in size, complexity and power consumption, and these are key limiting factors for receive diversity. As a result, in today's systems, receive diversity is mostly applied at the BS to compensate for low transmit power at MSs. All processing tasks are performed at BS side, therefore MS structure can be quite simple.

Being one of space diversity techniques, receive diversity requires that antenna separation be larger than the coherence distance of the channel, so that the spatial fading becomes uncorrelated. The coherence distance depends on the richness of scattering environment, i.e. how many multipath are available or whether LOS or a dominant reflection is present. The coherence distance of the channel is inversely proportional to the RMS angle spread - the larger the angle spread, the shorter the coherence distance [73].

There are two methods for receive diversity combining for OFDM systems, namely Post-DFT and Pre-DFT combining. In Post-DFT combining schemes, the time-domain OFDM samples from multiple receive antennas are first Discrete Fourier Transform (DFT) demodulated, and then combined on sub-carrier basis. As deep fades are distributed randomly among sub-carriers, combining at sub-carrier level enables the combination (or selection) of only the best-quality sub-carriers from different diversity branches. Therefore, Post-DFT MRC scheme is optimal in terms of BER performance. However, Post-DFT requires separate DFT processor for each antenna branch, which increases the computational complexity and power consumption at the receiver.

On the other hand, Pre-DFT combining techniques combine the diversity branches before performing OFDM demodulation. This reduces the complexity of the receiver, but at the expense of performance degradation. For instance, if the channel is flat over the entire OFDM spectrum, the performance of Pre-DFT MARC scheme is comparable to that of the Post-DFT MRC scheme. However, when the channel is frequency-selective fading, its performance is degraded and less diversity gain is achieved compared to Post-DFT MRC [77].

2.4.3.2 Considerations with Transmit Diversity

The implementation of multiple antennas at the transmitter side brings the possibility of exploiting redundancy of information by sending signals through different paths. Transmit diversity used alone falls under the group of Multiple Input Single Output (MISO) techniques and it is employed by using different ways to transmit the signal, separating them in time, frequency and/or space. However, applying diversity in time-domain only, e.g. repetition codes, considerably reduces the data rate [42]. Also, applying frequency-domain diversity alone, e.g. sending the same signal over different carriers, is not feasible due to the high cost of available spectrum [43]. Hence, space diversity, by applying more antennas is often a preferable option, given the decreasing cost of hardware. To overcome channel impairments, it is also beneficial to exploit diversity in more than one domain. The most common method employed to take advantage from transmit diversity is the Space-Time Codings (STCs), i.e. Space-Time Block Code (STBC) and Space-Time Trellis Code (STTC). Since the MS has more restrictions, in order to lower its cost, to save on battery consumption and to have small terminals, it may not be feasible to include multiple antennas at handsets. On the other hand, BS does not have such restrictions. It should also be noted that usually all contemporary BSs have more than one receive antennas for receive diversity purposes. These antennas can be used for transmit diversity purpose in the DL commonly used in 2G BSs, whereas transmit space diversity is proposed for The Third Generation Partnership Project 2 (3GPP2) specifications and in IEEE 802.16a standards.

In the group of STBC, the so-called Alamouti scheme, presented in [25], stands for being an optimal code to achieve both full data rate and full diversity gain by employing two transmit antennas and having no CSI at transmitter. STBC using more transmit antennas have been developed and an extended performance analysis presented in [78]. However, with more than two antennas there are no codes achieving both full rate and full diversity simultaneously. It should also be pointed out that, with the increase of order of STBC techniques, the latency of the transmission gets larger, e.g. with a four Transmitter (Tx) antennas STBC there is the need to wait for four symbol durations before decoding the same number of symbols. Even not affecting data rate, the block-by-block processing may introduce unacceptable delay in real time services. Another group of transmit diversity techniques are included in Space-Frequency Block Code (SFBC), exploiting frequency diversity [79]. This is employed across OFDM tones. Since in SFBC the time domain is not used, there is no latency. To make full use of diversity over the three domains (i.e time, frequency and space domains), more complex codes are required and they are referred to as Space-Time-Frequency Block Code (STFBC) [80].

It is worth noting here that if no CSI is available at transmitter, the array gain cannot be exploited at the transmitter. CSI is usually estimated at the receiver side, hence, to achieve transmit array gain, feedback should be sent from the MS. However, this option comprises a high amount of information to be exchanged and may not be feasible to implement, especially when the wireless channel is severely time-variant and when the usable data bandwidth is not sufficient. Nevertheless, it can be used in very low mobility situations such as indoor scenarios, where $T_s << T_c$. Two such systems are Institute of Electrical and Electronics Engineers (IEEE) 802.11a and IEEE 802.16a. Another option to have CSI at transmitter is using the CSI from the UL and apply it to DL. If the channel remains static for two symbol durations, this method can be easily implemented in Time

© Muhammad Imadur Rahman, 2007

Division Duplex (TDD) systems. On the other hand, in FDD systems the CSI from UL can not be directly re-used in DL, since the carrier frequency is different and usually not within the coherent bandwidth. In that case, a proper frequency calibration is required.

2.4.3.3 Choice of Diversity Technique

There is a great degree of freedom in combining OFDM and diversity techniques. Diversity gain can be obtained by employing either space, time or frequency diversity, or a combination of any of these three (i.e. space-time or space-frequency or time-frequency) or all three diversity techniques together (i.e. space-time-frequency) in an OFDM system. In general, obtaining space diversity would require additional antennas in the transmitter or receiver or at both. Obtaining time diversity would always introduce a time delay in service. Obtaining frequency diversity will always depend on the channel itself. It should also be noted that higher frequency diversity can be exploited in OFDM itself by using channel coding and interleaving. A careful choice of channel coding and interleaving can give a very good frequency diversity gain. In this section, the choice of diversity technique is considered for different scenarios, such as uplink vs downlink and indoor vs outdoor situations.

Uplink vs Downlink Scenario: Due to the limited dimensions of the mobile terminals, the complexity of processing has to be put in the BS, not in the MS. This trend seems to remain the same even in the future, since the economy of scale may allow more complex BS, thus the BS complexity may be the only trade space for achieving the requirements of next generation wireless systems. Considering the complexity issues, for UL (transmission from MS to BS), the preferable choice is receive diversity, while for DL (transmission from BS to MS) is transmit diversity. As shown in [25] both kinds of diversity can be combined, to achieve full diversity gain.

Outdoor vs Indoor Scenario: In a multipath channel, each ray arriving to an antenna element at the receiver has a specific angle of incidence of the plane wave, which is referred to as Direction of Arrival (DoA). Equivalently, each ray departing from a transmitter antenna has a Direction of Departure (DoD) [81]. The angle spread is a measure referring to the spread in DoA at the receive antenna arrays or the spread in DoD at the transmit antenna arrays. In an outdoor environment, the angle spread of the signals received by the MS is much lower than that of an indoor environment. This is mainly caused by the longer distance that separates BS and MS in outdoor situation, hence narrowing the angles of the multipaths of the received or transmitted signals. As a result, it is difficult to get the most out of angle diversity in outdoor scenario. Since BF performs better when desired signal arrives or departs from a single or narrow direction (i.e. having high spatial correlation) [82], this could be an interesting option to follow. On the other hand, in indoor channels, due to a broader angle spread, the spatial fading is uncorrelated, and therefore spatial diversity can be effectively exploited. Furthermore, BF may not be suitable for indoor scenario, since there is no narrow beam to increase SNR and separate from neighboring interferers [82].

Another important issue to diversity is the time variance of the channel. In order to implement STBC, the channel has to remain static over several symbol durations, depending on the code length, e.g. two symbols for Alamouti scheme. In addition, to achieve array gain in transmit

diversity, it is required that CSI is available at the transmitter. In indoor environment, the channel does not change so fast as in outdoor scenario, hence it is easier to implement such schemes. For instance, in IEEE 802.11a a bandwidth of 20 MHz corresponds a symbol period of 4 μs, while in Orthogonal Frequency Division Multiple Access - Fast Sub-Carrier Hopping (OFDMA-FSCH) (IEEE 802.16a Working Group) the symbol duration is 0.1 ms [13]. In WLAN environment with pedestrian mobility (i.e. 3 kmph velocity), the channel coherence time is 63.5 ms for 2.4 GHz carrier frequency [13, Appendix-A]. Thus, in ideal case, for $\frac{63.5ms}{4\mu s} = 15,875$ OFDM symbols, we need to transmit the CSI only once from MS to BS. This is reasonably low signalling overhead compared to other cases when the user mobility is very high. For fast-variant channel (e.g. outdoor environment) or when CSI feedback to transmitter is costly, receive diversity might be a better choice.

Special care needs to be taken into account in case of indoor scenario: it provides very little delay spread and this means the available frequency diversity may be very small, thus the system may suffer from flat fading situation (or very little frequency selective situation). This situation is worsened by the fact that indoor channels may experience very little fading in time domain also. This, in turns, means that when a terminal enters in flat fading scenario, it will remain there for some time. At this stage, the frequency diversity exploitation via channel coding and interleaving may not be enough. Thus, some intelligent techniques are required to combat this situation. [83] proposes CDD as a probable solution for this.

2.4.3.4 Considerations with Spatial Multiplexing

Depending on the final goal, different techniques have to be adopted. If the goal is to improve the SNR, this can be obtained by the increase of the array gain, provided e.g. by BF. If the objective is to achieve QoS, an improvement in link reliability is needed, obtained by the increase of diversity gain, and the right choice is employing diversity techniques. If the goal is the increase of throughput, the multiplexing gain has to be maximized, through SM techniques [84].

Indoor vs Outdoor If $T_s << T_c$, such as in indoor case, the CSI is available, so the non blind SM techniques are more suitable (e.g. MIMO with Singular Value Decomposition (SVD) or Adaptive Modulation and Coding (AMC)) than the blind ones. If T_s is comparable to T_c, as in the outdoor case (high mobility of the users) the feedback is expensive or impossible, and in this case it is better to choose the blind SM techniques, e.g. Bell labs LAyered Space Time (BLAST).

In indoor environment, there is a rich scattering (large Antenna Selection (AS)) such that the antennas are uncorrelated. This implies an high rank of $\overline{\mathbf{H}}$ (where $\overline{\mathbf{H}}$ is the equivalent channel matrix between the MIMO transmitter and receiver of size $Q \times P$, with P and Q are the number of transmit and receive antennas respectively) and since the SM performance depends on the rank, this case is suitable for high data rate applications. In outdoor the scattering is poor (small AS), so the antennas are correlated and this leads to a low rank of $\overline{\mathbf{H}}$: in this case the performance of SM is poor. In [85], it is shown that the presence of transmit correlation due to lack of scattering and/or insufficient transmit antenna spacing can have a detrimental impact on multi-antenna signaling techniques. In fact in case of antenna correlation, the diversity and multiplexing gains vanish, preserving only the receive array gain [86]. In general, antenna spacings of several wavelengths

© Muhammad Imadur Rahman, 2007

are required to achieve sufficient de-correlation. Antenna correlation causes rank loss, but the converse is not true.

SM is good at short distance from the BS (high SNR region), but the drawback here is the LOS situation (Ricean fading) that leads to rank decrease. Diversity techniques, such as STBC, perform better at large distance from the BS (low SNR). In Figure 2.13 this situation is visualized, where also a comparison with the Single Input Single Output (SISO) case is shown.

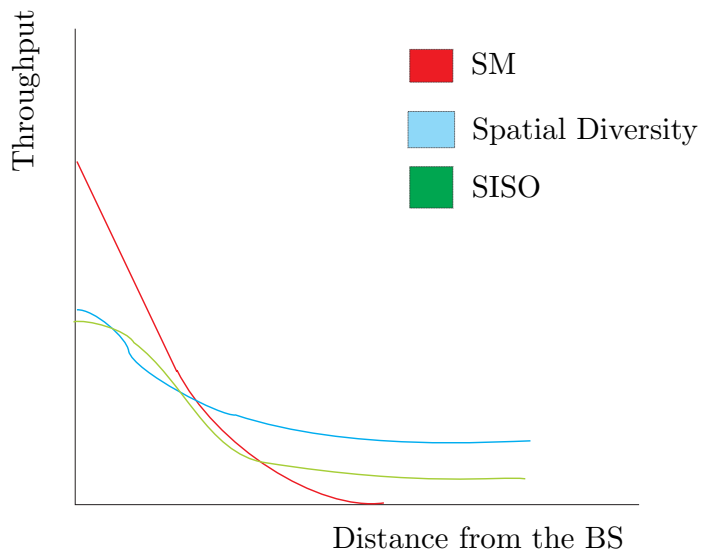

Figure 2.13: Qualitative representation of throughput versus distance from BS for SISO, SM and Spatial Diversity

Polarized Antennas Recently, the use of dual-polarized antennas has been proposed for SM as a cost-effective way of realizing significant multiplexing gain, where two spatially separated antennas are replaced by a single antenna structure with orthogonally polarized elements [87, 73]. Antennas with different polarizations at transmitter and receiver lead to a power imbalance between the elements of $\overline{\mathbf{H}}$ i.e. the power is not transmitted anymore all over the parallel pipes (the higher the power imbalance the higher the Cross Polarization Discrimination (XPD)). Low XPD hurts the information rate at low SNR and enhances rate at high SNR [73].

Multi-User SM can also be applied in a scenario where U users are present [73]. In the UL case, U users transmit each with a single antenna, and the transmitted signals arrive at a BS equipped with U antennas. The BS can separate the incoming signals to support simultaneous use of the channel by the users. This technique can also be termed as Space Division Multiple Access (SDMA). In the DL case, the BS can transmit U signals with spatial filtering so that each user can decode his own signal. This technique can also be called beamforming in multi-user context. In conclusion, a SM-Multi User (MU) system can achieve a capacity increase proportional to the number of antennas at the BS and the number of users.

3

Sub-Carrier and Band Hopped OFDMA

In this chapter, we describe our proposed channelization technique, Sub-Carrier and Band Hopped Orthogonal Frequency Division Multiple Access (SCBH-OFDMA). The main concentration of this chapter (and also in Chapter 4) is to study a channelization method for exploiting the time-frequency variability of wireless channel, experienced by users under wide-area cellular scenario, without requiring detailed Channel State Information (CSI) or Channel Quality Information (CQI) at the transmitter side. In another words, we would like to benefit from time-frequency diversity of wide-band channel with only a limited amount of CSI and/or CQI.

The background and motivation behind designing this channelization scheme is presented in Section 3.1. The multiple-access approach is described in Section 3.2. An analytical model of the SCBH-OFDMA in DL is presented in Section 3.3. We present our numerical results on system evaluations in Section 3.4. Relevant system parameters and assumptions related to the simulations scenarios are presented in Sections 3.4.1 and 3.4.2 respectively. The results in system level evaluations are presented in Section 3.4.5 onwards.

3.1 Background and Motivation

Orthogonal Frequency Division Multiple Access (OFDMA) is a multi-carrier based multiple access technique, where a part of the available sub-carriers is assigned to a single user. Thus, the users are

separated across sub-carriers, which bear orthogonal signals [53, 13, 9].

Different methods of allocating and re-allocating different sub-carriers to different users may be used:

Static: Sub-carriers are allocated to a user for a fixed time period without considering CSI. If the user is allocated sub-carriers that are in fade, the signal will remain faded until the user moves out of the fade or the sub-carriers are re-allocated.

Dynamic: Sub-carriers are allocated dynamically, assuming that the base station has instantaneous (or near-instantaneous) knowledge of the CSI for each user [14]. This is called Dynamic Sub-Carrier Allocation (DSA). In this case, the sub-carriers are allocated in real-time based on the knowledge of which sub-carriers are faded for which user.

Of these two methods, DSA has superior performance but requires excessive signalling, especially when the number of users and number of available sub-carriers are large, and when user mobility is very high (or when the channel is severely time-variant). DSA can be implemented only when the BS has the knowledge of CSI of all users in real time. Moreover, the allocation procedure is often computationally extensive when large number of sub-carriers and large number of users are present in the system. So, in some situations, the excessive signalling due to severely time-variant nature of physical wireless channel may prove prohibitive in implementing DSA algorithms [13].

Sub-Carrier Hopped Orthogonal Frequency Division Multiple Access (SCH-OFDMA) [1] is an alternative technique to Static OFDMA and comparable to DSA-OFDMA [14, 88]. In SCH-OFDMA, the users randomly (or pseudo-randomly) hop over the sub-carriers inside one OFDM symbol. This technique effectively averages the frequency-selective fading effects over all users.

Sub-carrier hopping provides significant frequency diversity and resistance to fading [89]. However, when the system bandwidth, B, is much smaller than or comparable to the coherence bandwidth, B_c, sub-carrier hopping will not provide this benefit. This is the case when the channel frequency selectivity is moderate (i.e. the maximum delay spread is not excessively high, resulting in B_c being much greater than the sub-carrier bandwidth, Δf; or B_c is comparable to B), or when the B is small (such as the 1.25 MHz used in the Flash-OFDM system [65]). In that case, band[2] hopping will be a good choice. In our novel multiple access scheme, together with Subcarrier hopping (SCH), we use OFDM symbol-by-symbol (or frame-by-frame) frequency band hopping in time domain (i.e. after IDFT modulation). We denote this kind of hopping as Band Hopping (BH). Thus, we have a system which can be denoted as Sub-Carrier and Band Hopped Orthogonal Frequency Division Multiple Access (SCBH-OFDMA).

[1] Some available literatures refer to SCH-OFDMA as Orthogonal Frequency Division Multiple Access - Frequency Hopping (OFDMA-FH), considering the fact that hopping across the sub-carriers amounts to frequency hopping, because the sub-carriers represent some specific frequencies. For example, Flarion's Flash-OFDM technology [65] uses Orthogonal Frequency Division Multiple Access - Fast Frequency Hopping (OFDMA-FFH) for DL, where the users' hopping patterns change at every OFDM symbol. Similarly, the same specification uses Orthogonal Frequency Division Multiple Access - Slow Frequency Hopping (OFDMA-SFH) for UL with a hopping rate of once per 7 OFDM symbols. In our scheme, both sub-carrier hopping and band hopping are actually frequency hopping, thus we use different terminology to differentiate between these two different frequency hopping techniques.

[2] Here we divide the total available spectrum to several frequency bands as shown in Figure D.1 and operate the OFDMA systems on the bands. Thus, B = band size. For example, if we have 60 MHz of available spectrum and if we would like to have OFDMA system with $B = 20$ MHz, then we can have 3 system bands and we can run 3 simultaneous OFDMA systems in the cell.

In addition to the less complex sub-carrier allocation procedure, as well as exploiting frequency diversity, BH also provides interference minimization and avoidance benefits. Another important feature of this proposed scheme is its adaptability with different user and propagation conditions. For example, in indoor scenario BH can be a good technique, whereas both SCH and BH can be applied in outdoor scenario. Similarly, because of different time-variability of the channel, we can design the hopping strategy to adapt to the specific channel condition with respect to time. Above all, if the available spectrum is spread over large frequency range (i.e. contiguous bands are not available), then BH will be a good solution to make use of all available spectrum.

3.1.1 Why Sub-carrier Hopping?

In an OFDMA system, each user is assigned a defined number of sub-carriers constituting the sub-channel for that user. Arising from the fact that the channel suffers from frequency selective fading, some of the sub-carriers will be faded. It may happen that a few consecutive sub-carriers are affected by fading. In a simple user sub-carrier assignment, the user sub-carriers are placed next to each other. When a burst error occurs due to consecutive sub-carriers in fade, the user performance will be highly affected. Hopping distributes the allocation of a sub-carrier to different users at different time. This necessarily means that a user will not be in deep fade for long duration. So, the Probability of error, P_b, performance is improved.

In other words, Subcarrier hopping (SCH) reduces the probability of burst errors without *a priori* knowledge of the channel. By dividing faded sub-carriers among all users, sub-carrier hopping increases the effectiveness of channel coding and increases the overall performance of an OFDMA system. In order to quantify the increase of system performance in terms of P_b, the type of channel coding used, as well as its recovery limitation, needs to be taken into account.

To summarize, SCH introduces the following advantages to a simple OFDMA system:

- Sub-carrier hopping minimizes the impact of fading. Users do not see burst errors due to severe fading effects. Thus, a considerable improvement in the average BER per user is expected at the price of very limited increment in signalling. This improvement over a conventional OFDMA system is presented in [90].
- With frequency hopping, channel state information is not needed for sub-channel allocation to users.
- With fast sub-carrier hopping, inter-cell interference is minimized [65].

3.1.2 Why Band Hopping?

In band hopping, the carrier frequency is changed on a regular basis. This is used to average out channel effects statistically where the coherence bandwidth is large enough to cover an entire FFT bandwidth (or coherence bandwidth is comparable to FFT bandwidth). Users are grouped according to channel conditions, so users requiring fast band hopping occupy the same band (FFT spectrum), while users not benefitting from fast sub-band hopping occupy other bands. When band hopping is implemented, then we effectively improve the outage scenario without knowing the channel information at the BS. Band hopping also mitigates narrowband interference.

© Muhammad Imadur Rahman, 2007

3.2 Multiple Access (or Channelization) Approach

The basic approaches behind SCBH-OFDMA can be summarized as follows:

1. The users are grouped according to a pre-defined criterion, for example, coherence time, T_c and coherence bandwidth, B_c. These two specific criteria will create user groups based on heterogeneous channel conditions.

2. The total available spectrum is divided into number of OFDM system bands, i.e. equivalent to a number of FFT bandwidth. If the available spectrum is W and if the number of user groups is G, then system bandwidth, $B = \frac{W}{G}$. Virtually, there are G number of OFDM systems existing in the cell area simultaneously.

3. Each user group is assigned to any of the G number of bands.

4. As a rule of thumb, sub-channels (or sub-carriers) are allocated to users without the CSI knowledge via predefined hopping sequence.

5. At every OFDM time slot (or after a number of time slots), the user groups are hopped across the bands.

The chosen approach of a combination of band and sub-carrier hopping is shown in Figures 3.1(a) - 3.1(d). Here, we have denoted fast and slow sub-carrier hopping when the hopping pattern changes once every OFDM symbol and once every coherence time (T_c), respectively[3]. Here it is assumed that $T_c \geq k * T_s$. That means, hopping pattern changes at every k^{th} OFDMA symbol for slow sub-carrier hopping. Fast and slow band hopping is defined as carrier frequency hopping once every *time-frequency frame* or hopping when a certain number of *time-frequency frames* have elapsed, respectively. This is explained graphically in Section 4.2. In the figures mentioned above, we also assume that $G = 3$. We have 4 sub-channels in each B with a width of Δf, and each sub-channel is assigned to one user. Users 1 to 4, 5 to 8 and 9 to 12 belong to user group 1, 2 and 3 respectively (i.e. yellow, green and grey groups respectively).

Grouping and hopping strategies define the proposed SCBH-OFDMA scheme. These are explained in the following sections.

3.2.1 User Grouping

The grouping strategies in SCBH-OFDMA should utilize the inherent flexibility of the multiple-access scheme. The grouping strategy for the access scheme should include the following criteria. For DL, we can group users that have similar channel profiles (in terms of B_c and T_c as shown in Tables 3.1 and 3.2). This will ensure a better channelization and thus, increase the throughput.

An example of this is shown in Figure 3.2. The figure illustrates a macrocell/microcell environment with differing channel conditions. Pedestrian outdoor users (red group) usually have a larger delay spread resulting in narrow coherence bandwidth (compared to indoor users). The same is true for the open building in the upper left side of the figure, which consists of open spaces.

[3]Slow sub-carrier hopping is actually defined as changes in sub-carrier hopping patterns once every *time-frequency frame*. Please refer to Section 4.2 for further details.

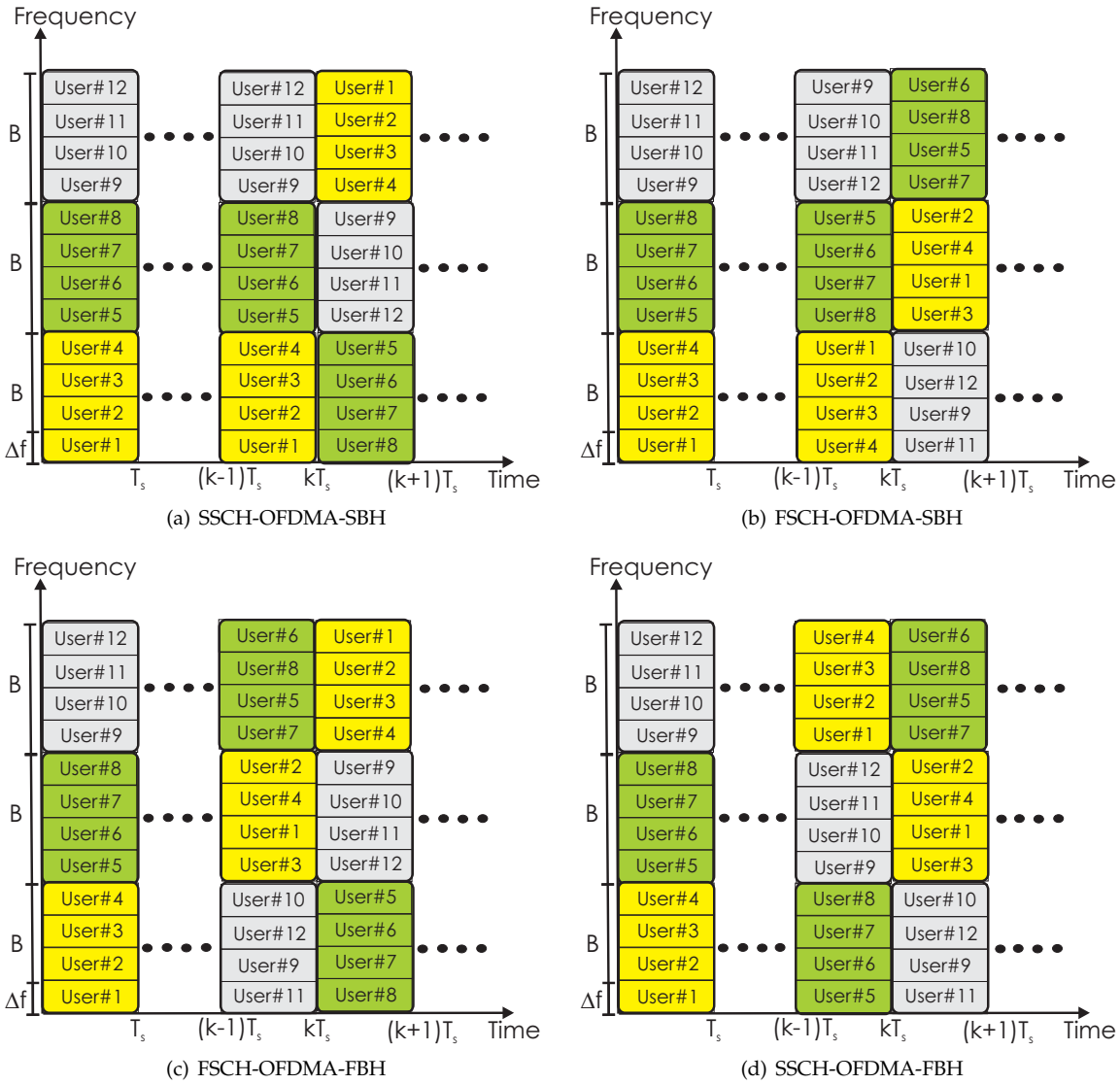

(a) SSCH-OFDMA-SBH (b) FSCH-OFDMA-SBH

(c) FSCH-OFDMA-FBH (d) SSCH-OFDMA-FBH

Figure 3.1: Different combinations of sub-carrier and band hopping in SCBH-OFDMA scheme.

© Muhammad Imadur Rahman, 2007

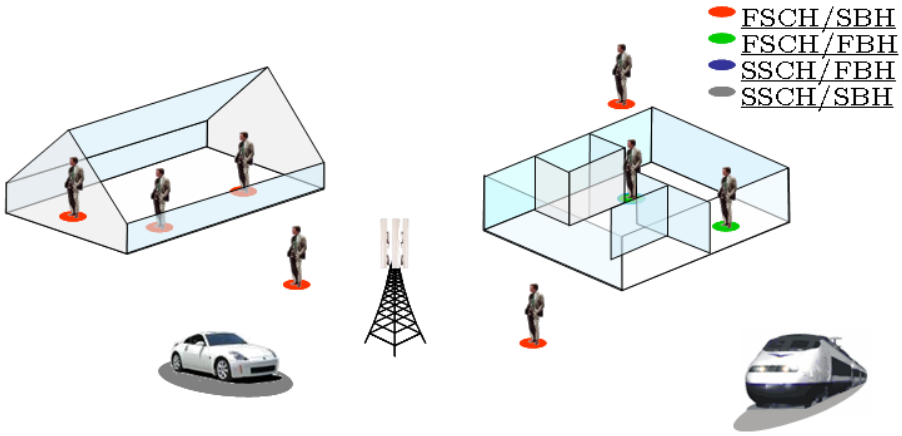

Figure 3.2: Illustration of grouping strategies.

Users in these areas will be put in the same group(s). As coherence bandwidth is low and coherence time is high (due to low mobility), fast sub-carrier hopping is used together with slow band hopping. The car and train (grey group) have similar propagation properties, i.e. the coherence time is lower due to the higher velocity. Therefore, slow hopping is employed as the benefits of fast hopping cannot be obtained in this case. Finally, the office building (right side of the figure) is a case of a microcell environment with a low delay spread and non-LOS propagation. This, combined with low mobility, this indoor environment makes fast sub-carrier and band hopping necessary to ensure the average channel quality for the users in the office (green group).

The instantaneous signal quality depends highly on the channel state for each OFDMA symbol. Assuming that the BS can correctly allocate the different users to the different groups, the average signal quality, however, is distributed fairly with only the required complexity (i.e. the sub-carrier or band is not hopped unless it is needed).

3.2.2 Sub-Carrier and Band Hopping Strategy

Sub-carrier hopping in and of itself reduces the complexity of resource allocation, as poor channel conditions will be distributed more fairly among different users. Besides this, band hopping provides interference minimization and avoidance. Required hopping rate in order to obtain an advantage from frequency diversity and/or interference mitigation depend on the characteristics of the mobile channel, i.e. coherence bandwidth, coherence time, etc.

These channel characteristics may be divided into four categories, depending on coherence time and bandwidth, i.e. high or low coherence bandwidth, B_c, and high or low coherence time, T_c. High (low) B_c refers to mild (severe) frequency selectivity of the wireless channel, which corresponds to short (long) delay spread compared to OFDM symbol duration, T_u. Similarly, high (low) T_c refers to mild (severe) time-variance of the channel, corresponding to low (high) user (and/or scatterer) mobility. The terms "high" and "low" should be seen as relative to OFDM symbol duration (T_u) in the case of T_c and sub-carrier spacing (Δf) in the case of B_c, as it is shown below:

Low T_c: On the order of one to few OFDM symbol durations

High T_c: Several OFDM symbol durations.

Low B_c: Partly covers an OFDM channel bandwidth, in another words, comparable to Δf and much smaller than B.

High B_c: Covers more than one OFDM sub-channels; i.e. much higher than Δf and comparable to B.

The different regimes (high/low B_c combined with high/low T_c) may be characterized according to propagation conditions, i.e. delay spread and relative velocity between MS and BS.

By using hopping to counter fading and outages instead of dynamically allocating channels based on channel estimation, system complexity is traded off for performance. By using random hopping, users do not get optimum channels. However, no user has a bad channel for more than a few OFDM symbols.

	Low T_c	High T_c
Low B_c	SSCH/SBH	FSCH/SBH
High B_c	SSCH/FBH	FSCH/FBH, SSCH/FBH

Table 3.1: Choice of hopping strategy depends on coherence bandwidth, B_c and coherence time, T_c.

B_c, T_c	Hopping	Typical scenario
Low T_c, low B_c	SSCH/SBH	Highway, suburban, tunnel, long bridge, i.e. outdoor macro cells
High T_c, low B_c	FSCH/SBH	Large office, shopping mall, airport, outdoor pedestrian, large stadium i.e. indoor micro cells and immediate outdoor micro cells
Low T_c, high B_c	SSCH/FBH	large production plant, city center in some cases
High T_c, high B_c	FSCH/FBH, SSCH/FBH	small office, home area, i.e. indoor picocells

Table 3.2: Division of hopping strategies

As for the case of low B_c and low T_c (i.e. outdoor micro cells), fast sub-carrier and band hopping will not yield any benefit compared to slow hopping, because we realize that the channel is very highly time-selective, thus a users' sub-carrier will not stay in deep fade for long period. and the rapid changes in channels' time characteristics will average the fade over the users. Similarly, for the case of high B_c and high T_c (i.e. indoor picocells), fast or slow sub-carrier hopping does not really bring the diversity effect due to comparable B_c to B. In this case, fast band hopping will be the prime reason for system performance improvement regardless of sub-carrier hopping scheme.

3.3 Analytical Model

In this section, we present an analytical system model of our proposed SCBH-OFDMA scheme.

© Muhammad Imadur Rahman, 2007

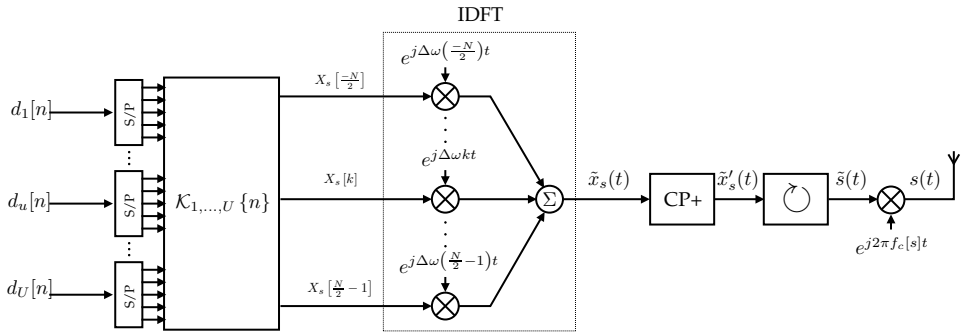

Figure 3.3: Transmitter diagram for the OFDM analytical model, given by Eq. (3.2) - (3.12). The data sequences for U users in one group are serial-to-parallel converted and allocated to the sub-carriers, shown in Eq. (3.2). The sub-carriers for the sth OFDM symbol each modulate a carrier, which are separated by $\Delta\omega$. The resulting waveforms are then summed, and the CP is added. The symbol $\circlearrowright$ represents the concatenation of the OFDM symbols, given by Eq. (3.11). The resulting signal is then converted to a carrier frequency and transmitted.

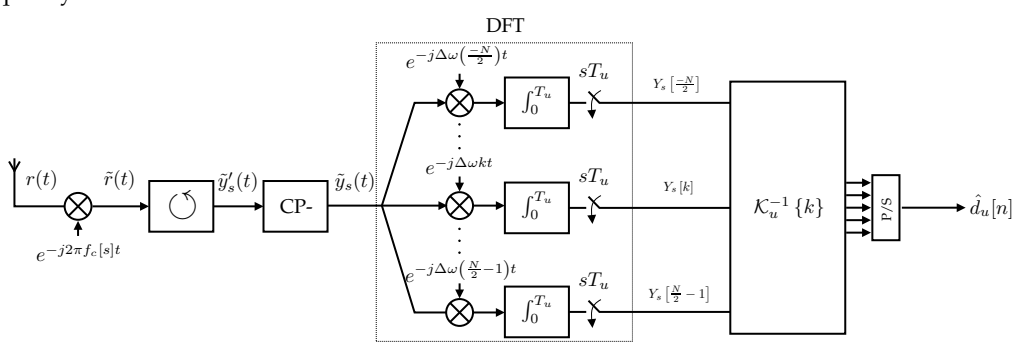

Figure 3.4: Downlink receiver diagram for the OFDM analytical model, given by Eq. (3.15) - (3.24). The received signal (suffering from multipath effects and AWGN) is converted down to baseband. The symbol $\circlearrowleft$ represents the division of the received signal into blocks, given by Eq. (3.17). The CP is removed from each block, and the signal is then correlated with each subcarrier frequency, as shown by Eq. (3.21). Finally, the sub-carriers belonging to user u are selected and parallel-to-serial converted, as seen from Eq. (3.29).

3.3.1 DL Transmitter

Considering a traditional OFDM scheme the difference is that the data input is a combination of different user data. Meaning that the user's data is partitioned into length that combined with error coding and baseband modulation fits the assigned number of sub-carriers.

For the sth OFDM symbol, and the uth user, each user is provided with a number of sub-carriers. The subcarrier indices for the uth user are found using the set Δ_u, i.e. the uth user uses $|\Delta_u|$ sub-carriers, where $|\Delta_u|$ denotes number of elements in Δ_u. Defining the indexing function for the uth user, $\mathcal{K}_u\{v\}$, as a function that bijectively maps a sequential index from 0 to $|\Delta_u|-1$ onto all subcarrier indices in Δ_u,

$$\begin{aligned} &\mathcal{K}_u\{v\} \in \Delta_u; \quad \forall v \in \{0,1,...,|\Delta_u|-1\} \\ &\mathcal{K}_u\{v\} \neq \mathcal{K}_u\{v'\}; \quad v \neq v, \end{aligned} \tag{3.1}$$

which means that there is a one-to-one correspondence between the sequential index and the sub-carrier index. As this scheme utilizes slow or fast subcarrier hopping, the indexing function of two distinct OFDM symbols may be different. In the following, the indexing function valid for the sth OFDM symbol is denoted as $\mathcal{K}_{u,s}\{v\}$. The inverse indexing function, i.e. the function that takes the subcarrier index and maps it onto a sequential index valid for the uth user is defined such that,

$$\begin{aligned} \mathcal{K}_{u,s}^{-1}\{k\} \in \{0,1,...,|\Delta_u|-1\} &\Leftrightarrow k \in \Delta_u; \\ \mathcal{K}_{u,s}\left\{\mathcal{K}_{u,s}^{-1}\{k\}\right\} &= k \\ \mathcal{K}_{u,s}^{-1}\{\mathcal{K}_{u,s}\{v\}\} &= v \end{aligned}$$

The kth subcarrier for the uth user and s^{th} OFDM symbol, $\mathbf{X}_{u,s}[k]$, is found by,

$$\mathbf{X}_{u,s}[k] = \begin{cases} d_u\left[sV_u^s + \mathcal{K}_{u,s}^{-1}\{k\}\right] & k \in \Delta_u \\ 0 & \text{otherwise} \end{cases} ; \quad k \in \{0,1,...,N-1\} \tag{3.2}$$

where $V_u^s = |\Delta_u|$ is the number of source symbols transmitted in every OFDM symbol for the uth user. The transmitted OFDM symbol for the uth user can then be written as,

$$\tilde{x}_{u,s}(t) = \frac{1}{\sqrt{T_u}} \sum_{k \in \Delta_u} \mathbf{X}_{u,s}[k] e^{j\Delta\omega k t}; \qquad 0 \leq t < T_u \tag{3.3}$$

In OFDMA, the users are combined into a OFDM symbol, where the sth OFDM symbol is,

$$\begin{aligned} \tilde{x}_s(t) &= \sum_{u=0}^{U-1} \tilde{x}_{u,s}(t) \\ &= \frac{1}{\sqrt{T_u}} \sum_{u=0}^{U-1} \sum_{k \in \Delta_u} \mathbf{X}_{u,s}[k] e^{j\Delta\omega k t}; \qquad 0 \leq t < T_u \end{aligned} \tag{3.4}$$

The sth OFDM symbol is found using the sth sub-carrier block, $\mathbf{X}_s[k]$. In practice, the OFDM

© Muhammad Imadur Rahman, 2007

signal is generated using an inverse DFT. In the following model, the transmitter is assumed ideal, i.e. sampling or filtering do not affect the signal on the transmitter side. Therefore, a continuous transmitter output signal may be constructed directly using a Fourier series representation within each OFDM symbol interval.

Each OFDM symbol contains N subcarriers, where N is an even number (frequently a power of two). The OFDM symbol duration is T_u seconds, which must be a whole number of periods for each subcarrier. Defining the subcarrier spacing as $\Delta\omega$, the relation between subcarrier spacing and the OFDM symbol duration is written as,

$$T_u = \frac{2\pi}{\Delta\omega} \Leftrightarrow \Delta\omega = \frac{2\pi}{T_u} = 2\pi\Delta f \tag{3.5}$$

Using this relation, the spectrum of the Fourier series for the duration of the sth OFDM symbol is written as,

$$\mathbf{X}_s(\omega) = \sum_{k=-N/2}^{N/2-1} \mathbf{X}_s[k]\delta_c(\omega - k\Delta\omega) \tag{3.6}$$

In order to provide the OFDM symbol in the time-domain, the spectrum in Eq. (3.6) is inverse Fourier transformed and limited to a time interval of T_u. The time-domain signal, $\tilde{x}_s(t)$, is therefore written as,

$$\begin{aligned}\tilde{x}_s(t) &= \mathcal{F}\left\{\mathbf{X}_s(\omega)\right\}\Xi_{T_u}(t) \\ &= \begin{cases} \frac{1}{\sqrt{T_u}} \sum_{k=-N/2}^{N/2-1} \mathbf{X}_s[k]e^{j\Delta\omega kt} & 0 \leq t < T_u \\ 0 & \text{otherwise} \end{cases} \end{aligned} \tag{3.7}$$

$$\tag{3.8}$$

where Ξ_{T_u} is a unity amplitude rectangular gate pulse of duration T_u. Following the frequency- to time-domain conversion, the signal is extended, and the CP is added,

$$\tilde{x}'_s(t) = \begin{cases} \tilde{x}_s(t + T_u - T_g) & 0 \leq t < T_g \\ \tilde{x}_s(t - T_g) & T_g < t < T_s \\ 0 & \text{otherwise} \end{cases} \tag{3.9}$$

where T_g is the cyclic prefix duration and $T_s = T_u + T_g$ is the total OFDM symbol duration. It should be noted, that Eq. (3.9) has the following property,

$$\tilde{x}'_s(t) = \tilde{x}'_s(t + T_u) \Leftrightarrow 0 \leq t < T_g \tag{3.10}$$

that is, a periodicity property within the interval $[0, T_g]$. The transmitted complex baseband signal, $\tilde{s}(t)$, is formed by concatenating all OFDM symbols in the time-domain,

$$\tilde{s}(t) = \sum_{s=0}^{S-1} \tilde{x}'_s(t - sT_s) \tag{3.11}$$

$$sT_s \leq t < (s+1)T_s$$

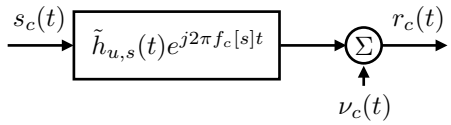

Figure 3.5: A diagram of the channel model given by Eq.(3.13). The transmitted signal passes through the channel, and noise is added.

This signal is finally up-converted to a carrier frequency and transmitted. As the system uses band hopping, the carrier frequency is changed at regular intervals. The RF signal is written as,

$$s(t) = \Re e\left\{\tilde{s}(t)e^{j2\pi f_c[s]t}\right\} \tag{3.12}$$

where $s(t)$ denotes the transmitted RF signal and $f_c[s]$ is the RF carrier frequency for the sth OFDM symbol. The period of $f_c[s]$ is χ, where χ is the hopping sequence period measured in whole OFDM symbols.

3.3.2 Wireless Channel

The baseband channel impulse response can be modeled as shown in Eq.(2.1). The channel is assumed to be static for the duration of one OFDM symbol, and the path gain coefficients for each path contribution are assumed to be uncorrelated. No assumption is made for the autocorrelation properties of each path, except in the case of frequency hopping systems. In such systems, the channel is assumed to be completely uncorrelated between two frequency hops, provided that the distance in frequency is sufficiently large.

As the channel is assumed to be static over each OFDM symbol, Eq.(2.1) is redefined as:

$$\tilde{h}_{u,s}(t) = \sum_{l=0}^{L-1} h_{u,l}[s]\delta_c(t-\tau_l) \tag{3.13}$$

where

$$h_{u,l}[s] = h_{u,l}(t); \qquad sT_s \leq t < (s+1)T_s$$

The corresponding frequency-domain channel transfer function, $H_{u,s}$, can then be found using Fourier transformation:

$$\begin{aligned} H_{u,s}(\omega) &= \mathcal{F}\left\{\tilde{h}_{u,s}(t)\right\} \\ &= \int_{-\infty}^{\infty} \tilde{h}_{u,s}(t)e^{-j\omega t}dt \end{aligned} \tag{3.14}$$

The time-domain channel model is illustrated in Figure 3.5.

© Muhammad Imadur Rahman, 2007

3.3.3 DL Receiver

The signal at the receiver side consists of multiple echoes of the transmitted signal, as well as thermal (white gaussian) noise and interference. The RF signal received by the uth user is written as,

$$r(t) = \Re e\left\{\left[\tilde{s}(t) * \tilde{h}_{u,s}(t)\right] e^{j2\pi f_c[s]t}\right\} + \nu(t); \qquad sT_s \leq t < (s+1)T_s \tag{3.15}$$

where $\nu(t)$ is a real valued, passband signal combining additive noise and interference. The receiver now has to recreate the transmitted signal. At this juncture, we should note that the reception procedure described in this section is essentially the reception in one particular user's receiver. Aside from noise and multipath effects, other imperfections in the receiver may also affect this process:

Timing error: In order to demodulate the signal, the receiver must establish the correct timing. This means that the receiver must estimate which time instant corresponds to $t = 0$ in the received signal (as seen from the transmitted signal point of view). As there are different uncertainties involved, a timing error of δt is assumed.

Frequency Error Similarly, the local oscillator of the receiver may oscillate at an angular frequency that is different from the angular frequency of the incoming signal. This difference is denoted $\delta\omega = 2\pi\delta f$.

The shifted time scale in the receiver is denoted $t' = t - \delta t$. Furthermore, due to the angular frequency error $\delta\omega$, the down-converted signal spectrum is shifted in frequency. The down-converted signal is therefore written as,

$$\tilde{r}(t) = \left[\tilde{s}(t') * \tilde{h}_{u,s}(t)\right] e^{j\delta\omega t} + \tilde{\nu}(t'); \qquad sT_s \leq t < (s+1)T_s \tag{3.16}$$

where $\tilde{\nu}(t')$ is the complex envelope of the down-converted Additive White Gaussian Noise (AWGN). We can write that $\tilde{\nu}(t') = \tilde{\nu}(t)$, due to Gaussian nature of the noise. The signal is divided into blocks of T_s each, and the CP is removed from each of them. The sth received OFDM symbol block, $y'_s(t)$ is defined as,

$$\tilde{y}'_s(t) = \tilde{r}(t' - sT_s); \qquad 0 \leq t < T_s \tag{3.17}$$

The signal block corresponding to $\tilde{x}_s(t)$, $\tilde{y}_s(t)$ is found by removing the CP from the each $\tilde{y}'_s(t)$,

$$\tilde{y}_s(t) = \tilde{y}'_s(t + T_g); \qquad 0 \leq t < T_s - T_g \tag{3.18}$$

which can be rewritten as,

$$\begin{aligned}
\tilde{y}_s(t) &= \tilde{y}'_s(t + T_g); \qquad 0 \leq t \leq T_u \\
&= \tilde{r}(t' + T_g - sT_s) \\
&= \left[\tilde{s}(t' + T_g - sT_s) * \tilde{h}_{u,s}(t)\right] e^{j\delta\omega t} + \tilde{\nu}(t + T_g - sT_s) \\
&= \left[\tilde{x}'_s(t' + T_g) * \tilde{h}_{u,s}(t)\right] e^{j\delta\omega t} + \tilde{\nu}_s(t) \\
&= \left[\tilde{x}_s(t') * \tilde{h}_{u,s}(t)\right] e^{j\delta\omega t} + \tilde{\nu}_s(t)
\end{aligned} \tag{3.19}$$

where $\tilde{\nu}_s(t)$ is the noise signal block of duration T_u corresponding to the sth OFDM symbol.

In order to recreate the transmitted sub-carriers, N correlators are used, each one correlating the incoming signal with the kth subcarrier frequency over an OFDM symbol period,

$$Y_s[k] = \frac{1}{\sqrt{T_u}} \int_0^{T_u} \tilde{y}_s(t') e^{j\Delta\omega k t} dt \tag{3.20}$$

where Eq.(3.20) is actually continuous Fourier transform of the received signals. Thus, In order to OFDM demodulate the sub-carriers, each signal block is DFT transformed. The DFT output for individual sub-carriers may be seen as taking the continuous Fourier transform of Eq.(3.19) multiplied by the rectangular pulse $\Xi_{T_u}(t)$ and evaluating it at the corresponding subcarrier frequency. Assuming that the timing error is low enough to avoid ISI,

$$0 \leq \delta t < T_g - \max(\tau_l)$$

the continuous Fourier transform can be written as,

$$\begin{aligned}
Y_s(\omega) &= \mathcal{F}\left\{\tilde{y}_s(t)\Xi_{T_u}(t)\right\} \\
&= \mathcal{F}\left\{(\tilde{x}_s(t') * \tilde{h}_{u,s}(t))e^{j\delta\omega t} + \tilde{\nu}_s(t')\right\} * T_u e^{j\pi\frac{\omega}{\Delta\omega}} \operatorname{sinc}\left(\frac{\omega}{\Delta\omega}\right) \\
&= \mathcal{F}\left\{(\tilde{x}_s(t') * \tilde{h}_{u,s}(t))e^{j\delta\omega t}\right\} * T_u e^{j\pi\frac{\omega}{\Delta\omega}} \operatorname{sinc}\left(\frac{\omega}{\Delta\omega}\right) + N_s(\omega) \\
&= \mathcal{F}\left\{\tilde{x}_s(t') * \tilde{h}_{u,s}(t)\right\} * \delta_c(\omega - \delta\omega) * T_u e^{j\pi\frac{\omega}{\Delta\omega}} \operatorname{sinc}\left(\frac{\omega}{\Delta\omega}\right) + N_s(\omega) \\
&= e^{-j\omega\delta t}\mathcal{F}\left\{\tilde{x}_s(t) * \tilde{h}_{u,s}(t)\right\} * \delta_c(\omega - \delta\omega) * T_u e^{j\pi\frac{\omega}{\Delta\omega}} \operatorname{sinc}\left(\frac{\omega}{\Delta\omega}\right) + N_s(\omega) \\
&= e^{-j\omega(\delta t + \frac{\pi}{\Delta\omega})} \sum_{k'=N/2}^{N/2-1} \mathbf{X}_s[k'] H_{u,s}(k'\Delta\omega) \operatorname{sinc}\left(\frac{\omega - k'\Delta\omega - \delta\omega}{\Delta\omega}\right) + N_s(\omega)
\end{aligned} \tag{3.21}$$

where

$$N_s(\omega) = \mathcal{F}\left\{\tilde{\nu}_s(t)\right\} * T_u e^{j\pi\frac{\omega}{\Delta\omega}} \operatorname{sinc}\left(\frac{\omega}{\Delta\omega}\right) \tag{3.22}$$

is the Fourier transform of the AWGN contribution. The DFT output at the kth sub-carrier is then found as,

$$\begin{aligned}
Y_s[k] &= Y_s(k\Delta\omega) \\
&= e^{-jk\Delta\omega(\delta t + \frac{\pi}{\Delta\omega})} \sum_{k'=N/2}^{N/2-1} \mathbf{X}_s[k'] H_{u,s}(k'\Delta\omega) \operatorname{sinc}\left(\frac{k\Delta\omega - k'\Delta\omega - \delta\omega}{\Delta\omega}\right) + N_s(k\Delta\omega)
\end{aligned} \tag{3.23}$$

For zero frequency error, Eq.(3.23) reduces to,

$$Y_s[k] = e^{-jk\Delta\omega(\delta t + \frac{\pi}{\Delta\omega})} \mathbf{X}_s[k] H_{u,s}[k] + N_s[k]; \quad \delta\omega = 0 \tag{3.24}$$

© Muhammad Imadur Rahman, 2007

where

$$N_s[k] = N_s(k\Delta\omega) \tag{3.25}$$

$$H_{u,s}[k] = H_{u,s}(k\Delta\omega) \tag{3.26}$$

From Eq.(3.23), it is seen that the kth correlator output, $Y_s[k]$ corresponds to the transmitted sub-carrier, $\mathbf{X}_s[k]$, with AWGN, ICI and a complex gain term (amplitude and phase shift) due to imperfect timing and channel effects. The analytical model for the receiver is illustrated in Figure 3.4.

When estimating the channel, the constant phase rotation term and the channel transfer function would be estimated jointly (as the receiver cannot discern between the two). In the following, the timing delay phase shift is omitted for clarity. Defining the equalization factor for the kth sub-carrier of the sth OFDM symbol and u^{th} user as $Z_{u,s}[k]$, the sub-carrier estimate is written as,

$$\begin{aligned}\hat{\mathbf{X}}_s[k] &= Z_{u,s}[k]\, Y_s[k] \\ &= Z_{u,s}[k]\, H_{u,s}[k]\, \mathbf{X}_s[k] + Z_{u,s}[k]\, N_s[k]\end{aligned} \tag{3.27}$$

Assuming a zero-forcing, frequency-domain equalizer (as well as perfect channel estimation and zero frequency error), the corresponding equalizer gain is written as,

$$Z_{u,s}[k] = \frac{1}{H_{u,s}[k]}$$

and Eq.(3.27) is rewritten as,

$$\hat{\mathbf{X}}_s[k] = \mathbf{X}_s[k] + \frac{N_s[k]}{H_{u,s}[k]} \tag{3.28}$$

It is observed, that although this is an unbiased estimator for $\mathbf{X}_s[k]$, the signal-to-noise ratio decreases drastically for sub-carriers in deep fades. From $\hat{\mathbf{X}}_s[k]$, only a fraction of the sub-carriers belong to the uth user. Using the uth user sub-carrier mapping information, the estimated data symbol sequence $\hat{d}_u$ is found using:

$$\hat{d}_u[sV_u^s + v] = \hat{\mathbf{X}}_s[\mathcal{K}_u\{v\}] \tag{3.29}$$

Sampling

Although the receiver may be modeled in the continuous time-domain, an OFDM receiver uses discrete signal processing to obtain the estimate of the transmitted sub-carriers.

When the received signal is modeled as a Dirac impulse train, i.e. an ideally sampled signal, Eq.(3.19) is instead written as,

$$\tilde{y}_{s,d}(t) = \sum_{n=0}^{N-1} \tilde{y}_s[n]\delta_c(t - nT) \tag{3.30}$$

where

$$T = \frac{T_u}{N} \tag{3.31}$$

is the sample duration and

$$\tilde{y}_s[n] = \tilde{y}_s(nT); \quad n \in \{0, 1, ..., N-1\} \tag{3.32}$$

is the discrete sequence corresponding to the sampled values of $\tilde{y}_s(t)$. When Eq.(3.30) is inserted into Eq.(3.20), the correlation becomes the Discrete Fourier Transform of the received signal. It can be shown, however, that Eq.(3.23) - (3.28) are still valid in the discrete-time case.

3.4 Numerical Evaluations

In this section, we describe our numerical evaluations of the proposed scheme in cellular scenario. We evaluate the scheme in a system level simulator that is specifically developed for evaluation of this scheme in MATLAB environment.

3.4.1 Simulation Parameters

Channel Parameters

Wireless channel parameters are chosen to support highly mobile (i.e highly time-variant) and severely frequency selective environment. This is exactly the scenario for outdoor wide area cellular system with high user data rate requirement.

Parameters	Units	Value	Comments
Maximum MS velocity, v	kmph	66	
Maximum RMS delay spread, τ_{rms}	μs	1	[91]
Coherence bandwidth, B_c	kHz	200	Section 2.1.1
Delay spread, τ_{max}	μs	5	$\tau_{max} \approx 5\tau_{rms}$
Maximum Doppler shift, f_d	Hz	185.19	Section 2.1.1
Coherence time, T_c	ms	2.3	Section 2.1.1

Multi-Carrier System Parameters

In this section, we explain the OFDM system related parameters. The number of required pilots and zero sub-carriers are very much of implementation related issue. We assigned some estimated numbers for those parameters for this moment, but it should be noted that as we will be designing pilot and pre-amble sequences, the number of frequency domain pilots and time-domain preambles will vary. In that case, a little tuning of the parameters will do.

Parameters	Units	Set-1	Set-2	Comments
System Bandwidth, B	MHz	40	20	
Carrier frequency, f_c	GHz	2.0	2.0	

© Muhammad Imadur Rahman, 2007

FFT size, N		2048	1024	
Number of non-zero sub-carriers, N_{nz}		1440	720	$= N_d + N_p$
Number of zero sub-carriers, N_z		608	304	$= N - N_{nz} = N - (N_d + N_p)$
Number of data sub-carriers, N_d		1299	650	$= N_{nz} - N_p$
Number of pilot sub-carrier, N_p		141	70	Once every coherence bandwidth for data sub-channels
Number of sub-bands		16	8	90 non-zero sub-carriers per band
Number of sub-channels		180	90	
Number of sub-carriers per sub-channel, N_{sch}		8	8	$180(90) * N_{sch} = N_d + N_p$
Sub-carrier spacing, $\Delta f = \frac{B}{N}$	kHz	19.53	19.53	Must be $f_d << \Delta f << B_c$
Sampling time, $T = \frac{1}{B}$	ns	25	50	$T * N = T_u$
DFT window time, T_d	μs	51.2	51.2	$= T * (N_d + N_z)$
Cyclic prefix samples, N_g		200	100	
Cyclic prefix duration, T_g	μs	5	5	$= N_g * T$
Total OFDM symbol duration, T_s	μs	56.2	56.2	$= T_d + T_g$
Number of OFDM symbols per basic time-frequency frame cell, S		9	9	
Basic frame duration, T_f	ms	0.5049	0.5049	$= S * T_s$

Simulation Assumptions

We made some generic assumptions for the simulations that we have performed without loosing any generality of the system:

1. The grouping of users, according to its channel characteristics, is needed to implement the SCBH-OFDMA scheme. The users are grouped based on statistical information. The users are assigned a multipath channel type[4] and velocity for the duration of the simulation. In the simulations, the grouping of these users is performed at the initial phase of the simulation. These groups are used throughout the simulations. Hence, there is no dynamic grouping of users in our evaluations.

2. We assume that the transmitter and the receiver is perfectly synchronized in time and frequency. Thus, we do not implement any synchronization algorithm.

3. No power control is performed in the DL.

[4]Here, a multipath channel type refers to the number of taps in the channel model.

3.4.2 System level Simulation

For the system level analysis, some considerations are made to check the improvements of our proposed SCBH-OFDMA scheme compared to other well known systems that allocates the sub-carriers in a blind manner. In this section, the system level assumptions are described, as well as the general view of the actions that need to be performed by such simulator.

3.4.2.1 Overall View

The general block diagram including the main functions identified to achieve a system level evaluation is depicted in Figure 3.6. The simulator generates a cellular scenario and analyzes the performance of a central cell surrounded by interfering cells. The communication under analysis is the DL from the BS to each user.

A database is built with information about each user, where several variables are stored, including user location and the channel gains experienced throughout the tested frames. The information about the channel gain at each sub-carrier and for all frames that will be tested is stored to be used at a later stage by the simulator. The channel generated is dependent on the environment where the user is.

When the system simulator initiates its action, it assumes constant data traffic arriving to the BS that needs to be sent to the users. The Scheduler plays the role, at the BS, of allocating resources in the OFDM frame to each user. Three types of scheduler have been implemented, as it will be mentioned in Section 3.4.2.4. After this process, the channel of each user is obtained, from the file where it was stored in the previous step, and the SINR is computed for each frame. When all the frames have been simulated, the performance of each user is measured and stored for analysis.

3.4.2.2 Scenario

A multiple cell scenario has been defined and the analysis will be done at a central cell surrounded by interfering neighbor cells employing the same system, as depicted in Figure 4.5. Moreover, the same user spatial density is assumed across all cells and a uniform distribution in the cell area was used to generate users position. It is assumed that all BSs employ the same scheduling algorithm.

When a user is generated in the scenario, it obtains a position index, used to calculate the distance to the serving BS and to interfering neighbor cells BS. Moreover, each user is characterized by experiencing a difference channel, i.e. path loss and fast fading. The fast fading channel that a user experiences depends on the environment assumed. Thus, three environments were identified to approximate a real world case:

- Indoor Stationary: Indoor comparatively lower delay spread environment, Low user mobility.
- Outdoor Stationary: Outdoor environment with both low and high delay spread situations, Low user mobility.
- Outdoor Mobile: Outdoor higher delay spread environment, high user mobility.

© Muhammad Imadur Rahman, 2007

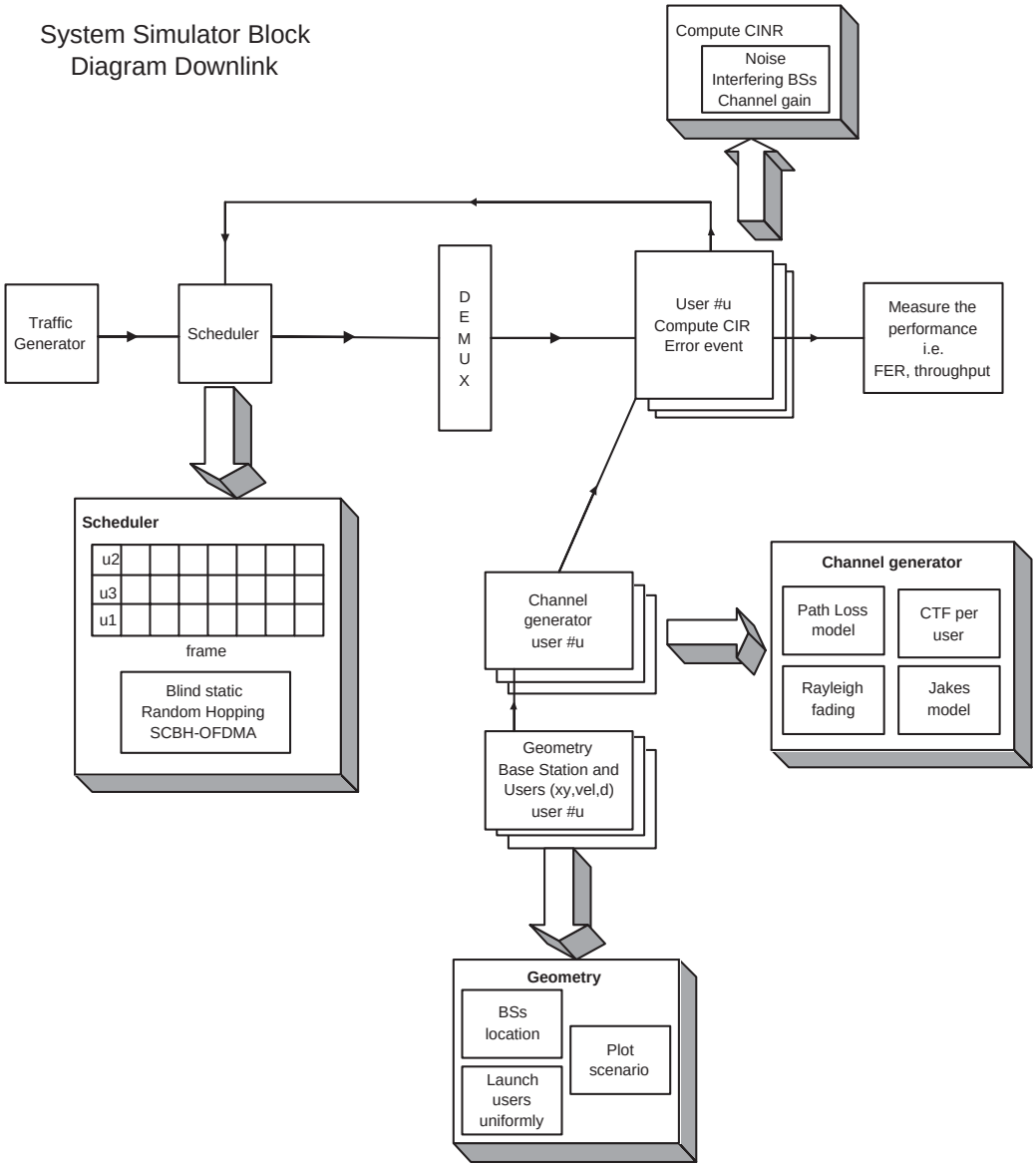

Figure 3.6: System level simulator flow

In Table 3.4, the distribution of users among the considered scenarios and its characteristics is shown. These parameters will be used to identify the features of fast fading channel, in Section 3.4.2.3.

Percent [%]	Type	v [kmph]	L [samples]
30%	Indoor St.	$50\% : 0.1$, $50\% : \mathcal{N}(5,1)$	$\mathcal{U}(5,20)$
30%	Outdoor St.	$50\% : 0.1$, $50\% : \mathcal{N}(5,1)$	$\mathcal{U}(5,20)$
40%	Outdoor Mob.	$100\% : \mathcal{N}(50,10)$	$\mathcal{U}(20,100)$

Table 3.4: Distribution of velocity and PDP length

The interference that limits the communication in a cellular scenario can be CCI, i.e. users using the same channel, or Adjacent Channel Interference (ACI), i.e. from users using neighbor (in spectrum) channels. We limit our analysis to a DL scenario. In this situation, the interference will be measured at the MS when it receives its desired signal and the signal to other users from its serving BS or from neighbor BS.

Depending on amount of CCI present in the system, we consider three different cases:

Full CCI: This scenario considers frequency re-use factor of 1.

Partial CCI: Roughly, this scenario corresponds to frequency re-use of 3.

No CCI: It corresponds to a single cell scenario, or a scenario with infinite re-use.

3.4.2.3 Channel Model

Path Loss

Depending on the user position in the cell, a path loss profile is identified, concerning the propagation loss that the signal suffers from the serving BS, as well as from interfering BSs. This propagation loss is mainly proportional to the distance between the terminal and the BS. The parameters employed for a preliminary analysis correspond to a model in which the signal power decreases with the distance with coefficients $n = 2.76$:

$$L_u \sim 10n \log(D_u) \tag{3.33}$$

where L_u is the pathloss for user u and D_u is the user's distance from the base station.

Short-Term Fading

The RMS delay spread for each user is defined based on Table 3.4. We use exponential channel model based on these RMS delay spread to generate corresponding CIR and Channel Frequency Response (CFR) of the channel. In our exponential model, channel impulse response in exponentially distributed with decay between the first and last impulse as -40dB.

© Muhammad Imadur Rahman, 2007

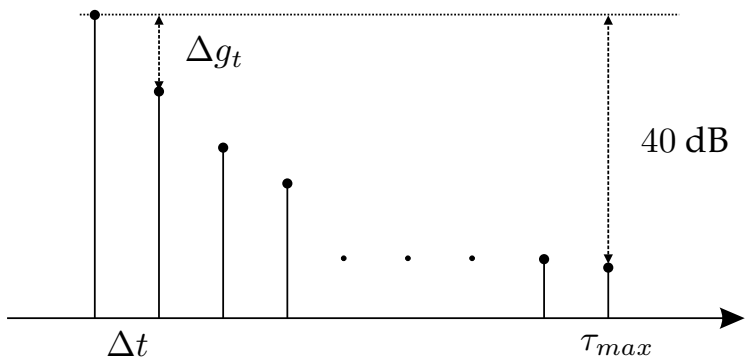

Figure 3.7: Power Delay Profile Model

Fast Fading

It is assumed that the channel maintains constant within a frame duration for all groups of users. The user mobility defines a correlation of the channel coefficients for each sub-carrier between two consecutive frames. This effect is dependent on the coherence time, affected by the Doppler frequency of the user. The normalized Doppler frequency per frame is then:

$$f_d = v_u \frac{f_c}{c} \Delta t N_{fr}(N + N_g) \tag{3.34}$$

where, v_u is the velocity of the user, f_c is the carrier frequency, c is the speed of light, Δt is the sample time, N_{fr} is the size of the frame (number of OFDM symbols), N is the FFT size and N_g is the guard size (number of sub-carriers used for CP).

3.4.2.4 Scheduler

An important assumption is that all users have equal data-rate request, hence they are allocated the same number of sub-carriers (or sub-channels) per frame. Two different scheduler algorithms were defined to make a term of comparison of the scheme SCBH-OFDMA:

Blind Static: In the Blind Static mode, the scheduler allocates the resources to the users in a permanent manner throughout the simulation. i.e. it is decided at the initial phase that first set of sub-channels are to be allocated to user 1, second set to user 2, and so on. This allocation is maintained throughout all the simulated frames. In the results section, this technique is denoted as '*Stat*'.

Random Hopping: In the Random scheduler, the sub-carriers are allocated randomly to the users. This allocation changes randomly at each frame. The users are allowed to perform sub-carrier (or sub-channel) hopping across the FFT bandwidth, B. This technique is denoted as '*Rand*'.

SCBH-OFDMA: SCBH-OFDMA scheduling is performed using the hooping mechanism explained in Section 4.7. This technique is denoted as '*SCBH*'. Groups employing slow band hopping

are assigned to the same bands in successive frames. The remaining bands are randomly redistributed to Fast Band Hopping (FBH) groups using random permutation. Sub-carrier hopping is achieved by randomly allocating the sub-carriers in a given band to different users. In fast subcarrier hopping, frequency rolling using a random index is performed every symbol. This is illustrated in Figure 4.3.

When grouping the users, each user is given a classification tag based on the preferred group type (fast or slow subcarrier hopping and fast or slow band hopping) based on coherence time and bandwidth. The users are grouped according to these tags according to the following method:

1. Determine the group size by dividing the number of user by the number of subbands (any remainder allocated to random groups).
2. Sort users based on classification tag. If the number of users tagged in a certain way exceeds the number of users per group, create a whole group. If the remainder of the users number more than the number of users per group, repeat.
3. When all group types have been allocated in this manner, the remaining groups are mixed. Starting with Fast Sub-Carrier Hopping (FSCH)-FBH, then Slow Sub-Carrier Hopping (SSCH)-FBH, followed by FSCH-Slow Band Hopping (SBH) and finally SSCH-SBH, the partial groups are filled with members from the next group (or groups). The hopping pattern is based on the ordering mentioned previously.

Example of SCBH-OFDMA Grouping: Sixty-four users must be grouped in 8 groups (8 users per group). There are 12 users preferring FSCH-FBH, 18 users preferring SSCH-FBH, 27 users preferring FSCH-SBH and 7 users preferring SSCH-SBH. By first grouping all whole groups, there is now one group using FSCH-FBH (4 users remaining), two groups using SSCH-FBH (2 users remaining), three groups using FSCH-SBH (3 users remaining) and no groups using SSCH-SBH. There are 4 FSCH-FBH users remaining, they are combined with the two remaining SSCH-FBH users and two of the three remaining FSCH-SBH users, the entire group using FSCH-FBH. The third FSCH-SBH user is then grouped with the seven SSCH-SBH users to form a FSCH-SBH group.

3.4.3 Interference Calculation

In order to estimate and/or emulate signal quality in a system scenario, the actual signal, noise and interference levels must be estimated separately and their relationship determined.

The average signal power per sub-carrier at a given user terminal can be found using:

$$\bar{p}_{s,u} = \frac{G_t G_r P_t \Delta P_u}{N L_u^0} \qquad \text{[Watt/sub-carrier]} \tag{3.35}$$

where P_t is the transmitted power, ΔP_u is the power control factor for user u, N is the number of sub-carriers, G_t is the transmit antenna gain, L_u^0 is the pathloss from the primary base station to user u and G_r is the receive antenna gain. Correspondingly, the average thermal noise power for a

© Muhammad Imadur Rahman, 2007

given sub-carrier is found using:

$$\bar{p}_{n,u} = \frac{kT_0BF_u}{N} \qquad \text{[Watt/subcarrier]} \tag{3.36}$$

where k is Boltzmann's constant, T_0 is the standard noise temperature (290 degrees Kelvin), P_n is the demodulator noise power, B is the system bandwidth and F_u is the noise figure for the receiver of user u.

Interference, strictly speaking, requires the simulation of any adjacent (or further) cells taken into consideration, then taking the pathloss from each cell to each user into account. In order to simplify the simulations considerably, the interference power per subcarrier from i^{th} interfering BS at the uth terminal can be found in a similar way as Eq.(3.35),

$$\bar{p}_{int,u,i} = \frac{G_tG_rP_t}{NL_u^i} \qquad \text{[Watt/sub-carrier]} \tag{3.37}$$

where L_u^i is the pathloss from the ith interfering base station to user u. Assuming a normalized average channel gain and signal power, the noise variance for user u is found using:

$$\sigma_u^2 = \frac{1}{\gamma} \tag{3.38}$$

where

$$\gamma = \frac{\bar{p}_{s,u}|h_{u,0}|^2}{\bar{p}_{n,u} + \sum_{i=1}^{I} \bar{p}_{int,u,i}|h_{u,i}|^2} \tag{3.39}$$

The combined noise plus interference can then be modeled by AWGN [92].

3.4.4 Outage SINR Analysis

In this section, we analyze the outage SINRs across the heterogeneous users. We simulate the systems for different levels of CCI by using the system level simulator described in Section 3.4.2. The sub-channel and band allocation is performed using three different schemes, described in Section 3.4.2.4. For every sub-channel, we record the resultant SINR for all users, and then we find the 10% outage SINR for all the users. Effectively, 10% outage SINR indicates that the user experiences higher SINR than the mentioned outage SINR for 90% of the time. Once the 10% outage SINRs of all users are found, the Cumulative Distribution Function (cdf) is plotted.

3.4.4.1 No CCI

Figure 3.8(a) shows the cdf of SINRs for all users when no CCI is used, i.e. an infinity re-use factor is assumed. In this case, the resultant SINRs of the users are high, due to the fact that the environment is interference free. Only a small part of the users experience lower range of SINRs. According to the cdf in Figure 3.8(a), some outage benefits are obtained by using SCBH-OFDMA for these small number of low SINR users. For the rest, the sub-carrier and band hopping does not provide much gain compared to static allocation.

3.4.4.2 In presence of CCI

Figures 3.8(b) and 3.8(c) present the cdfs when partial and full CCI is present in the system, respectively. These two cases correspond to re-use factor of 3 and 1 respectively. In presence of CCI, higher number of users experience lower SINR levels, thus the benefits out of frequency hopping is more evident. For random hopping case, the users that have very small coherence bandwidth, i.e. $B_c << B$, will only obtain the frequency diversity. When a user has a condition such that, $B_c \sim B$, i.e. the delay spread is very small, then only SCBH-OFDMA among these three schemes can be helpful for obtaining the benefit out of hopping. When the cellular interference is very high, i.e. re-use factor of 1, we can see that the benefits from SCBH-OFDMA technique is the most. This is logical as higher CCI level means that a large number of users may experience very low SINRs, hence there are higher possibilities to improve the outage by implementing combined sub-carrier and band hopping.

In table 3.5, we summarize the 10% and 20% outage users taken from Figures 3.8(a) - 3.8(c). For 20% outage values from the cdf of 10% outage SINRs show that SCBH-OFDMA obtains significant amount of gains in cellular environment compared to random hopping and static allocation cases. For re-use factor of 1 case, only 20% of the users experience outage SINRs of 3.5dB in SCBH-OFDMA, while it is approximately 42% and 51% for random hopping and static allocation respectively.

		10% outage	20% outage
SCBH	Full CCI	-4	3.5
	Partial CCI	6.5	8
	No CCI	8	12
Rand	Full CCI	-10	-7
	Partial CCI	2	4
	No CCI	7	10
Stat	Full CCI	-12	-9.5
	Partial CCI	-2	4
	No CCI	6	8

Table 3.5: 10% and 20% outage SINR values for different schemes with different levels of SINRs

3.4.5 Goodput Simulations

To evaluate the throughput performance of the schemes, the following metrics are analyzed:

Aggregate Frame Error Rate (FER): This is defined as, total number of frames that are erroneously received by any user, divided by the total number of transmitted frames.

Aggregate goodput: We denote $N_{bits,u}$ and T_f as aggregate FER of uth user, number of bits per user per frame and frame duration respectively. Then, we can define the aggregate goodput of any particular user as: $(1 - FER_u)\frac{N_{bits,u}}{T_f}$.

The FER results will show a similar pattern as seen in SINR results in Figures 3.8(a) - 3.8(c). These FER results are used to calculate the cell goodput as shown in Figures 3.9(a) and 3.9(b).

© Muhammad Imadur Rahman, 2007

3.4.5.1 Total Available Bandwidth, W = 20MHz

System bandwidth of 20MHz refers to '*Set-2*' of simulation parameters from Section 3.4.1. We have only presented the results related to complete CCI and no CCI case. We use QPSK, with $\frac{1}{2}$-rate convolutional coding for our simulations. Looking at Figure 3.8(a), almost all of our users experience an outage SINR of 5dB for all the schemes for no CCI scenario. Hence, following the trends from the outage SINR results, when no CCI is present, then the gain in aggregate goodput is very small when SCBH-OFDMA is used. This can also be seen in another way. When average SINR experienced by any user is higher, then hopping cannot increase the performance very much, provided that the user experiences either high frequency diversity due to delay spread, or high time diversity due to Doppler spread. In our case, we have large number of users who have either high delay spread, or high doppler spread, thus, at high average SINR conditions, e.g. no CCI situation, the resultant goodput cannot be improved much using hopping.

For CCI scenario, the gain out of SCBH-OFDMA scheme is very evident following the trends from SINR results. Almost 15% gain in goodput in terms of bps/Hz is seen when random hopping is used compared to static OFDMA system. SCBH-OFDMA scheme obtains almost 80% higher goodput compared to static allocation. Maximum goodput obtained by SCBH-OFDMA is around 1.35 bps/Hz, which is approximately 27Mbps on 20MHz of total used bandwidth.

3.4.5.2 Total Available Bandwidth, W = 40MHz

Using the'*Set-1*' of simulation parameters from Section 3.4.1, we have evaluated all three schemes using 40MHz of total available bandwidth. The goal is to investigate whether the users can exploit the possibility of higher frequency diversity when higher bandwidth is used. From Figures 3.9(a) and 3.9(b), it can be seen that not much of goodput improvement is achieved when 40MHz of system bandwidth is used, instead of 20MHz. The coherence bandwidth experienced by the users in the simulations, are much smaller compared to 20MHz, thus enough amount of frequency diversity is already obtained in 20MHz bandwidth.

It is worth noting here that we use $\frac{1}{2}$-rate convolutional code as our FEC code. It remains to be seen what level of performance improvement can be made by making use of stronger channel code, such as LDPC. It is expected that LDPC-type FEC codes can exploit the available frequency diversity more efficiently and improve the system throughput performance.

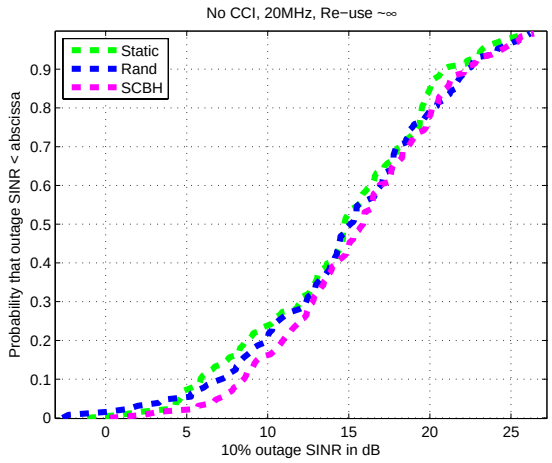

(a) No CCI

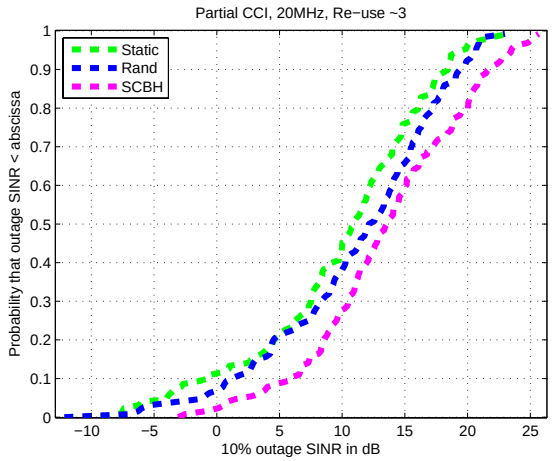

(b) Partial CCI

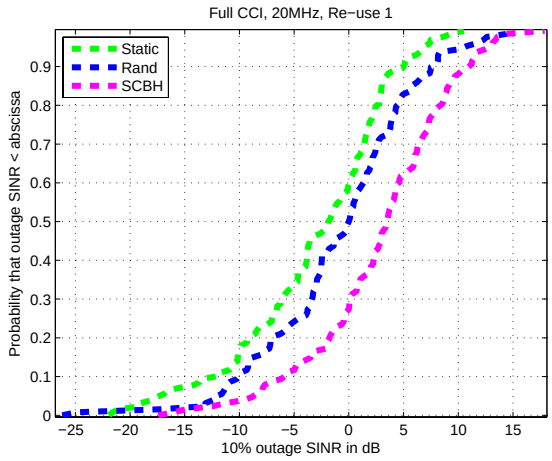

(c) Full CCI

Figure 3.8: cdf of 10% outage SNR for all users for different levels of CCI

© Muhammad Imadur Rahman, 2007

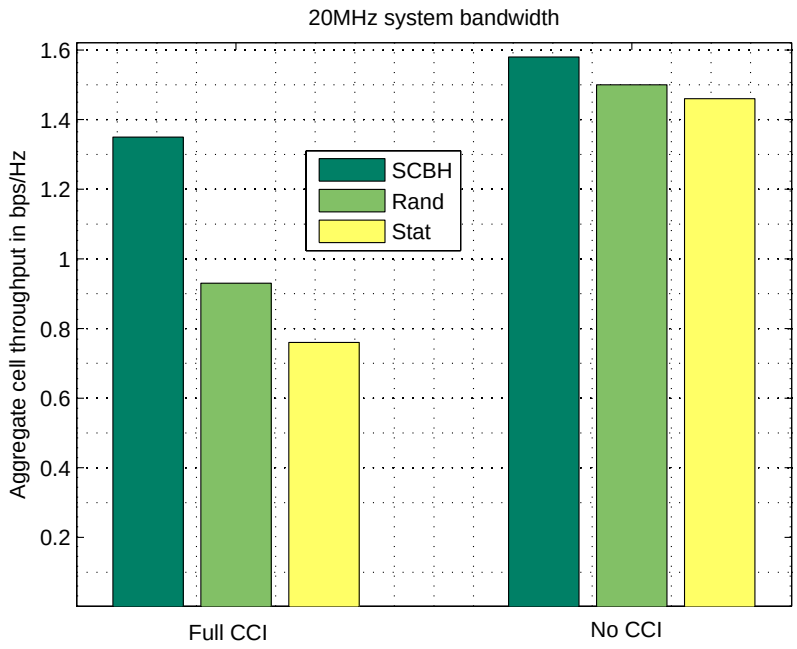

(a) $W = 20\text{MHz}$

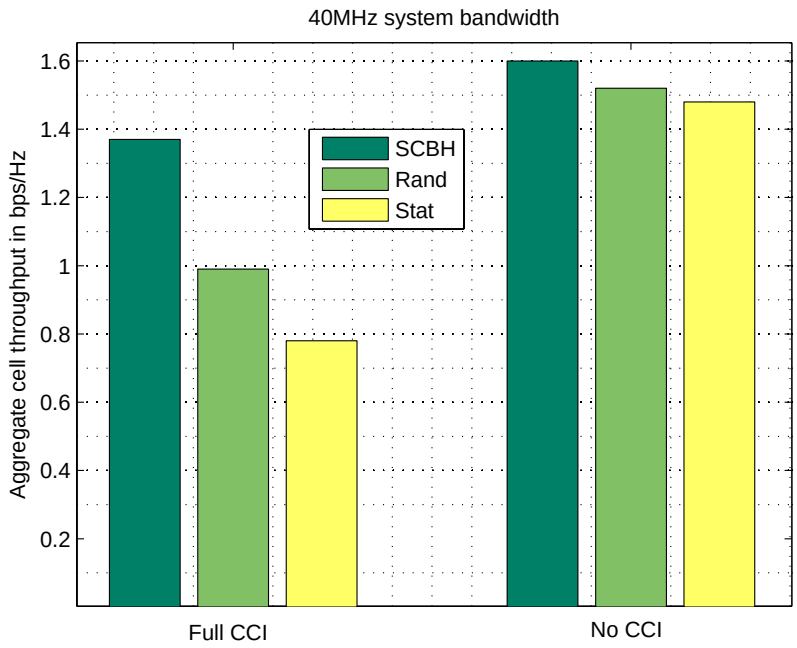

(b) $W = 40\text{MHz}$

Figure 3.9: Aggregate cell goodput for different levels of CCI and different system bandwidth

3.5 Chapter Summary

SCBH-OFDMA scheme

In SCBH-OFDMA scheme, we propose to accumulate the users in several groups based on certain predefined criteria. The total available spectrum is divided into a number of bands equal to the number of groups. For efficient time-frequency resource allocation, sub-carrier hopping and band hopping is simultaneously used in this novel multiple access scheme. Under some constraints, sub-carriers can also be assigned to different users based on known channel characteristics using dynamic sub-carrier allocation. Sub-carrier and band hopping are used for mitigating the frequency selectivity of the wireless channel and for minimizing and avoiding interference in the system. The novelty comes when users are grouped based on some pre-defined criteria and they are hopped on sub-carriers and on bands in a combined fashion. The proposed scheme is equally applicable to both downlink and uplink.

As it is shown in Table 3.2, by adopting sub-carrier and band hopping rate and pattern, we can increase the system throughput in almost all the practical user scenario. By making use of smaller bands, the multiple access capabilities of the system is increased and Multiple Access Interference (MAI) is avoided.

According to the best of our knowledge, this kind of combined sub-carrier and band hopping scheme is not found in any existing literature. Thus, we claim that a new multiple access technique is devised in this chapter which does not alter the basic properties of an OFDMA system without increasing much of the system complexities. The simulations have shown a good tradeoff between complexity and performance compared to other OFDMA scheduling methods.

Conclusion from Simulations

SCBH-OFDMA is an interesting solution to service users with heterogeneous channel conditions under one system architecture. We can conclude the following based on our simulations:

- Static allocation in a wideband fading channel will provide some users with favorable channel conditions and some users with non-favorable channel conditions. For decreasing SINR, the favorable users will have a non-zero throughput due to unfair distribution of resources.

- For random sub-carrier hopping, however, the diversity of the channel is spread in a fairer way, which means that for lower SINR, each user has equally *bad* conditions.

- For increasing SINR, random sub-carrier hopping provides a better channel for all users while static allocation lags slightly behind. It is to be noted that the frequency diversity to be provided by random hopping is somewhat limited due to fact that a user is only allowed to hop inside the bandwidth size of B.

- SCBH-OFDMA is a combination of sub-carrier hopping and band-wise allocation, which we have shown to be superior to random hopping and static allocation based systems. This is due to the additional band hopping that is done in SCBH-OFDMA scheme.

© Muhammad Imadur Rahman, 2007

- However, the SINR distribution in a system simulation scenario can be very wide, which makes the interpretation of results problematic.

Future outlook

Related to the analysis that we have performed in this chapter, we can perform a number of interesting issues in future:

Adaptive SCBH-OFDMA system: We can design an adaptive SCBH-OFDMA system, where the size of FFT bandwidth and OFDM symbol duration can be adapted in real-time based on user groups' mobility (i.e. Doppler) and delay spread. In this way, cell throughput can be optimized and optimum time-frequency resource allocation can be realized.

Link adaptation: Fast power adaptation and slow rate adaptation can be studied for SCBH-OFDMA system.

Multi-antenna techniques: Another way of increasing the system performance is to include spatial diversity to increase the link performances. Also, MIMO mode selection for different user groups can be implemented.

4

System Design Issues for SCBH-OFDMA Scheme

In Chapter 3, we have described our proposed SCBH-OFDMA channelization scheme. We have presented a system level evaluation of the proposed scheme in the previous chapter also.

In this chapter, different aspects of system design are discussed between Section 4.1 to Section 4.6, i.e. transceiver architecture, frame format, pilot sequences, preamble design, grouping, coordination of band hopping and complexity. A specific attention is given to hopping sequence design for SCBH-OFDMA in Section 4.7.

4.1 Transceiver Structure

Primarily, the MS transceiver architecture is not drastically different from any other OFDMA systems, at least the digital part. The RF front end must be able to follow the band-hopping pattern with sufficient speed and accuracy. The BS will need to have G distinct transceivers, including both the RF and digital part. A simple transceiver architecture DL is shown in Figures 4.1 and 4.2.

For the DL Transmitter (Figure 4.1), the BS has G parallel transmitters, one for each group of users. The data from each user is encoded, modulated and subsequently serial-to-parallel converted. The resulting signal blocks are then assigned to different sub-channels according to the SCH control block. The data is then parallel-to-serial converted and a CP is added. In the RF part of the transmitter, the carrier frequency is hopped according to the BH control.

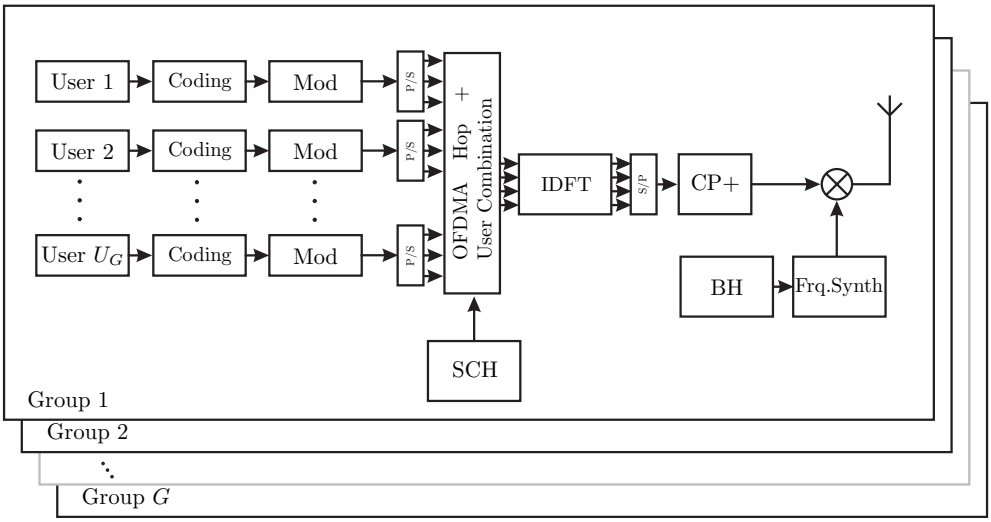

Figure 4.1: Downlink Transmitter.

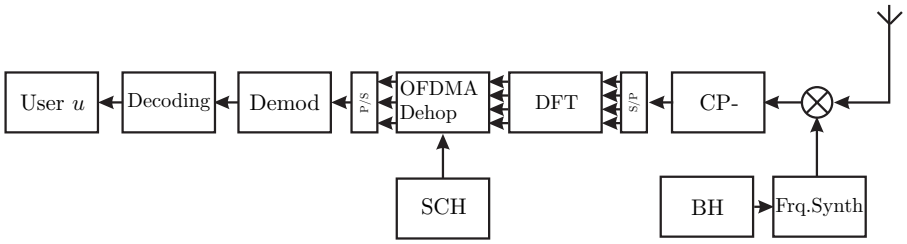

Figure 4.2: Downlink Receiver.

The DL receiver (Figure 4.2) is only interested in the signal from one user. The BH control block in the receiver side must be synchronized with the corresponding block in the transmitter side in order to downconvert the correct band. After CP removal, the signal is serial-to-parallel converted and FFT transformed. The OFDM Dehopping block then picks out the correct sub-carriers according to the SCH control block, which must also be synchronized with the corresponding block on the transmitter side. The selected (dehopped) sub-carriers are then parallel-to-serial converted, demodulated and decoded, yielding the user data.

4.2 Frame Format

We denote the basic time-frequency resource a *unit resource*, which is one sub-channel bandwidth for one OFDM symbol duration, T_s. One sub-channel bandwidth is denoted as, $\Delta f_{sch} = \alpha \times \Delta f$, where α is the number of contiguous sub-carriers that create a sub-channel. A *time-frequency frame* is defined as one system bandwidth, B (or FFT bandwidth) for k number of OFDM symbols. Fast band hopping is performed when the carrier frequency of any user is changed after every *time-frequency frame*, where as slow band hopping is performed when carrier frequency is changed after a number of *time-frequency frames*. This is decided due to the fact that the transmitter and receiver oscillators will take some time to settle down once the carrier frequency is changed. It is also noted

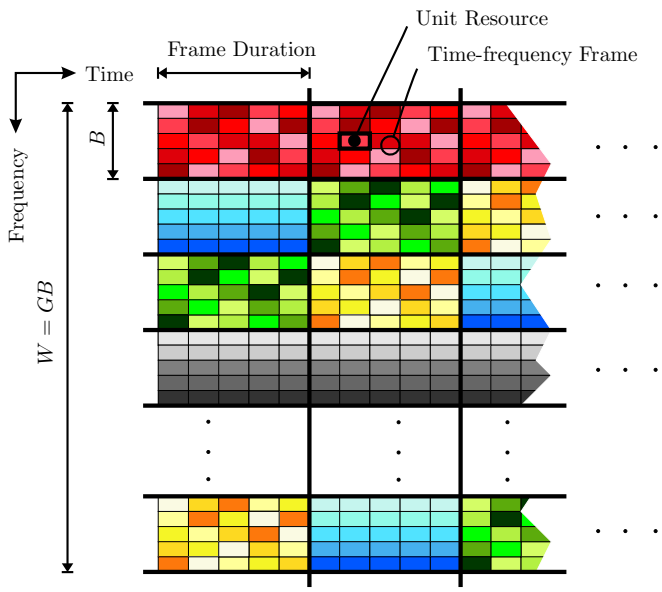

Figure 4.3: DL user data channel format for SCBH-OFDMA.

that frame duration must be much smaller than coherence time, i.e. $T_f \ll T_c$.

DL channels are as follows:

1. **Common control channel:** Used for broadcasting cell related information.
2. **DL pilot channel:** BS sends pilots at this channel for different synchronization purposes and partly for coarse channel estimation purposes.
3. **DL user data channel:** User data is transmitted via this channel.
4. **Resource assignment channel:** BS uses this channel to assign time and frequency resources to the users.

The organization of DL user data channel is shown in Figure 4.3. Different kinds of sub-carrier and band hopping are emphasized in the figure.

4.3 Pilot Sequence

We consider the case of non-contiguous sub-channel configuration in DL. In non-contiguous configuration, the sub-carriers that creates a single sub-channel are located sparsely in frequency dimension (i.e. sparsely located on the sub-carriers). The opposite is true for contiguous sub-channel configuration. Based on the B_c of the group, the number of pilot sub-carriers can be determined and they can be located accordingly. One pilot sub-carrier per B_c is sufficient for efficient system performance. Thus, total number of pilot sub-carriers for any particular group will be, $\frac{B}{B_c}$.

Pilots are spread in frequency domain, i.e, some pre-located sub-carriers are used for pilot transmission. In addition to this in UL, two pilot symbols are also placed in time domain (two

© Muhammad Imadur Rahman, 2007

OFDM symbol per time-frequency frame). The 1st and 9th OFDM symbols of all frames are reserved for pilot symbols. These two pilot symbols are used for frequency synchronization and additional channel estimation purposes.

In DL, all pilots are shared by all users, thus the number of pilots can be kept same in contiguous and non-contiguous sub-channel configuration. This cannot be assured in UL. This is only one possibility indeed, there can be other choices depending on other considerations as well.

4.4 Estimation of Coherence Bandwidth and Time

Using frequency domain pilots, the channel frequency response is estimated, by using Least Squares (LS) channel estimation methods followed with Minimum Mean Square Error (MMSE) criterion [93]. Then IFFT is used to determine the channel impulse response. The estimated CIR is used to find RMS delay spread. This RMS delay spread value is used to determine the coherence bandwidth.

We have not studied any specific methods for measuring coherence time. In our evaluations in Chapter 3 (Section 3.4), we have assigned a velocity to each user and use that velocity to determine the coherence time.

4.5 Grouping procedure

Although the grouping algorithms are conceptually simple, the system must determine which user has high or low coherence time and coherence bandwidth. In the downlink, channel measurements are carried out in the terminals, which means that some feedback is required.

Although this might seem like the problem is identical to DSA, where the CSI is regularly fed back to the base station, the signaling can be reduced to the four channel states (high/low coherence time, high/low coherence bandwidth). This assumes that the mobile terminals are capable of reducing channel estimate information to the four channel states before transmitting. Alternatively, the mobile terminal could transmit the estimated T_c and B_c, giving the BS more information to base the grouping on.

The basic grouping procedure can be designed as follows:

1. After the MS logs into the system, it will use Random Access Channel (RACH) to inform the BS its bandwidth requirement.

2. At the beginning, BS assigns the MS into a FSCH-FBH group.

3. At this phase, MS estimates DL channel characteristics, such as coherence time (T_c) and coherence bandwidth (B_c) etc, by using the pre-amble signals in broadcast channel.

4. Once the channel coherence estimates are ready, the MS sends these information to BS via the control channel.

5. With the information of T_c, B_c, and considering the bandwidth request with available resources, the BS decides on the correct group for the user.

Coherence time and bandwidth may e.g. be found using autocorrelation estimates on the channel transfer function (in both time and frequency). In our evaluations in Section 3.4, we have performed the grouping based on ideal channel statistics. The above grouping procedure is left for future system design.

4.6 System Complexity

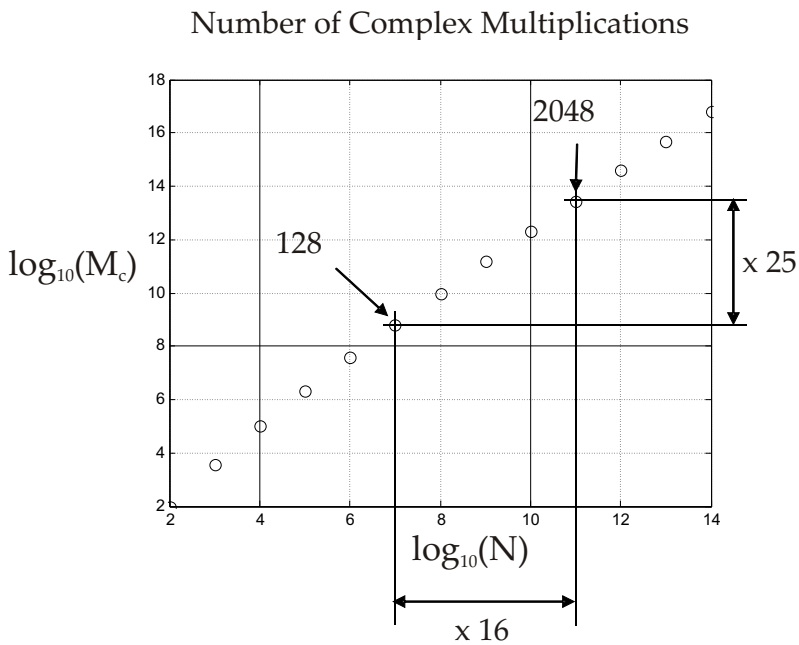

Figure 4.4: FFT complexity versus FFT size.

The hardware requirements for SCBH-OFDMA are similar to those of Orthogonal Frequency Division Multiplexing - Code Division Multiple Access - Slow Frequency Hopping (OFDM-CDMA-SFH) [52]. Sub-carrier hopping is performed in the digital domain by changing the OFDMA sub-carrier selection on a regular basis. Band hopping, on the other hand, places certain requirements on the RF hardware, as the frequency hopping must be performed using an agile frequency synthesizer that must provide adequate frequency stability and accuracy to ensure stable OFDM demodulation of the signal.

It is well known that OFDM receivers require superior frequency stability and phase noise performance compared to single-carrier systems [94], as frequency error causes loss of orthogonality between sub-carriers.

Band hopping may be implemented in two ways:

- Large FFT circuit and fixed oscillator
- Small FFT circuit and fast frequency synthesizer

A large FFT covers the entire system bandwidth, W, i.e. all sub-carriers for all groups ($= N_c \times G$). Each group has access to a contiguous block of N_c sub-carriers. The band hopping is

© Muhammad Imadur Rahman, 2007

then implemented by assigning the fast frequency hopping groups to different blocks in different frames, thus implementing the band hopping digitally.

The advantage of this approach is that it requires only one transmitter chain, and the frequency hopping can be implemented accurately (as it is done in the digital domain). The drawback to this method is that for the UL, the transmitter only utilizes a fraction of the FFT circuit. Furthermore, a single transmitter chain in the DL results in a high PAPR due to a high number of sub-carriers. Thus, we propose to use a single transmitter chain at the BS covering whole available spectrum (i.e. $= N_c \times G \times \Delta f$), while to use only the current band for transmission from MS side. This is possible to implement, as we know that BS can sustain more complexity and more hardware, while MS is required to be as simple as possible.

Using a small FFT, each group requires a separate transmitter at the BS. Here, the band hopping is implemented using frequency hopping synthesizers. For fast frequency hopping, the accuracy of the frequency synthesizer must be sufficiently high and the settling time must be low. PAPR is less of a problem here, as each FFT circuit is small. For the DL, the transmitter will require multiple transmitter chains, and a correspondingly complex combining at the antenna. The DL receiver is only interested in one band, so the only difference here is FFT size and oscillator. For the UL, the transmitter only transmits on one sub-band at a time. The UL receiver must receive multiple groups simultaneously, so multiple receiver chains are needed. For better system performance, some guard band may be required between received bands in the UL.

4.7 Hopping Sequence Design

4.7.1 Facts in Downlink

1. No MAI, i.e. no intra-cell interference is present in DL.

2. As the hopping sequence is decided at the BS, no user collision is expected inside any particular cell area.

3. For full re-use of spectrum, CCI cannot be totally avoided across cells.

4.7.2 Design Goal

The aim is to design a set of orthogonal hopping patterns for SCBH-OFDMA scheme that can be adopted at different BSs to provide an effect of interference averaging. The ultimate goal is to provide a fair distribution of the channel diversity among the users, using a minimum of complexity and system overhead.

4.7.3 Assumptions

1. The two-tier cell structure is shown in Figure 4.5. Knowledge about the cell system design for 1st and 2nd tiers are assumed to be available in operating BS. This knowledge includes, other cell locations, frequency-reuse characteristics, etc.

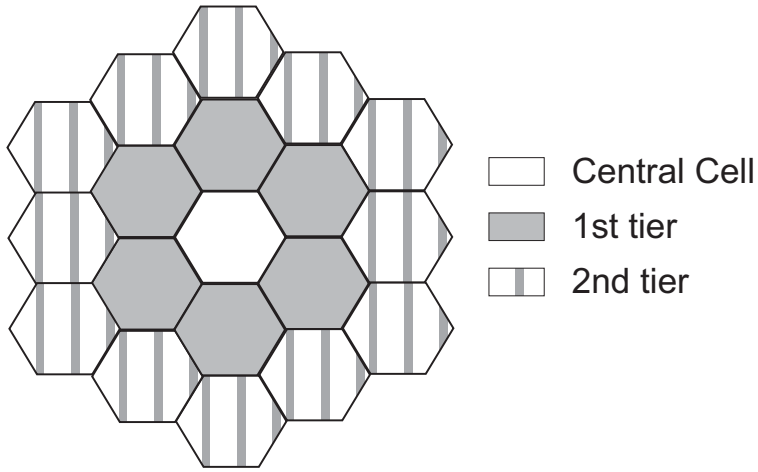

Figure 4.5: Two-tier cellular systems considered in the hopping sequence design.

2. SCH and BH intervals are one OFDM symbol duration and one frame duration respectively. In other words, for FSCH and FBH, a user changes its sub-carrier and band indices in every OFDM symbol and every transmission frame respectively.

3. For SBH and SSCH, the hopping duration is one superframe. A superframe consists of a number of frames, e.g. 16 frames. This is a design parameter. Definitions and relative durations of frame and superframe are shown in Figures 1.1 and 4.3.

4.7.4 Physical Considerations

According to the system design, we propose to perform SCH in digital domain and BH in RF domain, as explained in Sections 4.1 and 4.6. Indeed, it is possible to perform both the sub-carrier and band hopping in digital domain. Our proposal is intended to accommodate users with simpler transceivers (such as smaller bandwidth terminals, smaller FFT capabilities etc). In this way, a wide range of heterogenous terminals in terms of system complexity can be supported. For this hopping arrangements, we need to keep in mind certain physical constraints while designing the hopping sequence:

1. Slow hopping provides less complexity with respect to fast hopping

   (a) For BH, oscillator settling time becomes a consideration while determining BH frequency. Estimated channel coefficients are parameters that are affected by BH duration (or frequency), as lower BH rate means that the estimated channel can potentially be used for more OFDM symbols, provided that the channel does not change much in the BH duration. This is keeping in mind that when a user group moves to another RF band, they need to estimate the channel for new band frequency.

   (b) SCH is done in digital domain, thus, only signaling the hopping pattern is enough for this form of hopping. The hopping span for SCH is one FFT bandwidth. The implementation of this hopping is less critical than BH, as we know all users would at least have

© Muhammad Imadur Rahman, 2007

to have the capability to access the FFT bandwidth, which is defined in Eq.(4.2). FFT bandwidth is also described as band span in Figure D.1.

2. Slow hopping is preferred over fast hopping for economical reasons. Whenever fast hopping provides no benefit, slow hopping is used.

Based on these considerations, we can determine a upper level view of general hopping concepts for SCBH-OFDMA scheme, as shown in Tables 3.1 and 3.2.

4.7.5 Sequence Design Preliminaries

Assume that a SCBH-OFDMA system has N sub-carriers. The total available spectrum, W, is divided onto N_b bands and that each band has N_c sub-carriers:

$$N_c = \frac{N}{N_b} \tag{4.1}$$

Similarly, the band span, B, can be defined as FFT bandwidth on which each MS will perform. It can be written as

$$B = \frac{W}{N_b} \tag{4.2}$$

Figure D.1 explains the definitions related to total available spectrum, band span, sub-channel and sub-carrier bandwidth etc. Let $\mathcal{B}$ be the ordered set of all possible band indices and $\mathcal{S}_b$ the set of allowable sub-carrier indices within band b:

$$\mathcal{B} = \mathbb{N}_{N_b} \tag{4.3}$$

$$\mathcal{S}_b = \{s_{b,1}, s_{b,2}, ..., s_{b,N_c}\} \tag{4.4}$$

where $\mathbb{N}_N$ denotes a set which consists of all integer number between 1 to N. Note that

$$\mathcal{S}_b \subset \mathbb{N}_N \tag{4.5}$$

$$\mathcal{S}_{b_1} \cap \mathcal{S}_{b_2} = \emptyset; \qquad b_1 \neq b_2 \tag{4.6}$$

$$\bigcup_{b=1}^{N_b} \mathcal{S}_b = \mathbb{N}_N \tag{4.7}$$

When $N = 64$, $N_b = 4$, then we have, $N_c = 16$. For this case, $\mathcal{B} = \mathbb{N}_4 = \{1, 2, 3, 4\}$. If we assign 16 contiguous sub-carriers for each band, we can write that $\mathcal{S}_{b_1} = \{1, 2, \ldots, 16\}$, $\mathcal{S}_{b_2} = \{17, 18, \ldots, 32\}$, $\mathcal{S}_{b_3} = \{33, 34, \ldots, 48\}$ and $\mathcal{S}_{b_4} = \{49, 50, \ldots, 64\}$. Arguably, the sub-carrier set assigned to $\mathcal{S}_b$ may not be contiguous depending on system design considerations. Keeping in line with Eq.(4.7), we find that $\bigcup_{b=1}^{N_b} \mathcal{S}_b = \mathcal{S}_{b_1} \cup \mathcal{S}_{b_2} \cup \mathcal{S}_{b_3} \cup \mathcal{S}_{b_4} = \mathbb{N}_{64}$.

As a design principle, we decide on hopset size for SBH groups first and then, we allocate bands for FBH groups. This hopset size is dependant on system design constraints and system operating conditions etc.

4.7.6 Slow Band Hopping (SBH)

We denote, $N_{b,c}$, $N_{sbh,c}$ and $N_{fbh,c}$ as number of total allocated bands, number of SBH band and number of FBH bands allocated to c^{th} cell, respectively. Obviously, $N_{b,c} = N_{sbh,c} + N_{fbh,c}$. For unity re-use factor, $N_{b,c} = N_b,\ \forall c$.

Assume that the user groups in any cell hop between the bands contained in $\mathcal{B}_c \subset \mathcal{B}$. In case of unity re-use factor, $\mathcal{B}_c \equiv \mathcal{B}$. A subset of $\mathcal{B}_c$ is allocated to slow band hopping, denoted as $\mathcal{B}_{c,s} \subset \mathcal{B}_c$.

4.7.6.1 Principles of SBH

We have certain principle in assigning the SBH groups over the neighboring cells:

1. SBH allocations in neighboring cells are kept non-colliding. This is considering the fact that an SBH group remains in a certain band for an entire superframe. If a SBH group in one cell collides with a SBH group in an adjacent cell, users on the adjoining cell boundaries will experience excessive interference for an extended period of time.

2. SBH groups are interleaved with equal spacing across the whole spectrum (i.e. W, as defined in Section 4.7.5) for any particular cell. This will provide enough space for FBH groups to hop across the spectrum, W.

3. At the maximum, only a fraction of bands are allocated to SBH groups per cell. So,

$$N_{sbh,c} = \rho N_{b,c}, \qquad \text{where} \qquad 0 \leq \rho \leq 1 \tag{4.8}$$

   ρ is a system design parameter based on system load, hopping sequence etc. For band allocation process, it is desirable that $\frac{1}{\rho}$ is an integer.

4. When $\rho N_{b,c} > N_{sbh,c}$, i.e. when the number of active SBH groups is less than available SBH bands, then allocation of SBH bands from $\mathcal{B}_{c,s}$ hopset will preferably be interleaved. This means that when a part of SBH bands need to be used out of $\mathcal{B}_{c,s}$ hopset, then we do not take contiguous elements out of $\mathcal{B}_{c,s}$ set, rather we take non-contiguous elements from the set. As we know that $\mathcal{B}_{c,s}$ contains non-contiguous bands, the chosen non-contiguous assignment would make sure that SBH bands are spaced even further across W for any c^{th} cell.

For the current design process, we consider overall frequency re-use of 1. We can constitute an SBH hopping pattern when $\left\lfloor \frac{1}{\rho} \right\rfloor$ neighboring cells can use orthogonal band allocations for SBH bands. We can determine $\left\lfloor \frac{1}{\rho} \right\rfloor$ distinct (i.e. orthogonal) groups of SBH bands out of available N_b bands, such that

$$\mathcal{Q}_i \subset \mathcal{B} \qquad i \in 1, \ldots, \left\lfloor \frac{1}{\rho} \right\rfloor \tag{4.9}$$

where i is the SBH allocation index for a specific cell. Each cell is assigned a single SBH set, $\mathcal{Q}_i$, which contains the bands where SBH groups of that particular cell can hop over. If we assign the

© Muhammad Imadur Rahman, 2007

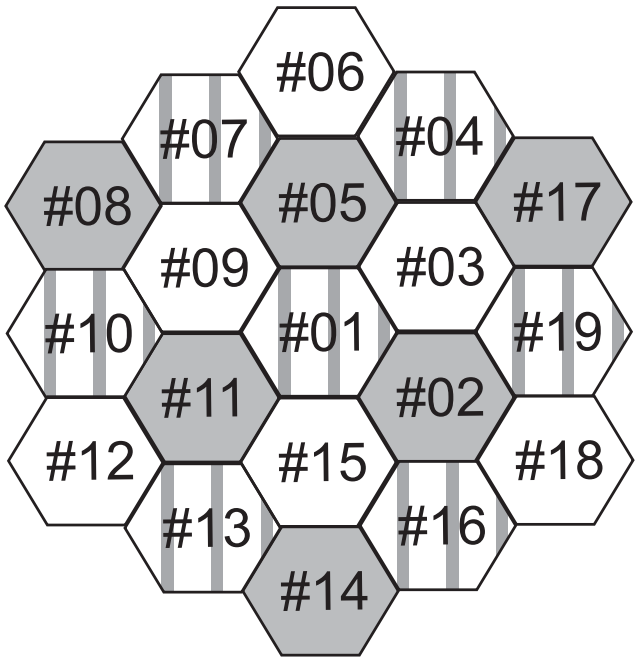

Figure 4.6: Band allocations for SBH groups in a two tier cellular system when $\rho = 0.33$. Cells with blank, stripes and shades are allocated similar set of bands for SBH allocations. Cell numbering and SBH hopset allocation is done according to Eq.(4.10) an Eq.(4.9), respectively.

cell number as c, then we can find the corresponding SBH allocation set assigned to the cth cell as

$$i(c) = ((c-1))_r + 1 \tag{4.10}$$

where $\left\lfloor \frac{1}{\rho} \right\rfloor = r$, and $((c-1))_r = (c-1) \mod r$.

4.7.6.2 Example of SBH Hopset Allocation across Cells

For example, when $\left\lfloor \frac{1}{\rho} \right\rfloor = 3$, then no collision will happen in SBH bands from another SBH band in the 1st tier. Figure 4.6 shows the SBH allocations when $\left\lfloor \frac{1}{\rho} \right\rfloor = 3$ in 19-cell based 1st and 2nd tier of a cellular system. The cell numbers are identified by using Eq.(4.10). Notice that the design parameter ρ in this specific SBH allocations gives us a constraint in the maximum number bands to be used for SBH groups according to Eq.(4.8). $\lfloor \rho N_b \rfloor$ bands per sets can be arranged in r sets, and can be allocated in neighboring cells, similar to the example in Figure 4.6.

If $N_b = 15$, then $\lfloor \rho N_b \rfloor = 5$ and we can write that $\mathcal{Q}_1 = \{1, 4, 7, 10, 13\}$, $\mathcal{Q}_2 = \{2, 5, 8, 11, 14\}$ and $\mathcal{Q}_3 = \{3, 6, 9, 12, 15\}$. One possible SBH hopset assignment option can be as follows. Based on Figure 4.6, all the cells with shaded color can be assigned with $\mathcal{Q}_1$ set, while cells with stripes and white color may get the sets $\mathcal{Q}_2$ and $\mathcal{Q}_3$, respectively. To be more specific, for the 5th cell, $\mathcal{Q}_1 = \{1, 4, 7, 10, 13\}$ bands are available for the SBH groups. Note that $\mathcal{B} \backslash \mathcal{Q}_1 = \{2, 3, 5, 6, 8, 9, 11, 12, 14, 15\} = \mathcal{Q}_2 \cup \mathcal{Q}_3$ are available for FBH groups in the same cell. Thus, an overall frequency reuse of 1 is assured for all cells.

4.7.6.3 Allocation of SBH Bands to User Groups

The SBH hopset for cell c, $\mathcal{B}_{c,s}$, is used to determine a hopping pattern by (pseudo-)randomly permuting the indices in $\mathcal{B}_{c,s}$:

$$\mathcal{H}_c = \mathbb{P}(\mathcal{B}_{c,s}) \tag{4.11}$$

where $\mathbb{P}(\mathcal{X})$ defines any kind of permutation of set $\mathcal{X}$. This hopset is updated (i.e. this permutation is performed) once every superframe. Each cell can act independently in deciding the allocation procedure. Some possibilities can be as follows:

1. The SBH bands can be allocated in a static manner for consecutive superframes. This is advantageous is a sense that the SBH groups do not need to re-synchronize to new band frequency. On the other hand, this may also increase CCI seen at the other cell for sustained period of time in some certain cases.

2. Simple PN sequences can be used for updating the SBH allocation in each cell.

3. Another alternative can be, simple band rolling across the hopset $\mathcal{B}_{c,s}$. If we denote a band index allocated to any SBH group at time t as X_t, we can write that

$$X_{t+1} = ((X_t + a))_{N_{sbh,c}} \tag{4.12}$$

with a constraint that $GCD(a, N_{sbh,c}) = 1$.

It is worth mentioning here that re-allocation of SBH hopset across superframes may not be very critical in terms of system outage performance.

4.7.7 Fast Band Hopping (FBH)

We denote the hopset for FBH groups in cell c as $\mathcal{B}_{c,f} \subset \mathcal{B}_c$. Relating to Eq.(4.8), it can be written that $\|\mathcal{B}_{c,f}\| = \lfloor (1-\rho)N_b \rfloor$, where $\|\mathcal{B}_{c,f}\|$ is the cardinality of hopset $\mathcal{B}_{c,f}$. All FBH groups can hop across $\mathcal{B}_{c,f}$ set using any orthogonal hopping sequence, such as Latin squares [95]. The hopping procedure is explained in Section 4.7.9.1.

4.7.7.1 FBH with Fixed Hopset

Based on system design procedure, it can be decided that $\|\mathcal{B}_{c,f}\|$ and $\|\mathcal{B}_{c,s}\|$ are constant. So, for all the system operation time, the available bands for FBH groups is constant for all the cells in the system area. Thus, the bands that are available for FBH in any particular cell are denoted as:

$$\mathcal{B}_{c,f} = \mathcal{B}_c \backslash \mathcal{B}_{c,s} = \bigcup_{\substack{q=1 \\ q \neq i(c)}}^{r} \mathcal{Q}_q \tag{4.13}$$

Here, $\mathcal{B}_{c,s} = \mathcal{Q}_{i(c)}$. At this stage, two situations can occur:

© Muhammad Imadur Rahman, 2007

$N_{fbh,c} \leq \lfloor (1-\rho)N_b \rfloor$: In this case, the required number of bands for FBH operation (i.e. number of active FBH groups in another words) is smaller than stipulated number of bands for FBH. Obviously, this is a trivial case, when FBH is performed only on a subset of $\mathcal{B}_{c,f}$ and all FBH groups are served.

$N_{fbh,c} > \lfloor (1-\rho)N_b \rfloor$: As we have mentioned earlier that this mode assumes a fixed amount of bands for SBH and FBH operations. Thus, even though all SBH bands are not used, we cannot serve $N_{fbh,c} - \lfloor (1-\rho)N_b \rfloor$ number of FBH groups.

Referring to the example explained in Section 4.7.6.2, the FBH hopset for 5th cell, $\mathcal{B}_{5,f}$ will be $\mathcal{Q}_2 \cup \mathcal{Q}_3$. Here, $\|\mathcal{B}_{5,f}\| = 10$. So only 10 FBH groups can be supported in each transmission frame.

It is clear that fixed amount of hopset makes it easier for system management, though it may not be an optimum solution in terms of spectrum usage and throughput. This is true when system load is high, i.e. when system is operating on closer to full load.

4.7.7.2 FBH with Adaptive Hopset

In Eq.(4.13), we do not consider the unused SBH bands in the cth cell. When we consider the unused SBH bands for using in FBH mode, we can say that we have an adaptive hopset for FBH in real-time. This gives more freedom for FBH, while it requires more complex system management from BS point of view. We can express the FBH hopset as the following:

$$\mathcal{B}_{c,f} = \mathcal{B}_c \backslash \mathcal{B}_{c,s} = \bigcup_{\substack{q=1 \\ q \neq i(c)}}^{r} \mathcal{Q}_q \bigcup \{\mathcal{B}_{c,s} \backslash \mathcal{B}_{c,s}^{(u)}\} \tag{4.14}$$

where $\mathcal{B}_{c,s}^{(u)} \subset \mathcal{B}_{c,s}$ is the set that contains a list of used bands for SBH operations. In this arrangement, now we again can have two situations:

$\mathcal{B}_{c,s}^{(u)} \equiv \mathcal{B}_{c,s}$: When all the SBH bands are used by SBH groups, then this occurs. This means that $\{\mathcal{B}_{c,s} \backslash \mathcal{B}_{c,s}^{(u)}\} = \emptyset$. Thus, Eq.(4.14) becomes equivalent to Eq.(4.13). So, both the situations explained in Section 4.7.7.1 apply for this case.

$\mathcal{B}_{c,s}^{(u)} \not\equiv \mathcal{B}_{c,s}$: When number of active SBH groups are smaller than $\|\mathcal{B}_{c,s}\|$, then this situation occurs. Now, $\{\mathcal{B}_{c,s} \backslash \mathcal{B}_{c,s}^{(u)}\} \neq \emptyset$, and we can support $\|\mathcal{B}_{c,s} \backslash \mathcal{B}_{c,s}^{(u)}\| + N_{fbh,c}$ number of FBH groups. We can write that $\mathcal{B}_{c,s}^{(u)} \equiv \mathcal{B}_{c,s}^{(u)}(t)$, so $N_{fbh,c} \equiv N_{fbh,c}(t)$ when the hopset for FBH is changed adaptively. This setup requires slightly more complex hopping arrangements, while a better spectrum usage is achieved.

A simple implementation of adaptive hopset for FBH can be realized as follows. For every superframe, we can send a $\lfloor \rho N_b \rfloor$ bits control information, which will indicate the SBH bands of any certain c^{th} cell that are currently being used for SBH groups. When this message is received at the MS from the BS control channel, the MS can figure out the additional bands for FBH in addition to $\mathcal{B}_{c,f}$. As an example, only 5 bits of control information can convey the message about $\mathcal{B}_{c,s} \backslash \mathcal{B}_{c,s}^{(u)}$ to all MSs when $\rho = 0.33$ and $N_b = 15$.

When Latin Square based orthogonal patterns are used for FBH groups, then realizing FBH with adaptive hopset may become a complicated process, due to constraints related to square size, frame size and number of neighboring cells etc [95]. In this situation, we propose to use the unused SBH bands in a non-orthogonal fashion, that means, we secure service for $\|\mathcal{B}_{c,s} \backslash \mathcal{B}_{c,s}^{(u)}\|$ number of FBH groups, but we cannot assure the interference averaging benefit for these groups. In this way, we are destroying the orthogonality of the hopping mechanism, but assuring the service availability of those groups.

4.7.8 Sub-Carrier Hopping (SCH)

SCH is performed in the digital domain, thus, it is much simpler to implement compared to BH. SCH is performed in one particular band of any cell. A band is defined in Eq.(4.2). So in designing sequence for SCH, we intentionally omit the cell notation from the description. As shown in Eq.(4.4), the SCH hopset for any b^{th} band is denoted as $\mathcal{S}_b$ and $\|\mathcal{S}_b\| = N_c$.

4.7.8.1 Fast Sub-Carrier Hopping (FSCH)

The hop duration for FSCH is one OFDM symbol. That means, a particular user occupies different sub-carriers at neighboring OFDM symbol, when the user belongs to an FSCH group. Latin square based orthogonal patterns can be used for this purpose [95].

The same orthogonal Latin square pattern is assigned to all FSCH groups in one cell. This means that different users in same cell will follow same sub-carrier hopping pattern, but will be separated by different band locations. This will ensure that when a certain FSCH group collides with any other group in neighboring cell, each user suffers collisions from an ensemble of users occupying same band in neighboring cell, rather than with one dominant interferer.

4.7.8.2 Slow Sub-Carrier Hopping (SSCH)

All users in an SSCH group are assigned a sub-carrier index at the beginning of every superframe. Throughout the transmission of the superframe, these users will maintain the same sub-carrier indices. Depending on whether they are assigned to an SBH or FBH group, their band indices will change.

1. If any user is assigned to an SBH group, then the sub-carrier and band indices will remain constant for whole superframe.

2. If any user belongs to any FBH group, then the sub-carrier indices will be unchanged for whole frame, but the band indices will change at every frame according to the hopping sequence explained in Section 4.7.7.

Similar to SBH in Section 4.7.6, we have several options for changing the sub-carrier allocation of SSCH users in neighboring superframes:

1. The sub-carriers can be allocated to the users statically to the users.

2. PN sequences can be used for indicating the changes of the allocation across superframes.

© Muhammad Imadur Rahman, 2007

3. Simple sub-carrier rolling can be used, similar to band rolling process shown in (4.12).

4.7.9 Implementation of Hopping Mechanism

4.7.9.1 Latin Square based Hopping

It is possible to obtain an orthogonal construction of sub-carrier and band hopping sequences for a matrix size corresponding to a prime number or a power of prime. Here, we consider this technique for FSCH and FBH operations. For FSCH, a Latin square of size N_c would be appropriate, while a Latin square of size $\|\mathcal{B}_{c,f}\|$ is required for FBH. Obtaining the required size for FSCH is fairly straight forward, while it is slightly tricky for FBH case, because it depends on a number of issues, such as:

1. The number of bands available for FBH, $N_{fbh,c}$;
2. The number of frames in a superframe;
3. the number of unused SBH bands in case of FBH with adaptive hopset as described in Section 4.7.7.2, etc.

In following discussions, the methods to obtain Latin Squares for each class of sizes (i.e. prime and power of primes) are described. The available sizes of matrices, for which Latin Squares can be constructed are listed as follows:

$$\begin{array}{cccccccccccc} 2 & 3 & 4 & 5 & 7 & 8 & 9 & 11 & 13 & 16 & 17 & 19 \\ 25 & 27 & 29 & 31 & 32 & \ldots & & & & & & \end{array}$$

Once a $n \times n$ Latin Square matrix is constructed, one can obtain $n-1$ mutually orthogonal matrices. According to [95] and [96] herein, two Latin squares are orthogonal to each other if n^2 ordered pairs (x, y), where x and y are the entries from the same position in the respective squares, exhaust n^2 possibilities, i.e. every ordered pair occurs exactly once. This property can be used to ensure that there is exactly only one frequency collision between two users in neighboring cells. This ensures that the effect of a strong interferer is shared among all users.

Prime Numbers: The Latin Squares are easily obtained, when the size of the square is a prime number. In that case, the matrix is obtained by simply rolling the sequence of numbers of the first row (or column) in subsequent row (or column), as shown in Table 4.1. We define the matrix, $\{a\}$, of size $n \times n$, using the following equation [95]:

$$\{a\}_{i,j} \equiv ((ai + j))_n \ , \quad a = 1, ..., n-1 \tag{4.15}$$

Table 4.1 shows a Latin square of order 5. If this is matrix $\{1\}$, then we can make specific permutations of rows (or columns) and obtain the other $n-2$ orthogonal matrices. We can see other orthogonal Latin squares of order 5 in Tables 4.2, 4.3 and 4.4.

Each of the orthogonal matrices can be assigned to a different cell, ensuring interference averaging among users in neighboring cells. Using Tables 4.1-4.4, we can explain the interference

0	1	2	3	4
1	2	3	4	0
2	3	4	0	1
3	4	0	1	2
4	0	1	2	3

Table 4.1: Construction of order 5, matrix $\{1\}$

0	1	2	3	4
2	3	4	0	1
4	0	1	2	3
1	2	3	4	0
3	4	0	1	2

Table 4.2: Matrix $\{2\}$ of order 5

0	1	2	3	4
3	4	0	1	2
1	2	3	4	0
4	0	1	2	3
2	3	4	0	1

Table 4.3: Matrix $\{3\}$ of order 5

0	1	2	3	4
4	0	1	2	3
3	4	0	1	2
2	3	4	0	1
1	2	3	4	0

Table 4.4: Matrix $\{4\}$ of order 5

averaging in a simple way. Matrices $\{1\}$-$\{4\}$ can be assigned to 4 neighboring cells with 4 users in each cell. Suppose, rows indicate the sub-carriers and columns indicates OFDM symbols. User-0 in cell-1 occupies sub-carriers [0,4,3,2,1] at consecutive OFDM symbols. In cell-2, user-3 is assigned sub-carriers set of [4,1,3,0,2]. We can see that these two users in two different cells collide with each other only in the 3rd OFDM symbol out of the five symbols. This is true for any user pairs in any two cell pairs. This means, the presence of any strong CCI is shared among users in all cells.

Power of Prime Numbers: It is also possible to obtain orthogonal matrices for sizes that are powers of prime numbers. One needs to employ Finite Field theory to do so. The study of algorithms to obtain the hopping sequence that implements Finite Field theory will be detailed here for two cases, $n = 4$ and $n = 8$ in GF(2).

For a size of $n = p^m$, the polynomial representation of this field, GF(p^m), has coefficients in the field of the prime p, GF(p).

Example of order 4 in GF(2): For order 4, the elements of this field are the roots of $f(x) = x^2 + x + 1 \in GF(2)$. The roots, α, are $\alpha^0 = 1$, $\alpha^0 = \alpha$, and $\alpha^2 = \alpha + 1$. To construct the matrix, we can use the additive operation, as depicted in Table 4.5 [97]. In Table 4.6, an example of Latin square from GF(2) is given for time/frequency indexes $\{0, \ldots, 3\}$, i.e. the order of the matrix is 4. In a similar fashion for prime numbers, the corresponding orthogonal matrices related to matrix $\{1\}$ (i.e. the matrix in Table 4.6) can be obtained.

$+$	0	1	α	$\alpha+1$
0	0	1	α	$\alpha+1$
1	1	0	$\alpha+1$	α
α	α	$\alpha+1$	0	1
$\alpha+1$	$\alpha+1$	α	1	0

Table 4.5: General construction of order 4 matrix in GF(2)

Example of order 8 in GF(2): For order 8, the elements of this field are the roots of $f(x) = x^3 + x + 1 \in GF(2)$. The roots, α, are $\alpha^0 = 1$, $\alpha^0 = \alpha$, $\alpha^2 = \alpha^2$, $\alpha^3 = \alpha + 1$, $\alpha^4 = \alpha^2 + \alpha$, $\alpha^5 = \alpha^2 + \alpha + 1$,

© Muhammad Imadur Rahman, 2007

0	1	2	3
1	0	3	2
2	3	1	0
3	2	0	1

Table 4.6: Construction of matrix $\{1\}$ of order 4 in GF(2)

0	1	2	3	4	5	6	7
1	0	4	7	2	6	5	3
2	4	0	5	1	3	7	6
3	7	5	0	6	2	4	1
4	2	1	6	0	7	3	5
5	6	3	2	7	0	1	4
6	5	7	4	3	1	0	2
7	3	6	1	5	4	2	0

Table 4.7: Construction of matrix $\{1\}$ of order 8

$\alpha^6 = \alpha^2 + 1$ [97]. To construct the matrix, we can use the additive operation similar to order 4 case. This is shown in Table 4.8. This general construction formula can be used to obtain matrix $\{1\}$ of order 8 as explained in Table 4.7.

As described earlier, we can obtain 7 orthogonal matrices of order 8 in GF(2). This is a good number in a sense that, there are 7 cells in the first tier of the network. Tables 4.9-4.14 lists the remaining orthogonal Latin squares for order 8. These 7 orthogonal matrices can be assigned to 7 neighboring cells. In this note, it is understood that if we require interference averaging across 1st and 2nd tier, we need to use Latin squares of order 25 or higher, as described in Section 4.7.9.1.

4.7.9.2 Pseudo-Random Sequence based Hopping

A frequency hopping sequence guaranteeing no collisions within the cell can be generated using a Pseudo-Random Number Generator (PRNG). For other cells, hopping sequences are generated in a similar manner. Provided that the correlation between the PRNG outputs of different cells is sufficiently low, this approach easily handles dynamic hopsets, and has interference averaging properties.

Overview: For cell c, an ordered list, $\mathcal{L}_c$, is used for keep track of hopping, either subcarrier or band. The list contains N_L elements. Let $\mathcal{L}_c^{(k)}$ denote the k'th iteration of the list. The first element in the list, $l_1^{(k)}$ is the index belonging to the first group for the duration of iteration k, the second element belongs to the second group, etc. There are N_g groups active at any one time, where $N_g \leq N_L$.

The next iteration in the list must is generated by a pseudo-random permutation of the current list. By transmitting the list to the mobile terminals, along with the state of the PRNG, the permutation sequence may be generated locally at the mobile side, using an identical PRNG. An overview of the hopping generation is shown in Figure 4.7.

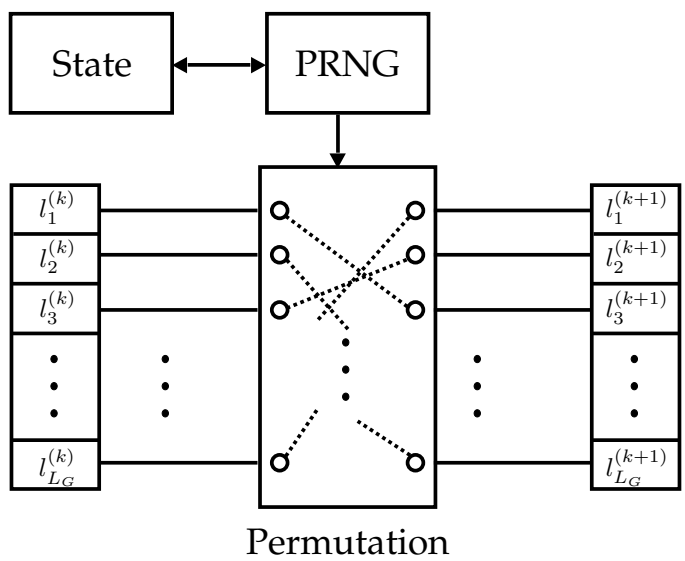

Figure 4.7: PRNG hopping

Permutation Algorithm: The permutation of the list can be generated with a simple algorithm [98].

$$\left.\begin{array}{l} l_i^{(k)} \longleftrightarrow l_{r_{i,N_L}}^{(k)} \\ l_i^{(k+1)} \longleftarrow l_i^{(k)} \end{array}\right\} \text{ for } 1 \leq i \leq N_G - 1 \tag{4.16}$$

where r_{i,N_L} is a uniformly distributed, (pseudo-)randomly generated integer between i and N_L. The algorithm runs through the list, starting with the first element, and swaps that element with a

© Muhammad Imadur Rahman, 2007

$+$	0	1	α	α^2	$\alpha+1$	$\alpha^2+\alpha$	$\alpha^2+\alpha+1$	α^2+1
0	0	1	α	α^2	$\alpha+1$	$\alpha^2+\alpha$	$\alpha^2+\alpha+1$	α^2+1
1	1	0	$\alpha+1$	α^2+1	α	$\alpha^2+\alpha+1$	$\alpha^2+\alpha$	α^2
α	α	$\alpha+1$	0	$\alpha^2+\alpha$	1	α^2	α^2+1	$\alpha^2+\alpha+1$
α^2	α^2	α^2+1	$\alpha^2+\alpha$	0	$\alpha^2+\alpha+1$	α	$\alpha+1$	1
$\alpha+1$	$\alpha+1$	α	1	$\alpha^2+\alpha+1$	0	α^2+1	α^2	$\alpha^2+\alpha$
$\alpha^2+\alpha$	$\alpha^2+\alpha$	$\alpha^2+\alpha+1$	α^2	α	α^2+1	0	1	$\alpha+1$
$\alpha^2+\alpha+1$	$\alpha^2+\alpha+1$	$\alpha^2+\alpha$	α^2+1	$\alpha+1$	α^2	1	0	α
α^2+1	α^2+1	α^2	$\alpha^2+\alpha+1$	1	$\alpha^2+\alpha$	$\alpha+1$	α	0

Table 4.8: General Construction of order 8 matrix in GF(2)

0	1	2	3	4	5	6	7
2	4	0	5	1	3	7	6
3	7	5	0	6	2	4	1
4	2	1	6	0	7	3	5
5	6	3	2	7	0	1	4
6	5	7	4	3	1	0	2
7	3	6	1	5	4	2	0
1	0	4	7	2	6	5	3

Table 4.9: Matrix $\{2\}$ of order 8 in GF(2)

0	1	2	3	4	5	6	7
3	7	5	0	6	2	4	1
4	2	1	6	0	7	3	5
5	6	3	2	7	0	1	4
6	5	7	4	3	1	0	2
7	3	6	1	5	4	2	0
1	0	4	7	2	6	5	3
2	4	0	5	1	3	7	6

Table 4.10: Matrix $\{3\}$ of order 8 in GF(2)

0	1	2	3	4	5	6	7
4	2	1	6	0	7	3	5
5	6	3	2	7	0	1	4
6	5	7	4	3	1	0	2
7	3	6	1	5	4	2	0
1	0	4	7	2	6	5	3
2	4	0	5	1	3	7	6
3	7	5	0	6	2	4	1

Table 4.11: Matrix $\{4\}$ of order 8 in GF(2)

0	1	2	3	4	5	6	7
5	6	3	2	7	0	1	4
6	5	7	4	3	1	0	2
7	3	6	1	5	4	2	0
1	0	4	7	2	6	5	3
2	4	0	5	1	3	7	6
3	7	5	0	6	2	4	1
4	2	1	6	0	7	3	5

Table 4.12: Matrix $\{5\}$ of order 8 in GF(2)

0	1	2	3	4	5	6	7
6	5	7	4	3	1	0	2
7	3	6	1	5	4	2	0
1	0	4	7	2	6	5	3
2	4	0	5	1	3	7	6
3	7	5	0	6	2	4	1
4	2	1	6	0	7	3	5
5	6	3	2	7	0	1	4

Table 4.13: Matrix $\{6\}$ of order 8 in GF(2)

0	1	2	3	4	5	6	7
7	3	6	1	5	4	2	0
1	0	4	7	2	6	5	3
2	4	0	5	1	3	7	6
3	7	5	0	6	2	4	1
4	2	1	6	0	7	3	5
5	6	3	2	7	0	1	4
6	5	7	4	3	1	0	2

Table 4.14: Matrix $\{7\}$ of order 8 in GF(2)

© Muhammad Imadur Rahman, 2007

random element in the list. The second element is swapped with a random element chosen from any but the (current) first element, the third element is swapped with any element except the first two, etc. In this way, the list is permuted in a random manner. If the sequence of random number is known, the reconstruction of the permutation is trivial.

Pseudo-Random Number Generator: Numerous methods for generating pseudo-random numbers have been developed, for many different purposes (e.g. cryptography, spread-spectrum, simulations, etc.). For this application, the PRNG is only required to generate random integers over a relatively narrow span. It is important that different cells may use the same PRNG to generate different or shifted sequences of uncorrelated random numbers, in order to avoid repeating collisions between the same groups in different cells.

The approach used in generating a pseudo-random integer in a given span is this:

1. Generate a unit uniformly distributed random number, $x[i] \in [0, 1)$.
2. Transform $x[i]$ onto $[a, a+1, ..., b]$ using

$$y[i] = a + \lfloor (b - a + 1)x[i] \rfloor \tag{4.17}$$

where it may easily be verified that $y[i]$ is uniformly distributed over the desired span. As stated earlier, the generation of x may be done in a number of ways. One example of a simple PRNG can be to employ a binary shift-register along with a linear feedback circuit (Linear Feedback Shift Register (LFSR)). The feedback consists of a number of XOR circuits, which calculate the modulo-2 sum of certain elements in the shift-register. The indices of these values are determined on the basis of a so-called "Generator Polynomial" For a LFSR, of length L_s, the value of the k'th bit is found using:

$$s_{k+1} = \bigoplus_{i=0}^{L_s} a_i s_{k-i}; \qquad a_{L_s} = 1 \tag{4.18}$$

where the a_i are the coefficients of the generator polynomial. Certain polynomials provide the maximum possible period of the sequence, $2^{L_s} - 1$. The resulting sequences are called Maximum Length sequences.

By generating β bits at a time, and subsequently transforming them to a unit uniformly distributed pseudo-random number, denoted $\hat{x}[i]$, can be generated:

$$\hat{x}[i] = 2^{-\beta} \sum_{b=0}^{\beta-1} 2^{s_{i\beta+b}} \tag{4.19}$$

This sequence can then be used in place of $x[i]$ in Step 1 of the permutation algorithm. For a given cell, this method may be used to generate band-hopping and subcarrier hopping sequences (albeit with two different PRNGs). For the mobiles in that cell, it is sufficient to transmit the L_s bits giving the state of the shift-register, and to indicate which generator polynomial is being used. As there are only a few polynomials out of the possible 2^{L_s-1} that generate maximum-length sequences, the

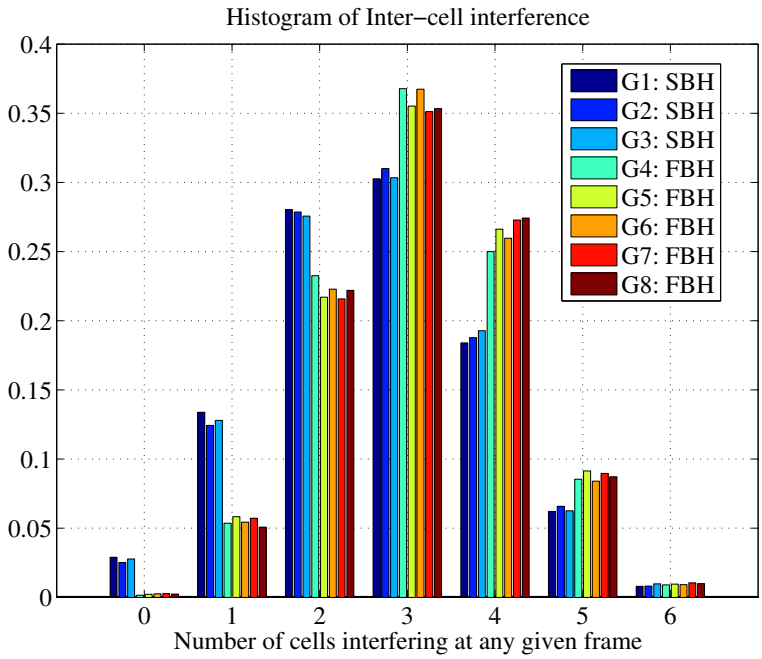

Figure 4.8: Number of interfering cells colliding with a group at a given time.

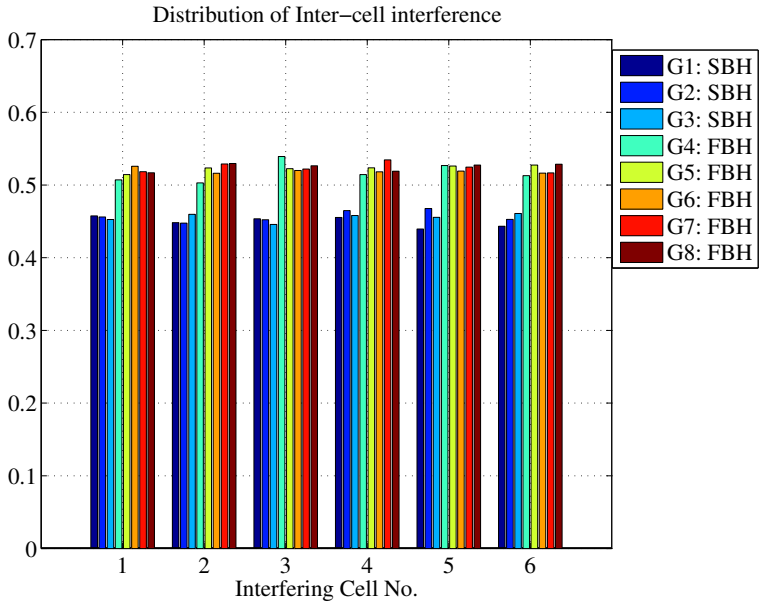

Figure 4.9: Probability of collision for different interfering cells.

© Muhammad Imadur Rahman, 2007

number of bits required to indicate the used polynomial is limited.

Simulations: A simple simulation, determining the validity of the claims made in this section, has been set up using Matlab. The setup emulates the hopping pattern of a central cell as well as 6 first-tier interfering cells. The PRNG consists of a 33-bit LFSR where 8 bits are used to generate each random number. The generating polynomial is a ML polynomial, where:

$$a_{32} = a_{31} = a_{30} = a_{10} = a_0 = 1$$

The same generator polynomial is used for all cells, while the starting state of the shift-register is randomized for each of the cells.

Using the nomenclature from Section 4.7.6.1 and 4.7.7, all cells are assumed to have $\rho = \frac{1}{3}$, $N_b = 16$ and $N_{sbh,c} = 5$. There are 8 bands in use at any given time for any given cell, 3 SBH bands and 5 FBH bands. Subcarrier hopping was not included in this investigation. The system was simulated for 5000 hops.

In Figure 4.8, the distribution of the number of interfering cells colliding with the different groups at any given frame is shown. From the figure, it is seen that for most frames, there are between 2-4 collisions from first-tier interfering cells. As there are 16 bands, where 8 are active at any given time, this is a reasonable result. Figure 4.9 shows the number of times a given interfering cell collides with a given group (proportionally to the total number of simulated frames). Here, it is seen that all interfering cells have an equal probability of collision, thereby obtaining interference averaging.

4.8 Chapter Summary

In this chapter, we have discussed several system design issues related to SCBH-OFDMA technique. We have designed a framework for sub-carrier and band hopping for SCBH-OFDMA scheme. The basic hopping mechanisms in two domains (i.e. sub-carrier and band domains) a re designed to ensure interference averaging among users in different cells. We have also explained two different forms of implementation for designed hopping procedure, one based on orthogonal Latin Squares and the other on Pseudo-random number generation and permutation. Both methods show promise for use in SCBH-OFDMA, the Latin square method being well suited for subcarrier hopping and the PRNG method for band-hopping.

5

Frequency Domain Rate and Power Allocation

In Chapters 3 and 4, we study a channelization method which makes use of only limited Channel State Information (CSI). In this chapter (and also in Chapter 6), we study methods for obtaining higher time-frequency diversity of the channel by exploiting more detailed CSI which are available at the transmitter.

The wireless channel condition is constantly changing, both in time and frequency. This is especially evident in cases when there is relative motion between transmitter and receiver, and when multipaths exist between the transmitter and receiver. The signal can experience high fluctuation in very short intervals of time and frequency. This makes it difficult to achieve high data rates while maintaining a target Bit Error Rate (BER) constraint. Thus, the variation in channel gain, which is termed as channel dynamics, has to be well exploited to maximize the data rate. One of the techniques to materialize this is Link Adaptation (LA), where system parameters are adapted according to the channel condition. This allows us to take advantage when channel conditions are favorable while optimizing bit and power resource during poorer conditions.

LA is a technique used to introduce a real-time balancing in the link budget in order to increase the spectral efficiency in bps/Hz of a system over fading channels [37, 99, 100, 20]. Parameters like transmitted power level, modulation scheme, coding rate, or any combination of these can be adapted according to the channel conditions. Channel conditions are estimated at the receiver and the Channel State Information (CSI) is sent to the transmitter to adapt the transmission accordingly.

Nearly all communication systems require some target BER not to be exceeded. It is possible to assume an average BER or an instantaneous BER (and FER or Block Error Rate (BLER)) as a constraint. However, an instantaneous value is more restrictive than an average constraint. Another assumption that we can make is the knowledge about the instantaneous CSI for each sub-carrier. With this knowledge, transmission parameters can be changed at the transmitter.

When no adaptation is done and the system presents low values of SNR, we should either increase the transmit power level, or decrease the modulation level, because transmission using high modulation levels in low SNR region leads to poor BER performance. To maintain the target BER it is necessary to compensate the state of the channel by adapting the transmitted power level. Again with no adaptation, when the SNR in the system increases, it can be interpreted as an improvement in the channel conditions which is not exploited. Under these considerations it is possible to "switch" to the next modulation level and increase the number of bits per symbol to be sent. Following the mentioned procedure it is possible to adapt the parameters in real-time at the transmitter to get an increased benefit from the dynamics of the channel. However, some reference points are required to "switch" from one constellation size to the next one. Theoretically these reference points correspond to the SNR required to achieve the target BER in AWGN channel conditions.

Defining the thresholds for switching between LA parameters are an interesting area of research. One possible criteria for switching points is described in [17]. A different approach can be found in [16], where the adaptation process is done considering the subcarrier fading statistics rather than instantaneous values. The adaptation can be done individually for each subcarrier as in [101, 19], or certain number of sub-carriers can be grouped to apply the same modulation technique, as described in [102]. An advantage of doing adaptation by using blocks is a reduction on the amount of information sent during the feedback to the transmitter. The effects of imperfect CSI in multi-carrier systems with adaptive modulation are studied in [103, 104, 105, 106].

Organization of this Chapter

The rest of this chapter is organized as follows. Sections 5.1 describes the basic ideas and constraints behind link adaptation process. Based on this understanding, we study a number of link adaptation algorithms in Section 5.2. The algorithms are compared in terms of spectral efficiency and complexity requirements for un-coded OFDM system in Section 5.3. From there we select a specific algorithm for further analysis. The link adaptation model is explained in Section 5.4. We study the interaction between multi-antenna techniques and LA procedure in Section 5.5.

5.1 Link Adaptation Preliminaries

In this section we describe a basic scenario of how the LA is done in an OFDM system. A block diagram of an adaptive modulation over one single sub-carrier (or sub-channel) is shown in Figure 5.1. However, the concept shown in Figure 5.1 can be extended to the multi-carrier scenarios by including the channels for the N sub-carriers (or N_{sch} sub-channels).

We assume that the entire frequency band is divided into N flat fading sub-carriers based

on the criteria that the symbol duration is less than the coherence time of the channel and the bandwidth of each sub-carrier is less than the coherence bandwidth of the system.

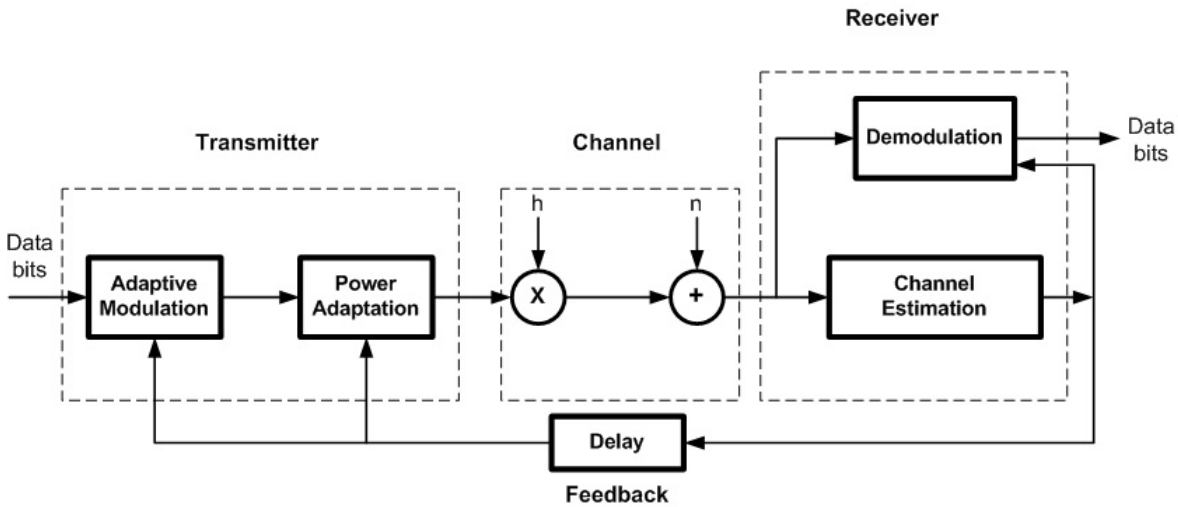

Figure 5.1: Block Diagram of a system using link adaptation, i.e. adaptive modulation and power adaptation

We denote h_k as the channel response for the kth sub-carrier. To simplify the study at the beginning, it is assumed that transmitter and receiver know the channel gain and an error free and instantaneous estimation of the channel is done at the receiver side. However, later on we will study the effects of delay and noisy estimations of the channel on the system.

Additive Gaussian noise $n(t)$ is assumed with σ_n^2 as its variance. At first, if we consider a constant average power, the average transmitted power will be denoted as $\overline{S}$ and γ_k the corresponding SNR at the kth sub-carrier, the relation between these two parameters can be described as [107],

$$\gamma_k = \overline{\gamma}|h_k|^2 = \frac{\overline{S}|h_k|^2}{\sigma_n^2} \tag{5.1}$$

where $\overline{\gamma}$ is the average SNR.

When power is not considered to be constant we will use the notation S_k for the power level at the kth sub-carrier, the instantaneous SNR then becomes [107],

$$\gamma_k = \frac{S_k|h_k|^2}{\sigma_n^2} \tag{5.2}$$

The process of LA implies to adapt the modulation and transmitted power according to the channel conditions. Channel conditions are evaluated for each sub-carrier based on Eq.(5.2).

Trade-offs and Optimization Target

Due to the requirements of high data rate for multimedia applications in current systems, one of the main concerns is to optimize the average spectral efficiency. Depending on the channel conditions, the power required to transmit data with a fixed rate will change with the time. Besides rate and power, it is necessary to consider that the system must meet some error rate requirement, thus these

© Muhammad Imadur Rahman, 2007

three parameters are the key to link adaptation.

Ideally, optimal S_k need to be found for all sub-carriers (or sub-channels), for $k \in [1, \ldots, N]$, so that,

$$\eta_t \approx \sum_k \mathfrak{R}_k \leq \log_2 \left(1 + \frac{S_k}{\sigma_n^2}|h_k|^2\right) \tag{5.3}$$

We omit the time notation from the right-hand side of Eq.(5.3) for clarity, without loosing any generality. For solving the power problem in this equation, $2^N - 1$ number of combinations can be found from all $S_k,\ \forall k \in [1, \ldots, N]$, on which the combination that provides highest rate need to be selected. This is a complex optimization problem, which can be solved using well-known *waterfilling* algorithm as describe below [73]. Assuming Gaussian input signal and perfect CSI feedback with no delay, the optimal power allocation to maximize the capacity (or supported rate) under total power constraint $\overline{S}$ can be solved as,

$$S_k = \left(\mu - \frac{\sigma_n^2}{|h_k|^2}\right)^+; \quad k = 1, \ldots, N, \tag{5.4}$$

where μ is chosen to satisfy $\sum_{k=1}^{N} S_k = N\overline{S}$, and where

$$(x)^+ = \begin{cases} x, & \text{if } x \geq 0 \\ 0, & \text{if } x < 0. \end{cases} \tag{5.5}$$

To understand the capacity regions, it is easier to study the optimization problem across two sub-carriers (or sub-channels). This problem can be explained as follows:

$$\mathfrak{R}_1 \leq \log_2 \left(1 + \frac{S_1}{\sigma_n^2}|h_1|^2\right) \tag{5.6}$$

$$\mathfrak{R}_2 \leq \log_2 \left(1 + \frac{\overline{S} - S_1}{\sigma_n^2}|h_2|^2\right) \tag{5.7}$$

$$\mathfrak{R}_1 + \mathfrak{R}_2 \leq \log_2 \left[\left(1 + \frac{S_1}{\sigma_n^2}|h_1|^2\right)\left(1 + \frac{\overline{S} - S_1}{\sigma_n^2}|h_2|^2\right)\right] \tag{5.8}$$

Eq.(5.8) can be solved to find a closed-form solution for S_1, which will give optimum rate. The rate region of two sub-carriers will be a two-dimensional plot, while capacity regions of more than two sub-carriers will be polyhedral. This means that, solving the optimum amount of power for k^{th} sub-carrier when N number of sub-carriers are present in the system, can be very complex, and virtually impossible to solve with any reasonable amount of complexity. Thus, sub-optimal algorithms need to be found, which are discussed in the next section.

Once the proper power level and bit allocation is done, then the average spectral efficiency, η can be written in bps/Hz [107],

$$\eta = \frac{1}{T}\sum_{t=1}^{T}\eta_t = \sum_t \frac{1}{BT_s}\sum_{k=1}^{N} ß_{k,t} \tag{5.9}$$

where $ß_{k,t}$ is the number of bits transmitted by the kth sub-carrier at t^{th} OFDM symbol. B and T_s are the system bandwidth and OFDM symbol duration, respectively. The power constraint is given by [107],

$$\frac{1}{N}\sum_{k=1}^{N} S_k \leqslant \overline{S} \tag{5.10}$$

5.2 Link Adaptation Algorithms

Based on the requirements mentioned in Section 5.1, we move to find a suitable LA algorithm for our analysis and studies. After extensive literature survey, we choose two algorithms for further review. One of them is Simple Rate Adaptation (SRA) [15]. SRA is a simple algorithm, where bit adaptation is done based on signal strength on any particular sub-carrier. The other chosen algorithm is Adaptive Power Distribution (APD) [18], because of its optimal performance. For this section, we assume that the gain of the channel is known and the estimation of this value is free of errors. Another assumption is that the feedback is instantaneous. The following sections describe the two algorithms mentioned above. Later, we propose a new algorithm based on the selected algorithms, but bringing about some improvements in terms of spectral efficiency and throughput.

5.2.1 Simple Rate Adaptation (SRA)

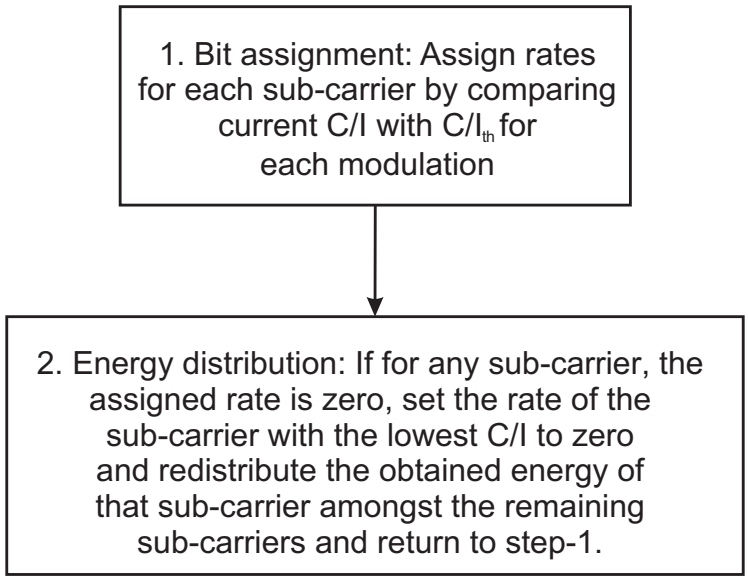

Figure 5.2: Flow Diagram for the SRA

This algorithm is fully described in [15]. It investigates the performance of HiperLAN/2. HiperLAN/2 uses the same modulation scheme across all the sub-carriers and the number of bits loaded is based on the average Carrier to Interference Ratio (C/I) of the system. OFDM along with BPSK, QPSK, 16QAM and 64QAM are used as in HyperLAN/2. The coherence time of the

© Muhammad Imadur Rahman, 2007

channel is considered as 0.7 ms. The total transmission time of one packet is 0.2 ms. The test of the algorithm is done using no coding scheme. The paper proposes a sub-carrier based adaptive modulation considering the C/I for each subcarrier individually and develops the SRA. The SRA doesn't necessarily assign the best modulation scheme based on the individual C/I of sub-carriers. The algorithm is based on the criteria of maximizing the throughput while keeping the total transmission power equal to the HiperLAN/2 system. The bit loading is performed by comparing the actual C/I condition for each subcarrier with pre-defined thresholds. A flow diagram for the SRA is shown in Figure 5.2.

This algorithm is designed for HiperLAN/2, but the criteria can be applied to any OFDM system. C/I vs. throughput for HiperLAN/2 with and without SRA are presented in [15]. The results show that, by doing adaptive modulation considering each subcarrier rather than all of them, the performance is better in terms of throughput. This is expected, since sub-carrier based adaptation corresponds to narrowband adaptation, thus better throughput is achieved. The solution for power is also simple since the power management is equally distributed among all the sub-carriers.

5.2.2 Adaptive Power Distribution (APD)

Adaptive Power Distribution (APD) proposes an adaptive power distribution algorithm whose objective is to improve the spectral efficiency in OFDM systems [18]. The BER target should be maintained and the total transmit power threshold should not exceed. QPSK, 16QAM and 64QAM are used as modulation schemes. The number of sub-carriers considered in [18] is 64 and a Wide Sense Stationary Uncorrelated Scattering (WSSUS) model for the channel is used. Noise is modeled as AWGN and the assumption of constant average noise power at each subcarrier is made. A flow diagram of the proposed algorithm is shown in Figure 5.3, where P_T is the transmit power threshold, P_L is the already distributed transmit power and P_{TL} is the distributed transmit power after a trial distribution. The trial distribution is used to check whether or not the threshold has overflowed.

According to Figure 5.3, the algorithm follows the following steps. Step 1 initializes the main parameters like initial power distribution and modulation schemes. The set of possible modulation schemes for each sub-carrier is collected in a vector $\mathfrak{B}$. Step 2 checks if there is a sub-carrier without assignment. If $\mathfrak{B}$ is empty the process ends. In every iteration sub-carriers and possible modulation schemes are evaluated. A sub-carrier can be excluded of use in two cases: First, if the incremental transmit power demanded by the kth sub-carrier to switch to the next modulation level yields to an excess on the power threshold, and second, when the number of bits per symbol in the next modulation level is smaller than the number of bits already loaded. This is applied in steps 5 and 7 (shown in Figure 5.3). The "BEST" modulation level for each sub-carrier and the "BEST" modulation mode are calculated in steps 3 and 4 (as shown in Figure 5.3). After these processes, power and the corresponding number of bits will be set to the sub-carrier which requires less average incremental transmit power per incremental bit to guarantee the pre-designated bit error rate.

It turns out that when no power is adapted the results are comparable to that in the first algorithm. In the SRA, only the bit loading is handled, whereas in APD, the total available power is also distributed dynamically. However, APD would require more calculations in determining

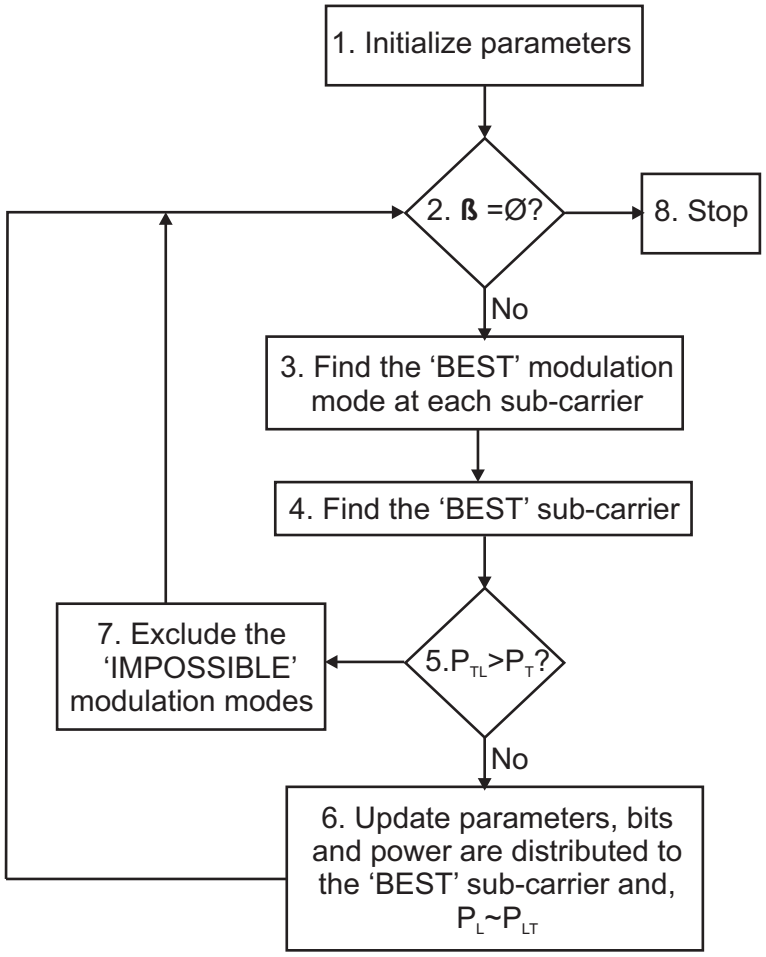

Figure 5.3: Flow Diagram for the Adaptive Power Distribution algorithm

power and modulation level compared to SRA.

5.2.3 The Proposed Link Adaptation Algorithm

In this section we will briefly present the modified LA algorithm based on SRA and APD that can balance between complexity and performance. As can be seen from previous sections, the SRA [15] is based on the equal power distribution and it follows an iterative mechanism. It is quite simple but not optimal while the APD algorithm adopts a optimum greedy approach, like [55], to obtain optimum throughput performance at the cost of high calculation complexity.

To find a balance between complexity and spectral efficiency, a new algorithm is proposed. It is a combination of the two algorithms discussed above, the greedy approach is still taken, but unlike the APD algorithm, instead of starting from 0 power and 0 bits as the beginning, it starts with equal power for all sub-carriers. Then by comparing received SNR with the SNR-lookup table, loaded bits for each subcarrier can be found, and power required for each subcarrier is recalculated. Then an approach similar to the APD algorithm is taken, to find the best bit and power

© Muhammad Imadur Rahman, 2007

distribution. We call such an algorithms as Simple Adaptive Modulation and Power Adaptation Algorithm (SAMPDA).

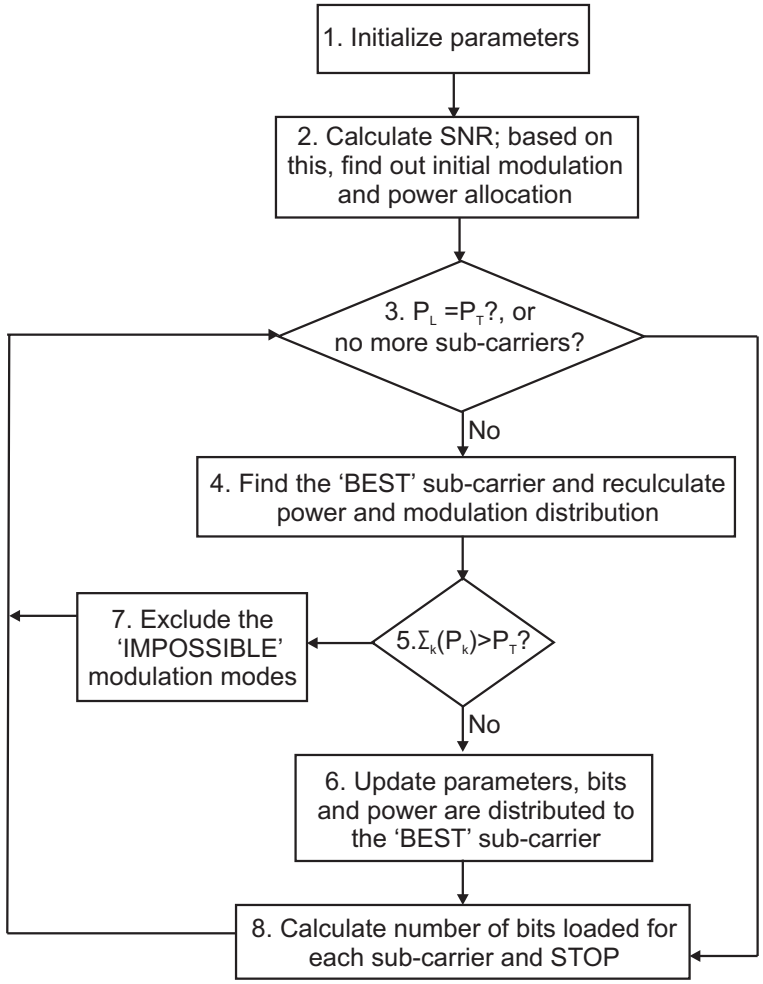

Figure 5.4: Flow diagram of the proposed algorithm

Different symbols that are used for describing SAMPDA are listed below:

- P_T Transmit power threshold
- P_L Loaded power
- N Number of sub-carriers
- F The highest modulation level
- $\psi_{mod} = [0, 1, ..., F]$ Usable modulation set
- $P_{1\times N}$ Vector of power for each sub-carrier
- $k_{1\times N}$ Vector of loaded bits for each sub-carrier
- $M_{1\times N}$ Vector of Modulation scheme for each sub-carrier

- k Sequence number of the sub-carrier
- h_k Channel frequency response at the kth sub-carrier
- $\frac{\Delta P}{\Delta k}_{1\times N}$ Incremental power per incremental bit
- γ_k Signal to noise ratio in each sub-carrier
- σ_n^2 Noise power in each sub-carrier
- SNR^f Required SNR to maintain the target BER for the fth modulation level
- NaN Not a number
- k^* Sequence number of the BEST subcarrier which has the minimum value of $\frac{\Delta P}{\Delta k}$.

5.2.3.1 SAMPDA Algorithm

SAMPDA works as follows:

- **Step 1: Initialization**

$$P_k = \frac{P_T}{N}$$

- **Step 2: Initial modulation scheme and power calculation**

$$\gamma_k = \frac{P_k h_k^2}{\sigma_n^2}$$

$$M_k = f_k \text{ where } SNR^{f_k} \leq ISNR_k < SNR^{f_k+1}$$

$$P_k = \frac{SNR^{M_k}\sigma_n^2}{h_k^2}$$

$$P_L = \sum_{k=1}^{N} P_k$$

$$\frac{\Delta P}{\Delta k}_k = \frac{(SNR^{M_k+1} - SNR^{M_k})\sigma_n^2}{2h_k^2} \text{ if } M_k \neq F$$

$$\frac{\Delta P}{\Delta k}_k = NaN \text{ if } M_k == F$$

- **Step 3: Check the Termination Condition**
  If $P_L = P_T$ or $min(M) = F$, go to step 6, else continue;

- **Step 4: Iteration starts**
  Find the BEST subcarrier:

$$k^* = argmin_k \frac{\Delta P}{\Delta k}$$

© Muhammad Imadur Rahman, 2007

Recalculate power and modulation scheme for the kth subcarrier:

$$M_{k^*} = M_{k^*} + 1$$
$$P_{k^*} = \frac{SNR^{M_{k^*}}\sigma_n^2}{h_{k^*}^2}$$

- **Step 5: Check Whether the Distributed Power Overflows**
  if $\sum_{k=1}^{N} P_k \geq P_T$, exclude the IMPOSSIBLE Modulations:

$$\frac{\Delta P}{\Delta k}_{k^*} = NaN$$
$$M_{k^*} = M_{k^*} - 1$$
$$P_{k^*} = \frac{SNR^{M_{k^*}}\sigma_n^2}{h_{k^*}^2}$$

  go to step 3;
  else update the parameters:

$$P_L = \sum_{k=1}^{N} P_k$$
$$\frac{\Delta P}{\Delta k}_{k^*} = \frac{(SNR^{M_{k^*}+1} - SNR^{M_{k^*}})\sigma_n^2}{2h_{k^*}^2} \;\; if \;\; M_{k^*} \neq F$$
$$\frac{\Delta P}{\Delta k}_{k^*} = NaN \;\; \text{if} \;\; M_{k^*} == F$$

  go to step 3;

- **Step 6: End**
  Calculate bits loaded for each subcarrier:

$$ß_k = log2(2^{2\times M_k}) = 2 \times M_k$$

  and stop.

After these six steps, bit and power for each subcarrier are stored in the two N length vectors $ß_{1\times N}$ and $P_{1\times N}$, which will be used for the transmission. A flow diagram is shown in Figure 5.4 to help understand this LA process.

5.3 Spectral Efficiency and Complexity Analysis in Un-coded system

As an initial evaluations, we have compared the three algorithms in terms of spectral efficiency and computational complexity. We have used a set of OFDM system parameters based on WiMAX system. The parameters are shown in Table 5.1.

Parameter	Value
Carrier Frequency	3.5GHz
Bandwidth	5MHz
Sampling Frequency	5.714MHz [64]
Sub-carrier Spacing	11.16kHz
RMS delay spread	0.5μs–2μs
FFT size	512
Useful Symbol period	89.6μs
Cyclic Prefix	11.2μs
OFDM symbol duration	100.8μs
FEC coding	Convolutional coding
Code rates	$\frac{1}{3}, \frac{1}{2}, \frac{2}{3}$
Modulation	4-QAM, 16-QAM, 64-QAM

Table 5.1: System parameters for evaluations of link adaptation algorithms

5.3.1 Analysis in Terms of Spectral Efficiency

Spectral efficiency is of vital importance in judging an algorithm. The spectral efficiency for the three algorithms can be seen from Figure 5.5. It can be seen that the proposed SAMPDA algorithm can achieve the same spectral efficiency as the APD algorithm, which is better than the SRA. The difference between them is especially large at medium SNR range, however it is not so significant when SNR goes higher or when SNR is very low. When SNR is very high, all the algorithms reach the highest spectral efficiency of $\frac{N*log_2(2^{2F})}{(T_s*B_W)} = \frac{512*8}{(10^{-4}*5*10^6)} = 8.1920bps/Hz$.

5.3.2 Complexity Analysis in Terms of Number of Iterations

It is easily understood that there will be a maximum 512 iterations for the SRA, and $\frac{N*log_2(F)}{2} = 2048$ iterations for the APD algorithm. Our proposed SAMPDA algorithm requires more number of iterations than SRA, but less than the number of iterations required by APD algorithm. This can be seen from Figure 5.6. At low SNR, our algorithm takes slightly more iterations than the APD algorithm, but much better than the SRA. For SNR between 4dB and 11dB, the proposed algorithm has the least iterations. For SNR higher than 11dB, the proposed algorithm takes a little more iterations than the SRA, but the distance goes less to zero as SNR increases.

5.3.3 Number of Loaded Sub-carriers

While designing a system, it could be better to have more sub-carriers being used, rather than transmitting with only a few sub-carriers at higher modulation level. Figure 5.7 shows the proposed algorithm and the APD algorithm have same number of available sub-carriers for all SNR, which is higher than the SRA. This is because Adaptive Power Distribution Algorithm tries to fill as many sub-carriers as it can, while SRA tries to fill each subcarrier maximally. However, for high SNR, all give the same performance because all sub-carriers are used.

From the comparison above, we find that the proposed SAMPDA algorithm can achieve almost the same spectral efficiency and number of available sub-carriers as the APD algorithm, while it is much more efficient with a lower calculation complexity. So, we will use SAMPDA algo-

© Muhammad Imadur Rahman, 2007

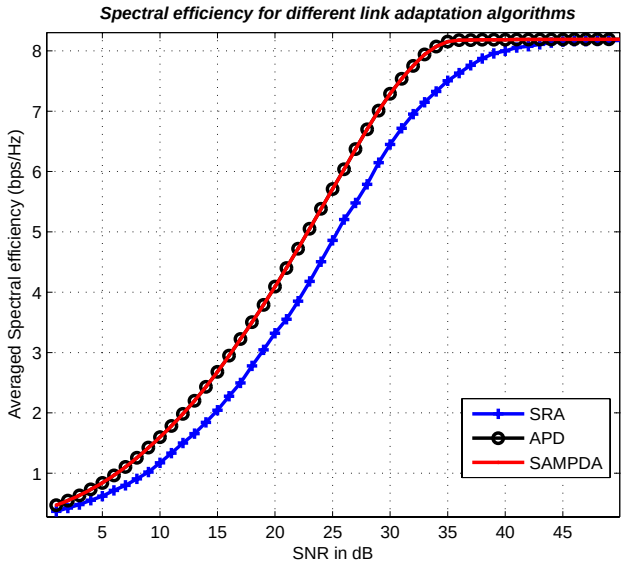

Figure 5.5: Spectral efficiency achievement of the adaptation algorithms

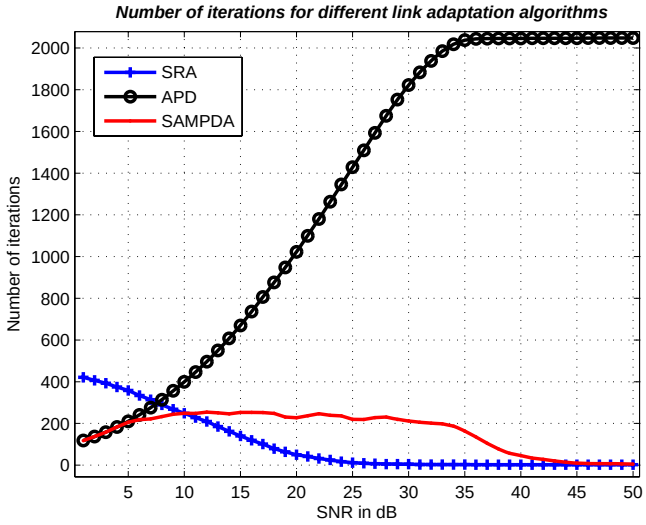

Figure 5.6: Number of iterations required by different adaptation algorithms

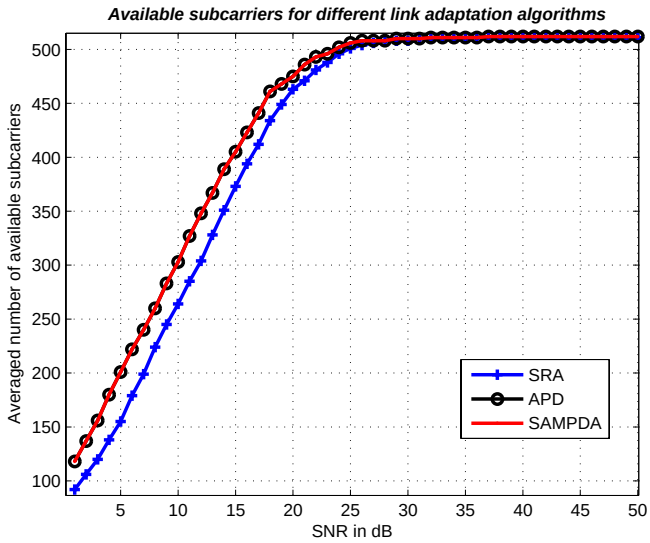

Figure 5.7: Sub-carrier loading for different algorithms

rithm in our system in the BER and/or BLER and throughput performance presented in following sections.

5.3.4 Adaptive SNR Lookup Table Method

Under different channel conditions, the SNR lookup table has to be different in order to achieve the target BER. To manually find a new SNR lookup table for each case is indeed very cumbersome, and so we propose an adaptive technique. In this technique, the link adaptation algorithm would automatically adapt the SNR lookup table to meet the target BER.

For each case of adaptation, achieved BER of the previous adaptation is compared against the target BER and the SNR lookup table is adjusted accordingly by increasing or decreasing the margin on top of the SNR table in AWGN channel. Adjustment steps are chosen accordingly to avoid possible ping-pong effect. The resultant BER after adaptation is taken over sufficient number of bits such that effects of instantaneous fluctuations are suppressed.

Once a suitable SNR lookup table margin is determined for certain conditions, it is fixed for that case. A high margin means more power has to be distributed for the same modulation scheme, which in the end means a low spectral efficiency or throughput. In a practical system however, the margin for worst case would be used, thus accommodating a certain degree of tolerance in the system.

5.3.5 Adaptive Sub-channel Size

In a multi-carrier system, adaptation across each sub-carrier can be very complex and overhead intensive, thus, a number of OFDM sub-carriers are grouped together to create sub-channels. The choice of sub-carrier number in one sub-channel depends on the system coherence bandwidth, as

© Muhammad Imadur Rahman, 2007

m	4	8
Margin	1.71dB	6.33dB
Number of sub-channels	128	64
MLI overhead	384kbps	192kbps

Table 5.2: SNR margin for different sub-channelization size

Δg	0.5%	1%	2%	3%
Margin	1.72dB	3.03dB	5.15dB	7.14dB
Number of possible sub-channels	151	112	78	64
MLI overhead	453kbps	336kbps	234kbps	192kbps

Table 5.3: SNR margin for adaptive sub-channelization with different threshold

bandwidth of each sub-channel should preferably be smaller than (or at least comparable to) the coherence bandwidth. Fulfilling the mentioned criterion, number of sub-carriers in one sub-channel is usually chosen to be the minimum possible, so that the coherence bandwidth is still larger (or comparable to) sub-channel bandwidth, and also maximum possible so that we can reduce system complexity and overhead requirements. Coherence bandwidth depends on the RMS delay spread, τ_{rms}, which is the measure of the spread of the multipath distortion. In mobile communication systems, Tx-Rx separation is not fixed and so is the τ_{rms}. Hence the coherence bandwidth is also varying with the user distance from the transmitter [44].

This characteristic can be exploited to add further adaptation to the system by 'bundling' together number of sub-carriers for cases when τ_{rms} is small, i.e. the coherence bandwidth is wider. Usually this is done by estimating the coherence bandwidth and grouping multiple sub-carriers accordingly. A common practice is to group adjacent sub-carriers into groups of m ($m = 2$, or its multiple) such that $M = N/m$ is a integer, and do link adaptation once for each sub-channel. This means same power and modulation level within each sub-channel, so less bits for Modulation Level Information (MLI) overhead are required. Further calculation complexity is reduced because of the reduction in number of groups to be adapted.

However, since the τ_{rms} and/or coherence bandwidth is a statistical measure, two adjacent sub-carriers across the whole spectrum are not always highly correlated. At times, sub-carrier condition is similar for a number of consequent sub-carriers, while otherwise, even adjacent sub-carriers may vary significantly. Thus it is not an easy task to meet the target BER while maintaining relatively high spectral efficiency if we choose a very large value for m. By using the adapt SNR lookup table method, the margin values and number of sub-channels for different m can be found, which is shown in Table 5.2.

In this analysis, we experiment a new technique which would group sub-carriers according to their relative gain and not based on the estimated τ_{rms}. Thus, the grouping is done on instantaneous basis, rather than on statistical information. This is in fact an adaptive sub-channelization technique. In this approach, consequent sub-carriers are grouped together, as long as their individual gain differs at most by a pre-specified level Δg. Then for different value of Δg, margins and average group number are found from simulation, as shown in Table 5.3.

From the two tables above, Tables 5.2 and 5.3, it is surprisingly observed that, by using fixed sub-channelization with $m = 4$, we can reduce MLI and complexity without loosing much in final

spectral efficiency. This can be seen from the first case of adaptive sub-channelization with $\Delta g = 0.5\%$ from Table 5.3 and $m = 4$ case from Table 5.2. In both cases, similar margin is required, but adaptive sub-channelization requires much higher MLI overhead. In adaptive sub-channelization, we need to transport information about instantaneous sub-channel size, which increases the MLI. However, in a scenario where τ_{rms} is not easy to find, the adaptive sub-channelization might be helpful.

5.4 Link Adaptation Scenario

In this section, we present the different system related issues that are considered in our investigation throughout the chapter.

5.4.1 Link Adaptation Process

We assume both TDD and FDD for this study. In case of TDD, the MS receives the pilot signals at the DL transmission slot, and then it measures the received SNR based on the used receiver technique. The received SNR is mapped to certain CQI, which is transported back to BS at UL time slot. For FDD case, the reporting of CQI is done via the UL frequency.

At the beginning of each adaptation window, the resulting SNR, γ_k, for all sub-channels are measured. This SNR is mapped back to BS as CQI, which is used to decide on the power allocation level, modulation bits and coding rate to be used for that sub-channel by using different LA algorithms. Naturally it is understood that for long adaptation window, the CQI will be somewhat invalid at the end of the adaptation window.

Figure 5.8 describes the LA model. An example of FDD is shown in this figure. We assume that there are 6 OFDM symbols in one frame (or block). If the processing time (i.e. time required by the MS to calculate the sub-channel gains and decide on the LA levels) is negligible compared to OFDM symbol duration, then there is a delay of 4 OFDM symbols in actual estimation of the CQI and its implementation in LA system. For TDD-based systems, the UL and DL are separated in time rather than frequency. So, the resultant delay in LA process will depend on the ratio of slots assigned to DL and UL.

5.4.2 Different LA Mechanisms Used in This Study

Three LA mechanisms are used here and they are discussed in the following:

5.4.2.1 AMC with Fixed Power:

In this LA mechanism, total power is divided equally among all the sub-channels. Given the feedback CQI, the received SNR level can be calculated. Comparing this received SNR and SNR threshold from a pre-defined lookup table, the highest supported modulation and coding rate for each sub-channel can be found. For 'weak' sub-channels, which cannot support even the lowest modulation and coding levels, no power is allocated. Because the SNR threshold values are discontinuous,

© Muhammad Imadur Rahman, 2007

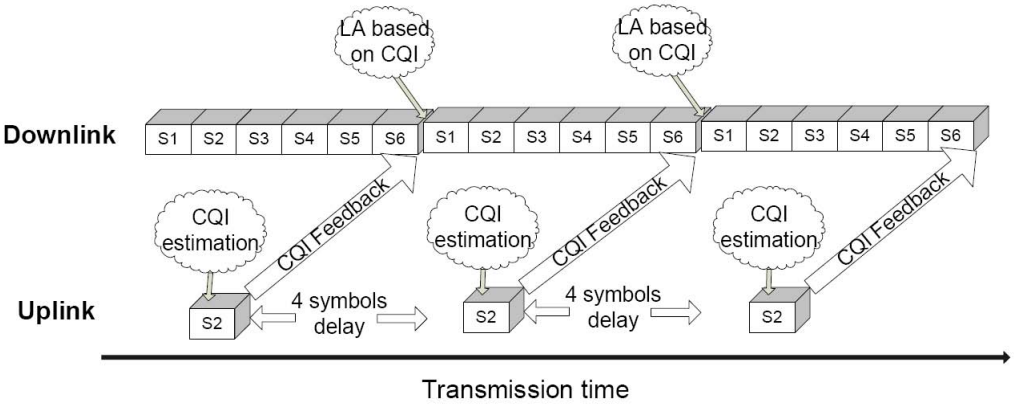

Figure 5.8: Link adaptation model; example of FDD scenario is shown.

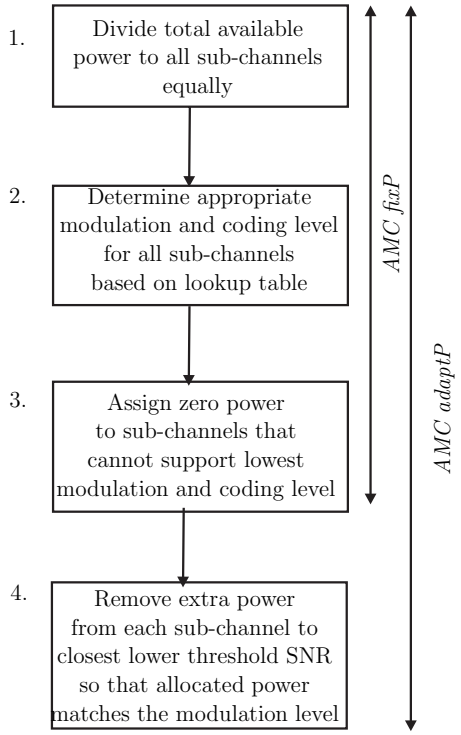

Figure 5.9: Flowchart of *AMC fixP* and *AMC adaptP* mechanism. Steps 1-3 corresponds to *AMC fixP* and steps 1-4 corresponds to *AMC adaptP*.

there is high probability that the power assigned to one sub-channel is much higher than the power required to support the selected modulation level.

5.4.2.2 AMC with Adapted Power:

Similar to AMC with fixed power, this technique starts with equal power distribution, and finds out which modulation and coding can be supported. Once this step is done, the power assigned for each sub-channel will be adjusted to the threshold values. In this way, extra power available at the sub-channel is removed. In a multi-cellular case, this means that interference is reduced to users in same sub-channel in neighboring cells. Also, in multi-user context, this saved power can be used for 'weaker' users. Similar to AMC with Fixed Power, no power is allocated to 'weak' sub-channels in this algorithms also. Figure 5.9 shows the definition of both AMC with fixed power and AMC with adapted power based LA mechanisms.

5.4.2.3 Adaptive Power, Modulation and Coding (APMC):

Unlike the two above mentioned algorithms, APMC will adapt power, modulation and coding rate all together. The degree of freedom is increased in this algorithm and it can achieve a better performance than AMC with fixed power and also AMC with adaptive power assignment. SAMPDA algorithm is one example of APMC-type LA mechanism, which is described in Section 5.2.

5.4.3 System Parameters

We use WiMAX system for our studies, as mentioned in Table 5.1. In addition to the ones mentioned in the table, we also use the following system parameters:

- The maximum channel RMS delay spread that is considered in this work is 2μs. This corresponds to highly frequency selective channel. We have also used other lower RMS delay spread values, such as 0.5μs and 1μs. The channel power delay profile is taken from [44].

- Sub-channelization is used according to WiMAX standard. A Sub-channel consists of 8, 16, 32 or 512 sub-carriers. We denote this as *subN* in the subsequent discussions.

- A frame is defined as one sub-channel across 6 consecutive OFDM symbols, thus a frame duration is around 0.6ms. For example, one frame has 96 Quadrature Amplitude Modulation (QAM) symbols, when the sub-channel size is 16.

- The LA adaptation window is taken to be 1, 2, 4, 10 and 20 frames, i.e. on each 6, 12, 24, 60 and 120 OFDM symbols, respectively. This gives us an adaptation window of 0.6ms, 1.2ms, 2.4ms, 6.0ms and 12.0ms respectively.

- The maximum Doppler spread is taken as 50Hz and 250Hz for two cases of our investigations. Corresponding user speeds are 15.43kmph and 77.14kmph respectively. Referring to Table 2.2, corresponding 50% coherence times are 8.5ms and 1.7ms respectively [42].

© Muhammad Imadur Rahman, 2007

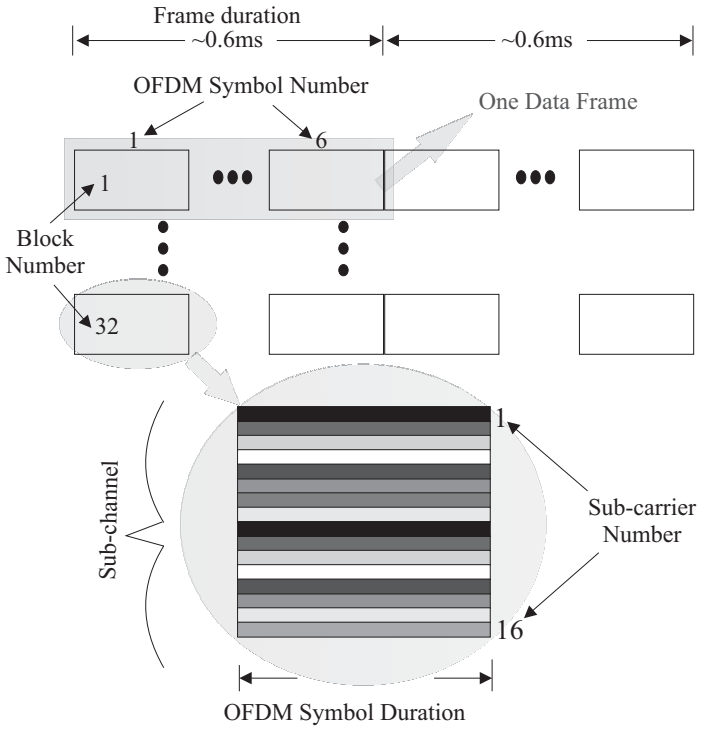

Figure 5.10: Link adaptation frame structure; an example of 6 OFDM symbols per frame (or block) and 16 sub-carrier per sub-channel is shown.

5.4.4 Frame Structure

The frame structure fundamental to LA being considered in this work is given in Figure 5.10. The minimum unit over which FEC and interleaving is applied is called a frame (or block). It is a set of consecutive sub-carriers which span a successive sequence of OFDM symbols over a period of 0.6ms. The sub-channel size is defined by the number of consecutive sub-carriers that make the frame. The modulation level, code rate and power level are applied at the frame level in this work. The frame size can be made to vary in the frequency domain, by changing the sub-channel size and in time domain by changing the number of symbols inside one frame. The modulation and coding level is adapted once every adaptation interval, which can be multiple of the block duration. Adaptation interval is the period in time over which the modulation and coding remains unchanged and power adaptation interval is the period between each power adaptation.

During LA, usually an adaptation window is defined in time and frequency domain, which can be multiple of the frames. Increasing the size of this window in time and frequency domain is expected to reduce the benefit of LA, but in some cases it might be of benefit, whereas overhead in signaling the LA configuration can be reduced, while there might not be significant change in throughput. The choice of this window is also influenced by channel parameters as mentioned before.

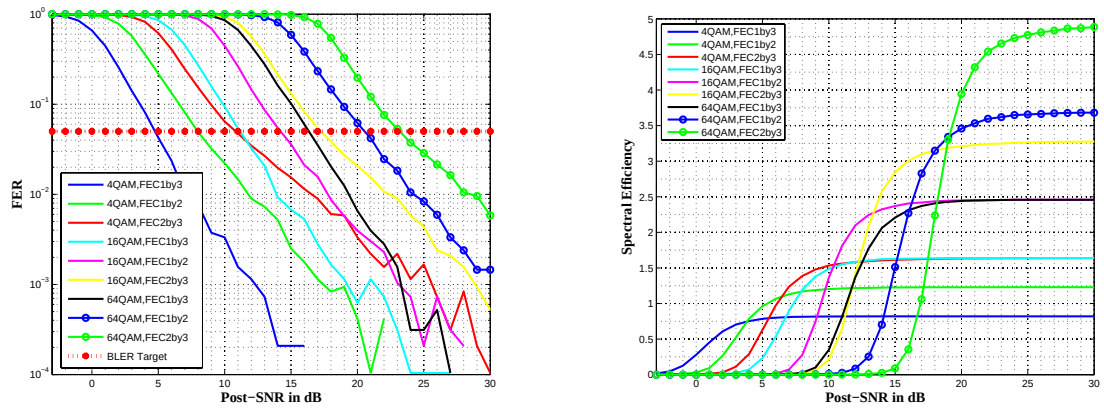

(a) FER

(b) Throughput

Figure 5.11: Non-adapted FER and throughput vs. Post-SNR for different modulation and coding combinations. Link Adaptation is done on every frame basis.

5.4.5 Threshold Measurement

The LA procedure is designed to provide a certain FER target, thus, a pre-defined SNR-to-FER lookup table is required. Different authors have used different methods in obtaining the lookup table. Ideal lookup table for AWGN channel conditions are used for performing LA in fading channels in [18]. According to our analysis, using such a table in fading channels will result in a failure in meeting the target error rate. Alternatively, margins for each rate level in fading channels can be found iteratively based on the original AWGN lookup table. The resultant spectral efficiency based on this new lookup table will be better, but this is not an efficient solution. In another way, for any specific transmit-SNR[1], a particular Post-SNR[2] can be forced by varying the assigned power level in every sub-channel, and corresponding FERs can be found for different modulation and coding level. Based on these FER results, the thresholds can be found corresponding to certain FER requirement.

In this work, we take a different approach in finding the thresholds lookup table:

Step-1: For any specific Pre-SNR, the resultant Post-SNR for all frames are measured, based on Eq.(5.1). Whether the frames are in error or not, is also checked.

Step-2: Step-1 is repeated for all values of Pre-SNRs, i.e. $0dB \leq \overline{\gamma} \leq 30dB$, and corresponding Post-SNRs for every frame and the error conditions are also checked.

Step-3: All the Post-SNR values are sorted and they are grouped together around certain Post-SNR values. For example, all the values between $5 \pm \epsilon$ dB can be grouped together as 5dB. ϵ can be chosen carefully so that realistic grouping is performed. For small values of ϵ, such as 0.5dB, the impact on the system link adapted system performance will be tolerable, as

[1]We use the term transmit-SNR the ratio between average transmit power and noise power, i.e. $\overline{\gamma} = \frac{\overline{S}}{\sigma_n^2}$. We also use the term, pre-SNR for the same definition.

[2]Post-SNR is defined in Eq. (5.1) as, $\gamma_k = \overline{\gamma}|h_k|^2$. In some places, we have described this as instantaneous SNR.

© Muhammad Imadur Rahman, 2007

shown in [108]. Now, for each Post-SNR reference value, i.e. γ_{post}, the corresponding FER is obtained.

Step-4 : From the γ_{post} vs. FER relationship, we can find the proper γ_{post} value that offers the required FER. This value is the switching threshold for the given **M** & **C** combination.

Step-5: All possible **M** & **C** combinations are tested using the above steps and the relevant switching thresholds are found.

Figure 5.11(a) shows the FER vs. post-SNR curves for different **M** & **C** combinations, for a SISO system. The corresponding spectral efficiency performance is shown in Figure 5.11(b).

With a given target FER of 0.05, the SNR threshold values can be found from this figure and are shown in Table 5.4. The $'NaN'$ in the table indicate the corresponding **M** & **C** combinations require more power while offering the same or less rate than some of the other combinations, so it is better not to use such combinations. However, for fixed coding rate schemes, these combinations might be applicable.

Modulation	4QAM			16QAM			64QAM		
Coding Rate	1/3	1/2	2/3	1/3	1/2	2/3	1/3	1/2	2/3
Threshold Values	5dB	8dB	11dB	NaN	14dB	17dB	NaN	21dB	23dB

Table 5.4: SNR Lookup Table for a SISO system with frame-by-frame adaptation

5.5 Interaction between Spatial Diversity and Link Adaptation

We have studied two different LA algorithms, namely Simple Rate Adaptation (SRA) and Adaptive Power Distribution (APD) algorithms, that are described in Section 5.2. Based on these two algorithms, we study another LA algorithm, e.g. Simple Adaptive Modulation and Power Adaptation Algorithm (SAMPDA), which is described in Section 5.2.3. Section 5.3 compares the three algorithms in terms of achievable spectral efficiency and computational complexity. Using these algorithms, we now move to study different aspects of link adaptation together in OFDM system.

Multiple antennas at the transmitter or receiver can provide a number of benefits for received signal enhancement. The available spatial degrees of freedom can be utilized to obtain spatial diversity. Besides, array gain is also obtained when coherently combined at the receiver, or when CSI is known at the transmitter. Depending on whether pre-processing or post-processing SNR is used for threshold determination, the diversity and array gains can be very important; as these can influence the thresholds required for different modulation, coding and power allocation levels.

In this section, we study the performance of different multi-antenna diversity techniques when used in a LA-based OFDM system.

5.5.1 Multi-Antenna Diversity Schemes

We include a number of spatial diversity techniques in this study. These techniques provide either array gain, or diversity benefits or both together in the system.

5.5.1.1 Maximum Ratio Combining

For MRC, link adaptation is performed based on the combined channel gain from the multiple links. Since this combined channel gain is greater than that of each individual link, a better performance is achieved compared to SISO. MRC can benefit the transmission in terms of both diversity gain and array gain.

We assume, Q as the number of receive diversity branches. For MRC, the received signal is:

$$\hat{X}_k = \frac{\sum_{q=1}^{Q}(d_k h_q h_q^* + N_q h_q^*)}{\sum_{q=1}^{Q}|h_q|^2} \tag{5.11}$$

$$= d_k + \frac{\sum_{q=1}^{Q} N_q h_q^*}{\sum_{q=1}^{Q}|h_q|^2} \tag{5.12}$$

The output SNR is:

$$\gamma_{mrc} = \frac{E_{ss}}{\sigma_n^2 \frac{\sum_{q=1}^{Q}|h_q|^2}{(\sum_{q=1}^{Q}|h_q|^2)^2}} = \gamma_{tx}\sum_{q=1}^{Q}|h_q|^2 \tag{5.13}$$

The equivalent channel gain is then found to be:

$$g_{mrc} = \frac{\gamma_{mrc}}{\gamma_{tx}} = \sum_{q=1}^{Q}|h_q|^2 \tag{5.14}$$

5.5.1.2 MISO Diversity Techniques

Single Input Multiple Output (SIMO) techniques, such as MRC, require multiple antennas at the receiver. The multiple antenna requirement at the receiver might not be possible to obtain for some user terminals. As an alternative approach, MISO employs multiple antennas in the transmitter part and improves the performance with less requirement on the receiver [73]. Two popular MISO techniques are used here, namely Alamouti's STBC and AS.

MISO Alamouti: Alamouti scheme is employed at the transmitter with two transmit antennas, without requiring the channel state information to be known at the transmitter [25]. The receiver complexity is reduced because diversity is achieved by multiple antennas at the transmitter part. Alamouti-based MISO performs similarly as MRC in terms of diversity gain. However, with no channel knowledge and in presence of total transmission power constraint, the transmission power has to be divided among the transmitter antennas.

The channel is assumed to be flat for at least two symbol durations. Alamouti scheme works as follows [25]: in the transmitter side, two symbols are transmitted at the same time from two different antennas, as can be seen from Table 5.5.

In the receiver side, we denote CTFs for 1st and 2nd antenna as h_1 and h_2 respectively. When channel is constant for two symbol duration, we can say that $h_1 = h_2$. The received signal and the output signal from an Alamouti receiver is shown in Table 5.6. The equivalent channel gain can be

© Muhammad Imadur Rahman, 2007

	T_1	T_2
$Antenna_1$	d_1	$-d_2^*$
$Antenna_2$	d_2	d_1^*

Table 5.5: Alamouti transmitter

written as:

$$g_{alt} = \frac{\sum_{p=1}^{P} |h_p|^2}{P} \tag{5.15}$$

where $P = 2$ is the number of transmit antennas.

	T_1
Received Signal	$X_1 = h_1 d_1 + h_2 d_2 + n_1$
Output Signal	$\hat{X}_1 = h_1^* r_1 + h_2 r_2^*$ $= (\lvert h_1\rvert^2 + \lvert h_2\rvert^2) d_1 + h_1^* n_1 + h_2 n_2^*$
	T_2
Received Signal	$X_2 = -h_1 d_2^* + h_2 d_1^* + n_2$
Output Signal	$\hat{X}_2 = h_2^* r_1 - h_1 r_2^*$ $= (\lvert h_1\rvert^2 + \lvert h_2\rvert^2) d_2 + h_2^* n_1 - h_1 n_2^*$

Table 5.6: Alamouti receiver

From Table 5.6, it can be seen that Alamouti-based MISO performs similarly as MRC in terms of diversity gain. The difference between SIMO and MISO is that, because the total transmission power has to be divided equally between the two transmit antennas in MISO, SIMO (e.g. MRC) obtains a 3dB of array gain given the same total power constraint, while MISO does not. Note that the array gain can be obtained in MISO systems, only when CSI is known at the transmitter and a closed-loop TxDiv is formed.

Transmit Antenna Selection: Transmit AS works by selecting the antenna with the highest channel gain at the transmitter part. There are two ways to do the selection, one is in frequency domain (i.e. selecting on narrowband or on sub-carriers or on sub-channels), the other one is in time domain (i.e. selecting on wideband signals). For an OFDM system, time domain selection will not give much performance improvement compared to a SISO system. The reason for this is that, it will do selection based on the channel gain for one OFDM symbol, which is the averaged information across all the sub-carriers. On the other hand, AS on frequency domain is a sub-carrier (or sub-channel) level selection, thus a better performance can be expected. Because of this reason, frequency domain antenna selection is used here. Because only one antenna is transmitting at one time, the total power need not be divided by the transmitting antenna number as in Alamouti. The equivalent channel gain can be written:

$$g_{as} = \max_p |h_p|^2 \qquad p \in \{1, \ldots, P\} \tag{5.16}$$

Transmit AS is similar as SIMO-AS, the difference is that the antenna selection is shifted from receiver to the transmitter part. This reduces the antenna requirements on mobile terminals,

while increasing the network requirement by the need of CQI at the transmitter. Figure 5.12 shows BER performance for non-adapted system in fading channel with Antenna selection in frequency domain and time domain, compared to SISO system. From this we can see the benefit of MISO-AS (frequency) over MISO-AS (time) and SISO system.

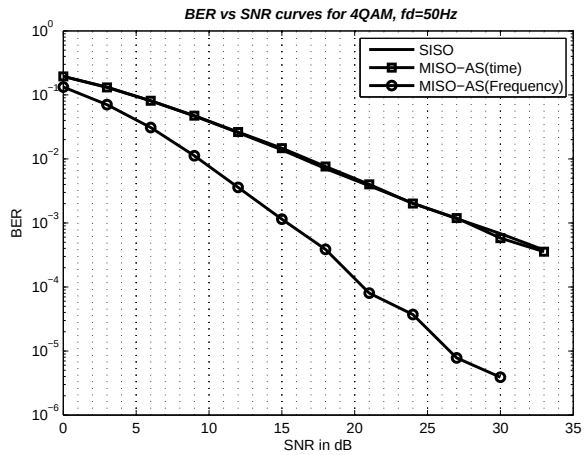

Figure 5.12: BER vs SNR curves for SISO, AS (time) and AS (frequency), with fd=50Hz

5.5.1.3 MIMO Diversity Techniques

Two kinds of Multiple Input Multiple Output (MIMO) diversity systems are considered for this study, where both the transmit and receive antennas are used for spatial diversity purposes. The available diversity order in MIMO diversity systems is $P \times Q$, while it is P and Q in MISO and SIMO systems respectively.

Alamouti-MRC MIMO: In this scheme, Alamouti-based transmit diversity is implemented at the transmitter and MRC combining is used at the receiver. The equivalent channel gain can be written as:

$$g_{alt-mrc} = \frac{\sum_{q=1}^{Q}\sum_{p=1}^{P}|h_{q,p}|^2}{P} \qquad p \in \{1,\ldots,P\} \;\&\; q \in \{1,\ldots,Q\} \tag{5.17}$$

where $P = 2$ because Alamouti scheme is used for space-time coding at the transmitter. So, the total available diversity order is $2Q$.

AS-MRC MIMO: In AS-MRC scheme, transmit AS is implemented while the received signal branches are combined by MRC. The equivalent channel gain can be written as:

$$g_{as-mrc} = \max_{p}\sum_{q=1}^{Q}|h_{q,p}|^2 \qquad p \in \{1,\ldots,P\} \;\&\; q \in \{1,\ldots,Q\} \tag{5.18}$$

© Muhammad Imadur Rahman, 2007

where the available diversity order is $P \times Q$. These diversity benefits are obtained at the expense of CQI at the transmitter.

For all the above multi-antenna schemes, the SNR look-up table is shown in Table 5.7. Frame-by-frame adaptation is assumed in the mentioned table, and the resultant FER and throughput performances for instantaneous adaptation, shown in the coming sections are based on this SNR lookup table.

5.5.2 FER and Throughput Performance of Multi-Antenna assisted LA Systems

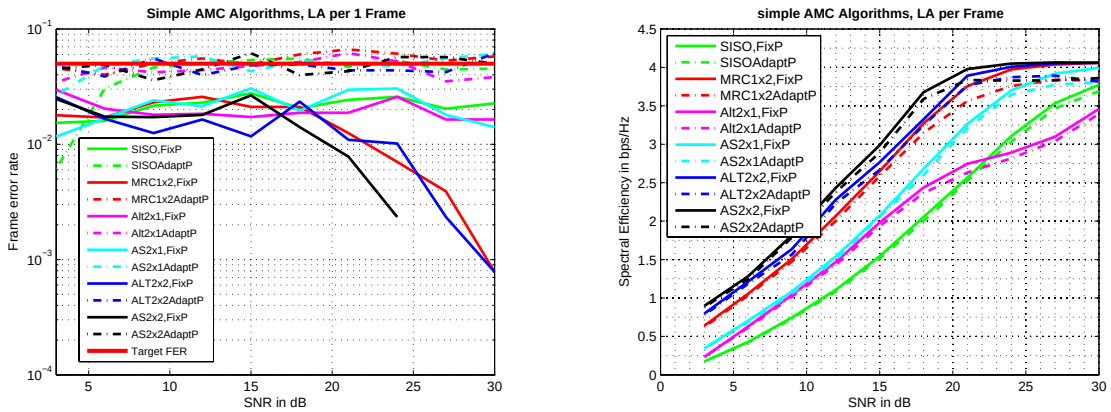

(a) FER results (b) Spectral efficiency

Figure 5.13: Performance results of *instantaneous link adaptation* in multi-antenna assisted OFDM systems

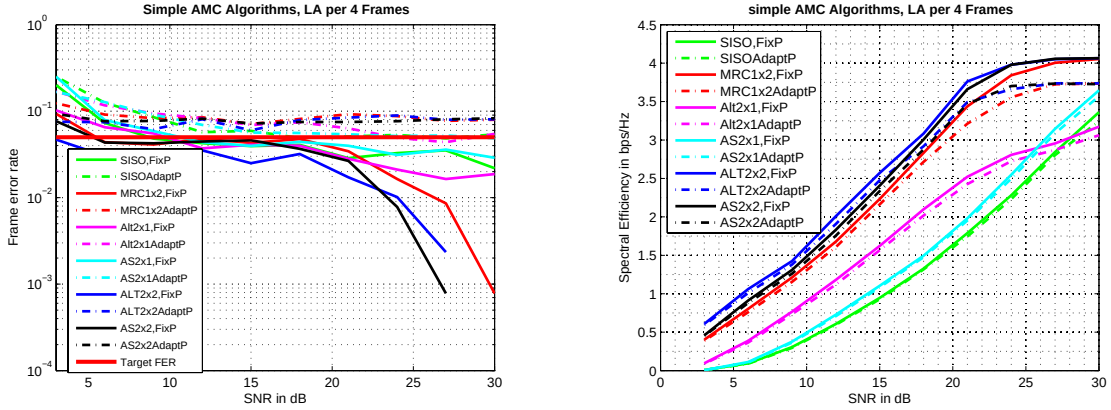

(a) FER results (b) Spectral efficiency

Figure 5.14: Performance results of *slower link adaptation* in multi-antenna assisted OFDM systems

Figures 5.13(a) and 5.13(b) show us the FER results and corresponding spectral efficiency curves for all the schemes when two different LA algorithms are implemented, namely AMC with fixed power and AMC with sub-sequent power adaptation. We have defined the FER requirement as 0.05. In these two LA cases, the LA operation is done for both AMC and power in frame-by-frame basis. In Figures 5.13(a) - 5.14(b), we have used *Pre-SNR* in the x-axis, which refers to the average

transmit SNR, $\overline{\gamma} = \frac{E_s}{N_0}$. This means that, when multiple transmit antennas are present, then a total of E_s is transmitted via all the antennas, e.g. for Alamouti transmission, $\frac{E_s}{2}$ is transmitted across each antenna. Thus, the Pre-SNR in our results is the total transmit SNR for corresponding system.

Notice that AS-MRC performs better than other multi-antenna schemes in frame-by-frame adaptation as seen in Figures 5.13(a) and 5.13(b). When AS is used at the transmitter, then we need additional CQI in collaboration with CQI required for link adaptation. When modulation level decisions are done in MS, then the CQI feedback contains the notification selected antenna branch and corresponding modulation level. If modulation decisions are done in BS, then MS needs to send the CQI corresponding to all antenna paths and their respective modulation levels. In our system setup, the best available multi-antenna scheme is AS-MRC, where both transmit-receive diversity gain and receive array gain is achieved. In this case, AS performs very well also, because the AS is done instantaneously and the best channel is always selected. This can be seen from the spectral efficiency results shown in Figure 5.13(b). For 2×1 Alamouti scheme, we can see that the throughput is degraded at high average SNR. This is because, at high SNR, only higher modulations are selected. At these modulation levels, the signal constellations are dense, so little difference in channel co-efficiencies between two OFDM symbols due to the time-variance of the channel causes relatively higher signal distortions. To summarize, we can conclude that the best available multi-antenna scheme needs to be chosen when frame-by-frame adaptation is possible.

Modulation	4QAM			16QAM			64QAM		
Coding Rate	1/3	1/2	2/3	1/3	1/2	2/3	1/3	1/2	2/3
SISO	5dB	8dB	11dB	NaN	14dB	17dB	NaN	21dB	23dB
MRC1x2	4dB	6dB	9dB	NaN	13dB	15dB	NaN	19dB	21dB
Alamouti2x1	4dB	6dB	9dB	NaN	13dB	15dB	NaN	19dB	21dB
AS2x1	4dB	7dB	9dB	NaN	13dB	16dB	NaN	19dB	21dB
Alamouti2x2	4dB	6dB	8dB	NaN	12dB	15dB	NaN	18dB	21dB
AS2x2	4dB	6dB	8dB	NaN	13dB	15dB	NaN	18dB	20dB

Table 5.7: SNR Lookup Table for MIMO systems, LA is performed on frame-by-frame basis.

Modulation	4QAM			16QAM			64QAM		
Coding Rate	1/3	1/2	2/3	1/3	1/2	2/3	1/3	1/2	2/3
SISO	12dB	16dB	18dB	NaN	22dB	25dB	NaN	28dB	31dB
MRC1x2	8dB	11dB	13dB	NaN	17dB	20dB	NaN	23dB	26dB
Alamouti2x1	8dB	11dB	13dB	NaN	17dB	20dB	NaN	23dB	26dB
AS2x1	14dB	17dB	20dB	NaN	23dB	26dB	NaN	29dB	32dB
Alamouti2x2	5dB	8dB	10dB	NaN	14dB	17dB	NaN	20dB	23dB
AS2x2	8dB	11dB	13dB	NaN	18dB	20dB	NaN	23dB	26dB

Table 5.8: SNR Lookup Table for MIMO systems, LA is performed on per 20 Frames

Figures 5.14(a) and 5.14(b) give us the FER and spectral efficiency results for slower adaptation rate corresponding to Figures 5.13(a) and 5.13(b) respectively. In these two figures, our adaptation rate is now 4 times slower than the frame rate. This means that we are adapting the channel in every 2.4ms. This is quite comparable to 50% coherence time mentioned in Section 5.4. Thus, we can say that now we are doing the adaptation based on outdated CQI information. In case of slower adaptation rate, the channel changes quite significantly inside the adaptation window, thus

© Muhammad Imadur Rahman, 2007

the AS completely fails to meet the FER requirement, as the selection is done incorrectly. This is the reason why 2×1 AS performs quite badly in Figures 5.14(a) and 5.14(b). The 2×2 AS-MRC obtains lower throughput compared to 2×2 Alamouti-MRC. Note that AS-MRC requires CQI feedback, while STBC-MRC does not. The lower rate of adaptation diminishes the gain to be obtained from CQI feedback in AS-MRC. The 2×2 STBC-MRC, 1×2 MRC and 2×1 STBC perform quite well corresponding to fast link adaptation case. Comparing Figure 5.14(b) and Figure 5.13(b), we can see that the throughput performance of these three techniques are not affected very much because of slower adaptation rate, while the other schemes are affected very highly. This is because of the averaging in terms of received SNR which is obtained due to the array gain, and we know that these two schemes (i.e. STBC and MRC) are quite suitable for this kind of scenario. Thus, it is concluded that, when both end of the transmission can exploit the available spatial degrees of freedom for diversity purposes, then it is satisfactory to reduce the LA rate. In that case, CQI-based transmit diversity, such as AS, can be avoided and comparatively simpler Alamouti based transmit diversity and MRC can be used at slower adaptation rate without loosing much in spectral efficiency. Alternatively, we can also conclude that, due to mobility and other reasons, if we do not have the possibility to obtain instantaneous (and reliable) CQI information, then it is more useful to choose multi-antenna schemes which do not require CSI or CQI at the transmitter.

5.5.3 Impact of LA Rates in Different Multi-Antenna Schemes

Note that Figures 5.13(a) - 5.14(b) show us the numerical results when AMC with fixed power (*'AMC fixP'*) and AMC with adapted power (*'AMC adaptP'*) is evaluated for different multi-antenna schemes. In those figures, only two adaptation rates, namely frame-by-frame adaptation and adaptation at every 4 frames are studied. In Figures 5.15(a) - 5.15(d), we have presented the spectral efficiency results for the studied MIMO schemes with different rate of adaptations at different pre-SNR values. In these results, APMC-type LA, such as SAMPDA is studied. These results are valid for a RMS delay spread of 0.5μs and Doppler frequency of 50Hz. Roughly, pre-SNR of 3dB corresponds to CCI-affected case and pre-SNRof 27dB corresponds to users located very close to the BS. As seen earlier, 50Hz of Doppler frequency corresponds to 3ms of coherence time. We can observe a few very important outcome by studying these results, as explained below:

- For lower SNRs, when the adaptation window is very large, i.e. 12ms, then the performance of AS 2×1 is very similar to SISO systems. This is logical and in coherence with Figure 5.12, where channel averaging is experienced for large adaptation window.

- Achievable diversity gain plays an important role in system performance. In low SNR regions, systems with higher diversity orders (i.e. AS-MRC, Alt-MRC etc) obtains much higher spectral efficiency compared to other schemes even at very large adaptation window.

- The array gain is also very important for improvement in spectral efficiency. In AS-MRC scheme, channel averaging effect is expected to be seen at large adaptation window, however, the achieved spectral efficiency at large adaptation window in this scheme is still much higher than transmit diversity and SISO schemes. This is because of the array gain and diversity gain

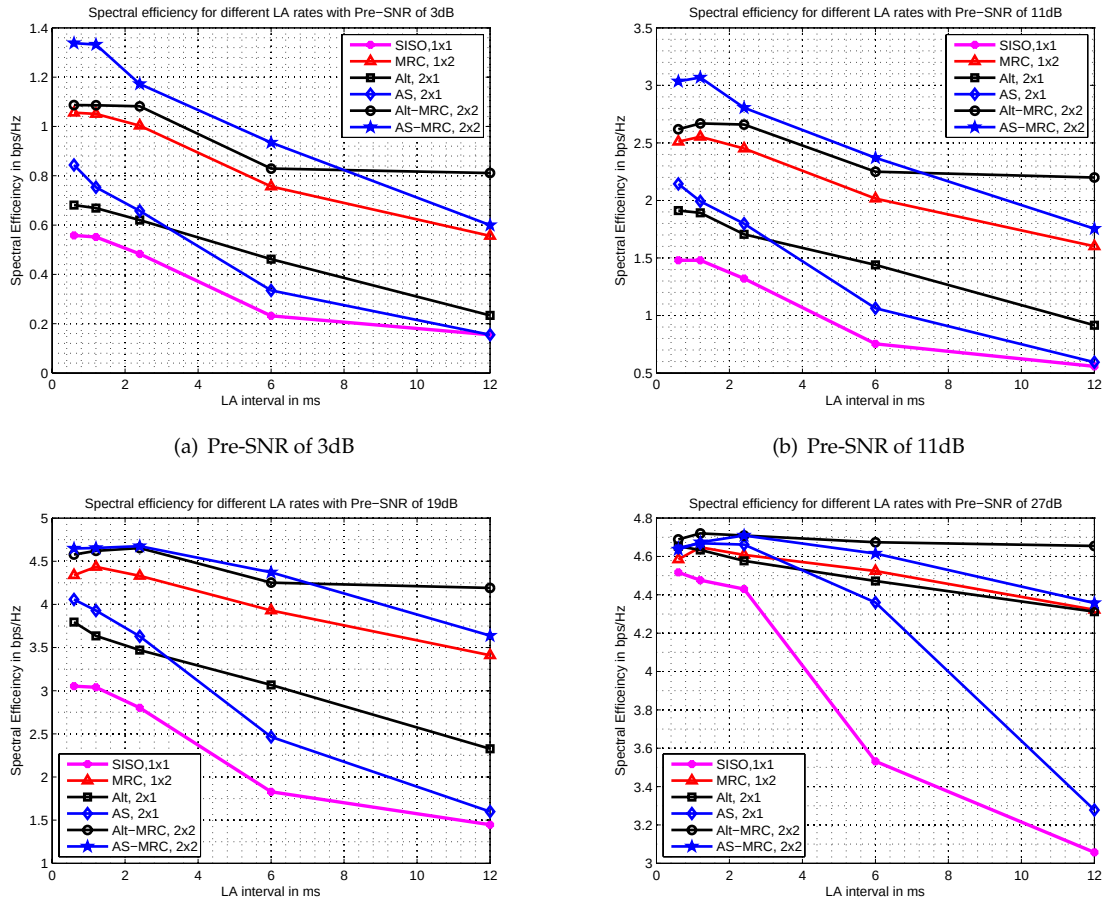

(a) Pre-SNR of 3dB

(b) Pre-SNR of 11dB

(c) Pre-SNR of 19dB

(d) Pre-SNR of 27dB

Figure 5.15: Spectral efficiency results for different MIMO schemes for different LA rates at different levels of Pre-SNRs

due to MRC at the receiver. Obviously, the performance of 1×2 MRC and 2×2 AS-MRC at 12ms adaptation window is very close for all the SNRs.

- As concluded earlier in Section 5.5.2, non-CSI based transmit diversity schemes are more suitable in terms of achievable spectral efficiency when the adaptation window is not very large. At larger adaptation window, the CQI from MS that is sent back to BS can be obtained by averaging the SNRs inside the window. In that case, the feedback SNR is an average parameter, thus, non-CSI based schemes perform better. If the CQI from first frame is used for AMC decisions, then we will actually use the outdated CQI, thus again, combination of Alamouti-based transmit diversity and MRC-based receive diversity is a good choice, as both of these schemes provides diversity without CSI and MRC also provides array gain. For all the SNR regions, we can see that the spectral efficiency loss due to increasing adaptation window in STBC-MRC scheme is much less compared to others. We can see that when the window in increased beyond the coherence time compared to a window equal to the coherence time, then the loss is insignificant.

© Muhammad Imadur Rahman, 2007

- At high SNR, the available diversity order and array gain play much more significantly compared to lower SNR regions. The gains from MRC and Alamouti are quite evident. In this case, 2×1 AS scheme fails with larger adaptation window as seen in Figure 5.15(d), as the chosen bit and power level is not correct anymore. For 2×2 AS-MRC, although the decided bit and power level is not correct, but the MRC gains are still beneficial, so we see that 2×2 AS-MRC approaches 1×2 MRC at higher SNRs.

5.6 Chapter Summary

In this chapter, we describe our studies related to suitable link adaptation algorithms to be used for broadband OFDM type systems. After that, we have studied the interaction between link adaptation scheme and spatial diversity techniques.

Simple Adaptive Modulation and Power Distribution Algorithm (SAMPDA)

An algorithm, namely Simple Adaptive Modulation and Power Adaptation Algorithm (SAMPDA), for bit and power loading in OFDM systems is presented. The algorithm has been compared against two other algorithms, namely Simple Rate Adaptation (SRA) and Adaptive Power Distribution (APD). One of the algorithms is highly efficient but needs very high number of iterations to assign the best bit and power load for the sub-carriers. The second algorithm has a lower spectral efficiency and uses very low number of iterations (low complexity). The studied algorithm is found to provide a spectral efficiency as good as the first one in the entire range of operation, which is 15% to 33% better than the low complexity algorithm. The number of iterations of the proposed algorithm is immensely lower than the more complex algorithm but slightly higher than the simple algorithm. Therefore it can be said that the proposed algorithm exploits the best of the two algorithms in attaining the highest throughput but at a much lower complexity making it more realizable.

An adaptive sub channelization scheme is proposed instead of regular fixed sub channel size. It is found to provide improved performance over fixed sub-channelization, but it is very difficult to evaluate the real gains since it is closely coupled to feedback mechanisms used. Impact of larger adaptation window in time (adaptation

Interaction between Link Adaptation and Spatial Diversity

We have studied several combinations of bit and power allocation approaches in multi-antenna systems in this chapter, so that the throughput can be optimized without increasing much of the system complexity. We conclude the following:

1. Multi-antenna techniques in general improve the resultant spectral efficiency of the system, compared to SISO systems.

2. for instantaneous link adaptation possibilities, it is always suitable to use the MIMO mode that depend on CQI. This will provide added array gain and will improve the system throughput performance.

3. When the window of LA procedure is large (i.e. T_c is smaller or comparable to LA window size in time), then MRC and Alamouti-type schemes are more useful, as the channel information is averaged due to the large window size, and only non-CQI based MIMO schemes are useful in this scenario.

© Muhammad Imadur Rahman, 2007

6

Multi-Dimensional Link Adaptation Strategies

In Chapter 5, we have studied different link adaptation algorithms and evaluated the gain obtained from multi-antenna techniques in collaboration with link adaptation algorithms.

In this chapter, we study link adaptation possibilities across several dimensions, such as bit allocation, power allocation, sub-channel size, channel coding level, AMC rate, adaptation window size etc. We have combined all these dimensions and analyzed them under one framework for a simplified, yet spectrally efficient link adaptation process for broadband OFDM system.

The potential of simultaneous power and bit allocation is studied in Section 6.1. In Section 6.2, we explain the hybrid strategies for LA in different channel and system conditions, by exploiting several degrees of freedom that OFDM provides. In Section 6.3, we have described the transmitter non-linearity issue in regard to link adaptation algorithms.

6.1 Role of Power Adaptation in Collaboration with Bit Adaptation

In a system where modulation, channel coding and transmit power across OFDM sub-channels are adapted in real time, the adaptation algorithms are usually quite complex. One such algorithm is proposed in Section 5.2.3 (and also in [109]). In this case, the algorithm has to take care of the fact that the total power is constant and a threshold BER, or FER needs to be met. There are other

sub-optimal algorithms where different combinations of bit and power adaptation can be done. It is much easier to assign equal power across all OFDM sub-channels and then determine the allowable modulation and coding level for any particular sub-channel, such a method is called Adaptive Modulation and Coding (AMC). In AMC, the complexity of LA procedure is reduced compared to AMC with dynamic power allocation[1]. Usually it is related that AMC and power allocation is not suitable to be carried out at the same rate in any wireless systems. Several authors previously suggested that, when a point-to-point wireless link is considered, then AMC with dynamic power allocation does not provide any significant improvement in throughput in comparison to only AMC-based systems [20, 110, 111, 112]. Some of these articles suggest that it is not recommended to perform the AMC in collaboration with adaptive power distribution due to excessive system complexity. In [14], the same is suggested for multi-user OFDM system.

In this section, we have studied bit and power allocation strategies for multi-antenna assisted OFDM systems. Contrary to the suggestions in the above mentioned articles, we have found that in some scenarios and in some system conditions, some form of power adaptations along with bit allocations across OFDM sub-channels are required together for efficient system performance. For broadband OFDM systems, the channel variations are quite high inside the OFDM system bandwidth, thus dynamic power distribution is advantageous together with AMC. This is in-line with the conclusions made in [113]. Using different LA mechanisms, we have found that, when we cannot find the exact SNR thresholds due to different reasons, such as reduced LA rate, CSI error, feedback delay etc., it is better to fix the transmit power across all sub-channels to guarantee the target FER. Then the power allocation will actually act as safety margin for the impairment up to a certain degree. Otherwise, we can use adaptive power distribution to save power, which can be used for other purposes, or we can increase the modulation level to increase the system throughput. These benefits are even more visible when multi-antenna schemes are used in the system.

Our investigation is mainly concentrated on different bit and power allocation rates in OFDM systems. In Section 6.1.1 we study the impact of both adaptations at the same rate and in Section 6.1.2, the adaptations at different rates are investigated.

6.1.1 AMC and Power Adaptation at Same Rate

In this section, we study bit and power adaptation in the same rate, so the adaptation window for bit and power allocation is always same. In this way, both of the allocations are impacted in the same way by the channel conditions and user mobility.

As we have seen in Section 5.4, when the adaptation window is only one frame long, then the channel conditions are quite static for the Doppler conditions that we are considering here. Thus, we can say that the feedback CQI is almost correct according to the channel condition when the LA decisions are implemented. Figure 5.13(a) points out that the resultant FER is well below the FER threshold when instantaneous AMC is done. Thus, we clearly see that some power is wasted when only AMC is done. When we also adapt the power after the AMC decisions are made, we find that the FER threshold is still maintained. Now, we need to look at the corresponding spectral

[1] We have described two LA mechanisms in Section 5.4.2, where AMC with dynamic power allocation is used. According to that description, *AMC with Adapted Power* and *Adaptive Power, Modulation and Coding (APMC)* fall into the category of *AMC with dynamic power allocation*.

efficiency curves as shown in Figure 5.13(b). Intuitively, when some power is removed after power adaptation, the spectral efficiency should be lower. But, we can observe that the spectral efficiency is almost equal with and without power adaptation. Note that, in this case, the power adaptation essentially means that we are saving some power, which is described in Figure 6.1(a) and discussed later.

For outdated feedback case as in Figures 5.14(a) and 5.14(b), we should find new AMC thresholds compared to the original AMC thresholds used in previous simulations. These new threshold margins can be found via monte-carlo simulations. In Figure 5.14(a), we can see that the FER threshold is not met when AMC is followed by power adaptation. This is the case when the adaptation window is equal to 2.4 ms, i.e. 4 frames. In the same scenario, the fixed power based mechanism works well. As we are having slower rate of adaptation, we practically need a a new threshold (which is obviously higher than the previous one) for the slower adaptation rate. In this case, extra power available after bit and coding rate allocation compensates for the required additional power when the adaptation is slowed down. As seen in Figure 5.14(b), the spectral efficiency is almost the same when the power is adapted and the power is fixed for all the schemes, but the FER threshold is not met when power adaptation follows the AMC procedure. Compared to Figure 5.13(b), a loss in spectral efficiency is experienced when wider adaptation window is used.

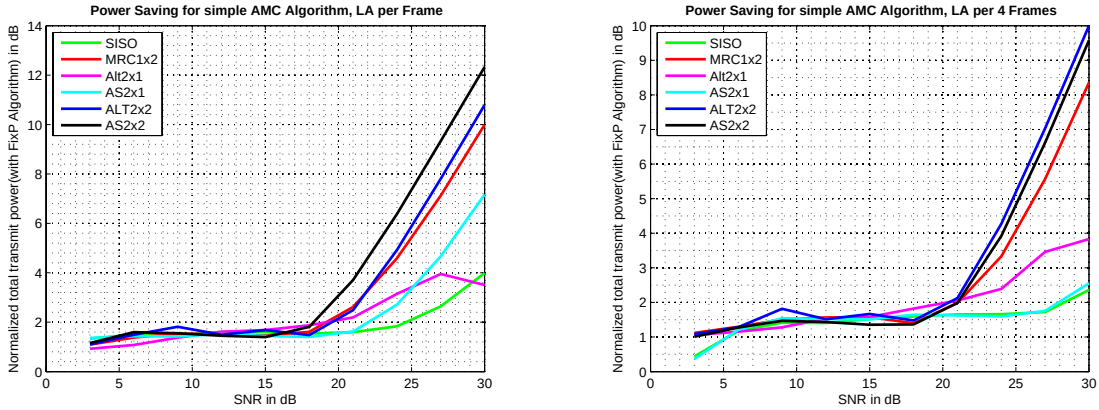

(a) Instantaneous adaptation

(b) Slower adaptation

Figure 6.1: Power savings of different link adaptation rate with and without power adaptation. Ensemble average of the ratio of total transmit power required between *AMC,AdaptP* and *AMC,FixP* is plotted against the average Pre-SNRs.

Figures 6.1(a) and 6.1(b) summarize the resultant saving of power when AMC followed by a power adjustment is done, in comparison to only AMC scheme. We can see that significant amount of power can be saved for instantaneous adaptation. When the system SNR is roughly more than 20dB, the power savings to meet the FER requirement is more than 2dB. When the average SNR increases, the power saving increases very much. This result demonstrates that power allocation also has a role to play in WiMAX like broadband OFDM systems, though it is originally claimed that power allocation does not bring much more benefit when AMC is already done [20],[107]. As expected, the power savings becomes irrelevant when the adaptation window is longer. In

© Muhammad Imadur Rahman, 2007

this case, the power saving is done, but the threshold FER is not met. Thus, we see a throughput degradation.

The saved transmit power can be used for many other purposes in the system. For example, more bits in particular sub-channel can be transmitted. Thus, a window of opportunity arises when we do the power adaptation in collaboration with AMC. In a multi-user scenario, the saved power can be allocated to a user with weaker SNR and system spectral efficiency can be improved in that way.

Impact of Different Power Adaptation Algorithms

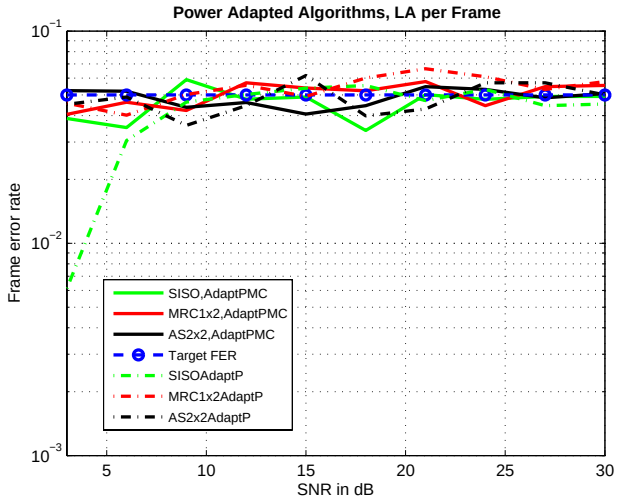

Figure 6.2: FER results of instantaneous link adaptation with different power adaptation

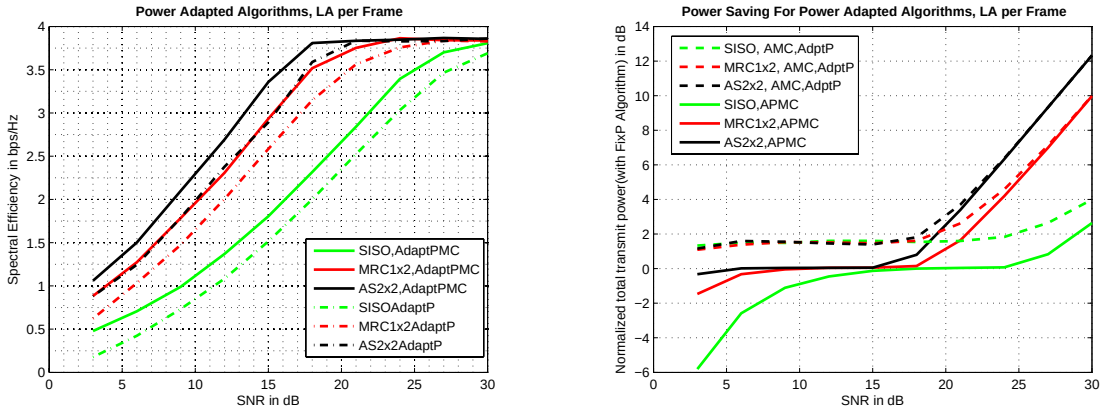

(a) Spectral Efficiency (b) Power Saving

Figure 6.3: Spectral efficiency and power saving of instantaneous link adaptation with different power adaptation mechanisms

Figures 6.2, 6.3(a) and 6.3(b) give us the FER, resultant spectral efficiency and power savings

respectively, when we use two different power adaptation mechanisms. In these results, APMC refers to our optimal SAMPDA algorithm as developed in [109] (and described in Section 5.2.3), and AMC with sub-sequent power adaptation refers to power adaptation applied after AMC decision is made (labeled as *'AMC,AdaptP'* in figures). At low SNR regime, APMC will utilize more power than AMC with power allocation. APMC algorithms (e.g. SAMPDA) do not assign any bit to any weaker sub-channel (i.e. withdraws power from the weaker sub-channels), rather it concentrates the available power across sub-channels where some bits can be transmitted. For the case of AMC with power adaptation, not many bits can be transmitted at low SNR, so throughput is very low (as seen in Figure 6.3(a)), although some power saving is seen in Figure 6.3(b). In the same figures, we can see that APMC is able to transmit significantly higher throughput even at very low average SNR, because APMC allocates most of available power at some sub-channels where some bits can be transmitted. So, we can conclude that APMC utilizes the total available power efficiently. This throughput optimization in APMC is obtained at the price of added complexity in the LA algorithm. At high SNR regime, both these algorithms can save power, but APMC will utilize the available power more efficiently than AMC with adapted power to achieve a better throughput performance.

In these results, we have only shown the FER, throughput and power saving performances for fast (or instantaneous) LA rate, because both AMC with adapted power and APMC can maintain the FER target at fast LA rates, while at low LA rate, an additional margin is needed, as seen in Figure 5.14(a).

6.1.2 AMC and Power Adaptation at Different Rates

Conventional wideband systems, such as Global System for Mobile communication (GSM) and Wideband Code Division Multiple Access (WCDMA), use a mixture of AMC and Power Control (PC), which can broadly be classified as Adaptive Power Fixed Rate (APFR) method, where one strives to adapt the power for maintaining required throughput over the duration of communication. On the other hand, systems like HSDPA, use another class of methods, namely Fixed Power Adaptive Rate (FPAR) method, where modulation and coding rate is adapted enabled by the momentary channel quality using fixed power [114]. In our previous discussions, we have studied different combinations of APFR and FPAR-type LA methods. For OFDM-like multi-carrier systems, APFR is not a good solution, because using APFR means we will not be able to exploit the available frequency diversity of the channel. OFDM enables us to exploit the channel gains up to sub-carrier level, and this degree of freedom should be exploited. Thus, a mixture of AMC and PC will always be a preferable solution.

Until now in our discussions, we have used the WiMAX system parameters for our analysis and evaluations for different LA issues. From this point onwards until the end of this chapter, we use another set of parameters taken from UMTS-LTE standard. The parameters are listed in Table 6.1.

In Section 6.1.1, we have studied the role of simultaneous power and bit adaptations (i.e. AMC and PC at the same rate). We have concluded that simultaneous bit and power allocations are needed at some scenarios to ensure power savings at the expense of insignificant throughput

© Muhammad Imadur Rahman, 2007

Carrier frequency	2GHz
Bandwidth	5MHz
FFT size	512
Sub-carrier spacing	15kHz
Useful part of OFDM symbol	66.67μs
Frame duration	0.5ms
Adaptation window size	[1,2,4,10,20] frames
Adaptation window durations	[0.5,1.0,2.0,5.0,10.0] ms
Maximum transmit power	38dBm

Table 6.1: Parameters from UMTS-LTE Standard

reduction. In Section 6.2.4, the results show that, even at lower Doppler frequency values, the system throughput is severely degraded when the LA window is very large. In both of these sections, it is explained that instantaneous (or near instantaneous) AMC and PC is the best solution in terms of spectral efficiency. In reality, this requires frequent feedback from the transmitter to receiver; which can be of large amount compared to the available spectrum and link capacity. This can be very difficult to achieve in FDD systems. In TDD systems, the required CQI can be obtained without using any feedback channel, but, it still remains an issue that, the transceivers need to perform complex calculations on every frame to find out the possible modulation, coding and power level. This may require high processing power and also large processing time. For some traffic conditions, e.g. delay-intolerant real-time traffic, this can even be an inefficient scenario. One possible solution can be to use a fast PC while using slow rate control (i.e. AMC). For AMC, the required amount of feedback is much higher compared to PC, because AMC needs multi-level feedback for selected modulation and coding rate, while PC requires only a single bit (power up or power down) feedback. Thus, In this section, the performance for reduced AMC rates but with fast PC rates is investigated.

Figure 6.4 shows the concept of reduced LA with fast PC rates. The idea is to use a fast PC to compensate the SNR mismatching loss due to the time domain channel variation caused by slow AMC. It works as following:

1. Assume a slow AMC rate of every $T_{amc}\ ms$, and a fast PC rate of every $T_{pc}\ ms$, $T_{amc}/T_{pc} = K$ and K is an integer. It is understood that k is always greater than one.

2. Within one single data block, the power, modulation and coding rate for each sub-channel is found out using above mentioned LA algorithms. These levels are kept constant during the whole LA window.

3. In the beginning of the kth PC window ($1 < k \leq K$), MS will compare the instantaneous channel gain with the previous PC window. If the difference between the two channel gains is within a certain limit L_{unchg}, no change in bit, power or coding level is performed.

4. BS collects all the requirements for each block. In first step, BS decreases the power level to those blocks which require a reduction in power. However, the blocks that require an increase in the transmission power due to worsening channel conditions, BS need to consider the total power constraints by taking into account the saved power after bringing down the ones

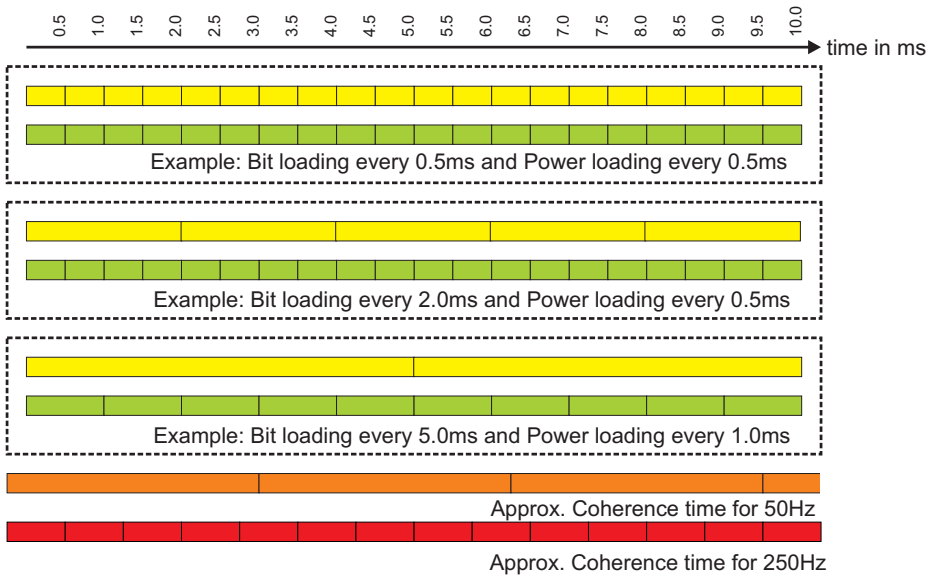

Figure 6.4: Examples of different power and bit allocations rates. For clarity, the coherence time related to 50 Hz and 250Hz is also shown.

mentioned before. Assume the granularity for bring down power is always G_{down} (which is typically 20% in our investigations) and the maximum granularity for increasing power is G_{up}. The increase in power, G_{up} can be decided dynamically. It can start from an increase of 20%, and then increase step-by-step until the the requirement of the sub-channel is met. Thus, the actual increasing in power level, $G_{up,actual}$, can be calculated as:

$$G_{up,actual} = \epsilon G_{pu} \quad \text{where } \epsilon = \min\{1, \frac{P_{av} + G_{down} \sum_{n=1}^{N_{down}} P_{k-1,n}}{G_{up} \sum_{n=1}^{N_{up}} P_{k-1,n}}\} \tag{6.1}$$

where N_{down} is the number of blocks which need less power and N_{up} is the number of blocks which need more power. $P_{k-1,n}$ is the power assigned for the nth block during the $k-1^{th}$ PC window. P_{av} is available power before redistributing the power and is calculated by:

$$P_{av} = P_T - \sum_{n=1}^{N} P_{k-1,n} \tag{6.2}$$

P_T is the total power constraint which indicates the up-limit for the total transmission power.

5. Step-3 is then repeated for each PC window within the same AMC window. Step-2 and Step-3 is repeated for each AMC window during the whole transmission time.

In this work, we take that $G_{up} = G_{down} = 0.2$. Figure 6.6(a) and 6.6(b) show the achievable spectral efficiency for different combination of AMC and PC rates, for low and high diversity conditions respectively. This analysis is valid when 16 consecutive sub-carriers are placed together in one sub-channel (i.e. $subN = 16$). For a better understanding of the ratio of time between the adaptation windows and channel characteristics, we can check Figure 6.4.

For low-diversity conditions, it can be seen that:

© Muhammad Imadur Rahman, 2007

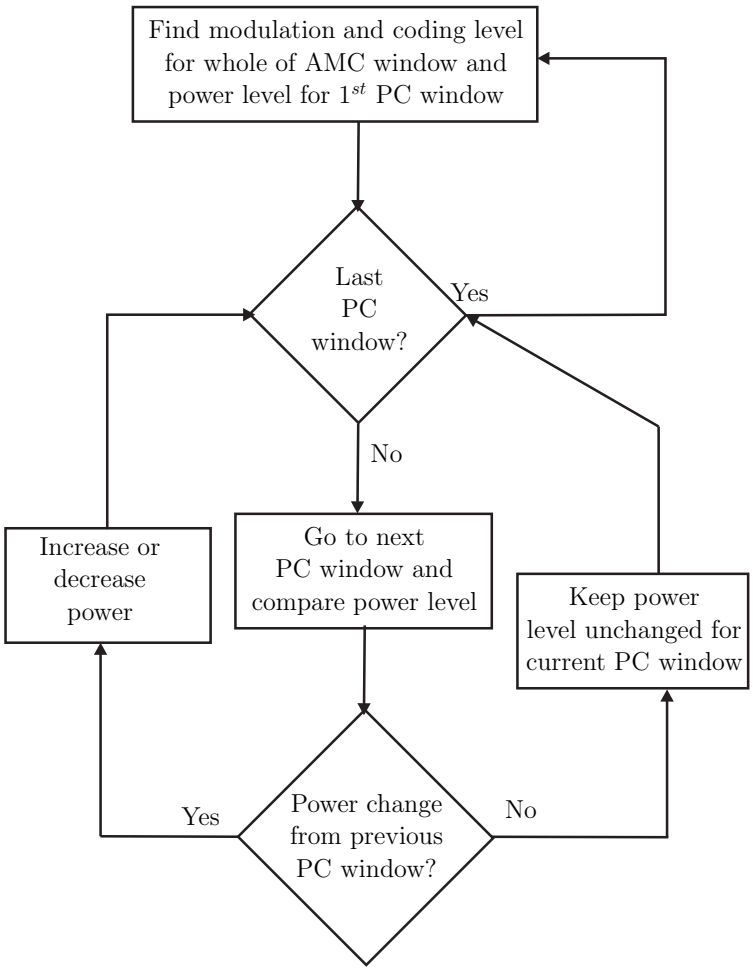

Figure 6.5: Flowchart of link adaptation mechanism when faster power control and slower AMC is used.

1. When AMC rate is less or equal to $1ms$, there is not much difference in performance compared to cases with faster power control.

2. When AMC is done every $2ms$, a faster PC rate of every $0.5ms$ can improve the performance compared to AMC at $2ms$ and PC at $1ms$ by $\sim 0.2dB$. It can also be noted that very fast power control (i.e. PC at $0.5ms$) reduces the need for faster AMC, which can be seen from the cases of AMC at $2ms$-PC at $0.5ms$, AMC at $1ms$-PC at $1.0ms$ and AMC at $1ms$-PC at $0.5ms$. These three cases are very similar in performance, thus, lower AMC rate can be chosen.

3. When AMC is done every $5ms$, both PC rates of every $0.5ms$ and $1ms$ give the same performance. For 50Hz of Doppler spread, the coherence time is $8.5ms$. So inside the AMC window of $5ms$, we will see some channel variations, thus, PC faster than $1ms$ is not beneficial. What is noticeable is that, when PC and AMC are both done at $5ms$, the spectral efficiency performance is degraded largely compared to AMC at $5.0ms$-PC at $1ms$. Once again, this proves that fast power control is striving to mitigate the SNR threshold imbalances caused by slower AMC rate.

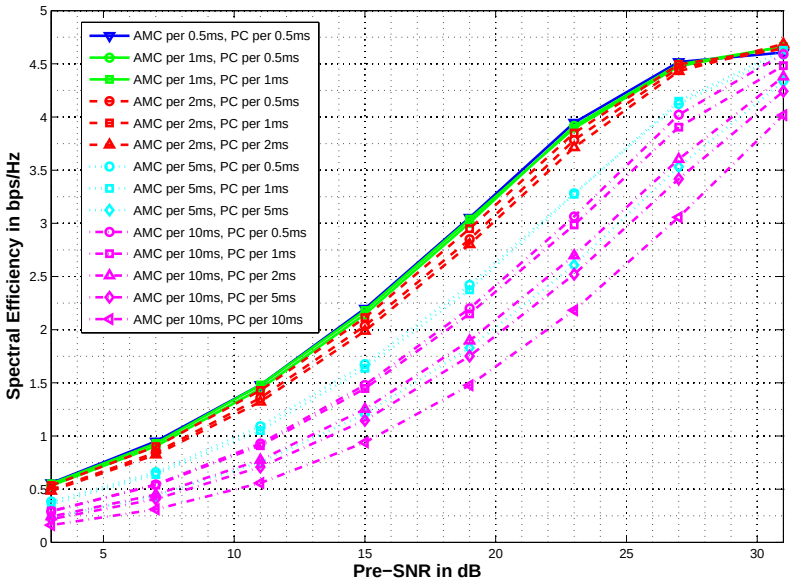

(a) Doppler 50Hz, RMS delay spread 0.5μs

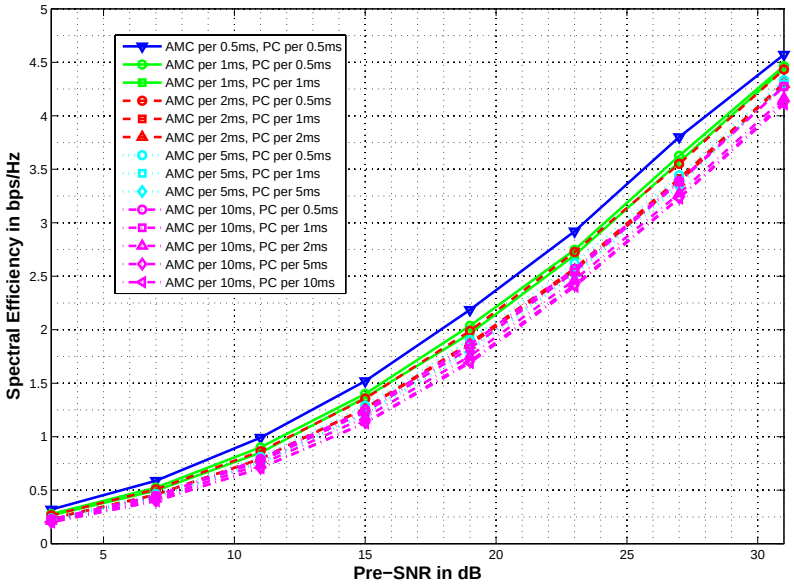

(b) Doppler 250Hz, RMS delay spread 2.0μs

Figure 6.6: Spectral Efficiency for Different AMC and PC Rates. PC rate is always higher than the AMC rate.

© Muhammad Imadur Rahman, 2007

4. Similar trends are seen for the case of AMC at $10ms$. The cases of AMC at $10ms$-PC at $0.5ms$ and AMC at $10ms$-PC at $1.0ms$ show that the resultant spectral efficiency is improved by almost 50% compared to the spectral efficiency of AMC at $10ms$-PC at $10ms$ case, as seen in the figure.

In essence, decreasing the AMC rate has severe impact on the system performance, as seen earlier also. In real-scenario, it may be required some times to reduce the AMC rate. In those cases, faster PC rates need to be implemented for acceptable level of system performance. For the particular system and user parameters as shown in Figure 6.6(a), PC rate of $1ms$ provides good performance for several AMC rate combinations.

Figure 6.6(b) shows the performance when $f_d = 250Hz$. As can be seen from this figure, with high Doppler frequency, PC gives very limited benefit as compared to low Doppler cases. This result is in accordance with Figure 6.10(b).

To conclude, reduced AMC rate can be used to reduce the system complexity. At high Doppler frequency, this reduced AMC rate will not affect performance much, while at low Doppler frequency, a large degradation can be observed for low AMC rate. By using PC at a fast rate, the combined performance can be improved at reasonably lower complexity than only fast AMC rate.

6.1.3 Overhead Analysis

In our work related to LA, we have mainly considering the gain in throughput obtained by bit and power adaptation, while this gain is obtained at a cost of increased overhead. For a proper system design, exact amount of overhead need to be measured, and also proper feedback mechanism needs to be found to minimize the feedback overheads while still maintaining the system performance at a satisfactory level. In this section, we do an initial evaluations of required feedback when different rates of AMC and PC are used.

Considering the discussions related to different rates of AMC and PC rates, we need to have a look at the required overhead bits for transporting the channel information between the transmitter and the receiver.

Following parameters are used for overhead estimates:

- N: total number of available sub-carriers,
- $subN$: Number of sub-carriers in one sub-channel,
- T_{amc}: AMC interval, i.e. $\frac{1}{T_{amc}}$ gives us the AMC rate
- T_{pc}: Power adaptation interval, i.e. $\frac{1}{T_{pc}}$ gives us the AMC rate
- $K = T_{amc}/T_{pc}$, an integer number representing AMC over PC duration,
- PC_{ix}: the index of power adaptation times within one AMC window.

We can divide the overhead in two parts, in Downlink (DL) and in Uplink (UL). Total overhead can be written as:

$$overhead_{total} = overhead_{ul} + overhead_{dl} \tag{6.3}$$

6.1.3.1 Overheads in Uplink

In the UL, we need to transmit two types of overhead information:

1. We need to transport the Channel Quality Information (CQI) from Mobile Station (MS) for informing the Base Station (BS) about the possible modulation and coding level that can be supported for each sub-channel. Thus, 5 bits (i.e. 2^5 levels of information) for one sub-channel will be fed back to the BS for the received SNR level.

2. For faster PC, we need to transport the $PA_{ix} = [2, ..., K]$. In this case, only 1 bit is needed per sub-channel per T_{pc} to indicate whether the power should go up or down. Note that, we are considering the situation when $T_{amc} > T_{pc}$.

So, we can express the overhead in UL as follows:

$$\begin{aligned} Overhead_{ul} &= \left[5 + \left(\frac{T_{amc}}{T_{pc}} - 1\right)\right] \frac{N}{subN} \frac{1}{T_{amc}} \\ &= \frac{(\frac{T_{amc}}{T_{pc}} + 4)N}{subN\ T_{amc}} \\ &= \frac{(K+4)N}{subN\ T_{amc}} \end{aligned} \tag{6.4}$$

6.1.3.2 Overheads in Downlink

In the DL, the BS needs to inform the MS about the modulation and coding level for each sub-channel. If we have 16 possible rate levels, then 4 bits for each sub-channel will be transmitted from BS via the control channels. This can be expressed as:

$$Overhead_{dl} = 4\frac{N}{subN}\frac{1}{T_{amc}} = \frac{4N}{subN\ T_{amc}} \tag{6.5}$$

6.1.3.3 Overhead Calculation corresponding to Our System Parameters

Using Eq.6.4 and Eq.6.5, we can write that the total system overhead expression as:

$$overhead_{total} = \frac{(K+8)N}{subN\ T_{amc}} \tag{6.6}$$

Table 6.2 presents amount of overhead signalling required for different combinations of AMC rate, PC rate and different sub-channel size. As seen in the table, highest amount of overhead is required in case of AMC at 1.0ms-PC at 1.0ms, while we have seen earlier that the achievable spectral efficiency is also very high at this adaptation rates. Depending on different channel conditions and different system complexity requirements, we can choose to increase both the AMC and PC rates. We can see that when AMC window is extended from 1.0ms to 10.0ms, we have approximately 80% less overhead requirement for all sub-channel sizes.

© Muhammad Imadur Rahman, 2007

T_{amc}	1.0ms	2.0ms		5.0ms		10.0ms
T_{pc}	1.0ms	0.5ms	1.0ms	0.5ms	1.0ms	1.0ms
subN=8	0.57	0.384	0.32	0.2302	0.1664	0.1152
subN=32	0.144	0.096	0.08	0.0575	0.0416	0.0288
subN=128	0.036	0.024	0.02	0.0144	0.0104	0.0072
subN=512	0.009	0.006	0.005	0.0036	0.0026	0.0018

Table 6.2: Overhead in Mbps for Adapt Power LA

6.2 Link Adaptation considering Several System Issues

As we have described in previous sections, Link Adaptation (LA) schemes adapt transmission parameters according to the channel conditions so that the maximum bit rate is achieved keeping the error rate below the target. Once the values of the adapted parameters are selected, they are kept constant over a region where the channel is relatively flat. OFDM with its fine granularity of the minimum allocation unit as a sub-carrier (or sub-channel), which experiences flat fading, provides the inherent support needed to exploit the advantage of LA techniques [109, 15] in multiple dimensions. The degrees of freedom that can be exploited by LA techniques increase when it is applied in OFDM systems and this leads to increase in complexity of the system with the benefit of improved spectral efficiency. LA involves adaptation of the modulation level (M), the FEC rate (C) and the power level (P) at the transmitter as per the channel state information fed back from the receiver. When applied in the OFDM framework, LA additionally includes selection of adaptation interval for M & C, adaptation interval for P, sub-channel size (a set of consecutive sub carriers that span across a few successive OFDM symbols), and choice of bit and power loading algorithms. Other than the fast fading of the channel gains, the dynamic variation of the channel parameters such as the RMS delay spread, Doppler frequency spread, average SNR condition, heavily influence the values to be selected for the LA parameters.

LA scheme, maximizing the throughput while maintaining a target error rate, is expected to become highly complex when it tries to adapt so many parameters optimally which depend on another large set of varying channel and system conditions. Therefore hybrid strategies, i.e. to limit to some of the degrees of freedom by slowly varying some parameters, while using fast adaptation for the others are investigated in this section. The objective is to analyze the tradeoff between spectral efficiency loss and complexity and overhead reduction that can be obtained by the hybrid strategies. When FEC with interleaving is considered in LA, as in this case, the interplay of sub-channel size, RMS delay spread, Doppler spread and adaptation window size becomes especially important. This is because, on one hand (frequency-time) diversity gain is brought by FEC while on the other hand LA with adaptive modulation and power loading exploits diversity in a different way. Therefore it is very interesting to study the synergy of these techniques, which is also one of the objectives of this section.

In this section, strategies for simplified LA, which reduce processing complexity but not compromising on throughput significantly, are presented. Results obtained in this perspective are also very important for multi-user resource allocation, since the resource unit to be allocated to one user must be such that there is maximum benefit in terms of overall throughput considering the signaling overhead. This work serves as a first step to such systems.

6.2.1 Strategies for Bit and Power Loading Algorithms

In this section, we examine different LA algorithms that can be used for OFDM-based systems. The goal is to understand their suitability in terms of throughput and power requirement, so that a good decision can be made about the LA mechanism to be used.

Three LA mechanisms, as it is explained in Section 5.4.2, are labeled in the forthcoming figures as follows:

1. Adaptive Modulation and Coding (AMC) with fixed power, denoted as *'AMC fixP'*
2. Adaptive Modulation and Coding (AMC) with adapted power, denoted as *'AMC adaptP'*
3. Adaptive Power, Modulation and Coding (APMC), denoted as *'APMC'*

6.2.1.1 Performance Comparison

The throughput comparison of the three algorithms mentioned above is shown in Figure 6.7(a). In the figures in this section, the legend '*u*' is used for '*micro seconds*, μs' which refers to the RMS delay spread of the channel. It can be seen that the three algorithms perform differently under different channel conditions. In all cases the APMC has the best throughput. The throughout results of *'AMC fixP'* is closely followed by *'AMC AdaptP'*. *'AMC fixP'* has almost similar performance to APMC, when there is high diversity in the channel condition, i.e. large Doppler and RMS delay spread, but it has notable performance loss in case of low Doppler and low RMS delay spread condition. Therefore it can be suggested that for low Doppler and low RMS delay spread condition (also moderate Doppler and moderate RMS delay spread conditions), APMC should be used. If APMC is computationally extensive for practical implementation, then we should use *'AMC adaptP'*, which will save some transmit power at the expense of negligible throughput loss compared to *'AMC fixP'*. When the diversity in the channel increases, i.e. high doppler and high RMS delay spread conditions, it is better to use *'AMC fixP'*. This is also in-line with our conclusions in Figures 5.13(a) - 5.14(b).

6.2.1.2 Power Utilization

Figure 6.7(b) shows the power utilization of the different algorithms. A low power utilization means low power transmission. This in turn means low interference condition in multi-cellular scenario, where aggressive frequency re-use is followed. In such a scenario, the algorithm which has the lowest power utilization, may be the best one to use. In this viewpoint the algorithm which brings down the transmit power to meet the threshold of the receive SNR, but avoids iterative power distribution seems to have the best performance under all channel conditions.

The power savings need to be studied together with throughput curves for making any decision about suitable LA procedure. We can observe a few issues by studying the power utilization results and throughput performances in Figure 6.7(b) and Figure, 6.7(a) respectively:

1. APMC makes best use of available power via the simultaneous power and bit allocations, because extra power from a 'strong' sub-channel is distributed to a 'weak' sub-channel so that

© Muhammad Imadur Rahman, 2007

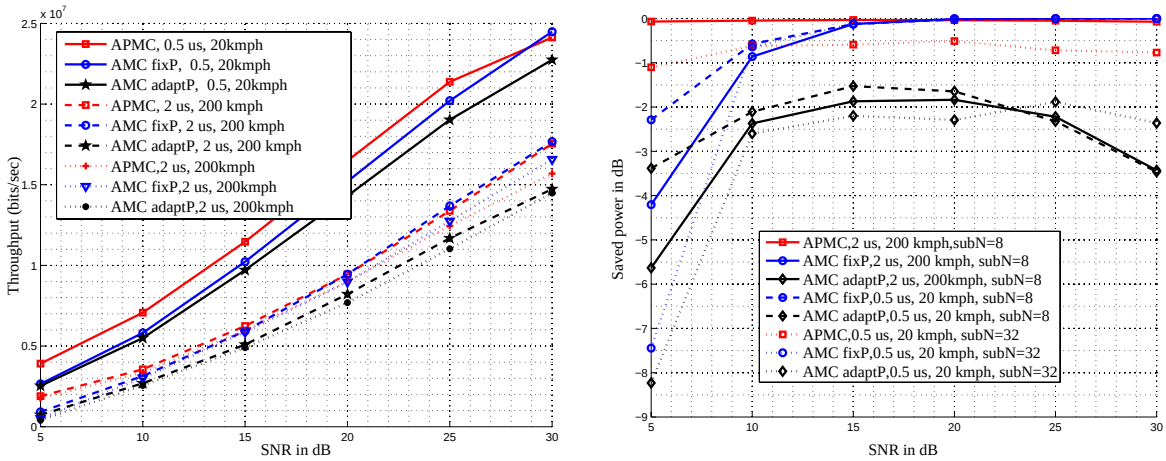

(a) Throughput performance (b) Power utilization

Figure 6.7: Throughput comparison (for subN = 8) and Power utilization of different Link adaptation algorithms at different RMS delay spread and Doppler conditions

some bits can be transmitted in that sub-channel. Thus, best results in terms of throughput is also achieved while all powers are used.

2. *'AMC adaptP'* saves a good amount of power at low SNRs, because all powers are withdrawn at 'weak' sub-channels (i.e. zero power allocation at 'weak' sub-channels), which cannot even support the lowest modulation scheme. This *saved* or *unused* power can be used for other purposes. At high SNRs, most sub-channels experience an SNR level which is higher than threshold power required for highest modulation scheme, thus, again significant amount of power is saved.

3. *'AMC fixP'* saves some power at low SNRs, because 'weak' sub-channels do not get any power, but, at high SNRs, all power is used and all sub-channels transmit at highest modulation and coding level.

6.2.2 Sub-Channelization

In this part the influence of RMS delay spread and Doppler velocity on different sub-channel sizes (8, 16, 32 and 64 sub-carriers in one sub-channel) is investigated. Figure 6.8 shows the spectral efficiency in terms of bps/Hz for LA system when AMC is done every 2ms while keeping P fixed (i.e. total available power is equally divided across all sub-channels for all frames). It can be seen from the figures that, when RMS delay spread is small and user velocity is low, i.e. coherence bandwidth and coherence time are large respectively, the sub-channel size of 8 sub-carriers has the highest throughput. At this sub-channel size, the channel is very flat inside whole of sub-channel, i.e. link adaptation gains will dominate over the frequency-time interleaving gains[2].

[2]Time-Frequency interleaving inside one sub-channel provides time-frequency diversity in any coded-OFDM systems, provided that the channel gains vary significantly inside the sub-channel duration and sub-channel bandwidth.

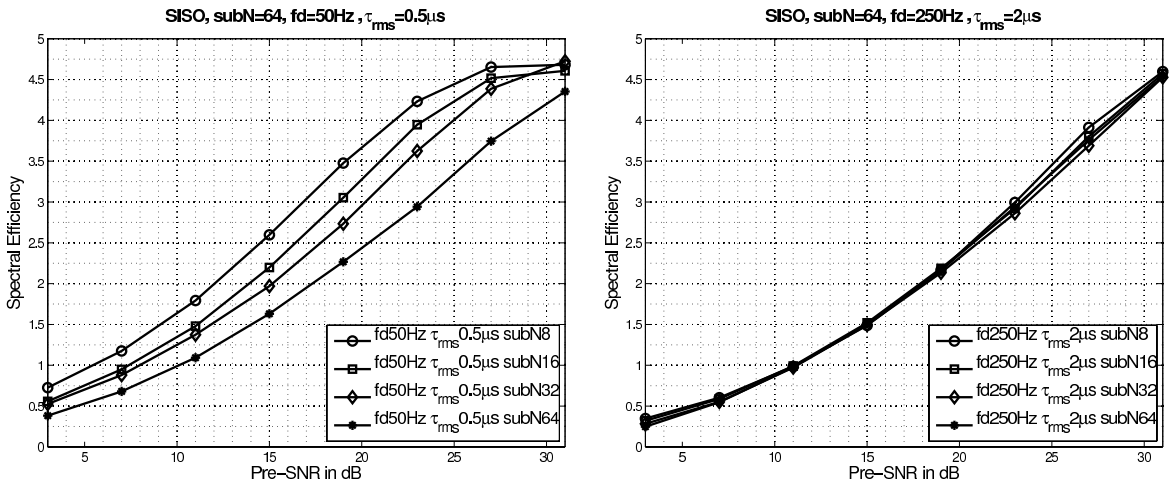

(a) Doppler 50Hz, RMS delay spread 0.5μs (b) Doppler 250Hz, RMS delay spread 2.0μs

Figure 6.8: Achievable spectral efficiency using different sub-channel sizes.

Interestingly at high velocity and high RMS delay spread i.e. small coherence bandwidth and small coherence time, the sub-channel size of 8 sub-carriers has very similar performance as that of sub-channel with 64 sub-carriers. This is because of the fact that the channel is already time- and frequency-selective inside the sub-channel space at low T_c and low B_c, even when only 8 sub-carriers are included inside one sub-channel. In this case, the interleaving gain is much higher compared to LA gain, thus, spectral efficiency is not improved for different sub-channel sizes.

Therefore, the LA performance is optimal in terms of throughput when the sub-channel size is small for low-diversity conditions. It can be concluded that for very high velocity and high RMS delay spread condition, it is better to use a large sub-channel size since it will somewhat lower the required overhead without reducing the achievable spectral efficiency, while on the opposite conditions of velocity and RMS delay spread, it is suggested to use small sub-channel size. It must be noted that sub-channel size selection can be a statistical adaptation in combination with instantaneous adaption of modulation and coding rate.

6.2.3 Fixed Coding Rate

In most references cited in this work, it is found that adaptive bit loading is considered without any constraint on user devices. The best bit loading may bring out a situation where more than one coding rate is allocated to one user. Though this might lead to a spectrally efficient system, this might not be feasible since it will put a heavy signal processing burden on the user equipment. Using multiple coding rates simultaneously in a dynamically fashion means that the user equipment needs multiple FECs and decoders, which would increase the complexity prohibitively. Therefore using only a single FEC coder (i.e only one FEC rate) for one user is highly desired. In a practical system, the FEC coding rate adaptation window can also be made long enough, to find a compromise between performance and signal processing requirements.

In this section, we would like to show the impact of channel coding on LA scenario. Thus

© Muhammad Imadur Rahman, 2007

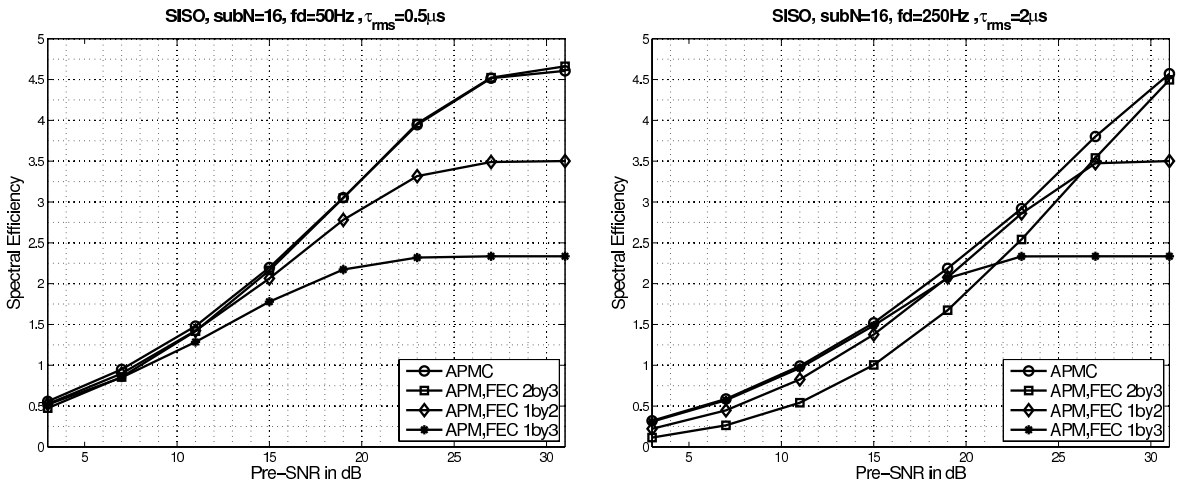

(a) Doppler 50Hz, RMS delay spread 0.5μs

(b) Doppler 250Hz, RMS delay spread 2.0μs

Figure 6.9: Spectral efficiency performance comparison for fixed coding with adaptive modulation vs adaptive modulation and coding.

we study the following:

1. All three dimensions, i.e. bit, power and code-rate is adapted dynamically on frame-by-frame basis;

2. Total transmit power is equally distributed across all sub-channels and coding rate is kept fixed while only modulation is varied on frame-by-frame basis, i.e. fixed P and C and varying M.

Figures 6.9(a) and 6.9(b) show the throughput comparison for different channel conditions when different form FEC-rates are used in the system. In the figures, *'APMC'* means adaptive power allocation, modulation and coding simultaneously, using our proposed SAMPDA algorithm. *'APM'* is used to denote adaptive bit and power allocation using the same algorithm, while the FEC rate is fixed. Figure 6.9(a) gives us the spectral efficiency results when low diversity channel (large B_c and T_c) is used, while Figure 6.9(b) presents the results when high diversity channel is used. In this case, 50Hz and 250Hz correspond to 15.43kmph and 77.14kmph respectively, similarly coherence time of 8.5ms and 1.7ms respectively.

As seen from the previous section, for the low diversity case as in Figure 6.9(a), the interleaving gain is non-existent, thus only coding gain is available. APMC always provides the optimal gain in all SNR ranges. Closer inspection reveals that rate-$\frac{2}{3}$ FEC approaches the performance of APMC when average SNR is higher than 12dB. For lower SNRs, rate-$\frac{1}{2}$ FEC is very close to the optimal results. This is because, in low diversity channels, coding gain plays the important role. For SNRs even lower than that, rate-$\frac{1}{3}$ performs a little worse in spectral efficiency compared to rate-$\frac{1}{2}$. For high-diversity channels, as seen in Figure 6.9(b), we can now see more gains due to channel coding and interleaving for different ranges of SNRs. Up to 18dB of average SNR, rate-$\frac{1}{3}$ can be used, while rate-$\frac{1}{2}$ can be used for SNRs between 18dB to 25dB. Beyond this, rate-$\frac{2}{3}$ can be used.

FEC		$\frac{1}{3}$	$\frac{1}{2}$	$\frac{2}{3}$	$\frac{1}{3}$	$\frac{1}{2}$	$\frac{2}{3}$	$\frac{1}{3}$	$\frac{1}{2}$	$\frac{2}{3}$	$\frac{1}{3}$	$\frac{1}{2}$	$\frac{2}{3}$
τ_{rms}	f_d	$subN = 8$			$subN = 16$			$subN = 32$			$subN = 64$		
0.5	50	NA	NA	-	NA	NA	-	-	16	24	-	18	27
	150	NA	-	19	-	13	19	-	18	25	-	19	27
	250	NA	-	18	-	16	23	-	17	26	-	20	28
1	50	-	11	16	-	15	24	-	18	27	-	19	28
	150	NA	-	19	-	13	19	-	19	27	-	20	28
	250	NA	-	21	-	16	24	-	17	27	-	20	29
2	50	-	14	23	-	17	26	-	20	27	-	20	28
	150	-	16	24	-	19	26	-	18	27	-	20	28
	250	-	17	24	-	19	27	-	19	27	-	20	27

Table 6.3: Average SNR thresholds (in dB) for switching coding rate for different RMS delay spread and Doppler condition

Figures 6.9(a) and 6.9(b) provide us the results when the sub-channel size is 16. As discussed in the previous section, we understand that different sub-channel sizes will also have an influence on thresholds for choosing different FEC rates. Table 6.3 summarizes the switching thresholds for all the sub-channel sizes, different doppler frequencies and delay spread values. The mark '-' indicates that coding rate is the default coding rate to start with, while the SNR values indicate the starting average SNR from where the particular coding rate can be used, and 'N.A.' indicates that the corresponding coding rate will not be used. In those code rates, the target FER is not achieved even at very high SNR, thus we exclude those code rates.

It can be seen that the performance of different fixed coding rate at different ranges of SNRs is not very far from the optimal APMC scheme. If average SNR is used as the threshold for switching between one coding to another, then one user can choose a coding rate based on the average channel SNR information and then use adaptive modulation.

6.2.4 AMC Rate

Modulation	4QAM			16QAM			64QAM		
Coding Rate	1/3	1/2	2/3	1/3	1/2	2/3	1/3	1/2	2/3
LA per 1	5dB	8dB	11dB	NaN	14dB	17dB	NaN	21dB	23dB
LA per 2	5dB	9dB	11dB	NaN	15dB	17dB	NaN	21dB	24dB
LA per 4	6dB	10dB	12dB	NaN	16dB	19dB	NaN	22dB	25dB
LA per 10	10dB	13dB	16dB	NaN	19dB	23dB	NaN	25dB	28dB
LA per 20	12dB	16dB	18dB	NaN	22dB	25dB	NaN	28dB	31dB

Table 6.4: SNR Lookup Table for SISO with Different AMC Rates

In Section 6.2.2, we have studied the impact of different size of adaptation space by varying the sub-channel size, i.e. the adaptation window was varied in frequency domain. In this section, we would like to investigate the impact of different AMC rates, i.e. we will study the varying adaptation in time-domain when the sub-channel size is fixed. The adaptation window can be varied in time by including varying number of OFDM symbols inside one LA space. Here, the power is kept constant, while modulation and coding rates are adapted.

© Muhammad Imadur Rahman, 2007

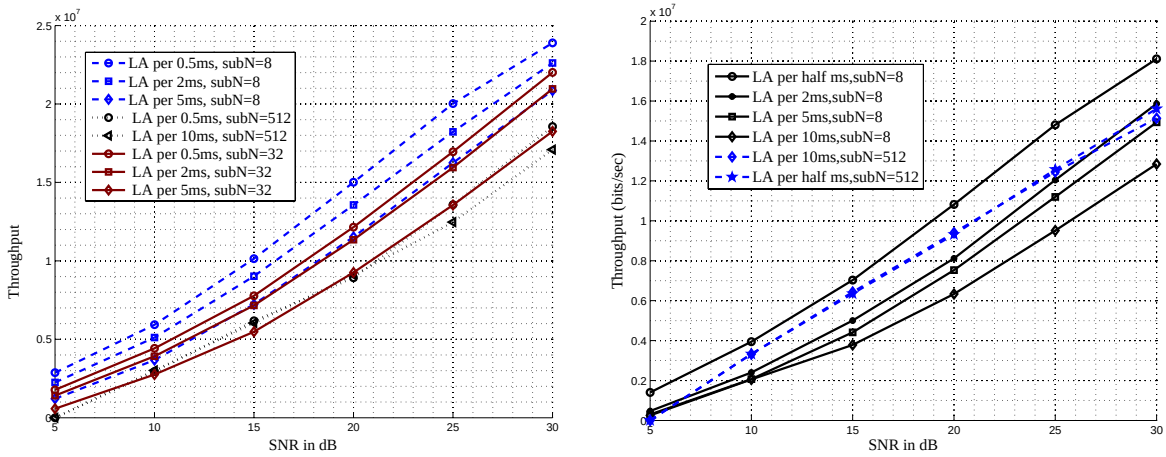

(a) Doppler 50Hz, RMS delay spread 0.5μs

(b) Doppler 250Hz, RMS delay spread 2.0μs

Figure 6.10: Throughput comparison for different bit adaptation rates

Figure 6.10(b) shows the impact of changing the adaptation rate for high-diversity channels. Corresponding SNR look up table is shown in Table 6.4. It can be observed that when the sub-channel size is small there is strong impact of the adaptation rate, but when the sub-channel size is very large, then adaptation rate has hardly any influence. It can also be seen that for low and moderate average SNR levels at this kind of channel conditions (RMS delay spread of 2 μs at 77.14kmph) a large sub-channel size can be good enough, in this way, the overhead for signaling the LA modulation and coding level can be minimized. It may also be concluded that with these channel conditions low rate link adaptation with a large sub-channel size may be selected, thus, the adaptation window in time and frequency can be quite large. This conclusion is in-line with our understanding from Figure 6.8.

Figure 6.10(a) shows similar performance comparison but for low diversity situation i.e. RMS delay spread of 0.5μs and 15.43kmph of velocity. It can be seen that there is a large impact of the decreased adaptation rate as in the earlier case for sub-channel size of 8 sub-carriers and also to some extent for sub-channel size of 32. When sub-channel size is made large there is little impact on the adaptation time interval; i.e. short term adaptation in time domain is not necessary when the adaptation window is large in frequency domain even in low mobility conditions. Compared to the previous case there is difference in performance between large and small sub-channel sizes.

6.3 Influence of Transmitter Non-linearities

Despite many advantages, OFDM suffers from the high Peak to Average Power Ratio (PAPR) problem. OFDM symbol is generated by superimposing several carriers when FFT based OFDM modulation is done at the transmitter. These carriers may add up constructively which results in high Peak to Average Power Ratio (PAPR). When this signal with high PAPR passes through the High Power Amplifier (HPA), which has a nonlinear transfer function [8], in-band and out-band regrowth occurs [115]. This in turn causes Frame Error Rate (FER) degradation and Adjacent Channel

Interference (ACI) [8], [36].

Backing off the operating power of the amplifier by a certain amount helps to reduce the non linear distortion effect [115]. The larger the power Back-Off (BO), the higher the reduction of the distortion effect. On the other hand, it reduces the total available transmit power which affects the coverage area and achievable throughput of the system. Therefore, it is aimed that minimum BO is used while optimizing the Block Error Rate (BLER) performance by limiting the signal distortion. It is also known that the amount of BO needed for optimum performance varies for different modulation and coding schemes [116]. Since LA employs varying modulation, power and coding rate, hence fixed value of BO power will not optimize the performance. So, it becomes important to analyze the impact of nonlinearity in OFDM system that uses rate, modulation and power adaptation.

To the best of our knowledge, very little attention is given to the performance of adaptive OFDM systems under the effect of non linear distortion. In [116], we have analyzed performance of uncoded system for a first hand analysis where significant influence of PAPR has been found on LA schemes. Although the implementation of FEC with interleaver improves the FER performance significantly, the effect of nonlinear distortion cannot be combated completely with it. It is therefore important that OFDM systems using LA with FEC and interleaver be investigated for practical implementation in WiMAX-like system which is the focus of this part of the thesis.

In this section, based on a well-known HPA model, we study the impact of HPA non-linearity and the required power BO on the FER results when different combinations of modulation levels are used for LA. Based on these results, we show the total degradations due to transmitter non-linearity and signal distortion for different combinations of modulation with coding schemes. We also study the Signal to Distortion and Noise Ratios (SDNRs) and it is shown that SDNR at the transmit side is independent of modulation and coding rate while dependent on amount of BO power employed. Based on the above mentioned results from these evaluations, it is identified that thresholds for switching between modulations need to be updated. Accordingly, new threshold values have been found for mitigating the HPA impacts. With these new threshold results, we study the throughput results when different combinations of modulation and coding rates are used. These results will serve as strong indication on how to design the LA thresholds when we consider the PAPR impairments.

6.3.1 Interaction between PAPR and Link Adaptation

6.3.1.1 Effect of HPA on signals with High PAPR

The HPA model used in this work is according to well-known Rapp's Model [117]. The HPA model for AM/AM conversion is simulated using the following relation [8]

$$g(x) = \frac{|x|}{(1 + |x|^{2\iota})^{\frac{1}{2\iota}}} \tag{6.7}$$

where x is the signal amplitude and the variable ι is used to tune the amount of nonlinearity. A good approximation of existing HPA can be obtained by choosing ι in the range of 2 to 3. For large values of ι, the model converges to a clipping amplifier. This clipping amplifier is perfectly

© Muhammad Imadur Rahman, 2007

linear until it reaches the maximum output power level, which is very hard to achieve in practical systems. The available literature suggests that the AM/PM conversion for Solid State Power Amplifier (SSPA) is small enough to be neglected [8].

If we denote the discrete time-domain samples at the output of Inverse Fast Fourier Transform (IFFT) in an OFDM system as $x(t)$, then the PAPR can be defined as,

$$PAPR = \frac{\max[|x(t)|^2]}{E[|x(t)|^2]} \tag{6.8}$$

The signal is fed to the input of the HPA. The output of the HPA depends on the nonlinearity parameter p given by the Eq.(6.7). Output of the HPA can be written as

$$y(t) = \alpha \cdot |x(t)|^2 \cdot e^{j\angle x} + n(t) = f(|x|^2, \alpha), \tag{6.9}$$

where α is an attenuation constant depending on the power BO value and $x(t)$ and $n(t)$ are uncorrelated. $n(t)$ is the additive white Gaussian noise present at the receiver.

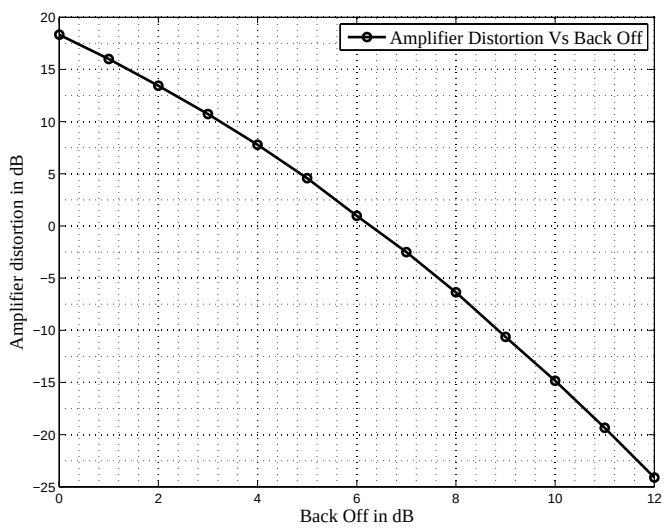

Figure 6.11: Amplifier distortion with different power BO

The variance of the distortion caused by the amplifier is given by,

$$\sigma_D^2 = E[x(t)|^2 - f(|x|^2, \alpha)] \tag{6.10}$$

Figure 6.11 shows the relation between distortion with power BO of the HPA. This is clear from the figure that with increasing power BO, the signal operates more in the linear region and hence decreases the amount of distortion, at the cost of amplifier inefficiency.

Using the above definitions, the SDNR at the transmitter side can be written as,

$$SDNR_{Tx} = \frac{f(|x|^2, \alpha)}{\sigma_D^2 + \sigma_w^2} \tag{6.11}$$

where σ_w^2 is the variance of white gaussian noise. This SDNR expression takes distortion due to amplifier in to account. Since this distortion is due to nonlinearity of power amplifier, it is independent of modulation scheme used.

Figure 6.12 shows the SDNR plots when 64-QAM modulation is used. For any certain BO, the SDNR saturates when operating SNR is increased beyong a certain value. This means that, for this BO condition, the SDNR cannot be increased any more by simply increasing the operating SNR. For lower BO, this saturation point is reached much faster compared to higher BO cases. Since with different power BO, SDNR behaves differently, the selection of BO should be done carefully to achieve optimum performance.

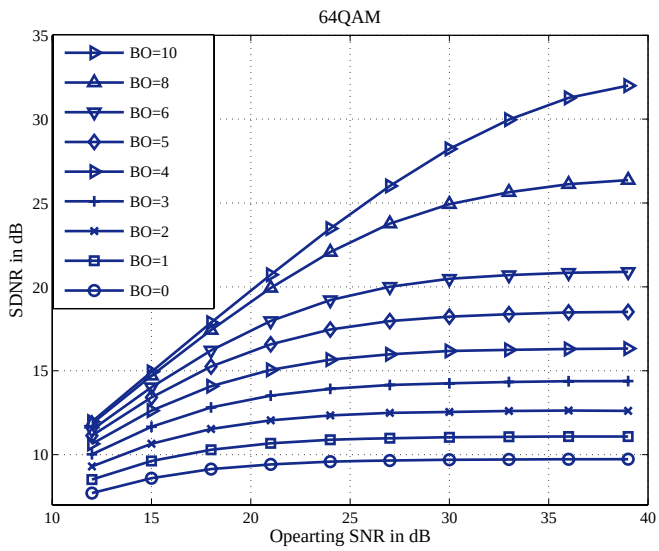

Figure 6.12: SDNR plot for 64-QAM in AWGN channel.

For LA based system, thresholds are the function of SNR distribution [20]. Since the Eq.(6.11) clearly shows that the SDNR is function of α which influences the amount of amplifier power BO, thus, the switching thresholds for adaptive modulation also become dependent on α. This means that the Look-Up Table (LUT), which contains the threshold values for different modulation and coding rate at certain FER constraints, needs to be updated. For uncoded system, it is possible to obtain analytical expression for revised threshold. However, this is not applicable to coded system. Since almost all practical system, as well as system under investigation, i.e. WiMAX, uses FEC coding, analytical expression obtained for uncoded system will not be usable. Therefore, computer based simulations are used in this work in order to find the additional margin needed to update LUT in order to maintain the QoS constraint.

6.3.1.2 Impact of HPA on Coded and Uncoded OFDM System

Figure 6.13 shows the symbol constellation for 16QAM with 1/2-rate convolutional coding for two different BO values of 3dB and 6dB respectively. $HPA = 1$ in Figure 6.13 means that HPA is used in the evaluations. It is clearly seen that the impact of BO on symbol error probability is severe which justifies further investigation into the impact of HPA and BO on LA system performance.

© Muhammad Imadur Rahman, 2007

In the forthcoming discussions, we always take the non-linearity tuning parameter as, $\iota = 2$, as seen from Eq.(6.7). This is the worst case scenario in terms of linear region of power amplifier operation curve. Following the HPA-affected constellations diagrams shown in Figure 6.13, we have tested the BERs and FER of uncoded and coded OFDM system.

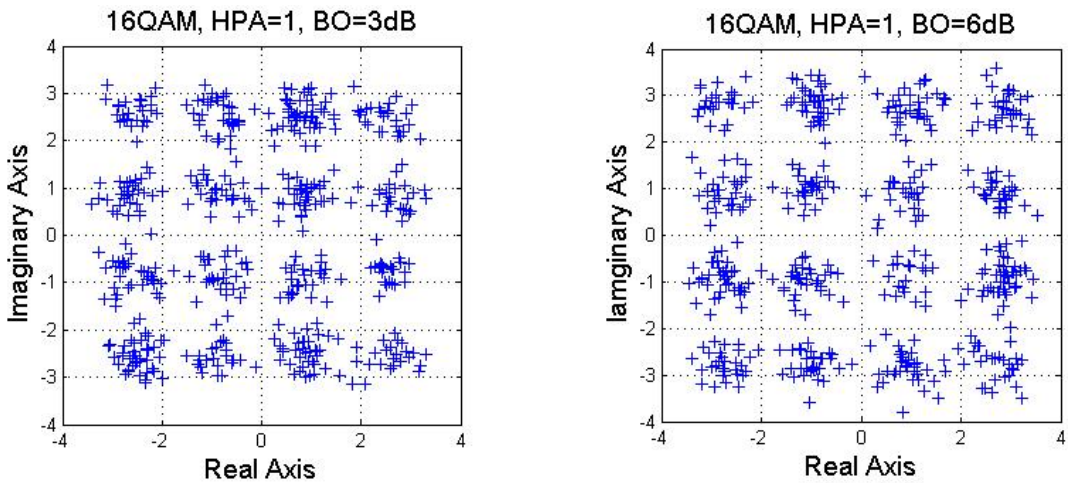

Figure 6.13: Effect of HPA and BO on 16QAM constellation points

Figures 6.14 and 6.15 show the performance comparison for uncoded and coded system respectively. The results are shown for QPSK, 16-QAM and 64-QAM; and also for different BO values, such as 10dB, 6dB and 2dB. For coded curves, code rate of $\frac{1}{2}$ is used. In both coded and uncoded system, there is impact of HPA in the system performance, however there is some performance improvement for FEC coding gain. Coding rates in conjunction with different modulation schemes have different impacts on system performance. The higher the modulation rate, the greater the impact of BO values to mitigate the HPA non-linearity. Figure 6.15 also shows that FEC tries to compensate the distortion effect. For uncoded case, 16-QAM and 64-QAM schemes show error floor when lower BO values (hence higher distortion) are applied. At lower modulations like QPSK, coding does not alter the impact of different BO values in the error rate. At higher modulation rate, e.g. at 64-QAM, coding rate gives significant gain at the cost of throughput reduction due to FEC.

As stated earlier, power BO shifts the operating point of HPA more to the linear region and thereby reduces the nonlinear distortion but at the cost of coverage reduction. From Figure 6.15, it is clear that the performance improvement due to higher BO in low modulation rate is quite limited. However for 16QAM modulation, power BO of 2dB gives us almost the same performance comparing to no BO case. This is inline with other available literatures [8]. In those works, it is reported that increasing the BO values for more than the mean of PAPR (which is nearly 6dB) does not make much difference, as the cdf of PAPR is quite steep. For higher modulation, the impact of different BOs is more visible, as we know that distortions are more detrimental to dense constellation diagrams.

Since different modulation and coding rate shows different behavior for variation in BO power, the choice of suitable BO point for different modulations are different. Also it is highly

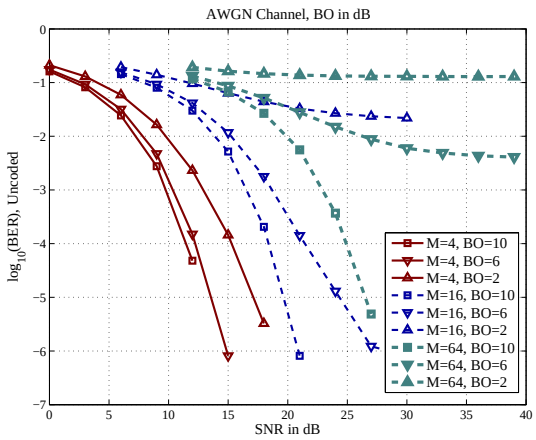

Figure 6.14: Effect of HPA and BO on uncoded system in AWGN channel

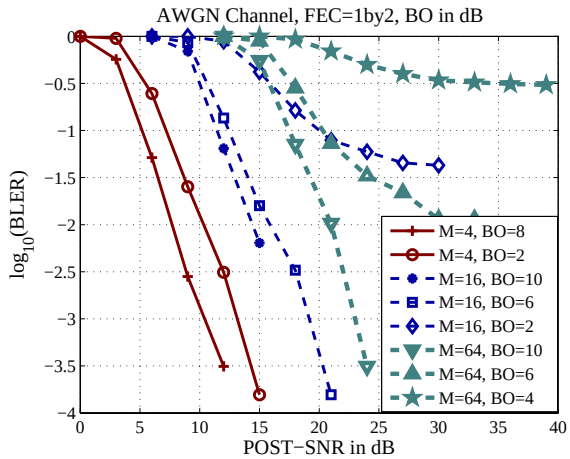

Figure 6.15: Effect of HPA and BO on coded system in AWGN channel

BO Values	Ideal	10	8	6	5	4
Measured SNR	5.1	5.67	5.7	5.79	5.91	6.33
Degradation	0.0	0.57	0.6	0.69	0.91	1.33
Total Degradation	-	10.57	8.60	6.69	5.91	5.33

Table 6.5: Table for Calculation of Total Degradation in dB

complex, if not impossible, to change the BO power frequently with the change in modulation and coding rate in link adapted system. So finding an optimum BO point considering modulation with coding rate becomes necessary for optimum performance.

6.3.1.3 Total degradation analysis

Total degradation for a certain FER threshold is defined as the amount of BO plus the SNR degradation due to non-linearity in FER performance as compared to the performance in basic system [115].

Total degradation curve is very useful to find this optimum operating BO. The Table 6.5 shows how the Total degradation values are calculated. For a certain value of BER or FER, the corresponding SNR for without HPA system is used as the basic reference point. Then for that BER or FER threshold, corresponding SNR value for different BO values are noted. The difference between these values and basic reference values represent the degradation. Figure 6.16 represents the total degradation curve for FER threshold of 0.1. The amount of degradation can vary for different modulation, coding as well as for FER threshold. From Figure 6.16, we can see that for 64 QAM, 16QAM and 4-QAM, optimum BO is 6dB, 4dB and 0dB respectively. So, it becomes important to draw total degradation curves for different FER threshold as well as different coding and modulation rate to find the best operating BO.

We showed that SDNR at transmitter side is independent of modulation and code rate. However, if it is measured at the receiver considering the constellation point, then it will be dependent on modulation also.

© Muhammad Imadur Rahman, 2007

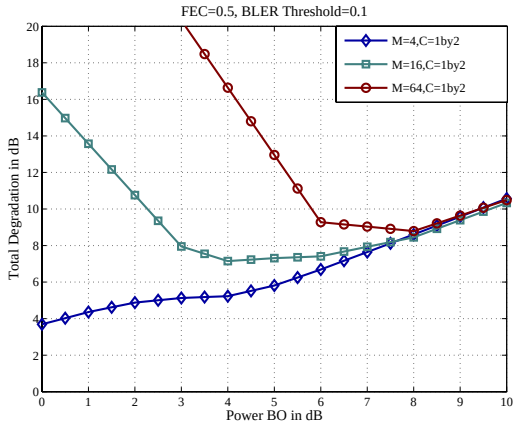

Figure 6.16: Total Degradation Plot for FER Threshold of 0.1

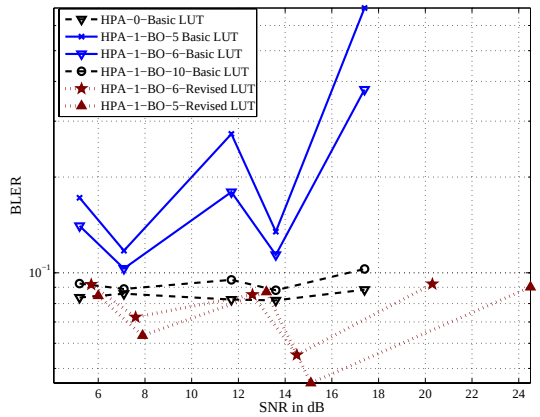

Figure 6.17: BLER Performance of Link Adapted System with and without HPA

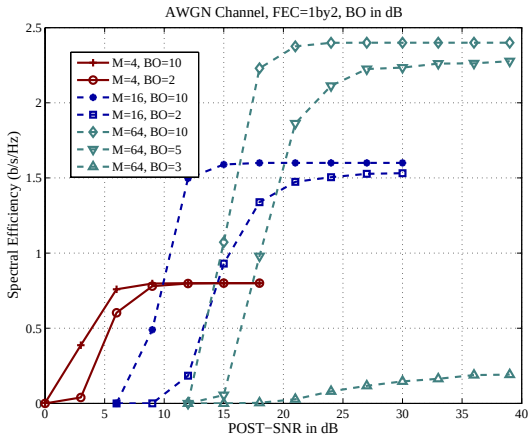

Figure 6.18: Spectral Efficiency Comparison for different BO values

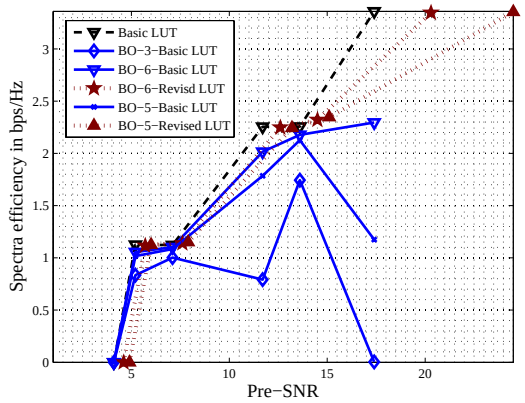

Figure 6.19: Spectral Efficiency for Link Adapted System in AWGN Channel

We define the SDNR at receiver as:

$$SDNR_{Rx} = \frac{1}{N}\sum_{i=0}^{N-1}\frac{|X_i|^2}{|X_i - \hat{X}_i|^2} \tag{6.12}$$

Here, X_i is the transmitted constellation point, $\hat{X}_i$ is the received constellation point and N is the number of sub-carriers in the system.

6.3.2 Link Adaptation with HPA in Coded OFDM System

The first row of the Table 6.6 shows the threshold for ideal system, i.e. without HPA for LA system at FER threshold of 0.1 with $\frac{1}{2}$ rate coding. It also shows the additional margin required to satisfy the FER threshold when HPA is used and since decreasing BO leads to increase in distortion, higher additional margin is required for lower BO values.

Figure 6.17 shows the performance of LA with ideal system clearly satisfies the FER thresh-

Power BO	None	QPSK	16QAM	64QAM
Ideal	0	5.1	11.6	17.3
6	0	5.1+0.5	11.6+0.9	17.3+2.9
5	0	5.1+0.8	11.6+1.5	17.3+7.1

Table 6.6: LUT with basic and updated values for system with FEC= $\frac{1}{2}$ in AWGN Channel (Values in dB)

old. However, when HPA is added to the system, using the same LUT the FER requirement can not be met except with a very high Power BO of 10dB. However, this can not be used as solution since it will reduce the coverage drastically. Obviously alternative solution is to modify the LUT by adding some extra margin to satisfy the threshold.

For coded system, Table 6.6 shows the amount of margin required to satisfy the FER requirement. The LA performance with the updated LUT is shown in Figure 6.17 where it clearly satisfies the FER requirement. The zigzag nature of the curves when HPA is employed is due to the power adaptation algorithm used in the system. For each sub-channel, SNR is measured and checked which modulation scheme threshold it satisfies. Power for that sub-channel is reduced to the threshold level. However, reducing power of the sub-channel is in a way, backing of power by that amount which means it is operating in more linear region that definitely improves the performance. So for two different operating SNR, amount of power reduction is different and therefore FER performance for same LUT is different accordingly. Thats why the zigzag nature is found in the figure.

6.3.2.1 Effect of HPA on Throughput

Throughput is the most important key parameter to measure performance. Figure 6.18 shows the spectral efficiency of the system with HPA. With low modulations as QPSK, there is almost no effect of BO. However this effect gradually increases with increase in modulation and coding rate. At low SNR for 16-QAM rate $\frac{1}{2}$, throughput for BO of 3dB is lower than that without HPA. The impact is severe for 64-QAM. For example, Spectral Efficiency (SE) at 22dB SNR with BO of 10dB, 5dB are 2.4 b/s/Hz and 2 b/s/Hz respectively; and for 3dB BO, SE falls almost to zero. It is therefore very much important to carefully select the BO point considering throughput as well as FER and other parameters which again shows the importance of total degradation curves for different threshold.

For LA based system, if it fails to maintain the target FER, then throughput performance is severely affected that results in a loss in spectral efficiency. Thus it becomes very important to maintain the target FER. The Figure 6.19 shows the spectral efficiency of the system for different conditions. The figure also shows that if the revised LUT with added margin is used, then the system can have nearly the same spectral efficiency of the basic system.

6.3.3 Results for Fading Channel

The discussions and results presented so far are based on AWGN channel. In this section, we evaluate the performance in fading channel conditions with realistic channel parameters.

Figure 6.20 shows the basic system performance in Fading channel with different modulation and power BO. It is worth mentioning that in all the figures the performance is shown against

© Muhammad Imadur Rahman, 2007

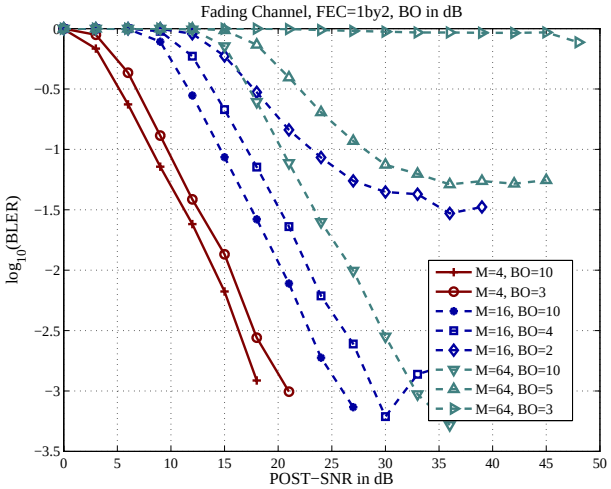

Figure 6.20: Effect of HPA and BO in Fading Channel

Power BO	None	QPSK	16QAM	64QAM
Ideal	0	8.31+1.6	14.34+0.6	18.6
6	0	(8.31+1.6)+0.0	(14.34+0.6)+0.2	18.6+0.5
4	0	(8.31+1.6) + 0.4	(14.34+0.6)+0.4	18.6+1.8

Table 6.7: LUT with basic and updated values for system with FEC $= \frac{1}{2}$ in Fading Channel(Values in dB)

post SNR, i.e. the SNR measured at the receiver for each sub-channel.

The performance with power BO of 10dB can be considered as the basic system performance as with this amount of BO the system mostly operates in the linear region. However, this will reduce the coverage of the system significantly. Like AWGN channel, the effect of HPA gradually increases with the increase in modulation rate.

The first row of the Table 6.7 shows the basic LUT for fading channel. In link adaptation system, channel information is extracted from one symbol of a frame and is used not only in the next one symbol but also over the whole next frame. Thus a certain amount of error due to delay and averaging is introduced. To compensate this effect, some margins are added for some of the modulation schemes (which is shown as addition within the bracket).

With this LUT basic system maintains the target FER as shown in Figure 6.21. However, when HPA is employed behavior is same as in AWGN channel and it fails to meet target FER which results in a severe reduction in SE at high SNR which is shown in Figure 6.22. Hence extra margin is required to satisfy the QoS constraint. Smaller the power BO, higher the degradation and hence more margin is required which may make some higher modulation and and lower coding rate invalid.

Figure 6.23 shows SDNR plot which shows that for higher order modulation with low BO, SDNR saturates at certain value. This means increasing SNR beyond this value will not improve performance. So SDNR plot plays a vital role in choosing the highest operating SNR and thereby saves power. On the other hand, increase in BO causes decrease in the cell coverage. So a trade off between this two should be made. Total degradation curve, in Figure 6.24, can help to find the

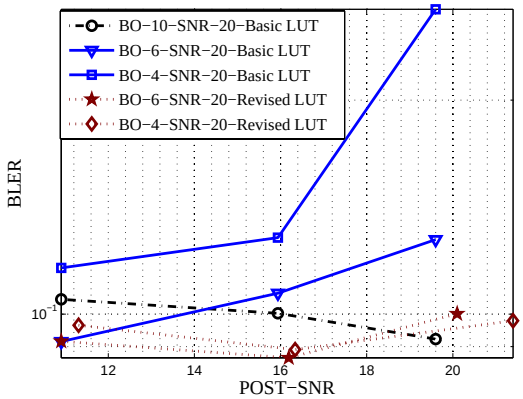

Figure 6.21: FER Performance of Link Adaptation with and without HPA

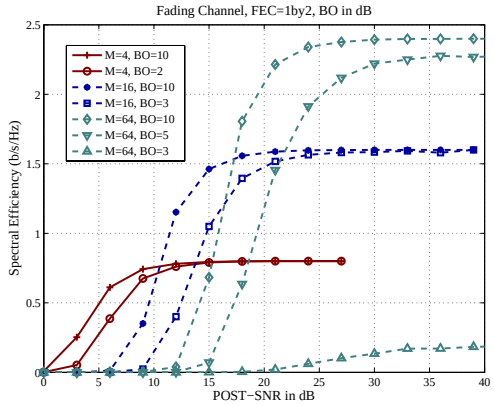

Figure 6.22: Spectral Efficiency Comparison for different BO values in Fading Channel

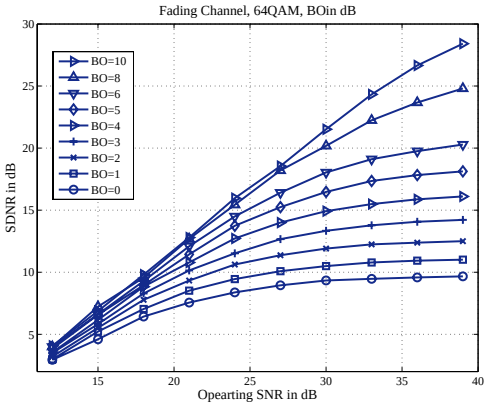

Figure 6.23: SDNR for 64QAM in fading channel

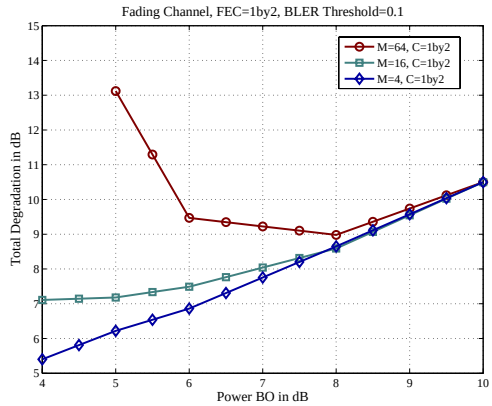

Figure 6.24: Total Degradation Plot for FER Threshold of 0.1 in fading channel

optimum BO value.

6.4 Chapter Summary

In this chapter, several aspects of link adaptation in OFDM systems have been presented. Below, we present a short summary of the studies performed in this chapter:

Guidelines for Hybrid Link Adaptation

It is seen that there are a large number of options to maximize the throughput in link-adapted OFDM systems. If all of these options are intended to be optimized in the same rate, then the system becomes very complex since it involves optimization of several parameters. From wireless channel point of view, Doppler conditions, RMS delay spread, average SNR range etc are the statistical measures and channel gain values for each sub-channel in real-time are the instantaneous information that provides a number of opportunities for improving the system performance.

© Muhammad Imadur Rahman, 2007

Hybrid LA strategies do not exploit all degrees of freedom simultaneously at the same rate. As mentioned, several parameters can be adapted, namely, modulation level (M), the FEC rate (C), power level (P), adaptation interval for M and C, adaptation interval for P, sub-channel size and choice of bit and power loading algorithms. Different combinations of slow and fast adaptation can be made between these parameters so that only few parameters are adapted instantaneously using immediate channel gains, while others are adapted statistically, i.e. using some average information such as RMS delay spread, Doppler conditions, average SNRs etc.

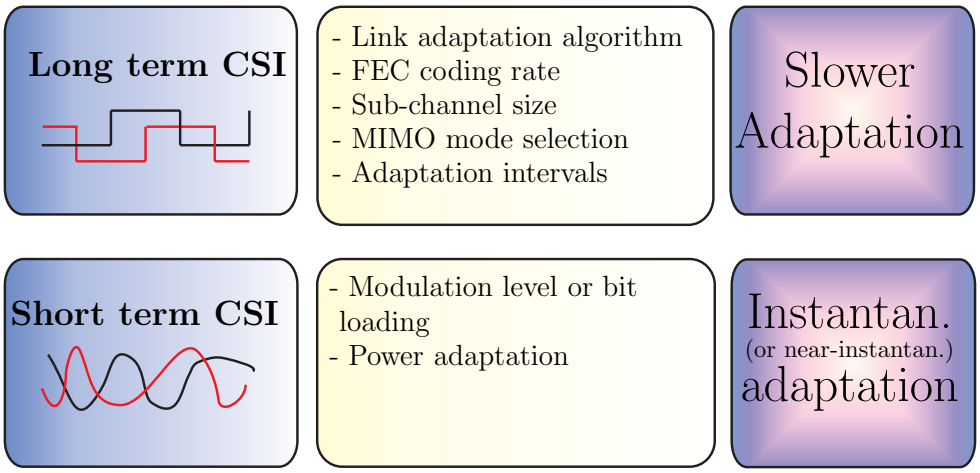

Figure 6.25: Summary of hybrid link adaptation approach

We can summarize our findings as shown in Figure 6.25. From the results presented it can be said that bit and power loading algorithm can be selected based on the average SNR conditions. For optimum throughput performance, APMC-type algorithm is the best, while it also requires highest complexity. Thus, sub-optimal methods can be taken as shown in this chapter. In general, AMC with adapted power should be used for low-diversity channel (i.e. low RMS delay spread and low Doppler values), while AMC with fixed power algorithms can be used in opposite conditions. The coding rate can also made quasi static which adapts based on the average SNR criteria, which includes shadowing loss of the channel. The selection of sub-channel, which influences the overhead easily, is dependent on channel time and frequency correlation factors. It suggests that, significant gain can be obtained in case of low Doppler by using small sub-channel size, where as for high velocity making sub-channel size large does not reduce throughput but decreases the overhead, which can be of great advantage. It must be remembered that each case is dependent on the coherence bandwidth, coherence time of the channel and the sub-channel size.

It is seen that using hybrid strategies, i.e. using a combination of slow and fast adaptation of different parameters can simplify the LA process while there is little impact on the spectral efficiency performance. This understanding will give a significant information on resource allocation strategies where users may have different channel conditions and then selecting different LA parameters for different users will be very important. Results, such as the ones presented in this chapter, will play a key role in identifying such cases. These results are also expected to trigger a lot of investigation in to resource allocation algorithms for future broadband wireless systems, such as

UMTS-LTE and IMT-Advanced kind of systems.

Conclusion from Bit and Power Allocation Analysis

We have studied several combinations of bit and power allocation rates, so that the throughput can be optimized without increasing the system complexity. Popularly it is believed that simultaneous bit and power allocation at the same rate is not very much useful in terms of system throughput. Contrary to this popular belief, we have found that in some scenarios and in some system conditions, some kind of power adaptations along with bit allocations across OFDM sub-channels are required together for efficient exploitation of wireless channel. In case of multi-antenna schemes, the benefits of simultaneous bit and power allocation is even higher compared to bit allocation only schemes. We have tested different link adaptation algorithms in different multi-antenna systems. We have found that, if we cannot find the exact SNR thresholds due to different reasons, such as reduced LA rate, CSI error, feedback delay etc., it is better to fix the transmit power across all sub-channels to guarantee the target FER. Otherwise, we can use adaptive power distribution to save power, which can be used for other purposes, or to increase the throughput of the system by transmitting higher number of bits.

Due to system complexity requirements, if we need to reduce the adaptation rates, then modulation and coding can be adapted at a slower rate if fast power control is applied in time domain. This provides a satisfactory system performance compared to the required system complexity. We conclude the following:

1. If LA window is quite narrow (i.e. short in time domain), then we practically waste the transmit power if we fix the amount of power for each sub-channel. If we can adjust the power, once the FER threshold is met based on our AMC threshold table, then there will be power saving without losing much of spectral efficiency.

2. For power-non-adapted cases, if we adapt both FEC and modulation, then by introducing more switchable rates, the difference in wastage power for with and without power adaptation cases will be smaller, thus less power will be wasted. This can be done by introducing more channel-coding rates. But, this will also bring other system level complexities.

3. If LA window is quite wide (i.e. long in time domain), then faster PC rates can be used to compensate for the mismatch between actual SNR and modulation level assigned to any sub-channel.

Future Work: In future, the impact of different sub-channel size in collaboration with different bit and power allocation rates can be studied. More importantly, studying these issues in multi-user scenario will show us the benefit of the power savings more significantly.

Transmitter Non-Linearities in LA

It has been shown that the LA algorithms fail to meet FER requirement if the non linear distortion from HPA due to high PAPR is not considered which has severe impact on throughput performance. A solution to this problem is proposed where SNR LUT is adapted. It is shown that with

© Muhammad Imadur Rahman, 2007

the new threshold, the LA meets the target FER. however, since change in threshold sometimes set some of the modulation and code rate invalid, it may affect the throughput performance. Performance degradation varied quite a lot for different coding and modulation. So both coded and uncoded system has been compared. It is also found that the SDNR plot has some correlation with the additional margin needed to maintain the FER. Total degradation curve is a nice way to find the optimum BO; and since BO reduces the cell coverage and it is shown that BO has severe impact on throughput performance, it becomes very important to carefully select the BO for different FER thresholds which can easily be managed by total degradation curve.

7

Transmit Diversity Vs Beamforming

In Chapters 3-6, we study different methods to obtain as much time-frequency diversity as possible, based on different amount of Channel State Information (CSI) available at the transmitter side. From this chapter onwards, we also include the spatial domain in our studies, so that spatial diversity gains can also be achieved together with time-frequency diversity of wireless channel.

In this chapter, we study the impact of spatial diversity and array gain obtained from transmit diversity and beamforming respectively in the resultant system performance for indoor and outdoor cellular systems. Following a brief overview of the multi-antenna techniques considered in this study, to be found in Section 7.2, we analyze the impact of the two above multi-antenna gain components in terms of downlink capacity and error probability in Section 7.3. The way to employ DL-BF in multi-user OFDM systems is explained in Section 7.4. Performance analysis and comparison of the techniques are explained in Section 7.5. Finally conclusions are drawn in Section 7.6.

7.1 Introduction

Wireless systems which operate at high data rate, providing higher multi-user capabilities, are always impaired by harsh wireless channel. Multi-antenna techniques can be used to overcome these unwanted situations, e.g. diversity techniques can be used to obtain reliable transmission systems or beamforming can be used to increase the signal strength towards a particular user, thus reducing interference to others. Traditionally spatial diversity is exploited involving multiple antennas in transmitter (Transmit Diversity) and/or receiver (Receive Diversity). Transmit diversity is a lu-

crative and reasonable choice for Downlink (DL), i.e. Base Station (BS)-to-Mobile Station (MS), especially for portable receivers where current drain and physical size are important constraints.

Orthogonal Frequency Division Multiplexing (OFDM) itself does not pose any built-in diversity, thus it is necessary to install some forms of diversity in an OFDM system for the purpose of achieving higher link quality and link availability without using any extra bandwidth. For example, channel coding and interleaving are used in IEEE 802.11a to obtain frequency diversity. Contrary to this, BF techniques can be used to achieve similar performance.

In this chapter, we compare the usability of transmit diversity and BF for DL of OFDM based cellular systems at indoor (micro and picocells) and outdoor urban macrocell scenarios. As seen in subsequent analysis in this chapter, the tradeoff between transmit diversity and Transmit Beamforming (TxBF) is actually a trade-off between diversity gain and array gain. *Diversity Gain* relates to shape of the pdf of instantaneous Signal to Noise Ratio (SNR), while *Array Gain* is related to the improvement in the average SNR. In both approaches the configuration used is Multiple Input Single Output (MISO), since it is supposed that multiple antennas are employed at the BS transmitter and a single antenna at the MS receiver. The target is to define the conditions in which one of the two techniques is preferred to the other for DL cellular systems. We compare the schemes based on BER performance, on various angular spread values and corresponding channel correlation status.

In any OFDM-type multi-carrier system, downlink beamforming can be implemented either before IDFT (frequency domain) or after IDFT (time domain) module in a base station transmitter. We denote the former scheme as Pre-IDFT downlink beamforming, and the latter as Post-IDFT downlink beamforming. In this chapter, we have compared Pre-IDFT downlink beamforming with Space-Time Block coded and Space-Frequency block coded transmit diversity schemes for 4×1 downlink OFDM systems. The study is performed for indoor microcells and picocells and urban macro cells. The studies can also be adapted to multi-users scenarios, e.g. Orthogonal Frequency Division Multiplexing - Time Division Multiple Access (OFDM-TDMA) and Orthogonal Frequency Division Multiple Access (OFDMA) systems. Regardless of the multiple access scheme, it is found that beamforming always performs better in outdoor environment, where angular spread is lower, thus spatial correlation is higher. Similarly, indoor environment (high angular spread and low spatial correlation) suggests that transmit diversity schemes performs better than beamforming strategies.

7.2 A Brief Look at Diversity and Beamforming

7.2.1 Beamforming

In a BF system, the weights to be multiplied with the signals have to be carefully chosen. From antenna theory, an array with P antenna elements has different excitation currents according to the angle of direction of the waves arriving or departing from each element of the array. Considering linear phase progression, the weights have a phase that increases the same amount from one

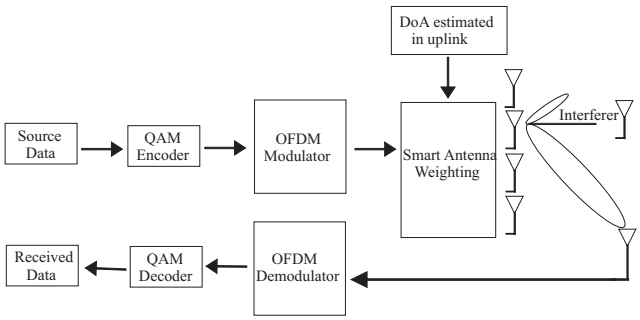

(a) OFDM system with beamforming operation

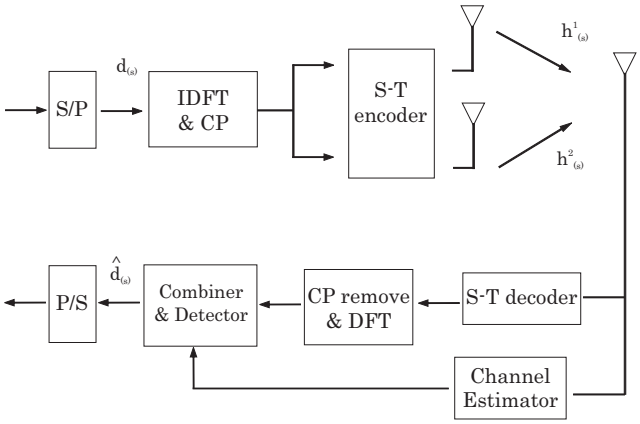

(b) Space-Time diversity in OFDM system

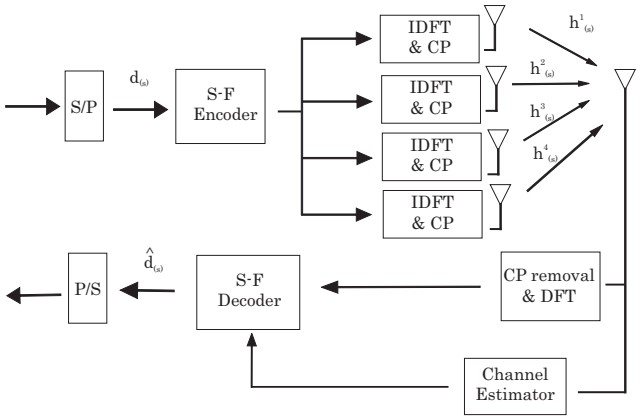

(c) Space-Frequency diversity in OFDM system

Figure 7.1: Beamforming and transmit diversity systems in OFDM system

element to the next. For Uniform Spaced Linear Arrays (USLA), the array factor becomes,

$$\mathbf{F}(\theta) = \sum_{p=0}^{P-1} A_p e^{j2\pi(p-1)\frac{d}{\lambda}\sin\theta} \tag{7.1}$$

where θ is the Direction of Arrival (DoA), d is inter-element distance, λ is the wavelength of the transmitted signal, and A_p is the instantaneous signal amplitude at p^{th} transmit antenna element [73]. This assumption is termed as *Narrow-band Antenna Array* condition, where neighboring antenna elements see same signal amplitude and only a progressive rotations in corresponding signal phases.

Usually, BF is treated in literature as a method of increasing array gain when receiving signals from a specific direction. DoA is the angle of the wave arriving to the antenna. However, in this study it is intended to analyze the DL case, placing the beamformer at the transmitter side, i.e. at the BS, since it is more feasible to have multiple antennas at the BS than at the MS. This will bring additional complications if it is assumed that there is complete channel knowledge at the receiver, but not at the transmitter. In order to solve this problem, the DL-BF technique to be employed in this analysis will extract the weights to be used in DL from the weights calculated in UL. This method can be used in Time Division Duplex (TDD) systems without losing performance. However, in Frequency Division Duplex (FDD) systems, as a consequence of the frequency dependent steering array response and uncorrelated fading, the weights determined in UL cannot be directly used in in DL, because the system performance will be degraded. So, for FDD systems, a proper frequency calibration technique is required, for determining the DL BF weight vectors based on received signals in the UL.

A block diagram showing the implementation of DL-BF in an OFDM transmitter is presented in Figure 7.1(a). In order to concentrate most of the transmit energy towards the DoA, Minimum Mean Square Error (MMSE) criterion can be used for determining the BF weight criterion. There are a number of other BF algorithms, that can be used also. We consider a beamformer with weight vector, $\mathbf{w} = [\ w_1 \quad w_2 \quad \dots \quad w_P\ ]$, with $|\mathbf{w}| = 1$ (i.e. BF weights are chosen so that $\mathbf{w}$ is an unit vector) and P is the number of transmit antennas. We denote the instantaneous SNR at the receiver after reception of the BF signals, γ as,

$$\gamma = \overline{\gamma}|\alpha|^2 = \frac{\overline{S}}{\sigma_n^2}\left|\sum_{p=1}^{P} w_p h_p\right|^2 \tag{7.2}$$

where $\overline{\gamma} = \frac{\overline{S}}{\sigma_n^2}$ is the average SNR with $\overline{S}$ as the average transmit power and σ_n^2 is the variance of AWGN. $\alpha = \sum_{p=1}^{P} w_p h_p$ is a Zero Mean Circularly Symmetric Complex Gaussian (ZMCSCG) random variable with a variance g of,

$$g = \mathbf{w}^H \mathbf{R} \mathbf{w} \tag{7.3}$$

where $\mathbf{w}^H$ is the conjugate transpose of $\mathbf{w}$, and $\mathbf{R}$ is the covariance matrix of the channel transfer vector, $\mathbf{h} = [\ h_1 \quad h_2 \quad \dots \quad h_P\ ]$. All these statements are true when the channel experienced between the transmit antenna elements and the receiver is frequency flat. Thus, we should be able to

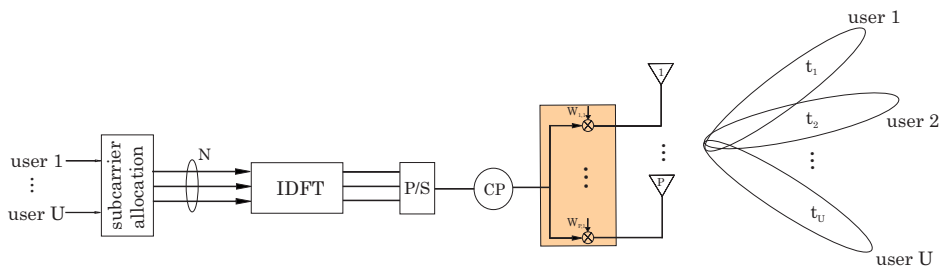

(a) Time-domain beamforming approach

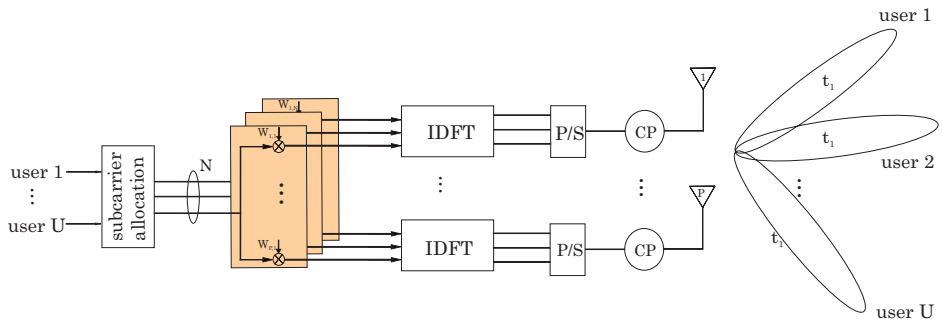

(b) Frequency-domain beamforming approach

Figure 7.2: Time- and Frequency-domain beamforming approach on an OFDMA system

use this analysis in sub-carrier basis of an OFDM system. Depending the fading correlation across different transmit antenna elements, we can find two extreme cases:

Independent fading: When independent fading across the transmit antennas is observed, then $\mathbf{R} = \mathcal{E}\{\mathbf{h}\mathbf{h}^H\} = \mathbf{I}$ and $g = 1$. This means that the transmit BF array provides no gain compared to any single antenna transmitter. So, $\mathcal{E}\{\gamma\} = \overline{\gamma}$.

Correlated fading: When the transmit antennas are completely correlated, we have $\mathbf{R} = \mathcal{E}\{\mathbf{h}\mathbf{h}^H\} \neq \mathbf{I}$. Indeed, $\mathbf{R} = [\mathbf{1}]_P$, where $[\mathbf{1}]_P$ is a $P \times P$ square matrix with all unity entry. So, $g = \mathbf{w}^H[\mathbf{1}]_P\mathbf{w} = P$. In this case, we can write that [118]

$$\gamma = P\frac{\overline{S}}{\sigma_n^2}|\varsigma|^2 \tag{7.4}$$

where ς is zero mean and unit variance complex Gaussian random variable, i.e. γ has a chi-square distribution, i.e. χ_2^2 distribution. This also means that $\mathcal{E}\{\gamma\} = P\overline{\gamma}$. Thus, the pdf of the received SNR for BF system at full correlation across the transmit antennas can be written as:

$$\mathfrak{f}(\gamma) = \frac{1}{P\overline{\gamma}}\exp\left(-\frac{\gamma}{P\overline{\gamma}}\right) \tag{7.5}$$

Looking at the above expressions, we can see that BF obtains complete array gain when the antennas are completely correlated, while spatial diversity techniques require independent fading across different spatial branches for obtaining complete diversity gain. For a better comparison

© Muhammad Imadur Rahman, 2007

of BF and SISO systems, we can envision that BF and SISO would require $\frac{\overline{S}}{\sigma_n^2}$ and $\frac{\overline{S}}{\sigma_n^2} + 10log_{10}P$ amount of power respectively to obtain the same SNR level at the receiver.

7.2.2 Space-Time Block Coding (STBC)

STBC consists of applying STC on blocks of data symbols instead of individual symbols. Its implementation in an OFDM system is shown in Figure 7.1(b). A special case of STC is Alamouti's STBC [25], which is actually a full diversity and full rate STBC scheme for 2×1 system. In this process, where two transmitter antennas and one receiver antenna are used, two symbols are being transmitted through two transmitting antennas at every symbol duration. Tarokh et al. [78] proved that full rate and full diversity is only achievable for 2×1 transmit diversity system, when only linear receiver is considered. They proposed partial rate and full diversity codes for 4×1 space-time transmit diversity system. One such example of code is described here in Table 7.1.

OFDM Symbol	Ant 1	Ant 2	Ant 3	Ant 4
T_n	s_n	s_{n+1}	s_{n+2}	s_{n+3}
$T_n + 1$	$-s_{n+1}$	s_n	$-s_{n+3}$	s_{n+2}
$T_n + 2$	$-s_{n+2}$	s_{n+3}	s_n	$-s_{n+1}$
$T_n + 3$	$-s_{n+3}$	$-s_{n+2}$	s_{n+1}	s_n
$T_n + 4$	s_n^*	s_{n+1}^*	s_{n+2}^*	s_{n+3}^*
$T_n + 5$	$-s_{n+1}^*$	s_n^*	$-s_{n+3}^*$	s_{n+2}^*
$T_n + 6$	$-s_{n+2}^*$	s_{n+3}^*	s_n^*	$-s_{n+1}^*$
$T_n + 7$	$-s_{n+3}^*$	$-s_{n+2}^*$	s_{n+1}^*	s_n^*

Table 7.1: Tarokh's $\frac{1}{2}$ rate Space-Time Block Encoding Scheme; s_n denotes the transmitted symbol at n^{th} OFDM symbol duration.

By combining the received eight symbols and applying Maximum Likelihood (ML) detector, the four transmitted symbols can be obtained [78]. The abstract transceiver structure of this scheme in an OFDM system is shown in Figure 7.1(b).

Using the notations from the earlier sections, we can write for any open-loop transmit diversity scheme that:

$$\gamma = \frac{\overline{S} \sum_{p=1}^{P} |h_p|^2}{P\sigma_n^2} \tag{7.6}$$

where $\overline{S}$ is the total transmitted from one sub-carrier and divided equally across all P transmit antennas. $\sum_{p=1}^{P} |h_p|^2$ has a χ_{2P}^2 distribution, thus, we can write the pdf of SNR for open-loop transmit-diversity scheme as:

$$\mathfrak{f}(\gamma) = \frac{\gamma^{P-1}}{(P-1)! \left(\frac{\overline{\gamma}}{P}\right)^P} \exp\left(-\frac{P\gamma}{\overline{\gamma}}\right) \tag{7.7}$$

We can write that:

$$\mathcal{E}\{\gamma\} = \frac{\overline{S}}{\sigma_n^2} = \overline{\gamma} \tag{7.8}$$

This is the case when independent fading is assumed across the antenna elements, thus, $\mathcal{E}\{\sum_{p=1}^{P}|h_p|^2\} = P$. So, it is clear that the independent spatial branches are a requirement for obtaining the transmit diversity benefits. Although there is no difference in the average SNR when a SISO and open-loop MISO is compared, the probability distribution of SNR for MISO system is very different corresponding to the number of transmit antennas available at the system. *Channel tightening* impact is seen when the number of transmit branches is increased. As the order of the distribution $2P$ increases, the pdf is concentrated more and more around the average SNR, $\overline{\gamma}$; thus the change in the shape of the SNR distribution provides us the diversity gain.

Space-Frequency Block Coding (SFBC)

STBC algorithms can be implemented in OFDM systems with a condition that the channel is time-invariant for the duration of the orthogonal transmission block (i.e. coherence time, $T_c \geq \frac{PT_s}{R_{td}}$, where T_s is total OFDM symbol duration including the cyclic prefix) and R_{td} is the STBC code rate. This can be a bottleneck for highly time-variant mobile environment. Besides, effectively the latency that the receiver incurs because of STBC algorithm is essentially equal to $\frac{PT_s}{R_{td}}$. This can also be unsatisfactory for some particular real-time services.

An alternative to Space-Time Block Coded OFDM (STBC-OFDM) system in this regard is Space-Frequency Block Coded OFDM (SFBC-OFDM) system. In SFBC-OFDM system, the orthogonal code blocks are designed across OFDM sub-carriers. Thus, as long as neighboring sub-carriers have similar frequency response, there will be no problems with SFBC algorithms. It is worth noting here that SFBC-OFDM systems will suffer in performance in situations where $\Delta f \leq B_c \leq \frac{P\Delta f}{R_{td}}$. Here, Δf is the subcarrier spacing of the OFDM systems. For cases when $\frac{P}{R_{td}}$ is large, special care needs to be taken in SFBC system design, so that degradation due to change of CSI inside the coding span in frequency does not occur. Moreover, the orthogonal coding is not done across OFDM symbols, rather in one OFDM symbol, so as long as the channel remains static for one OFDM symbol duration (i.e. T_s), the coding should provide optimum diversity gain to the system [79]. Its implementation in OFDM system is shown in Figure 7.1(c). The orthogonal space-frequency blocks can be defined in a similar fashion like Table 7.1. All the considerations related to array gain and diversity gain done in case of STBC also hold for SFBC system.

7.2.3 Receive Diversity System

As a comparison, we also introduce the receive diversity scheme, namely Single Input Multiple Output (SIMO) systems, in this section. In a SIMO system, the signal is transmitted from a single transmit antenna and received at multiple antennas. After that, they are combined using Maximal Ratio Combining (MRC). So, the instantaneous SNR can be written as,

$$\gamma = \overline{\gamma}\sum_{q=1}^{Q}|h_q|^2 = \frac{\overline{S}}{\sigma_n^2}\sum_{q=1}^{Q}|h_q|^2\,, \tag{7.9}$$

© Muhammad Imadur Rahman, 2007

where Q is the number of receive antennas. The pdf of instantaneous SNR at the output of the MRC combiner can be written as,

$$\mathfrak{f}(\gamma) = \frac{\gamma^{Q-1}}{(Q-1)!\,\overline{\gamma}^{Q}} \exp\left(-\frac{\gamma}{\overline{\gamma}}\right). \tag{7.10}$$

We can see from Eq.(7.9) that the instantaneous SNR is increased by the number of spatial branches in MRC, which is the direct result of *array gain* obtained in MRC receiver. The average SNR after the receiver combining can be written as:

$$\mathcal{E}\{\gamma\} = Q\overline{\gamma} \tag{7.11}$$

Thus, array gain can be defined as:

$$\begin{aligned} Array\,gain &= \frac{Average\,SNR\,at\,the\,output\,of\,the\,linear\,combiner}{Average\,SNR\,at\,the\,input\,i.e.\,at\,the\,transmitter} \\ &= \frac{\mathcal{E}\{\gamma\}}{\overline{\gamma}} \end{aligned} \tag{7.12}$$

7.2.4 MIMO Diversity System

A particular interest regarding the array gain and diversity gain is MIMO diversity system, with P number of transmit branches while the combiner has Q branches. When open-loop transmit (e.g. Alamouti's STBC) is used at the transmitter and MRC combining is done at the receiver, then the resultant SNR, γ and the pdf of γ at the output of the combiner can be written as:

$$\gamma = \frac{\overline{\gamma}}{P}\sum_{p=1}^{P}\sum_{q=1}^{Q}|h_{p,q}|^2 \tag{7.13}$$

$$\mathfrak{f}(\gamma) = \frac{\gamma^{PQ-1}}{(PQ-1)!\left(\frac{\overline{\gamma}}{P}\right)^{PQ}} \exp\left(-\frac{P\gamma}{\overline{\gamma}}\right) \tag{7.14}$$

Channel tightening due to the transmit diversity scheme, together with receive diversity and array gains are seen in MIMO diversity schemes.

7.2.5 SNR Statistics of Diversity and Beamforming Systems

We present the pdf of instantaneous SNRs in Figure 7.3 for all the four schemes that are described in the above sections. For brevity, we have only shown the cases with 2 and 8 antennas for BF, transmit diversity and MRC schemes, and 2×4 and 4×2 transmit-receive diversity schemes. This figure highlights different aspects of diversity and array gain that can be obtained by exploiting the available spatial degrees of freedom in different ways. Looking at the pdfs, we can summarize the following:

1. We obtain complete array gain in an ideal MRC receiver, while we obtain no array gain in open-loop transmit diversity. That is the reason that 2×1 and 8×1 transmit diversity has al-

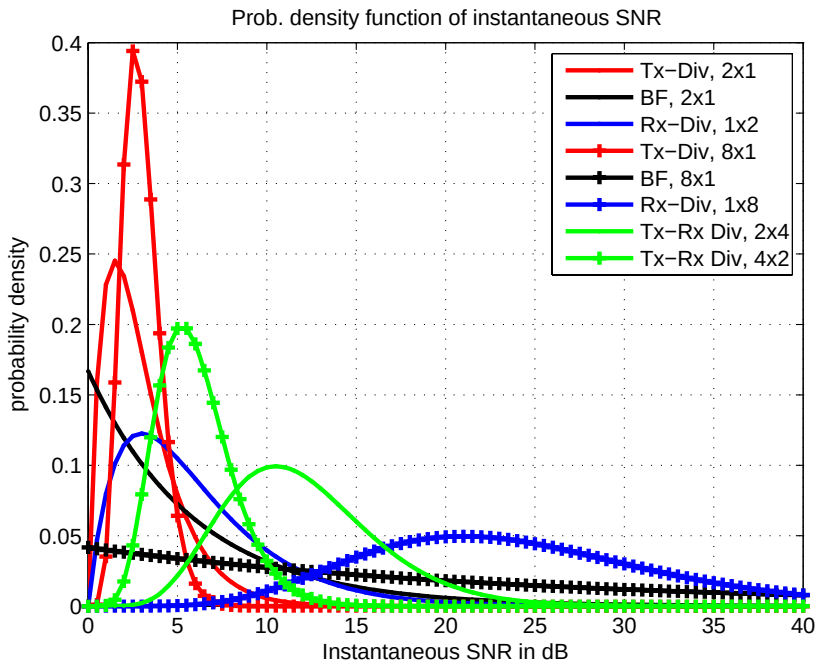

Figure 7.3: Probability density function (pdf) of SNR for different combinations of diversity and beamforming systems.

most similar average SNR, while 8×1 transmit diversity has more 'concentrated' pdf, coming from channel tightening due to 8-order of diversity.

2. Beamforming obtains full array gain when spatial branches are completely correlated. In this case, no diversity gain is obtained.

3. 4×2 and 2×4 transmit-receive diversity has same diversity order of 8. But, they have different array gain of 3dB and 6dB respectively. Thus, the pdf is right-shifted for 2×4 system. Similarly, 4×2 also experiences higher channel tightening compared to 2×4 system, thus, we see that pdf of 4×2 system is more concentrated compared to that of 2×4 system.

7.3 Downlink Capacity and Error Probability Analysis

7.3.1 Ergodic Capacity

For any specific system, when the received SNR can be characterized by γ, the well-known Shannon capacity formula for non-fading Gaussian channel can be used [34], as shown below:

$$\mathcal{C} = \log_2(1 + \gamma) \tag{7.15}$$

The capacity in $\mathcal{C}$ is also referred as error-free deterministic spectral efficiency for any specific γ, or the data rate per unit bandwidth that can be sustained reliably over the link with instantaneous SNR of γ [73].

© Muhammad Imadur Rahman, 2007

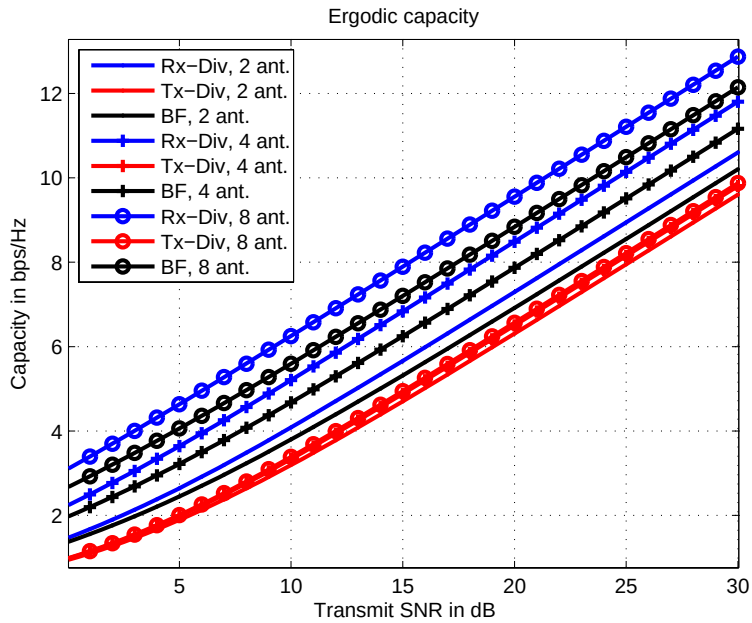

Figure 7.4: Ergodic channel capacity for transmit diversity, receive diversity and beamforming techniques with 2, 4 and 8 antennas.

Since the wireless channel coefficients are random variables, so is the parameter γ, which means that the information rate associated with the capacity is also a random variable. That is why we use a term called *Ergodic Capacity* of the system for further analysis. The ergodic capacity, $\overline{\mathcal{C}}$, of any wireless channel is the ensemble average of the deterministic capacity, $\mathcal{C}$ over the distribution of the elements of the random channel parameter. When we use asymptotically optimal transmit codebooks, then we can send the information at the channel at a rate of $\overline{\mathcal{C}}$ with vanishing error, thus, ergodic capacity is equal to shannon capacity in this sense.

Based on some well-known works, we can write the ergodic capacity of receive diversity schemes as [119]:

$$\overline{\mathcal{C}} = \mathcal{E}\{\mathcal{C}\} = \mathcal{E}\{\log_2(1 + \overline{\gamma}\sum_{q=1}^{Q}|h_q|^2)\} = \mathcal{E}\{\log_2(1 + \frac{\overline{S}}{\sigma_n^2}\sum_{q=1}^{Q}|h_q|^2)\} \tag{7.16}$$

Similar to this, we can write the ergodic capacity of open-loop transmit diversity scheme (i.e. no CSI present at the transmitter) as [74]:

$$\overline{\mathcal{C}} = \mathcal{E}\{\mathcal{C}\} = \mathcal{E}\{\log_2(1 + \frac{\overline{\gamma}}{P}\sum_{p=1}^{P}|h_p|^2)\} = \mathcal{E}\{\log_2(1 + \frac{\overline{S}}{P\sigma_n^2}\sum_{p=1}^{P}|h_p|^2)\} \tag{7.17}$$

For beamforming, we can consider the system to be equivalent to a single antenna system

with an increased average gain. So, the capacity of the beamformer can be written as [118]:

$$\overline{\mathcal{C}} = \mathcal{E}\{\log_2(1 + P\overline{\gamma}|h|^2)\} = \mathcal{E}\{\log_2(1 + \frac{P\overline{S}}{\sigma_n^2}|\varsigma|^2)\} \tag{7.18}$$

The notations in the above equations are same as the ones used before. Note that the capacity expression for BF case is valid when the transmit antenna elements are completely correlated, while they are assumed to completely independent for both the diversity methods. Figure 7.4 shows us the ergodic capacity of all three schemes when 2, 4 and 8 antennas are used either at transmitter, or at receiver. The ergodic capacity is an average parameter, thus, only the impact of array gain can be seen here. Receive diversity offers both diversity and array gain, thus, it always achieves higher capacity than other two techniques for the same antenna configuration. Beamforming performs better than transmit diversity, because it achieves array gain.

7.3.2 Outage Capacity

One problem with Shannon capacity parameters is that, it assumes very ideal scenario, thus, it only provides an upper bound for any practical system. The underlying assumptions are, infinite block length, vanishing error probability, etc. Thus, outage capacity is used in several literature for determining a more realistic capacity parameter. Outage capacity can be defined as the capacity with outage probability p, so that the random capacity $\mathcal{C}$ always resides below the outage capacity with a probability of p.

In this section, we only concentrate on transmit diversity and beamforming for our studies, as these two techniques are the focus of our analysis. For receive diversity and transmit-receive diversity, the outage capacity expression can be derived in the similar fashion.

If we define, the pdf of $\mathcal{C}$ as $\mathfrak{f}(\mathcal{C})$, then outage capacity, $\mathcal{C}_{out}(\mathfrak{p}_c)$ is related to corresponding outage probability $\mathfrak{p}_c$ as:

$$\mathfrak{p}_c = \int_{-\infty}^{\mathcal{C}_{out}(\mathfrak{p}_c)} \mathfrak{f}(\mathcal{C})\, d\mathcal{C} \tag{7.19}$$

For brevity, we denote the following:

$$\text{Tx-Div:} \qquad \mathcal{C} = \log_2\left(1 + \tfrac{\overline{\gamma}}{P}\phi\right); \qquad \text{where } \phi = \sum_{p=1}^{P} |h_p|^2 \tag{7.20}$$

$$\text{Tx-BF:} \qquad \mathcal{C} = \log_2\left(1 + P\overline{\gamma}\psi\right); \qquad \text{where } \psi = |\varsigma|^2 \tag{7.21}$$

As mentioned earlier, the pdf of ϕ and ψ are known as χ^2_{2P} and χ^2_2 respectively.

© Muhammad Imadur Rahman, 2007

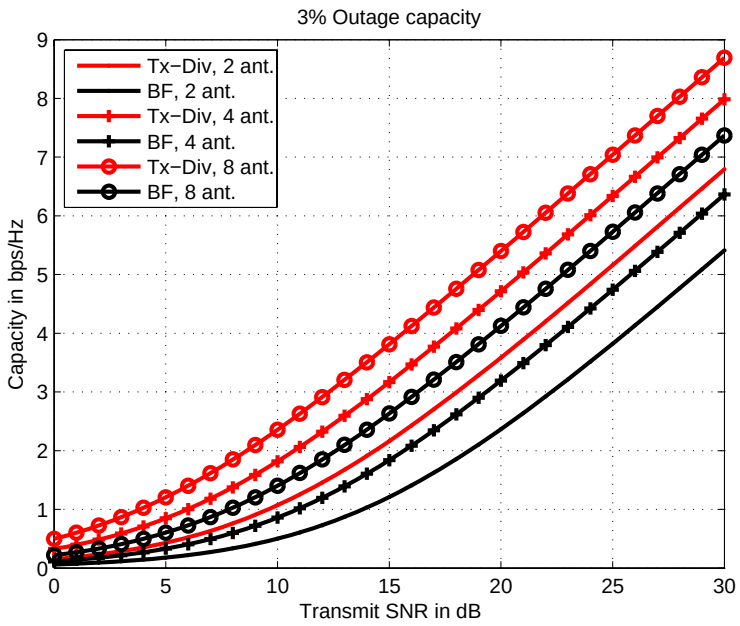

(a) Outage capacity for 3% outage probability

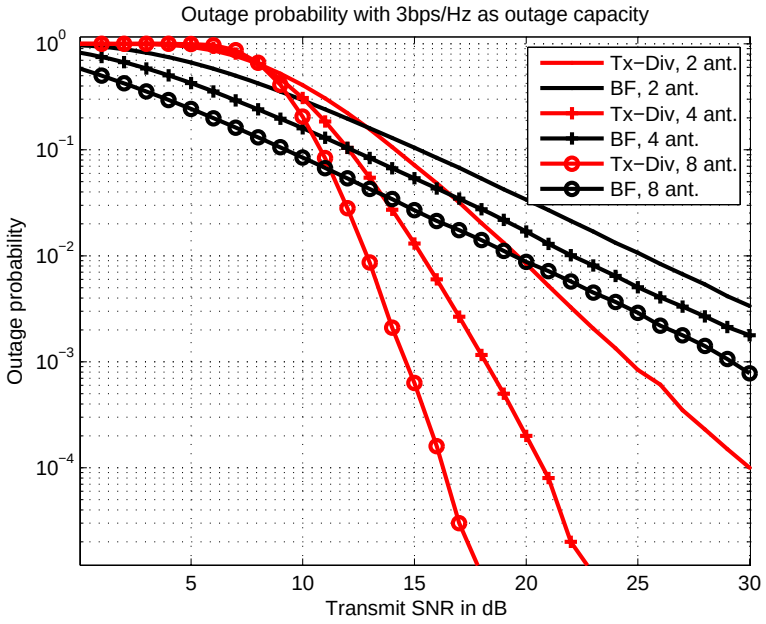

(b) Outage probability for 3 bps/Hz outage capacity

Figure 7.5: Outage capacity and outage probability for transmit diversity and beamforming with varying number of transmit antennas.

7.3.2.1 Case Study: Transmit Diversity

Using standard random variable transform formula as in [118], we can write the following for transmit diversity:

$$\mathfrak{f}(\mathcal{C}) = \frac{\chi^2_{2P}(\phi)}{\frac{d\mathcal{C}}{d\phi}} \tag{7.22}$$

where

$$\frac{d\mathcal{C}}{d\phi} = \frac{1}{\left(1+\frac{\overline{\gamma}}{P}\phi\right) ln2}\frac{\overline{\gamma}}{P} = \frac{\overline{\gamma}}{2^{\mathcal{C}} P\, ln2} \tag{7.23}$$

using $\phi = \left(2^{\mathcal{C}}-1\right)\frac{P}{\overline{\gamma}}$. So, pdf of $\mathcal{C}$ can be written as:

$$\begin{aligned}
\mathfrak{f}(\mathcal{C}) &= \frac{2^{\mathcal{C}} P\, ln2}{\overline{\gamma}}\chi^2_{2P}\left(\left(2^{\mathcal{C}}-1\right)\frac{P}{\overline{\gamma}}\right) \\
&= \frac{2^{\mathcal{C}} P\, ln2}{\overline{\gamma}}\frac{1}{(P-1)!}\left[\left(2^{\mathcal{C}}-1\right)\frac{P}{\overline{\gamma}}\right]^{P-1}\exp\left(-\frac{(2^{\mathcal{C}}-1)P}{\overline{\gamma}}\right) \\
&= \frac{2^{\mathcal{C}}\, ln2}{(P-1)!}\left(\frac{P}{\overline{\gamma}}\right)^{P}\left(2^{\mathcal{C}}-1\right)^{P-1}\exp\left(-\frac{(2^{\mathcal{C}}-1)P^2}{\overline{\gamma}}\right)
\end{aligned} \tag{7.24}$$

The $\mathfrak{p}_c$ can actually be calculated from the cdf of the capacity. So, from here, we can find the $\mathfrak{p}_c$ by using a known result from [34, Section 2.1.4]:

$$\mathfrak{p}_c = e^{\left(\frac{P}{\overline{\gamma}}\right)}\left[\sum_{p=0}^{\lfloor\frac{P}{2}\rfloor-1}\frac{1}{p!}\left(\left(-\frac{P}{\overline{\gamma}}\right)^{p} - \left((2^{\mathcal{C}_{out}}-1)\frac{P}{\overline{\gamma}}\right)^{p} e^{(1-2^{\mathcal{C}_{out}})}\right)\right] \tag{7.25}$$

7.3.2.2 Case Study: Beamforming

Using the same procedure, we can define the pdf of $\mathcal{C}$ for BF case as the following:

$$\mathfrak{f}(\mathcal{C}) = \frac{\chi^2_2(\psi)}{\frac{d\mathcal{C}}{d\psi}} \quad \text{with } \frac{d\mathcal{C}}{d\psi} = \frac{P\overline{\gamma}}{2^{\mathcal{C}}\, ln2} \tag{7.26}$$

Thus, for beamforming systems,

$$\begin{aligned}
\mathfrak{f}(\mathcal{C}) &= \frac{2^{\mathcal{C}}\, ln2}{P\overline{\gamma}}\chi^2_2\left(\frac{2^{\mathcal{C}}-1}{P\overline{\gamma}}\right) \\
&= \frac{2^{\mathcal{C}}\, ln2}{P\overline{\gamma}}\exp\left(-\frac{2^{\mathcal{C}}-1}{P\overline{\gamma}}\right)
\end{aligned} \tag{7.27}$$

From here, we can calculate the outage probability corresponding to any outage capacity

© Muhammad Imadur Rahman, 2007

values as follows:

$$\begin{aligned}\mathfrak{p}_c &= \int_{-\infty}^{\mathcal{C}_{out}} \frac{2^{\mathcal{C}}\, ln2}{P\overline{\gamma}} \exp\left(\frac{2^{\mathcal{C}}-1}{P\overline{\gamma}}\right) d\mathcal{C} \\ &= \exp\left(-\frac{1}{P\overline{\gamma}}\right) - \exp\left(-\frac{2^{\mathcal{C}_{out}}-1}{P\overline{\gamma}}\right) \end{aligned} \tag{7.28}$$

Using Eq.(7.25) and Eq.(7.28), we produce the outage capacity for specific outage probability and outage probability for specific outage capacity in Figures 7.5(a) and 7.5(b) respectively. In terms of outage capacity, we can see that the outage capacity is almost two times higher than the BF scheme for all antenna configurations. Note that this result is valid for independent fading for transmit diversity and fully correlated fading for beamforming. Thus, favorable conditions for both the schemes. For a fixed outage capacity of 3bps/Hz, we obtain the outage probability in Figure 7.5(b). At higher outage probability, the array gain is more useful compared to diversity gain, thus, BF performs better. As the outage probability decreases, the advantage of BF diminishes and transmit diversity schemes starts to perform better. For example, at an outage probability of 1%, the 8×1 transmit diversity outperforms 8×1 BF system by around 7dB.

7.3.3 Error Probability

In this section, we derive the average bit error probability expressions for transmit diversity and beamforming. The average BER can be computed for any system using the the following expression:

$$\overline{\mathbf{p}}_b = \int_0^{\infty} \mathbf{p}_b \mathbf{f}(\gamma) d\gamma \tag{7.29}$$

where $\mathbf{p}_b$ is the instantaneous BER for any M-QAM system in AWGN channel. $\mathbf{p}_b$ for M-QAM system can be written as [34]:

$$\mathbf{p}_b \approx 4\left(1 - \frac{1}{\sqrt{(M)}}\right) \mathbb{Q}\left(\sqrt{\frac{3\overline{\gamma}}{M-1}}\right) \tag{7.30}$$

where $\mathbb{Q}(x) = \frac{2}{\sqrt{\pi}} \int_x^{\infty} \exp\left(-t^2\right) dt$ is called complimentary error function. It is difficult to obtain close-form expressions when $\mathbb{Q}$-function is involved in calculation, so we take an approximation of $\mathbf{p}_b$ from [20]. Here it is shown that the instantaneous BER of an M-QAM system, with coherent detection and gray coding over AWGN channel, can be approximated within 1dB tight and for BER$\leq 10^{-3}$ by, $\mathbf{p}_b \approx 0.2 \exp\left(-\frac{1.6\gamma}{M-1}\right)$.

For a transmit diversity system, we can write the average BER as:

$$\begin{aligned}\overline{\mathbf{p}}_b &= \frac{0.2}{(P-1)!\left(\frac{\overline{\gamma}}{P}\right)^P} \int_0^{\infty} \gamma^{P-1} \exp\left[-\left(\frac{1.6}{M-1} + \frac{P}{\overline{\gamma}}\right)\gamma\right] d\gamma \\ &= 0.2\left(\frac{1}{1+\frac{1.6\overline{\gamma}}{P(M-1)}}\right)^P \end{aligned} \tag{7.31}$$

using the following identity: $\int_0^\infty x^k \exp(-\xi x) d\,x = \frac{k!}{\xi^{k+1}}$.

Similarly, we can obtain the average BER expression for beamforming as:

$$\begin{aligned} \overline{\mathbf{p}}_b &= \frac{0.2}{P\overline{\gamma}} \int_0^\infty \exp\left[-\left(\frac{1.6}{M-1} + \frac{1}{P\overline{\gamma}}\right)\gamma\right] d\,\gamma \\ &= \frac{0.2}{1 + \frac{1.6P\overline{\gamma}}{(M-1)}} \end{aligned} \tag{7.32}$$

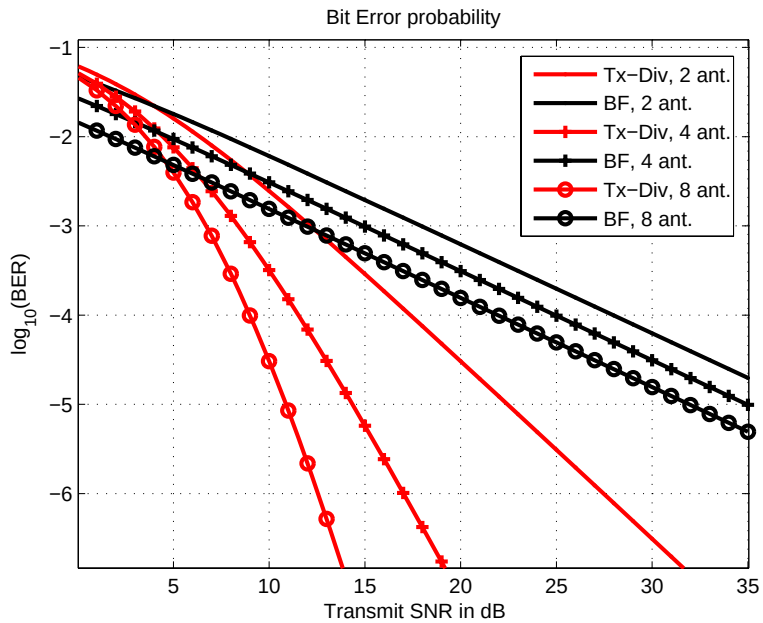

Figure 7.6: Theoretical average bit error probabilities for transmit diversity and beamforming systems.

The average BERs of transmit diversity and beamforming systems are shown in Figure 7.6, by using Eq.(7.31) and Eq.(7.31) respectively. The BERs for different number of transmit antennas are presented. Similar to the case of outage probability for 3bps/Hz outage capacity in Figure 7.5(b), transmit diversity obtains the diversity gain, while beamforming only shows the array gain benefits. So, roughly for BER of 10^{-2}, the diversity gain is more dominant and transmit diversity performs better than beamforming. Below that range, the array gain is more important and beamforming outperforms transmit diversity systems.

7.4 Downlink Beamforming and Transmit Diversity in Multi-User OFDM Systems

7.4.1 Issues in OFDM-TDMA

In an OFDM-TDMA system, one complete OFDM symbol at a certain time is allocated to a user [120]. If there are U users in the system and if all users require same bit rate services, we can assign every

© Muhammad Imadur Rahman, 2007

$(lU+1)^{\text{th}}$ OFDM symbol to U^{th} user ($l = 0, 1, \ldots$). The number of OFDM symbols per TDMA frame can be varied according to each user requests. Its main drawback is the increase of the latency when the number of users gets higher in the cell.

Keeping in mind that STBC algorithm requires more than one consecutive OFDM symbols for orthogonal transmission (to be exact, P number of consecutive OFDM symbols for $P \times 1$ STBC-OFDM-TDMA system), it is clear that STBC orthogonal blocks need to be implemented with data from different users, when TDMA slots are consists of less than P consecutive OFDM symbols. This will mean that though an OFDM symbol slot is not allocated to any user, that particular user has to receive the data in that slot to decode STBC blocks. This is not desired, so we propose to use SFBC algorithms in OFDM-TDMA systems for transmit diversity purposes. In this case, only one user at a time is involved in the transmission process and so the benefits of OFDM-TDMA are preserved.

It is fairly easy to implement beamforming algorithms in OFDM-TDMA systems. Because the data carried by one whole OFDM symbol is intended for one single user, it is possible to direct the transmitted signal at that symbol duration to the direction of respective user. So, the goals of beamforming are preserved, i.e. only the involved user's data is directed to concerned user and interference to other users is reduced. If the beamformer is placed before the IDFT, the problem is that the number of IDFTs must be equal to the number of transmitting antennas P, instead of only one as if the beamformer was placed after the IDFT. It is therefore better to allocate the beamformer after the IDFT, in fact in this case the complexity of the system is lower (one IDFT is needed instead of P).

7.4.2 DL-BF in OFDMA

In OFDMA system, users are separated across sub-carriers. BS allocates the available sub-carriers to users while transmitting in the DL. After that IDFT modulation is performed on frequency domain data. So, if the subcarrier allocation is kept static for at least μP number of OFDM symbols (or even if it is dynamic allocation via sub-carrier hopping for each OFDM symbol), then the creation and transmission of orthogonal transmit block is done simply by implementing the algorithm across OFDM symbols. Here, we denote transmit diversity coding rate as μ. As usual, it will not change any OFDMA properties, only that it will increase the latency of detection process (which is typical to any STBC algorithm). Similar to this, SFBC can also be used in OFDMA system, satisfying the condition that the users are allocated contiguous sub-carriers and the number of sub-carriers assigned to one user, $\eta = l\mu P$, where $l \in [1, \ldots, \lfloor \frac{N}{\mu P} \rfloor - 1]$.

After IDFT modulation, time-domain sampled data are transmitted towards the user. It is obvious that based on the CSI of each user, we can apply the BF weights either before IDFT modulation, or after IDFT modulation. These are called Post-IDFT Beamforming and Pre-IDFT Beamforming respectively.

7.4.2.1 Post-IDFT Downlink Beamforming

A block diagram of an implementation of Post-IDFT BF technique in an OFDMA system is shown in Figure 7.2(a). After the IDFT operation in the transmitter, the signal is indeed wideband time-

domain signal, so any wideband BF technique can be used. A multi-tap beamformer can be used for this purpose. The wideband OFDM signal is frequency selective, thus the weight vectors are required for each user which can be used to steer the signal towards the user. The BF problem can be expressed as [121],

$$\frac{\mathbf{w}_u^H \mathbf{R}_u \mathbf{w}_u}{\sum_{l=1;l\neq u}^{U} \mathbf{w}_l^H \mathbf{R}_u \mathbf{w}_l + \sigma_u^2} \geq \gamma_u, \qquad u = 1, 2, \ldots, U \tag{7.33}$$

Here, $\mathbf{R}$ denotes the co-variance matrix as it is shown in Section 7.5. γ_u, $\mathbf{w}_u$ and σ_u^2 denote the required SNR, beamformer tap weights and additive white gaussian noise variance of uth user respectively. Solving this problem with algorithm proposed by [121] will give us the beamformer weights $\mathbf{w}_u$ for all users.

For this purpose, the channel needs to be estimated in time domain. Once the beamformer weights are decided, then the received signal at the MS, $\tilde{y}_s$, can be written as

$$\tilde{y}_s = \mathbf{w}_u * \tilde{x}_s \tag{7.34}$$

7.4.2.2 Pre-IDFT Downlink Beamforming

Before applying the IDFT, the BF can be implemented across OFDM sub-carriers, as shown in Figure 7.2(b). Sub-carriers poses narrowband frequencies and thus, any narrowband scheme can be used in this case. Similar to Eq.(7.33), we can write,

$$\begin{gathered}\frac{w_{u,k}^H \mathbf{R}_{u,k} w_{u,k}}{\sum_{l=1;l\neq u}^{U} w_{l,k}^H \mathbf{R}_u w_{l,k} + \sigma_u^2} \geq \gamma_u^k, \\ u = 1, 2, \ldots, U \ \& \ k = 0, \ldots, N-1\end{gathered} \tag{7.35}$$

Here, the number of sub-carriers is identified by N and γ_u^k defines required SNR for u^{th} user's N^{th} subcarrier.

7.4.3 DL-BF in Clustered OFDMA

Both the Pre- and Post-IDFT BF schemes clearly show that the user data is not separated before steering the beams to user's location, rather all the OFDM modulated signal is sent towards all users. In this way, it is made sure that the users receive the transmitted data with higher SNR, but they also receive other users' data at the same time. In a sense, it can be said that using these kind of BF schemes, it is not possible to obtain all the goals of BF.

In order to reduce the power inefficiency of BF in OFDMA, in the way that user individual highly directive beams are carrying data from all users in the cell, we take another approach which partially solve this issue. If using a number of IDFTs equal to the number of antennas, the BS can transmit through that same number of beams to groups of users. So, what we do is to create clusters of users who are co-located. This means grouping the users spatially, i.e. define clusters of users that are close to each other, each beam can be set to acquire a shape that covers the users in that set and protects them from interference coming from other user sets in the cell. The process of

© Muhammad Imadur Rahman, 2007

grouping users into clusters, shall be undertaken by the BS using an algorithm that identifies DoA from the CSI and organizes the transmission radiation pattern according to an error minimization criterion like MMSE. This clustering beamforming approach is employed in our studies.

7.5 Performance Analysis and Comparison

7.5.1 Channel Model

Indoor (micro and picocells) and outdoor (macro cells) wireless channels for low and high user mobility are considered at 5GHz carrier frequency. For indoor channel delay profiles, we use HiperLan/2 channel model A, corresponding to a typical office environment for Non Line Of Sight (NLOS) conditions and 50ns average rms delay spread [122]. For outdoor delay profiles, we use typical urban 12-path channel model [123, Appendix-E].

7.5.2 Angular Spread and Spatial Correlation

Angular spread is a measure of the angular dispersiveness of DoAs. Angular spread is usually higher in indoor scenario, whereas it is smaller in urban macrocell scenario. Thus, indoor channel provides enough angular diversity so that transmit diversity schemes can be easily implemented. Angular spread can be measured as:

$$AS^j = \sqrt{\frac{\sum_i \left(\phi_i^j - E[\phi^j]\right)^2 |A_i^j|^2}{\sum_i |A_i^j|^2}} \tag{7.36}$$

where ϕ^j is the Angle of Arrival (AoA) of a certain mobile user j and A_i is the field amplitude, hence $|A_i|^2$ is the power of a signal coming from that scatterer i. In an indoor environment, the angular spread of the signals received by the MS is much higher than when the communication is established in an outdoor environment. This is mainly caused by the longer distance that separates BS and MS in outdoor situation, hence narrowing the angles of the received signals from multipath [124].

This characteristic makes it difficult to get the most out of angle diversity in outdoor channels, thus BF could be an interesting option to follow. On the other hand, in indoor channels, due to a broader angular spread, the multipath signals have low correlation between them, therefore angle diversity can be effectively exploited. Furthermore, BF may not be suitable for indoor scenarios, since there is no narrow beam to increase SNR and separate from neighboring interferers.

The rays departing from BS are spread over a certain angular spread. The spatial covariance matrix is characterized on the geometry relevant to a certain Direction of Departure (DoD) profile

which is represented by Eq.(7.37) [125].

$$\mathbf{R} = \sum_{l=1}^{L} \mathbf{a}^H(\theta_l)\mathbf{a}(\theta_l) \tag{7.37}$$

$$\mathbf{a}(\theta_l) = [1, \exp(-j\alpha_l), ..., \exp(-j(P-1)\alpha_l)] \tag{7.38}$$

$$\alpha_l = \frac{2\pi}{\lambda} d \sin\theta_l \tag{7.39}$$

where L is the number of rays emitted from the BS, $\mathbf{a}(\theta_l)$ is the directional vector dependent on azimuth direction θ_l of the lth ray and P is the number of transmit antennas.

The channel covariance matrix $\mathbf{R}$ can be decomposed into eigenvectors and eigenvalues; and the correlated channel vector for multiple transmit antennas and single receive antenna can now be written as [125]:

$$\mathbf{h}^R = \mathbf{Q}\mathbf{\Sigma}^{1/2}\mathbf{h} \tag{7.40}$$

where $\mathbf{h}$ and $\mathbf{h}^R$ are independent channel frequency response vector and correlated frequency response vector respectively. $\mathbf{Q}$ stands for the matrix which is composed with eigenvectors and $\mathbf{\Sigma}$ contains eigenvalues in diagonal locations for covariance matrix.

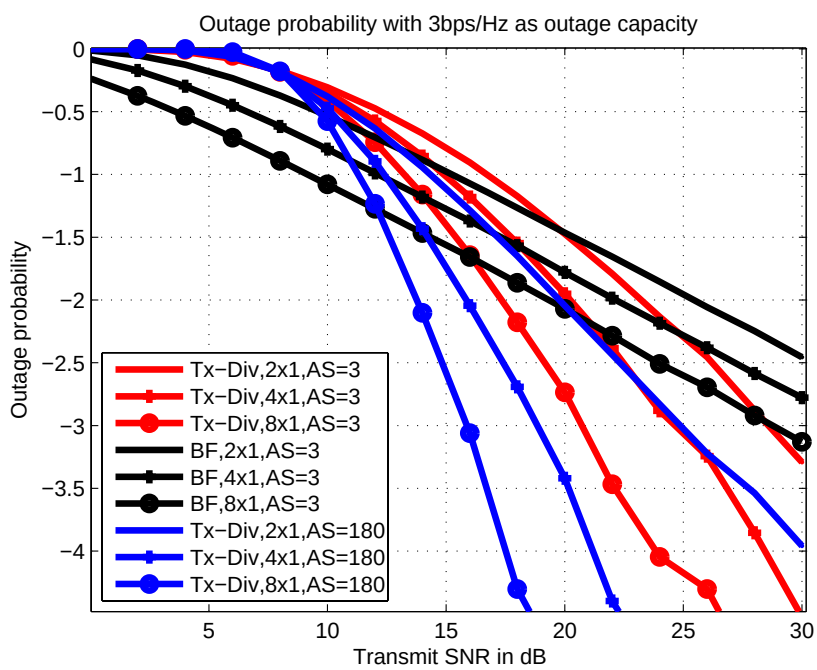

Figure 7.7: Impact of antenna correlation corresponding to different angle spread on transmit diversity and beamforming.

Using the spatial correlation model described above, we investigate the impact of transmit antenna correlation on transmit diversity and beamforming schemes. We use a semi-analytical method to calculate the outage probability corresponding to 3bps/Hz outage capacity. The chan-

© Muhammad Imadur Rahman, 2007

nel coefficients are generated so that they are zero-mean unit-variance independent Gaussian random variables. The channel is taken to be un-correlated in time between two consecutive symbol durations. Then, using Eq.(7.38) and (7.39), we can introduce the spatial correlation corresponding to different angle spread values. 10^7 number of channel capacity values are calculated using Eq.(7.17) and (7.18) for transmit diversity and beamforming respectively. From these capacity values, we determine the outage probability for 3bps/Hz outage capacity, which is shown in Figure 7.7. This figure should be seen in collaboration with Figure 7.5(b), where independent fading for transmit diversity and complete correlation for BF is assumed. Comparing the result in Figure 7.7, we can see that for an angular spread of 3°, the performance of transmit diversity suffers hugely. Only for outage probability less than 1%, the transmit diversity performs better compared to BF for 2×1 and 4×1 systems. when the angular spread is 180°, then the diversity gains are more visible in transmit diversity schemes. In a nutshell, when spatial correlation is high due to very small angular spread, the beamforming scheme should perform very closely (or even better) at least for 2×1 and 4×1 systems.

7.5.3 Simulation Parameters

Indoor micro-cell and outdoor macro-cell scenarios are considered for DL in our simulations. Simulations are performed for a single cell system to simplify the analysis. Obviously this means that no CCI is present in the system. The simulation parameters are listed in Table 7.2.

	Indoor	Outdoor
Max delay spread [124]	$\leq$0.5μs	5μs
Max angular spread [124]	360°	20°
System bandwidth	20MHz	
Carrier frequency	5.0GHz	
OFDM sub-carriers, N	64	1024
Data sub-carriers	52	832
Null sub-carriers	12	192
Subcarrier spacing, kHz	312.5	19.53125
CP length, N_g	16	200
OFDM Symbol Duration, $T_s = T_u + T_g$, μs	4	61.2
Useful data period, T_u, μs	3.2	51.2
CP period, T_g, μs	0.8	10
Sampling duration, T, ns	50	50
Symbol mapping	QAM	QAM
Channel coding	$\frac{1}{2}$-rate Convolutional coding	
Data rate, Mbps	13	14.2
User velocity, kmph	3	50
Doppler spread, Hz	13.9	231.5
Coherence time, T_c, ms	30.5	1.8

Table 7.2: Parameters for comparison between diversity and beamforming

Four antennas at the transmitter side is chosen for BF system. By looking at the outage capacity results in previous sections, we have seen that two transmit antennas can provide at best

3dB of array gain for BF, while this gain may not be enough for some scenarios. With four transmit antennas, the maximum achievable array gain will be 6dB. More number of antennas are also possible to use for the simulations, but, in that case, we may not be able to ensure that the channel is constant for a duration of $\frac{PT_s}{R_{td}}$ seconds.

We use the $\frac{1}{2}$-rate Tarokh code described in Table 7.1, which is suitable for any 4×1 system, giving full diversity but losing in bandwidth efficiency. In both transmit diversity approaches, STBC and SFBC, the antenna spacing has to be such that low correlation between signals is achieved at MS, hence it is chosen to use $d = 5\lambda$, since at the BS there are no space constraints as at the MS. However, since the performances of STBC and SFBC do not differ much, we have only included STBC for this simulations. Regarding BF, in order to obtain a narrow beam, the antenna elements must be placed closely, hence the spacing chosen was $d = \lambda/4$.

7.5.4 BER Results and Discussions

STBC and BF applied to the multi-access schemes OFDM-TDMA and OFDMA are compared regarding their performance and implementation complexity. We assume that the synchronization requirement of the OFDM receiver is perfectly met and perfect CSI is present at the receiver. When comparing the systems using different techniques, it is assumed that they are using the same number of antennas, as well as the same transmit power level. The performance is measured in terms of raw BER.

Based on [124], angular spread is chosen for indoor channel as $[120^o, 240^o, 360^o]$. On the other hand, for outdoor channel, the angular spread is made to vary within $[5^o, 10^o, 20^o]$.

For these different values of angular spread, BER curves for STBC-OFDM system are presented in Figure 7.8. The STBC is implemented with four antennas using Tarokh's orthogonal code with half-rate. By analyzing the results in that same figure, it can be seen that for indoor scenarios (i.e. higher angular spread), the BER performance of transmit diversity is generally better than for outdoor scenarios (i.e. lower angular spread). This means that the advantage that can be taken out of the use of STBC is more significant in indoor environments than in outdoor scenarios, due to higher angular spread that makes the arriving signals from different spatial location less correlated. Hence, more reliability is achieved by combining those different sources of data.

The simulations are performed in an analogous way for BF-OFDM system and the results are shown in Figure 7.9. Unlike the previous case, it can now be seen that for BF, a smaller angular spread results in better performance of the system.

In order to compare which method better fits to each environment, the results for outdoor and indoor cases are shown in Figures 7.10 and 7.11 respectively.

From the results obtained in this work, it can be highlighted that in outdoor scenarios, BF performs better than transmit diversity in OFDM systems. It is found that transmit diversity increases reliability of the received signals with the increase of angular spread. It has been noticed that in an outdoor environment, targeting an error rate of 10^{-2} with 20° of angular spread (i.e. in outdoor scenario), BF has a gain of more than 7dB compared to transmit diversity. Although the complexity of employing BF is much higher than the one for transmit diversity, it can be said that for outdoor environments, it is worthy.

© Muhammad Imadur Rahman, 2007

For indoor environments, it is seen that transmit diversity does not always perform better than BF. In some particular cases where the user is located in LOS in indoor environment, then BF certainly performs better than transmit diversity. However, even when it seems that employing BF would easily improve system's performance, one has to bear in mind that the complexity of this method is much higher than the simple transmit diversity scheme. Since the gain of employing BF in indoor scenarios is not significantly higher as in outdoor, the strategy could pass for targeting a cheaper cost by employing transmit diversity.

Although we have not investigated the immediate outdoor scenario, the user mobility is higher than indoor in this case and the feedback channels may not be quite efficient to provide the CQI at the beamformer and/or closed-loop transmit diversity system, so that close-loop schemes can be implemented. So, it is our suggestion that open loop system should be used for immediate outdoor channels.

Although it is suggested that BF is a better option compared to transmit diversity in outdoor scenario, BF requires some form of closed-loop information, and the fact that higher user speed in outdoor scenario can somewhat preclude the possibility of closed-loop operation. This provides a conflicting scenario, which may become a hindrance in using closed-loop BF even in outdoor scenario. Thus, BF methods that utilizes the long-term channel statistics may become more useful in outdoor scenario due to system complexity constraints, rather than the ones that require 'short'-term channel information.

7.5.5 Pilot Design Issue

For a satisfactory system performance, proper design of pilot channels are very important. In case of transmit diversity and beamforming systems, the total available power is shared among all transmit antennas. This means that a pilot in these systems will have $\log_{10}(P)$ dB less power, on the average. This is not advantageous for transmit diversity schemes, as the receiver needs to estimate all P number of channels based on these pilots which has an average transmit power reduced by $\log_{10}(P)$ dB. For beamforming schemes, the pilots also obtain the array gain, provided that proper beamforming technique is employed and thus, the received power at the pilots is $\log_{10}(P)$ dB higher compared to the case of transmit diversity scenario. Thus, we can see that beamforming has an advantage in terms of pilot design compared to transmit diversity schemes.

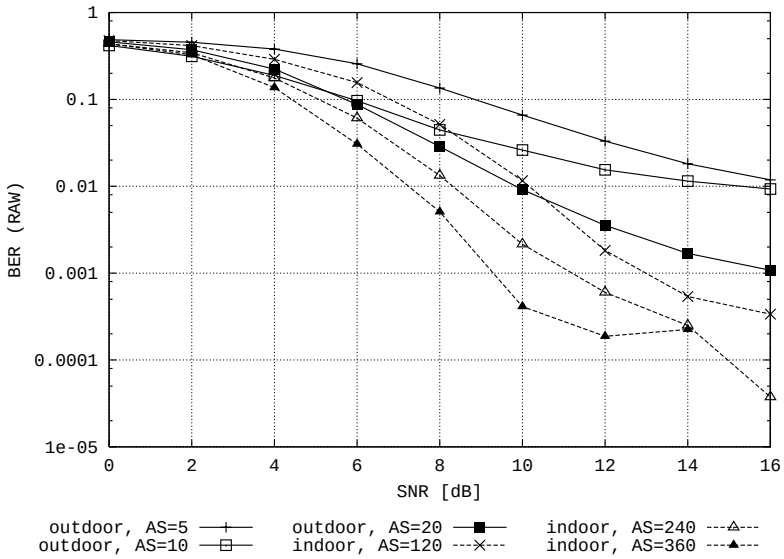

Figure 7.8: BER performance for STBC/SFBC for different AS

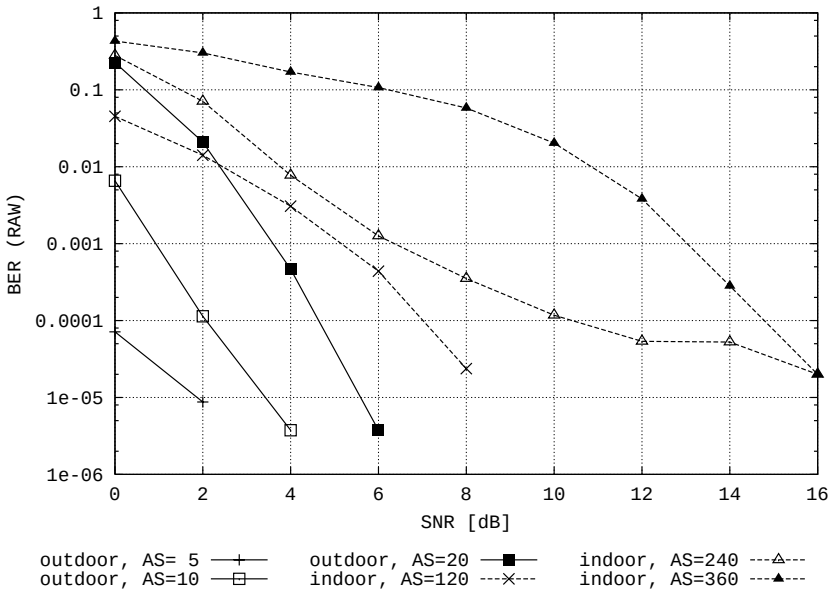

Figure 7.9: BER performance for BF for different AS

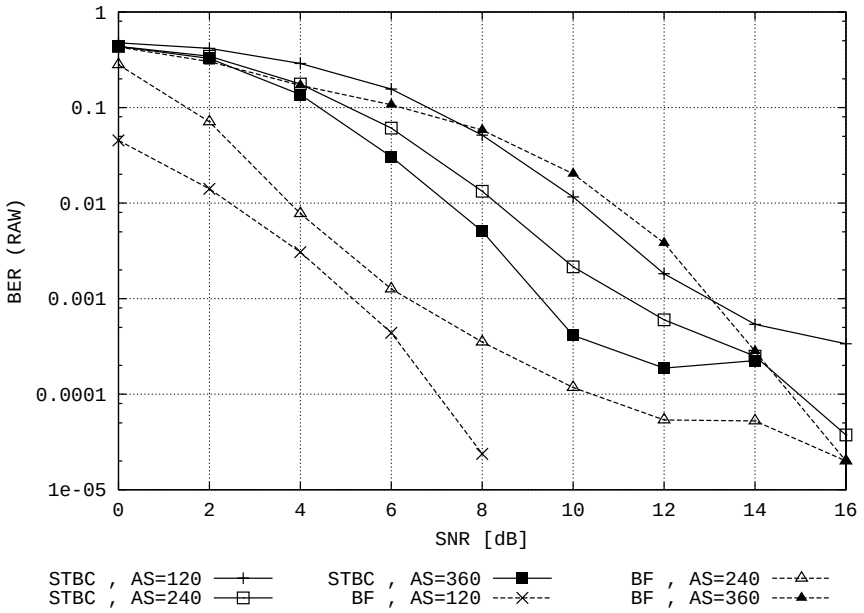

Figure 7.10: BER comparison between BF and STBC for Indoor channel

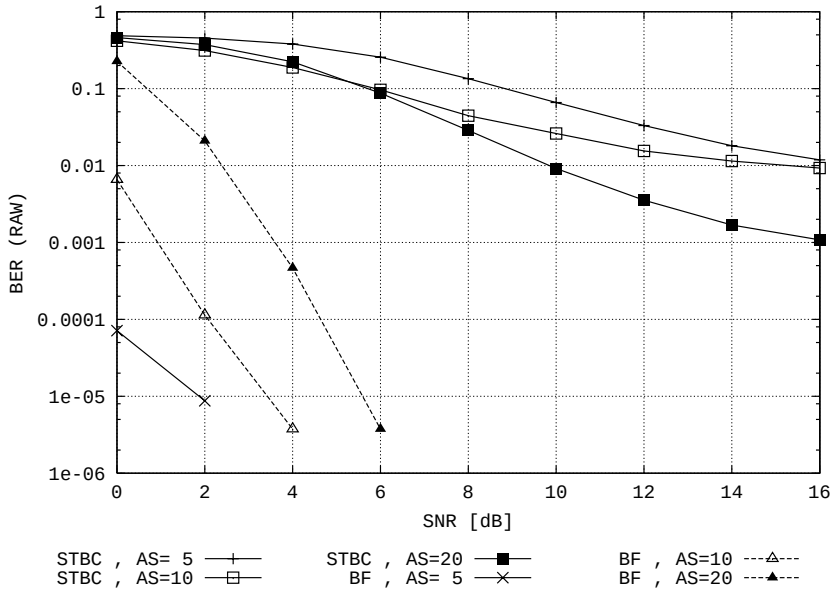

Figure 7.11: BER comparison between BF and STBC for Outdoor channel

7.6 Chapter Summary

Space-Time Block Code (STBC) [25] is an open loop transmit diversity scheme where the diversity is achieved at the receiver without the knowledge of the channel at the transmitter. A complementary to this kind of transmit diversity scheme is BF [126]. TxDiv and BF are two techniques that describes the trade-off between diversity and array gain respectively.

When the wireless channels between transmit and receive antennas are correlated to each other, then transmit diversity scheme is not expected to perform well, i.e. if independent fading among the antenna signals cannot be achieved, BF is preferred over transmit diversity. In BF we exploit the fact that the antenna elements are close together so that appreciable coherence between the antenna signals is present.

In this chapter, we have studied the transmit diversity and beamforming strategies from diversity and array gain perspective. Special attention is given in outage probability for certain outage capacity for the systems. From this point onwards, we have performed numerical evaluations to compare the usability of diversity and array gain in indoor and outdoor scenario.

Regardless of the multiple access scheme, it is found that BF always performs better in outdoor environment, where angular spread is lower, thus spatial correlation is higher. Similarly, indoor environment (high angular spread and low spatial correlation) suggests that transmit diversity schemes are more suitable to be employed than BF strategies.

In a practical cellular system, the total system performance depends on a number of issues that provides different forms of diversity, such as spatial diversity, multi-user diversity, retransmission diversity, macro diversity etc. It is understood that, when different forms of diversity benefits are available, e.g. when macro-diversity is achieved using handover between neighboring cells, then the benefits out of spatial degrees in transmit diversity scheme diminishes and BF may become more preferable, as array gain becomes more important. In the end, the system design depends on available angular spread and number of antennas available at the terminals.

© Muhammad Imadur Rahman, 2007

8

Exploiting Cyclic Delay Diversity in OFDM System

Cyclic Delay Diversity (CDD) is an interesting way to transform the available spatial diversity into extended frequency diversity in an OFDM system. Due to its simplicity in its implementation and its conformance with any established standard, recently CDD has obtained a lot of consideration for broadband OFDM system.

In this chapter we study the exploitation of Cyclic Delay Diversity (CDD) properties in an OFDM system. The basic OFDM system model is given in Section 8.2. We briefly explain the well-known Post-DFT MRC scheme in Section 8.3. Section 8.4 presents the basic mechanisms of CDD technique, and the system capacity of CDD based transmit diversity systems. Our proposed Pre-DFT MARC scheme is described in Section 8.5. We analyze the optimum SNR for maximum cyclic shift and optimum gain factors in this section. We also present a simple case of a dual receive antenna system. Performance results and discussions are placed in Section 8.5.4. This section also describes the comparison of computational complexity between Post-DFT MRC and Pre-DFT MARC techniques and the effect of time-variance in the combining scheme.

Exploiting CDD in SM systems are described in Section 8.6. We have out lined the system architecture in Section 8.6.1. The ergodic capacity analysis of Cyclic Delay Assisted Spatially Multiplexed Orthogonal Frequency Division Multiplexing (CDA-SM-OFDM) system is described in Section 8.6.2. We have presented the simulation results in terms of FER in Section 8.6.3.

Finally, the chapter summary in presented in Section 8.7.

8.1 Introduction

Orthogonal Frequency Division Multiplexing (OFDM) has been successfully used in Wireless Local Area Network (WLAN), such as IEEE 802.11a, European HiperLAN/2 or Japanese Multimedia Mobile Access Coomunication (MMAC) standards as high-data rate physical layer transmission scheme for local area coverage. All three of these standards are almost similar in their PHY layers. Higher data rate along with higher Quality-of-Service (QoS) are one of the prime demands for next generations of wireless communications systems. The omnipresent WLANs standards are capable of providing data rates up to 54 Mbps for local area coverage. The IEEE 802.11a WLAN standard specifies channel coding ($\frac{1}{2}$ rate convolutional coding with a constraint length of 7) and frequency interleaving to exploit the frequency diversity of the wideband channel. Efficiency can only be achieved if the channel is sufficiently frequency-selective, corresponding to long channel delay spreads. In a flat fading situation (or in relatively lesser frequency-selective fading situation which we often encounter in indoor wireless scenario), all or most sub-carriers are attenuated simultaneously leading to long error bursts. In this case, frequency interleaving does not provide enough diversity to significantly improve the decoding performance as reported in [127].

Traditionally space domain is exploited at the receiver to obtain multipath diversity, so schemes like Maximal Ratio Combining (MRC), Equal Gain Combining (EGC), or Selection Combining (SC) are used to obtain a better link quality. MRC is more complex compared to SC and EGC, but yields the highest SNR [34],[35]. In case of MRC, The signals at the output of the receivers are linearly combined so as to maximize the instantaneous SNR. The linear combining in MRC is achieved by combining the co-phased signals, which requires that the CSI is known at the receiver. The SNR of the combined signal is equal to the sum of the SNRs of all the branch signals [34].

For an MRC-OFDM system as shown in Figure 8.1, the combining operations are performed at subcarrier level after the DFT operation, thus we denote the process as Post-DFT MRC or subcarrier combining receiver [77]. The received OFDM signals at different antenna branches are first transformed via Q separate DFTs, when Q is the number of receive branches. Their outputs are assigned to N diversity combiners where N refers to number of OFDM sub-carriers. Note that, similar to MRC, all of the above spatial diversity schemes in an OFDM system requires multiple DFT blocks in the receiver.

STC, such as Alamouti's STBC [25] can be implemented in an OFDM system that takes advantage of flat fading channel and thus achieve full diversity [128],[79]. Using Alamouti's scheme, the source symbols are transmitted in such a way that they can be combined in the receiver using an MRC like method.

Another way of achieving transmit diversity is using a simple Delay Diversity (DD) scheme [129]. Using DD, the original signal is transmitted via the first antenna and a (several) linearly time-delayed version(s) of original signal is (are) transmitted via one (or more) additional antenna elements. The limiting factor for such a diversity system is that the introduced delay should always be shorter than the Cyclic Prefix (CP) to make sure that ISI is avoided.

To overcome this limiting problem, Cyclic Delay Diversity (CDD) has been proposed in [23],[130],[131]. In this case, the signal is not truly delayed between respective antennas but cyclically shifted and thus, there are no restrictions for the delay times. The receiver structure in the DD and CDD

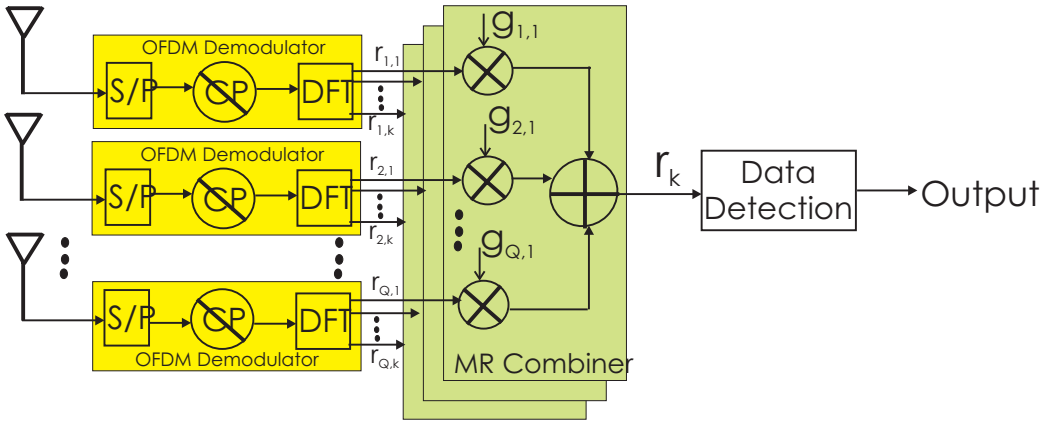

Figure 8.1: Multiple Antenna Receiver Diversity with MRC at sub-carrier level

schemes are similar to each other. It is worth noting here that, similar to Alamouti scheme, it is possible to apply CDD as a transmit diversity technique without knowing the CSI at the transmitter.

Our Contribution: In this chapter, CDD concept is exploited and implemented in OFDM receiver [132], to obtain receiver diversity like MRC. All the signal processing needed is performed in *time domain* when CDD is used to exploit multiple receive antennas, so the duplication of the DFT operation for each receiving antenna branch is not a requirement any more, thus the receiver has lower computational cost compared to Post-DFT MRC (Figure 8.1). At the receiver, the antenna branch signals can be used for estimating the channel responses for each individual receiver antenna in order to optimize the diversity combining based on the instantaneous channel behavior. This allows for an optimized diversity combining using cyclic delays in received data samples and complex gain factors [132].

We have studied a scheme named MARC, which is basically application of CDD in an OFDM receiver. In effect, we obtain partial array gain by employing the weight estimation method explained in this chapter. A detailed discussion on the scheme is presented, where the optimum weighting factors and cyclic shifts are derived for the multiple antenna case, based on the estimated CSI in the receiver. We present a comparative study between MRC receiver diversity and CDD in the IEEE 802.11a and/or HiperLAN/2 WLAN context. The traditional use of MRC is studied along with usage of CDD in both OFDM transmitter and receiver. Special attention is given to the application of CDD at a dual antenna receiver, where the optimum weighting factors and cyclic shifts are derived for the two antenna case, based on the known CSI at the receiver side. Thus, our receive-CDD technique performs better compared to transmit (or receive) CDD techniques studied in [130]. Simulations based on the WLAN standard are performed to compare the different diversity schemes in terms of BER with and without error correction coding.

The Pre-DFT combining simplifies the receiver operations, but it also costs the system performance, because the operations are done on wideband, thus, proper receiver combining gain cannot be archived for highly frequency-selective channels. Thus, an alternative is proposed in [77], where Pre-DFT combining is used together with sub-carrier combining after the DFT operation.

© Muhammad Imadur Rahman, 2007

In this way, the loss due to wideband combining is gained back using sub-carrier level combining, but it also costs in spectral efficiency, because symbols need to be re-transmitted across many sub-carriers, so that sub-carrier level combining can be done. Compared to this work, we do not re-transmit same symbols across many sub-carriers to avoid the loss in spectral efficiency, rather we employ the CDD property at the receiver, so that transformed frequency diversity via CDD principle can be exploited for recovering the loss incurred from wideband Pre-DFT combining.

8.2 OFDM System Model

The OFDM signal consists of N orthogonal sub-carriers modulated by N parallel data streams. Denoting the frequency and complex source symbol of the kth subcarrier as f_k and d_k respectively, the baseband representation of an OFDM symbol is

$$x(t) = \frac{1}{\sqrt{N}} \sum_{k=-\frac{N}{2}}^{\frac{N}{2}-1} d_k e^{j2\pi f_k t}, \quad -\frac{N}{2}T \leq t \leq \left(\frac{N}{2} - 1\right) T. \tag{8.1}$$

d_k is typically taken from a Phase Shift Keying (PSK) or QAM symbol constellation, and NT is the duration of the OFDM symbol. The subcarrier frequencies are equally spaced at $f_k = k/NT$. The OFDM signal in Eq.(8.1) can be derived by using a single (inverse) DFT operation rather than using a bank of oscillators. Thus the discrete time representation of an OFDM symbol is

$$x(t) = \frac{1}{\sqrt{N}} \sum_{k=-\frac{N}{2}}^{\frac{N}{2}-1} d_k W_N^{kn}, \quad -\frac{N}{2} \leq n \leq \frac{N}{2} - 1, \tag{8.2}$$

where $W_N = e^{j2\pi/N}$. Assuming that the channel impulse response is shorter than the guard interval and that perfect synchronization is achieved, the received signal constellations after OFDM demodulation (which includes the removal of the guard interval and a DFT operation) can be related to the data symbols d_k by [127]

$$r_k = d_k h_k + n_k, \tag{8.3}$$

where h_k is the (complex-valued) channel transfer function at frequency f_k and n_k denotes an AWGN sample with variance $\sigma^2 = \mathcal{E}\{n_k^2\}$. The BER performance depends on the SNR at a certain sub-carrier, which is given by

$$\gamma_k = \frac{\mathcal{E}\{|d_k|^2\}|h_k|^2}{\sigma^2} \infty |h_k|^2. \tag{8.4}$$

Note that the SNR is proportional to the squared magnitude of transfer function; therefore, maximizing h_k will yield improved performance.

8.3 Post-DFT Maximum Ratio Combining

In a traditional wireless system, MRC is widely used as a receiver diversity combining technique where multiple receive antennas are used along with a single transmit antenna. In MRC, the signals at the output of the receivers are linearly combined so as to maximize the instantaneous SNR, array gain and diversity gain [34]. The signals are co-phased and combined together. The assumption here is that the CSI must be known perfectly at the receiver.

For an MRC-OFDM system as shown in Figure 8.1 above, the combining operations are performed at subcarrier level after the DFT operation, thus we denote the process as Post-DFT MRC-OFDM system. Recognizing the fact that combining is performed at subcarrier level, the Post-DFT MRC-OFDM receiver can also be termed as subcarrier combining receiver [77]. The received OFDM signals at different antenna branches are first transformed via separate DFT processors and the values of kth data subcarrier in an OFDM symbol ($r_{1,k}$ up to $r_{Q,k}$) are introduced to diversity combiner, given Q receive antennas are present. The combiner combines the signals based on SC, EGC or MRC on sub-carrier basis. We will focus on MRC in the following discussions.

Ignoring the noise present in the reception process, the received signal in Q^{th} antenna for k^{th} data subcarrier can be expressed as $r_{q,k}$. In the linear combiner, the subcarrier data in each branch is multiplied by

$$g_{q,k} = \alpha_{q,k} e^{-j\theta_{q,k}} \tag{8.5}$$

This multiplication is performed such that each of the signal branches are co-phased (i.e. all branches have zero phase). Here, $g_{q,k}$ is a complex number with $\theta_{q,k}$ is the corresponding phase of received signal branch, and $\alpha_{q,k}$ is the weighting factor defined as

$$\sum_{q=1}^{Q} \mid \alpha_{q,k} \mid^2 = 1 \tag{8.6}$$

Then co-phased branches are added together. The resultant signal envelope is

$$r_k = \sum_{q=1}^{Q} r_{q,k} g_{q,k} \tag{8.7}$$

The above-mentioned Post-DFT combining diversity scheme is optimum in terms of its BER performance [77]. As deep fades are often uniformly distributed among sub-carriers, combining at subcarrier level enables the selection and combination of only the best-quality sub-carriers from uncorrelated antenna branches. For Post-DFT combining schemes, the OFDM signal is treated in the same way as in the single carrier system.

On the other hand, the computational complexity of Post-DFT combining schemes increases with the number of receive antennas and number of sub-carriers used. As shown in Figure 8.1, the Post-DFT combining scheme requires Q independent OFDM demodulators, one for each receive antenna. In many cases, the number of receive antennas is limited to 2, since the largest diversity gain is obtained with $Q = 2$, and diminishing returns are realized with increasing of Q [133]. In addition, the number of diversity combining modules is equal to the number of

© Muhammad Imadur Rahman, 2007

sub-carriers of interest at the receiver. For instance, in the DL, the number of diversity combiners is equal to the number of sub-carriers assigned to that particular user. In the UL, the BS needs N diversity combining module, one for each subcarrier. These requirements will result in a very complex and power-hungry receiver, as 4G wireless system is expected to operate with large number of sub-carriers [134]. In Section 8.5, a less complex diversity combining technique is introduced, which is important for MS whose low hardware and algorithm complexity as well as low power consumption are the key requirements.

8.4 Benefitting from Cyclic Delay Property in OFDM System

In this section, we describe the effect of CDD on an OFDM system. CDD is a simple, efficient and effective way to achieve diversity in such a flat fading scenario. The technique is originally proposed as a transmit diversity [23],[130],[131]. As mentioned earlier, when we shift the OFDM signals cyclically and add them up in the receiver linearly, we actually insert some virtual echoes on the channel response. This effect increases the channel frequency-selectivity, thus higher order frequency diversity can be achieved, which is effectively exploited by a COFDM system.

Figures 8.2(a)-8.2(d) explain the effect of employing CDD seen at the receiver with two diversity paths. Here, we assume that we have 2 transmit antennas (i.e. $P = 2$). The second path is assumed to be cyclically shifted by $\frac{N}{2}$ number of samples, where N denotes total number of OFDM sub-carriers in the system. The 1st and 2nd SISO paths show a frequency flat (or less frequency selective) wideband scenario in Figure 8.2(a) and Figure 8.2(b) respectively. When we linearly add the paths, we do not obtain much diversity, because linear addition of two short channel impulse responses creates another short channel impulse response, thus the frequency selectivity remains same. On the other case, when cyclic delays are applied in the transmitter branches, CDD is achieved and the resulting channel response seen from the receiver is equivalent to frequency selective channel.

8.4.1 System Model with Cyclic Delay Diversity

Figure 8.3 shows the transmission scheme using cyclic delays at the transmitter antenna branches. At first, user data is FEC coded and baseband modulated from any PSK or QAM constellation points. Then the modulated symbols are used at the IFFT inputs and $\tilde{x}_s[n],\ \forall n$ is produced at the IFFT output. The time-domain samples are parallel-to-serial converted. At this stage, an antenna specific cyclic delay, Ω_p, is inserted. So the transmit symbol from p^{th} transmit antenna at s^{th} OFDM symbol time window is written as

$$\tilde{x}_{s,p}[n] = \tilde{x}_s[\big((n - \Omega_p)\big)_N] \tag{8.8}$$

where $\big((n - \Omega_p)\big)_N$ means $(n - \Omega_p) mod N$. The delay Ω_p is shown here in samples, it's equivalent to $T\Omega_p$ seconds in time scale. After this step, CP is inserted at all the antenna branches separately before transmission.

These cyclically delayed branches together convert a MISO channel into a SISO channel.

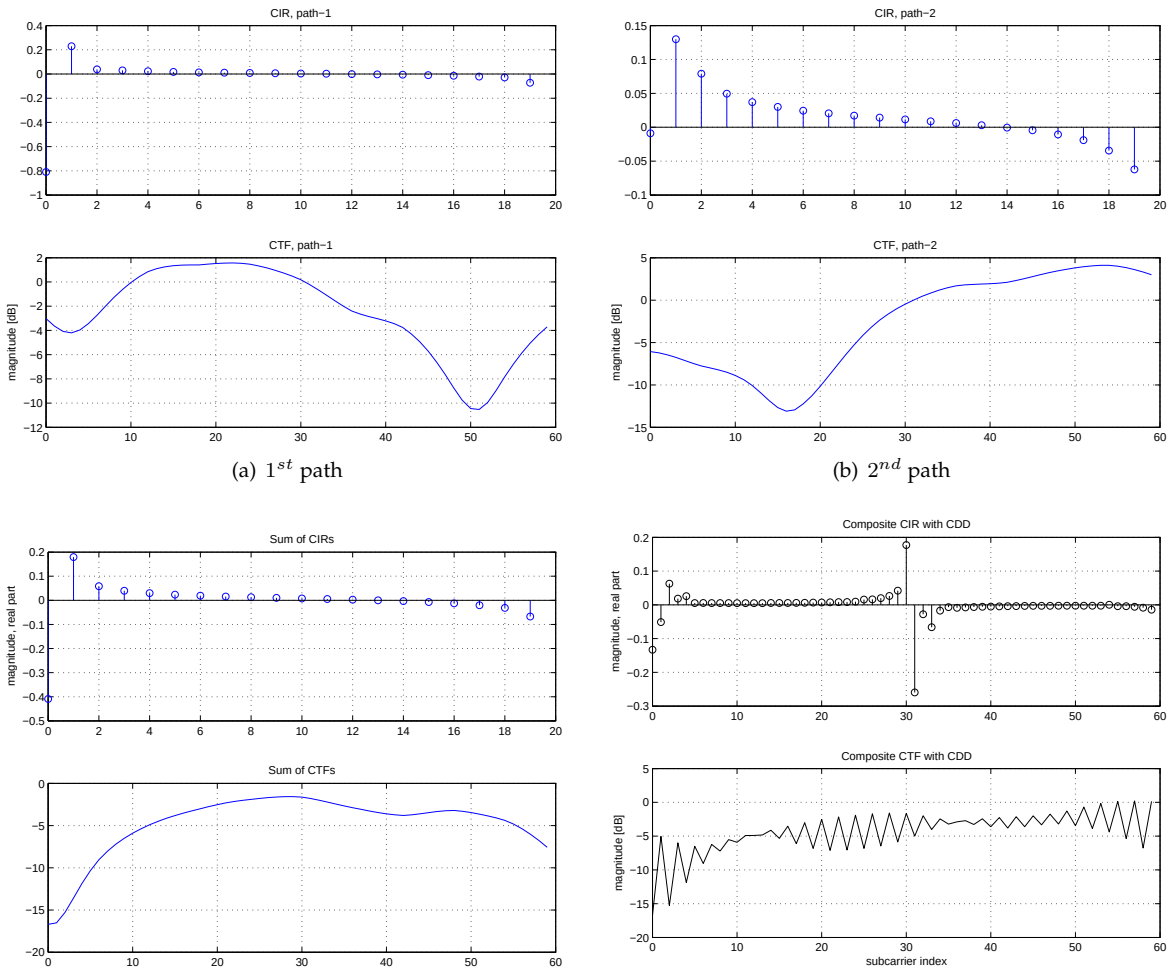

(a) 1st path

(b) 2nd path

(c) Linear sum of the two paths

(d) The combined channel after applying CDD

Figure 8.2: CIR and CTF of two separate paths, their linear sum and the combined channel after applying cyclic delay principle

Similarly, a MIMO channel will become SIMO channel when CDD is applied at the transmitter [135]. This is because, the addition of all cyclically delayed transmit branches at each receive antenna will equivalently 'see' a more frequency selective SISO wireless channel. The equivalent CIR seen at the qth receive antenna can be written as

$$\mathbf{g}_{q,equ} = \frac{1}{\sqrt{P}} \sum_{p=1}^{P} \mathbf{g}_{q,p}[\big((n - \Omega_p)\big)_N] \tag{8.9}$$

Here, $\mathbf{g}_{q,equ}$ is a $(L + max(\Omega)) \times 1$ vector, whose l^{th} element is $g_{q,equ}[l]$, i.e. the CIR of lth tap for the corresponding channel. The normalization factor $\frac{1}{\sqrt{P}}$ is used to keep the transmission power constant. $max(\Omega)$ is the maximum amount of cyclic delay inserted in the transmit branches.

© Muhammad Imadur Rahman, 2007

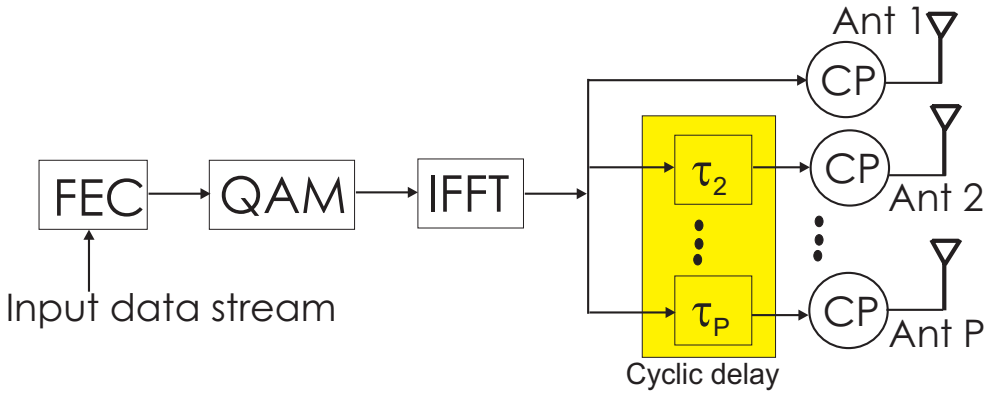

Figure 8.3: Transmitter Model for CDD based MISO-OFDM Transmission Scheme.

The CTF of the equivalent CIR can be obtained as

$$\mathbf{h}_{q,equ} = \mathbb{F}\{\mathbf{g}_{q,equ}\} \tag{8.10}$$

where $\mathbb{F}$ shows the DFT operation. Equivalently,

$$\begin{aligned} h_{q,equ}[k] &= \sum_{l=0}^{L+max(\Omega)-1} g_{q,equ}[l]e^{-j2\pi\frac{k}{N}l} \qquad k = 0, 1, \ldots, N-1 \\ &= \sum_{l=0}^{L+max(\Omega)-1} \frac{1}{\sqrt{P}} \sum_{p=1}^{P} g_{q,p}[\big((l-\Omega_p)\big)_N]e^{-j2\pi\frac{k}{N}l} \\ &= \frac{1}{\sqrt{P}} \sum_{p=1}^{P} \sum_{l=0}^{L+max(\Omega)-1} g_{q,p}[\big((l-\Omega_p)\big)_N]e^{-j2\pi\frac{k}{N}l} \\ &= \frac{1}{\sqrt{P}} \sum_{p=1}^{P} h_{q,p}[k]W_N^{-k\Omega_p} \end{aligned} \tag{8.11}$$

As mentioned above, Figure 8.2(d) shows the corresponding time and frequency response of equivalent SISO channel as described in Eq.(8.9) and Eq.(8.11). It is worth noting that the increased frequency diversity at the receiver is originated from available spatial diversity from the transmitter, thus it can be said that CDD utilizes the available spatial diversity for better frequency de-correlation for the OFDM system. When the frequency selectivity is increased, then it is understood that the average BER can be improved when CDD can be used in co-ordination with FEC coding in near frequency flat (or less frequency selective) scenario.

8.4.1.1 Choice of Delay Parameter in Tx-CDD

As we noted that no CSI is available at the transmitter, we have to insert the cyclic delays in a blind manner. As it is shown in [21] that, if Ω is chosen to be equal to or smaller than L, then the delay diversity cannot convert the available spatial diversity into frequency diversity, because the delayed channel impulse responses will 'fall' on each other in the equivalent CIR. Thus, a good

choice of cyclic delay can be [136]

$$\Omega_p = \frac{N(p-1)}{P} = \frac{N}{P} + \Omega_{p-1} \tag{8.12}$$

8.4.1.2 Diversity Order in CDD

The orthogonal STBCs (and corresponding SFBCs) that are designed in [78, 25] obtain full diversity, which can also be seen from Eq.(7.6). This is ensured by utilizing linear receivers that adds the channel coefficients only constructively (i.e. MRC like receiver). Thus, the full diversity is already obtained before the constellation de-mapper. As opposed to this, when we look at Eq.(8.11), we can see that the channel is added up incoherently for CDD systems. It can be easily shown that $h_{q,equ}[k]$ has a normal distribution with zero mean and unity variance, i.e. $h_{q,equ}[k] \sim \mathfrak{c}\mathcal{N}(0,1)$. This is the reason that we do not see any gain in terms of BER between SISO and CDD system in Figure 8.10 for uncoded case. Thus, the available frequency diversity can only be picked up when the FEC coding and de-interleaving is performed. In this way, in collaboration with FEC, CDD systems obtain full diversity [136, 131, 130]. For original CDD proposals [23, 130], the delay parameter is inserted blindly either at transmitter or at receiver. In both of these cases, the diversity gain is full, i.e. the diversity order is always P and Q for the cases, when blind CDD is employed in transmitter and receiver, respectively .

Note that, for any arbitrary number of antennas, it is possible to obtain full rate and full diversity in CDD with linear receivers, while original STBCs cannot obtain full rate and full diversity simultaneously with linear receivers when $P > 2$ [78].

8.4.2 Capacity of CDD Based OFDM System

In the following we assume that for each channel use, we obtain an independent realization of channel response vectors for all channels between transmit and receive antennas, thus, no spatial correlation is present. It is also assumed that the channel remains constant for one OFDM channel use. When we use CDD, then the equivalent CTF of P number of CDD branches can be treated like any SISO channel CTF. As we use a normalization constant in Eq.(8.11), the total transmitted power is constant in all CDD branches compared to a single SISO channel. We can write the capacity for any k^{th} sub-carrier of the equivalent CDD channel as

$$\mathcal{C}_k^{CDD} = log_2\left[1 + \overline{\gamma} h_{q,equ}[k] h^*_{q,equ}[k]\right] \tag{8.13}$$

where γ is the average received SNR, and $h^*_{q,equ}[k]$ means the complex conjugate of $h_{q,equ}[k]$.

© Muhammad Imadur Rahman, 2007

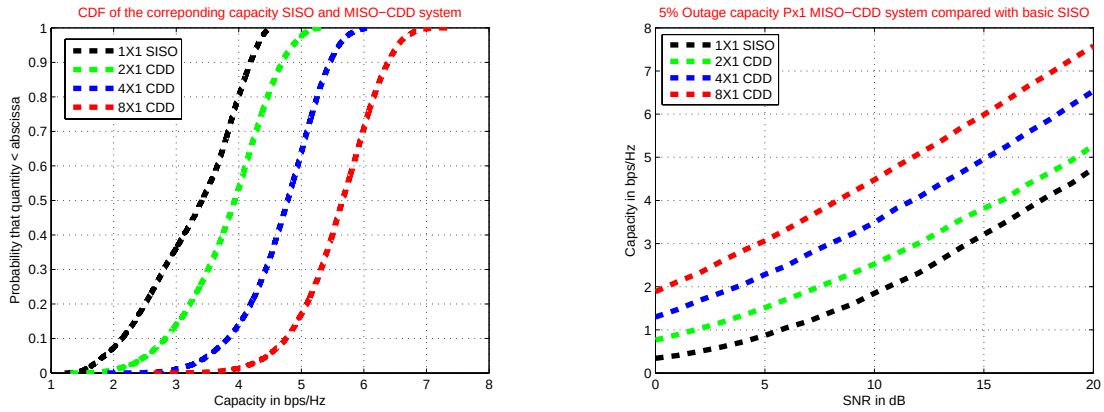

(a) *cdf* of system capacity

(b) 5% Outage capacity

Figure 8.4: cdf of system capacity and 5% outage capacity for SISO and $P \times 1$ CDD systems.

The total capacity of the broadband channel can be written as

$$\begin{aligned}
\mathcal{C}^{CDD} &= \frac{1}{N}\sum_{k=0}^{N-1}\mathcal{C}_k^{CDD} \\
&= \frac{1}{N}\sum_{k=0}^{N-1} log_2\left[1+\overline{\gamma}h_{q,equ}[k]h^*_{q,equ}[k]\right] \\
&= \frac{1}{N}\sum_{k=0}^{N-1} log_2\left[1+\overline{\gamma}\left(\frac{1}{\sqrt{P}}\sum_{p=1}^{P}h_{q,p}[k]W_N^{-k\Omega_p}\right)\left(\frac{1}{\sqrt{P}}\sum_{p=1}^{P}h_{q,p}[k]W_N^{-k\Omega_p}\right)^*\right] \\
&= \frac{1}{N}\sum_{k=0}^{N-1} log_2\left[1+\frac{\overline{\gamma}}{P}\sum_{p=1}^{P}\sum_{p'=1}^{P}h_{q,p}[k]h_{q,p'}[k]W_N^{-k(\Omega_p-\Omega_{p'})}\right] \qquad (8.14)
\end{aligned}$$

The capacity expression in Eq.(8.14) is in fact the average instantaneous capacity across OFDM sub-carriers. This average is the instantaneous capacity of the whole wideband system. To obtain the ergodic capacity, we average this instantaneous wideband capacity over long time.

Figure 8.4(a) shows the Cumulative Distribution Function (CDF) considering capacity of SISO and various CDD systems. Corresponding outage capacity is seen in Figure 8.4(b). These curves are taken against the following parameters: $N = 64$, $\tau_{rms} = 100ns$, $T_s = 4.0\mu s$ and $T_g = 0.8\mu s$. In the ergodic capacity results, the diversity effect cannot be seen, as the time average introduces the time diversity. This diversity effect is added to all the spatial diversity schemes, thus the impact of spatial diversity on ergodic capacity cannot be seen. From the outage capacity results in Figure 8.4(b), it is seen that outage capacity is improved when higher number of CDD branches are used. It should be noted here that the diversity effect is captured in the CDD system capacity without increasing the system complexity too much, i.e. no extra processing is required in the receiver and a minimal processing is needed at the transmitter. Compared to other transmit diversity techniques, such as Alamouti's STBC, the CDD is much simpler and easier to implement.

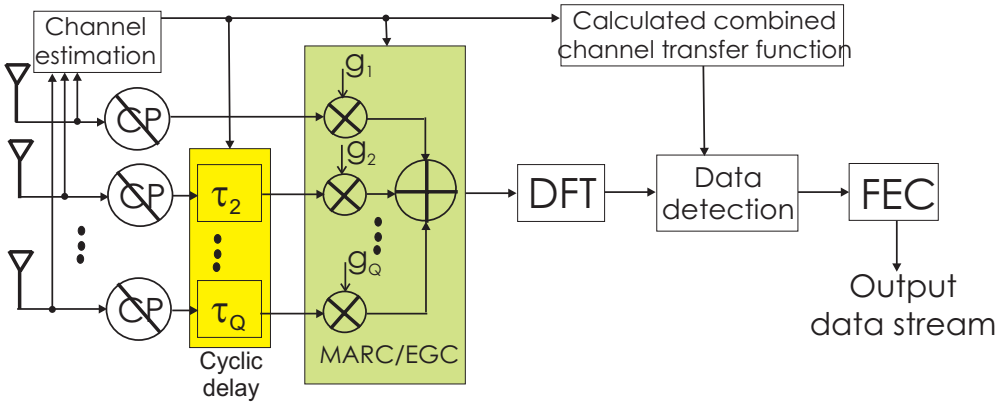

Figure 8.5: OFDM receiver with Pre-DFT Combining CDD. The instantaneous channel is estimated from the received signals to determine the optimum cyclic shifts (and gain factors, if MARC combining is performed).

8.5 Pre-DFT Maximum Average Ratio Combining

Introducing CDD in an OFDM system (either in the transmitter or in the receiver) amounts to increasing the frequency-selectivity of a relatively flat fading channel seen from the receiver side [127]. When CDD is introduced at the receiver, the diversity combining is performed prior to the DFT operation [127, Section 8.3], as shown in Figure 8.5. At the receiver, the antenna branch signals can be used to estimate the channel responses for each individual receiver antenna in order to optimize the diversity combining based on the instantaneous channel behavior. This allows for an optimized diversity combining using cyclic delays, $\tau_n^{(q)}$ in received data samples and complex gain factors, $g_q = a_q e^{j\phi_q}$, where $a_q = |g_q|$, $\phi_q = \angle g_q$ and $\sum_{q=1}^{Q} |g_q|^2 = 1$, for $q = 1, 2, ..., Q$.

We denote this combining technique in the OFDM receiver as Pre-DFT Maximum Average (signal-to-noise) Ratio Combing (Pre-DFT MARC). If we select equal values for the gain magnitudes (i.e. $|g_q| = \sqrt{\frac{1}{Q}}$), the combining technique is named as Pre-DFT EGC.

8.5.1 Optimum SNR for the Combined Signal

We denote the discrete time and discrete frequency index as l and k respectively; and define, $r_q(l)$, $r_{q,CDD}(l)$ and $r_{comb}(l)$ as received signal in time-domain at q^{th} receive antenna, signal after applying CDD at q^{th} diversity branch and combined signal after the combining respectively. All of these vectors are defined for one OFDM symbol, so they have a dimension of $[N, 1]$. Denoting the complex valued time-invariant Channel Impulse Response (CIR) of the qth diversity branch as $\mathbf{c}_q(l)$, we can write that [34]

$$r_q(l) \quad = \quad \left[d(l) \overset{N}{\circledast} c_q(l) \right] \tag{8.15}$$

where $\overset{N}{\circledast}$ denotes N-point circular convolution, and by definition, $0 \leqslant l \leqslant N-1$. The length of $c_q(l)$ is actually the length of the CIR for q^{th} diversity branch which is obviously less than N, so the length is extended to N by padding zeros at the end of the vector.

© Muhammad Imadur Rahman, 2007

The signals at each diversity branch after applying CDD can be written as

$$r_{q,CDD}(l) = \left[d(l) \overset{N}{\circledast} c_q((l - \tau_n^{(q)}))_N \right] \tag{8.16}$$

where $c_q((l))_N = c_q((l) mod N)$. The CDD signal, $r_{q,CDD}(l)$ is multiplied with the gain factor g_q to obtain the combined signal,

$$r_{comb}(l) = \frac{1}{\sqrt{Q}} \sum_{q=1}^{Q} g_q \left[d(l) \overset{N}{\circledast} c_q((l - \tau_n^{(q)}))_N \right] \tag{8.17}$$

The data part of the convolution in Eq.(8.17) is the same for all diversity branches, so we can write the effective channel impulse response of the combined channel as

$$c_{comb} = \sum_{q=1}^{Q} g_q c_q((l - \tau_n^{(q)}))_N \tag{8.18}$$

We assume, independent additive white gaussian noise with equal powers are present at the branches, $\sigma_1 = \sigma_2 = \ldots = \sigma_Q = \sigma$. After diversity combining, the noise powers are scaled by the squared magnitude of the gain factors and summed up. Since we choose $\sum_{q=1}^{Q} g_q^2 = 1$, the resulting noise level after diversity combining is constant and equal to the noise power of each antenna branch. Therefore we can derive a measure that is proportional to the SNR after diversity combining as $SNR \propto w[0]$, where $w[l]$ is

$$\begin{aligned}
w[l] &= c_{comb}[l] \overset{N}{\circledast} c_{comb}^*[N-l] \\
&= \sum_{q=1}^{Q} g_q c_q[((l - \tau_n^{(q)}))_N] \overset{N}{\circledast} \sum_{n=1}^{Q} g_n^* c_n^*[((\tau_n^{(n)} - l))_N] \\
&= \sum_{q=1}^{Q} |g_q|^2 c_q[l] \overset{N}{\circledast} c_q^*[N-l] \\
&+ \sum_{q=1}^{Q} \sum_{n=q+1}^{Q} \Big\{ g_q g_n^* c_q[((l - \tau_n^{(q)}))_N] \overset{N}{\circledast} c_n^*[((\tau_n^{(n)} - l))_N] \\
&\qquad + g_n g_q^* c_n[((l - \tau_n^{(n)}))_N] \overset{N}{\circledast} c_q^*[((\tau_n^{(q)} - l))_N] \Big\} \\
&= \sum_{q=1}^{Q} |g_q|^2 c_q[l] \overset{N}{\circledast} c_q^*[N-l] && (8.19) \\
&+ 2 \sum_{q=1}^{Q} \sum_{n=q+1}^{Q} \Re \Big\{ g_q g_n^* c_q[((l - \tau_n^{(q)}))_N] \\
&\qquad \overset{N}{\circledast} c_n^*[((\tau_n^{(n)} - l))_N] \Big\} && (8.20)
\end{aligned}$$

where * denotes the conjugate complex.

It is evident that the first part of Eq.(8.19) of this expression is independent of the cyclic

delays and the phases of the gain factors. Thus the SNR can be optimized with respect to these parameters by maximizing the second part Eq.(8.20). Unfortunately it is not possible to optimize these parameters independently, for the following reasons.

Between each pair of signals q and n, $n \neq q$, the cyclic delay leading to maximum SNR is given by the index of the maximum value in the respective summation term of Eq.(8.20),

$$(\tau_n^{(q)} - \tau_n^{(n)})_{opt} = \arg\max_l \left| c_q[((l - \tau_n^{(q)}))_N] \overset{N}{\circledast} c_n^*[((\tau_n^{(n)} - l))_N] \right| . \tag{8.21}$$

This optimum SNR would be reached by selecting the phase terms according to

$$\angle(g_q g_n^*) = -\angle \left\{ \max_l \left[c_q[((l - \tau_n^{(q)}))_N] \overset{N}{\circledast} c_n^*[((\tau_n^{(n)} - l))_N] \right] \right\} . \tag{8.22}$$

It becomes visible at this point that an independent optimization of the parameters $\angle(g_q)$ and $\tau_n^{(q)}$ is *not* possible if $Q > 2$. E.g. if we optimize the delays and phase-rotations for the antenna pairs 1-2 and 1-3, the corresponding parameters of pair 2-3 will be determined implicitly. We suggest to use the $Q - 1$ largest terms obtained by Eq.(8.21) for optimizing the cyclic delays. The gain factors will then be optimized using the approach described in the next section (i.e. Section 8.5.2).

8.5.2 Optimum Diversity Weights

As we have derived an optimum way to determine the cyclic delays for respective antennas, now the next step should be to determine the diversity branch weight factors. A method to derive optimum diversity weight factors for multiple antenna Pre-DFT processing OFDM receiver is presented in [77]. We adopt a similar weight estimation scheme for our Pre-DFT MARC with CDD receiver diversity scheme.

The SNR after sub-channel diversity combining can be written as:

$$SNR = \Gamma \mathbf{g}^H \mathbf{C} \mathbf{g} \tag{8.23}$$

where Γ is the average SNR per diversity branch, $\mathbf{C}$ is the covariance matrix of the CIRs of all the diversity branches, and $\mathbf{g}$ is the weight vector, defined as $\mathbf{g} = [g_1, g_2, \ldots, g_Q]^T$. Eigen analysis can be performed on the Hermitian matrix $\mathbf{C}$ according to $\mathbf{C} = \mathbf{Z}\mathbf{\Lambda}\mathbf{Z}^H$, where $\Lambda = \mathrm{diag}\,(\lambda_1, \lambda_2, \ldots, \lambda_Q)^T$ is the diagonal matrix whose diagonal elements consist of eigenvalues λ_q of $\mathbf{C}$ and $\mathbf{Z}$ is the unitary matrix whose columns are the eigenvectors corresponding to λ_q. It is found that the optimum diversity weight vector $\mathbf{g}_{opt}$ is the eigenvector, which corresponds to maximum eigenvalue from diagonal matrix $\mathbf{\Lambda}$.

In the method described above, the covariance matrix $\mathbf{C}$ is derived from the CIRs of all diversity branches. The time-domain CIR estimators that are found in literature impose a high computational complexity, thus utilizing the correlation among the signals of the diversity branches directly in time domain instead of explicitly estimating the CIRs or the CTFs of all the diversity branches yields a satisfactory trade-off solution.

We denote the sampled received signal vector at l^{th} sampling instant as $\mathbf{r}^{(l)} = \left[r_1^{(l)}, r_2^{(l)}, \ldots, r_Q^{(l)} \right]^T$.

© Muhammad Imadur Rahman, 2007

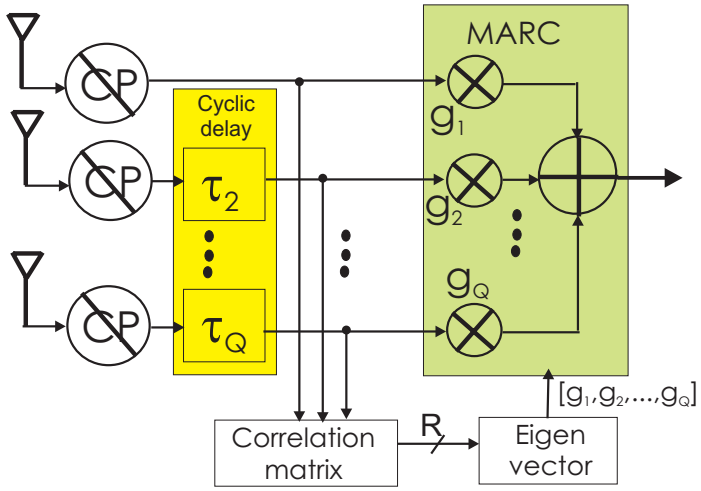

Figure 8.6: Diversity weight estimation method for Pre-DFT MARC with CDD receiver diversity scheme; for clarity, channel estimation procedure and COFDM part of the receiver is not shown in the Figure

The correlation matrix of the received signal vector at any sampling instant is given by

$$\mathbf{R} = \frac{1}{2} E\{\mathbf{r}^{(l)} \mathbf{r}^{(l)H}\} = [\rho_{p,q}] \tag{8.24}$$

where $\rho_{p,q}$ is the $[p,q]^{th}$ element of $\mathbf{R}$ matrix, that represents the correlation among received signal sample for l^{th} instant between p^{th} and q^{th} receive diversity branches, $\rho_{p,q} = \frac{1}{2} E[r_p^{(l)} r_q^{(l)H}]$. Denoting σ_x^2 as the variance of the transmitted signal and σ_n^2 as the variance of the noise component, we find from Eq.(8.24) that

$$\mathbf{R} = \sigma_x^2 \mathbf{C} + \sigma_n^2 \mathbf{I} \tag{8.25}$$

The equation above shows that the eigenvectors of $\mathbf{R}$ and $\mathbf{C}$ are the same, hence we can estimate the optimum weight factors based on the correlation matrix [77]. As it is shown in Figure 8.6, the received signals corresponding to all diversity branches for any sampling instant are put together in a vector ($\mathbf{r}^{(l)}$) and the autocorrelation of that vector is calculated according to Eq.(8.24). After that the optimum weights for all the receive antenna branches are determined using Eigen analysis as described in Eq.(8.25).

8.5.3 System Analysis with Dual Antenna Receiver

In the following analysis, we will concentrate on two branch diversity. Analysis on two-branch receiver is simpler and easier to understand. The channel transfer functions of the two branches are denoted as $\mathbf{h}_1$ and $\mathbf{h}_2$, where

$$\mathbf{h}_q = \begin{bmatrix} h_{q,0} & h_{q,1} & \ldots & h_{q,N-1} \end{bmatrix}^T \tag{8.26}$$

$h_{q,k}$ are samples of the Channel Transfer Function (CTF). Using the above vector notation,

we can obtain a measure that is proportional to the average SNR over all sub-carriers as

$$SNR_i = \mathbf{h}_i^H \mathbf{h}_i \tag{8.27}$$

where $(.)^H$ denotes the complex conjugate of a transposed vector $(.)$. For dual antenna system (i.e. $M = 2$), we denote the complex gain factors as $g_1 = \sqrt{a}$ and $g_2 = \sqrt{1-a}\, e^{j\phi}$, $0 \leq a \leq 1$. $\tau_n^{(2)} = n^{(2)}$ (in more general term, $\tau_n^{(q)} = n^{(q)}$ in data samples) is the inserted cyclic delay in branch two (in samples). The combined channel frequency response as a function of inserted cyclic delay, $n^{(2)}$, and diversity weight factor, g, can be written as

$$\mathbf{h} = \sqrt{g}\mathbf{h}_1 + \sqrt{1-g}e^{j\phi}\mathbf{W}_N^{n^{(2)}}\mathbf{h}_2 \tag{8.28}$$

where $\mathbf{W}_N^{n^{(q)}} = \text{diag}([W_N^{0^{(q)}}, W_N^{n^{(q)}}, W_N^{2n^{(q)}}, ..., W_N^{(N-1)n^{(q)}}])$, $W_N = e^{j2\pi/N}$, represents the cyclic delay in the qth branch.

Following Eq.(8.27) and Eq.(8.28), we can obtain an expression that is proportional to the average SNR over all sub-carriers in terms of a and $n^{(2)}$ as:

$$\gamma(a,n) = a\mathbf{h}_1^H\mathbf{h}_1 + (1-a)\mathbf{h}_2^H\mathbf{h}_2 + 2\Re\Big(e^{j\phi}\sqrt{a}\sqrt{1-a}\mathbf{h}_1^H\mathbf{W}_N^{n^{(2)}}\mathbf{h}_2\Big) \tag{8.29}$$

The phase, ϕ, for maximum SNR is found as

$$\phi_{max} = -\angle(\mathbf{h}_1^H\mathbf{W}_N^{n^{(2)}}\mathbf{h}_2) \tag{8.30}$$

which maximizes the additive third term in Eq. (8.29). Substituting this phase, the optimum SNR can be calculated as

$$\gamma(a,n) = a\mathbf{h}_1^H\mathbf{h}_1 + (1-a)\mathbf{h}_2^H\mathbf{h}_2 + 2\sqrt{a}\sqrt{1-a}|\mathbf{h}_1^H\mathbf{W}_N^{n^{(2)}}\mathbf{h}_2| \tag{8.31}$$

8.5.3.1 Optimum Weight Factors for Maximum SNR when $Q = 2$

We will achieve two sets of g for any given n, $g_{q|n}$ for $q \in \{1,2\}$ by setting the first derivative of Eq.(8.31) to zero with respect to g. After some manipulations, we obtain:

$$g_{q|n} = \frac{1}{2} \pm \frac{A}{2}\sqrt{\frac{1}{4B^2 + A^2}} \quad \text{for } q \in \{1,2\} \tag{8.32}$$

where $A = \mathbf{h}_1^H\mathbf{h}_1 - \mathbf{h}_2^H\mathbf{h}_2$ and $B = |\mathbf{h}_1^H\mathbf{W}_N^{n^{(2)}}\mathbf{h}_2|$. It is found that the maximum SNR is obtained using the $+$ sign. A simple observation from Eq.(8.32) shows that when both channels have equal average SNR, then $A = 0$ and the two weight factors are equal, being $g_{1|n} = g_{2|n} = 0.5$.

If the channel transfer functions $\mathbf{h}_1$ and $\mathbf{h}_2$ are orthogonal to each other for some specific cyclic delay n, then $B = 0$ leading to $g_{1|n} = 0, g_{2|n} = 1$ or $g_{1|n} = 1, g_{2|n} = 0$, unless $A = 0$. This means that for these particular channel realizations, nothing can be gained on the average over all sub-carriers compared to a single channel system. In another words, only one diversity branch can be exploited effectively in this case.

For one set of channel realizations, the average SNR as a function of the shift parameter

© Muhammad Imadur Rahman, 2007

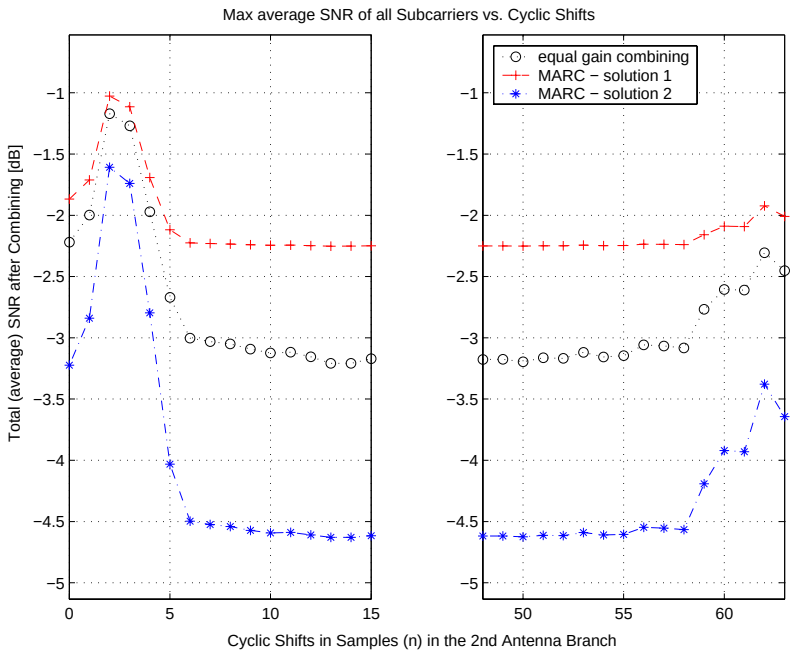

Figure 8.7: Average SNR with two-branch Pre-DFT MARC and Pre-DFT EGC with cyclic delays as a function of the delay parameter n (in samples).

n is shown in Figure 8.8. Pre-DFT MARC yields two solutions of weighting factors as indicated by Eq.(8.32), corresponding to the minimum and maximum average SNR. With respect to n, the maximum is reached with a cyclic shift of 2, for this particular set of channels. There is a gain of about 0.9dB compared with the best solution without CDD (i.e., when $n^{(2)} = 0$). The maximum SNR is always achieved for a very small or very large value of n as analyzed below.

8.5.3.2 Optimum Cyclic Shift for Maximum SNR when $Q = 2$

The maximum SNR with respect to n can be found from Eq.(8.31) by determining the maximum of B with respect to n (because A does not depend on n). $B(n)$ is in fact the IFFT of the product of two CTFs. So, to determine the delay n for maximum average SNR efficiently, we can compute

$$\mathbf{c} = \|\mathbb{F}_N^H\{\mathbf{h}_1^*.\mathbf{h}_2\}\| \tag{8.33}$$

where the IFFT is zero padded to N points and . denotes element-wise multiplication of two vectors. The index to the maximum of the resulting vector $\mathbf{c}$ equals the cyclic delay n_{max} that provides maximum average SNR. Figure 8.8 presents the histogram of the optimum cyclic shifts for maximum average SNR, calculated by using Eq.(8.33). The figure confirms that the optimum delays are confined to small values of n between $0-4$ and $60-63$. Note that the number of sub-carriers in the OFDM system in 64. This is due to the fact that the IFFT of the product of two CTFs is equivalent to the cyclic convolution of the respective channel impulse responses (where the impulse response corresponding to the conjugated transfer function is time-reversed). For relatively flat fading indoor wireless channel scenario, the channel impulse responses span over a few samples each, so

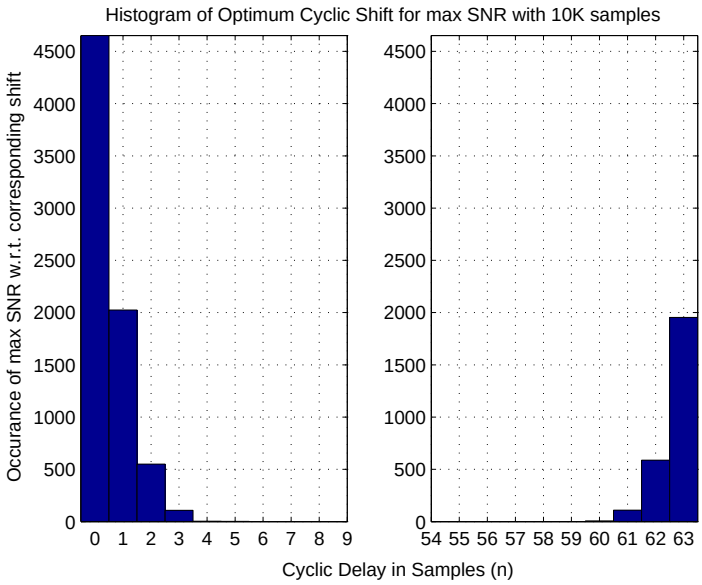

Figure 8.8: Histogram of Cyclic Shifts obtained for Maximum Average SNR with 10000 samples.

their convolution is roughly twice the length of one impulse response, located around both sides of 0. Note that, for the channel parameters used, in more than 50% of the simulated channel realizations some gain was obtained by introducing the cyclic delay. For the readers information, without cyclic delays, Pre-DFT diversity combining was studied in [77].

8.5.4 Numerical Analysis and Discussions

8.5.4.1 Channel Model

A second order stochastic channel model (WSSUS model) suitable for Rayleigh and Ricean fading distributions was used in this work. The frequency-selectivity is described by the spaced-frequency correlation function and by the delay power spectrum (DPS) [127]. In the simulations, realizations of channel transfer functions are generated directly, based on well-defined channel parameters, such as the normalized (or average) received power P_0, the Ricean parameter K and the RMS delay spread τ_{rms}. Indoor WLAN channels with $\tau_{rms} = 5ns$ to $50ns$ are generated. This corresponds to 0.1 to 1 sample considering a sampling frequency of 20MHz as used in IEEE 802.11a. Rayleigh fading scenarios (i.e. $K = 0$) and Ricean fading scenarios with $K = 4$ were considered.

8.5.4.2 Simulation Parameters

Simulations are performed with parameters stipulated by the IEEE 802.11a WLAN standard: number of OFDM sub-carriers, $N = 64$, length of Cyclic Prefix (CP), $N_{CP} = 16$ samples, OFDM symbol duration, $T_S = 4\mu s$ (consists of useful data period of $3.2\mu s$ and CP duration of $0.8\mu s$), QPSK symbol mapping with half-rate convolutional coding (corresponds to 12Mbps raw bit rate at the receiver), system bandwidth of 20MHz and operating at the 5GHz band. Our simulations only considered the dual antenna case (i.e. $M = 2$).

© Muhammad Imadur Rahman, 2007

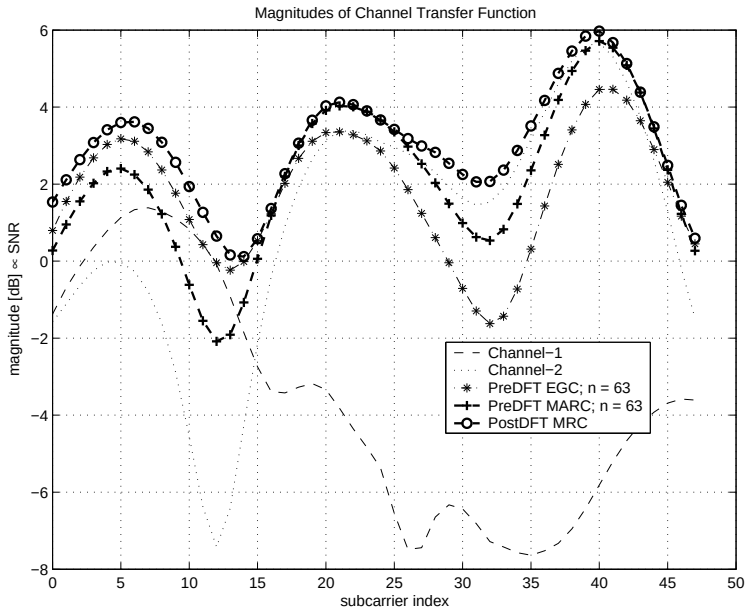

Figure 8.9: Magnitudes of Channel Transfer Functions before and after diversity combining. Pre-DFT MARC, Post-DFT MRC, and Pre-DFT EGC are shown in the figure.

8.5.4.3 Analysis of Channel Responses After Combining

The analysis shows that the amount of cyclic shift and the combiner weight factors can be determined effectively in order to achieve optimum SNR in all cases for a Pre-DFT *Receiver* CDD system, because the CSI can be estimated. Figure 8.9 shows the magnitude response of the combined channels (equivalent to the SNR per subcarrier) for several receiver diversity schemes, along with the channel responses of the branch channels. It is seen that the Post-DFT MRC scheme shows better SNR characteristics, though the responses for Pre-DFT MARC and Pre-DFT EGC are also very close.

8.5.4.4 Performance Results and Discussions

BER simulations have been performed for dual antenna receiver diversity using Post-DFT MRC, Pre-DFT MARC and Pre-DFT EGC. For comparison, pure CDD at the transmitter (Tx-CDD) with fixed cyclic delay of 16 samples [131] and Pre-DFT MARC without cyclic delay (which is equivalent to the technique described in [77]) are also simulated.

Figures 8.10 and 8.11 show uncoded BER results, which were calculated in a semi-analytical way as follows. For the various receiver concepts compared, the SNR values on the OFDM subcarriers were simulated. Based on these simulated channels, the BERs were determined analytically, using the Q-function, and averaged. The E_b/N_0 shown is the ratio of the average symbol energy per sub-carrier to the noise power density. Coherently detected QPSK with perfect channel estimation is assumed in this analysis.

On the Rayleigh channel, Tx-CDD does not give any performance advantage in terms of uncoded BER compared with a single antenna receiver, because the channel gains are added up

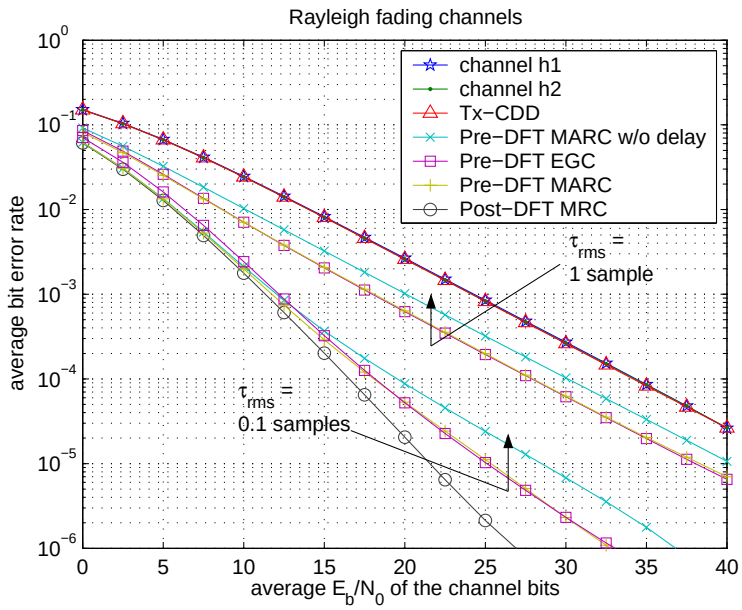

Figure 8.10: Uncoded BER with and without application of diversity, Rayleigh fading channels with various τ_{rms}.

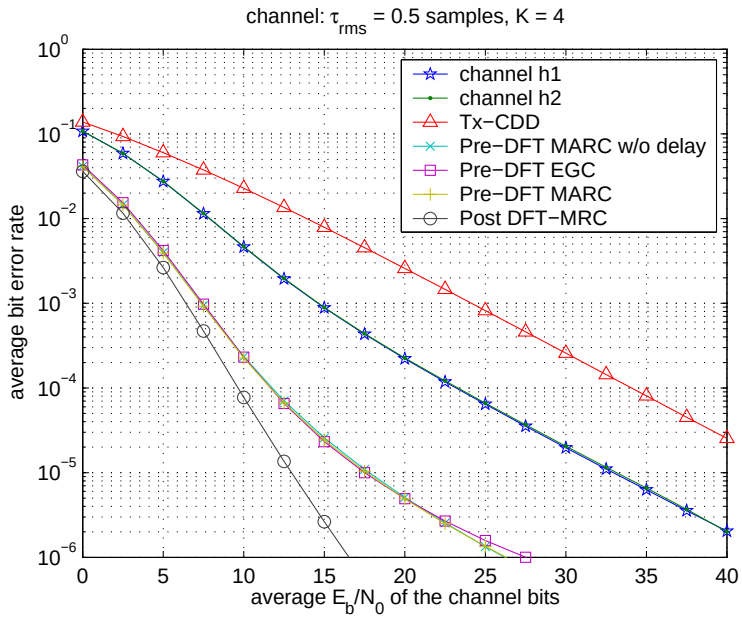

Figure 8.11: Uncoded BER with and without application of diversity, Ricean channel with $K = 4$.

© Muhammad Imadur Rahman, 2007

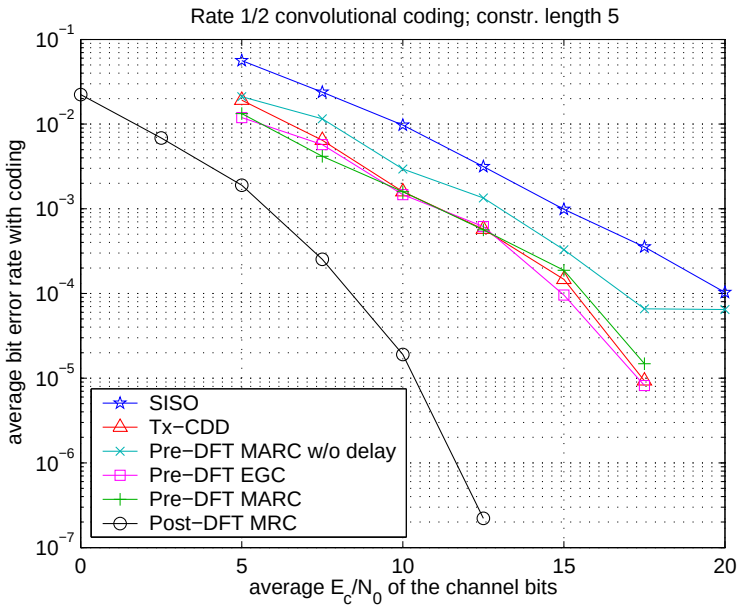

Figure 8.12: Performance results in terms of coded BER; Rayleigh channel, $\tau_{rms} = 1$ sample; rate $\frac{1}{2}$ convolutional coding with constraint length 5.

incoherently just like the noise. On the Ricean channel, the performance with Tx-CDD is even worse, because the combined channel has deeper fades than the component channels. This is one of the main drawbacks of Tx-CDD. The best performance is achieved with Post-DFT MRC at the cost of high computational complexity. The Pre-DFT receiver diversity schemes lie in between those results. It is evident that more can be gained over 'flatter' channels (lower τ_{rms} and/or higher K), which is not surprising since in these cases the Pre-DFT combining schemes can add up the channel transfer functions constructively over a wider frequency range. Under the same condition, we observe less performance difference among the Pre-DFT schemes exploiting the CSI. Pre-DFT MARC and Pre-DFT EGC show very similar performance although the average SNR over the sub-carriers is significantly higher using MARC. The gain over Pre-DFT MARC without delay can be significant, but it reduces on channels with a very short channel impulse response.

In Figure 8.12, performance results are given in terms of bit error rate for the coded OFDM system. The source data is FEC-coded with a $\frac{1}{2}$ rate convolutional coder, whose constraint length is 5, i.e., the effect of each information bit is spread over roughly 10 FEC coded bits. A block interleaver (with interleaver depth = 4) is used to exploit the available frequency diversity. After interleaving the FEC-related bits are spread over 40 sub-carriers in an OFDM symbol (which consists of 48 data sub-carriers). Note that the constraint length was reduced compared with the WLAN standard in order to speed up the computer simulations. Although this affects the absolute results, we expect the general trends and conclusions to be equivalent. BER performance shows that the largest gain is achieved with the 'traditional' Post-DFT MRC technique, amounting to almost 7dB at $BER = 10^{-4}$. About 3-4dB gain are observed from the Pre-DFT diversity combining techniques, whose performance is remarkably similar. Only MARC without delay is slightly weaker. In particular, after coding, the 'optimized' techniques applied at the receiver, which can use CSI, perform

not much better than the 'unsupervised' combining technique using a fixed cyclic delay.

It is evident from Figures 8.10, 8.11 and 8.12 that the scheme works better in situation where the RMS delay spread is quite small, which means that, in a typical indoor WLAN environment, Pre-DFT MARC will perform well. It is a prolific advantage that our scheme works better even if the diversity branches are correlated to each other due to LOS scenario. This brings another benefit, i.e. usually the size constraint in MS causes insufficient spatial separation between antennas. When the antennas are closely placed to each other, then the diversity branches will experience sufficient correlation which will destroy the benefits that the diversity schemes (such as Post-DFT MRC or EGC or SC) bring. In those cases, Pre-DFT MARC scheme can be used to combine the signals efficiently from correlated diversity branches.

8.5.4.5 Efficient Implementation

We compared the complexity of the schemes in terms of number of multiplications required. Considering that we have a channel which is time-invariant for considerable amount of time, so that N_{pkt} number of OFDM symbols can be put in one OFDM packet, then the number of multiplications required for one OFDM symbol are

$$X_{pre} = \frac{Q(Q-1)N_o}{2} + N_{pkt}\left(\frac{N}{2}log_2N + QN\right) \tag{8.34}$$

$$X_{post} = N_{pkt}\left(\frac{QN}{2}log_2N + QN\right) \tag{8.35}$$

where $\frac{N}{2}log_2N$ multiplications are required for FFT module per OFDM symbol [8]. The 1st term of Eq.(8.34) corresponds to the calculation of covariance matrix shown in Figure 8.6. N_o is the number of time-domain data samples that need to be acquired to obtain the correlation matrix. The computational complexity associated with Eigen analysis for gain factors is not taken into account, as it is only required once for complete OFDM packet [77].

Figures 8.13(a) and 8.13(b) show the relative processing cost between Pre-DFT MARC and Post-DFT MRC in comparison to N and N_{pkt} respectively for different values of Q. In both figures, we can see that the processing cost is drastically reduced in our scheme when N or N_{pkt} or Q increases.

8.5.4.6 Effect of Channel Time-Variance

Referring to Figure 8.5, our scheme requires channel estimates in time domain for delay insertion and gain factor estimation; and in frequency domain for data detection. If the channel is severely time variant, then the channels need to be estimated very frequently, and thus the savings in complexity due to time-domain combining will be lost in excessive channel estimation burden. Table 8.1 summarizes the relationship between channel coherence time with respect to user velocity in the context of IEEE 802.11a WLAN system. If the coherence time is defined as the time over which the time correlation function is 0.5, then the coherence time is approximately, $T_c = \sqrt{\frac{9}{16\pi f_d^2}} = \frac{0.423}{f_d}$ [38, Section 4.4.3], when f_d is maximum doppler shift. In the last column of Table 8.1, we have shown the number of OFDM symbols that can be transmitted during T_c at corresponding user velocity.

© Muhammad Imadur Rahman, 2007

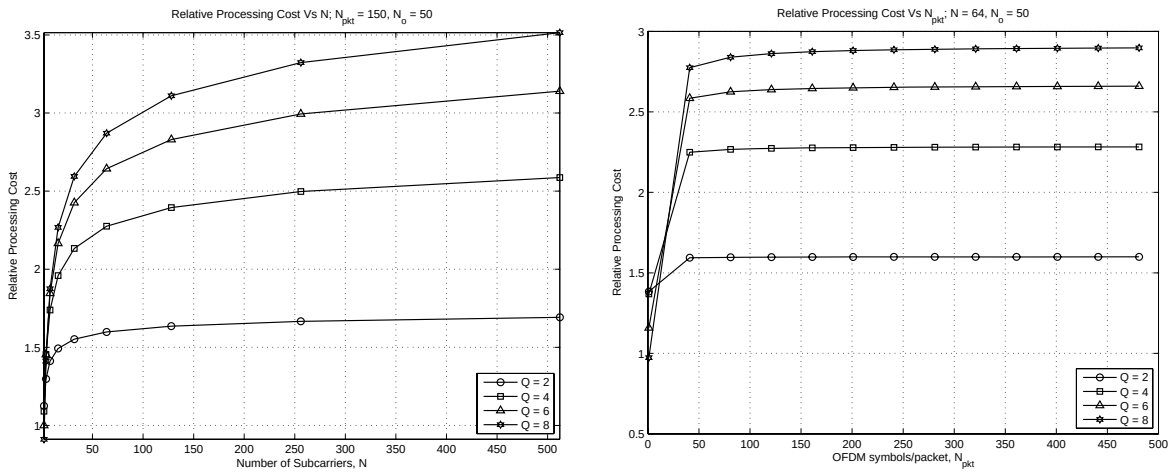

(a) Cost vs number of OFDM sub-carriers; $N_{pkt} = 150$ and $N_o = 50$

(b) Cost vs number of OFDM symbols/packet; $N = 64$ and $N_o = 50$

Figure 8.13: Relative Processing cost for Pre-DFT MARC and Post-DFT MRC in comparison to number of OFDM sub-carriers and number of OFDM symbols/packet.

Table 8.1: Comparison of channel coherence time with OFDM packet duration for IEEE 802.11a WLAN Standard

v, km/h	f_d, Hz	T_c, ms	max N_{pkt}
3	54	7.83	1957.5
10	180	2.35	587.5
20	360	1.175	293.75
50	900	0.47	117.5
100	1800	0.235	58.75
250	4500	0.094	23.5

In this case, we have taken that one OFDM symbol duration is $4\mu s$. The standard specifies a test case of 1000 octets in one OFDM packet, this corresponds to $\frac{1000\times 8}{24} = 333.3$ OFDM symbols in a packet with BPSK modulation and $\frac{1}{2}$ rate convolutional coding at the best-case scenario. We can see from the table that a velocity up to 20km/h will have a coherence time that equals to 293.75 OFDM symbols. 20km/h is quite a high velocity (if not impractical) for a WLAN user. When the velocity is increased (in the order of tens of km/h), then obviously the complexity will go higher. In general, when the channel is less time-variant, then the coherence time is larger and so the packet duration can be made arbitrarily larger, so the channel estimation frequency will be smaller.

8.6 Cyclic Delay Assisted Spatial Multiplexing

SM is a promising and powerful technique to dramatically increase the system capacity in terms of throughput. The independent spatial channels in rich scattering environment can be exploited to send multiple signals at the same time and frequency, thus it is also spectrally very efficient. Most

of the available SM techniques are effective in frequency flat scenario [73, 124]. Thus, in frequency selective environment, amalgamation of SM and OFDM techniques can provide a high data rate system where the spectral efficiency can also be high. All the algorithms can now be implemented on OFDM sub-carrier level, since OFDM converts a wideband frequency selective channel into a number of narrowband sub-carriers [22, 75].

Original SM techniques are proposed for increasing spatial data rate [74, 137]. These algorithms do not require any CSI at the transmitter, but require complete CSI at the receiver. The performance of such systems are always under investigation, because, for a sufficient FER performance, we need to have ML detection schemes, but the ML schemes are always very complex to implement. Thus, VBLAST is proposed, as a sub-optimal solution, and as a trade off between performance and cost [24]. Recently there are some approaches of incorporating the VBLAST technique with some well known STC techniques, so that both diversity and multiplexing benefits can be obtained in one transmission structure [138, 139]. We call such a system as JDM system. Arguably, the performance of JDM system would be better compared to original SM system (as in [24]). In [138], the Spatial Multiplexed Orthogonal Frequency Division Multiplexing (SM-OFDM) system uses two independent STC for two sets of transmit antennas. Thus, an original 2×2 SM-OFDM system is now extended to 4×2 STC aided SM-OFDM system. In the receiver, the independent STC are decoded first using pre-whitening, followed by maximum likelihood detection. Again, this increases the receiver complexity tremendously, though the system performance gets much better.

In this work, we discuss using CDD as the way to introduce the STC on SM-OFDM system. We denote the combined system as CDA-SM-OFDM system. Introducing CDD in SM system only requires changes in the transmitter and the receiver remains intact. Thus, the complexity increment is very minimal, but an improvement in performance is expected. We have compared the proposed CDA-SM-OFDM system with original SM schemes and have shown significant improvement in error rate.

8.6.1 Transmission Structure

Figure 8.14 shows the basic transmitter and receiver structure, when cyclic delays are used at the transmission side of a SM-OFDM system. The source data is FEC coded and baseband modulated. We denote this baseband modulated symbols as m_k. Then IFFT modulation is performed and time domain samples, $x[n]$, are placed for appropriate STC. For example, the sequence of $x[n]$ is de-multiplexed into $\mathbf{x}_1, \ldots, \mathbf{x}_P$ signal vectors. After that $\mathbf{x}_p$ for each p is cyclically delayed. In Figure 8.14, the blocks noted by, $\Omega_1, \Omega_2, \ldots, \Omega_\Delta$ perform the cyclic delay operation. The amount of delays for δ^{th} delayed branch for p^{th} SM branch is given by Eq.(8.39). $\mathbf{x}_p$ and its cyclically delayed branches are transmitted via Δ number of antennas, so we denote the transmitted symbol vectors as, $\mathbf{x}_p^{(\delta)} = \mathbf{x}[\big((n - \Omega_\delta)\big)_N]$. This means that total number of transmit antennas in the transmitter is $P\,\Delta$. For any p, all corresponding Δ number of cyclic delay branches are named together as p^{th} group of transmit antennas. The receiver is similar to the original VBLAST receiver as explained in [24].

We denote the received signal vectors at q^{th} receive antenna as $\mathbf{y}_q$ and the corresponding OFDM demodulated symbol vector as $\mathbf{z}_q$. For the following description, we use the notations, $g_{q,p}^{(\delta)}$

© Muhammad Imadur Rahman, 2007

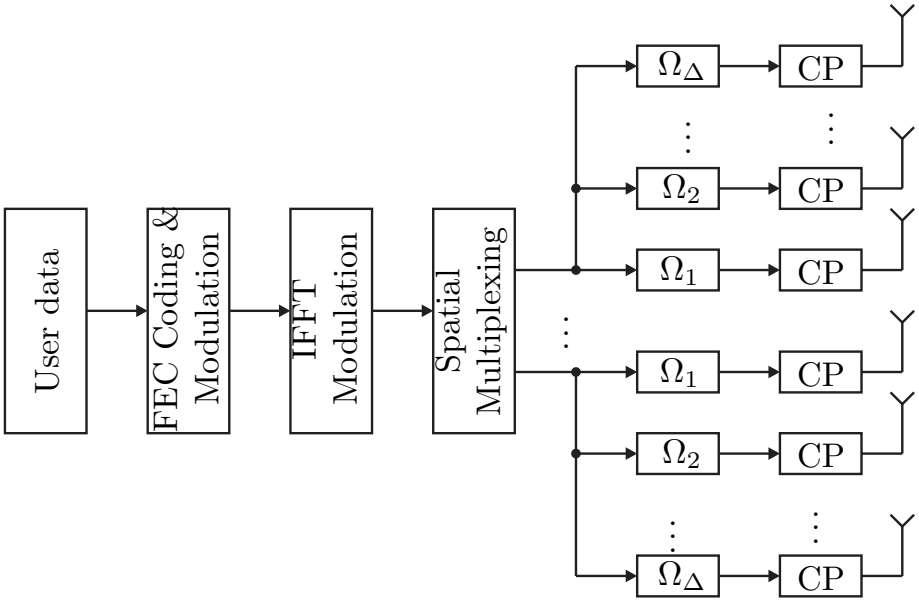

(a) CDA-SM-OFDM Transmitter

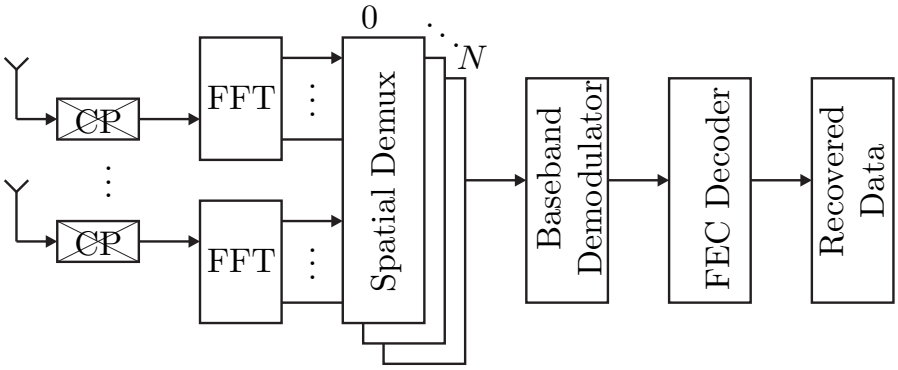

(b) CDA-SM-OFDM Receiver

Figure 8.14: Transceiver Architecture for CDA-SM-OFDM System

and $h_{q,p}^{(\delta)}$, as the CIR and CTF between δ^{th} cyclic delay branch of pth transmit antenna group and q^{th} receive antenna respectively. $\overset{N}{\circledast}$ denotes cyclic convolution operation of N size. The received signals at q^{th} receive antenna can be written as,

$$\begin{aligned}
y[n]_q &= \frac{1}{\sqrt{\Delta}}\left[g_{q,1}^{(1)} \overset{N}{\circledast} x[n]_1 + g_{q,1}^{(2)} \overset{N}{\circledast} x[\big((n-\Omega_2)\big)_N]_1 + \ldots + g_{q,1}^{(\Delta)} \overset{N}{\circledast} x[\big((n-\Omega_\Delta)\big)_N]_1\right] + \ldots \\
&\quad + \frac{1}{\sqrt{\Delta}}\left[g_{q,P}^{(1)} \overset{N}{\circledast} x[n]_P + g_{q,P}^{(2)} \overset{N}{\circledast} x[\big((n-\Omega_2)\big)_N]_P + \ldots + g_{q,P}^{(\Delta)} \overset{N}{\circledast} x[\big((n-\Omega_\Delta)\big)_N]_P\right] \\
&\quad + v[n]_q \qquad (8.36) \\
&= \frac{1}{\sqrt{\Delta}}\left[g_{q,1}^{(1)} + g_{q,1}^{(2)}[\big((n-\Omega_2)\big)_N] + \ldots + g_{q,1}^{(\Delta)}[\big((n-\Omega_\Delta)\big)_N]\right] \overset{N}{\circledast} x[n]_1 + \ldots \\
&\quad + \frac{1}{\sqrt{\Delta}}\left[g_{q,P}^{(1)} + g_{q,P}^{(2)}[\big((n-\Omega_2)\big)_N] + \ldots + g_{q,P}^{(\Delta)}[\big((n-\Omega_\Delta)\big)_N]\right] \overset{N}{\circledast} x[n]_P \\
&\quad + v[n]_q \qquad (8.37) \\
&= \frac{1}{\sqrt{\Delta}}\left[\sum_{\delta=1}^{\Delta} g_{q,1}^{(\delta)}[\big((n-\Omega_\delta)\big)_N]\right] \overset{N}{\circledast} x[n]_1 + \ldots \\
&+ \frac{1}{\sqrt{\Delta}}\left[\sum_{\delta=1}^{\Delta} g_{q,P}^{(\delta)}[\big((n-\Omega_\delta)\big)_N]\right] \overset{N}{\circledast} x[n]_P \\
&+ v[n]_q \qquad (8.38)
\end{aligned}$$

Eq.(8.38) basically gives us the equivalent CIR of the wireless channel between q^{th} receive antenna and all P^{th} transmit multiplexing branches, where $p \in \{1, \ldots, P\}$. For the above formulation, we took the CDD branches to be equal for all transmit antenna groups (i.e. $= \Delta$) for simplicity of expressions. In practice, there should not be any problem in choosing different number of antennas for each transmit antenna group. The amount of cyclic delays for Δ number of antennas in any transmit group can be chosen based on the analysis in [140] as,

$$\Omega_\delta = \frac{N(\delta-1)}{\Delta} = \frac{N}{\Delta} + \Omega_{\delta-1} \qquad (8.39)$$

Now we can obtain the equivalent frequency response of the system from Eq.(8.38). We define the following relationships:

1. $\mathbb{F}\{\mathbf{y}_q\} = \mathbf{z}_q$ and $\mathbb{F}\{y[n]_q\} = z_k^q$

2. $\mathbb{F}\{\mathbf{x}_p\} = \mathbf{m}_p$ and $\mathbb{F}\{x[n]_p\} = m_k^p$

3. $\mathbb{F}\{\mathbf{v}_q\} = \mathbf{n}_q$ and $\mathbb{F}\{v[n]_q\} = n_k^q$

where z_k^q, m_k^p and n_k^q are elements of $\mathbf{z}_q$, $\mathbf{m}_p$ and $\mathbf{n}_q$ respectively. Using above definitions and Eq.(8.38), the DFT demodulated symbols at k^{th} sub-carrier (i.e. in frequency-domain) of qth receive

© Muhammad Imadur Rahman, 2007

antenna can be written as

$$\begin{aligned} z_k^q &= \frac{1}{\sqrt{\Delta}}\left[\sum_{\delta=1}^{\Delta} h_{q,1}^{(\delta)}[k]W_N^{-k\Omega_\delta}\right] m_k^1 + \dots \\ &+ \frac{1}{\sqrt{\Delta}}\left[\sum_{\delta=1}^{\Delta} h_{q,P}^{(\delta)}[k]W_N^{-k\Omega_\delta}\right] m_k^P + n_k^q \end{aligned} \tag{8.40}$$

So, the simplified system response for CDD assisted SM-OFDM system can be written as

$$\begin{bmatrix} z_k^1 \\ \vdots \\ z_k^Q \end{bmatrix} = \mathbf{H}^{CDD}[k] \begin{bmatrix} m_k^1 \\ \vdots \\ m_k^P \end{bmatrix} + \begin{bmatrix} n_k^1 \\ \vdots \\ n_k^P \end{bmatrix} \tag{8.41}$$

where

$$\mathbf{H}^{CDD}[k] = \frac{1}{\sqrt{\Delta}} \begin{bmatrix} \sum_{\delta=1}^{\Delta} h_{1,1}^{(\delta)}[k]W_N^{-k\Omega_\delta} & \dots & \sum_{\delta=1}^{\Delta} h_{1,P}^{(\delta)}[k]W_N^{-k\Omega_\delta} \\ \vdots & \ddots & \vdots \\ \sum_{\delta=1}^{\Delta} h_{Q,1}^{(\delta)}[k]W_N^{-k\Omega_\delta} & \dots & \sum_{\delta=1}^{\Delta} h_{Q,P}^{(\delta)}[k]W_N^{-k\Omega_\delta} \end{bmatrix} \tag{8.42}$$

In the receiver, Ordered Successive Interference Cancelation (OSIC) approach as devised in [24] can be used in straight-forward manner. The key idea of the non-linear OSIC receiver is to decode the symbol streams successively and extract them away layer by layer. At the beginning of each stage, the stream with the highest SNR for peeling is extracted. Once one particular layer is decoded, then the effect of the detected layer is subtracted from the received signal and the next branch in terms of SNR strength is chosen. This is continued until the last layer is decoded.

OSIC is performed on a sub-carrier by sub-carrier basis. On each sub-carrier, the detection scheme appears to be very similar to VBLAST detection, as derived in [24]. OSIC improves the detection quality compared to detection without ordering and is shown to be the optimal Successive Interference Cancellation (SIC) approach in terms of error rate performance [73].

8.6.2 System Capacity of CDA-SM-OFDM

One can easily notice the difference between the effective channel response matrix of kth sub-carrier for CDA-SM-OFDM system (as in Figure 8.14) and SM-OFDM system [24] by looking at Eq.(8.41)

and Eq.(8.44) respectively. The channel matrix for SM-OFDM scheme, $\mathbf{H}[k]$, is shown below,

$$\mathbf{H}^{CDD}[k] = \frac{1}{\sqrt{\Delta}} \begin{bmatrix} \sum_{\delta=1}^{\Delta} h_{1,1}^{(\delta)}[k] W_N^{-k\Omega_\delta} & \dots & \sum_{\delta=1}^{\Delta} h_{1,P}^{(\delta)}[k] W_N^{-k\Omega_\delta} \\ \vdots & \ddots & \vdots \\ \sum_{\delta=1}^{\Delta} h_{Q,1}^{(\delta)}[k] W_N^{-k\Omega_\delta} & \dots & \sum_{\delta=1}^{\Delta} h_{Q,P}^{(\delta)}[k] W_N^{-k\Omega_\delta} \end{bmatrix} \tag{8.43}$$

$$\mathbf{H}[k] = \begin{bmatrix} h_{1,1}[k] & h_{1,2}[k] & \dots & h_{1,P}[k] \\ h_{2,1}[k] & h_{2,2}[k] & \dots & h_{2,P}[k] \\ \vdots & \vdots & \ddots & \vdots \\ h_{Q,1}[k] & h_{Q,2}[k] & \dots & h_{Q,P}[k] \end{bmatrix} \tag{8.44}$$

Here, we recall the well-known channel capacity equations for any SM system when CSI is unknown at the transmitter. This is given by [73, Section 4.3]

$$\mathcal{C}_k = log_2 \left[det \left(\mathbf{I}_Q + \frac{\overline{\gamma}}{P} \mathbf{H}[k] \mathbf{H}^H[k] \right) \right] \tag{8.45}$$

where $\mathbf{H}^H[k]$ denotes the complex conjugate transpose (or Hermitian transpose) of $\mathbf{H}[k]$. Equivalently, we can write that[1]

$$\mathcal{C}_k = \sum_{i=1}^{r} log_2 \left(1 + \frac{\overline{\gamma}}{P} \lambda_i \right) \tag{8.46}$$

where r is the rank of the channel and λ_i are the positive eigenvalues of $\mathbf{H}[k]\mathbf{H}^H[k]$. Thus, the total MIMO system capacity is actually the sum of r SISO channels (or spatial modes) with a power gain of λ_i. In the absence of CSI at the transmitter, we cannot exploit the different channel gain for different spatial modes, and thus, the power division by P appears in Eq.(8.45) and Eq.(8.46). Similar system capacity expressions can be obtained for CDA-SM-OFDM system based on Eq.(8.45) and Eq.(8.46) as

$$\mathcal{C}_k = log_2 \left[det \left(\mathbf{I}_Q + \frac{\overline{\gamma}}{P\Delta} \mathbf{H}^{CDD}[k] \mathbf{H}^{CDD,H}[k] \right) \right] \tag{8.47}$$

$$= \sum_{i=1}^{r} log_2 \left(1 + \frac{\overline{\gamma}}{P\Delta} \lambda_i^{CDD} \right) \tag{8.48}$$

where $\mathbf{H}^{CDD,H}[k]$ is Hermitian transpose of $\mathbf{H}^{CDD}[k]$, and λ_i^{CDD} are the positive eigenvalues of $\mathbf{H}^{CDD}[k]\mathbf{H}^{CDD,H}[k]$.

For a better understanding of the system capacity, we have examined the statistical characteristics of the eigenvalues of both channel structures. We define the *normalized eigenvalue spread* as the difference between the maximum and the minimum eigenvalues, normalized by mean eigenvalue. When the eigenvalue spread is higher, then it is understood that one or more of the spatial modes are far weaker than others, or one or more spatial modes are far stronger than others. So

[1] For derivation of this expression, interested readers are requested to read the above mentioned reference (i.e. [73, Section 4.3])

© Muhammad Imadur Rahman, 2007

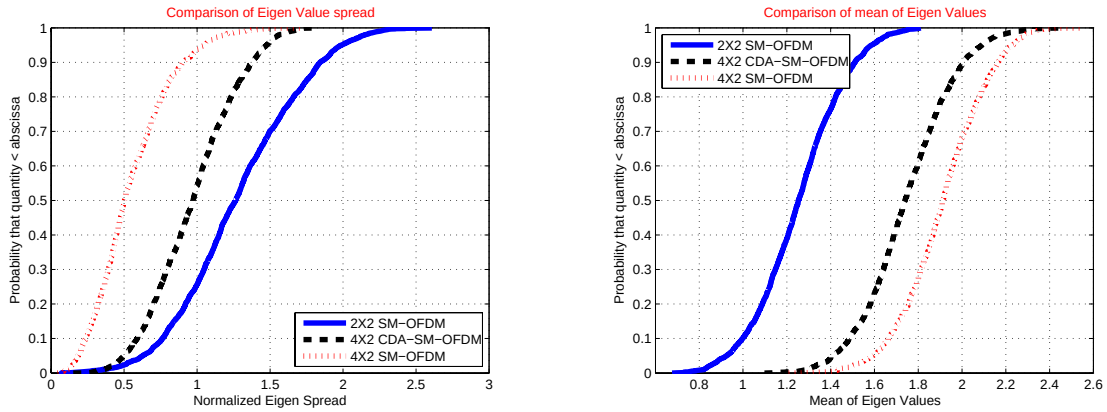

(a) Normalized eigenvalue spread

(b) Mean eigenvalue

Figure 8.15: Comparison of normalized eigenvalue spread and mean eigenvalue for 4×2 CDA-SM-OFDM system with 2×2 and 4×2 SM-OFDM system

when the spread goes very high, we may end up with available spatial modes less than $min(P, Q)$. This means that the effective capacity gain of the MIMO channel is reduced. One other property that can be checked very closely with normalized eigenvalue spread is *mean eigenvalue*. This is defined as mean of $\lambda_i; \forall i$. Though this parameter may be very misleading about the system capacity, it gives some valuable information when studied along with eigenvalue spread information.

Figures 8.15(a) and 8.15(b) shows the CDFs of normalized eigenvalue spread and mean eigenvalue for the case when $P = 2$, $Q = 2$ and $\Delta = 2$. Figure 8.15(a) shows that the normalized eigenvalue spread for 4×2 CDA-SM-OFDM system is in between 2×2 and 4×2 SM-OFDM systems. For mean eigenvalue for the two 4×2 system are much higher compared to 2×2 system, as shown in Figure 8.15(b). This is because of the extra spatial diversity effect that is available in 4×2 system. Note that 2 receive antennas means only 2-spatial branches can be transmitted for all the systems, thus, the increase in capacity for 4×2 system is logarithmic, rather than linear. We know that when the eigenvalue spread is the same for two channel matrices, if the mean eigenvalue is higher for one of them, the capacity will be higher for that channel too. Thus, the system capacity is increased in 4×2 system compared to 2×2 system as shown in Figure 8.16(a). As expected, the capacity curves show that the system capacity for 4×2 CDA-SM-OFDM system is in between the capacity curve for 2×2 and 4×2 SM-OFDM systems.

The above comparison refers to the ergodic capacity of the respective systems. Now, from these ergodic capacity curves, we can obtain the outage capacity values. We define the *outage capacity* as the capacity in b/s/Hz obtained below 10% of the times. If we look at Figure 8.16(a), 10% of the times, the system capacity will be below 4.5 b/s/Hz approximately for 2×2 SM-OFDM system. For the same capacity level, the outage will be less than 1% for 4×2 CDA-SM-OFDM system and almost 0% for 4×2 ideal SM-OFDM system. Thus, the outage probability is also greatly reduced in CDA-SM-OFDM system compared to simple SM-OFDM system. Figure 8.16(b) shows us the outage capacity vs Pre-SNR for the systems, where we can see that outage capacity is increased when higher diversity order is available and when the Pre-SNR is increased.

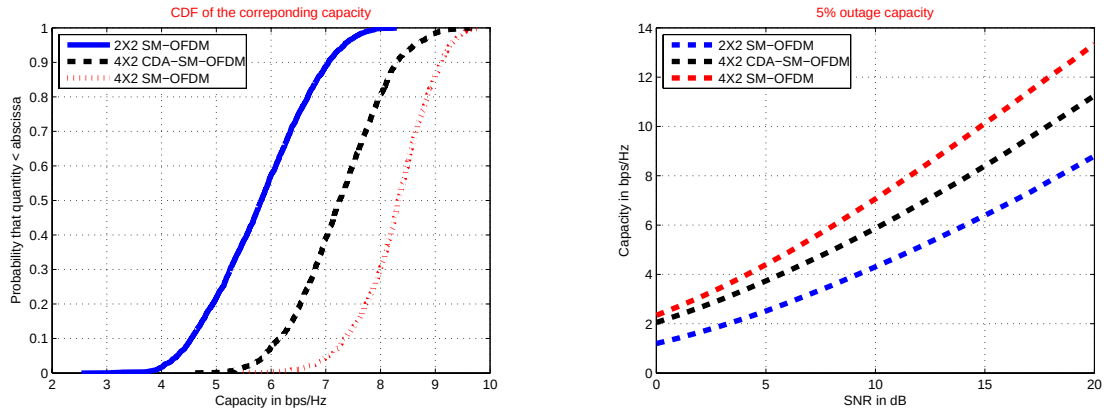

(a) Ergodic Capacity

(b) 5% outage capacity

Figure 8.16: Comparison of system capacity and 5% outage capacity for 4×2 CDA-SM-OFDM system with 2×2 and 4×2 SM-OFDM system

It should be noted here that capacity for 4×2 and 2×2 SM-OFDM systems can be achieved when the best possible STCs (or Space-Frequency Codings (SFCs)) and channel coding are available in corresponding antenna configurations. Thus, the capacity curves in Figure 8.16(a) shows an upper limit of capacity for any 4×2 SM-OFDM system. In contrast to this, 4×2 CDA-SM-OFDM achieves a capacity closer to this upper limit with a simple STC, i.e. CDD. Introducing CDD does not require any change in the receiver, changes are required only in the transmitter. In this case, two more transmit antenna branches are required and the delay element need to be inserted in all the transmit branches.

8.6.3 Simulation Results and Discussions

8.6.3.1 Wireless Channel Model

Indoor wireless channels for low user mobility will be considered at 5.4GHz. For indoor channels, we use the channel PDP model provided by HiperLan/2 WLAN standard.

8.6.3.2 System Scenario

Link level simulations are performed for a single cell OFDM system with a moderate speed. We are simulating for a single cell system to simplify the analysis, obviously this means that no Co-Channel Interference (CCI) is present in the system. The simulation parameters are listed in Table 8.2. The parameters are exactly similar to IEEE 802.11a standard. According to the standard, the parameters listed in the table corresponds to 12Mbps raw bit rate at the user receiver for SISO systems.

© Muhammad Imadur Rahman, 2007

Table 8.2: OFDM Simulation Parameters, taken similar to $IEEE$ 802.11a standard

OFDM sub-carriers, N	64
Data sub-carriers, N_{data}	48
Pilot sub-carriers, N_{pilot}	4
Null sub-carriers, N_{null}	12
CP length, N_{CP}	16
OFDM Symbol Duration, T_s	4μs
Useful data period, T_{data}	3.2μs
CP period, T_{CP}	0.8μs
Data Symbol mapping	QAM
Pilot Symbol mapping	BPSK
Channel coding scheme	$\frac{1}{2}$-rate Convolutional coding
System bandwidth	20MHz
Carrier frequency	5.4GHz

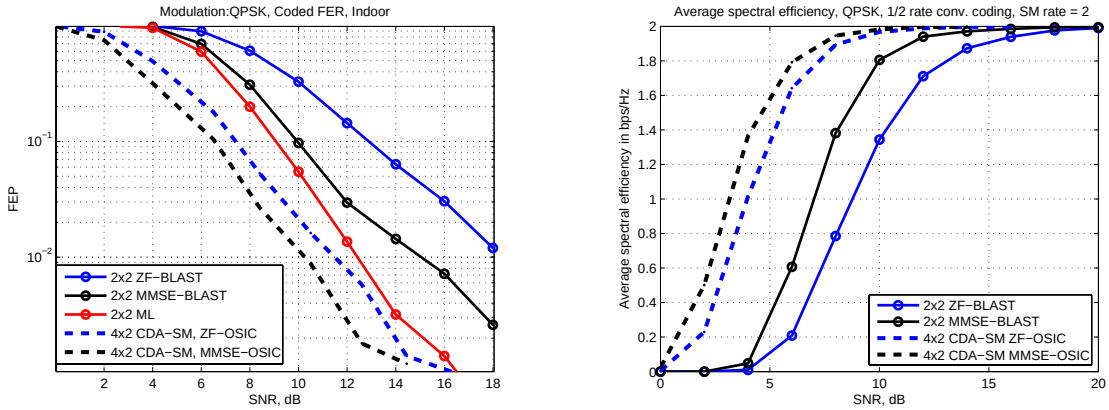

(a) FER results

(b) Average spectral efficiency

Figure 8.17: Average FER and spectral efficiency in bps/Hz of different types of spatial multiplexing schemes.

8.6.4 Performance Results and Discussions

Figure 8.17(a) shows the Frame Error Rate (FER) performance of the schemes in our simulation scenario. In indoor scenario, a frame consists of $N \times L_f \times M \times P \times R_c = 64 \times 16 \times 2 \times 2 \times 0.5 = 2048$ source bits. The tags used to describe the systems in the figures are listed in Table 8.3. All the transmission schemes use QPSK. Total transmitted power is always kept constant, so that comparison is done on equal footing. So the power transmitted via any branch is always $\frac{P_T}{P\Delta}$ and $\frac{P_T}{P}$ for all CDA-SM-OFDM and SM-OFDM schemes respectively, where P_T is the total transmitted power. As a reference, FER performance of ML receiver is plotted along with the other schemes, so that the benefit out of the optimal receiver is also compared. We have simulated both ZF and MMSE based OSIC receivers for original VBLAST and our proposed CDA-SM-OFDM system. As seen from Figure 8.17(a), CDA-SM-OFDM scheme obtains a gain of about 5dB and 4dB for ZF and MMSE based OSIC receivers respectively, at an FER of 10^{-2}. This gain is the direct result of exploitation of the additional antennas at the transmitter side via the CDD principle.

Table 8.3: Tags used in figures for corresponding schemes

the scheme	Tag
2×2 SM-OFDM scheme with horizontal coding and Zero Forcing (ZF)-VBLAST receiver [24]	2×2 *ZF-BLAST*
2×2 SM-OFDM scheme with horizontal coding and MMSE-VBLAST reception [24]	2×2 *MMSE-BLAST*
2×2 SM-OFDM scheme with horizontal coding and optimum ML reception	2×2 *ML*
4×2 CDA-SM-OFDM scheme with CDA-SM-OFDM transmitter and non-linear ZF based OSIC reception (Figure 8.14)	4×2 *CDA-SM, ZF-OSIC*
4×2 CDA-SM-OFDM scheme with CDA-SM-OFDM transmitter and non-linear MMSE based OSIC reception (Figure 8.14)	4×2 *CDA-SM, MMSE-OSIC*

Figure 8.17(b) shows us the average spectral efficiency of the studied systems in indoor scenario. The maximum rate with 1/2-rate convolutional coding, QPSK modulation and two spatially-multiplexed branches is, $R_b = \frac{\text{Number of bits per frame}}{\text{frame duration}} = \frac{NMPR_cN_f}{N_fT_s} = \frac{64\times2\times2\times0.5\times16}{16\times4\times10^{-6}}$ bps = 32Mbps, thus, a spectral efficiency of 1.6 bps/Hz at 20MHz system bandwidth. We define the practical spectral efficiency as $SE = R_b(1 - FER)$. At the best case with current modulation and coding level along with MIMO rate, the maximum spectral efficiency can be 1.6 bps/Hz. It can be seen that the average spectral efficiency of the proposed schemes is much higher than the 2×2 SM schemes at comparatively low SNR. As the SNR increases, the average spectral efficiency approaches the maximum value (i.e. 1.6 bps/Hz) for all the schemes. It is noticed that for CDA-SM-OFDM schemes, maximum achievable spectral efficiency is obtained faster than the VBLAST schemes when compared to increment in SNR.

Outage spectral efficiency results via simulations may offer more insights into the practical outage scenario, when all the mentioned schemes are compared. It is an issue that is under investigation at the moment.

© Muhammad Imadur Rahman, 2007

8.7 Chapter Summary

Cyclic Delay Diversity (CDD) is shown to be a good technique for exploiting the available spatial diversity either at transmitter, or at receiver, or at both locations simultaneously. The technique can be implemented at the transmitter without altering the receiver technique. Similarly, when applied at receiver, significant performance gain can be achieved by exploiting the known channel information at the receiver. We have shown that the proposed receive CDD scheme performs considerably well in some scenarios considering the trade-off between performance and complexity. Because of the low complexity our approach will allow low cost wireless modules targeting the mass market. For less frequency-selective channel, which is very similar to typical indoor or immediate outdoor wireless channel, Pre-DFT MARC with CDD combining is a lucrative option for cost effective, efficient and reliable diversity reception. In situations where diversity branches are correlated to each other because of the presence of LOS conditions, Pre- DFT MARC scheme works very well and efficiently combines the diversity branches to increase the transmission quality. It has also been understood that the scheme works well in severely time-variant situations.

We have only studied a single-tap weight estimation for Pre-DFT MARC scheme. The goal was to limit the system complexity, but still obtain a reasonable performance. For better performance, we can use multi-tap weight estimation, thus the scheme can become more robust to highly frequency-selective channels. Also, more taps in weight estimator can ease the receiver equalization process. But, one needs to keep in mind that, multi-tap time-domain weight estimation may require high equalization complexities and may jeopardize the simple single-tap equalization benefit that OFDM offers on every flat sub-carriers. Also, the proposed receiver Pre-DFT MARC principle can be implemented at the transmitter with similar system performance, but, it would require the channel information to be transported at the transmitter, thus system overhead would increase.

In collaboration to receive CDD proposed in this chapter, we can also use transmit-CDD with fixed delays simultaneously, so that the diversity principle can be used at both locations of the transmission. The improvement of the system performance in this case needs to be investigated.

When CDD is used in collaboration with any standard Spatial Multiplexing (SM) system, it increases the complexity marginally, but gives much better channel capacity values compared to basic SM-OFDM systems. CDD-based STC on SM-OFDM is much less complex compared to any other well-established STC techniques, such as Alamouti's 2×1 block codes. It is understood that CDA-SM-OFDM can be easily incorporated with any standard SM-OFDM system and can be directly used for DL using the proposed structure in Figure 8.14. When applied at the receiver, the scheme can also be used for UL.

However, it needs to be mentioned that channel estimation modules need to be taken care of, when CDD is used in the system. The technique essentially destroys the frequency correlation across neighboring sub-carriers, while channel estimation schemes sometimes exploit the correlation between the channel coefficients of adjacent sub-carriers in order to reduce the noise floor of the channel estimates [127]. Thus, eliminating this correlation would cause failure to some channel estimation schemes, and would require a re-design when CDD is used. Several solutions regarding channel estimation in CDD-based systems are proposed [141, 142] and can be modified to be used

with our proposed receive CDD technique in this chapter. In [143], it is shown that the required additional pilot symbol overhead for channel estimation in CDD systems is the same compared to other STBC systems with same number of transmit antennas.

Future Work:

The impact of spatial correlation across the antennas at both transmitter and receiver on the proposed scheme can be studied in future. Incorporation of such a scheme in a multi-user scenario can also be investigated. It is also understood that the rate control across different multiplexing streams will yield throughput improvement for CDA-SM-OFDM system. For Bit-Interleaved Coded Modulation (BICM) systems, proper interleaver design together with efficient FEC coding can be studied for CDD based systems.

© Muhammad Imadur Rahman, 2007

9

Joint Diversity and Multiplexing Systems

We present our studies related to combination of spatial diversity and multiplexing schemes in this chapter. Sections 9.2 and 9.3 explain the system model for Spatially-Multiplexed Orthogonal SFBC (SM-OSFBC) and Spatially-Multiplexed Quasi-orthogonal SFBC (SM-QSFBC) systems respectively. We have explained Least Squares (LS)-based linear receiver for SM-OSFBC scheme and Ordered Successive Interference Cancelation (OSIC)-based non-linear receiver for both the systems. Numerous simulations are done to evaluate the systems and their performances under certain realistic wireless scenarios. The results of those simulations and the discussions can be found in Section 9.4. The numerical evaluations include comparison in terms of FER and outage spectral efficiency in realistic wireless channel scenario, such as spatial correlation at both ends of the transmission link and presence of LOS. Conclusions are drawn in Section 9.5.

9.1 Introduction

Multiple antennas can be used at both ends of a MIMO wireless transmission system to exploit the benefits of spatial dimension. Two benefits can be obtained, namely Space Diversity (SD) and Spatial Multiplexing (SM). STC and MRC can be used at the transmitter side and/or receiver side respectively, to exploit the maximum spatial diversity available in the channel. This can be used to increase the system reliability [73]. Similarly, parallel spatial channels between multiple antennas

can be exploited for increasing the transmission rate without increasing required bandwidth. In rich scattering environment, the independent spatial channels can be exploited to send multiple signals at the same time and frequency, resulting in higher spectral efficiency [22].

SD schemes provide higher SNR at the receiver, whereas SM schemes provide higher rate [26]. Transmit SD schemes have multiple antennas at the transmitter, and may have only one or more than one receive antennas, whereas SM schemes must have multiple antennas at both sides. A subset of SD schemes uses some sort of STBC (or SFBC) coding at the transmitter (i.e. $\Delta \times 1$ system, where Δ is the number of antennas at the transmitter side; conversely we define Q as the number of receive antennas). Depending on different Δ, we can classify the SD systems into three different categories:

P **= 2** orthogonal (i.e. full diversity, full rate) [25];

$P >$ **2** quasi-orthogonal (i.e. partial diversity, full rate) [144];

$P >$ **2** orthogonal (i.e. full diversity, rate loss) [78].

These SD schemes do not require any channel information at the transmitter, thus, they can be implemented at fairly low system complexity and signaling overhead.

SM schemes are two fold,

CSI assisted: SVD-MIMO, eigen-mode MIMO etc. These schemes provide higher system capacity, but require a feedback path, thus they are more complex and difficult to implement;

Blind: BLAST, they are easier to implement compared to SVD-MIMO.

Blind SM schemes can have different kinds of receivers:

1. Linear ZF or MMSE receiver: simple receiver, but poor performance [22];
2. Non-linear ML receiver: optimal and most complex receiver [73, 75];
3. Non-linear OSIC receiver with ZF or MMSE nulling: sub-optimal receiver [24].

In wideband scenarios, OFDM can be combined with MIMO systems, for both diversity and multiplexing purposes [145]. In frequency selective environments, amalgamation of SM and OFDM techniques can be a potential source of high spectral efficiency at reasonable complexity, because MIMO-OFDM drastically simplifies equalization in frequency-selective environments.

9.1.1 What are JDM Schemes?

The trade-off between diversity and multiplexing has been studied in recent times, as in [146, 147, 148]. The trade-off studies are triggered based on the fact that none of the schemes mentioned above can become an absolute choice for better system performance in all scenarios. To be exact, a user located very close to access point can exploit the multiplexing benefits, while a user at farther location may benefit more by using MIMO diversity schemes. That's why MIMO switching schemes, such as [27], are well studied and examined. In switching schemes, either SD or SM schemes are optimally chosen based on some specific selection criterion, so that optimum benefits

from both type of schemes can be obtained in the system. This kind of combination is actually performed in time domain. In recent years, combining SM and SD schemes in space domain has gained a lot of interest, because these schemes are beneficial in effect that both diversity and multiplexing benefits are available at the same time. In this chapter, we study such MIMO structures which simultaneously exploit diversity and multiplexing gains at the same signalling scheme.

In a cellular wireless system, the STBC-OFDM [128] and SFBC-OFDM [79] can be used to increase the resultant SNR at the receiver, thus, increasing the coverage area. In contrast to this, as SM requires high receive SNR for reliable detection [27], it is evident that users at farther locations from BS cannot use SM techniques to enhance the spectral efficiency. Thus, it is required to combine both of these two techniques in one structure so that both the diversity and multiplexing benefits can be achieved at farther locations from transmission source. We call such schemes as JDM schemes.

To be specific, blind SD schemes enhance the receive SNR, thus they are good for users at locations farther from the BS; while blind SM schemes require higher SNR to efficiently decode the multiplexing branches, thus only users located near to the BS can get the services [26]. We can combine SM and SD, in one structure in the following ways (by P we mean the number of SM branches):

1. P, Q = arbitrary; Δ =2; Alamouti scheme at every SM branch, thus, $2P \times Q$ Spatially-Multiplexed Orthogonal SFBC (SM-OSFBC) systems. Here, we denote Δ as the number of antennas per SM branch where SFBC is applied;

2. P, Q = arbitrary; $\Delta > 2$; Orthogonal partial rate SFBC scheme at every SM branch, thus, $P\Delta \times Q$ SM-OSFBC systems. These schemes lose SM benefits because of partial rate SFBC, so they are not considered in this work;

3. P, Q = arbitrary; $\Delta > 2$; Quasi-orthogonal full rate SFBC scheme at every SM branch, thus, $P\Delta \times Q$ Spatially-Multiplexed Quasi-orthogonal SFBC (SM-QSFBC) systems.

When coding across S-T is envisioned, we can have Spatially-Multiplexed Orthogonal STBC (SM-OSTBC) or Spatially-Multiplexed Quasi-orthogonal STBC (SM-QSTBC) systems.

9.1.2 State-of-the-Art on JDM Schemes

Recently there are some approaches of incorporating the VBLAST technique with some well known STC techniques. One such work is described in [138], where a combination of SD and SM for MIMO-OFDM system is proposed. Arguably, the performance of such a JDM system would be better than SD only and SM only schemes. In [138], the SM-OFDM system uses two independent STC for two sets of transmit antennas. Thus, an original 2×2 SM-OFDM system is now extended to 4×2 STC aided SM-OFDM system. In the receiver, the independent STCs are decoded first using pre-whitening, followed by maximum likelihood detection. Again, this increases the receiver complexity quite a lot, though the system performance gets much better. In later work, Alamouti's STBC is combined with SM for OFDM system in [149], and a linear receiver is designed for such a combination. Non-linear receiver for similar SM-OSTBC scheme is mentioned in [150], though the receiver structure is not detailed. The main concentration of [150] is on switching between MIMO

© Muhammad Imadur Rahman, 2007

techniques, i.e. between SD only, SM only and SM-OSTBC schemes. Choosing antenna pairs in SM-OSTBC scheme based on correlation criterion is studied in [151], while again receiver structures are not discussed at all. AMC on SM-OSTBC is studied in [152]. Detection schemes for SM-OSTBC system are analyzed in [153], where linear ZF and QR decomposition based receiver is discussed.

Our Contributions

Following these trends, we have combined SFBC with SM and obtained a linear receiver similar to [149] in this work. One advantage in using SFBC instead of STBC is that, in SFBC, the coding is done across the sub-carriers inside one OFDM symbol duration, while STBC applies the coding across a number of OFDM symbols equal to number of transmit antennas, thus, an inherent processing delay is unavoidable in STBC [154]. We have analyzed Linear receiver for SM-OSFBC system with ZF and MMSE criterion: this linear receiver is very similar to the receiver structure for SM-OSTBC scheme in [149]. We have derived OSIC receiver with ZF and MMSE criterion, and their FER performance is compared with linear receivers via simulations. For SM-QSFBC scheme, OSIC receiver with ZF and MMSE is derived, analyzed and simulated. To the best of our knowledge, SM-QSFBC scheme has not been studied and analyzed before this work. It is worth noting here that the OSIC approach that we have taken in this work is similar to original BLAST algorithm in [24]. With the understanding of different receiver structures, we have investigated the impact of spatial correlation at both sides of transmission and the impact of LOS component in wireless channel.

9.2 SM-OSFBC Transmission Scheme

In this section, we will explain the transmission structure of the JDM scheme based on combining SM and Orthogonal Space-Frequency Block Code (OSFBC). Following this, we propose a linear two-stages receiver, which is an extension of LS receiver in [149], where the linear reception technique is used for SM-OSTBC system based on ZF and MMSE criteria, on sub-carrier by sub-carrier basis. After this, we derive a non-linear SIC receiver where the detection is based on both ZF and MMSE nulling.

9.2.1 Transmitter

We denote the number of available transmit SM branches and receive antennas as P and Q respectively. We have N number of sub-carriers in the system. We denote p, q and k as indices for transmit SM branch, receive antenna and sub-carrier group respectively. For every p^{th} SM branch, we implement an orthogonal block coding across the sub-carriers.

Figure 9.1 explains the basic transceiver architecture, while referring to a linear receiver. At first source bits are FEC coded. The coded bit stream is baseband modulated using an appropriate constellation diagram, such as BPSK, QAM etc. We denote these baseband modulated symbols as $\mathbf{m}$. The sequence of $\mathbf{m}$ is demultiplexed in to $\mathbf{m}_1, \ldots, \mathbf{m}_P$ vectors. $\mathbf{m}_p$ is transmitted via p^{th} spatial channel, which can be written as, $\mathbf{m}_p = \begin{bmatrix} m_{p,1} & m_{p,2} & \ldots & m_{p,N-1} & m_{p,N} \end{bmatrix}^T$.

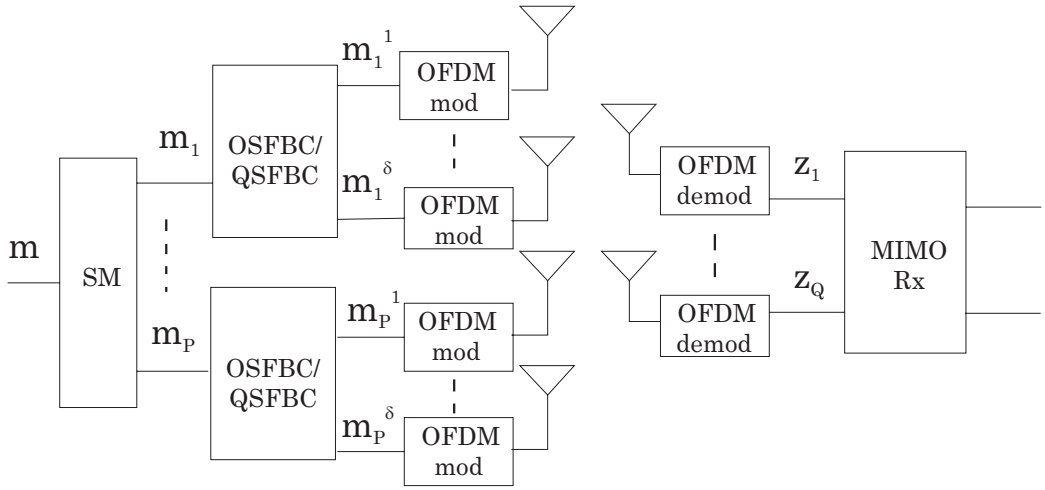

Figure 9.1: Simplified System Model for SM-OSFBC/SM-QSFBC Transmission Scheme

For every p^{th} SM branch, we implement a block coding across the sub-carriers, thus SFBC is included in the system. For p^{th} SM branch, we have Δ_p number of antennas where SFBC can be implemented. When $\Delta_p = \Delta,\ \forall p$, then we have $\Delta \cdot P$ number of transmit antennas at the transmission side. If we use well-known Alamouti coding [25] across the sub-carriers, then $\Delta = 2$.

For p^{th} SM branch, $\mathbf{m}_p$ is coded into two vectors, $\mathbf{m}_p^{(\delta)};\ \delta = 1, 2$. Thus, the output of the SFBC encoder block of the pth SM branch will be

$$\mathbf{m}_p^{(1)} = \begin{bmatrix} m_{p,1} & -m_{p,2}^* & \dots & m_{p,N-1} & -m_{p,N}^* \end{bmatrix}^T \tag{9.1}$$

$$\mathbf{m}_p^{(2)} = \begin{bmatrix} m_{p,2} & m_{p,1}^* & \dots & m_{p,N} & m_{p,N-1}^* \end{bmatrix}^T \tag{9.2}$$

Following this, we define

$$\mathbf{m}_{p,o} = \begin{bmatrix} m_{p,1} & m_{p,3} & \dots & m_{p,N-3} & m_{p,N-1} \end{bmatrix}^T \tag{9.3}$$

$$\mathbf{m}_{p,e} = \begin{bmatrix} m_{p,2} & m_{p,4} & \dots & m_{p,N-2} & m_{p,N} \end{bmatrix}^T \tag{9.4}$$

Using these equations, we can write that

$$\mathbf{m}_{p,o}^{(1)} = \mathbf{m}_{p,o}; \qquad \mathbf{m}_{p,e}^{(1)} = -\mathbf{m}_{p,e}^* \tag{9.5}$$

$$\mathbf{m}_{p,o}^{(2)} = \mathbf{m}_{p,e}; \qquad \mathbf{m}_{p,e}^{(2)} = \mathbf{m}_{p,o}^* \tag{9.6}$$

After SM and SFBC operations, IFFT modulation is performed and CP is added before transmission via the respective transmit antenna. Transmitted time domain samples, $\mathbf{x}_p^{(\delta)}$, can be related to $\mathbf{m}_p^{(\delta)}$ as, $\mathbf{x}_p^{(\delta)} = \mathbb{F}^H\{\mathbf{m}_p^{(\delta)}\}$, where $\mathbb{F}^H$ is the IFFT matrix.

© Muhammad Imadur Rahman, 2007

9.2.2 Two-Stage Linear Receiver

In [155], a two stage interference cancelation receiver scheme for STBC is presented. This receiver treats one of the branches as the interfering source for the other one. This receiver is used to derive a linear reception technique for SM-OSTBC system in [149]. In this work, we adopt a similar receiver structure for our SM-OSFBC system.

In the receiver, the signals are down-converted after reception at the respective antennas. The time-domain signal at q^{th} after CP removal can be written as

$$\begin{aligned}\mathbf{y}_q &= \mathbf{g}_{q,1}^{(1)} \overset{N}{\circledast} \mathbf{x}_1^{(1)} + \mathbf{g}_{q,1}^{(2)} \overset{N}{\circledast} \mathbf{x}_1^{(2)} + \ldots + \mathbf{g}_{q,p}^{(1)} \overset{N}{\circledast} \mathbf{x}_p^{(1)} + \mathbf{g}_{q,p}^{(2)} \overset{N}{\circledast} \mathbf{x}_p^{(2)} + \mathbf{v}_q \\ &= \sum_{\delta=1}^{2} \sum_{p=1}^{P} \mathbf{g}_{q,p}^{(\delta)} \overset{N}{\circledast} \mathbf{x}_p^{(\delta)} + \mathbf{v}_q \end{aligned} \tag{9.7}$$

where $\mathbf{y}_q$ denotes the received signal vector at q^{th} receive antenna branch of size $N \times 1$, and $\mathbf{g}_{q,p}^{(\delta)}$ denotes the CIR vector of the wireless channel between q^{th} receive antenna and δ^{th} SFBC branch of pth SM channel. The size of $\mathbf{g}_{q,p}^{(\delta)}$ is $L \times 1$. $\mathbf{v}_q$ is the time-domain sample of the received noise at q^{th} received branch.

After DFT demodulation, we can express the frequency-domain sub-carrier signal as

$$\mathbf{z}_q = \sum_{\delta=1}^{2} \sum_{p=1}^{P} \mathbf{h}_{q,p}^{(\delta)} \odot \mathbf{m}_p^{(\delta)} + \mathbf{n}_q \tag{9.8}$$

where $\mathbf{h}_{q,p}^{(\delta)}$ denotes the CTF vector of the wireless channel between q^{th} receive antenna and δ^{th} SFBC antenna of pth SM branch, $\mathbf{n}_q$ is the frequency-domain sample of the received noise at q^{th} received branch, and $\odot$ means element-wise multiplication.

We can divide $\mathbf{z}_q$ in odd and even components $\forall q;\ q = 1, 2$. Using Eq. (9.3) and Eq. (9.4), we can express

$$\begin{aligned}\mathbf{z}_{q,o} &= \mathbf{h}_{q,1,o}^{(1)} \odot \mathbf{m}_{1,o} + \mathbf{h}_{q,1,o}^{(2)} \odot \mathbf{m}_{1,e} + \ldots + \ldots \\ &\quad \mathbf{h}_{q,P,o}^{(1)} \odot \mathbf{m}_{P,o} + \mathbf{h}_{q,P,o}^{(2)} \odot \mathbf{m}_{P,e} + \mathbf{n}_{q,o} \end{aligned} \tag{9.9}$$

$$\begin{aligned}\mathbf{z}_{q,e} &= -\mathbf{h}_{q,1,e}^{(1)} \odot \mathbf{m}_{1,e}^{*} + \mathbf{h}_{q,1,e}^{(2)} \odot \mathbf{m}_{1,o}^{*} + \ldots - \ldots \\ &\quad \mathbf{h}_{q,P,e}^{(1)} \odot \mathbf{m}_{P,e}^{*} + \mathbf{h}_{q,P,e}^{(2)} \odot \mathbf{m}_{P,o}^{*} + \mathbf{n}_{q,e} \end{aligned} \tag{9.10}$$

From this point onwards, we use $P = 2$ and $Q = 2$. It is fairly simple to extend this analysis to higher number of transmit and receive antennas. Let us introduce the following $Q \times 1$ column vectors, $\mathbf{h}_{p,o}^{(\delta)}, \mathbf{h}_{p,e}^{(\delta)}, \mathbf{z}_o, \mathbf{z}_e$, whose q^{th} components are respectively, the odd and even elements of CTF between δ^{th} transmit antenna of the pth SM branch and q^{th} receive antenna, and the odd and even elements of received frequency domain signal at q^{th} receive antenna. Furthermore, we denote the following $Q \times 1$ column vectors, $\mathbf{n}_o, \mathbf{n}_e$, whose q^{th} components are respectively, the odd and even elements of frequency-domain noise at q^{th} receive antenna.

Using these notations above, we can write Eq. (9.11): in this equation, we have a sub-carrier

notation, where it is understood that such a system model is intended $\forall k \in [1, \ldots, \frac{N}{2}]$.

$$\begin{aligned}
\mathbf{z}_k &= \begin{bmatrix} z_{1,o} \\ z_{2,o} \\ z_{1,e}^* \\ z_{2,e}^* \end{bmatrix} = \begin{bmatrix} h_{11,o}^{(1)} & h_{11,o}^{(2)} & h_{12,o}^{(1)} & h_{12,o}^{(2)} \\ h_{21,o}^{(1)} & h_{21,o}^{(2)} & h_{22,o}^{(1)} & h_{22,o}^{(2)} \\ h_{11,e}^{(2)*} & -h_{11,e}^{(1)*} & h_{12,e}^{(2)*} & -h_{12,e}^{(1)*} \\ h_{21,e}^{(2)*} & -h_{21,e}^{(1)*} & h_{22,e}^{(2)*} & -h_{22,e}^{(1)*} \end{bmatrix} \begin{bmatrix} m_{1,o} \\ m_{1,e} \\ m_{2,o} \\ m_{2,e} \end{bmatrix} + \begin{bmatrix} n_{1,o} \\ n_{2,o} \\ n_{1,e}^* \\ n_{2,e}^* \end{bmatrix} \\
&= \begin{bmatrix} \mathbf{z}_o \\ \mathbf{z}_e^* \end{bmatrix}_k = \begin{bmatrix} \mathbf{h}_{1,o}^{(1)} & \mathbf{h}_{1,o}^{(2)} & \mathbf{h}_{2,o}^{(1)} & \mathbf{h}_{2,o}^{(2)} \\ \mathbf{h}_{1,e}^{(2)*} & -\mathbf{h}_{1,e}^{(1)*} & \mathbf{h}_{2,e}^{(2)*} & -\mathbf{h}_{2,e}^{(1)*} \end{bmatrix}_k \begin{bmatrix} m_{1,o} \\ m_{1,e} \\ m_{2,o} \\ m_{2,e} \end{bmatrix}_k + \begin{bmatrix} \mathbf{n}_o \\ \mathbf{n}_e^* \end{bmatrix}_k
\end{aligned} \tag{9.11}$$

We denote coherence bandwidth and sub-carrier spacing as B_c and Δf respectively. We define severely frequency-selective scenario when coherence bandwidth is smaller than a pair of sub-carrier bandwidth, i.e. $B_c < 2\Delta f$. In this case, we use a tool called companion matrix explained below.

Let us define a matrix $\mathbf{A}$ as

$$\mathbf{A} = \begin{bmatrix} \mathbf{a}_{11} & \mathbf{a}_{12} \\ \mathbf{a}_{21} & \mathbf{a}_{22} \end{bmatrix} \tag{9.12}$$

We can define another pair matrix $\widetilde{\mathbf{A}}$ as

$$\widetilde{\mathbf{A}} = \begin{bmatrix} -\mathbf{a}_{22}^T & \mathbf{a}_{12}^T \\ \mathbf{a}_{21}^T & -\mathbf{a}_{11}^T \end{bmatrix} \tag{9.13}$$

The matrix pair $\mathbf{A}$ and $\widetilde{\mathbf{A}}$ identifies a so called orthogonal pair. $\mathbf{a}_{ij},\ \forall i, j$, are column vectors of size $m \times 1$, thus $\mathbf{A}$ and $\widetilde{\mathbf{A}}$ are matrices of sizes $2m \times 2$ and $2 \times 2m$, respectively.

Let us omit from now on the sub-carrier index k. We can represent Eq.(9.11) as

$$\mathbf{z} = \mathbf{H}\mathbf{m} + \mathbf{n} = \begin{bmatrix} \mathbf{H}_i \,|\, \mathbf{H}_j \end{bmatrix} \mathbf{m} + \mathbf{n} \tag{9.14}$$

with

$$\mathbf{H}_i = \begin{bmatrix} \mathbf{h}_{1,o}^{(1)} & \mathbf{h}_{1,o}^{(2)} \\ \mathbf{h}_{1,e}^{(2)*} & -\mathbf{h}_{1,e}^{(1)*} \end{bmatrix},\ \mathbf{H}_j = \begin{bmatrix} \mathbf{h}_{2,o}^{(1)} & \mathbf{h}_{2,o}^{(2)} \\ \mathbf{h}_{2,e}^{(2)*} & -\mathbf{h}_{2,e}^{(1)*} \end{bmatrix} \tag{9.15}$$

We denote the companion matrices of $\mathbf{H}_i$ and $\mathbf{H}_j$ as $\widetilde{\mathbf{H}}_i$ and $\widetilde{\mathbf{H}}_j$ respectively. We define a new matrix, $\widetilde{\mathbf{H}} = \begin{bmatrix} \widetilde{\mathbf{H}}_i^T & \widetilde{\mathbf{H}}_j^T \end{bmatrix}^T$, with

$$\widetilde{\mathbf{H}}_i = \begin{bmatrix} \mathbf{h}_{1,e}^{(1)H} & \mathbf{h}_{1,o}^{(2)T} \\ \mathbf{h}_{1,e}^{(2)H} & -\mathbf{h}_{1,o}^{(1)T} \end{bmatrix},\ \widetilde{\mathbf{H}}_j = \begin{bmatrix} \mathbf{h}_{2,e}^{(1)H} & \mathbf{h}_{2,o}^{(2)T} \\ \mathbf{h}_{2,e}^{(2)H} & -\mathbf{h}_{2,o}^{(1)T} \end{bmatrix} \tag{9.16}$$

Now, at the beginning of the receiver, we can filter the received signal $\mathbf{z}$ with $\widetilde{\mathbf{H}}$ as it is

© Muhammad Imadur Rahman, 2007

shown below,

$$\mathbf{z}' = \widetilde{\mathbf{H}}\mathbf{z} = \begin{bmatrix} \widetilde{\mathbf{H}}_i \\ \widetilde{\mathbf{H}}_j \end{bmatrix} \begin{bmatrix} \mathbf{H}_i \,|\, \mathbf{H}_j \end{bmatrix} \mathbf{m} + \widetilde{\mathbf{H}}\mathbf{n} \tag{9.17}$$

The part, $\widetilde{\mathbf{H}}\mathbf{H}$, can be extended as in Eq. (9.18)

$$\widetilde{\mathbf{H}}\mathbf{H} = \begin{bmatrix} \mathbf{h}_{1,e}^{(1)H}\mathbf{h}_{1,o}^{(1)} + \mathbf{h}_{1,o}^{(2)T}\mathbf{h}_{1,e}^{(2)*} & 0 & \mathbf{h}_{1,e}^{(1)H}\mathbf{h}_{2,o}^{(1)} + \mathbf{h}_{1,o}^{(2)T}\mathbf{h}_{2,e}^{(2)*} & \mathbf{h}_{1,e}^{(1)H}\mathbf{h}_{2,o}^{(2)} - \mathbf{h}_{1,o}^{(2)T}\mathbf{h}_{2,e}^{(1)*} \\ 0 & \mathbf{h}_{1,e}^{(1)H}\mathbf{h}_{1,o}^{(1)} + \mathbf{h}_{1,o}^{(2)T}\mathbf{h}_{1,e}^{(2)*} & \mathbf{h}_{1,e}^{(2)H}\mathbf{h}_{2,o}^{(1)} - \mathbf{h}_{1,o}^{(1)T}\mathbf{h}_{2,e}^{(2)*} & \mathbf{h}_{1,e}^{(2)H}\mathbf{h}_{2,o}^{(2)} + \mathbf{h}_{1,o}^{(1)T}\mathbf{h}_{2,e}^{(1)*} \\ \mathbf{h}_{2,e}^{(1)H}\mathbf{h}_{1,o}^{(1)} + \mathbf{h}_{2,o}^{(2)T}\mathbf{h}_{1,e}^{(2)*} & \mathbf{h}_{2,e}^{(1)H}\mathbf{h}_{1,o}^{(2)} - \mathbf{h}_{2,o}^{(2)T}\mathbf{h}_{1,e}^{(1)*} & \mathbf{h}_{2,e}^{(1)H}\mathbf{h}_{2,o}^{(1)} + \mathbf{h}_{2,o}^{(2)T}\mathbf{h}_{2,e}^{(2)*} & 0 \\ \mathbf{h}_{2,e}^{(2)H}\mathbf{h}_{1,o}^{(1)} - \mathbf{h}_{2,o}^{(1)T}\mathbf{h}_{1,e}^{(2)*} & \mathbf{h}_{2,e}^{(2)H}\mathbf{h}_{1,o}^{(2)} + \mathbf{h}_{2,o}^{(1)T}\mathbf{h}_{1,e}^{(1)*} & 0 & \mathbf{h}_{2,e}^{(1)H}\mathbf{h}_{2,o}^{(1)} + \mathbf{h}_{2,o}^{(2)T}\mathbf{h}_{2,e}^{(2)*} \end{bmatrix} \tag{9.18}$$

We define that

$$\widetilde{\mathbf{H}}\mathbf{H}(1:2,1:2) = \underbrace{\left(\mathbf{h}_{1,e}^{(1)H}\mathbf{h}_{1,o}^{(1)} + \mathbf{h}_{1,o}^{(2)T}\mathbf{h}_{1,e}^{(2)*}\right)}_{\alpha_1^{'}} \mathbf{I} = \alpha_1^{'}\mathbf{I} \tag{9.19}$$

$$\widetilde{\mathbf{H}}\mathbf{H}(3:4,3:4) = \underbrace{\left(\mathbf{h}_{2,e}^{(1)H}\mathbf{h}_{2,o}^{(1)} + \mathbf{h}_{2,o}^{(2)T}\mathbf{h}_{2,e}^{(2)*}\right)}_{\alpha_2^{'}} \mathbf{I} = \alpha_2^{'}\mathbf{I} \tag{9.20}$$

$$\widetilde{\mathbf{H}}\mathbf{H}(1:2,3:4) = \begin{bmatrix} \mathbf{h}_{1,e}^{(1)H}\mathbf{h}_{2,o}^{(1)} + \mathbf{h}_{1,o}^{(2)T}\mathbf{h}_{2,e}^{(2)*} & \mathbf{h}_{1,e}^{(1)H}\mathbf{h}_{2,o}^{(2)} - \mathbf{h}_{1,o}^{(2)T}\mathbf{h}_{2,e}^{(1)*} \\ \mathbf{h}_{1,e}^{(2)H}\mathbf{h}_{2,o}^{(1)} - \mathbf{h}_{1,o}^{(1)T}\mathbf{h}_{2,e}^{(2)*} & \mathbf{h}_{1,e}^{(2)H}\mathbf{h}_{2,o}^{(2)} + \mathbf{h}_{1,o}^{(1)T}\mathbf{h}_{2,e}^{(1)*} \end{bmatrix} = \mathbf{G}_{12} \tag{9.21}$$

$$\widetilde{\mathbf{H}}\mathbf{H}(3:4,1:2) = \begin{bmatrix} \mathbf{h}_{2,e}^{(1)H}\mathbf{h}_{1,o}^{(1)} + \mathbf{h}_{2,o}^{(2)T}\mathbf{h}_{1,e}^{(2)*} & \mathbf{h}_{2,e}^{(1)H}\mathbf{h}_{1,o}^{(2)} - \mathbf{h}_{2,o}^{(2)T}\mathbf{h}_{1,e}^{(1)*} \\ \mathbf{h}_{2,e}^{(2)H}\mathbf{h}_{1,o}^{(1)} - \mathbf{h}_{2,o}^{(1)T}\mathbf{h}_{1,e}^{(2)*} & \mathbf{h}_{2,e}^{(2)H}\mathbf{h}_{1,o}^{(2)} + \mathbf{h}_{2,o}^{(1)T}\mathbf{h}_{1,e}^{(1)*} \end{bmatrix} = \mathbf{G}_{21} \tag{9.22}$$

We can see that $\mathbf{G}_{12}$ and $-\mathbf{G}_{21}$ form an orthogonal pair as mentioned in the definition of companion matrix above.

Now, Eq. (9.17) can be written as

$$\mathbf{z}' = \begin{bmatrix} \alpha_1^{'}\mathbf{I}_2 & \mathbf{G}_{12} \\ \mathbf{G}_{21} & \alpha_2^{'}\mathbf{I}_2 \end{bmatrix} \mathbf{m} + \widetilde{\mathbf{H}}\mathbf{n} \tag{9.23}$$

We define an LS receiver $\mathbf{W}$ as

$$\mathbf{W} = \frac{1}{\gamma} \begin{bmatrix} \alpha_2^{'}\mathbf{I}_2 & -\mathbf{G}_{12} \\ -\mathbf{G}_{21} & \alpha_1^{'}\mathbf{I}_2 \end{bmatrix} \tag{9.24}$$

where $\gamma = \alpha_1^{'}\alpha_2^{'} - [\mathbf{G}_{12}(1,1)\mathbf{G}_{12}(2,2) - \mathbf{G}_{12}(1,2)\mathbf{G}_{12}(2,1)]$. Thus, the estimated symbol vector can be written as

$$\widehat{\mathbf{m}} = \mathbf{W}\mathbf{z}' = \mathbf{m} + \mathbf{W}\widetilde{\mathbf{H}}\mathbf{n} \tag{9.25}$$

In relation to frequency-selective scenario, when $B_c > 2\Delta f$, we can easily say that neigh-

boring sub-carriers have identical channel frequency response. In this case $\mathbf{h}_{p,o}^{(\delta)} = \mathbf{h}_{p,e}^{(\delta)} = \mathbf{h}_{p,oe}^{(\delta)}$. So we can write Eq.(9.11) as

$$\mathbf{z} = \begin{bmatrix} \mathbf{z}_o \\ \mathbf{z}_e^* \end{bmatrix} = \begin{bmatrix} \mathbf{H}_1 \,|\, \mathbf{H}_2 \end{bmatrix} \mathbf{m} + \mathbf{n} \tag{9.26}$$

where

$$\mathbf{H}_1 = \begin{bmatrix} \mathbf{h}_{1,oe}^{(1)} & \mathbf{h}_{1,oe}^{(2)} \\ \mathbf{h}_{1,oe}^{(2)*} & -\mathbf{h}_{1,oe}^{(1)*} \end{bmatrix}, \; \mathbf{H}_2 = \begin{bmatrix} \mathbf{h}_{2,oe}^{(1)} & \mathbf{h}_{2,oe}^{(2)} \\ \mathbf{h}_{2,oe}^{(2)*} & -\mathbf{h}_{2,oe}^{(1)*} \end{bmatrix} \tag{9.27}$$

are two orthogonal matrices, so we can write that

$$\mathbf{H}_1^H \mathbf{H}_1 = \left(|\mathbf{h}_{1,oe}^{(1)}|^2 + |\mathbf{h}_{1,oe}^{(2)}|^2 \right) \mathbf{I}_2 = \alpha_1 \mathbf{I}_2 \tag{9.28}$$

$$\mathbf{H}_2^H \mathbf{H}_2 = \left(|\mathbf{h}_{2,oe}^{(1)}|^2 + |\mathbf{h}_{2,oe}^{(2)}|^2 \right) \mathbf{I}_2 = \alpha_2 \mathbf{I}_2 \tag{9.29}$$

where $\alpha_1 = |\mathbf{h}_{1,oe}^{(1)}|^2 + |\mathbf{h}_{1,oe}^{(2)}|^2$ and $\alpha_2 = |\mathbf{h}_{2,oe}^{(1)}|^2 + |\mathbf{h}_{2,oe}^{(2)}|^2$. Similarly,

$$\mathbf{H}_1^H \mathbf{H}_2 \left(\mathbf{H}_1^H \mathbf{H}_2 \right)^H = \mathbf{H}_1^H \mathbf{H}_2 \mathbf{H}_2^H \mathbf{H}_1 = (a+b)\mathbf{I}_2 \tag{9.30}$$

where $a = |\mathbf{h}_{1,oe}^{(1)H} \mathbf{h}_{2,oe}^{(1)} + \mathbf{h}_{1,oe}^{(2)T} \mathbf{h}_{2,oe}^{(2)*}|^2$ and $b = |\mathbf{h}_{1,oe}^{(1)H} \mathbf{h}_{2,oe}^{(2)} - \mathbf{h}_{1,oe}^{(2)T} \mathbf{h}_{2,oe}^{(1)*}|^2$.

Now we can write the estimated symbol vector by using LS estimator, i.e. by multiplying the received symbol vector with Moore-Penrose pseudo-inverse matrix for $\mathbf{H}$,

$$\begin{aligned} \widehat{\mathbf{m}} &= \left(\mathbf{H}^H \mathbf{H} \right)^{-1} \mathbf{H}^H \mathbf{z} \\ &= \frac{1}{\alpha_1 \alpha_2 - (a+b)} \begin{bmatrix} \mathbf{H}_2^H \mathbf{H}_2 & -\mathbf{H}_1^H \mathbf{H}_2 \\ -\mathbf{H}_2^H \mathbf{H}_1 & \mathbf{H}_1^H \mathbf{H}_1 \end{bmatrix} \begin{bmatrix} \mathbf{H}_1^H \\ \mathbf{H}_2^H \end{bmatrix} \mathbf{z} \end{aligned} \tag{9.31}$$

Using some definitions described above, we can express the former equation as following,

$$\widehat{\mathbf{m}} = \frac{1}{\alpha_1 \alpha_2 - (a+b)} \begin{bmatrix} \alpha_2 \mathbf{I}_2 & -\mathbf{H}_1^H \mathbf{H}_2 \\ -\mathbf{H}_2^H \mathbf{H}_1 & \alpha_1 \mathbf{I}_2 \end{bmatrix} \begin{bmatrix} \mathbf{H}_1^H \\ \mathbf{H}_2^H \end{bmatrix} \mathbf{z} \tag{9.32}$$

The MMSE receiver can be implemented in the same simple way. Defining ρ_n as the average SNR at each of the receive antennas, and the new constants $\beta_1 = \alpha_1 + \frac{\Delta P}{\rho_n}$, $\beta_2 = \alpha_2 + \frac{\Delta P}{\rho_n}$ then we can rewrite Eq. (9.32) as

$$\widehat{\mathbf{m}} = \frac{1}{\beta_1 \beta_2 - (a+b)} \begin{bmatrix} \beta_2 \mathbf{I}_2 & -\mathbf{H}_1^H \mathbf{H}_2 \\ -\mathbf{H}_2^H \mathbf{H}_1 & \beta_1 \mathbf{I}_2 \end{bmatrix} \begin{bmatrix} \mathbf{H}_1^H \\ \mathbf{H}_2^H \end{bmatrix} \mathbf{z} \tag{9.33}$$

9.2.3 OSIC-based Non-Linear Receiver

The basic transceiver architecture has been shown in Figure 9.1. In the case of OSIC-based non-linear receiver, the detection part is shown in Figure 9.2. The key idea of the non-linear receiver is to decode the symbol streams successively and extract them away layer by layer. At the beginning of each stage, the stream with highest SNR is chosen using ZF or MMSE detection for peeling. Once

© Muhammad Imadur Rahman, 2007

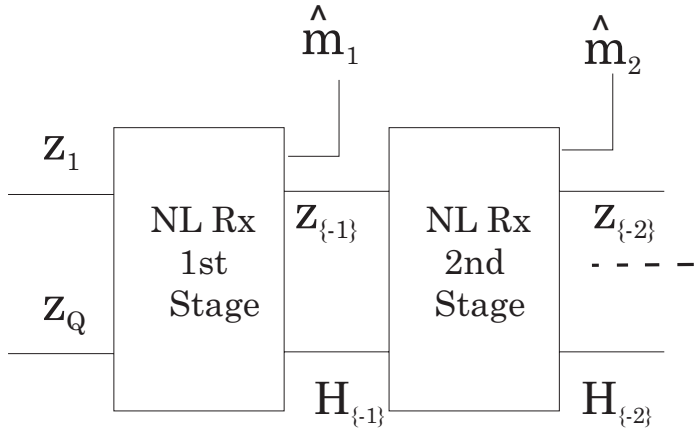

Figure 9.2: Simplified data flow for OSIC receiver

one particular layer is decoded, then the effect of the detected layer is subtracted from the received signal. From the remaining signal, the next branch in terms of SNR strength is chosen. This is continued until the last layer is decoded. This kind of non-linear detection is called OSIC [73],[24]. OSIC is performed on sub-carrier by sub-carrier basis. On each sub-carrier, the detection scheme appears to be very similar to VBLAST detection, as derived in [24]. OSIC improves the detection quality compared to detection without ordering and is shown to be optimal for SIC approach [73].

We consider $P = 2$, $\Delta = 2$ and $Q = 2$. Considering the frequency domain, it can be written

$$\mathbf{z}_k = \mathbf{H}_k \mathbf{m}_k + \mathbf{n}_k \tag{9.34}$$

where

$$\mathbf{H}_k = \begin{bmatrix} h^{(1)}_{11,o} & h^{(2)}_{11,o} & h^{(1)}_{12,o} & h^{(2)}_{12,o} \\ h^{(2)*}_{11,e} & -h^{(1)*}_{11,e} & h^{(2)*}_{12,e} & -h^{(1)*}_{12,e} \\ h^{(1)}_{21,o} & h^{(2)}_{21,o} & h^{(1)}_{22,o} & h^{(2)}_{22,o} \\ h^{(2)*}_{21,e} & -h^{(1)*}_{21,e} & h^{(2)*}_{22,e} & -h^{(1)*}_{22,e} \end{bmatrix}_k \tag{9.35}$$

and $\mathbf{z}_k = \left[z_{1,o}\,,\, z^*_{1,e}\,,\, z_{2,o}\,,\, z^*_{2,e}\right]^T_k$; $\mathbf{m}_k = [m_{1,o}\,,\, m_{1,e}, m_{2,o}\,,\, m_{2,e}]^T_k$; $\mathbf{n}_k = \left[n_{1,o}\,,\, n^*_{1,e}\,,\, n_{2,o}\,,\, n^*_{2,e}\right]^T_k$ with $k \in [1, \ldots, \frac{N}{2}]$.

The OSIC receiver consists of two steps: nulling and cancelation. While implementing the nulling operation, we consider two options, ZF and MMSE.

For ZF, we calculate the Moore-Penrose pseudo-inverse of the CTF

$$\begin{aligned} \mathbf{G}_k &= [\mathbf{g}_1\, \mathbf{g}_2\, \mathbf{g}_3\, \mathbf{g}_4]_k = \sqrt{\frac{\Delta P}{P_T}} \left\{ \mathbf{H}^H_k \mathbf{H}_k \right\}^{-1} \mathbf{H}^H_k \\ &= \sqrt{\frac{4}{P_T}} \left\{ \mathbf{H}^H_k \mathbf{H}_k \right\}^{-1} \mathbf{H}^H_k \end{aligned} \tag{9.36}$$

where P_T is the total transmit power from all transmit antennas, while for the MMSE we consider

a kind of pseudo-inverse that considers also the noise term

$$\mathbf{G}_k = \sqrt{\frac{4}{P_T}}\left\{\mathbf{H}_k^H\mathbf{H}_k + \frac{4\sigma^2}{P_T}\mathbf{I}_4\right\}^{-1}\mathbf{H}_k^H \tag{9.37}$$

where $[\mathbf{g}_i]_k$ is the ith column of $\mathbf{G}_k$, σ^2 is the noise variance at each receive antenna and $\mathbf{I}_4$ is the 4×4 identity matrix, and for both ZF and MMSE we have considered that $\Delta = 2$ and $P = 2$. At this stage, we calculate the metric:

$$l = arg\ \min_l\{d_1, d_2\} \tag{9.38}$$

where

$$d_1 = \mathbf{c}(1) + \mathbf{c}(3),\ d_2 = \mathbf{c}(2) + \mathbf{c}(4). \tag{9.39}$$

For ZF the vector, $\mathbf{c}$ is

$$\mathbf{c} = [\mathbf{c}(1)\ \mathbf{c}(2)\ \mathbf{c}(3)\ \mathbf{c}(4)] = diag\left(\{\mathbf{H}_k^H\mathbf{H}_k\}^{-1}\right) \tag{9.40}$$

and for MMSE the vector, $\mathbf{c}$ is

$$\mathbf{c} = [\mathbf{c}(1)\ \mathbf{c}(2)\ \mathbf{c}(3)\ \mathbf{c}(4)] = diag\left(\{\mathbf{H}_k^H\mathbf{H}_k + \frac{4\sigma^2}{P_T}\mathbf{I}_4\}^{-1}\right). \tag{9.41}$$

If $l = arg\ \min_l\{d_1, d_2\} = 1$ then we decode first the stream associated to $p = 1$ by doing

$$\widehat{\mathbf{m}}_{1,k} = \begin{bmatrix} \widehat{m}_{1,o} \\ \widehat{m}_{1,e} \end{bmatrix}_k = \begin{bmatrix} \mathbf{g}_1^H \\ \mathbf{g}_2^H \end{bmatrix}_k \mathbf{z}_k \tag{9.42}$$

and the second stream by doing the following steps (in Eq. (9.43) the cancelation operation is performed)

$$\mathbf{z}_k^{'} = \mathbf{z}_k - [\mathbf{h}_1\ \mathbf{h}_2]_k \begin{bmatrix} \widehat{m}_{1,o} \\ \widehat{m}_{1,e} \end{bmatrix}_k \tag{9.43}$$

$$\mathbf{H}_k^{'} = [\mathbf{h}_3\ \mathbf{h}_4]_k \tag{9.44}$$

$$\begin{aligned} \mathbf{H}_k^{'H}\mathbf{H}_k^{'} &= \frac{1}{\mid h_{12,o}^{(1)} \mid^2 + \mid h_{12,o}^{(2)} \mid^2 + \mid h_{22,o}^{(1)} \mid^2 + \mid h_{22,o}^{(2)} \mid^2}\mathbf{I}_2 \\ &= \frac{1}{\alpha}\mathbf{I}_2 \end{aligned} \tag{9.45}$$

$$\widehat{\mathbf{m}}_{2,k} = \begin{bmatrix} \widehat{m}_{2,o} \\ \widehat{m}_{2,e} \end{bmatrix}_k = \frac{1}{\alpha}\mathbf{H}_k^{'H}\mathbf{z}_k^{'} \tag{9.46}$$

where $[\mathbf{h}_i]_k$ is the ith column of $\mathbf{H}_k$ and $\mathbf{I}_2$ is the 2×2 identity matrix. In Eq.(9.45) we assume that neighboring sub-carriers have identical channel frequency response. Exactly the dual procedure of Eq.(9.42-9.46) has to be applied if $l = arg\ \min_l\{d_1, d_2\} = 2$, i.e. decoding the second SM branch at the beginning and then the first one.

© Muhammad Imadur Rahman, 2007

9.3 SM-QSFBC Transmission Scheme

9.3.1 Transmitter

Similar to SM-OSFBC scheme, Figure 9.1 explains the basic transmitter architecture for proposed SM-QSFBC system, with the receiver depicted in Figure 9.2. As mentioned earlier, this scheme is not studied and analyzed before we have performed this work, to the best of our knowledge based on extensive literature survey of public literatures. At first source bits are FEC coded and bit interleaved. The interleaved bit stream is baseband modulated using an appropriate constellation diagram, such as BPSK, QAM etc. We denote this baseband modulated symbols as $\mathbf{m}$. The sequences of $\mathbf{m}$ is demultiplexed in to $\mathbf{m}_1, \ldots, \mathbf{m}_P$ vectors. $\mathbf{m}_p$ is transmitted via p^{th} spatial channel, which can be written as,

$$\mathbf{m}_p = \begin{bmatrix} m_{p,1} & m_{p,2} & m_{p,3} & m_{p,4} & \ldots & m_{p,N-3} & m_{p,N-2} & m_{p,N-1} & m_{p,N} \end{bmatrix}$$

For every p^{th} SM branch, we implement a block coding across the sub-carriers, thus SFBC is included in the system. For p^{th} SM branch, we have Δ_p number of antennas where SFBC can be implemented. When $\Delta_p = \Delta, \ \forall p$, then we have $\Delta * P$ number of transmit antennas at the transmission side. When $\Delta = 2$, we can use well-known Alamouti coding [25] across the sub-carriers [156, 157], which are described in the previous section. For higher Δ, such as $\Delta = 4$, we can use orthogonal block codes as in [78], or quasi-orthogonal block codes as in [144]. The orthogonal code in [78] is not full rate, thus, the goal of SM in terms of data rate increment would be lost. So we use quasi-orthogonal codes in [144] for the studied Spatially-Multiplexed Quasi-orthogonal Space-Frequency Block Coded Orthogonal Frequency Division Multiplexing (SM-QSFBC-OFDM) system.

For p^{th} SM branch, $\mathbf{m}_p$ is coded into four vectors, $\mathbf{m}_p^{(\delta)}; \ \delta = 1, \ldots, 4$. Thus, the output of the Quasi-orthogonal Space-Frequency Block Code (QSFBC) encoder block of the pth SM branch will be

$$\begin{aligned}
\mathbf{m}_p^{(1)} &= \begin{bmatrix} m_{p,1} & -m_{p,2}^* & -m_{p,3}^* & m_{p,4} & \ldots & m_{p,N-3} & -m_{p,N-2}^* & -m_{p,N-1}^* & m_{p,N} \end{bmatrix} \\
\mathbf{m}_p^{(2)} &= \begin{bmatrix} m_{p,2} & m_{p,1}^* & -m_{p,4}^* & -m_{p,3} & \ldots & m_{p,N-2} & m_{p,N-3}^* & -m_{p,N}^* & -m_{p,N-1} \end{bmatrix} \\
\mathbf{m}_p^{(3)} &= \begin{bmatrix} m_{p,3} & -m_{p,4}^* & m_{p,1}^* & -m_{p,2} & \ldots & m_{p,N-1} & -m_{p,N}^* & m_{p,N-3}^* & -m_{p,N-2} \end{bmatrix} \\
\mathbf{m}_p^{(4)} &= \begin{bmatrix} m_{p,4} & m_{p,3}^* & m_{p,2}^* & m_{p,1} & \ldots & m_{p,N} & m_{p,N-1}^* & m_{p,N-2}^* & m_{p,N-3} \end{bmatrix}
\end{aligned} \tag{9.47}$$

After SM and SFBC operations, IFFT modulation is performed and CP is added before transmission via respective transmit antenna. Transmitted time domain samples, $\mathbf{x}_p^{(\delta)}$, can be related to $\mathbf{m}_p^{(\delta)}$ as, $\mathbf{x}_p^{(\delta)} = \mathbb{F}^H\{\mathbf{m}_p^{(\delta)}\}$.

Note that N sub-carriers are divided into $N/4$ groups of 4 sub-carriers and on each group QSFBC is performed. Note that $P \leq Q$.

9.3.2 OSIC Receiver

The OSIC receiver for SM-QSFBC scheme is similar to the OSIC receiver for SM-OSFBC scheme described in Section 9.2.3.

We consider $P = 2$, $\Delta = 4$ and $Q = 2$. We assume perfect time and frequency synchronization is achieved in the system. Thus, we can represent the system in frequency domain notations. To represent the SFBC part of the scheme, here we write the received symbol at 4 consecutive sub-carriers, where the transmit symbols are coded using quasi-orthogonal block coding:

$$\begin{aligned} z_{q,a} &= h^{(1)}_{q1,a} m_{1,a} + h^{(2)}_{q1,a} m_{1,b} + h^{(3)}_{q1,a} m_{1,c} + h^{(4)}_{q1,a} m_{1,d} \\ &+ h^{(1)}_{q2,a} m_{2,a} + h^{(2)}_{q2,a} m_{2,b} + h^{(3)}_{q2,a} m_{2,c} + h^{(4)}_{q2,a} m_{2,d} + n_{q,a} \end{aligned} \tag{9.48}$$

$$\begin{aligned} z_{q,b} &= -h^{(1)}_{q1,b} m^*_{1,b} + h^{(2)}_{q1,b} m^*_{1,a} - h^{(3)}_{q1,b} m^*_{1,d} + h^{(4)}_{q1,b} m^*_{1,c} \\ &- h^{(1)}_{q2,b} m^*_{2,b} + h^{(2)}_{q2,b} m^*_{2,a} - h^{(3)}_{q2,b} m^*_{2,d} + h^{(4)}_{q2,b} m^*_{2,c} + n_{q,b} \end{aligned} \tag{9.49}$$

$$\begin{aligned} z_{q,c} &= -h^{(1)}_{q1,c} m^*_{1,c} - h^{(2)}_{q1,c} m^*_{1,d} + h^{(3)}_{q1,c} m^*_{1,a} + h^{(4)}_{q1,c} m^*_{1,b} \\ &- h^{(1)}_{q2,c} m^*_{2,c} - h^{(2)}_{q2,c} m^*_{2,d} + h^{(3)}_{q2,c} m^*_{2,a} + h^{(4)}_{q2,c} m^*_{2,b} + n_{q,c} \end{aligned} \tag{9.50}$$

$$\begin{aligned} z_{q,d} &= h^{(1)}_{q1,d} m_{1,d} - h^{(2)}_{q1,d} m_{1,c} - h^{(3)}_{q1,d} m_{1,b} + h^{(4)}_{q1,d} m_{1,a} \\ &+ h^{(1)}_{q2,d} m_{2,d} - h^{(2)}_{q2,d} m_{2,c} - h^{(3)}_{q2,d} m_{2,b} + h^{(4)}_{q2,d} m_{2,a} + n_{q,d} \end{aligned} \tag{9.51}$$

where $a = 4k - 3,\ b = 4k - 2,\ c = 4k - 1,$ and $d = 4k,$ with $k \in [1, \ldots, \frac{N}{4}]$ and $q \in [1, 2]$. Using these four equations above, we can write the equivalent system model as the following:

$$\mathbf{z}_k = \mathbf{H}_k \mathbf{m}_k + \mathbf{n}_k \qquad k \in \left[1, \ldots, \frac{N}{4}\right] \tag{9.52}$$

where $\mathbf{z}_k$ and $\mathbf{n}_k$ are the concatenations of the received signals and noise respectively, for the kth group of sub-carriers. Here $\mathbf{z}_k = \left[\mathbf{z}^{(1)}_k \ldots \mathbf{z}^{(Q)}_k\right]^T$, with $\mathbf{z}^{(q)}_k = \left[z^{(q)}_{4k-3}\ z^{(q)*}_{4k-2}\ z^{(q)*}_{4k-1}\ z^{(q)}_{4k}\right]^T$. Similarly, $\mathbf{m}_k = \left[\mathbf{m}^{(1)}_k \ldots \mathbf{m}^{(P)}_k\right]^T$, with $\mathbf{m}^{(p)}_k = \left[m^{(p)}_{4k-3}\ m^{(p)}_{4k-2}\ m^{(p)}_{4k-1}\ m^{(p)}_{4k}\right]$. $\mathbf{m}^{(y)}_x$ and $\mathbf{z}^{(y)}_x$ denote transmitted and received samples respectively, for x^{th} sub-carrier group on y^{th} SM branch and receive antenna respectively. $\mathbf{H}_k$ is shown in Eq.(9.53) as,

$$\mathbf{H}_k = \begin{bmatrix} [\mathbf{H}_{11}]_k & \ldots & [\mathbf{H}_{1P}]_k \\ \vdots & \ddots & \vdots \\ [\mathbf{H}_{Q1}]_k & \ldots & [\mathbf{H}_{QP}]_k \end{bmatrix} \tag{9.53}$$

where $[\mathbf{H}_{ij}]_k$ with $i \in \{1, \ldots, Q\}$ and $j \in \{1, \ldots, P\}$ is,

$$[\mathbf{H}_{ij}]_k = \begin{bmatrix} h^{(1)}_{ij,4k-3} & h^{(2)}_{ij,4k-3} & h^{(3)}_{ij,4k-3} & h^{(4)}_{ij,4k-3} \\ h^{(2)*}_{ij,4k-2} & -h^{(1)*}_{ij,4k-2} & h^{(4)*}_{ij,4k-2} & -h^{(3)*}_{ij,4k-2} \\ h^{(3)*}_{ij,4k-1} & h^{(4)*}_{ij,4k-1} & -h^{(1)*}_{ij,4k-1} & -h^{(2)*}_{ij,4k-1} \\ h^{(4)}_{ij,4k} & -h^{(3)}_{ij,4k} & -h^{(2)}_{ij,4k} & h^{(1)}_{ij,4k} \end{bmatrix} \tag{9.54}$$

© Muhammad Imadur Rahman, 2007

For ZF, we calculate the Moore-Penrose pseudo-inverse, $\mathbf{G}_k$, of the equivalent CTF, $\mathbf{H}_k$,

$$\begin{aligned}\mathbf{G}_k &= [\mathbf{g}_1 \dots \mathbf{g}_{4Q}]_k = \sqrt{\frac{\Delta P}{P_T}}\left\{\mathbf{H}_k^H\mathbf{H}_k\right\}^{-1}\mathbf{H}_k^H \\ &= \sqrt{\frac{8}{P_T}}\left\{\mathbf{H}_k^H\mathbf{H}_k\right\}^{-1}\mathbf{H}_k^H \end{aligned} \tag{9.55}$$

where P_T is total transmit power from all transmit antennas.

For the MMSE nulling operator, the pseudo-inverse is defined considering the noise variance [73], $\mathbf{G}_k = \sqrt{\frac{4P}{P_T}}\{\mathbf{H}^H\mathbf{H} + \frac{4P}{\rho}\mathbf{I}_{4P}\}^{-1}\mathbf{H}^H$. Note that in our case, the number of transmit antennas is $\Delta P = 4P$. The SNR is $\rho = \frac{P_T}{\sigma^2}$, with σ^2 noise variance at each receive antenna. Using this definition of ρ, we finally obtain the MMSE nulling operator as

$$\begin{aligned}\mathbf{G}_k &= [\mathbf{g}_1 \dots \mathbf{g}_{4Q}]_k = \sqrt{\frac{\Delta P}{P_T}}\left\{\mathbf{H}_k^H\mathbf{H}_k + \frac{\Delta P\sigma^2}{P_T}\mathbf{I}_{\Delta P}\right\}^{-1}\mathbf{H}_k^H \\ &= \sqrt{\frac{8}{P_T}}\left\{\mathbf{H}_k^H\mathbf{H}_k + \frac{8\sigma^2}{P_T}\mathbf{I}_8\right\}^{-1}\mathbf{H}_k^H \end{aligned} \tag{9.56}$$

where $[\mathbf{g}_i]_k$ is the ith column of $\mathbf{G}_k$, $\mathbf{I}_8$ is the 8×8 identity matrix and we have considered that $\Delta = 4$ and $P = 2$.

At this stage, we define a vector, $\mathbf{\Omega}$ as:

$$\text{ZF} \quad : \quad \mathbf{\Omega} = diag\left[\{\mathbf{H}_k^H\mathbf{H}_k\}^{-1}\right] \tag{9.57}$$

$$\text{MMSE} \quad : \quad \mathbf{\Omega} = diag\left[\{\mathbf{H}_k^H\mathbf{H}_k + \frac{4P\sigma^2}{P_T}\mathbf{I}_{4P}\}^{-1}\right] \tag{9.58}$$

where $diag\,[\mathbf{X}]$ is the vector containing all the diagonal components of matrix $\mathbf{X}$.

After that, the ordering for layer-by-layer detection is done, by determining the strongest received signal branch. For this, we calculate the component of a vector,

$$\begin{aligned}\mathbf{d}(p) &= \mathbf{\Omega}(p) + \mathbf{\Omega}(p+P) + \mathbf{\Omega}(p+2P) + \dots \\ &\quad + \mathbf{\Omega}(p + (\Delta - 1)P) \end{aligned} \tag{9.59}$$

where $\mathbf{\Omega}(p)$ and $\mathbf{d}(p)$ are the pth element of vector $\mathbf{\Omega}$ and $\mathbf{d}$ respectively. Clearly, $\mathbf{\Omega} \in \mathbb{C}^{[4P\times 1]}$ and $\mathbf{d} \in \mathbb{C}^{[P\times 1]}$. For example, when $\Delta = 4$ and $P = 2$, we can write that

$$\mathbf{d}(1) = \mathbf{\Omega}(1) + \mathbf{\Omega}(3) + \mathbf{\Omega}(5) + \mathbf{\Omega}(7) \tag{9.60}$$

$$\mathbf{d}(2) = \mathbf{\Omega}(2) + \mathbf{\Omega}(4) + \mathbf{\Omega}(6) + \mathbf{\Omega}(8) \tag{9.61}$$

Using the vector $\mathbf{d}$, we define a new vector $\mathbf{\Phi}$, which indicates the received strength of transmitted branches in descending order, i.e. the SM branches are arranged in descending order in this vector. We define, $\mathbf{\Phi}(1) = arg\ \min_l\{\mathbf{d}(l)\}, \forall\ l \in [1, \dots, P]$. Similarly, $\mathbf{\Phi}(2) = arg\ \min_l\{\mathbf{d}(l)\}, \forall\ l \in [1, \dots, P]\backslash\mathbf{\Phi}(1)$. This is continued until all P transmit branches are ordered. The metric to define the descending order of received SM branches in $\mathbf{\Phi}$ is found based on OSIC approach as explained

in [73].

If $\mathbf{\Phi}(1) = 1$, then we extract the first receive stream by using ZF or MMSE nulling criterion, i.e. $\widehat{\mathbf{m}}_k^{(1)} = \mathbf{G}_{1,k}\mathbf{z}_k$, where $\widehat{\mathbf{m}}_k^{(1)} = \left[\widehat{m}_{4k-3}^{(1)}\ \widehat{m}_{4k-2}^{(1)}\ \widehat{m}_{4k-1}^{(1)}\ \widehat{m}_{4k}^{(1)}\right]_k^T$ and $\mathbf{G}_{1,k} = [\mathbf{g}_1\ \mathbf{g}_2\ \mathbf{g}_3\ \mathbf{g}_4]_k^T$.

Once the strongest branch is extracted, then the contribution of this branch is subtracted from the remaining signal, and the new equivalent CTF is obtained:

$$\mathbf{z}_k^{'} = \mathbf{z}_k - [\mathbf{h}_1\ \mathbf{h}_2\ \mathbf{h}_3\ \mathbf{h}_4]_k\ \widehat{\mathbf{m}}_k^{(1)} = \mathbf{H}_k^{'}\left[\mathbf{m}_k^{(2)}\ \ldots\ \mathbf{m}_k^{(P)}\right]^T \tag{9.62}$$

where $\mathbf{H}_k^{'} = [\mathbf{h}_5\ \mathbf{h}_6\ \ldots\ \mathbf{h}_{4P}]_k$ and $[\mathbf{h}_i]_k$ is the ith column of $\mathbf{H}_k$.

The next strongest branch is found as $\mathbf{\Phi}(2)$. We define a new nulling operator as $\mathbf{G}_{\mathbf{\Phi}(2),k} = \left[\mathbf{g}_{4\mathbf{\Phi}(2)-3}\ \mathbf{g}_{4\mathbf{\Phi}(2)-2}\ \mathbf{g}_{4\mathbf{\Phi}(2)-1}\ \mathbf{g}_{4\mathbf{\Phi}(2)}\right]_k^T$. With this nulling operator and new CTF matrix as in (9.62), a new nulling criterion is defined and the second strongest branch is extracted from the remaining signal as shown below for ZF and MMSE solutions respectively:

$$\begin{aligned}\widehat{\mathbf{m}}_k^{(\mathbf{\Phi}(2))} &= \mathbf{G}_{\mathbf{\Phi}(2),k}\mathbf{z}_k^{'} = \sqrt{\frac{\Delta P}{P_T}}\left\{\mathbf{H}_k^{''H}\mathbf{H}_k^{''}\right\}^{-1}\mathbf{H}_k^{''H}\mathbf{z}_k^{'} \\ &= \sqrt{\frac{8}{P_T}}\left\{\mathbf{H}_k^{''H}\mathbf{H}_k^{''}\right\}^{-1}\mathbf{H}_k^{''H}\mathbf{z}_k^{'}\end{aligned} \tag{9.63}$$

and for MMSE

$$\begin{aligned}\widehat{\mathbf{m}}_k^{(\mathbf{\Phi}(2))} &= \sqrt{\frac{\Delta P}{P_T}}\left\{\mathbf{H}_k^{''H}\mathbf{H}_k^{''} + \frac{\Delta P\sigma^2}{P_T}\mathbf{I}_\Delta\right\}^{-1}\mathbf{H}_k^{''H}\mathbf{z}_k^{'} \\ &= \sqrt{\frac{8}{P_T}}\left\{\mathbf{H}_k^{''H}\mathbf{H}_k^{''} + \frac{8\sigma^2}{P_T}\mathbf{I}_4\right\}^{-1}\mathbf{H}_k^{''H}\mathbf{z}_k^{'}\end{aligned} \tag{9.64}$$

where $\mathbf{H}_k^{''} = \left[\mathbf{h}_{4\mathbf{\Phi}(2)-3}\ \mathbf{h}_{4\mathbf{\Phi}(2)-2}\ \mathbf{h}_{4\mathbf{\Phi}(2)-1}\ \mathbf{h}_{4\mathbf{\Phi}(2)}\right]_k^T$ in both (9.63) and (9.64), $\mathbf{I}_4$ is the 4×4 identity matrix and we have considered that $\Delta = 4$ and $P = 2$. When there are more than $P = 2$ transmitted streams, the whole procedure is continued until the last branch is detected.

9.4 Numerical Results

9.4.1 System Parameters

We have used simulation scenarios with following system parameters: System bandwidth, B = 1.25 MHz, Carrier frequency, f_c = 3.5 GHz, OFDM sub-carriers, N = 128, CP length, N_{CP} = 16, Sampling rate, f_s=1.429 Msps, Symbol duration, $T_s = (N + N_{CP})/f_s$ = 100.77 μs, number of symbols in a frame, $N_f = 5$ and Frame duration, $T_f = N_f T_s$ = 503.85 μs. QPSK modulation with $\frac{1}{2}$-rate convolutional coding is used for all the schemes. For all our analysis and simulations, we have two SM branches and dual receive antennas in all systems, i.e. $P = Q = 2$. We have confined ourselves to the case of $\Delta = 2$ and 4 for each pth SM branch in SM-OSFBC and SM-QSFBC systems respectively. Thus, we have 4×2 and 8×2 systems for SM-OSFBC and SM-QSFBC schemes respectively. The tags used to denote different transmission and reception configurations are shown in Table 9.1.

© Muhammad Imadur Rahman, 2007

We assume that perfect channel estimation values for each sub-carrier for all the spatial channels are available at the receiver. We use the exponential model to generate the corresponding CIR and CTF of the channel. In our model, the power delay profile of the channel is exponentially distributed with decay between the first and the last impulse as -40 dB.

Scheme	Tag
2×1 Alamouti SFBC scheme [79]	2×1 *SFBC*
2×2 VBLAST with ZF nulling [24]	2×2 *ZF-BLAST*
2×2 VBLAST with MMSE nulling [24]	2×2 *MMSE-BLAST*
2×2 SM system optimum ML reception	2×2 *ML*
4×2 SM-OSFBC transmitter and ZF based linear receiver	4×2 *SM-OSFBC, ZF-Lin*
4×2 SM-OSFBC transmitter and MMSE based linear receiver	4×2 *SM-OSFBC, MMSE-Lin*
4×2 SM-OSFBC transmitter and ZF based OSIC receiver	4×2 *SM-OSFBC, ZF-OSIC*
4×2 SM-OSFBC transmitter and MMSE based OSIC receiver	4×2 *SM-OSFBC, MMSE-OSIC*
8×2 SM-QSFBC transmitter and ZF based OSIC receiver	8×2 *SM-QSFBC, ZF-OSIC*
8×2 SM-QSFBC transmitter and MMSE based OSIC receiver	8×2 *SM-QSFBC, MMSE-OSIC*

Table 9.1: Tags used in figures for corresponding schemes

9.4.2 System Capacity Analysis

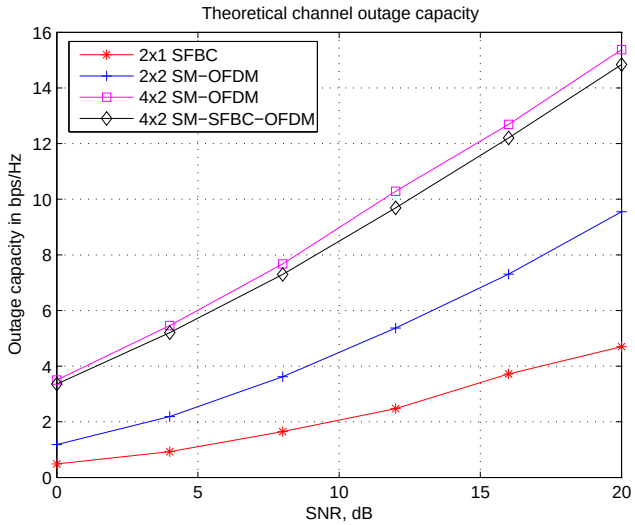

Figure 9.3: 10% channel outage capacity for reference systems

The theoretical instantaneous capacity (i.e. deterministic capacity) of SFBC-OFDM, STBC-OFDM, SM-OFDM and SM-SFBC-OFDM systems are evaluated in this section via a semi-analytical Monte-Carlo simulation approach. The instantaneous channel capacity is obtained based on the

following equation:

$$C = \frac{1}{N}\sum_{k=0}^{N-1} log_2\left[det\left(\mathbf{I}_Q + \frac{\overline{\gamma}}{P}\mathbf{H}_k\mathbf{H}_k^*\right)\right] \tag{9.65}$$

where $\overline{\gamma}$ is the average transmit SNR and $\mathbf{H}_k$ is the equivalent effective CTF of kth sub-carrier. Equivalent CTF means the CTF at the particular sub-carrier at the receiver, such as shown in Eq.(8.44) and Eq.(9.35). The above instantaneous capacity is derived for each channel realizations.

Outage analysis is a form of reliability analysis. We define 10% outage channel capacity as the information rate that is guaranteed for 90% of the channel realizations, such that the probability that outage rate falls below the certain threshold rate is at most 10% [73]. The 10% outage channel capacities for SFBC-OFDM, SM-OFDM and Spatially-Multiplexed Orthogonal Space-Frequency Block Coded Orthogonal Frequency Division Multiplexing (SM-OSFBC-OFDM) are given in Figure 9.3. For reference purpose, *2x1 SFBC* outage channel capacity is plotted in the figure. *4x2 SM-OFDM* shows the optimum achievable outage channel capacity derived from Shannon limit. We can see that the upper bound in outage channel capacity of our scheme (i.e. *4x2 SM-SFBC-OFDM*) approaches very close to the Shannon limit. As expected, the difference in 10% outage channel capacity of SM and JDM scheme is 3 bps/Hz at comparatively low SNR (i.e. at 4dB of SNR) and is more than 5 bps/Hz at comparatively high SNR (i.e. at 16dB of SNR). For system SNR of 10dB, diversity only scheme (i.e. SFBC) has an outage capacity of approximately 2.0 bps/Hz. In contrast to this, 2×2 spatial multiplexing only scheme has 10% outage capacity of 4.2 bps/Hz, compared to our 4×2 hybrid schemes at 8.2 bps/Hz. The maximum outage capacity of any 4×2 'open loop' MIMO schemes can be 8.9 bps/Hz approximately. The last outage capacity value is an upper bound for any 4×2 'open loop' MIMO scheme. This is achievable with best available source, channel and S-F coding. In our case, even though we have simple Alamouti as the S-F code, it can be seen that the capacity performance is very close to the optimum boundary.

9.4.3 FER Performance

Figure 9.4 shows us the coded FER results for the schemes in WiMAX scenario. For various transmit antenna configurations, the total transmit power is kept constant, thus, the SNR at the x-axis reflects total SNR of the systems. We have used QPSK modulation for all the systems. We know that 2×2 SM [24] performs worse in terms of FER compared to 2×1 SFBC system: in fact in the SM system, we get an higher rate, but we lose in diversity [26]. Considering this, we can see that 4×2 SM-OSFBC with OSIC receiver performs better than SFBC system in terms of FER. In this case, not only the diversity gain is achieved, but spatial multiplexing gain is also realized. We can see an even better gain in FER is obtained when 8×2 SM-QSFBC system is used. This clearly shows the benefits of increased spatial dimensions at the transmitter and OSFBC or QSFBC used in the transmission system. For instance, SM-QSFBC-MMSE-OSIC and SM-OSFBC-MMSE-OSIC achieve a gain of 9dB and 5dB respectively, compared to MMSE-BLAST at an FER of 10^{-2}.

© Muhammad Imadur Rahman, 2007

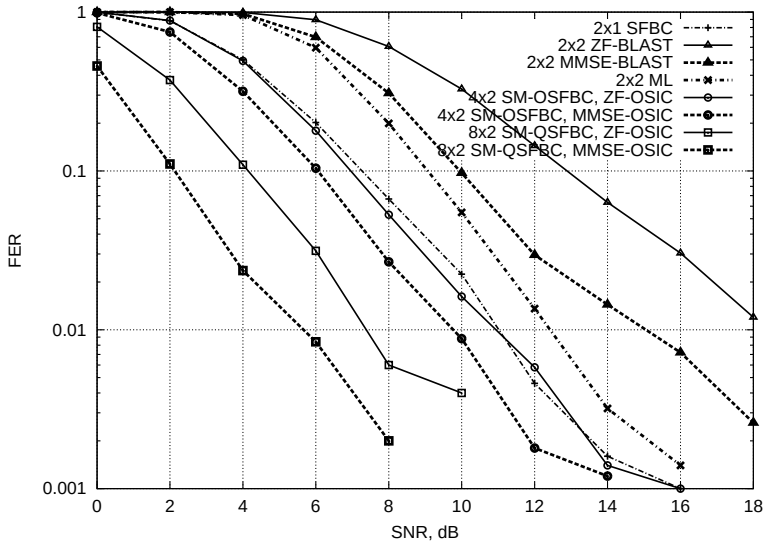

Figure 9.4: FER performance for the schemes

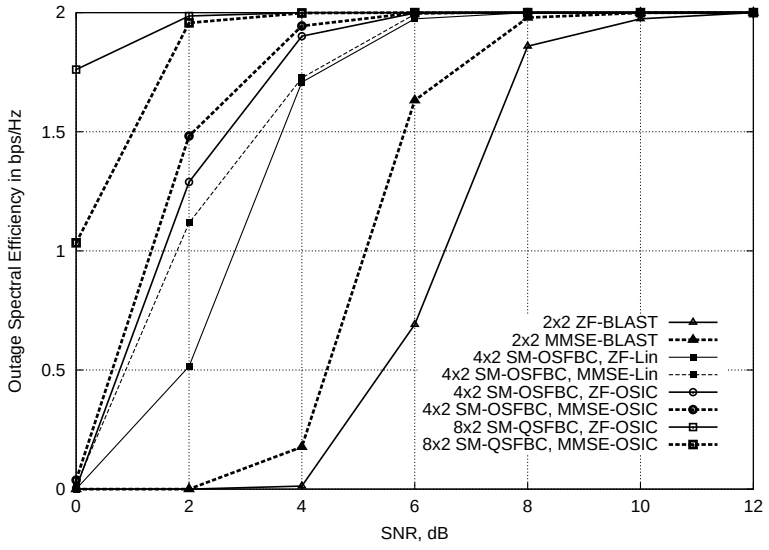

Figure 9.5: 10% Outage spectral efficiency

9.4.4 10% Outage Spectral Efficiency

The 10% outage spectral efficiencies for SM, SM-OSFBC and SM-QSFBC with different receiver configurations are given in Figure 9.5. At 0dB of SNR, 10% outage spectral efficiency of SM-QSFBC-MMSE-OSIC and SM-QSFBC-ZF-OSIC schemes are 1.75 and 1 bps/Hz respectively. The maximum achievable spectral efficiency with the set of parameters that we have used for these simulations is 2 bps/Hz (achieved with spatial rate of 2, QPSK modulation, channel coding rate of 1/2). For SM-QSFBC-OSIC schemes, the 10% outage spectral efficiency is almost close to maximum at any SNR more than than 4dB. At that SNR, SM system obtains very low efficiency, whereas SM-OSFBC schemes obtain between 1.7 and 1.9 bps/Hz, which is quite impressive also. One conclusion that can be easily made is that added spatial dimensions at the transmitter side are exploited well in JDM schemes to improve system performance in terms of FER and outage spectral efficiency as seen in Figure 9.4 and Figure 9.5 respectively.

9.4.5 Effect of Spatial Correlation

R	0.90	0.82	0.70	0.61	0.51	0.40	0.29	0.22	0.15
d(cm)	0.56	0.78	1.00	1.17	1.33	1.50	1.67	1.78	1.89

Table 9.2: Correlation for corresponding spatial separation among antennas at 3.5GHz of carrier frequency. R and d denote spatial correlation and separation in cm across two neighboring elements respectively.

We model the spatial correlation in $\mathbf{H}$ based on the inter-element distances in the transmit and receive antenna arrays, as it is done in [151]. We can model the spatial correlation across all sub-carriers as

$$\mathbf{H}_k = \sqrt{\mathbf{R}_{k,rx}}\mathbf{H}_{w,k}\sqrt{\mathbf{R}_{k,tx}} \tag{9.66}$$

where $\mathbf{R}_{k,rx}$, $\mathbf{H}_{w,k}$ and $\mathbf{R}_{k,tx}$ are receive correlation matrix, uncorrelated channel matrix and transmit correlation matrix respectively. The correlation coefficient between p_1 and p_2 transmit antennas can be written as

$$[\mathbf{R}_{k,tx}]_{p_1,p_2} = \mathcal{J}_0\left(\frac{2\pi(p_1 - p_2)d}{\lambda}\right) \tag{9.67}$$

where $p_1, p_2 \in [1, \ldots, P\Delta]$. $\mathcal{J}_0$ denotes the 0th order Bessel function of 1st kind, d is the distance between the elements and λ is the wavelength corresponding to the carrier frequency. Similar spatial correlation can be defined for receiver also.

In this section, we investigate the impact of spatial correlation on FER and on outage spectral efficiency. For this, the receive (transmit) correlation is fixed to 0.3 and transmit (receive) correlation is varied as shown in Table 9.2. This 0.3 of receive spatial correlation corresponds to off-diagonal components in $\mathbf{R}_{k,rx}$, i.e. the spatial correlation between the neighboring elements is 0.3. The same applies for transmit side. The results are obtained for a particular SNR value, i.e. 12dB.

In Figures 9.6 and 9.7, we produce the FER results of the schemes, in presence of spatial correlation due to insufficient spatial separation between antenna elements. In [153], impact of

© Muhammad Imadur Rahman, 2007

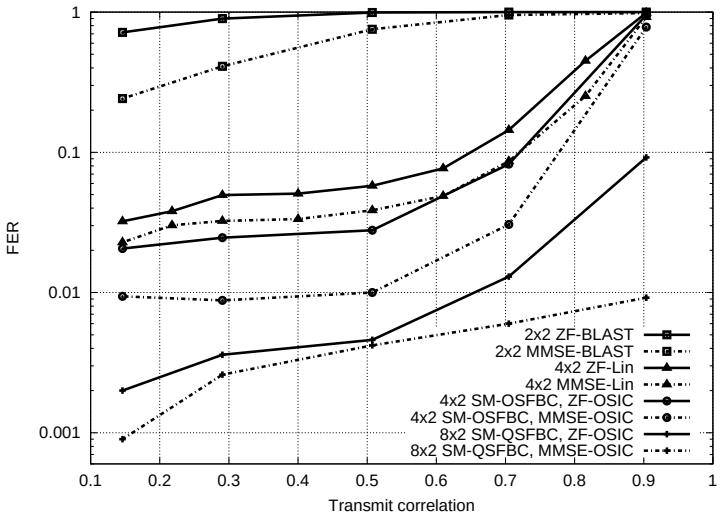

Figure 9.6: FER with respect to increasing transmit correlation (i.e. decreasing antenna spacing) and fixed receive correlation at system SNR of 12dB

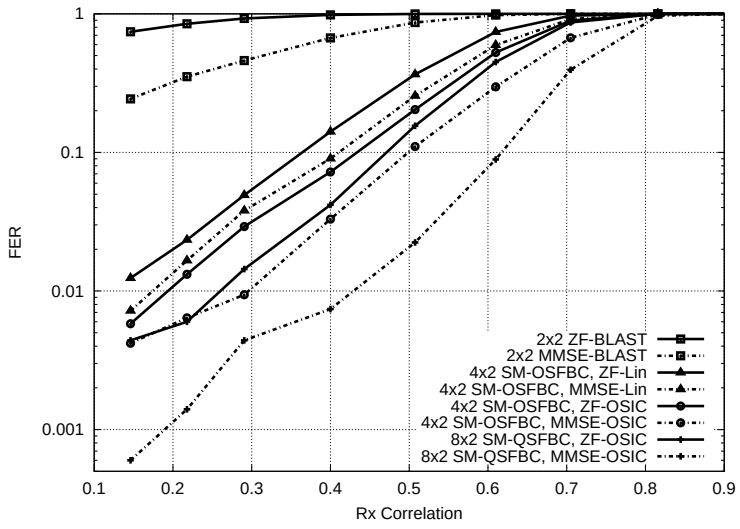

Figure 9.7: FER with respect to increasing receive correlation (i.e. decreasing antenna spacing) and fixed transmit correlation at system SNR of 12dB

spatial correlation is studied for a system similar to SM-OSTBC scheme: however it is not clear in [153], whether the spatial correlation is considered at the transmitter or at the receiver or at both locations. For Figure 9.6, we varied the transmit correlation and fixed the receive correlation to 0.3, and the opposite is done for Figure 9.7. One interesting conclusion that can be drawn from these figures is that receive correlation affects these systems much more than transmit correlation. This is because no extra diversity measures are taken at the receiver. From Figure 9.7, we see that the FERs increase very fast when the receive correlation increases. This is true for all the systems. From Figure 9.6, for increasing transmit correlation with a fixed receive correlation, the degradation in JDM schemes is gradual. Up to 60% of spatial correlation between the transmit antennas, the JDM schemes perform quite consistently, they worsen only when the spatial correlation is increased more than this. Thus, as long as the transmit elements are separated by a spacing of at least 1.17 cm for our system (according to Table 9.2), the effect of spatial correlation in FER performance is not quite significant for JDM systems. While SM-QSFBC-OSIC with ZF and MMSE equalization perform the best for increasing transmit correlation, ZF-BLAST and MMSE-BLAST perform quite badly, when the spatial correlation is increased. Thus, it is evident that original VBLAST systems are not so robust in spatially correlated scenario as it was previously reported in [73].

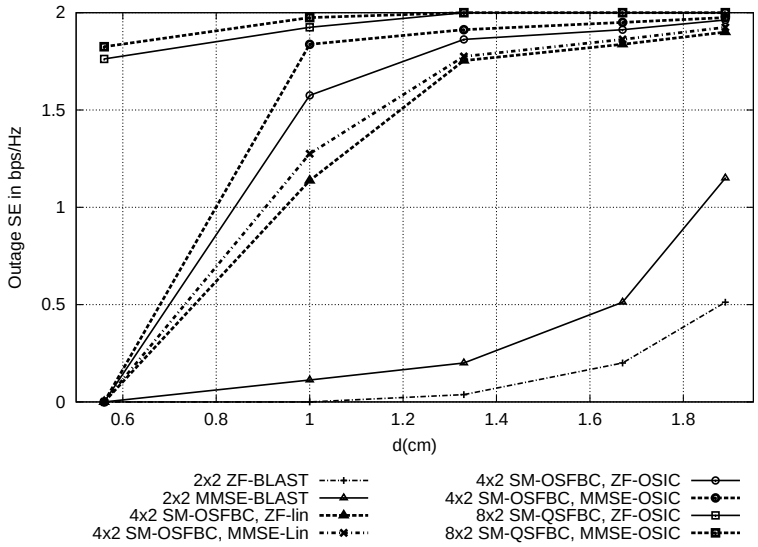

Figure 9.8: Outage spectral efficiency with respect to decreasing transmit correlation (i.e. increasing antenna spacing) and fixed receive correlation at system SNR of 12dB

To obtain more insight into the impact of transmit correlation, we have also performed simulations to measure the 10% outage spectral efficiency for all the schemes when transmit spatial correlation is increased steadily with a fixed receive spatial correlation. In Figure 9.8, the antenna spacing at the transmitter side is shown on x-axis: the higher the antenna spacing, the lower the spatial correlation experienced in the system. As shown in Figure 9.8, as soon as the antenna spacing at the transmitter starts to increase (i.e. the correlation starts to decrease), the outage efficiency

© Muhammad Imadur Rahman, 2007

for SM-QSFBC schemes reaches the highest spectral efficiency. Other JDM schemes also have high outage spectral efficiency. The reason for good outage spectral efficiency is the diversity benefits obtained in JDM schemes in parallel with the multiplexing gains. We know that any form of diversity benefits is bound to improve the outage scenario. It is worth noticing here that SM schemes provide very low outage efficiency even at low level of transmit correlation.

9.4.6 Performance in Presence of LOS

We model the wireless channel response having two distinct components [158],

1. a specular component (or LOS component) that illuminates the arrays uniformly and is thus spatially deterministic from antenna to antenna, we denote such a component as $\mathbf{H}_c$;

2. a scattered Rayleigh-distributed component that varies randomly from antenna to antenna, this component is denoted as $\mathbf{H}_w$.

The MIMO channel model for each sub-carrier with the effect of LOS component can now be written as

$$\mathbf{H}_k = \sqrt{\frac{K}{K+1}}\mathbf{H}_{c,k} + \sqrt{\frac{1}{K+1}}\mathbf{H}_{w,k} \tag{9.68}$$

where K is the Ricean K-factor of the system that is essentially the ratio of the power in the LOS component of the channel to the power in the fading component. $K = 0$ corresponds to pure Rayleigh fading, while $K = \infty$ corresponds to a non-fading channel. The elements of normalized scattering component $\mathbf{H}_{w,k}$ are modeled as ZMCSCG with unit variance [73]. The specular component is given by

$$\mathbf{H}_c = \mathbf{a}(\theta_r)^T\mathbf{a}(\theta_t) \tag{9.69}$$

where $\mathbf{a}(\theta_t)$ and $\mathbf{a}(\theta_r)$ are the specular array responses at the transmitter and receiver respectively. The array response corresponding to the transmit $P\Delta = 4P$ (or receive Q)-element linear array is given by $\left[1\ e^{j2\pi d\cos(\theta)}\ \ldots\ e^{j2\pi d(P\Delta-1)\cos(\theta)}\right] = \left[1\ e^{j2\pi d\cos(\theta)}\ \ldots\ e^{j2\pi(4P-1)\cos(\theta)}\right]$, where θ is the Angle of Departure (AoD) in the transmitter (or AoA in the receiver) of the specular component and d is the antenna spacing in wavelengths [158].

This investigation is intended for outdoor micro cell scenario, therefore θ_t and θ_r are taken to be 120 and 360 degrees [124]. Spacing between arrays at both ends is taken as 0.56 cm (i.e. spatial correlation of 0.3). After obtaining the FER, we calculated the corresponding average spectral efficiency loss when LOS component becomes stronger, compared to NLOS scenario (corresponding FER results for NLOS scenario are given in Figure 9.4). The average SE is defined as $SE = R\,(1 - FER_{coded})$, where $R = 2\ bps/Hz$ is the maximum achievable SE. For brevity, we have presented the results for MMSE based receivers only. The impact of LOS on SM-QSFBC systems is much less compared to BLAST and SM-OSFBC schemes. Figure 9.9 shows the loss because of the LOS component in average spectral efficiency. It is seen that spectral efficiency loss in *SM-QSFBC* system is 25% less compared to other schemes at $K = 50$ (i.e. ≈ 17 dB).

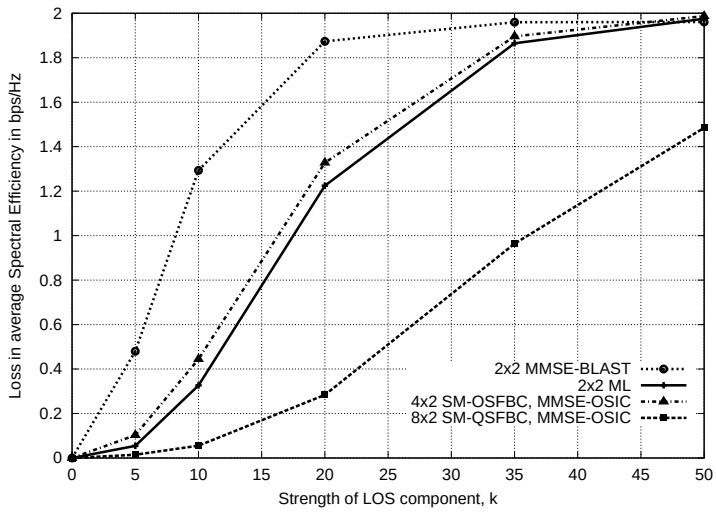

Figure 9.9: Loss in average spectral efficiency with respect to increasingly strong LOS component

9.5 Chapter Summary

In this chapter, we have studied different joint schemes where both diversity and multiplexing benefits are exploited at the same time. We have analyzed the performance of different receiver strategies in realistic wireless conditions. JDM schemes are in general robust to spatial correlation caused by the inadequate spatial separation between antenna elements. When spatial correlation is caused by the LOS scenario, then only SM-QSFBC type JDM schemes show robustness in performance. All other JDM schemes fail with little increment in strength of LOS component in the wireless channel. For both ZF and MMSE, the VBLAST-based SM schemes [24] perform poorly in realistic wireless conditions.

It is clear that JDM schemes are a suitable solution when SM is used at any cellular access point, as JDM schemes in effect increase the coverage in terms of radius where SM can be supported. Thus, it can be said that JDM schemes can be effectively used to increase the system throughput.

Future Work: In future, more system level analysis of the studied schemes is required. This will give us concrete understanding of these schemes' impact on multi-user throughput. Several others issues that can be studied in conjunction with multi-user MIMO scenario are as follows:

1. Resource allocation and multi-user detection using JDM scenario in distributed MIMO-OFDM systems
   (a) Spatial separation (i.e. SDMA component)
   (b) Sub-carrier allocation (i.e. OFDMA component)
   (c) Antenna selection/allocation

© Muhammad Imadur Rahman, 2007

(d) Resource allocation in heterogeneous scenario

2. If CSI is available, we can incorporate beamforming in the JDM structure for distributed MIMO scenario.

10

Impact of MIMO Co-channel Interference

In the chapter, we study the impact of Co-Channel Interference (CCI) caused by any MIMO scheme on the same or other MIMO schemes. In Section 10.2, we describe the cellular system scenario used for the forthcoming analysis in this chapter. Symbol-by-symbol based linear receivers used in this analysis is explained in Section 10.3. The SINR expressions corresponding to different link combinations and its statistics are presented in Section 10.4 and 10.5 respectively. Section 10.6 presents the probability of error analysis for CCI affected MIMO systems when STBC is used (and not used) as an interference. In Section 10.7, we have presented the BER results when different link combinations are used. The conclusions are drawn in Section 10.8.

10.1 Introduction

In a cellular scenario, the transmission from any BS is heavily dependent on frequency planning of the network. Specific frequency planning parameters relate to certain amount of interference seen at any receiver (i.e. Mobile Station (MS) in Downlink (DL), this interference from neighboring cells, namely Co-Channel Interference (CCI), limits the system performance. In future wireless systems, the number of users requiring high data rate will also be very high. Thus, highly spectral systems are desired, that means, optimum re-use of spectrum is also envisioned. In this context, aggressive spatial re-use of available spectrum in a cellular system will be a necessity in future wireless system

design. So, the network and/or the user equipments will have to be equipped with interference management, avoidance and/or cancellation capabilities. In general, users located at the cell edge can be heavily affected by CCI. When multiple antennas are used for transmission from interfering BSs, the interference scenario is even more complicated. Different Multiple Input Multiple Output (MIMO) schemes are affected in different ways in the presence of CCI, and inversely, different MIMO schemes cause different interference.

Performance of multi-antenna schemes, or MIMO schemes, for OFDMA systems without any interference are well-known. For universal frequency re-use factor based system, CCI, introduced by the same and/or another MIMO schemes at the same sub-channel (or sub-carriers) from neighboring cells, plays an important role in system performance. Recent studies related to effects of CCI on MIMO based cellular systems include the impact on cell capacity [28, 29], impact on any specific MIMO scheme with regard to CCI [31], optimal theoretical signalling techniques [30] etc. Angle diversity based null-steering beamformer is proposed in [32] for CCI suppression when STBC is used in both links.

All the discussions and analysis in current literatures are done considering the fact that both the interfering and desired link uses the same MIMO scheme. To the best of our knowledge, none of the work investigates the impact of interfering MIMO schemes on other MIMO schemes. So, it is an important issue to study the MIMO techniques to be used at a user who is experiencing a CCI-limited situation. In this chapter, we have studied the SINR statistics and BER performances when different combination of MIMO schemes are used at desired and interfering BS transmitters.

We define the term 'logical stream' as the data stream that is transmitted from any transmitter. Thus, a Space-Time Block Code (STBC) transmitter [25] sends one logical stream and multiple physical streams. The number of logical streams is more important than the number of physical streams as interferers [33]. Besides, the number of logical streams has more impact on the desired link than the power of the interferers. Also, the nature (i.e. spatial signature) of logical interfering streams are important in interference cancelation schemes. Using this knowledge, it is found that single stream interferers, such as SIMO, AS or TxBF provide similar impact on any type of desired link. When SIMO, AS or TxBF is used at the desired link, a symbol by symbol processing is usually sufficient. However, if STBC is an interfering link, a symbol by symbol processing becomes inadequate as the STBC signal is correlated over several symbols. If symbol-by-symbol processing is used when STBC is present as an interferer, the 'apparent' logical streams from the STBC interferer is seen to be more than one, thus, the receiver might not cope with the number of available antennas.

In this chapter, we have classified MIMO schemes in terms of their tolerance to CCI and in terms of the severity of the CCI they cause to other MIMO schemes. Based on the current analysis, it is found that STBC is a severe interferer compared to others, and specific attention is needed to counter the interference introduced by STBC interfering link.

10.2 Assumptions and Definitions

10.2.1 Assumptions

Following assumptions are made to conduct this study:

1. Frequency re-use factor of 1 is assumed.
2. We only consider first tier, i.e. one operating cell with six neighboring interfering cell.
3. Interference analysis is only performed for DL in reference cell.
4. Time slot refers to the DL slot when DL frames are transmitted. When DL slots are aligned in both cells, we define it as synchronized case. So, for synchronized FDD system, the amount of interference power is constant during whole DL slot.
5. For synchronized TDD, we can also assume that the amount and the number of interferers are fixed during the whole time-slot, if all the neighboring cells uses DL transmission in the same slot.

10.2.2 Link Definitions

We denote P, Q and R as the number of antennas at the desired BS, the desired MS and the interfering BSs respectively. Following MIMO Techniques are considered:

1. **SIMO:** Multiple Rx antenna combining, we use Maximal Ratio Combining (MRC), as described in Section 5.5.1.1 and Minimum Mean Square Error (MMSE) combining as described in this chapter.
2. **AS:** Multiple Rx antenna combining with antenna selection from multiple Tx antenna,
3. **TxBF:** We have also used the term Transmit Maximum Ratio Combining (TxMRC) for Transmit Beamforming (TxBF) technique. This basically means the same method. This is used from dual Tx antenna as described in [73, Section 11.6]. If the desired BS has the channel information of its own user, then TxMRC technique can be implemented.
4. **STBC:** Alamouti coding at Tx as described in Section 5.5.1.2 and Multiple Rx combining [25, 128],
5. **SM:** Dual stream spatial multiplexing [24]

We always assume that $Q > 1$, except the case of TxBF. In this case, by definition, $Q = 1$[1]. For AS, TxBF and STBC case, we always have $P = 2$ when the scheme is used at desired transmitter and, also $R = 2$ when the scheme is used at interfering transmitter.

Notations: In the following text, we define the 'operating cell' as the cell which contains the desired link as shown in Figure 10.1, and we define 'interfering cell' as the cell from which the interfering signals arrive at the operating cell. We define the term 'Technique1-Technique2',

[1] TxMRC scheme used in this analysis is taken from [73, Section 11.6] which defines a $P \times 1$ system. Here, the CSI of P number of channels are assumed to be known fully at the transmitter.

© Muhammad Imadur Rahman, 2007

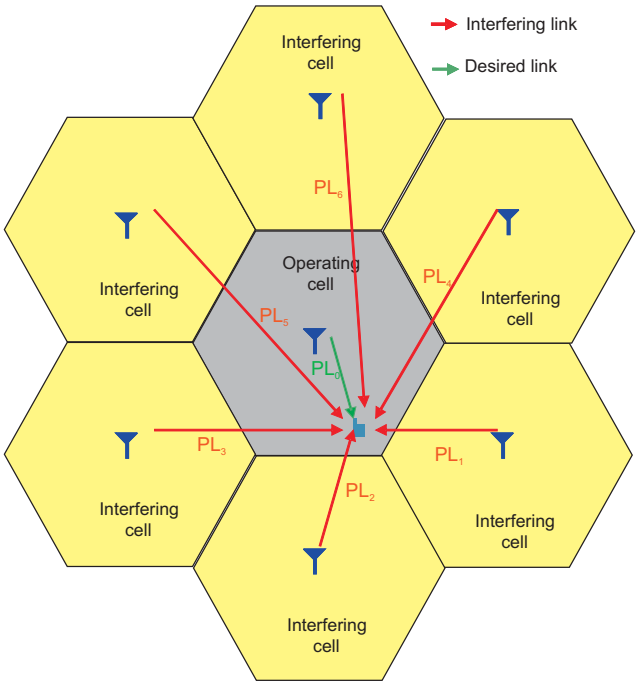

Figure 10.1: Cell Scenario for interference studies

PL_0	136.6632 dB
PL_1	136.9914 dB
PL_2	138.6452 dB
PL_3	145.2387 dB
PL_4	146.1309 dB
PL_5	148.8530 dB
PL_6	149.1105 dB

Table 10.1: An example of pathloss values from different interfering BSs and the desired BS

as 'Technique1' used in the desired link in operating cell (i.e. the green link in Figure 10.1) and 'Technique2' are the interfering links from interfering cells experienced at desired MS (i.e. all red links in Figure 10.1). 'Technique1' and 'Technique2' can take any value from all the considered schemes: SIMO, AS, TxBF, STBC, SM. For example, SIMO-STBC: SIMO in desired link and STBC in interfering links.

10.2.3 Scenario Definition

We consider, one tier of cells for the studies. Figure 10.1 shows us the six interfering BSs around the operating cell. An example of pathloss values of six interfering links together with the desired link is also placed in Table 10.1. It is clear that, when MS is located near the cell edge, signals from 2 to 3 interfering BSs are very strong, while the rest 3 BSs provide weaker interferes. Besides the cellular scenario, we have also considered a case where all the interferers arrive at the desired MS

with similar power compared to the desired BS. For the second tier of the cellular systems, we assume that the amount of interference caused by cells in second tier in frequency reuse factor of 1 scenario is not very significant compared to the cells in first tier.

10.3 Symbol by-Symbol Linear Receivers

Received signal is processed at every OFDM symbol duration. Two types of combining are studied: MRC receiver and MMSE nulling receiver.

1. MRC receiver

2. MMSE nulling receiver

10.3.1 MRC Receiver

For example, we present a simple case of SIMO-SIMO scenario. The received signal can be written as:

$$\mathbf{z} = \mathbf{H}\mathbf{m} + \mathbf{v} \tag{10.1}$$

where the channel matrix is, $\mathbf{H} = \begin{bmatrix} \mathbf{h}_0 & \mathbf{h}_1 & \dots & \mathbf{h}_I \end{bmatrix}$. The channel vector corresponding to desired link, $\mathbf{h}_0 = \sqrt{E_{s,0}} \begin{bmatrix} h_{11} & h_{21} & \dots & h_{Q1} \end{bmatrix}^T$ and the interfering links (i.e. links between i^{th} interfering BSs and the MS), $\mathbf{h}_i = \sqrt{E_{s,i}} \begin{bmatrix} h^i_{11} & h^i_{21} & \dots & h^i_{Q1} \end{bmatrix}^T$ $\forall i \in [1, I]$. I is the number of interferers in the system, in this case, it is 6. The vector containing all transmitted symbols from all BSs is $\mathbf{m} = \begin{bmatrix} m_0 & m_1 & \dots & m_I \end{bmatrix}^T$. The noise vector is $\mathbf{v} = \begin{bmatrix} v[1] & v[2] & \dots & v[Q] \end{bmatrix}^T$.

The MRC operator can be written as:

$$G_{MRC} = (\mathbf{h}_0^H \mathbf{h}_0)^{-1} \mathbf{h}_0^H \tag{10.2}$$

The estimated symbol is:

$$\widetilde{m} = G_{MRC}\mathbf{z} = (\mathbf{h}_0^H \mathbf{h}_0)^{-1} \mathbf{h}_0^H \mathbf{H}\mathbf{m} + (\mathbf{h}_0^H \mathbf{h}_0)^{-1} \mathbf{h}_0^H \mathbf{v} \tag{10.3}$$

Note that the receiver acts on receive signal samples on symbol- by-symbol basis.

10.3.2 MMSE Receiver

The signal model is similar to MRC case, as shown in Eq.(10.1). The MMSE operator is:

$$G_{MMSE} = \mathbf{h}_0^H \mathbf{R}_{\mathbf{zz}}^{-1} \tag{10.4}$$

© Muhammad Imadur Rahman, 2007

where,

$$\begin{aligned}\mathbf{R_{zz}} &= E_{s,0}\mathbf{h}_0\mathbf{h}_0^H + \sum_i E_{s,i}\mathbf{h}_i\mathbf{h}_i^H + N_0\mathbf{I}_Q \\ &= \mathbf{H}\mathbf{H}^H + N_0\mathbf{I}_Q \end{aligned} \tag{10.5}$$

The difference between Eq.(10.2) and Eq.(10.4) is the covariance matrix $\mathbf{R_{zz}}$. Inclusion of $\mathbf{R_{zz}}$ in MMSE operator provides the interference nulling capabilities. The estimated symbol is:

$$\widetilde{m} = \mathbf{h}_0^H\mathbf{R}_{\mathbf{zz}}^{-1}\mathbf{H}\mathbf{m} + \mathbf{h}_0^H\mathbf{R}_{\mathbf{zz}}^{-1}\mathbf{v} \tag{10.6}$$

10.4 SINR Expressions

Based on the two linear receivers that we have described in Section 10.3, we now derive the expressions for SINR for several different link combinations.

10.4.1 SIMO in Desired Link

10.4.1.1 SIMO-SIMO

MRC Receiver: The SINR for MRC receiver can be written as, taken from [73, eq. 11.9]:

$$\gamma_t = \frac{E_{s,0}\|\mathbf{h}_0\|_F^2}{\sum_i E_{s,i}\alpha_i + N_0} \qquad \text{where} \quad \alpha_i = \frac{|\mathbf{h}_0^H\mathbf{h}_i|^2}{\|\mathbf{h}_0\|_F^2} \tag{10.7}$$

This is derived from the system model shown in Section 10.3.

MMSE Receiver: The SINR expression can be written as, following the derivation from [159]:

$$\gamma_t = \frac{det(\mathbf{R_{zz}})}{det(\mathbf{R_{zz}} - E_{s,0}\mathbf{h}_0\mathbf{h}_0^H)} - 1 \tag{10.8}$$

Related to different kind of receivers for SIMO-SIMO systems, we can summarize the system performance and complexity requirement as shown in Table 10.2, taken from [73, Section 11.4.1]. We can make the following observations based on the table:

1. ML requires maximum knowledge and practically impossible to implement in real systems.

2. Though remaining diversity order is less in MMSE receiver, it performs better than MRC because of interference nulling effect.

3. If interference is uniformly distributed in space (i.e. spatially white interference scenario), the diversity order of MMSE will converge to MRC receiver.

Scheme	Remaining diversity order	Noise enhancement loss	Knowledge required
Optimum ML	Q	None	$\mathbf{h}_0$, $\mathbf{h}_i$, $\forall i$
MMSE	$Q - I$	Medium	$\mathbf{R_{zz}}$, $\mathbf{h}_0$
MRC	Q	None	$\mathbf{h}_0$

Table 10.2: Receivers for CCI cancellation in frequency flat channels.

10.4.1.2 SIMO-AS

The SINR expression is very similar to SIMO-SIMO case. In case of SIMO-AS, the interfering channels will be,

$$[\mathbf{h}_{j(i)}]_q = h^{j(i)}_{qx_q} \quad \text{and} \quad x_q = \arg\max_r |h^{j(i)}_{qr}|^2 \tag{10.9}$$

The antenna selection in i^{th} cell is done based on j^{th} user in i^{th} cell, thus, the desired MS will randomly experience a strong or weak interferer.

10.4.1.3 SIMO-STBC

The interference channel is:

$$\mathbf{H}_i = \begin{bmatrix} h^i_{11} & h^i_{21} & \dots & h^i_{Q1} \\ h^i_{12} & h^i_{22} & \dots & h^i_{Q2} \end{bmatrix}^T \tag{10.10}$$

MRC Receiver: The SINR expression for MRC receiver is:

$$\gamma_t = \frac{E_{s,0}\|\mathbf{h}_0\|^2_F}{\sum_i \frac{E_{s,i}}{2}\alpha_i + N_0} \qquad \text{where} \quad \alpha_i = \frac{|\mathbf{h}_0^H \mathbf{H}_i|^2}{\|\mathbf{h}_0\|^2_F} \tag{10.11}$$

MMSE Receiver: For MMSE Receiver in SIMO-STBC case, the SINR expression is similar to SIMO-SIMO, as shown in Eq.(10.8), only that the definition of $\mathbf{R_{zz}}$ is changed due to the change of interfering source,

$$\gamma_t = \frac{det(\mathbf{R_{zz}})}{det(\mathbf{R_{zz}} - E_{s,0}\mathbf{h}_0\mathbf{h}_0^H)} - 1 \tag{10.12}$$

$$\mathbf{R_{zz}} = E_{s,0}\mathbf{h}_0\mathbf{h}_0^H + \sum_i \frac{E_{s,i}}{2}\mathbf{H}_i\mathbf{H}_i^H + N_0\mathbf{I}_Q \tag{10.13}$$

When the interferer is STBC, then the interfering signals over several time slots are correlated. In a symbol-by-symbol based receiver, this transmit signal correlation is not exploited.

© Muhammad Imadur Rahman, 2007

10.4.1.4 SIMO-TxBF

The effective channel from interfering BSs will be:

$$\mathbf{H}_i = \begin{bmatrix} h^i_{11} & h^i_{12} & \dots & h^i_{1R} \\ h^i_{21} & h^i_{22} & \dots & h^i_{2R} \\ \vdots & \vdots & \ddots & \vdots \\ h^i_{Q1} & h^i_{Q2} & \dots & h^i_{QR} \end{bmatrix} \tag{10.14}$$

MRC Receiver:

$$\gamma_t = \frac{E_{s,0}\|\mathbf{h}_0\|^2_F}{\sum_i E_{s,i}\alpha_i + N_0} \tag{10.15}$$

$$\tag{10.16}$$

$$\text{with} \quad \alpha_i = \frac{|\mathbf{h}_0^H \mathbf{H}_i \mathbf{w}^T_{j(i)}|^2}{\|\mathbf{h}_0\|^2_F} \tag{10.17}$$

where $\mathbf{w}_{j(i)}$ is chosen such that:

$$\mathbf{w}_{j(i)} = \frac{\mathbf{h}^H_{j(i)}}{\sqrt{\|\mathbf{h}_{j(i)}\|^2_F}} \tag{10.18}$$

MMSE Receiver:

$$\gamma_t = \frac{det(\mathbf{R_{zz}})}{det(\mathbf{R_{zz}} - E_{s,0}\mathbf{h}_0\mathbf{h}_0^H)} - 1 \tag{10.19}$$

$$\mathbf{R_{zz}} = E_{s,0}\mathbf{h}_0\mathbf{h}_0^H + \sum_i E_{s,i}\mathbf{H}_i\mathbf{w}^T_{j(i)}\mathbf{w}^*_{j(i)}\mathbf{H}_i^H + N_0\mathbf{I}_Q \tag{10.20}$$

10.4.2 AS in the Desired Link

10.4.2.1 AS-SIMO

By using AS at the transmitter, the best channel is selected from the desired BS as shown below:

$$x(q) = \arg\max_p \{|h_{qp}|^2, \forall\, p \in [1, \dots, P]\} \tag{10.21}$$

$$\mathbf{h}_0 = [h_{1x(1)}\ h_{2x(2)}\ \dots\ h_{Qx(Q)}] \tag{10.22}$$

MRC Receiver: Similar to SIMO-SIMO case, we can define the SINR expression using the new $\mathbf{h}_0$ defined in Eq.10.22:

$$\gamma_t = \frac{E_{s,0}\|\mathbf{h}_0\|^2_F}{\sum_i E_{s,i}\alpha_i + N_0} \quad \text{with} \quad \alpha_i = \frac{|\mathbf{h}_0^H \mathbf{h}_i|^2}{\|\mathbf{h}_0\|^2_F} \tag{10.23}$$

MMSE Receiver:

$$\gamma_t = \frac{det(\mathbf{R_{zz}})}{det(\mathbf{R_{zz}} - E_{s,0}\mathbf{h}_0\mathbf{h}_0^H)} - 1 \tag{10.24}$$

$$\mathbf{R_{zz}} = E_{s,0}\mathbf{h}_0\mathbf{h}_0^H + \sum_i E_{s,i}\mathbf{h}_i\mathbf{h}_i^H + N_0\mathbf{I}_Q \tag{10.25}$$

10.4.2.2 AS-TxBF

The channel matrix will be:

$$\mathbf{H}_i = \begin{bmatrix} h_{11}^i & h_{12}^i & \dots & h_{1R}^i \\ h_{21}^i & h_{22}^i & \dots & h_{2R}^i \\ \vdots & \vdots & \ddots & \vdots \\ h_{Q1}^i & h_{Q2}^i & \dots & h_{QR}^i \end{bmatrix} \tag{10.26}$$

MRC Receiver:

$$\gamma_t = \frac{E_{s,0}\|\mathbf{h}_0\|_F^2}{\sum_i E_{s,i}\alpha_i + N_0} \tag{10.27}$$

$$\tag{10.28}$$

$$\text{with} \quad \alpha_i = \frac{|\mathbf{h}_0^H\mathbf{H}_i\mathbf{w}_{j(i)}^T|^2}{\|\mathbf{h}_0\|_F^2} \tag{10.29}$$

MMSE Receiver:

$$\gamma_t = \frac{det(\mathbf{R_{zz}})}{det(\mathbf{R_{zz}} - E_{s,0}\mathbf{h}_0\mathbf{h}_0^H)} - 1 \tag{10.30}$$

$$\mathbf{R_{zz}} = E_{s,0}\mathbf{h}_0\mathbf{h}_0^H + \sum_i E_{s,i}\mathbf{H}_i\mathbf{w}_{j(i)}^T\mathbf{w}_{j(i)}^*\mathbf{H}_i^H + N_0\mathbf{I}_Q \tag{10.31}$$

10.4.2.3 AS-AS

When AS is used at the interfering BSs, the MS does not see any difference compared to SIMO interferers, because the AS in interfering cells are done based on the best channel of another user.

10.4.2.4 AS-STBC

AS-STBC scheme is very similar to SIMO-STBC explained in Section 10.4.1.3. The only difference is the best channel selection in the desired link, as shown in Eq.(10.21).

© Muhammad Imadur Rahman, 2007

10.4.3 TxBF in the Desired Link

10.4.3.1 TxBF-SISO

$\mathbf{w}_0$ applied to transmitted signals from desired cell:

$$\gamma_t = \frac{E_{s,0}\|\mathbf{h}_0\|_F^2}{\sum_i E_{s,i}|h_i|^2 + N_0} \tag{10.32}$$

$\mathbf{w}_0$ is chosen such that:

$$\mathbf{w}_0 = \frac{\mathbf{h}_0^H}{\sqrt{\|\mathbf{h}_0\|_F^2}} \tag{10.33}$$

10.4.3.2 TxBF-TxBF

$\mathbf{w}_0$ applied to transmitted signals from desired cell and $\mathbf{w}_{j(i)}$ applied to interfering BS:

$$\gamma_t = \frac{E_{s,0}\|\mathbf{h}_0\|_F^2}{\sum_i E_{s,i}\|\mathbf{w}_{j(i)}\mathbf{h}_i\|_F^2 + N_0} \tag{10.34}$$

$\mathbf{w}_0$ is chosen such that:

$$\mathbf{w}_0 = \frac{\mathbf{h}_0^H}{\sqrt{\|\mathbf{h}_0\|_F^2}} \tag{10.35}$$

$\mathbf{w}_{j(i)}$ is chosen in the ith cell for j^{th} user such that:

$$\mathbf{w}_{j(i)} = \frac{\mathbf{h}_{j(i)}^H}{\sqrt{\|\mathbf{h}_{j(i)}\|_F^2}} \tag{10.36}$$

10.4.3.3 TxBF-STBC

$$\gamma_t = \frac{E_{s,0}\|\mathbf{h}_0\|_F^2}{\sum_i \frac{E_{s,i}}{2}\left(\mathbf{h}_i^T\mathbf{h}_i^*\right) + N_0} \tag{10.37}$$

10.4.3.4 TxBF-AS

$$\gamma_t = \frac{E_{s,0}\|\mathbf{h}_0\|_F^2}{\sum_i E_{s,i}|h_i|^2 + N_0} \tag{10.38}$$

10.4.4 STBC in the Desired Link

10.4.4.1 STBC-STBC

MRC Receiver:

$$\gamma_t = \frac{\frac{E_{s,0}}{2}\|\mathbf{H}_{0,eff}\|_F^2}{\sum_i \frac{E_{s,i}}{2}\alpha_i + N_0} \quad \text{with} \quad \alpha_i = \frac{\|\mathbf{H}_{0,eff}^H\mathbf{H}_{i,eff}\|_F^2}{\|\mathbf{H}_{0,eff}\|_F^2} \tag{10.39}$$

The equivalent channel matrix can be written as:

$$\mathbf{H}_{x,eff}, \qquad x\forall\{0,i\}$$
$$= \begin{bmatrix} h^x_{11} & h^x_{21} & \dots & h^x_{Q1} & h^{x*}_{12} & h^{x*}_{22} & \dots & h^{x*}_{Q2} \\ h^x_{12} & h^x_{22} & \dots & h^x_{Q2} & -h^{x*}_{11} & -h^{x*}_{21} & \dots & -h^{x*}_{Q1} \end{bmatrix}^T \tag{10.40}$$

$$\mathbf{H}_{x,eff} = \begin{bmatrix} h^x_{11} & h^x_{12} \\ h^x_{21} & h^x_{22} \\ \vdots & \vdots \\ h^x_{Q1} & h^x_{Q2} \\ h^{x*}_{12} & -h^{x*}_{11} \\ h^{x*}_{22} & -h^{x*}_{21} \\ \vdots & \vdots \\ h^{x*}_{Q2} & -h^{x*}_{Q1} \end{bmatrix} \tag{10.41}$$

MMSE Receiver:

$$\gamma_t = \frac{det(\mathbf{R_{zz}})}{det(\mathbf{R_{zz}} - \frac{E_{s,0}}{2}\mathbf{H}_{0,eff}\mathbf{H}^H_{0,eff})} - 1 \tag{10.42}$$

$$\mathbf{R_{zz}} = \frac{E_{s,0}}{2}\mathbf{H}_{0,eff}\mathbf{H}^H_{0,eff} + \sum_i \frac{E_{s,i}}{2}\mathbf{H}_{i,eff}\mathbf{H}^H_{i,eff} + N_0\mathbf{I}_{2Q} \tag{10.43}$$

10.4.4.2 STBC-SIMO

MRC Receiver:

$$\gamma_t = \frac{\frac{E_{s,0}}{2}\|\mathbf{H}_{0,eff}\|^2_F}{\sum_i E_{s,i}\alpha_i + N_0} \quad \text{with} \quad \alpha_i = \frac{|\mathbf{H}^H_{0,eff}\mathbf{h}_{i,eff}|^2}{\|\mathbf{H}_{0,eff}\|^2_F} \tag{10.44}$$

The channel matrices are:

$$\mathbf{h}_{i,eff} = \begin{bmatrix} \mathbf{h}_i \\ \mathbf{h}^*_i \end{bmatrix}; \quad \mathbf{h}_i = \begin{bmatrix} h^i_1 & h^i_2 & \dots & h^i_Q \end{bmatrix}^T \tag{10.45}$$

MMSE Receiver: the SINR expression is similar to Eq. (10.42), only the $\mathbf{R_{zz}}$ expression is changed, as seen below:

$$\gamma_t = \frac{det(\mathbf{R_{zz}})}{det(\mathbf{R_{zz}} - \frac{E_{s,0}}{2}\mathbf{H}_{0,eff}\mathbf{H}^H_{0,eff})} - 1 \tag{10.46}$$

$$\mathbf{R_{zz}} = \frac{E_{s,0}}{2}\mathbf{H}_{0,eff}\mathbf{H}^H_{0,eff} + \sum_i E_{s,i}\mathbf{h}_{i,eff}\mathbf{h}^H_{i,eff} + N_0\mathbf{I}_{2Q} \tag{10.47}$$

10.4.4.3 STBC-AS

When AS is used in interfering BSs while STBC is used in desired BS, h^i_q in Eq. (10.45) will be chosen based on AS selection procedure in intf. BS.

© Muhammad Imadur Rahman, 2007

10.4.4.4 STBC-TxBF

The equivalent channel will be:

$$\mathbf{h}_{i,eff} = \begin{bmatrix} \mathbf{h}_i \\ \mathbf{h}_i^* \end{bmatrix} \quad \text{with} \quad \mathbf{h}_i = \begin{bmatrix} w_{j(i)}^1 h_1^i & w_{j(i)}^2 h_2^i & \dots & w_{j(i)}^Q h_Q^i \end{bmatrix}^T \tag{10.48}$$

MRC Receiver:

$$\gamma_t = \frac{\frac{E_{s,0}}{2}\|\mathbf{H}_{0,eff}\|_F^2}{\sum_i E_{s,i}\alpha_i + N_0} \quad \text{with} \quad \alpha_i = \frac{|\mathbf{H}_{0,eff}^H \mathbf{h}_{i,eff}|^2}{\|\mathbf{H}_{0,eff}\|_F^2} \tag{10.49}$$

MMSE Receiver:

$$\gamma_t = \frac{det(\mathbf{R_{zz}})}{det(\mathbf{R_{zz}} - \frac{E_{s,0}}{2}\mathbf{H}_{0,eff}\mathbf{H}_{0,eff}^H)} - 1 \tag{10.50}$$

$$\mathbf{R_{zz}} = \frac{E_{s,0}}{2}\mathbf{H}_{0,eff}\mathbf{H}_{0,eff}^H + \sum_i E_{s,i}\mathbf{h}_{i,eff}\mathbf{h}_{i,eff}^H + N_0\mathbf{I}_{2Q} \tag{10.51}$$

10.5 SINR Analysis

We use a semi-analytical method to determine the SINR statistics. The process is as follows:

1. We randomly locate a user at the cell edge.
2. Calculate the pathloss from all 7 BSs.
3. Generate channel coefficients for all 7 links.
4. Use the SINR expression as in Section 10.4 to calculate instantaneous SINR.

The main parameters used in the semi-analytical evaluation are explained in Table 10.5.

cell radius, R_c	750m
BS transmit power	43dBm
User location	randomly between $0.9R_c$ and R_c

Table 10.3: Parameters used in Semi-Analytical evaluations of SINR expressions

10.5.1 Cellular Scenario

Figures 10.2 - 10.5 show the *pdf*s of SINR with all different combinations of desired and interfering links. Tables 10.4 - 10.7 give us the average SINR values corresponding to the schemes. As it is seen from the results: MRC provides much lower average SINR compared to MMSE receiver. When desired link uses SIMO and processes the received signal in symbol-by-symbol basis, then STBC provides multiple interfering source from a single interfering BS. AS and TxMRC in the interfering

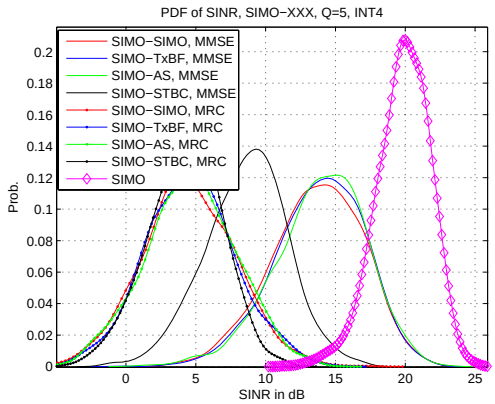

Figure 10.2: *pdf* of SINR with SIMO as the desired link in cellular scenario

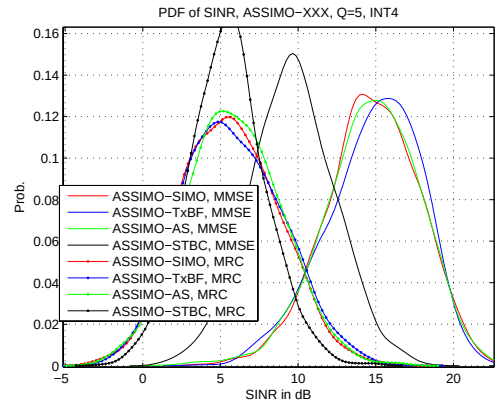

Figure 10.3: *pdf* of SINR with AS as the desired link in cellular scenario

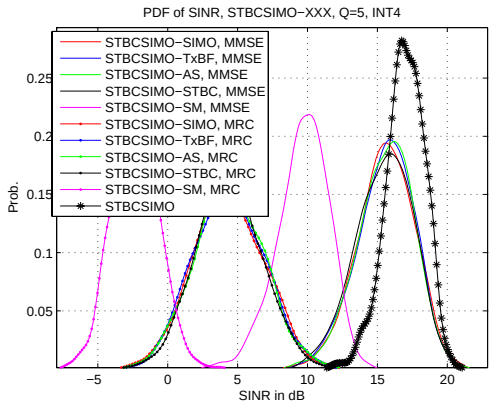

Figure 10.4: *pdf* of SINR with STBC as the desired link in cellular scenario

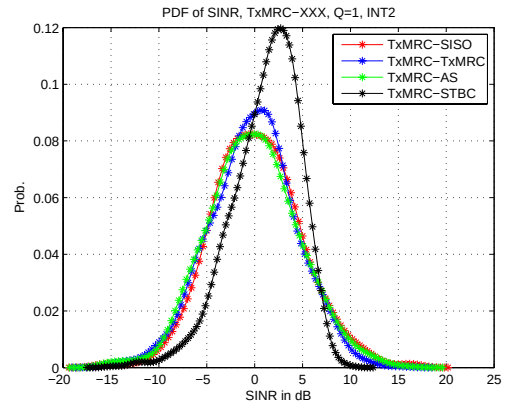

Figure 10.5: *pdf* of SINR with TxMRC as the desired link in cellular scenario

link affect the desired link in a similar fashion to interfering SIMO link. This is true for both MRC and MMSE receiver.

When AS is used in the desired link, the average SINR is improved compared to SIMO in the desired link, i.e Between SIMO-XXX and ASSIMO-XXX[2], there is a gain on approx. 1dB in ASSIMO-XXX. This is because of the array gain obtained via AS.

It is worth noting the case of TxMRC in the desired link. We have used TxMRC as our transmit beamforming technique. This means, we have multiple antennas at desired BS and a single antenna at desired MS. Obviously, MS has no capabilities to suppress the interfering signals from other BSs, so the average SINR for all interfering cases are very low. We need to study more advanced beamforming technique for this case, e.g. Transmit Matched Filtering can be a reasonable scheme to investigate for further understanding.

[2]SIMO-XXX and ASSIMO-XXX mean, SIMO and **ASSIMO!** (**ASSIMO!**) in the desired link respectively and any other scheme in the interfering links.

© Muhammad Imadur Rahman, 2007

SIMO-XXX, $I = 4, Q = 5$		
	Mean SINR in dB	
Link	MRC	MMSE
SIMO	19.8433	
SIMO-SIMO	4.4974	13.6794
SIMO-TxMRC	4.5982	13.8468
SIMO-AS	4.6593	13.9255
SIMO-STBC	4.2435	8.6058

Table 10.4: Mean SINR in dB with SIMO as the desired link in cellular scenario

ASSIMO-XXX, $I = 4, Q = 5$		
	Mean SINR in dB	
Link	MRC	MMSE
ASSIMO-SIMO	5.6215	14.7806
ASSIMO-TxMRC	5.7813	14.8947
ASSIMO-AS	5.8043	14.7453
ASSIMO-STBC	5.4070	9.6112

Table 10.5: Mean SINR in dB with AS as the desired link in cellular scenario

STBC-XXX, $I = 4, Q = 5$		
	Mean SINR in dB	
Link	MRC	MMSE
STBC-SIMO	4.3462	15.5925
STBC-TxMRC	4.3675	15.5865
STBC-AS	4.4181	15.5898
STBC-STBC	4.3687	15.4787
STBC-SM	-2.3015	11.6800

Table 10.6: Mean SINR in dB with STBC as the desired link in cellular scenario

TxMRC-XXX, $I = 2, Q = 1$	
	Mean SINR in dB
Link	MRC
TxMRC-SISO	0.2266
TxMRC-TxMRC	-0.1910
TxMRC-AS	-0.1497
TxMRC-STBC	1.1463

Table 10.7: Mean SINR in dB with TxMRC as the desired link in cellular scenario

10.5.2 Equal Power Scenario

For the purpose of testing, we have considered the case when all the interferes arrive at the MS with equal power. The results are very similar to cellular scenario, except that the average SINRs in equal power scenario is smaller compared to corresponding cases in cellular scenario. This confirms that the interference power is also an important factor in system performance in interference limited systems like the one we are considering.

Figures 10.6 - 10.9 and Tables 10.8 - 10.11 provide the *pdf* of SINRs and mean SINR respectively, for all the combinations in equal power scenario. As in the case of cellular scenario, when the interfering link bears STBC, the average SINR performance is quite bad.

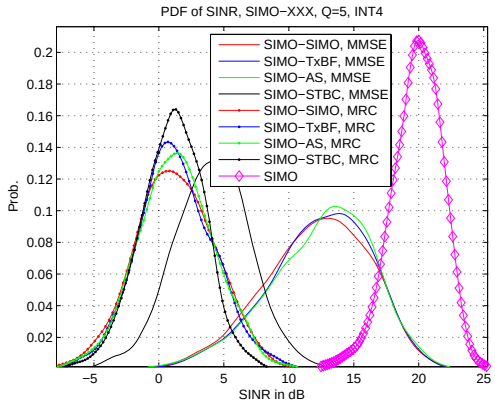

Figure 10.6: *pdf* of SINR with SIMO as the desired link in equal power scenario

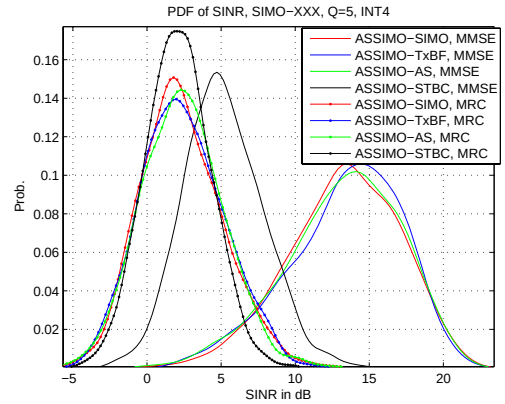

Figure 10.7: *pdf* of SINR with AS as the desired link in equal power scenario

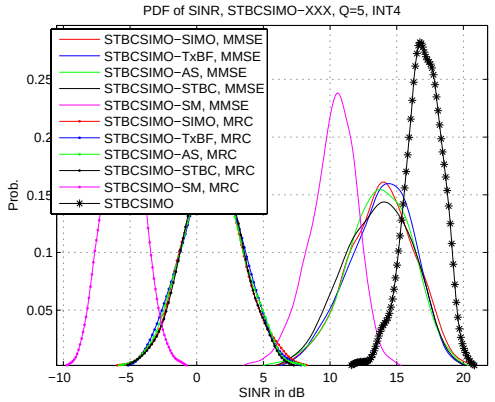

Figure 10.8: *pdf* of SINR with STBC as the desired link in equal power scenario

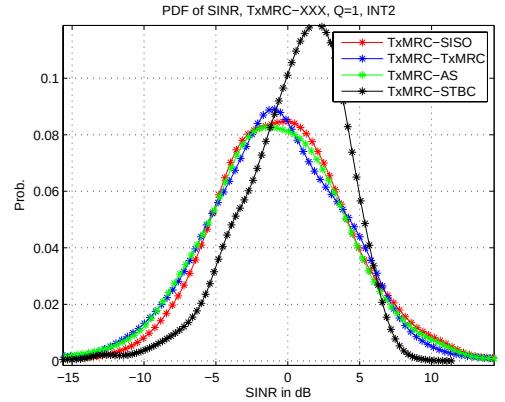

Figure 10.9: *pdf* of SINR with TxMRC as the desired link in equal power scenario

SIMO-XXX, $I = 4, Q = 5$		
	Mean SINR in dB	
Link	MRC	MMSE
SIMO	19.8433	-
SIMO-SIMO	1.2670	12.1580
SIMO-TxMRC	1.3124	12.3692
SIMO-AS	1.3335	12.4550
SIMO-STBC	1.0356	4.0912

Table 10.8: Mean SINR in dB with SIMO as the desired link in equal power scenario

ASSIMO-XXX, $I = 4, Q = 5$		
	Mean SINR in dB	
Link	MRC	MMSE
ASSIMO-SIMO	2.2670	13.2792
ASSIMO-TxMRC	2.4030	13.4038
ASSIMO-AS	2.4048	13.2471
ASSIMO-STBC	2.0957	5.1520

Table 10.9: Mean SINR in dB with AS as the desired link in equal power scenario

STBC-XXX, $I = 4, Q = 5$		
	Mean SINR in dB	
Link	MRC	MMSE
STBC	16.9878	-
STBC-SIMO	1.2080	13.8182
STBC-TxMRC	1.1834	13.7822
STBC-AS	1.1913	13.6754
STBC-STBC	1.1735	12.5502
STBC-SM	-5.4749	10.1919

Table 10.10: Mean SINR in dB with STBC as the desired link in equal power scenario

TxMRC-XXX, $I = 2, Q = 1$	
	Mean SINR in dB
Link	MRC
TxMRC-SISO	-0.3572
TxMRC-TxMRC	-0.8587
TxMRC-AS	-0.7689
TxMRC-STBC	0.4260

Table 10.11: Mean SINR in dB with TxMRC as the desired link in equal power scenario

10.6 Probability of Error

10.6.1 When Interferer is not STBC

The following assumptions are taken for this section:

1. STBC is not used as an interferer: consideration below does not hold for STBC, because the covariance matrix of the symbols is rank deficient.

2. Number of receive antennas must be equal to or higher than number of receive logical streams

The received signals can be written as:

$$\mathbf{z} = \mathbf{H}\mathbf{m} + \mathbf{v}; \text{ with } \mathbf{H} = \begin{bmatrix} \mathbf{h}_0 & \dots & \mathbf{h}_I \end{bmatrix} \tag{10.52}$$

Here, $\mathbf{h}_u$ = channel for u^{th} user, for TxMRC and AS, the user channel is composite channel, and user of interest is user 0.

Multi-user linear MMSE receiver operator can be shown as:

$$\begin{aligned} \mathbf{G}_{MMSE} &= \mathbf{R}_{\mathbf{mm}}\mathbf{H}^H \left[\mathbf{H}\mathbf{R}_{\mathbf{mm}}\mathbf{H}^H + \mathbf{R}_{\mathbf{vv}}\right]^{-1} && (10.53) \\ &= \left[\mathbf{R}_{\mathbf{mm}}^{-1} + \mathbf{H}^H\mathbf{R}_{\mathbf{vv}}^{-1}\mathbf{H}\right]^{-1}\mathbf{H}^H\mathbf{R}_{\mathbf{vv}}^{-1} && (10.54) \end{aligned}$$

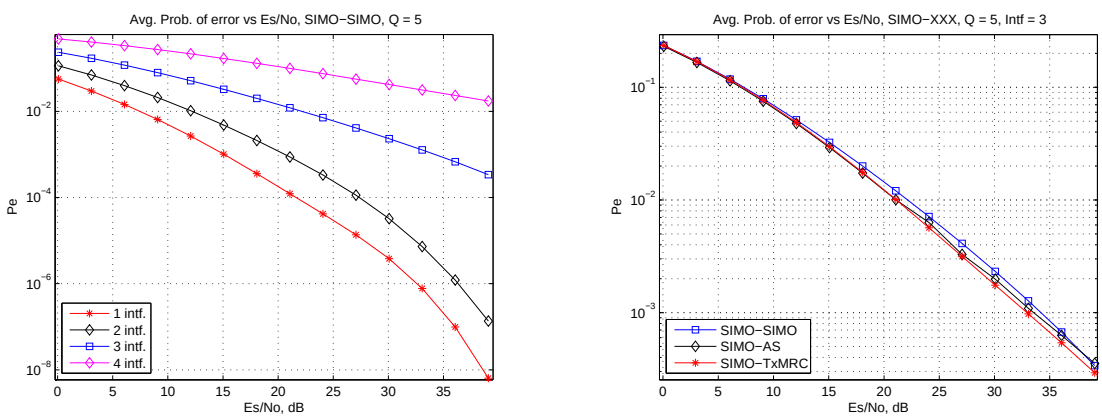

(a) SIMO-SIMO

(b) SIMO-XXX with 3 interferes

Figure 10.10: Probability of error comparison for SIMO at desired link and other schemes (except STBC) at interfering link. In both cases, 5 antennas are assumed at the receiver.

The second line in previous equation is obtained using matrix inversion lemma. The receiver we have been considering corresponds to the first line of $\mathbf{G}_{MMSE}$. We can determine the P_e for ZF, which is the same as MMSE at high SNR.

For $\mathbf{R}_{\mathbf{vv}} = N_0\mathbf{I}$,

$$\mathbf{G}_{MMSE} = \left[\mathbf{R}_{\mathbf{mm}}N_0 + \mathbf{H}^H\mathbf{H}\right]^{-1}\mathbf{H}^H \tag{10.55}$$

© Muhammad Imadur Rahman, 2007

When $N_0 \to 0$,

$$\mathbf{G}_{MMSE} = \left[\mathbf{H}^H\mathbf{H}\right]^{-1}\mathbf{H}^H = \mathbf{G}_{ZF} \tag{10.56}$$

For ZF, the Mean Squared Error (MSE) is, $N_0\left(\left[\mathbf{H}^H\mathbf{H}\right]^{-1}\right)_{1,1}$. The Probability of error, P_e is

$$P_e = \alpha Q\left(\beta\sqrt{\frac{E_{s,0}}{MSE}}\right) \tag{10.57}$$

where α and β depend on the input constellation.

Figures 10.10(a) and 10.10(b) presents the average bit error probability when SIMO is used at the desired link and other schemes except STBC is used at the interfering link. As seen from SINR statistics in Section 10.5, the single stream MIMO interferes, such as SIMO, AS or TxBF provides similar kind of interferences. Note that these results are valid of uncoded systems only.

10.6.2 When Interferer is STBC

The P_e presented in previous section are valid when STBC is not used in the interfering link. Due to the reason that the transmitted symbol from interfering link are correlated for successive symbol period (i.e. covariance matrix of transmitted symbols from interfering links are rank-deficient), we have analyzed using decomposition of real and imaginary parts of interfering signals.

Using eigen decomposition of $\mathbf{R_{mm}}$, We define $\mathbf{R_{mm}} = \mathbf{U\Lambda U}^H$.

Both $\mathbf{R_{mm}}$ and $\mathbf{U}$ are block diagonal. $\mathbf{H}, \mathbf{U}, \mathbf{R_{mm}}$ assume decomposition in real and imaginary part of the data.

MSE can be written as:

$$MSE = N_0\left(\mathbf{U}\left[\mathbf{U}^H\mathbf{H}^H\mathbf{HU}\right]^{-1}\mathbf{U}^H\right)_{1,1} \tag{10.58}$$

$$= N_0\left(\left[\mathbf{UU}^H\mathbf{H}^H\mathbf{HUU}^H\right]^{-1}\right)_{1,1} \tag{10.59}$$

This MSE expression can be used now to find out P_e as it is shown in Eq.(10.57). Then, the BER curves similar to Figures 10.10(a) and 10.10(b) can be drawn for the case, when STBC is used as an interferer.

10.7 BER Evaluations via Numerical Simulations

10.7.1 Simulation Parameters

Following system parameters are used for simulations, as in Table 10.12:

cell radius, R_c	2 km
BS transmit power	43dBm
User location	randomly between $0.9R_c$ and R_c
Number of sub-carriers	128
System bandwidth	1.25 MHz
Sampling frequency	1.429 MHz
Sample time	700 ns
Sub-carrier spacing	11.161 kHz
Useful symbol time	89.6 μs
Guard time	11.2 μs
OFDMA symbol time	100.8 μs
User speed	150 kmph
Frame duration	8×100.8 μs = 800.64 μs
Channel coding	half-rate convolutional coding

Table 10.12: Simulation parameters used in Simulations

The received power levels of both cellular and equal power scenario are shown in Table 10.13. In cellular scenario, the transmit power from all BSs are kept the same and denoted as P_{tx}. The values of P_{tx} in simulations are between 20dBm to 50dBm. The pathloss values, PL_0 up to PL_6 are taken as shown in Table 10.1.

	Equal power	Cellular
$E_{s,0}/N_0$	-10dB to 20dB	$(P_{tx} - PL_0)/N_0$
$E_{s,1}/N_0$	$E_{s,0}/N_0$	$(P_{tx} - PL_1)/N_0$
$E_{s,2}/N_0$	$E_{s,0}/N_0$	$(P_{tx} - PL_2)/N_0$
$E_{s,3}/N_0$	$E_{s,0}/N_0$	$(P_{tx} - PL_3)/N_0$
$E_{s,4}/N_0$	$E_{s,0}/N_0$	$(P_{tx} - PL_4)/N_0$
$E_{s,5}/N_0$	$E_{s,0}/N_0$	$(P_{tx} - PL_5)/N_0$
$E_{s,6}/N_0$	$E_{s,0}/N_0$	$(P_{tx} - PL_6)/N_0$

Table 10.13: Power levels in Simulations

As for the current simulations, we have used a time-invariant channel for MMSE processing, this is advantageous to the estimation of $\mathbf{R_{zz}}$ matrix. In this way, the estimation of $\mathbf{R_{zz}}$ is almost equal to the ideal (i.e. calculated) value. It is worth noting here that in cellular scenario, we have 2 interferers (out of a total of 6 interferers in first tier) who are very close in signal strength compared to the desired signal. In Figures 10.11 - 10.14, when '1 int' is used in the legend, it means that the strongest among all the interfering BSs are used in the simulations. The same is applied for others number of interferers in the simulations.

© Muhammad Imadur Rahman, 2007

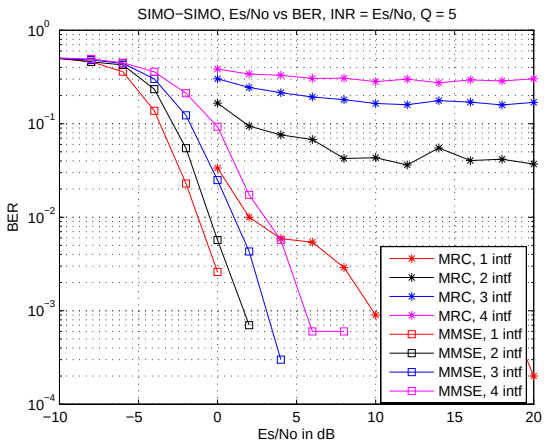

Figure 10.11: BER vs SNR with SIMO-SIMO combination and symbol-by-symbol based receiver in equal power scenario

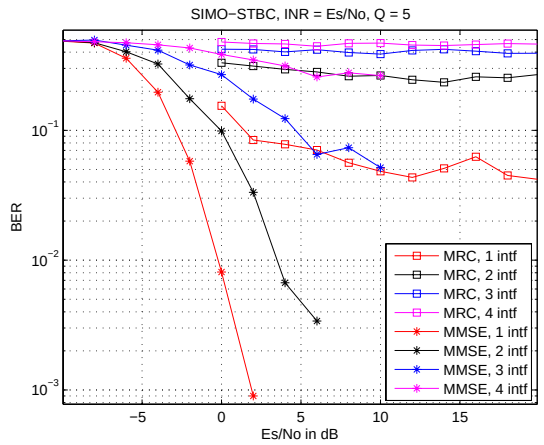

Figure 10.12: BER vs SNR with SIMO-STBC combination and symbol-by-symbol based receiver in equal power scenario

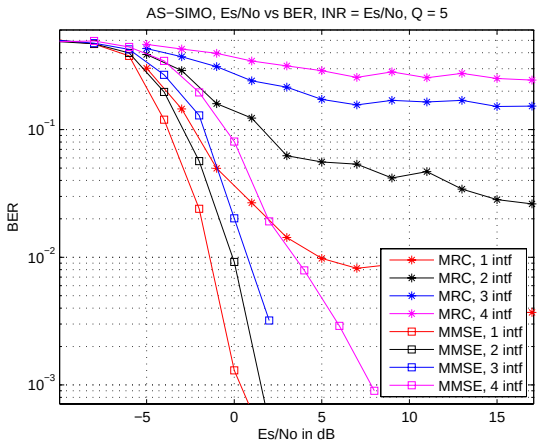

Figure 10.13: BER vs SNR with AS-SIMO combination and symbol-by-symbol based receiver in equal power scenario

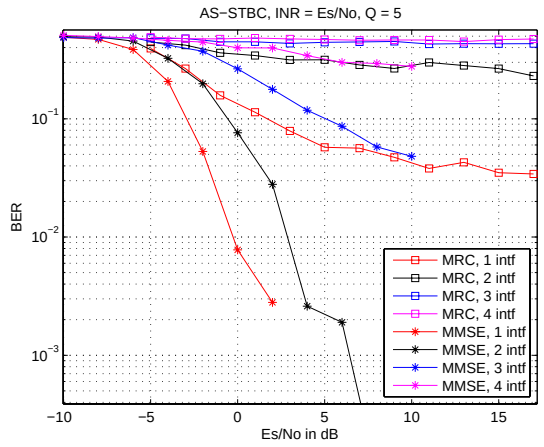

Figure 10.14: BER vs SNR with AS-STBC combination and symbol-by-symbol based receiver in equal power scenario

10.7.2 Equal Power Scenario

Figures 10.11 and 10.12 provide us the BER vs SNR curve for SIMO-SIMO and SIMO-STBC cases respectively, when symbol-by-symbol processing is used at the receiver. Similarly, Figures 10.13 and 10.14 show us the corresponding BERs when AS is used as the desired link. All these results are simulated using 5 antennas at the desired MS.

10.7.2.1 SIMO-XXX Case

Looking at Figure 10.11, MRC performs very unsatisfactorily as expected, specially when the number of interferers are increased. Four of SIMO interferers mean four interfering streams, thus, the desired MS is able to resolve the interferers and detect the desired signal when MMSE receiver is used. Coming to the case of SIMO-STBC in Figure 10.12, as seen previously, MRC performs very

bad for high number of interferers. MMSE receiver with 2 interferers (i.e. 4 streams) performs quire reasonably. This is logical as two STBC interferers mean the desired MS has 4 streams to null and one stream to detect. Beyond this, the receiver cannot resolve the interferers, as it is seen that, when more than 2 STBC interferers are present, the BER is quite high even at high SNR.

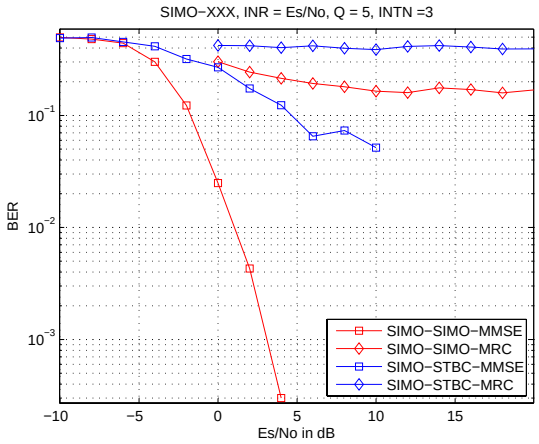

Figure 10.15: BER vs SNR with SIMO-XXX combination, Q=5, I=3, and symbol-by-symbol based receiver in equal power scenario

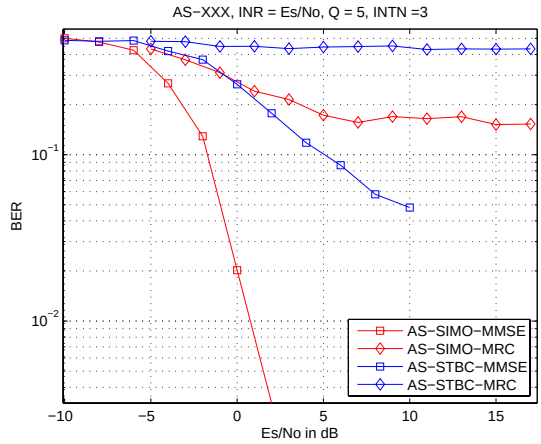

Figure 10.16: BER vs SNR with AS-XXX combination, Q=5, I=3, and symbol-by-symbol based receiver in equal power scenario

10.7.2.2 AS-XXX Case

For AS-SIMO case as shown in Figure 10.13, MRC performs very bad for higher number of interfering signals as seen in SIMO-XXX case (i.e. Figure 10.11). Compared to SIMO-XXX schemes, AS-XXX schemes obtain 2-order transmit diversity. Similar to SIMO-SIMO case, 5 receive antennas can resolve 4 SIMO interferers in AS-SIMO system when MMSE receiver is used. For AS-STBC case as in Figure 10.14, up to 2 STBC interferers, the MMSE receiver performs very well. There is a huge performance loss when one more STBC interferer is added, then 5 receive antennas are overloaded with 7 streams. Once again, STBC is more detrimental as an interferer compared to SIMO when symbol-by-symbol processing is used.

10.7.2.3 Comparison XXX-SIMO and XXX-STBC Cases

For better understanding of a particular scenario, when $Q = 5$ and $I = 3$, we have plotted the corresponding BER plots in Figures 10.15 and 10.16, derived from Figures 10.11-10.12 and Figures 10.13-10.14 respectively. In line with the *pdf*s of SINR before, STBC is much more detrimental to BER as an interferer compared to SIMO. It is expected that SIMO-AS and SIMO-TxMRC should follow same BER pattern as SIMO-SIMO. Similarly, as seen in Figure 10.16, AS-STBC impacts BER performance more than AS-SIMO case. As seen in SINR *pdf*s, AS-AS and AS-TxMRC should follow BER curves of AS-SIMO case.

© Muhammad Imadur Rahman, 2007

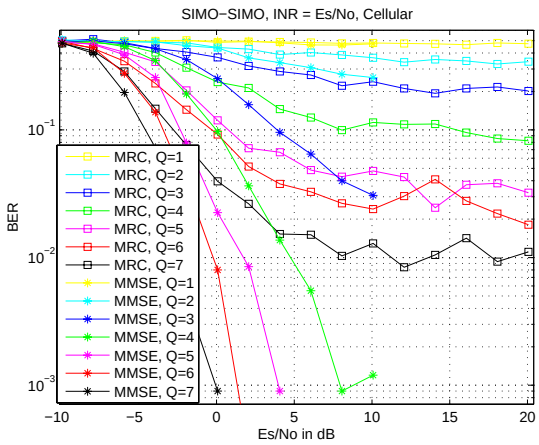

Figure 10.17: BER vs SNR with SIMO-SIMO combination and symbol-by-symbol based receiver in cellular scenario

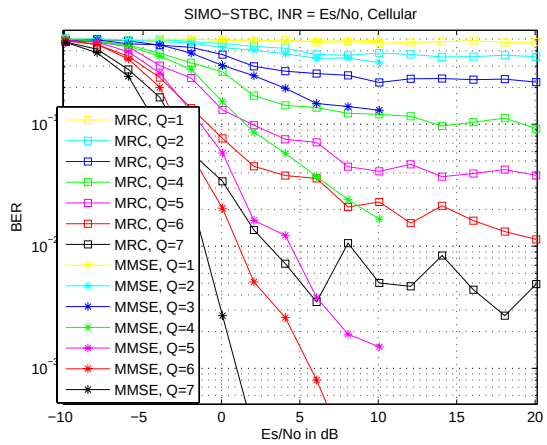

Figure 10.18: BER vs SNR with SIMO-STBC combination and symbol-by-symbol based receiver in cellular scenario

10.7.3 Cellular Scenario

It is worth noting here that in cellular scenario, we have 2 interferers (out of a total of 6 interferers in first tier) who are very close in signal strength compared to the desired signal (please refer to Table 10.1).

In this section, we present the BER results for different combinations of the systems when SIMO and AS are used in the desired link. According to Figure 10.17, we observe that MRC receiver obtains a BER of 10^{-2} only when there are 7 receive antennas at the MS. The interference nulling is not done in MRC, thus the BER floor is seen at high SNR even for the case of 7 receive antennas at MS. As for the MMSE receiver, the BER results are quite good with 4 receive antennas. This means that when 3 of the interferers are nulled, the BER performance is already quite good.

Same pattern of performance is also expected for AS-XXX cases.

10.8 Chapter Summary

The impact of cellular CCI on different multi-antenna schemes in terms of system capacity is well-studied in literature. In a real cellular system, existence of a number of multi-antenna schemes in neighboring cells means that different multi-antenna schemes will experience CCI from the same or other multi-antenna schemes. In this chapter, we have studied the impact of different MIMO schemes on the same or other MIMO schemes for cell-edge users in terms of SINR pdf and BER. Depending on receiver scheme, number of logical streams are more important than number of physical streams as interferers. In this sense, SIMO, AS and TxMRC are of similar type in terms of interference. So following groups have similar BER and SINR performances:

1. SIMO-SIMO, SIMO-AS, SIMO-TxMRC

2. AS-SIMO, AS-AS, AS-TxMRC

When STBC is an interferer, then a symbol-by-symbol processing receiver experiences multiple interfering streams, because then a single STBC interferer becomes an SM interferer. This makes the receiver unable to nullify the interfering signals. In that scenario, a more intelligent solution for interference cancelation needs to be found. In this case, we have transmit symbol correlations in interfering signals in consecutive symbol durations. Thus, a multiple symbol receive processing is required, which would exploit the transmit symbol correlation from the interfering source. When STBC is in the desired link, then regardless of the interference, 2-symbol processing is always done, thus, this concern is removed.

Thus we classify the MIMO schemes based on interference to other MIMO scheme as:

Case-1	1. SIMO 2. AS 3. TxMRC	1. Impacts similarly in BER performance 2. Symbol-by-symbol receive processing is sufficient
Case-2	STBC	Multiple symbol receive processing is required.

Table 10.14: Classification of MIMO schemes based on its interfering impact

To the best of our knowledge, none of the previous work investigates the impact of interfering MIMO schemes on other MIMO schemes. To be specific, none of the solutions handle the case when STBC (i.e. single logical stream, but multiple physical stream with correlated interfering signals across multiple-symbol durations) is present as the interferer together with any single logical stream desired link (i.e. SIMO, AS or TxBF). Thus, this issue is an interesting problem to solve, which is handled in the next chapter.

© Muhammad Imadur Rahman, 2007

11

MIMO Systems at Cell Edge: Robust Receiver Design

Chapter 10 describes our analysis on the impact of MIMO co-channel interference. Our conclusion is that special attention is needed for certain kind of MIMO interferers. In this chapter, we design a robust multiple-symbol based linear MMSE receiver for countering CCI caused by different MIMO interferers.

Our proposed multiple symbol processing is described in Section 11.2. The impact of the proposed receiver technique on the system level is also discussed in this section. We have designed a suitable interference detection block which can be used to reduce the system complexity. We have presented our numerical evaluations in Section 11.3. We have analyzed the systems in terms of Signal to Interference and Noise Ratio (SINR) and Bit Error Rate (BER) is Sections 11.3.2 and 11.3.4 respectively. The technique is studied in time-variant channel condition in Section 11.3.6. We describe our proposed fractional frequency reuse method to be used in collaboration with the multiple-symbol based robust receiver for the cell-edge users in Section 11.4. Finally, the conclusions are drawn in Section 11.5.

11.1 Introduction

In the previous chapter, we have analyzed the impact of Co-Channel Interference (CCI) when caused by the same or another MIMO scheme. Using a number of well-known multi-antenna algo-

rithms, we have found that some MIMO modes are more detrimental in terms of CCI compared to others. Our conclusion is that effective number of logical streams is very important in terms of interference management and/or avoidance mechanisms. Using this knowledge and understanding obtained in the previous chapter, we design an interference management mechanism, which takes advantage of both the interference cancelation and avoidance.

State-of-the-Art

MRC and MMSE nulling based receivers are proposed in [73, Section 11.4] when SIMO is used in both interfering and desired link. In these receivers, symbol-by-symbol interference cancellation is done, so when STBC is present as an interferer, the symbol-by-symbol based receiver fails as seen in our analysis in [160]. When STBC is used as the desired link and as the interferers, then MMSE based processing can be used for interference suppression together with ML decoding scheme as shown in [31]. The nulling method in [31] effectively suppresses the STBC interferers while providing the desired user the diversity benefit from STBC link. Angle diversity based null-steering beamformer is proposed in [32] for CCI suppression when STBC is used in both links.

Our Contribution

In this chapter, we propose an interference cancellation receiver robust to different types of MIMO interferers at cell edge for the downlink of cellular Orthogonal Frequency Division Multiple Access (OFDMA) systems. The receiver systematically performs a linear MMSE multiple-symbol processing. The number of symbols processed is equal to the least common multiple of the different STBC code lengths used. Thus, this receiver becomes robust to any kind of single logical stream interferer. A module detecting the presence of a STBC interferer is proposed. The multiple-symbol processing is switched to single symbol processing if no STBC interferer is detected.

Based on this linear interference cancelation scheme, We propose a frequency sharing for the downlink of a cellular OFDMA at cell edge. This frequency sharing among the main interfering BSs ensures that the number of receive antennas for each MS is larger or equal to the number of desired and interfering links. The proposed method uses the knowledge of the number of available receive antennas at the MS and ensures that the interference order is always kept under control so that the desired MS is not severely affected by CCI.

11.2 Multiple Symbol Processing

11.2.1 Scenario and Assumptions

We consider a cellular scenario as depicted in Figure 10.1. In our analysis, we make the following assumptions:

1. Frequency re-use factor of 1 (i.e. universal re-use factor) is assumed.
2. We only consider first tier, i.e. one operating cell with six neighboring interfering cells as shown in Figure 10.1.

3. STBC transmission starts at same time for all BSs.

11.2.2 Linear MMSE receiver: Multiple symbol processing

We will consider the case where $P \times Q$ system with either single-stream transmission or STBC scheme at the transmitter [78, 25] and receive diversity at the receiver is used. The interferer has R number of transmit antennas. So depending on the type of interferers, a R-symbol processing scheme can be performed at the MS. The proposed treatment can be generalized to the case where the interferers use different STBC lengths. In the following, $(.)^*$, $(.)^T$ and $(.)^H$ denote conjugate, transpose and conjugate transpose operations respectively.

11.2.2.1 Case-1: STBC is not an interferer

For notational convenience, we restrict ourselves to Alamouti's STBC algorithm [25]. For two-symbol processing case, we can write the received base-band signal at the desired MS as:

$$\mathbf{z} = \sqrt{E_0}\mathbf{H}_0\mathbf{m}_0 + \sum_{i=1}^{I}\sqrt{E_i}\mathbf{H}_i\mathbf{m}_i + \mathbf{v} \tag{11.1}$$

- When the user of interest in SIMO, AS or TxBF, $\mathbf{H}_0 = \begin{bmatrix} \mathbf{h}_0(t) & 0 \\ 0 & \mathbf{h}_0(t+1) \end{bmatrix}$: $\mathbf{h}_0(t)$ is the $Q \times 1$ channel vector at time t of the user of interest. Q is the number of receive antenna. In the case of TxBF, $\mathbf{h}_0(t)$ incorporates the transmit weights.
- $\mathbf{H}_i$ is the channel matrix of ith interferer with $i \in [1, \ldots, 6]$ and has a similar definition as $\mathbf{H}_0$; i.e. $\mathbf{H}_i = \begin{bmatrix} \mathbf{h}_i(t) & 0 \\ 0 & \mathbf{h}_i(t+1) \end{bmatrix}$.
- When the user of interest is STBC, $\mathbf{H}_0 = \frac{1}{\sqrt{2}}\begin{bmatrix} \mathbf{h}_{01}(t) & \mathbf{h}_{02}(t) \\ -\mathbf{h}_{02}^*(t+1) & \mathbf{h}_{01}^*(t+1) \end{bmatrix}$: $\mathbf{h}_{01}(t)$ is the channel vector from the first transmit antenna, $\mathbf{h}_{02}(t)$ is the channel vector from the second transmit antenna.
- $\mathbf{m}_0 = \begin{bmatrix} X_0(t) \\ X_0(t+1) \end{bmatrix}$ and $\mathbf{m}_i = \begin{bmatrix} X_i(t) \\ X_i(t+1) \end{bmatrix}$ contain the transmitted symbols at time t and $t+1$ for the user of interest and the interferers. The variance of the constellation symbols is assumed equal to σ_x^2.
- $\mathbf{v}$ is an additive complex circular white Gaussian noise: $\mathbf{v} \sim \mathcal{CN}(0, N_0\mathbf{I}_Q)$.
- E_i is the transmit power from any transmitting BS i.

We propose to use a linear MMSE multiple-symbol processing at MS receiver. This will provide robustness against STBC interferers. The linear MMSE estimate of the symbols for two consecutive durations can be written as:

$$\widehat{\mathbf{m}}_0 = \sqrt{E_0}\sigma_x^2\mathbf{H}_0^H\mathbf{R}_{\mathbf{zz}}^{-1}\mathbf{z} \tag{11.2}$$

© Muhammad Imadur Rahman, 2007

$\mathbf{R_{zz}}$ is the correlation matrix of the received signal. It can be expressed as:

$$\mathbf{R_{zz}} = \sigma_x^2 E_0 \mathbf{H}_0 \mathbf{H}_0^H + \sigma_x^2 \sum_{i=1}^{i} E_i \mathbf{H}_i \mathbf{H}_i^H + N_0 \mathbf{I}_{2Q} \tag{11.3}$$

11.2.2.2 Case-2: STBC is an interferer but is not the user of interest

We assume that interferer i is STBC and that the receiver knows when an STBC code starts. Here we assume that it starts at time t, so we can write that; $\mathbf{H}_i = \begin{bmatrix} \widetilde{\mathbf{H}}_i(t) & \mathbf{0} \\ \mathbf{0} & \widetilde{\mathbf{H}}_i(t+1) \end{bmatrix}$, where $\widetilde{\mathbf{H}}_i(t)$ and $\widetilde{\mathbf{H}}_i(t+1)$ is the $Q \times 2$ channel matrices from interferer i to the MS of interest; and $\mathbf{m}_i = \begin{bmatrix} X_1 & X_2 & -X_2^* & X_1^* \end{bmatrix}^T$. It can be verified that $\mathcal{E}\{\mathbf{m}_i \mathbf{m}_i^H\}$ and then $\mathcal{E}\{\mathbf{z}\mathbf{z}^H\} \neq 0$, i.e. $\mathbf{z}$ is not circular and the complex signal representation is not equivalent to the real one. So, we consider real and imaginary part of $\mathbf{z}$:

$$\mathbf{z}^R = \begin{bmatrix} \Re[\mathbf{z}] \\ \Im[\mathbf{z}] \end{bmatrix} = \sum_{i=0}^{I} \underbrace{\begin{bmatrix} \Re[\mathbf{H}_i] & -\Im[\mathbf{H}_i] \\ \Im[\mathbf{H}_i] & \Re[\mathbf{H}_i] \end{bmatrix}}_{\mathbf{H}_i^R} \underbrace{\begin{bmatrix} \Re[\mathbf{m}_i] \\ \Im[\mathbf{m}_i] \end{bmatrix}}_{\mathbf{m}_i^R} + \underbrace{\begin{bmatrix} \Re[\mathbf{v}] \\ \Im[\mathbf{v}] \end{bmatrix}}_{\mathbf{v}^R} = \sum_{i=0}^{I} \mathbf{H}_i^R \mathbf{m}_i^R + \mathbf{v}^R \tag{11.4}$$

with, $\Re(.)$ and $\Im(.)$ are the real and imaginary parts of $(.)$ respectively. The linear MMSE estimate of the input symbols is:

$$\widehat{\mathbf{m}}_0^R = \sqrt{E_0} \sigma_x^2 \mathbf{H}_0^{R^T} \mathbf{R}_{\mathbf{z}^R \mathbf{z}^R}^{-1} \mathbf{z}^R \tag{11.5}$$

with:

$$\mathbf{R}_{\mathbf{z}^R \mathbf{z}^R} = \mathcal{E}\{\mathbf{z}^R \mathbf{z}^{R^T}\} = \sigma_x^2 E_0 \mathbf{H}_0^R \mathbf{H}_0^{R^T} + \sum_{i=1}^{i} \frac{E_i}{2} \mathbf{H}_i^R \mathcal{E}\{\mathbf{m}_i^R \mathbf{m}_i^{R^T}\} \mathbf{H}_i^{R^T} + \frac{1}{2} N_0 \mathbf{I}_{2Q} \tag{11.6}$$

Here, we can write that:

$$\mathcal{E}\{\mathbf{m}_i^R \mathbf{m}_i^{R^T}\} = \begin{bmatrix} \mathcal{E}\{\Re[\mathbf{m}_i]\Re[\mathbf{m}_i]^T\} & \mathbf{0} \\ \mathbf{0} & \mathcal{E}\{\Im[\mathbf{m}_i]\Im[\mathbf{m}_i]^T\} \end{bmatrix} \tag{11.7}$$

$$\mathcal{E}\{\Re[\mathbf{m}_i]\Re[\mathbf{m}_i]^T\} = \frac{1}{2}\sigma_x^2 \begin{bmatrix} 1 & 0 & 0 & 1 \\ 0 & 1 & -1 & 0 \\ 0 & -1 & 1 & 0 \\ 1 & 0 & 0 & 1 \end{bmatrix} \tag{11.8}$$

$$\mathcal{E}\{\Im[\mathbf{m}_i]\Im[\mathbf{m}_i]^T\} = \frac{1}{2}\sigma_x^2 \begin{bmatrix} 1 & 0 & 0 & -1 \\ 0 & 1 & 1 & 0 \\ 0 & 1 & 1 & 0 \\ -1 & 0 & 0 & 1 \end{bmatrix} \tag{11.9}$$

$\mathcal{E}\{\mathbf{m}_i^R \mathbf{m}_i^{R^T}\}$ is rank deficient: the rank is 4 and so is $\mathcal{E}\{\mathbf{z}^R \mathbf{z}^{R^T}\}$ (if the null space of $\mathcal{E}\{\mathbf{m}_i^R \mathbf{m}_i^{R^T}\}$ is included in the row space of $\mathbf{H}_i^R$). This observation confirms the fact that STBC interferer is

equivalent to a single interferer in case of multiple-symbol processing. So, for multiple-symbol receiver, the receiver now needs to estimate the correlation of received signals across multiple-symbol durations and use this knowledge (i.e. the covariance matrix of received signals across multiple symbols) to null out the interferers. This receiver is robust in a sense that the system performs satisfactorily whatever the nature of the interferers.

11.2.3 Impact on System Level and Implementation Related Issues

11.2.3.1 Detection of STBC interferers

At start, a multiple symbol processing is performed. If no STBC interferers are detected and the user of interest is not STBC, then a switching is done to single symbol processing. Indeed, single symbol processing requires less received samples for a given estimation performance of the covariance matrix $\mathbf{R}_{\mathbf{z}^R\mathbf{z}^R}$ compared with a multiple symbol processing. So, it is also less sensitive to channel variations. Let us consider the Alamouti STBC case; t indicates the start of the code. When an STBC interferer is present, then the correlation of received signals $\mathbf{z}^R(t)$ and $\mathbf{z}^R(t+1)$ is non zero, whereas it is zero when no STBC interferers are present. Note that $\mathcal{E}\{\mathbf{z}^R(t)\mathbf{z}^{R^T}(t+1)\}$ is the off diagonal block element of $\mathbf{R}_{\mathbf{z}^R\mathbf{z}^R}$, so the STBC detection module does not require additional complexity.

In practice, the off-diagonal element of the estimated covariance matrix is not strictly equal to 0 when no STBC interferers are present. So detection thresholds have to be carefully designed. These thresholds may depend on several items, such as

1. the number of interferers,
2. their receive power,
3. the number of STBC interferers vs number of non STBC interferers.

We denote $\mathcal{E}\{\Re[\mathbf{m}_i]\Re[\mathbf{m}_i]^T\} = \mathbf{A}$ and $\mathcal{E}\{\Im[\mathbf{m}_i]\Im[\mathbf{m}_i]^T\} = \mathbf{B}$, thus, $\mathbf{A}$ and $\mathbf{B}$ take values as shown in Eq.(11.8) and Eq.(11.9) respectively when the concerned interferer is an STBC interferer. For a SIMO interferer, $\mathbf{A} = \mathbf{B} = \mathbf{I}_{2Q}$. We denote, the receive power from any STBC interfering source as $\frac{E_i}{2}$, the power is split equally between two transmitting antennas, when Alamouti scheme is used [25]. The contribution to the $\mathbf{R}_{\mathbf{z}^R\mathbf{z}^R}$ from any STBC interfering source can be written as:

$$\mathbf{R}^i_{\mathbf{z}^R\mathbf{z}^R} = \frac{E_i}{2}\begin{bmatrix} \Re(\mathbf{H}_i) & -\Im(\mathbf{H}_i) \\ \Im(\mathbf{H}_i) & \Re(\mathbf{H}_i) \end{bmatrix}\begin{bmatrix} \mathbf{A} & \mathbf{0}_{2R} \\ \mathbf{0}_{2R} & \mathbf{B} \end{bmatrix}\begin{bmatrix} \Re(\mathbf{H}_i)^T & \Im(\mathbf{H}_i)^T \\ -\Im(\mathbf{H}_i)^T & \Re(\mathbf{H}_i)^T \end{bmatrix} \tag{11.10}$$

$$= \frac{E_i}{2}\begin{bmatrix} \Re(\mathbf{H}_i)\mathbf{A} & -\Im(\mathbf{H}_i)\mathbf{B} \\ \Im(\mathbf{H}_i)\mathbf{A} & \Re(\mathbf{H}_i)\mathbf{B} \end{bmatrix}\begin{bmatrix} \Re(\mathbf{H}_i)^T & \Im(\mathbf{H}_i)^T \\ -\Im(\mathbf{H}_i)^T & \Re(\mathbf{H}_i)^T \end{bmatrix} \tag{11.11}$$

$$= \frac{E_i}{2}\begin{bmatrix} \Re(\mathbf{H}_i)\mathbf{A}\Re(\mathbf{H}_i)^T + \Im(\mathbf{H}_i)\mathbf{B}\Im(\mathbf{H}_i)^T & \Re(\mathbf{H}_i)\mathbf{A}\Im(\mathbf{H}_i)^T - \Im(\mathbf{H}_i)\mathbf{B}\Re(\mathbf{H}_i)^T \\ \Im(\mathbf{H}_i)\mathbf{A}\Re(\mathbf{H}_i)^T - \Re(\mathbf{H}_i)\mathbf{B}\Im(\mathbf{H}_i)^T & \Im(\mathbf{H}_i)\mathbf{A}\Im(\mathbf{H}_i)^T + \Re(\mathbf{H}_i)\mathbf{B}\Re(\mathbf{H}_i)^T \end{bmatrix} \tag{11.12}$$

The off-diagonal components of Eq. 11.12 can be analyzed further to differentiate between a SIMO and STBC interferer. The size of the off-diagonal components is of $2Q \times 2Q$. We can write

© Muhammad Imadur Rahman, 2007

that

$$\begin{aligned}
\Re(\mathbf{H}_i)\mathbf{A}\Im(\mathbf{H}_i)^T &= \frac{1}{2}\sigma_x^2 \begin{bmatrix} \Re(\mathbf{H}_i(t)) & \mathbf{0}_{Q\times R} \\ \mathbf{0}_{Q\times R} & \Re(\mathbf{H}_i(t+1)) \end{bmatrix} \begin{bmatrix} \mathbf{I}_R & \mathbf{X} \\ \mathbf{Y} & \mathbf{I}_R \end{bmatrix} \begin{bmatrix} \Im(\mathbf{H}_i(t)^T) & \mathbf{0}_{R\times Q} \\ \mathbf{0}_{R\times Q} & \Im(\mathbf{H}_i(t+1)^T) \end{bmatrix} \\
&= \frac{1}{2}\sigma_x^2 \begin{bmatrix} \Re(\mathbf{H}_i(t)) & \Re(\mathbf{H}_i(t))\mathbf{X} \\ \Re(\mathbf{H}_i(t+1))\mathbf{Y} & \Re(\mathbf{H}_i(t+1)) \end{bmatrix} \begin{bmatrix} \Im(\mathbf{H}_i(t)^T) & \mathbf{0}_{R\times Q} \\ \mathbf{0}_{R\times Q} & \Im(\mathbf{H}_i(t+1)^T) \end{bmatrix} \\
&= \frac{1}{2}\sigma_x^2 \begin{bmatrix} \Re(\mathbf{H}_i(t))\Im(\mathbf{H}_i(t)^T) & \Re(\mathbf{H}_i(t))\mathbf{X}\Im(\mathbf{H}_i(t+1)^T) \\ \Re(\mathbf{H}_i(t+1))\mathbf{Y}\Im(\mathbf{H}_i(t)^T) & \Re(\mathbf{H}_i(t+1))\Im(\mathbf{H}_i(t+1)^T) \end{bmatrix} \qquad (11.13)
\end{aligned}$$

where $\mathbf{X} = \begin{bmatrix} 0 & 1 \\ -1 & 0 \end{bmatrix}$ and $\mathbf{Y} = \begin{bmatrix} 0 & -1 \\ 1 & 0 \end{bmatrix}$ when the interferer is STBC. Similarly,

$$\Im(\mathbf{H}_i)\mathbf{A}\Re(\mathbf{H}_i)^T = \frac{1}{2}\sigma_x^2 \begin{bmatrix} \Im(\mathbf{H}_i(t))\Re(\mathbf{H}_i(t)^T) & \Im(\mathbf{H}_i(t))\mathbf{X}\Re(\mathbf{H}_i(t+1)^T) \\ \Im(\mathbf{H}_i(t+1))\mathbf{Y}\Re(\mathbf{H}_i(t)^T) & \Im(\mathbf{H}_i(t+1))\Re(\mathbf{H}_i(t+1)^T) \end{bmatrix} \qquad (11.14)$$

$$\Im(\mathbf{H}_i)\mathbf{B}\Re(\mathbf{H}_i)^T = \frac{1}{2}\sigma_x^2 \begin{bmatrix} \Im(\mathbf{H}_i(t))\Re(\mathbf{H}_i(t)^T) & \Im(\mathbf{H}_i(t))\mathbf{U}\Re(\mathbf{H}_i(t+1)^T) \\ \Im(\mathbf{H}_i(t+1))\mathbf{V}\Re(\mathbf{H}_i(t)^T) & \Im(\mathbf{H}_i(t+1))\Re(\mathbf{H}_i(t+1)^T) \end{bmatrix} \qquad (11.15)$$

$$\Re(\mathbf{H}_i)\mathbf{B}\Im(\mathbf{H}_i)^T = \frac{1}{2}\sigma_x^2 \begin{bmatrix} \Re(\mathbf{H}_i(t))\Im(\mathbf{H}_i(t)^T) & \Re(\mathbf{H}_i(t))\mathbf{U}\Im(\mathbf{H}_i(t+1)^T) \\ \Re(\mathbf{H}_i(t+1))\mathbf{V}\Im(\mathbf{H}_i(t)^T) & \Re(\mathbf{H}_i(t+1))\Im(\mathbf{H}_i(t+1)^T) \end{bmatrix} \qquad (11.16)$$

where $\mathbf{U} = \begin{bmatrix} 0 & -1 \\ 1 & 0 \end{bmatrix}$ and $\mathbf{V} = \begin{bmatrix} 0 & 1 \\ -1 & 0 \end{bmatrix}$ when the interferer is STBC.

We denote the matrix $\mathbf{D}$ of size $2Q\times 2Q$ and is either upper or lower off-diagonal component of $\mathbf{R}^i_{\mathbf{z}^R\mathbf{z}^R}$ matrix. From Eq. 11.12, taking the upper off-diagonal matrix of $\mathbf{R}^i_{\mathbf{z}^R\mathbf{z}^R}$, $\mathbf{D}$ can be written as:

$$\mathbf{D} = \Re(\mathbf{H}_i)\mathbf{A}\Im(\mathbf{H}_i)^T - \Im(\mathbf{H}_i)\mathbf{B}\Re(\mathbf{H}_i)^T \qquad (11.17)$$

Defining upper and lower off-diagonal matrices of $\mathbf{D}$ as $[\mathbf{D}]^U$ and $[\mathbf{D}]^L$. We can now write that:

$$[\mathbf{D}]^U = \Re(\mathbf{H}_i(t))\mathbf{X}\Im(\mathbf{H}_i(t+1)^T) - \Im(\mathbf{H}_i(t))\mathbf{U}\Re(\mathbf{H}_i(t+1)^T) \qquad (11.18)$$

$$[\mathbf{D}]^L = \Re(\mathbf{H}_i(t+1))\mathbf{Y}\Im(\mathbf{H}_i(t)^T) - \Im(\mathbf{H}_i(t+1))\mathbf{V}\Re(\mathbf{H}_i(t)^T \qquad (11.19)$$

Similarly, taking the lower off-diagonal component of $\mathbf{R}^i_{\mathbf{z}^R\mathbf{z}^R}$, it can be defined that:

$$\mathbf{E} = \Im(\mathbf{H}_i)\mathbf{A}\Re(\mathbf{H}_i)^T - \Re(\mathbf{H}_i)\mathbf{B}\Im(\mathbf{H}_i)^T \qquad (11.20)$$

$$[\mathbf{E}]^U = \Im(\mathbf{H}_i(t))\mathbf{X}\Re(\mathbf{H}_i(t+1)^T) - \Re(\mathbf{H}_i(t))\mathbf{U}\Im(\mathbf{H}_i(t+1)^T) \qquad (11.21)$$

$$[\mathbf{E}]^L = \Im(\mathbf{H}_i(t+1))\mathbf{Y}\Re(\mathbf{H}_i(t)^T) - \Re(\mathbf{H}_i(t+1))\mathbf{V}\Im(\mathbf{H}_i(t)^T) \qquad (11.22)$$

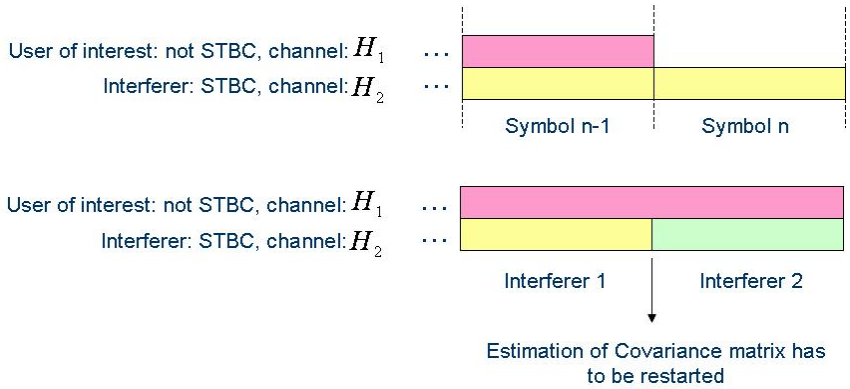

Figure 11.1: Estimation of covariance matrix

Now, we can exploit the fact that when the interfering source is a SIMO source, then, $\mathbf{X} = \mathbf{Y} = \mathbf{U} = \mathbf{V} = \mathbf{0}_R$. So, $Q \times Q$ off-diagonal matrices of matrix $\mathbf{D}$ and $\mathbf{E}$ are $\mathbf{0}_Q$, i.e. $[\mathbf{D}]^U = [\mathbf{D}]^L = [\mathbf{E}]^U = [\mathbf{E}]^L = \mathbf{0}_Q$ when the interferer is of SIMO type and non-zero when the interferer is of STBC type.

Using this analysis, we can determine a threshold when we assume that only one strong interferer is present in the system. We assume that received energy from the interferer is known, i.e. E_i is known to the receiving MS. Note that E_i indicates the received signal power from i^{th} interferer, thus the pathloss is included in this parameter. Since the E_i is known, we can easily write that the threshold values for the components in $[\mathbf{D}]^U$, $[\mathbf{D}]^L$, $[\mathbf{E}]^U$ and $[\mathbf{E}]^L$ will be $\|\frac{E_i+N_0}{2}\|$.

Assuming only received interference power is known, the threshold is only is in average sense. What we need to do is: check the values on off-diagonal component of $\mathbf{D}$ and $\mathbf{E}$ for sufficient number of samples, then we can verify with the threshold of $\|\frac{E_i+N_0}{2}\|$ provided that the channel gain is 0dB. In that way, the channel impact is taken into account. For instantaneous cases, we cannot find any threshold unless we use the known values of the channel coefficients of interfering source.

The above threshold is only valid for a simple scenario with only one interferer. It should be fairly simple to extend this model to more complex scenario. Once the system is in single-symbol processing mode, the receiver can periodically perform the STBC interference detection as mentioned above. If a presence of STBC interference is detected in later stages, the receiver will switch to 2-symbol processing; otherwise the single-symbol processing mode will be maintained. This will ensure that the system performance will be maintained above some satisfactory level.

11.2.3.2 Covariance Matrix Estimation: allocation of different time slot length

A SIMO, AS or TxBF user of interest might be allocated an odd number of symbols. If an STBC user is interfering, then 2 symbol processing has to be modified. An example is shown in Figure 11.1, where the interferer is STBC and the user of interest is not STBC. We assume here that the channel is time invariant. The received signal at time t and $t+1$ for the user of interest is (we do not include

© Muhammad Imadur Rahman, 2007

the noise here):

$$\mathbf{z}_0^R = \sqrt{E_0} \begin{bmatrix} \mathbf{h}_0^R & 0 \\ 0 & 0 \end{bmatrix} \begin{bmatrix} X_0^R \\ 0 \end{bmatrix} \tag{11.23}$$

and for the interferer:

$$\mathbf{z}_1^R = \sqrt{E_1} \mathbf{H}_1^R \mathbf{m}_1^R \tag{11.24}$$

For brevity, we mention only one interferer. It should be fairly simple to extend to multiple interferers. The theoretical covariance matrix is:

$$\begin{aligned} \mathbf{R}_{\mathbf{z}^R\mathbf{z}^R} &= \mathbf{R}_{\mathbf{z}_0^R\mathbf{z}_0^R} + \mathbf{R}_{\mathbf{z}_1^R\mathbf{z}_1^R} \\ &= \sigma_{m_1}^2 E_0 \begin{bmatrix} \mathbf{h}_0^R \mathbf{h}_0^{R^T} & 0 \\ 0 & 0 \end{bmatrix} + \mathbf{h}_1^R \mathbf{R}_{m_1^R m_1^R} \mathbf{h}_1^{R^T} + \frac{1}{2} N_0 \mathbf{I}_Q \end{aligned} \tag{11.25}$$

We assume that the estimation of the covariance matrix is done based on the received signal until time $t-1$. This covariance matrix is equal to:

$$\begin{aligned} \mathbf{R}_{\mathbf{z}^R\mathbf{z}^R}^{(t-1)} &= \mathbf{R}_{\mathbf{z}_0^R\mathbf{z}_0^R} + \mathbf{R}_{\mathbf{z}_1^R\mathbf{z}_1^R} \\ &= \sigma_{m_1}^2 E_0 \begin{bmatrix} \mathbf{h}_0^R \mathbf{h}_0^{R^T} & 0 \\ 0 & \mathbf{h}_0^R \mathbf{h}_0^{R^T} \end{bmatrix} + \mathbf{h}_1^R \mathbf{R}_{m_1^R m_1^R} \mathbf{h}_1^{R^T} + \frac{1}{2} N_0 \mathbf{I}_{2Q} \end{aligned} \tag{11.26}$$

Based on $\widehat{\mathbf{h}}_0^R$, the estimate of $\mathbf{h}_0^R$ and $\widehat{\mathbf{R}}_{\mathbf{z}^R\mathbf{z}^R}^{(t-1)}$, the estimate of $\mathbf{R}_{\mathbf{z}^R\mathbf{z}^R}^{(t-1)}$, we can compute:

$$\widehat{\mathbf{R}}_{\mathbf{z}^R\mathbf{z}^R} = \widehat{\mathbf{R}}_{\mathbf{z}^R\mathbf{z}^R}^{(t-1)} - \sigma_x^2 E_0 \begin{bmatrix} 0 & 0 \\ 0 & \widehat{\mathbf{h}}_0^R \widehat{\mathbf{h}}_0^{R^T} \end{bmatrix} \tag{11.27}$$

With the above estimate, now we can detect the desired transmitted symbol,

$$\widehat{\mathbf{m}}_0^R = \begin{bmatrix} \widehat{\mathbf{h}}_0^{R^T} & 0 \end{bmatrix} \widehat{\mathbf{R}}_{\mathbf{z}^R\mathbf{z}^R}^{-1} \mathbf{z}^R \tag{11.28}$$

To avoid this processing, it is recommended to schedule users across even number of slots.

11.2.3.3 Co-existence of Diversity and AMC channels in WiMAX systems

As defined in WiMAX standard, AMC channels consist of neighboring sub-carriers, while diversity channel consists of interleaved sub-carriers. It is possible to use the CSI (or CQI) feedback from AMC sub-channels, thus MIMO mode can also be selected for these sub-channels. Diversity channels will be used for non-CSI assisted MIMO schemes, as it is not possible to obtain instantaneous CSI or CQI of these channels. It is worth mentioning here that it is possible to have one CSI or CQI value for diversity channels. In this case, it represents the average channel quality over the whole bandwidth.

Interference from the same or another MIMO scheme brings us the question whether AMC and diversity channels of neighboring cells can collide in the same band or not. According to our

Table 11.1: Simulation parameters

cell radius, R_c	2 km
BS transmit power	43dBm
User location	randomly between $0.9 * R_c$ and R_c
Number of sub-carriers	128
System bandwidth	1.25 MHz
Sampling frequency	1.429 MHz
Sample time	700 ns
Sub-carrier spacing	11.161 kHz
Useful symbol time	89.6 μs
Guard time	11.2 μs
OFDMA symbol time	100.8 μs
User speed	150 kmph
Frame duration	8×100.8 μs = 800.64 μs
Channel coding	half-rate convolutional coding
Modulation	QPSK

multiple-symbol receiver design, the robustness provided by the receiver will ensure that diversity channels and AMC channels can co-exist in same frequency across neighboring cells when the concerned interference is of STBC type. When multiple-stream interference is present, then we need to adopt other solutions for interference management. The multiple-symbol receiver design ensures better protection only against STBC interference. In AMC channels, multiple streams transmissions can occur, without correlation over 2 consecutive symbols. In this case, the fractional frequency reuse method must be used as proposed Section 11.4, because, the receiver alone cannot guarantee sufficient protection if the number of receive antennas is too small.

11.3 Numerical Evaluations

11.3.1 Simulations Parameters

The simulation parameters are shown in Table 11.1.

11.3.2 SINR statistics

11.3.2.1 SINR definition

We define the SINR as follows:

$$\mathcal{SINR} = \frac{\mathcal{E}\{|X_0(t)|^2\}}{[\mathbf{R}_{\tilde{\mathbf{m}}_0\tilde{\mathbf{m}}_0}]_{t,t}} - 1 = \frac{\mathcal{E}\{|X_0(t+1)|^2\}}{[\mathbf{R}_{\tilde{\mathbf{m}}_0\tilde{\mathbf{m}}_0}]_{t+1,t+1}} - 1 \tag{11.29}$$

.

We define, the estimation error after MMSE interference cancelation as, $\tilde{\mathbf{m}}_0 = \widehat{\mathbf{m}}_0 - \mathbf{m}_0$. So,

© Muhammad Imadur Rahman, 2007

$\mathbf{R}_{\tilde{\mathbf{m}}_0\tilde{\mathbf{m}}_0}$ in Eq. (11.29) can be written as:

$$\begin{aligned}\mathbf{R}_{\tilde{\mathbf{m}}_0\tilde{\mathbf{m}}_0} &= \mathcal{E}\{\tilde{\mathbf{m}}_0\tilde{\mathbf{m}}_0^H\} \\ &= \mathcal{E}\{(\widehat{\mathbf{m}}_0 - \mathbf{m}_0)(\widehat{\mathbf{m}}_0 - \mathbf{m}_0)^H\} \\ &= \mathbf{R}_{\mathbf{m}_0\mathbf{m}_0} - \mathbf{R}_{\mathbf{m}_0\mathbf{z}}\mathbf{R}_{\mathbf{zz}}^{-1}\mathbf{R}_{\mathbf{z}\mathbf{m}_0} \qquad (11.30)\end{aligned}$$

where

$$\mathbf{R}_{\mathbf{m}_0\mathbf{m}_0} = \mathcal{E}\{\mathbf{m}_0\mathbf{m}_0^H\} = \sigma_x^2 E_0 \qquad (11.31)$$

$$\mathbf{R}_{\mathbf{m}_0\mathbf{z}} = \mathcal{E}\{\mathbf{m}_0\mathbf{z}^H\} = \mathcal{E}\{\mathbf{m}_0\left(\sqrt{E_0}\mathbf{H}_0\mathbf{m}_0 + \sum_{i=1}^{I}\sqrt{E_i}\mathbf{H}_i\mathbf{m}_i + \mathbf{v}\right)^H\} = \sigma_x^2 E_0\mathbf{H}_0^H \qquad (11.32)$$

$$\mathbf{R}_{\mathbf{z}\mathbf{m}_0} = \mathcal{E}\{\mathbf{z}\mathbf{m}_0^H\} = \mathcal{E}\{\left(\sqrt{E_0}\mathbf{H}_0\mathbf{m}_0 + \sum_{i=1}^{I}\sqrt{E_i}\mathbf{H}_i\mathbf{m}_i + \mathbf{v}\right)\mathbf{m}_0^H\} = \sigma_x^2 E_0\mathbf{H}_0 \qquad (11.33)$$

The MSE for both symbols are expected to be equal. Thus, the SINR is also same for both durations.

11.3.2.2 pdfs and cdfs SINR for different combinations

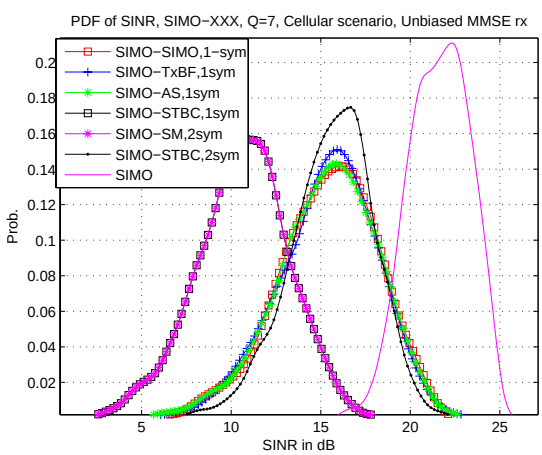

Figure 11.2: pdf of SINR with different combinations for 2-symbol processing when SINR definition of 'unbiased' MMSE is used

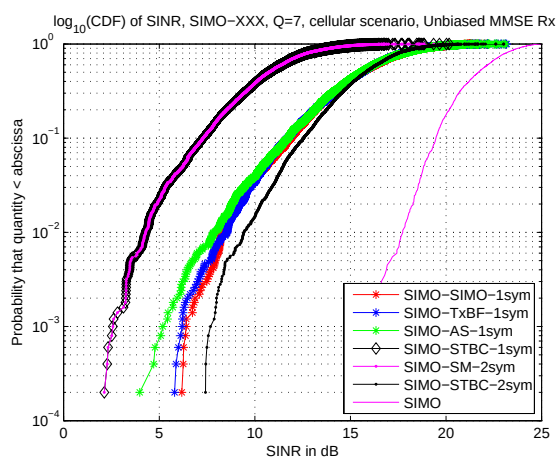

Figure 11.3: $log_{10}(cdf)$ SINR with different combinations for 2-symbol processing when SINR definition of 'unbiased' MMSE is used

The statistics for 'unbiased' MMSE is shown in Figures 11.2 and 11.3. Corresponding mean SINRs are shown in Table 11.2. These statistics are based on semi-analytical computations: theoretical SINR can be expressed as a function of the different instantaneous channels involved, then these statistics are evaluated by simulations. Rayleigh channel model is used to generate the channel coefficients. The delay spread values used in the simulations are taken from WiMAX literature. As seen from Table 11.2, the SINR statistics for SIMO-SIMO, SIMO-AS and SIMO-TxBF does not differ between single-symbol and two symbol processing. This is logical, as in both single-symbol

Table 11.2: Mean SINR for different cases with 7 Rx-antenna

SIMO-XXX, cellular scenario, $Q = 7$, Linear MMSE receiver		
	Mean SINR in dB	
Link	2-sym proc.	1-sym proc.
SIMO	-	21.6170
SIMO-SIMO	15.2176	15.4314
SIMO-TxBF	15.2756	15.1531
SIMO-AS	15.3717	15.1952
SIMO-STBC	15.6138	10.3778
SIMO-SM	10.6463	-

and multiple-symbol processing cases, the logical interfering stream is always only one for both the receiver processing cases. Thus, for clarity of figure, we have only plotted single-symbol processing plots for these three cases in Figures 11.2 - 11.3. As for SIMO-STBC case, when single-symbol processing is used, then the STBC interferer is similar to an SM an interferer with double streams, this is verified in case of SIMO-SM case when double-symbol processing is used. With dual antenna SM transmitter at the interfering BSs, we have 4 interfering streams per interfering BS for 2-symbol processing receiver. Thus, SIMO-SM system with 2-symbol processing receiver gives an equal average SINR compared to SIMO-STBC system with symbol-by-symbol processing receiver as seen in Table 11.2. This should also be the the same for AS-SM case.

Note that in practice, the 2 symbol processing will have lower performance than the single processing case if the estimation of covariance matrix of the received signal is based on the same number of samples.

As seen in Table 11.2, the average SINR for the cases SIMO-SIMO, SIMO-AS and SIMO-TxBF is comparable for both single-symbol and multiple-symbol processing. This is also true for the distribution of the SINR. Compared with these 3 cases, SIMO-STBC with 2-symbol processing gives equal performance with single-symbol processing for SIMO-SIMO, SIMO-AS and SIMO-TxBF. This proves our earlier conclusion that multiple-symbol processing converts an STBC interferer to a single-stream interferer. Note that when SIMO-STBC case with 2-symbol processing is used, the pdf of SINR is slightly narrow compared to SIMO-SIMO/SIMO-AS/SIMO-TxBF with 1-symbol processing. The same effect is also seen in cdf. We could verify by simulations for the SIMO-SIMO and SIMO-STBC case the following: on average, the norm of the projection of the signal subspace of STBC onto the signal subspace of SIMO is smaller than the norm of the projection of the signal subspace of SIMO onto the signal subspace of (another user) SIMO. As the interference cancelation is done in the noise subspace of the user of interest, cancelation is less for SIMO-SIMO than SIMO-STBC. This impact is slightly seen the cdf and pdf.

11.3.3 Mean SINR

In Figures 11.4 and 11.5, mean SINRs for different combinations of STBC-XXX and SIMO-XXX with 1-symbol and 2-symbol processing is shown. These results are obtained for a cellular scenario with all 6 interferers present in the system. Mean SINR can only indicate the performance of any case

© Muhammad Imadur Rahman, 2007

in the average sense. Still, it provides some useful indication about the performance of any case. As expected, MMSE receivers perform better than MRC receivers for both cases. For STBC-XXX, an SM interferer is seen as 2 interferers in case of dual branch SM. For all single-stream interferers, the mean SINR is same. Similar to this, when 2-symbol processing is used in SIMO-STBC scheme, the mean SINR is same compared to all other single-logical stream interferers with single-symbol processing. This is in line with the pdf and cdf in Figure 11.2 and 11.3 respectively.

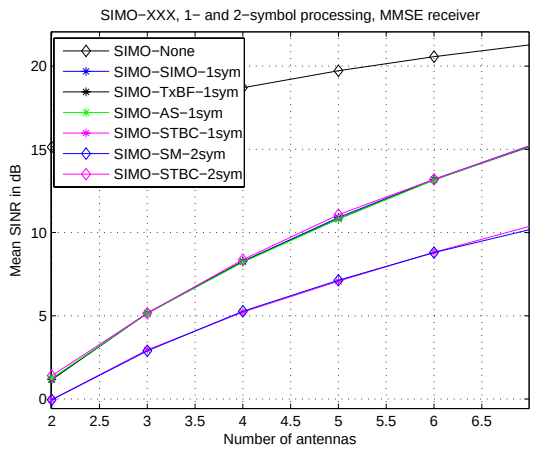

Figure 11.4: Mean SINR for SIMO-XXX cases with 1- and 2-symbol processing.

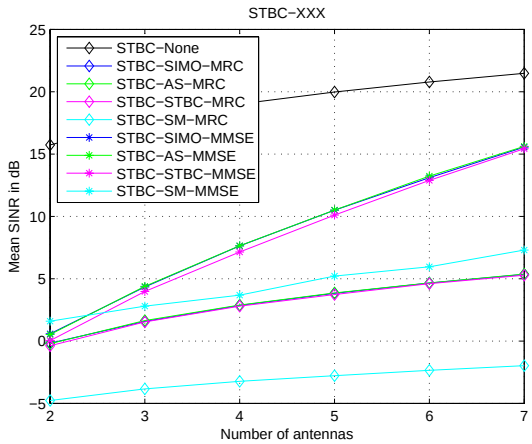

Figure 11.5: Mean SINR for different STBC-XXX cases.

11.3.4 Initial Investigations in Time-Invariant Channel

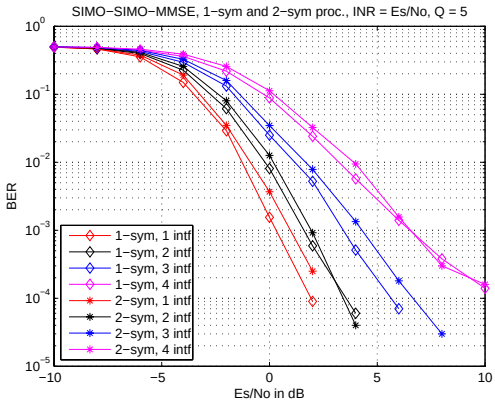

Figure 11.6: BER results for SIMO-SIMO with single-symbol and 2-symbol processing with linear MMSE receiver

As a test case, we have conducted simulations for 1-symbol and 2-symbol based MMSE processing for different link combinations. Figures 11.6 and 11.7 show the BER results for single-symbol and 2-symbol processing for SIMO-SIMO case and SIMO-STBC case respectively. The channel is taken as time-invariant. For each set of channels, we have used 600 number of terms in sample covariance matrix of received signal samples for estimating the $\mathbf{R_{zz}}$ matrix for single-symbol processing, while 300 terms are used while simulating the 2-symbol processing based linear MMSE

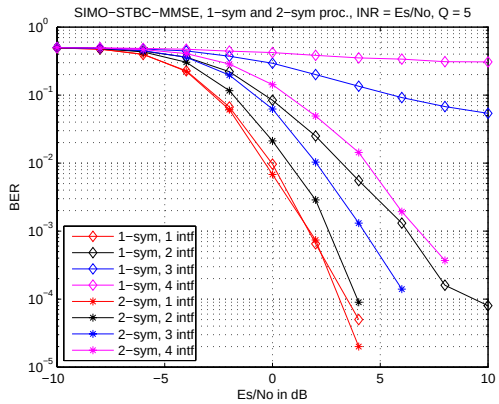

Figure 11.7: BER results for SIMO-STBC with single-symbol and 2-symbol processing with linear MMSE receiver

receiver. When the interfering link is SIMO, then increasing the MMSE processing duration (in number of symbols) does not give any added advantage. This is logical, as we know that when the received samples between two consecutive OFDM symbols are put together in one vector which is used to find covariance matrix, it indeed gives us an extended covariance matrix compared to the symbol-by-symbol basis operation. We can explain it like this: if we denote symbol-by-symbol based covariance matrix as $\mathbf{R}^1_{\mathbf{zz}}$ and 2-symbol based covariance matrix as $\mathbf{R}^2_{\mathbf{zz}}$, then we can easily find out that:

$$\mathbf{R}^2_{\mathbf{zz}} = \begin{bmatrix} \mathbf{R}^1_{\mathbf{zz}} & \mathbf{O}_Q \\ \mathbf{O}_Q & \mathbf{R}^1_{\mathbf{zz}} \end{bmatrix} \tag{11.34}$$

This easily shows that there should not be any performance improvement when multiple symbol processing is used in SIMO-SIMO/AS/TxMRC case.

The BER difference between single-symbol and 2-symbol processing in SIMO-SIMO case is caused by the fact that less terms in sample covariance matrix is used for $\mathbf{R}_{\mathbf{zz}}$ estimation in 2-symbol processing compared to single-symbol processing. It is understood that with equal number of terms for $\mathbf{R}_{\mathbf{zz}}$ estimation, BER performance will be same for SIMO-SIMO case in both single-symbol and 2-symbol processing. For Figure 11.7, we can see that as long as the 'apparent' logical streams in SIMO-STBC with single-symbol processing is lower than the available degree of freedom in terms of interference rejection (in this case, it is 4, because Q = 5, thus 2 STBC interferers can be rejected when single-symbol processing is used for SIMO-STBC receiver), the BER performance is quite satisfactory. When AS is used instead on SIMO in desired link, then we also see similar trends in AS-SIMO and AS-STBC cases corresponding to SIMO-SIMO and SIMO-STBC respectively. Obviously, only difference is that AS is desired link provides transmit diversity gain compared to SIMO case.

11.3.5 Simulation with Different Type of MIMO Interferers

In this section, we present the BER simulations when different kinds of interferers are present from different interfering BSs. We have 6 different BSs and we simulated for several numbers of channel realizations. Once again, the channel is taken as time-invariant. The cellular simulation scenario is

© Muhammad Imadur Rahman, 2007

similar to the one as shown in Figure 10.1. For each set of channel realizations (i.e. time-invariant condition), 500 iterations are done to estimate the interference nulling matrix, i.e. 500 samples of receive signals are used for al three cases for estimating the $\mathbf{R_{zz}}$ matrix. In another words, 500 sets of transmitted symbols and noise samples are used to estimate the $\mathbf{R_{zz}}$ matrix for each set of channel realizations. For the case of SIMO-Diff, SIMO, AS, TxBF and STBC interferers are equally likely to be present throughout the simulations. 2-symbol processing is used for all the cases. When a single-stream interferer other than STBC is present (i.e. SIMO, AS or TxBF), then the interference type from the particular interference source remains same for two-symbol durations, i.e. the interference type does not change in between two-symbol durations. Desired link uses SIMO scheme. For SIMO-SIMO and SIMO-Diff cases, the BER is same for all the ranges of BERs. This confirms our previous conclusion that multiple-symbol processing linear MMSE receiver provides a robust receiver solution to all kinds of single-stream interferers.

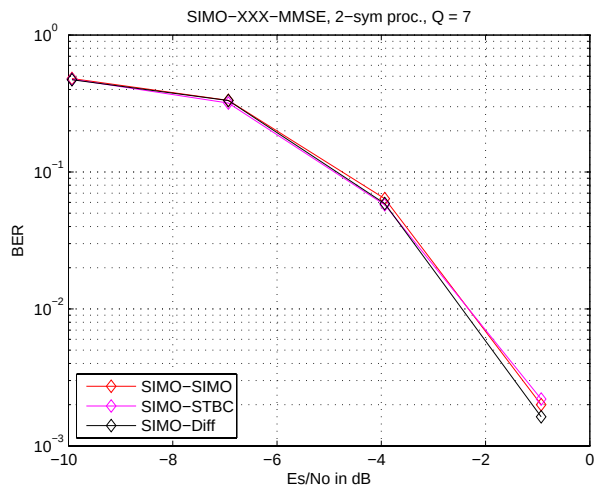

Figure 11.8: BER results for SIMO-SIMO, SIMO-STBC and SIMO-Diff cases with 2-symbol processing in cellular scenario

11.3.6 Time-Variant Case

All the simulation results that are presented so far are done for time-invariant channel. In time-variant case, the estimation of $\mathbf{R_{zz}}$ plays a big role in system performance.

We define a term, $\chi = \frac{T_c^{90\%}}{T_s}$, where $T_s = T_u + T_g$. T_u and T_g are the duration of OFDM data part and cyclic prefix respectively. T_s is the total OFDM symbol duration. So, following expressions can be written:

$$\chi = \frac{9}{16\pi f_d T_s} = \frac{0.179}{f_d T_s} \tag{11.35}$$

$$f_d = \frac{9}{16\pi \chi T_s} = \frac{0.179}{\chi T_s} \tag{11.36}$$

According to our simulation parameters, we have $T_u = 102.4\mu s$ and $T_g = \frac{T_u}{8} = 12.8\mu s$. So, $T_s = 115.2\mu s$. Using these parameters, we obtain the parameters in Table 11.3:

Table 11.3: Channel time-variance related parameters

χ	f_d, Hz	v, m/s	v, kmph
10	155.3819	9.3229	33.5625
25	62.1528	3.7292	13.4250
50	31.0764	1.8646	6.7125
100	15.5382	0.9323	3.3562
200	7.7691	0.4661	1.6781
500	3.1076	0.1865	0.6713

For simulations with time-variant channels, $\mathbf{R_{zz}}$ is estimated in two different methods:

1. using sliding window, i.e. $\mathbf{R_{zz}}$ is a time-average.
2. Using exponential average of $\mathbf{R_{zz}}$

For the time-averaging sliding window method, the averaging of $\mathbf{R_{zz}}$ can be defined as follows:

$$\mathbf{R}_{\mathbf{zz}}^{avg} = \frac{1}{N}\sum_{t=0}^{N-1} W_t \mathbf{R}_{\mathbf{zz}}^{(t)} \tag{11.37}$$

where $W_t = 1;\ \forall t$.

For Exponential average method, the average of $\mathbf{R_{zz}}$ is defined as:

$$\mathbf{R}_{\mathbf{zz}}^{avg} = \sum_{t=0}^{N-1} \frac{e^{-\frac{\alpha t}{N}}}{\xi} \mathbf{R}_{\mathbf{zz}}^{(t)} \tag{11.38}$$

where $\xi = \sum_{t=0}^{N-1} e^{-\frac{\alpha t}{N}}$ is the normalizing factor. α is the factor by which we determine the impact of 'older' $\mathbf{R_{zz}}$ values. For example, when the ratio between the 0th and $(N-1)^{\text{th}}$ components of $\mathbf{R}_{\mathbf{zz}}^{avg}$ is 10^{-2}, then $\alpha = -4.6052$.

We implement the $\mathbf{R_{zz}}$ estimator as described above across certain number of OFDM symbol durations. This number is denoted as $\mathbf{R_{zz}}$ window size. Figure 11.9 shows the BER when the number of receive antennas are varied for a velocity of 0.6713kmph (i.e. very static scenario). According to Table 11.3, at this velocity, 500 OFDM symbols reside inside a single 90% coherence time. So, channel should be very constant inside one $\mathbf{R_{zz}}$ window of 100 OFDM symbols. In these conditions, we can see that the moving average estimation of $\mathbf{R_{zz}}$ matrix produces an interference nulling performance very close to non-time-variant situation. Naturally, when the number of receive antennas are reduced, then the system performance becomes worse, because.

We have experimented the systems with different velocities. Different velocities impose different $\mathbf{R_{zz}}$ estimation window size. Figure 11.10 gives us the BERs when the user velocity in increased, for SIMO-SIMO system with single symbol processing. The length of the $\mathbf{R_{zz}}$ estimation block is 200. As Seen from Table 11.3, when the velocity is increased then the time-variance inside the estimation block (i.e. 200 OFDM symbol durations) increases, thus the resulting interference nulling becomes equivalent to MRC receiver. At a velocity of 3.3563kmph, we already have a duration equals to two coherence time inside the $\mathbf{R_{zz}}$ estimation window, so we see a significant per-

© Muhammad Imadur Rahman, 2007

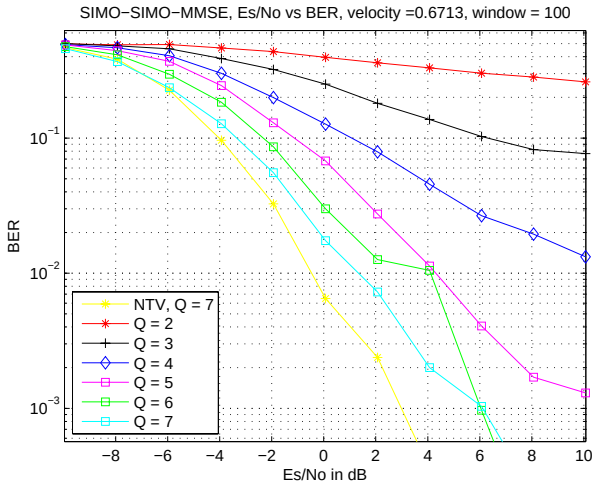

Figure 11.9: BER results for SIMO-SIMO-MMSE system, $\mathbf{R_{zz}}$ Window size =100, velocity = 0.6713kmph

formance drop. When the velocity is increased even more, the moving average estimation window contains more channel variations, and the resultant BER becomes very high. The conclusion that the BER performance at high velocity becomes equivalent to MRC receiver is in synchronization with our previous results, as seen from Figures 10.17 and 10.18.

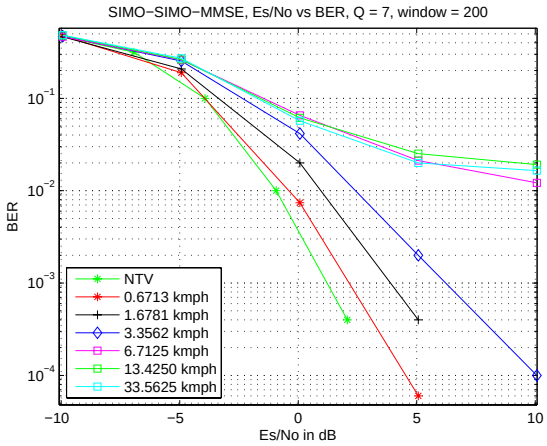

Figure 11.10: BER results for SIMO-SIMO case in time-variant channel scenario

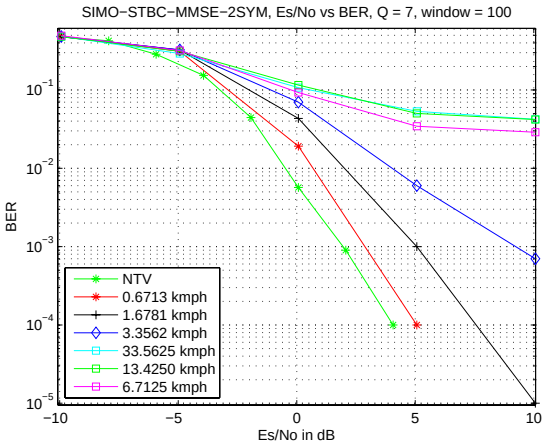

Figure 11.11: BER results for SIMO-STBC case in time-variant channel scenario

On the other hand, Figure 11.11 gives us the BER performance results for SIMO-STBC case when 2-symbol processing is used. For SIMO-STBC scenario, we have used the estimation window equal to 100. In this way, the averaging duration is equal to SIMO-SIMO case in Figure 11.10. As understood earlier, the BER performance of SIMO-STBC compared to SIMO-SIMO schemes for same velocity conditions will be little worse, because the number of samples for nulling operator estimation in SIMO-STBC is half of that in SIMO-SIMO case. In BER performance curves in Figure 11.11, a similar trend compared to SIMO-SIMO case is seen.

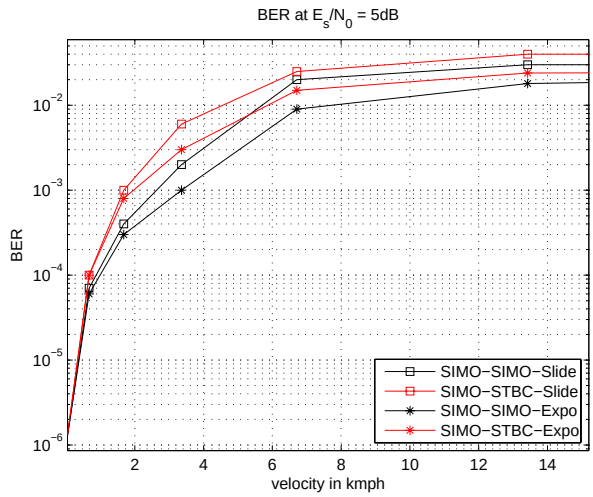

Figure 11.12: BER results for different $\mathbf{R_{zz}}$ estimation method, at 5dB of E_s/N_0

Figures 11.10 and 11.11 provide us the impact of time-variance on the $\mathbf{R_{zz}}$ estimation process when sliding window average method is used. We have also explained the exponential averaging method in this section. Figure 11.12 shows us the BER results at E_s/N_0 = 5dB when both sliding window and exponential averaging window method are used on SIMO-SIMO with single-symbol processing and SIMO-STBC with 2-symbol processing cases. As seen t'previously, the number of samples for $\mathbf{R_{zz}}$ estimation is SIMO-SIMO and SIMO-STBC cases are 200 and 100 respectively. We can see that in lower velocity, both exponential and sliding window averaging method performs quite similarly. This is logical, as we know that the channel is less time-variant inside the estimation window for lower velocities. For higher velocities (i.e. starting from pedestrian mobility), the exponential averaging method puts a lower 'weighting' coefficients to 'older' channel coefficients, thus, the BERs are improved with exponential averaging method.

11.3.7 STBC Detection Module

As explained in Section 11.2.3.1, we define that, if the values of at least $2Q$ points in $[\mathbf{D}]^U$ and $[\mathbf{D}]^L$ are inside the range of $\| \frac{E_i}{4} + \frac{N_0}{2} \|$ and $\| \frac{E_i+N_0}{2} \|$, then SIMO-STBC interferer is detected. Similarly, when the values are in the range of $\| \frac{N_0}{2} \|$ and $\| \frac{E_i}{4} + \frac{N_0}{2} \|$, then we decide that the interference is of SIMO type. We simulated the detection module in following way:

1. **Symbol index-1:** Either SIMO or STBC interferer is assigned randomly. Receiver starts 2-symbol processing mode, so 100 pairs of $\mathbf{R_{zz}}$ matrix is obtained.

2. **Symbol index-200:** receiver averages the mentioned elements of $\mathbf{R_{zz}}$ matrix and decides whether SIMO or STBC interferer is present. If STBC is detected, then 2-symbol processing is continued. If not, then receiver switches to single-symbol processing. In that case, the diagonal components of $\mathbf{R_{zz}}$ matrix of 100 pairs, i.e. 200 previous $\mathbf{R_{zz}}$ matrices are used for further $\mathbf{R_{zz}}$ estimation.

© Muhammad Imadur Rahman, 2007

3. **Symbol index-2000:** The assignment of SIMO or STBC interferer is changed randomly again. Then the receiver switches to 2-symbol processing if the processing at previous 5000 symbols were single-symbol processing. Receiver now again starts to look at the off-diagonal elements and decides the interference type. By symbol index-2200, a new decision is made and procedures as described for symbol index-200 is done.

4. A total of 50,000 symbols are simulated in this way.

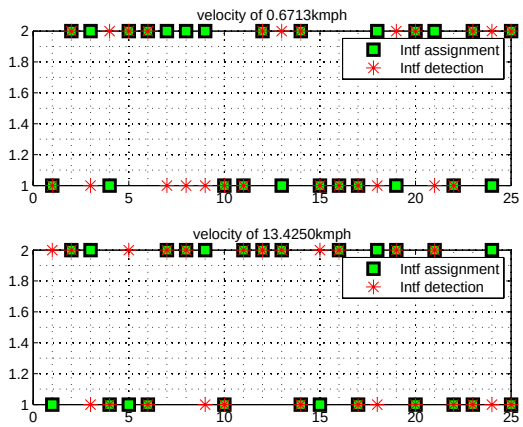

Figure 11.13: Successful detection and false detection when STBC module is used

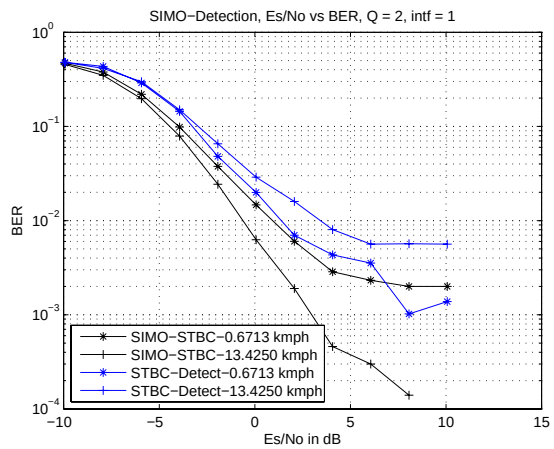

Figure 11.14: BER results for SIMO-STBC case with and without the STBC detection module in time-variant channel scenario

Figure 11.13 shows us the STBC detection instants whether a correct or false detection is seen. 1 and 2 on y-axis refers to random SIMO and STBC assignment in the simulation respectively. 1 to 25 on x-axis refers to 25 blocks of 2000 symbols where the interference type is same. Green color shows the interference assignment at simulation run, and red color shows the detection at that block. Two velocities are simulated, 0.6713kmph (3Hz of Doppler) and 13.4250kmph (62Hz of Doppler). Sliding window averaging is used for $\mathbf{R_{zz}}$ estimation. False detection is denoted as, when STBC is detected while the interferer is SIMO, and Failure is denoted as, when SIMO is detected while the interferer is STBC and the false detections. We can see that, for low velocity, false detection rate is $\frac{4}{11}$ and failure rate is $\frac{10}{25}$. At low velocity, channel is quite constant, thus false detection and failure may become higher. For higher velocity, the channel averaging due to Doppler happens, thus, false detection and failure reduces compared to lower velocity scenario, here it is $\frac{3}{12}$ and $\frac{7}{25}$ respectively.

Figure 11.14 shows us the BER when detection module is used. Only one interferer is considered for this simulations. Number of receive antennas at MS is 2. So the strongest interferer from cellular scenario is taken into consideration. As mentioned earlier, we assume that the received interference power is known to the MS. 'SIMO-STBC' curve is for SIMO-STBC-MMSE with 2-symbol processing. For this, the window size is 200, so 100 samples are used for $\mathbf{R_{zz}}$ estimation. Corresponding velocity curve is used as reference. 'STBC-Detect' curve is for STBC detection method. The detection method is as described in this section. The receiver processing is switched between

single and multiple symbol processing according to detection. It is worth noting here that false detection does not impact the BER, as it enables 2-symbol processing which is robust against both interference type. For lower velocity, the failure causes the BER degradation, while the channel averaging is the reason for BER degradation in general for higher velocity. Although the failure is less in higher velocity, the degradation in BER is present due to the channel variance.

11.4 Fractional Frequency Reuse at Cell Edge

11.4.1 Motivation and Problem Definition

With increasing demand for more extensive frequency reuse, new methods for utilizing available frequency bands are of great importance. One of the main concerns for designing the frequency channel assignment at the cell border is available number of receive antennas at the interfered receiver. It has been reported previously [33],[73] that the maximum number of streams (both desired and interfering) that a receiver can resolve using linear receive techniques is equal to number of receive antennas. As we have defined 'the logical stream' as the interfering data streams in Chapter 10, receive diversity, e.g. SIMO, transmit Antenna Selection, i.e. AS, or TxBF links are termed to be single-link logical stream. When STBC is used at the interfering link, then the desired link experiences more than one 'apparent' logical stream if the signals are processed on symbol-by-symbol basis. We have shown in Section 11.2 that the linear MMSE receiver based on multi-symbol processing cancels out the interferers provided that the number of receive antennas is larger or equal to the number of received logical streams (i.e. addition of desired and interfering streams). These interfering logical streams may include STBC. This multiple-symbol based receiver technique provides us robustness against any single stream interferer.

In this section, we propose a novel frequency assignment technique among the cell edge users which exploits the knowledge of number of the available receive antennas and the multiple-symbol based linear MMSE technique. Each cell is assigned one set of frequencies for cell-edge users, which are shared among users of different interference rejection capabilities. Orthogonal frequency channels are used across the cells only for the cell-edge users, thus a fractional re-use factor is achieved. The novelty of the proposal is that it is not only adapted to the number of interfering base stations, but to the total number of transmitted logical streams. This may be done at cell site deployment, or adaptively in time with cell sites cooperation.

11.4.2 Prior Arts

A Fractional Frequency Reuse (FFR) method for severely CCI affected users at the cell edge is proposed in [161]. The FFR method in [161] assigns frequency channels to any particular user based on its location. Unrestricted usable frequency channel sets for all users in a cell are defined for users located inside the cell area (i.e. much closer compared to cell edge). When a user is located around the cell edge, then the allocation also takes care of the nearest CCI source, i.e. nearest BS that is also transmitting in DL. So, based on the information about the location of any cell edge user, a decision on the available frequency set for that particular user is made. This FFR method

© Muhammad Imadur Rahman, 2007

does not take care of the impact of the type of interferer, rather it only concentrates on the fact that more than one CCI interferers are present for a cell edge user. When the interference rejection capabilities via MIMO antennas are not taken into account in the FFR design, it is clear that the benefit of MIMO systems will not be exploited in the frequency assignment. The performance of the system can be greatly improved when MIMO interference cancelation capabilities is taken into account for frequency reuse assignment.

11.4.3 The FFR method

We denote the number of receive antenna at the desired MS as Q and the number of DL interferers as I. As mentioned earlier, the linear MMSE receiver can cancel out at least $Q - 1$ number of interferers. This is true even for the case when STBC is present as interferer. To satisfy this condition (i.e. enough diversity order to null out the interferers) and exploit our proposed multiple-symbol processing, we propose a frequency sharing among the main interfering BSs.

The main assumptions are:

1. There are 2 main interfering BSs, as shown in Figure 1: the other interfering BSs are assumed negligible. It is worthy to mention here that the scheme should be extendable to more interfering BSs.

2. A frequency band is reserved for users located at cell edge and shared by the interfering BS. Each BS does not know the nature of the interfering links.

3. Spatial Multiplexing is not used for transmission to cell edge users. Only single logical link transmission is used.

4. Maximum length of the STBC codes used by the interfering BS is known to the MS: this assumption is not strictly necessary as the MS could estimate this maximum length.

5. STBC transmissions are synchronized for all the BSs (i.e. starts at the same time for all BS).

As shown in Figure 11.15, the proposed assignment scheme ensures that the concerned MS always has sufficient orders of spatial degree of freedom to nullify the interfering signals. The principle is as follows:

1. **For $\mathbf{Q} = 1$:** no sharing of the bands is allowed, as the MS cannot nullify any interfering signal.

2. **For $\mathbf{Q} = 2$:** channel sharing between 2 BSs is allowed, because the MS can now efficiently nullify one interferer.

3. **For $\mathbf{Q} \geq 2$**, sharing between 2 or more BSs is allowed.

Transmission towards one MS in the DL can cause interference for other MSs. In another words, assigning some resources to any user located in cell edge area can also mean that some interference is generated for users located at the neighboring cells, thus, existence of one particular MS can become the reason of interference for other MS. With the knowledge of the interference rejection capability (i.e. number of receive antennas available at the MS), unwanted interference

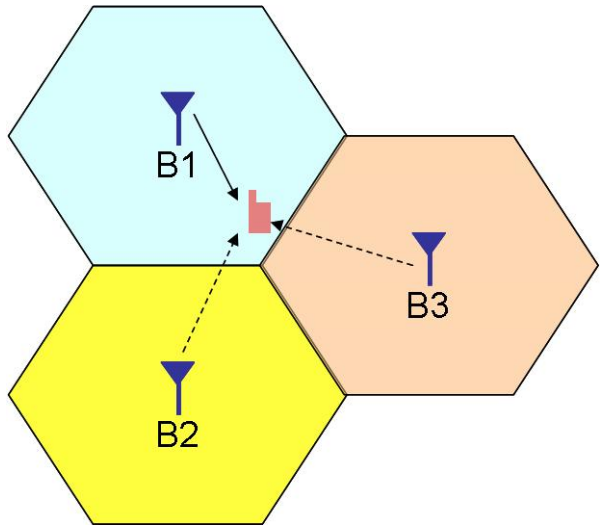

Figure 11.15: Scenario Description. Only 2 interfering BSs are considered.

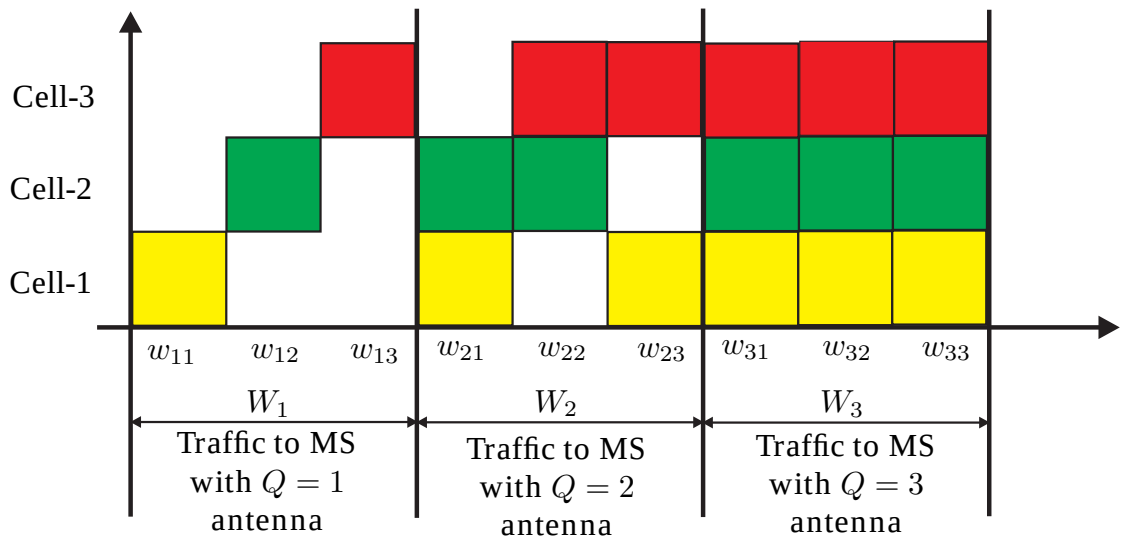

Figure 11.16: Example of frequency assignment between 3 neighboring cells as shown in Figure 11.15

can be avoided for other users in the neighboring cells. In a nutshell, the main motivation of our proposed channel assignment design is to avoid the interferences from other interfering BSs and also to ensure that one particular MS does not become source of interference for others.

Let's denote the total available frequency sets for all three BSs as W. We define three disjoint sets of frequencies, such as:

1. W_1, W_2 and $W_3 \subset W$

2. $W_i \cap W_j = \emptyset$, where $\emptyset$ means an empty set and this is true for all $i, j \in \{1, 2, 3\}$

3. As one of the possible solutions, the users located inside the cell area of al cells can use the same frequency band. That band can be denoted as $W \cap \left[\cup_{i=1}^{3} W_i\right]$.

© Muhammad Imadur Rahman, 2007

These three bands are identified with three classes that are mentioned before with respect to the number of available receive antennas at the desired MS. For the example shown in Figures 11.15 and 11.16, we have three different cells and we need to allocate the frequencies in all of three bands mentioned above. Thus, we define another three sub-sets of frequencies under all the above three sets, such that

1. $W_{i1} \cup W_{i2} \cup W_{i3} = W_i$
2. $W_{ix} \cap W_{iy} = \emptyset;\ \forall\ i, x, y \in \{1, 2, 3\}$

As shown in Figure 11.16, the proposed assignment scheme ensures that the concerned MS always has sufficient orders of spatial degree of freedom to nullify the interfering signals. By utilizing the classes, and the frequency set definitions defined in the previous page, the frequency allocations principle can be described as follows:

1. Users with $Q = 1$ antennas are scheduled in the band W_1 where no frequency sharing between BS is allowed.
2. Users with $Q = 2$ antennas are scheduled in the band W_2 where frequency sharing between 2 BSs is allowed
3. Users with $Q \geq 3$ antennas are scheduled in the band W_3 where frequency sharing between 3 BSs is allowed.

The sizes of these frequency sets and subsets depend on the number of available users located at cell edge with certain receive antenna classes. As the load factor for all these three classes are always random (or at least not deterministic), we can safely say that depending on system load, $W_1,\ W_2$ and W_3 (and sub-channel bandwidth inside each band) might be adapted. This provides us an opportunity to design an adaptive FFR method based on the number of severely interfered users at the cell-edge.

Frequency hopping can be used to reassign the bands and subbands. The sharing is described in Figure 11.16 in frequency only, but it can be done in time or in a time-frequency plane or both.

11.4.4 Evaluation of proposed FFR method

We have explained that the proposed method will ensure the available degree of freedom in any MS receiver will always be sufficient to efficiently nullify all the interferers. This is done by considering the MIMO mode that is supported at the MS. In Section 11.2.2, we have shown that as long as the number of logical interfering streams is kept less than $(Q - 1)$, the interference cancelation is possible. We have also shown the method to nullify the special interference case of STBC, where two-symbol processing can be used.

11.5 Chapter Summary

In this chapter, we have designed a robust MIMO interference cancelation receiver and also proposed a frequency-reuse scheme that can be used at the cell-edge for CCI avoidance, on top of

the CCI cancelation via the multiple-symbol based receiver. The following observations are made regarding these two issues:

Robust linear receiver design

1. Multiple-symbol processing based linear MMSE receiver provides robustness against all single-stream interferers, such as STBC, SIMO etc.

2. Combined with suitable frequency re-sue scheme, the proposed multiple-symbol processing can be effectively used to manage multiple-logical-stream interferers.

3. Via the STBC detection block, when the presence of STBC as an interferer is detected, savings in terms of processing is achieved while the interference rejection is ensured.

4. The proposed scheme can be used to adopt to any length of STBC interference block length.

FFR method based on number of interfering MIMO links

1. By considering the available degrees of freedom at the cell edge users, the proposed FFR method provides a CCI avoidance mechanism when the interference to and from the same and/or other MIMO schemes are present. This is done by assigning orthogonal sets of frequencies for neighboring BSs for different groups of users. The user grouping is done based on number of degrees of freedom available at the MS receiver.

2. Very good frequency utilization can be achieved for cell edge users who are capable of MIMO techniques in parallel to CCI avoidance.

3. Based on the load at the cell edge, an adaptive FFR method can be achieved.

Future Work

Multi Cell BS Communication for interference avoidance is a challenging task that can be taken upon. Interference power/type feedback between BSs can be used for interference reduction. A few issues related to this is described below:

1. e.g., knowledge of type of interfering links from neighboring links can be used to inform desired MS about multiple symbol processing. Not strictly necessary, multiply symbol processing can be done by default, or there could be a mechanism where the MS switches to Multiple link processing based on P_e.

2. In AMC channels, procedures such as bit loading may be affected by severe STBC interferer: STBC should be considered for 2 symbol processing, in that case STBC interference is approximately equivalent to the other transmit techniques

3. The knowledge of current studies can be used to make sure that AMC channels should not collide with STBC channels from interfering cells.

© Muhammad Imadur Rahman, 2007

4. At lower velocity, the MMSE parameter estimation works, but at higher velocity, proper estimation methods need to be studied.

"You never finish a job, unless a deadline is set."

Anonymous

12

Conclusions and Future Outlook

12.1 Overall Summary

OFDM paves way for numerous possibilities of implementing multiple access to provide services to multiple users simultaneously. In the first contribution part of this thesis, i.e. Chapters 3 and 4, we have studied a specific channelization technique, Sub-Carrier and Band Hopped Orthogonal Frequency Division Multiple Access (SCBH-OFDMA), where we allocate sub-carrier (or sub-channel) based resources to users who experience heterogenous channel conditions, but require services under the same system configurations. We propose to accumulate the users in several groups based on certain predefined criteria. The total available spectrum is divided into a number of bands equal to the number of user groups. For efficient time-frequency resource allocation, sub-carrier hopping and band hopping is simultaneously used in this novel multiple access scheme. Under some constraints, sub-carriers can also be assigned to different users based on known channel characteristics using dynamic sub-carrier allocation. Sub-carrier and band hopping are used for mitigating the frequency selectivity of the wireless channel and for minimizing and avoiding interference in the system. The novelty comes when users are grouped based on some pre-defined criteria and they are hopped on sub-carriers (or sub-channels) and on bands. By using unified hopping mechanisms, we support heterogeneous users under the same system and we also improve the outage scenario. The proposed scheme is equally applicable to both DL and UL, though we have concentrated mainly on DL scenario.

When CSI is available at the transmitter, LA techniques exploit the fine granularity of OFDM systems to optimize the achievable spectral efficiency. We have studied hybrid strategies to

tradeoff achievable efficiency and complexity for practical LA solutions in Chapters 5 and 6. The choice for adapting link parameters are investigated which are highly dependent on dynamically changing channel parameters such as delay spread, Doppler frequency spread, average SNR and instantaneous channel gains. Besides, we have also examined the performance of link adaptation process under several system impairments, such as transmitter non-linearities, etc.

We have studied several multi-antenna techniques in collaboration with OFDM systems in Chapters 7 - 9. Our first focus is on studying the tradeoff between diversity and array gain in terms of open-loop transmit diversity and beamforming systems in Chapter 7. We have studied the systems in terms of outage capacity, corresponding outage probability and BER. We have compared Pre-IDFT downlink beamforming (i.e. sub-carrier domain transmit beamforming) with Space-Time Block coded and Space-Frequency block coded transmit diversity schemes for downlink OFDM systems. The study is performed for indoor micro and pico cells and urban macro cells. It is found that beamforming always performs better in outdoor environment, where angular spread is lower, thus spatial correlation is higher. Similarly, indoor environment (high angular spread and low spatial correlation) suggests that transmit diversity schemes performs better than beamforming strategies.

In Chapter 8, we focus on a simplified diversity technique, namely CDD technique. In our work, CDD is applied in OFDM receiver to increase the frequency-selectivity of the channel seen at the receiver for flat (or less frequency-selective) channels. The diversity combining is performed prior to the DFT operation. A new method has been studied to optimize the Pre-DFT diversity combining by selecting the cyclic shifts and weight factors based on known channel state information. The optimum signal to noise ratio for maximum cyclic delay and optimum weight factors for multiple antenna receiver diversity are analyzed. A performance comparison is presented in terms of BER with and without coding, between MRC for receiver diversity and CDD for transmitter and receiver diversity in the context of IEEE 802.11a and/or HiperLAN/2 WLAN systems. CDD yields good diversity gains although the performance of MRC on subcarrier level is not reached. On Ricean channels, the optimized schemes perform much better than CDD with fixed delays, while the gain in Rayleigh channels is surprisingly small. Finally, it is found that the scheme advocated in this thesis drastically reduces the computational complexity comparing to traditional receiver diversity schemes. With this knowledge and understanding of basic CDD benefits, we have used the CDD technique on top of a spatial multiplexing based OFDM system. We have shown significant improvement in the FER by using this scheme in comparison to a simple spatial multiplexing scheme. This is achieved with little changes at any standard spatial multiplexing system. In addition, the number of transmit antennas can be increased to increase the link capacity without making any changes to the receiver. Thus, the proposed technique can be used with any existing MIMO-OFDM system.

In line with these studies of MIMO signalling techniques, we have studied two JDM structures where both diversity and multiplexing benefits are available for OFDM-MIMO systems in Chapter 9. Two types of JDM architectures, namely SM-OSFBC system and SM-QSFBC systems are studied in the work. Linear and non-linear receivers based on well-known ZF, MMSE and OSIC techniques are derived and analyzed. The systems are compared in terms of FER and outage spectral efficiency in realistic wireless channel scenario, such as spatial correlation at both ends of

the transmission link and presence of LOS. It is found that due to added diversity via SFBC at the transmitter, JDM schemes are more robust compared to original spatial multiplexing schemes (such as VBLAST) when high spatial correlation is present at any end of the link, or when LOS component is present in the system.

In the last part of this thesis in Chapters 10 and 11, we have summarized our studies, analysis and simulations related to interference of some specific MIMO schemes on the same and other MIMO schemes. The goal is to study the impact of interference from MIMO schemes at a user located in the cell edge. Semi-analytical evaluations of SINR is done to find out the SINR statistics of different combinations of desired-interfering links. We have studied single- and multiple-symbol duration receiver processing for all the link combinations. Based on the current analysis, it is found that STBC is a severe interferer compared to others, and specific attention is needed to counter the interference introduced by STBC interfering link. Based on these conclusions, we propose an interference cancelation receiver robust to different types of MIMO interferers at cell edge for the DL of cellular OFDMA systems. The receiver systematically performs a multiple symbol processing which is the appropriate processing, especially when a co-channel interferer using STBC is present. We have found that the proposed multiple-symbol based receiver is a suitable solution for efficient cancelation of CCI originated from different MIMO interfering sources. A module detecting the presence of a STBC interferer is proposed: when no STBC interferer is detected, the receiver switches to a single symbol processing. After that, we propose a frequency sharing for the DL of a cellular OFDMA at cell edge. This frequency sharing among the main interfering BSs ensures that the number of receive antennas for each MS is larger or equal to the total of received streams, i.e. the addition of number of desired and interfering links. The proposed method uses the knowledge of the number of available receive antennas at the MS and ensures that the interference order is always kept under control so that the desired MS is not severely affected by CCI.

12.2 Contribution of Thesis

Channelization: SCBH-OFDMA

Under the same cell area, different users experience different time and frequency selectivity characteristics depending on their distance from BS, their velocities and the wireless multi-path scenario that they observe. Using this heterogeneous channel scenario, we have designed a flexible channelization technique, namely SCBH-OFDMA, by making use of sub-carrier and band hopping which can be adapted in different scenarios, thus creating an adaptive system.

Frequency Domain Link Adaptation

By using a less-complex and more spectrally efficient LA algorithm, we have performed an unified investigation of different channel and system related parameters under one framework in WiMAX/UMTS-LTE context for link adaptation. We have investigated the impact of a number of parameters. Based on these results, we have suggested a simplified implementation where parameters are adapted at different stages, and not simultaneously. In most other works, the adaptations across different domains are done simultaneously.

© Muhammad Imadur Rahman, 2007

Transmit Diversity and Beamforming

Using theoretical analysis, we have motivated the use of transmit diversity and beamforming in different scenarios. Based on the theoretical analysis and numerical simulations, we propose to use transmit diversity schemes in high angular spread scenario, such as indoor or immediate outdoor scenario, while beamforming for low angular spread scenario, e.g. outdoor macro cell scenario.

Cyclic Delay Diversity

Exploiting the cyclic delay diversity, we have proposed a simplified receive diversity architecture, which obtains receive diversity gains without increasing the system complexity very much. We have also proposed an SM technique, where CDD properties are used on top of a basic SM scheme. In both of the cases, we have found that some gain are obtained.

Joint Diversity and Multiplexing

Two types of JDM systems, namely SM-OSFBC system and SM-QSFBC systems are studied in the work. Linear and non-linear receivers based on well-known ZF, MMSE and OSIC techniques are derived and analyzed. It is found that due to added diversity via SFBC at the transmitter, JDM schemes are more robust compared to only spatial multiplexing schemes (such as VBLAST) when high spatial correlation is present at any end of the link, or when LOS component is present in the system.

MIMO Techniques at Cell Edge

We have analyzed the impact of CCI caused by different MIMO schemes. Our proposed multiple symbol processing is robust to any single stream interferer. STBC detection block has been designed to reduce the unnecessary processing at the receiver. Detailed analysis of the usage of th multiple symbol processing is done. Based on this understanding and knowledge, a proper frequency re-use pattern is designed for cell-edge users, where the number of spatial degrees of freedom is considered for designing the frequency-reuse pattern.

12.3 Future Outlook

Based on our analysis and discussions, following future items can be studied:

Channelization and Link Adaptation

Due to practical system conditions, there will be different levels of reliability of the CSI that can be achieved at the BS in a cellular system, thus, a combination of blind and CSI based resource-allocation (e.g. link adaptation and scheduling) in multi-user context need to be studied. Our studies can provide significant guidelines in designing such a resource allocation mechanism.

Multi-Antenna Techniques

We can extend our investigation in multi-antenna techniques in a number ways:

1. There is a need to study the usability of transmit diversity and beamforming in link adapted system, because, the available array gain in beamforming may become very important in link adaptation scheme.

2. The studies related to transmit diversity and link adaptation can be extended to multi-user scenario, where opportunistic beamforming can be used to introduce multi-user diversity.

3. The diversity and multiplexing trade-off needs to be studied together in multi-user scenario.

4. If partial or full CSI is available at the transmitter, we can use transmit pre-filtering (like Transmit-MRC) across SM branches, thus joint beamforming and multiplexing schemes can be designed. In this way, transmission will be done on the eigenmodes when full CSI available, and on eigenmodes of transmit covariance matrix when partial CSI is present. These kind of schemes can be compared with multi-user MIMO techniques.

CCI Management in Cellular System

Based on our studies, novel and efficient interference management schemes, i.e. combination of interference cancelation and avoidance, need to be designed. Proper BS communications can be designed to distribute information about interference scenario and conduct the interference management algorithm.

Using the knowledge of MIMO schemes and interference management, cooperative MIMO algorithms can be designed to best-utilize the multi-antenna capabilities in network for countering the CCI and increase the overall spectral efficiency.

© Muhammad Imadur Rahman, 2007

The Prophet Muhammad (peace be upon him) said: "There are two (kinds of) people worth envying: Someone whom God has made rich and who spends his money righteously; and someone whom God has given wisdom and who acts according to it and teaches it to others."

- Sahih Al-Bukhari, Volume 9, Hadith 255

A

List of IPRs, Publications and Technical Reports

Selected IPRs and Publications related to this Thesis

Chapter-3 & 4: Sub-Carrier and Band Hopped OFDMA (SCBH-OFDMA)

1. **Muhammad Imadur Rahman**, Ragnar V. Reynisson, Frank Fitzek, Ramjee Prasad, "Apparatus and Method for Operating Frequency Resources in a Mobile Communication System", assigned by Korean Intellectual Property Office with serial no. 2005-89562, September 2005, applied in USPTO on October 2006.

2. **Muhammad Imadur Rahman**, Ragnar V. Reynisson, Daniel V.P. Figueiredo, Ramjee Prasad, "Coordinated Sub-Carrier and Band Hopping in OFDMA based Systems", in proceedings of IEEE International Symposium on Wireless Communication Systems, ISWCS'07, held in Norway on 17-19 October 2007.

3. **Muhammad Imadur Rahman**, Ragnar V. Reynisson, Daniel V.P. Figueiredo, Ramjee Prasad, "Sub-Carrier and Band Hopped OFDMA", selected for publication in a special issue of the Springer journal ŞWireless Personal Communications (WPC)Ť based on selected papers from the IEEE ISWCS 2007 conference, to be published in 4Q, 2008.

Chapter-5 & 6: Frequency Domain Link Adaptation

1. **Muhammad Imadur Rahman**, Suvra Sekhar Das, Yuanye Wang, Flemming Bjerge Frederiksen, Ramjee Prasad, "Bit and Power Loading Approach for Broadband Multi-Antenna OFDM System", in proc. of IEEE VTC, Fall 07, Baltimore, USA, 2-4 October 2007.

2. Suvra Sekhar Das, **Muhammad Imadur Rahman**, Nidcha Pongsuwanich, Yuanye Wang, Nurul Huda Mahmood, Carlos Leonel Flores, Bayu Anggoro Jati, Ramjee Prasad, "Impact of PAPR Reduction Mechanism on Bit and Power Loading Strategies for UMTS-LTE/WiMAX systems", in proc. of IEEE VTC Spring'07, Dublin, Ireland, 22-25 April 2007.

3. Suvra Sekhar Das, **Muhammad Imadur Rahman**, Yuanye Wang, Flemming Bjerge Frederiksen, Ramjee Prasad, "Hybrid Strategies for Link Adaptation exploiting several degrees of freedom in OFDM based Broadband Wireless Systems", in proc. of IEEE VTC, Fall 07, Baltimore, USA, 2-4 October 2007.

Chapter-7: Transmit Diversity vs Beamforming

1. Daniel V.P. Figueiredo, **Muhammad Imadur Rahman**, Nicola Marchetti, Frank H.P. Fitzek, Marcos D. Katz, Youngkwon Cho & Ramjee Prasad, "Transmit Diversity Vs Beamforming for OFDM Based Wireless Systems", in proc. 7th WPMC'04, 12-14 September, 2004, Italy.

Chapter-8: Cyclic Delay Diversity in OFDM Systems

1. **Muhammad Imadur Rahman**, Klaus Witrisal, Suvra Sekhar Das, Frank H.P. Fitzek, Ole Olsen & Ramjee Prasad, "Optimum Pre-DFT Combining with Cyclic Delay Diversity for OFDM Based WLAN Systems", in the proceedings of IEEE VTC Spring '04, May, 2004.

2. **Muhammad Imadur Rahman**, Suvra Sekhar Das, Frank H.P. Fitzek, Ramjee Prasad, "Pre- and Post-DFT Combining Space Diversity Receiver for Wideband Multi-Carrier Systems", in proc. 8th WPMC'05, 19-21 September, 2005, Aalborg, Denmark.

3. **Muhammad Imadur Rahman**, Suvra Sekhar Das, Elisabeth de Carvalho, Ramjee Prasad, "Spatial Multiplexing in OFDM Systems with Cyclic Delay Diversity ", in proc. of IEEE VTC Spring'07, Dublin, Ireland, 22-25 April 2007.

4. **Muhammad Imadur Rahman** et al., "Cyclic Delay Diversity based Pre-DFT Combining Receiver for Multi-carrier Systems", to be submitted to IEEE transactions of wireless communications.

Chapter-9: Joint Diversity and Multiplexing Schemes

1. **Muhammad Imadur Rahman**, Nicola Marchetti, Elisabeth de Carvalho, Ramjee Prasad, "Joint Diversity and Multiplexing for MIMO-OFDM System", accepted subjected to revisions in EURASIP journal on Wireless Communications and Networking.

2. **Muhammad Imadur Rahman**, Nicola Marchetti, Elisabeth de Carvalho, Ramjee Prasad, "Spatially Multiplexed Quasi-Orthogonal SFBC Systems", IEE Electronics Letter, August 2006.

3. **Muhammad Imadur Rahman**, Nicola Marchetti, Elisabeth de Carvalho, Ramjee Prasad, "Joint Quasi-Orthogonal SFBC and Spatial Multiplexing in MIMO-OFDM Systems", in proc. IEEE VTC Fall 2006, Montreal, Canada, 25-28 September, 2006.

4. **Muhammad Imadur Rahman**, Nicola Marchetti, Frank H.P. Fitzek, Ramjee Prasad, "Non-Linear Detection for Joint Space-Frequency Block Coding and Spatial Multiplexing in MIMO-OFDM Systems", in the proc. of 2nd IEEE International Symposium of Wireless Communications Systems (ISWCS '05), Siena, Italy, 5-9 September, 2005.

5. **Muhammad Imadur Rahman**, Nicola Marchetti, Suvra Sekhar Das, Frank H.P. Fitzek, Ramjee Prasad, "Combining Orthogonal Space-Frequency Block Coding and Spatial Multiplexing in MIMO-OFDM System", in proc. of 10th International OFDM-Workshop (InOWo '05), Hamburg, Germany, 31 Aug-01Sep, 2005.

Chapter-10 & 11: MIMO Systems at Cell Edge

1. Elisabeth de Carvalho, **Muhammad Imadur Rahman**, Ramjee Prasad, "Interference cancelation robust to various MIMO interferers via multiple-symbol processing at the cell edge of a cellular OFDM(A) system ", filed in USPTO and Korean Intellectual Property office by May 2007, by Samsung Electronics, Korea.

2. Elisabeth de Carvalho, **Muhammad Imadur Rahman**, Ramjee Prasad, "Fractional frequency reuse at cell edge based on the number of interfering MIMO links for OFDM(A) systems ", filed in USPTO and Korean Intellectual Property office by May 2007, by Samsung Electronics, Korea.

3. **Muhammad Imadur Rahman**, Elisabeth de Carvalho, Ramjee Prasad, "Impact of MIMO Co-Channel Interference", in proc. of IEEE PIMRC'07, held in Athens, Greece, 3-7 September 2007.

4. **Muhammad Imadur Rahman**, Elisabeth de Carvalho, Ramjee Prasad, "Mitigation of MIMO Co-channel Interference using Robust Interference Cancelation Receiver", in proc. of IEEE VTC, Fall 07, Baltimore, USA, 2-4 October 2007.

5. **Muhammad Imadur Rahman**, Elisabeth de Carvalho, Ramjee Prasad, "Robust Interference Cancelation at Cell Edge for Cellular OFDMA Systems", submitted to IEEE Transactions on Wireless Communications.

6. **Muhammad Imadur Rahman**, Elisabeth de Carvalho, Ramjee Prasad, "Interference cancelation robust to various MIMO interferers via multiple-symbol processing at the cell edge of a cellular OFDM(A) system", under preparation, to be submitted to IEEE Transactions on Communications.

© Muhammad Imadur Rahman, 2007

Other IPRs during PhD Studies

1. Suvra Sekhar Das, **Muhammad Imadur Rahman**, Frank H.P. Fitzek, Ramjee Prasad, "Process and a system for transmission of data: Enhancing Spectral Efficiency of OFDM Systems by Data Transmission over Pilot Tones", Indian Patent Office application No 963/MUM/2004, published 2005-12-09, filed 2004-09-08; currently filed in USPTO, serial no. 20060088112.

2. Suvra Sekhar Das, **Muhammad Imadur Rahman**, Frank H.P. Fitzek; Ramjee Prasad, "A Novel Multirate Orthogonal Frequency Division Multiplexing System Proposal to Reduce Inter-Carrier Interference", Indian Patent Office application No 964/MUM/2004, filed 2004-09-08; currently filed in USPTO.

Other Publications & Technical Reports during PhD Studies

1. **Muhammad Imadur Rahman**, Suvra Sekhar Das & Frank H.P. Fitzek, "OFDM Based WLAN Systems", Aalborg University, Denmark, January, 2004, Technical Report R-04-1002, ISSN 0908-1224, ISBN 87-90834-43-7

2. **Muhammad Imadur Rahman**, Søren Skovgaard Christensen, Suvra Sekhar Das, Basak Can, Ragnar V. Reynisson, Anders Brødløs Olsen, Jesper Michael Kristensen, Nicola Marchetti, Daniel V. P. Figueiredo, Petar Popovski, "Comparison of Various Modulation and Access Schemes Under Ideal Channel Conditions", Jade Project Deliverable D3.1[1], July, 2004, 104 pages

3. Suvra Sekhar Das, Ratnam V.Rajakumar, **Muhammad Imadur Rahman**, Arpan Pal, Frank H.P.Fitzek, Ole Olsen, Ramjee Prasad, "Low Complexity Residual Phase Tracking Algorithm for OFDM-based WLAN Systems", in proc. 4th IEEE CSNDSP Symposium, 20-22 July 2004, pp. 128-131.

4. Frank H. P. Fitzek, Basak Can, Nguyen Cong Huan, **Muhammad Imadur Rahman**, Ramjee Prasad and Changhoi Koo, "Cross Layer Optimization of OFDM Systems for 4G Wireless Communications", in proc. of 9th International OFDM-Workshop (InOWo '04), Dresden, Germany, September, 2004.

5. **Muhammad Imadur Rahman**, Huan Cong Nguyen, Daniel V.P. Figueiredo, Ragnar V. Reynissen, Elisabeth de Carvalho, "Initial Recommendations for Access techniques and Duplexing for Cellular Systems ", Jade Project Deliverable B-2005-06-02, June 2005, 47 pages

6. **Muhammad Imadur Rahman**, Elisabeth de Carvalho, "MIMO Techniques at Cell Edge ", Chapter-3 of Jade Project Annual Deliverable, JADE MIMO Work Package 2006, December 2006, 33 pages

7. Suvra Sekhar Das, **Muhammad Imadur Rahman**, Frank H.P. Fitzek, Ramjee Prasad, "Multi Rate Orthogonal Frequency Division Multiplexing", in proc. of IEEE ICC '05, Seoul, Korea, May, 2005.

8. **Muhammad Imadur Rahman**, Ragnar Reynissen, Daniel Figueiredo, Elisabeth de Carvalho, "Sub-Carrier and Band-Hopped Orthogonal Frequency Division Multiple Access", Jade Project Technical Note TN-WPB-WA4-Dec05, December 2005, 96 pages

9. Suvra Sekhar Das, **Muhammad Imadur Rahman**, Frank H.P. Fitzek, Ramjee Prasad, "On Performance of SCH-OFDMA-CDM in Frequency Selective Indoor Environment", in the proceedings of IEEE VTC Spring '05, Stockholm, Sweden, May, 2005.

10. **Muhammad Imadur Rahman**, Nicola Marchetti, Elisabeth de Carvalho, "Joint Diversity and Multiplexing Schemes for MIMO-OFDM Systems", Jade Project Deliverable B-2005-06-03, June 2005, 47 pages

11. Suvra Sekhar Das, **Muhammad Imadur Rahman**, Frank H.P. Fitzek, Ramjee Prasad, "Variable Guard Interval for OFDM based WLANs", in proc. 8th IEEE PIMRC'05, 11-14 September, 2005, Berlin, Germany.

12. Suvra Sekhar Das, **Muhammad Imadur Rahman**, Suvra Sekhar Das, Frank H.P. Fitzek, Ramjee Prasad, "Low Complexity Residual Phase Tracking for Semi-Blind OFDM WLANs", in proc. 8th WPMC'05, 19-21 September, 2005, Aalborg, Denmark.

13. **Muhammad Imadur Rahman**, Nuno Silva, Flemming B. Frederiksen, Ramjee Prasad, "Spectral Efficiency Analysis for Multi-Carrier Based 4G Systems", in proc. 9th WPMC '06, San Diego, USA, 19-22 September 2006.

Supervision of MSc Thesis Students

1. Daniel V.P. Figueiredo: Diversity vs Beamforming in OFDM systems, Spring 2004, masters thesis co-supervised with Assoc. Prof. Frank H.P. Fitzek.

2. Nuno Silva: Spectral Efficiency Analysis for Multi-Carrier based 4G Systems, Spring 2005, masters thesis co-supervised with Assoc. Prof. Flemming B. Frederiksen.

3. Nurul Huda Mahmood, Yuanye Wang, Carlos Leonel and Bayu A. Jati: Exploiting Channel Dynamics for Bit and Power Allocation, Spring 2006, 8-semster project co-supervised with Assoc. Prof. Flemming B. Frederiksen, Suvra Sekhar Das and Daniel V.P. Figueiredo.

4. Nidcha Pongsuwanich: PAPR Issues in Link Adaptation for WiMAX-like OFDM Systems, Spring 2006, ongoing masters thesis to be completed in September 2006, masters thesis co-supervised with Assoc. Prof. Flemming B. Frederiksen and Suvra Sekhar Das.

5. Nurul Huda Mahmood, Yuanye Wang and Carlos Leonel: Link Adaptation in WiMAX-like MIMO-OFDM Systems, Summer 2006, CTIF internal student project co-supervised with Assoc. Prof. Flemming B. Frederiksen and Suvra Sekhar Das.

6. Maciej Portalski, Hugo Leberton: Implementation Aspects of Cooperative Diversity Schemes for Wireless Communications, Fall 2006-Spring 2007, 9-semester project co-supervised with Assist. Prof. Yannick Le Moullec and Basak Can.

© Muhammad Imadur Rahman, 2007

7. Sri Hanuma Chitti, Shradha Shradha, Gaurav Kulkami, Shabanpreet Warar: SDR Implementation of Link Adaptation Algorithm for OFDM based Mobile Broadband Wireless Access (WiMAX/UMTS-LTE), Fall 2006, 9-semester project co-supervised with Assist. Prof. Yannick Le Moullec and Suvra Sekhar Das.

8. Faisal Tariq: Joint Link Adaptation and Scheduling for Cellular MIMO OFDMA Systems (WiMAX, 3GPP LTE), Fall 2006- Spring 2007, masters thesis co-supervised with Prof. Ramjee Prasad and Suvra Sekhar Das.

9. Yuanye Wang: Evaluation of Multi-User Scheduling and MIMO Precoding Techniques for UMTS-LTE Downlink, Spring 2007, co-supervised with Assoc. Prof. Troels B. Sørensen and Suvra Sekhar Das.

B

List of Abbreviations

2G	2nd Generation
3G	3rd Generation
3GPP2	The Third Generation Partnership Project 2
4G	4th Generation
ACI	Adjacent Channel Interference
ADC	Analog-to-Digital Converter
AMC	Adaptive Modulation and Coding
AoA	Angle of Arrival
AoD	Angle of Departure
APFR	Adaptive Power Fixed Rate
APMC	Adaptive Power, Modulation and Coding
APD	Adaptive Power Distribution
ARQ	Automatic Repeat reQuest
AS	Antenna Selection

ATM	Asynchronous Transfer Mode
AWGN	Additive White Gaussian Noise
BER	Bit Error Rate
BF	Beamforming
BH	Band Hopping
BICM	Bit-Interleaved Coded Modulation
BLAST	Bell labs LAyered Space Time
BLER	Block Error Rate
BO	Back-Off
BPSK	Binary Phase Shift Keying
BS	Base Station
BWA	Broadband Wireless Access
C/I	Carrier to Interference Ratio
cdf	Cumulative Distribution Function
CCI	Co-Channel Interference
CDA-SM	Cyclic Delay Assisted Spatial Multiplexing
CDA-SM-OFDM	Cyclic Delay Assisted Spatially Multiplexed Orthogonal Frequency Division Multiplexing
CDD	Cyclic Delay Diversity
CDF	Cumulative Distribution Function
CDMA	Code Division Multiple Access
CFR	Channel Frequency Response
CIR	Channel Impulse Response
COFDM	Coded Orthogonal Frequency Division Multiplexing
CP	Cyclic Prefix
CQI	Channel Quality Information
CSI	Channel State Information
CTF	Channel Transfer Function

DAC	Digital to Analogue Converter
DD	Delay Diversity
DFT	Discrete Fourier Transform
DL	Downlink
DoA	Direction of Arrival
DoD	Direction of Departure
DSA	Dynamic Sub-Carrier Allocation
EGC	Equal Gain Combining
FDMA	Frequency Division Multiple Access
FDD	Frequency Division Duplex
FDM	Frequency Division Multiplexing
FEC	Forward Error Correction
FER	Frame Error Rate
FFT	Fast Fourier Transform
FBH	Fast Band Hopping
FFR	Fractional Frequency Reuse
FPAR	Fixed Power Adaptive Rate
FSCH	Fast Sub-Carrier Hopping
FWA	Fixed Wireless Access
GSM	Global System for Mobile communication
HPA	High Power Amplifier
HSPA	High Speed Packet Access
HSDPA	High Speed Downlink for Packet Access
HSUPA	High Speed Uplink for Packet Access
ICI	Inter-Carrier Interference
IEEE	Institute of Electrical and Electronics Engineers
IFFT	Inverse Fast Fourier Transform
ISI	Inter-Symbol Interference

© Muhammad Imadur Rahman, 2007

JDM	Joint Diversity and Multiplexing
LA	Link Adaptation
LDPC	Low Density Parity Check
LFSR	Linear Feedback Shift Register
LMS	Least Mean Square
LOS	Line of Sight
LS	Least Squares
LUT	Look-Up Table
MAC	Medium Access Control
MAI	Multiple Access Interference
MARC	Pre-DFT Maximal Average Ratio Combining
MBS	Mobile Broadband System
MC-CDMA	Multi-Carrier Code Division Multiple Access
MIMO	Multiple Input Multiple Output
MISO	Multiple Input Single Output
ML	Maximum Likelihood
MLI	Modulation Level Information
MMAC	Multimedia Mobile Access Coomunication
MMSE	Minimum Mean Square Error
MRC	Maximal Ratio Combining
MS	Mobile Station
MSE	Mean Squared Error
MU	Multi User
NLOS	Non Line Of Sight
OFDM	Orthogonal Frequency Division Multiplexing
OFDM-CDMA-SFH	Orthogonal Frequency Division Multiplexing - Code Division Multiple Access - Slow Frequency Hopping
OFDM-TDMA	Orthogonal Frequency Division Multiplexing - Time Division Multiple Access

OFDMA	Orthogonal Frequency Division Multiple Access
OFDMA-FH	Orthogonal Frequency Division Multiple Access - Frequency Hopping
OFDMA-FFH	Orthogonal Frequency Division Multiple Access - Fast Frequency Hopping
OFDMA-SFH	Orthogonal Frequency Division Multiple Access - Slow Frequency Hopping
OFDMA-FSCH	Orthogonal Frequency Division Multiple Access - Fast Sub-Carrier Hopping
OSFBC	Orthogonal Space-Frequency Block Code
OSIC	Ordered Successive Interference Cancelation
PAPR	Peak to Average Power Ratio
PC	Power Control
pdf	probability density function
PDP	Power Delay Profile
PHY	Physical Layer
PRNG	Pseudo-Random Number Generator
PSK	Phase Shift Keying
QAM	Quadrature Amplitude Modulation
QoS	Quality of Service
QPSK	Quadrature Phase Shift Keying
QSFBC	Quasi-orthogonal Space-Frequency Block Code
RACH	Random Access Channel
RF	Radio Frequency
RLS	Recursive Least Squares
RMS	Root Mean Square
SAMPDA	Simple Adaptive Modulation and Power Adaptation Algorithm
SBH	Slow Band Hopping
SC	Selection Combining
SCBH-OFDMA	Sub-Carrier and Band Hopped Orthogonal Frequency Division Multiple Access
SCH-OFDMA	Sub-Carrier Hopped Orthogonal Frequency Division Multiple Access

© Muhammad Imadur Rahman, 2007

SCH	Subcarrier hopping
SCH-OFDMA	Sub-Carrier Hopped Orthogonal Frequency Division Multiple Access
SD	Space Diversity
SDMA	Space Division Multiple Access
SDNR	Signal to Distortion and Noise Ratio
SE	Spectral Efficiency
SFBC	Space-Frequency Block Code
SFBC-OFDM	Space-Frequency Block Coded OFDM
SFC	Space-Frequency Coding
SIC	Successive Interference Cancellation
SIMO	Single Input Multiple Output
SINR	Signal to Interference and Noise Ratio
SISO	Single Input Single Output
SM	Spatial Multiplexing
SM-OFDM	Spatial Multiplexed Orthogonal Frequency Division Multiplexing
SM-OSFBC	Spatially-Multiplexed Orthogonal SFBC
SM-OSTBC	Spatially-Multiplexed Orthogonal STBC
SM-QSFBC	Spatially-Multiplexed Quasi-orthogonal SFBC
SM-QSTBC	Spatially-Multiplexed Quasi-orthogonal STBC
SM-OSFBC-OFDM	Spatially-Multiplexed Orthogonal Space-Frequency Block Coded Orthogonal Frequency Division Multiplexing
SM-QSFBC-OFDM	Spatially-Multiplexed Quasi-orthogonal Space-Frequency Block Coded Orthogonal Frequency Division Multiplexing
SNR	Signal to Noise Ratio
SRA	Simple Rate Adaptation
SSCH	Slow Sub-Carrier Hopping
SSPA	Solid State Power Amplifier
SVD	Singular Value Decomposition
STBC	Space-Time Block Code

STBC-OFDM	Space-Time Block Coded OFDM
STC	Space-Time Coding
STFBC	Space-Time-Frequency Block Code
STTC	Space-Time Trellis Code
TDD	Time Division Duplex
TDMA	Time Division Multiple Access
Tx	Transmitter
TxBF	Transmit Beamforming
TxDiv	Transmit Diversity
TxMRC	Transmit Maximum Ratio Combining
UL	Uplink
UMTS-LTE	Universal Mobile Telecommunications Systems- Long Term Evolution
VBLAST	Vertical - Bell Labs LAyered Space-Time Architecture
VoIP	Voice over IP
VSF-OFCDMA	Variable Spreading Factor - Orthogonal Frequency and Code Division Multiple Access
USLA	Uniform Spaced Linear Arrays
WCDMA	Wideband Code Division Multiple Access
WiMAX	Worldwide Interoperability for Microwave Access
WLAN	Wireless Local Area Network
WSSUS	Wide Sense Stationary Uncorrelated Scattering
XPD	Cross Polarization Discrimination
ZF	Zero Forcing
ZMCSCG	Zero Mean Circularly Symmetric Complex Gaussian

© Muhammad Imadur Rahman, 2007

C
List of Symbols

Functions & Operations

$\mathcal{F}\{\cdot\}$	Continuous Fourier Transform
$\mathcal{F}^{-1}\{\cdot\}$	Continuous Inverse Fourier Transform
$\mathcal{F}_d\{\cdot\}$	Discrete Fourier Transform
$\mathcal{F}_d^{-1}\{\cdot\}$	Inverse Discrete Fourier Transform
$\mathcal{K}_u\{v\}$	OFDMA subcarrier index function
$\mathcal{K}_u^{-1}\{k\}$	Inverse OFDMA subcarrier index function

Indexing

v	Source symbol index
s	OFDM symbol index
k	Subcarrier index
l	Multi-path index
n	Time-domain index
u	User index
p	Transmitting antenna index
q	Receiving antenna index
V	Number of source symbols
V_u^s	Number of source symbols per OFDM symbol for the uth user
N	Number of sub-carriers

η	Number of sub-carriers assigned to each user
S	Number of OFDM symbols
L	Number of multi-paths
U	Number of users
N_g	Number of samples in the CP
P	Number of transmitting antennas
Q	Number of receiving antennas
ß	The number of bits per data symbol loaded in sub-carrier

Matrix/Vector model

$\mathbf{m}$	Subcarrier vector (transmit side)
$\mathbf{x}$	Transmitted OFDM symbol vector (without CP)
$\mathbf{s}$	Transmitted signal vector (including CP)
$\mathbf{v}$	Noise vector (time-domain)
$\mathbf{n}$	Noise vector (frequency-domain)
$\mathbf{r}$	Received signal vector
$\mathbf{y}$	Received symbol vector (guard interval/CP removed)
$\mathbf{z}$	Sub-carrier vector (receiver-side)
$\mathbf{g}$	Channel impulse response vector
$\mathbf{G}$	Channel impulse response convolution matrix
$\mathbf{H}$	Channel frequency response matrix
$\mathbf{A}$	Frequency hopping set matrix
$\mathbf{M}$	Subcarrier mapping matrix (transmit side)
$\mathbb{F}$	Discrete Fourier Transform matrix
$\mathbb{F}^H$	Inverse Discrete Fourier Transform matrix

Discrete sequences

$\mathbf{X}_s[k]$	Sub-carrier (IDFT input) sequence
$Y_s[k]$	Received subcarrier (DFT output) sequence
$\hat{\mathbf{X}}_s[k]$	Estimated subcarrier sequence
$N_s[k]$	Subcarrier noise block
$h_{u,l}[s]$	The lth multipath component of the uth user's impulse response during the sth OFDM symbol
$H_u[k]$	The frequency response component of kth user subcarrier for the uth user
$Z_u[k]$	The frequency-domain equalizer gain for the kth subcarrier for the uth user
$\delta_{\mathbf{g}}$	Number of samples between first and last considered path

Continuous signals

t	Time
f	Frequency
ω	Angular frequency
$\tilde{x}_s(t)$	OFDM symbol block (IDFT output over one OFDM symbol)

$\tilde{x}'_s(t)$	OFDM symbol block with CP added
$\tilde{y}'_s(t)$	Received OFDM symbol sequence (DFT input over one OFDM symbol)
$\tilde{y}_s(t)$	Received OFDM symbol sequence after CP removal
$\tilde{s}(t)$	Transmitted complex baseband signal
$\tilde{r}(t)$	Received complex baseband signal
$\tilde{\nu}(t)$	Complex baseband noise signal
$\tilde{\nu}_s(t)$	Received complex baseband noise block for the sth OFDM symbol
$s(t)$	Transmitted RF signal
$r(t)$	Received RF signal
$\nu(t)$	RF Noise (continuous time)
$\tilde{h}_u(t)$	Channel impulse-response
τ_l	Delay of the lth multipath response
$Y_s(\omega)$	Fourier spectrum of $\tilde{y}_s(t)$
$H_{u,s}(\omega)$	Continuous channel transfer function of $\tilde{h}_u(t)$ for the uth user during the sth OFDM symbol
$N_s(\omega)$	Fourier spectrum of $\tilde{\nu}(t)$

System Parameters

T_d	Data symbol duration
T_s	Total OFDM symbol duration
T_u	OFDM symbol duration without guard interval
Δf	OFDM sub-carrier spacing
$\Delta\omega$	OFDM sub-carrier spacing (angular)
T_g	Guard interval duration
T_c	Channel coherence time
B_c	Channel coherence bandwidth
W	Total available spectrum
B	System bandwidth, i.e. FFT bandwidth for OFDM systems
f_c	Carrier frequency
$f_{c,0}$	System central frequency
f_h	Hopping frequency (displacement from carrier frequency)
Ψ	Hopping pattern length
Υ	Number of hopping patterns in use
χ	Hop duration/symbol duration ratio
T_h	Hopping sequence duration
δt	Receiver timing error
δf	Receiver frequency error
$\delta\omega$	Receiver timing error (angular frequency)
N_0	Noise variance/single sided noise density
γ	Instantaneous Signal to Noise Ratio
$\overline{\gamma}$	Average Signal to Noise Ratio, i.e. $\mathcal{E}\{\gamma\} = \overline{\gamma}$
P_b	Bit error probability

© Muhammad Imadur Rahman, 2007

P_s	Symbol error probability
M	Modulation order
ß	Number of bits per symbol
Δ_u	Set of sub-carriers assigned to the uth user

Symbols Used in Interference Studies

γ_t	SINR after receiver processing
$\mathbf{h}_0$	frequency response of channel between desired user and central BS
$\mathbf{h}_i$	frequency response of channel between desired user and i^{th} interfering BS
$E_{s,0}$	Source power from desired BS
$E_{s,i}$	Interfering power from interfering BS
$\mathbf{z}$	Received vector
$\|\mathbf{h}\|_F^2$	Frobenius norm of $\mathbf{h}$
N_0	Noise variance
P	No. of Tx ant. in desired BS
Q	No. of Rx ant. in desired MS
R	No. of Tx ant. in intf. BS
I	No. of interferes
$\mathbf{R}_{aa}$	Covariance matrix of a
$\mathbf{w}_0$	Weights applied to desired user from central cell
$\mathbf{w}_{j(i)}$	Weights applied to j^{th} user in i^{th} intf. cell
$\mathbf{h}_j$	frequency response of channel between j^{th} user in i^{th} intf. BS and i^{th} BS
p	Index for Tx ant. in desired BS
q	Index for Rx ant. in desired MS
r	Index for Tx ant. in intf. BS
i	Index for intf. BS
h_{xy}	Channel coefficient between x^{th} Rx ant. and y^{th} Tx ant.
$[\mathbf{a}]_x$	x^{th} component of vector $\mathbf{a}$
$[\mathbf{A}]_{xy}$	$[x, y]^{\text{th}}$ component of matrix $\mathbf{A}$

D
Useful Definitions

In this thesis, numerous terms regarding various aspects of the multiple access schemes and their corresponding systems are used. Here, the nomenclature used in this deliverable is expanded and defined in detail. An overview of the mathematical notation conventions used in this report is also given.

Frequency spectrum

The frequency spectrum definitions described here are explained graphically in Figure D.1.

Sub-carrier: This is the atomic unit of any OFDM system. A subcarrier is the spectral component of an OFDM signal corresponding to one point of the Discrete Fourier Transform.

Sub-channel: A logical group of Sub-carriers. These groups may be contiguous, or non-contiguous.

Sub-band: A Sub-band is a subset of the entire band, either contiguous or non-contiguous. Externally defined sub-bands (defined by licensing authorities) are usually contiguous.

Band: This term denotes the entire system bandwidth as seen from the RF transmitter or receiver. In an FDD system, the uplink and downlink usually take place in two separate bands, denoted the UL and DL bands, respectively.

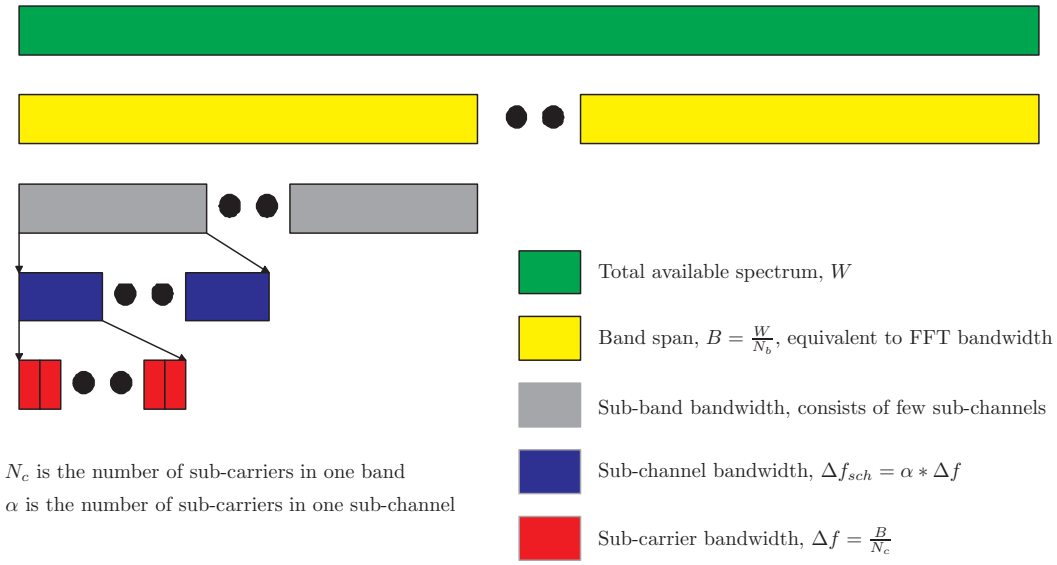

Figure D.1: Spectrum definitions. The total available bandwidth is divided into bands, which is the system bandwidth, or Band. This is equivalent to FFT bandwidth. Band is divided into one or more Sub-bands. The Sub-bands, in turn, contain one or more sub-channels. The sub-channel consists of a number of sub-carriers.

Data and modulation

Source symbol: A bit (or group of bits) modulated according to the baseband modulation form used, e.g. BPSK, 16-QAM, etc.)

OFDM symbol: A group of N_d source symbols modulated onto an OFDM carrier signal using DFT. An OFDM symbol also includes pilot and zero sub-carriers.

Cyclic Prefix: A guard interval inserted at the front of an OFDM symbol, copying the last part of the OFDM symbol to the start of the signal.

OFDM Block or OFDM Frame: A continuous group of OFDM symbols, frequently containing training sequences and signaling.

System

Base Station: An immobile transceiver connected to the fixed network infrastructure, e.g. a WLAN access point.

Mobile Station: A mobile transceiver carried by a user, e.g. a mobile phone, PDA, laptop PC etc. Also referred to as terminal unit or mobile terminal.

Downlink: Signal transmission going from base station to mobile station.

Uplink: Signal transmission going from mobile station to base station.

Mathematical notation

In order to make the mathematical descriptions in this deliverable more legible, the same notation has been used throughout the document. Here, a short overview of the mathematical notation used in this deliverable is given.

Discrete sequences are denoted with the argument in square brackets (e.g. $d_u[v]$, $\mathbf{X}_u[k]$), and are most frequently assumed to be complex. Continuous signals (i.e. continuous in time or frequency) are denoted with the argument in parentheses (e.g. $\tilde{x}_s(t)$, $N_s(\omega)$). Continuous-time complex baseband signals are indicated by a tilde over the symbol, while real-valued (passband) signals are not.

Time-domain sequences (both discrete- and continuous-time) are denoted using lower case letters, while frequency-domain (Fourier-transformed) signals are capitals. Subgroups of signals, either pertaining to individual users or a time-limited signal block containing information for a single OFDM symbol are denoted with subscripts.

Running indices for sums or sequences are shown using lower case letters, while sum limits are denoted using capital letters (most frequently the capital letter corresponding to the index). Time constants are denoted using T with the appropriate subscript (i.e. T_ξ for chip duration, T_s for OFDM symbol duration, etc.).

Matrices and vectors are denoted using bold letters, lower case letters for vectors, capitals for matrices. Blackboard-bold denotes either extended time-domain matrices or well-defined sets of numbers (such as the set of natural numbers $\mathbb{N}$ or the set of complex numbers, $\mathbb{C}$). Functions defined inside the deliverable, as well as Fourier transforms, are denoted using a calligraphic font.

© Muhammad Imadur Rahman, 2007

"Seek knowledge from the cradle to the grave."

- Prophet Muhammad (Peace be Upon Him)

Bibliography

[1] R. Prasad, W. Konhauser & W. Mohr (Editors), *Third Generaion Mobile Communications Systems*, 1st ed. Artech House Publishers, June 2000.

[2] T. Ojanpera & R. Prasad, *Wideband CDMA for Third Generaion Mobile Communications*, 1st ed. Artech House Publishers, Ocotber 2001.

[3] H. Holma & A. Toskala (Editors), *HSDPA/HSUPA for UMTS: High Speed Radio Access for Mobile Communications*, 1st ed. Wiley Publishers, June 2006.

[4] R. Prasad & L. Munoz, *WLANs and WPANs Towards 4G Wireless*. Artech House Publishers, Jan 2003.

[5] Y.K. Kim & R. Prasad, *4G Roadmap and Emerging Communications Technologies*, 1st ed. Artech House Publishers, Jan 2006.

[6] D. Astèly, E. Dahlman, et al., "A Future Radio-Access Framework," *IEEE Journal on Selected Areas on Communications*, vol. 24, no. 3, pp. 693–706, March 2006.

[7] K.R. Santhi & G.S. Kumaran, "Migration to 4G: Mobile IP based Solutions," *proc. IEEE AICT-ICIW'06*, February 2006.

[8] R. Prasad, *OFDM for Wireless Communications Systems*. Artech House Publishers, September 2004.

[9] H. Sari et al., "An Analysis of Orthogonal Frequency-Division Multiple Access," in *GLOBECOM*, vol. 3, November 1997, pp. 1635–1639.

[10] H. Rohling & R. Grunheid, "Performance of an OFDM-TDMA Mobile Communication System," in 46th *VTC*, vol. 3, April-May 1996, pp. 1589 – 1593.

[11] N. Yee, J.P. Linnartz et al., "Multicarrier CDMA in Indoor Wireless Networks," in *IEEE PIMRC*, Yokohama, Japan, September 1993, pp. 109–113.

[12] H. Atarashi and S. Abeta and M. Sawahashi, "Variable Spreading Factor-Orthogonal Frequency and Code Division Multiplexing (VSF-OFCDM) for Broadband Packet Wireless Access," *IEICE Trans. Commun.*, vol. E86-B, no. 1, pp. 291–299, January 2003.

[13] M.I. Rahman, S.S. Christensen, R.V. Reynisson, S.S. Das, B. Can, A.B. Olsen, J.M. Kristensen, N. Marchetti, D.V.P. Figueiredo, H.C. Nguyen, P. Popovski & F. Fitzek, "Comparison of Various Modulation and Access Schemes under Ideal Channel Conditions," Aalborg University, Denmark, JADE project Deliverable, D3.1[1], July 2004.

[14] W. Rhee & J. M. Cioffi, "Increase in Capacity of Multiuser OFDM System Using Dynamic Subchannel Allocation," in *IEEE VTC Spring'00*, Tokyo, Japan, May 2000, pp. 1085 – 1089.

[15] A.T. Toyserkani, S. Naik, J. Ayan, Y. Made & O. Al-Askary, "Sub-carrier based Adaptive Modulation in HIPERLAN/2 System," *IEEE ICC'04*, vol. 6, pp. 3460 – 3464, June 2004.

[16] Z. Song, K. Zhang & Y.L. Guan, "Statistical Adaptive Modulation for QAM-OFDM Systems," *proc. IEEE GLOBECOM'02*, vol. 1, pp. 706 – 710, Nov 2002.

[17] M. Siebert & O. Stauffer, "Enhanced Link Adaptation Performance Applying Adaptive Subcarrier Modulation in OFDM Systems," *IEEE VTC Spring'03*, vol. 57, no. 2, pp. 920 – 924, April 2003.

[18] M. Lei, P. Zhang, H. Harada & h.Wakana, "An Adaptive Power Distribution Algorithm for Improving Spectral Efficiency in OFDM," *IEEE Trans. on Broadcasting*, vol. 50, no. 3, pp. 347 – 351, September 2004.

[19] Li Zhen, and et al., "Link Adaptation of Wideband OFDM Systems in Multi-path Fading Channel," *IEEE CCECE*, vol. 3, pp. 1295 – 1299, May 2002.

[20] S. T. Chung and A. J. Goldsmith, "Degrees of Freedom in Adaptive Modulation: A Unified View," *IEEE Trans. Commun.*, vol. 49, no. 9, pp. 1561–1571, September 2001.

[21] J. H. Winters, "The Diversity Gain of Transmit Diversity in Wireless Systems with Rayleigh Fading," *IEEE Trans. Veh. Technol.*, vol. 47, no. 1, pp. 119–123, February 1998.

[22] G. L. Stuber et al., "Broadband MIMO-OFDM Wireless Communications," in *Proceedings of the IEEE*, vol. 92, no. 2, February 2004, pp. 271–294.

[23] K. Witrisal, Y.H. Kim et al., "Antenna Diversity for OFDM using Cyclic Delays," in *Proc. IEEE 8th Symposium on Communications and Vehicular Technology in the Benelux, SCVT-2001*, October 2001.

[24] P.W. Wolniansky et al., "V-BLAST: An Architecture for Realizing Very High Data Rates Over the Rich-Scattering Wireless Channel," in *Proc. IEEE-URSI International Symposium on Signals, Systems and Electronics*, Pisa, Italy, May 1998.

[25] S. M. Alamouti, "A Simple Transmit Diversity Technique for Wireless Communications," *IEEE JSAC*, vol. 16, no. 8, October 1998.

[26] H. Bolcskei, D. Gesbert, C.B. Papadias, A.-J. van der Veen (Editors), Ed., *Space-Time Wireless Systems: From Array Processing to MIMO Communications*. Cambridge University Press, UK, Spring 2006.

[27] R. W. Heath and A. J. Paulraj, "Switching Between Diversity and Multiplexing in MIMO Systems," *IEEE Trans. Comm.*, vol. 53, pp. 962–968, June 2005.

[28] R.S. Blum, "MIMO Capacity with Interference," *IEEE JSAC (Special Issue on MIMO Systems)*, vol. 21, no. 5, pp. 793–801, June 2003.

[29] M. Webb, M. Beach & A. Nix, "Capacity Limits of MIMO Channels with Co-Channel Interference," in *proc. IEEE VTC Spring*, Milan, Italy, May 2004.

[30] S. Ye & R.S. Blum, "Optimized Signaling for MIMO Interference Systems with Feedback," *IEEE JSAC (special issue on MIMO Systems)*, vol. 51, no. 11, pp. 2839–2848, November 2003.

[31] A. Naguib et al., "Applications of Space-Time Block Codes and Interference Suppression for High-Capacity and High Data rate Wireless Systems," in *proc. Asilomar conference on Signals, Systems and Computers*, vol. 2, Pacific Grove, CA, USA, 1998, pp. 1803–1810.

[32] J. Li et al., "Co-Channel Interference Cancellation for Space-Time Coded OFDM Systems," *IEEE Trans. Wirless Comm.*, vol. 2, no. 1, pp. 41–49, January 2003.

[33] J. H. Winters et al., "The Impact of Antenna Diversity on the Capacity of Wireless Communication Systems," *IEEE Trans. Comm.*, vol. 42, no. 2/3/4, pp. 119–123, February/March/April 1994.

[34] J. G. Proakis, *Digital Communications*, 4th ed. McGraw-Hill, August 2000.

[35] W.C.Y. Lee, *Mobile Cellular Telecommunications Systems*. New York, USA: McGraw Hill Publications, December 1989.

[36] Andreas Molisch, *Wireless Communications*. Wiley-Interscience, 2006.

[37] Andrea Goldsmith, *Wireless Communications*. Cambridge University Press, 2005.

[38] T.S. Rappaport, *Wireless Communications Principles and Practice*, 2nd ed. Prentice-Hall, January 2002.

[39] J. Heiskala and J. Terry, *OFDM Wireless LANs: A Theoretical and Practical Guide*, 2nd ed. Sams Publishing, July 2001.

[40] D. Matic, "OFDM Synchronization and Wideband Power Measurements at 60 GHz for Future Wireless Broadband Multimedia Communications," Ph.D. dissertation, Aalborg University, Denmark, September 2001.

[41] H. Rohling et al., "Broad-band OFDM Radio Transmission for Multimedia Applications," in *Proc. of the IEEE*, vol. 87, no. 10, October 1999, pp. 1778 –1789.

[42] T.S. Rappaport, *Wireless Communications Principles and Practice*. Prentice-Hall, January 1996.

[43] W.C. Jakes Jr., *Microwave Mobile Communications*. New York: John Wiley & Sons, May 1994.

[44] V Erceg et al., "A Model for the Multipath Delay Profile of Fixed Wireless Channels," *IEEE JSAC*, vol. 17, no. 3, pp. 399–410, March 1999.

© Muhammad Imadur Rahman, 2007

[45] V. Erceg, K.V.S. Hari et al, "Channel Models for Fixed Wireless Applications," IEEE 802.16 Working Group," Technical Report, IEEE 802.16a-03/01, June 2003.

[46] S. Haykin, *Adaptive Filter Theory*, 3rd ed. Prentice-Hall, December 1996.

[47] J.H. Scott, "The How and Why of COFDM," BBC Research and Development," EBU Technical Review, Winter 1999.

[48] C.R. Nassar et al., *Multi-carrier Technologies for Wireless Communication*. Kluwer Academic Publishers, 2002.

[49] J. Geier, *Wireless LANs, Implementing High Performance IEEE 802.11 Networks*, 2nd ed. Sams Publishing, July 2001.

[50] U.S. Jha, "Low Complexity Resource Efficient OFDM Based Transceiver Design," Ph.D. dissertation, Aalborg University, Denmark, September 2002.

[51] R. Prasad & M. Ruggieri, *Technology Trends in Wireless Communications*. Artech House Publishers, April 2003.

[52] M. Jankiraman, "Wideband Multimedia Solution Using Hybrid OFDM/CDMA/SFH Techniques," PhD Thesis, Delft university of Technology, The Netherlands, July 2000.

[53] H. Sari and Y. Levy and G. Karam, "Orthogonal Frequency-Division Multiple Access for the Return Channel on CATV Networks," in *IEEE ICT*, Istanbul, April 1996.

[54] C.Y. Wong, R.S. Cheng, K.B. Letaief & R.D. Murch, "Multiuser OFDM with Adaptive Subcarrier, Bit, and Power Allocation," *IEEE J. Select. Areas Commun.*, October 1999.

[55] C.Y. Wong, C.Y. Tsui, R.S. Cheng & K.B. Letaief, "A Real-time Subcarrier Allocation Scheme for Multiple Access Downlink OFDM Transmission," in *IEEE VTC*, Houston, USA, May 1999.

[56] D. Kivanc and H. Liu, "Subcarrier Allocation and Power Control for OFDMA," in *IEEE Signals, Systems and Computers*, Pacific Grove, USA, October 2000.

[57] D. Galda and H. Rohling, "A Low Complexity Transmitter Structure for OFDM-FDMA Uplink Systems," in *IEEE VTC*, Birmingham, USA, May 2002.

[58] A. Persson, T. Ottosson and E.G. Strom, "Analysis of the Downlink BER Performance for Coded OFDMA with Fading Co-Channel Interference," Chalmers University of Technology, Sweden, SE-412 96 Goteborg Sweden, Technical Report R001/2004 ISSN 1403-266X, January 2004.

[59] The IEEE 802.16 Working Group on Broadband Wireless Access Standards, "Part 16: Air Interface for Fixed and Mobile Braodband Wireless Access Systems," Tech. Rep., IEEE P802.16e Standard Document, December 2005.

[60] Steven J. Vaughan-Nichols, "Achieving Wireless Broadband With WiMAX," *IEEE Computer Magazine*, vol. 37, no. 6, pp. 10 – 13, June 2004.

[61] H. Wei & S. Ganguly, "Design of 802.16 WiMAX-based Radio Access Network," in *proc. IEEE PIMRC'06*, Helsinki, Finland, September 2006.

[62] R. Baines, "The Roadmap to Mobile WiMAX," *IEE Journal of Communications Engineering*, vol. 3, no. 4, pp. 30 – 34, Aug - Sept 2005.

[63] Z. Abichar, Y. Peng & J.M. Chang, "WiMAX: The Emergence of Wireless Broadband," *IEEE IT Magazine, published by IEEE Computer Society*, vol. 8, no. 4, pp. 44–48, Jul-Aug 2006.

[64] Hassan Yaghoobi, "Scalable OFDMA Physical Layer in IEEE 802.16 WirelessMAN," *Intel Technology Journal, ISSN 1535-864X*, vol. 8, no. 3, pp. 201 – 212, August 2004.

[65] P. Carson, "Flash-OFDM Technology," Flarion Whitepaper, November 2001.

[66] S. Kapoor et al., "Initial Contribution on a Sytem Meeting MBWA Characteristics," *IEEE 802.20 Working Group on Mobile Broadband Wireless Access*, March 2003.

[67] F. Daffara and O. Adami, "A New Frequency Detector for Orthogonal Multicarrier Transmission Techniques," *IEEE VTC*, pp. 804–809, July 1995.

[68] 3GPP Technical Report, "Physical layer aspects for evolved Universal Terrestrial Radio Access (UTRA), (release 7)," 3GPP, Technical Report TR 25.814, v7.0.0 June,2006.

[69] A. Toskala, H. Holma et al, "UTRAN Long Term Evolution in 3GPP," in *proc. 17th IEEE PIMRC*, Helsinki, Finland, 9-11 September 2006.

[70] H. Ekström, A. Furuskär et al., "Technical Solutions for the 3G Long-Term Evolution," *IEEE Comm. Magazine*, pp. 38–45, March 2006.

[71] E. Dahlman, H. Ekström et al., "The Long-Term Evolution of 3G," *Ericsson Review*, no. 2, pp. 118–125, 2005.

[72] N. Marchetti, E. Cianca & R. Prasad, "Low Complexity Transmit Diversity Scheme for SCFDE Transmissions over Time-Selective Channels," in *proc. IEEE ICC (accepted for publication)*, Glasgow, Scotland, June 2007.

[73] A.J. Paulraj, R. Nabar & D. Gore, *Introduction to Space-Time Wireless Communications*, 1st ed. Cambridge University Press, September 2003.

[74] G. J. Foschini and M. J. Gans, "On Limits of Wireless Communications in a Fading Environment When Using Multiple Antennas," *Wireless Personnal Communications*, vol. 6, pp. 311–335, March 1996.

[75] H. Bolcskei, D. Gesbert, and A. J. Paulraj, "On the Capacity of OFDM-Based Spatial Multiplexing Systems," *IEEE Trans. Commun.*, vol. 50, no. 2, pp. 225–234, February 2002.

[76] S. Sandhu, R. Nabar, D. Gore, and A. J. Paulraj, "Introduction to Space-Time Codes," Smart Antenna Research Group, Stanford University, Tech. Rep., 2004.

© Muhammad Imadur Rahman, 2007

[77] M. Okada and S. Komaki, "Pre-DFT Combining Space Diversity Assisted COFDM," *IEEE Trans. Veh. Tech.*, vol. 50, no. 2, March 2001.

[78] V. Tarokh, H. Jafarkhani, and A. R. Calderbank, "Space-Time Block Coding for Wireless Communications: Performance Results," *IEEE JSAC*, vol. 17, no. 3, March 1999.

[79] K.F. Lee, & D.B. Williams, "A Space-Frequency Transmitter Diversity Technique for OFDM Systems," in *IEEE GLOBECOM*, vol. 3, November-December 2000, pp. 1473–1477.

[80] A.F. Molisch, M.Z. Win & J. H. Winters, "Space-Time-Frequency (STF) Coding for MIMO-OFDM Systems," *IEEE Comm. Lett.*, vol. 6, no. 9, pp. 370–372, September 2002.

[81] J. C. Liberti and T. S. Rappaport, *Smart Antennas for Wireless Communications*. Prentice-Hall, April 1999.

[82] D.V.P. Figueiredo, M.I. Rahman et al., "Transmit Diversity Vs beamforming for Multi-User OFDM Systems," in *WPMC*, Abano Terme, Italy, September 2004.

[83] M. I. Rahman et al., "Performance Comparison between MRC Receiver Diversity and Cyclic Delay Diversity in OFDM WLAN Systems," in *proc.* 6th *WPMC*, vol. 2, Yokosuka, Japan, October 2003, pp. 198–202.

[84] D. Schafhuber, "MIMO-OFDM Systems," Austria, June 2004.

[85] H. Bolcskei and A.J. Paulraj, "Performance Analysis of Space-Time Codes in Correlated Rayleigh Fading Environments," in *ACSSC*, October 2000.

[86] D. Gesbert et al., "Outdoor MIMO Wireless Channels: Models and Performance Prediction," *IEEE Trans. Commun.*, July 2000.

[87] H. Bolcskei et al., "Performance of Spatial Multiplexing in the presence of Polarization Diversity," in *ICASSP*, May 2001.

[88] E.P. Lawrey, "Adaptive Techniques for Multiuser OFDM," Ph.D. dissertation, James Cook University, Australia, December 2001.

[89] R. Laroia, J. Li & M.C. Vanderveen, "Orthogonal Frequency Devision Multiplexing Based Spread Sprectrum Multiple Access," US Patent no. 6,473,418, October 29 2002.

[90] S. Zhou, G.B. Ginnakis & A. Scglione, "Long Codes for Generalized FH-OFDMA Through Unknown Multipath Channels," *IEEE Trans. Commun.*, vol. 49, no. 4, pp. 721–733, April 2001.

[91] X. Zhao, J. Kivinen, P. Vainikainen & K. Skog, "Propagations Characteristics for Wideband Outdoor Mobile Communications at 5.3 GHz," *IEEE J. Select. Areas Commun.*, vol. 20, no. 3, pp. 507–514, April 2002.

[92] S. Plass and A. Dammann and S. Kaiser, "Analysis of Coded OFDMA in a Downlink Multi-Cell Scenario," in *9th International OFDM Workshop*, Dresden, Germany, September 2004.

[93] Jan-Jaap van de Beek, "Synchronization and Channel Estimation in OFDM Systems," PhD thesis, Lulea University of Technology, Sweden, September 1998.

[94] C. Muschallik, "Influence of RF oscillators on an OFDM signal," *IEEE Transactions on Consumer Electronics*, vol. 41, no. 3, pp. 592 – 602, August 1995.

[95] G.J. Pottie & A.R. Calderbank, "Channel Coding Strategies for Cellular Radio," *IEEE Trans. Veh. Tech.*, vol. 44, no. 4, pp. 763–770, November 1995.

[96] D.R. Hughes and F.C. Piper, *Projective Planes*. New York: Springer Verlag, 1973.

[97] P. Östergård, "Lecture notes on S-72.341: Coding Methods course," Helsinki University of Technology, Finland, available at http://users.tkk.fi/∼pat/341.html, Spring 2005.

[98] L.E. Moses and R.V. Oakford, *Tables of Random Permutations*. Stanford, California: Stanford University Press, 1963.

[99] P.S.Chow, J. Cioffi, and J.A.C.Bingham, "A practical discrete multitone transceiver loading algorithm for data transmission over spectrally shaped channel," *IEEE Transaction on Communication*, pp. 773 – 775, Feb - April 1995.

[100] J. Hayes, "Adaptive Feedback Communications," *IEEE Trans. Comm.*, vol. 16, no. 1, pp. 29–34, Feb. 1968.

[101] Y. O. . T. H. H. Tase, S. Ohno, "Bit-rate maximization for multiuser ofdm systems," *MWSCAS '04*, vol. 47, no. 3, pp. 239 – 242, July 2004.

[102] Y.-T. Hwang, C.-Y. Tsai & C.-C. Lin, "Block Wise Adaptive Modulation for OFDM WLAN Systems," *IEEE International Symposium on Circuits and Systems*, vol. 6, pp. 6098 – 6101, 2005.

[103] C.-J. Ahn and I. Sasase, "The effects of modulation combination, target ber, doppler frequency, and adaptation interval on the performance of adaptive ofdm in broadband mobile channel," *IEEE Transactions Consumer Electronics*, vol. 48, no. 1, pp. 167 – 174, 2002.

[104] A. Leke and J. M. Cioffi, "Multicarrier systems with imperfect channel knowledge," *The Ninth IEEE International Symposium on Personal, Indoor and Mobile Radio Communications*, vol. 2, pp. 549 – 553, Sept 1998.

[105] M. R. Souryal and R. Pickholtz, "Adaptive modulation with imperfect channel information in ofdm," *IEEE International Conference on Communications*, vol. 6, pp. 1861 – 1865, June 2001.

[106] S. Ye, R. Blum, and J. Cimini, L.J., "Adaptive modulation for variable-rate ofdm systems with imperfect channel information," *VTC Spring '02*, vol. 55, no. 2, pp. 767 – 771, May 2002.

[107] S.T. Chung & A.J. Goldsmith, "Adaptive Multicarrier Modulation for Wireless Systems," *in proc. 34-th Asilomar Conference on Signals, Systems and Computers*, vol. 2, pp. 1603 – 1607, Oct - Nov 2000.

[108] A.J. Goldsmith & L. Greenstein, "Effect of Average Power Estimation Error on Adaptive MQAM Modulation," *in proc. IEEE ICC'97*, vol. 2, pp. 1105 – 1109, June 1997.

© Muhammad Imadur Rahman, 2007

[109] S.S. Das, M.I. Rahman et al., "Influence of PAPR on Link Adaptation Algorithms in OFDM Systems," in *proc. IEEE VTC Spring'07*, Dublin, Ireland, 22-25 April 2007.

[110] A. Czylwik, "Adaptive OFDM for Wideband Radio Channels," in *proc. Global Telecommunications Conf.*, vol. 2, 1996, pp. 713–718.

[111] T. Hunziker & D. Dahlhaus, "Optimal Power Adaptation for OFDM Systems with Ideal Bit-Interleaving and Hard-Decision Decoding," in *proc. IEEE ICC'03*, vol. 5, June 2003, pp. 3392–3397.

[112] D.V.P. Figueiredo et al., "Impact of Feedback Delay on Rate Adaptation for Multiple Antenna Systems," in *proc. IEEE PIMRC'06*, Helsinki, Finland, September 2006.

[113] M. Bohge, J. Gross & A. Wolisz, "The Potential of Dynamic Power and Sub-carrier Assignments in Multi-User OFDM-FDMA Cells," in *IEEE GlobeComm'05*, St. Louis, MO, USA, December 2005, pp. 2932 – 2936.

[114] P. Larsson, "Joint Power and Rate Control for Delay Tolerant Traffic in a Wireless System," in *proc. IEEE VTC Spring'07*, Dublin, Ireland, 22-25 April 2007.

[115] P. Banelli, G. Baruffa & S. Cacopardi, "Effect of HPA Non Linearity on Frequency Multiplexed OFDM Signals," *IEEE Trans. on Broadcasting*, vol. 47, no. 2, pp. 123–136, June 2001.

[116] S.S. Das, M.I. Rahman et al., "Influence of PAPR on Link Adaptation Algorithms in OFDM Systems," in *proc. IEEE VTC Spring'07*, Dublin, Ireland, 22-25 April 2007.

[117] C. Rapp, "Effects of HPA-nonlinearity on 4-DPSK-OFDM-signal for a Digital Sound Broadcasting System," in *Proc. 2nd European Conference on Satellite Communications*, Liege, Belgium, October 1991, pp. 179–184.

[118] B. Friedlander & S. Scherzer, "Beamforming Versus Transmit Diversity in the Downlink of a Cellular Communications System," *IEEE Trans. Vehicular Technology*, vol. 53, no. 4, pp. 1023–1034, July 2004.

[119] I. Telatar, "Capacity of Multi-Antenna Gaussian Channels," *European Trans. Tel.*, November 1999.

[120] H. Rohling et al., "Comparison of Multiple Access Schemes for An OFDM Downlink System," *in Multi-Carrier Spread Spectrum, edited by K. Fazel & G.P. Fettewis, published by Kluwer Academic Publishers*, pp. 23–30, 1997.

[121] M. Schubert and H. Boche, "An Efficient Algorithm for Optimum Joint Downlink Beamforming and Power Control," in *Proc. of VTC Spring*, May 2002, pp. 1911–1915.

[122] J. Medbo et al., "Channel Models for HIPERLAN/2 in Different Indoor Scenarios," in *COST 259 TD(98)70*, EURO-COST, Ed., Bradford, UK, April 1998.

[123] M. Pätzold, *Mobile Fading Channels*. John Wiley & Sons, June 2002.

[124] A.J. Paulraj & C.B.Papadias, "Space-time Processing for Wireless Communications," *IEEE Signal Processing Magazine*, vol. 14, pp. 49–83, November 1997.

[125] H.-C. Kim, J.-H. Park, Y. Shin, and W.-C. Lee, "Transmit Eigen-Beamformer with Space-Time Block Code for MISO Wireless Communication Systems," in *ITC-CSCC*, Phuket, Thailand, July 2002.

[126] B. Friedlander and S. Scherzer, "Beamforming vs. Transmit Diversity in the Downlink of a Cellular Communications System," in *Proc. of* 35th *Asilomar Conference on Signals, Systems and Computers*, vol. 2, November 2001, pp. 1014 – 1018.

[127] K. Witrisal, "OFDM Air-Interface Design for Multimedia Communications," Ph.D. dissertation, Delft University of Technology, the Netherlands, April 2002.

[128] K.F. Lee, & D.B. Williams, "A Space-time Coded Transmitter Diversity Technique for Frequency Selective Fading Channels," in *IEEE Sensor Array and Multichannel Signal Processing Workshop*, Cambridge, USA, March 2000, pp. 149–152.

[129] Y. Li, J.C. Chuang & N.R. Sollenberger, "Transmitter Diversity for OFDM Systems and Its Impact on High-Rate Data Wireless Networks," *IEEE JSAC*, vol. 17, no. 7, July 1999.

[130] A. Dammann & S. Kaiser, "Performance of Low Complex Antenna Diversity Techniques for Mobile OFDM Systems," in *proc.* 3rd *International Workshop on MC-SS*, Oberpfaffenhofen, Germany, September 2001.

[131] M. Bossert et al., "On Cyclic Delay Diversity in OFDM Based Transmission Schemes," in *proc.* 7th *International OFDM Workshop*, Hamburg, Germany, September 2002.

[132] M. I. Rahman et al., "Optimum Pre-DFT Combining with Cyclic Delay Diversity for OFDM Based WLAN Systems," in *proc. VTC Spring*, Milan, Italy, May 2004.

[133] G. L. Stuber, *Principles of Mobile Communications*. Kluwer Academic Publisher, January 1996.

[134] S. B. Slimane, "A Low Complexity Antenna Diversity Receiver for OFDM Based Systems," in *IEEE ICC*, vol. 4, Helsinki, Finland, June 2001, pp. 1147–1151.

[135] G. Bauch, "Differential Modulation and Cyclic Delay Diversity in Orthogonal Frequency-Division Multiplex," *IEEE Trans. on Comm.*, vol. 54, no. 5, pp. 798–801, May 2006.

[136] G. Bauch & J.S. Malik, "Cyclic Delay Diversity with Bit-Intereaved Coded Modulation in Orthogonal Frequency-Division Multiple Access," *IEEE Trans. on Wireless Comm.*, vol. 5, no. 8, August 2006.

[137] G. J. Foschini, "Layered Space-Time Architecture for Wireless Communication in a Fading Environment When Using Multiple Antennas," *Bell Labs Technical Journal*, pp. 41–59, Autumn 1996.

[138] Y. Li et al., "MIMO-OFDM for Wireless Communications: Signal Detection with Enhanced Channel Estimation," *IEEE Trans. Comm.*, vol. 50, no. 9, September 2002.

© Muhammad Imadur Rahman, 2007

[139] M.I. Rahman, N. Marchetti et al., "Joint Quasi-orthogonal SFBC and Spatial Multiplexing in MIMO-OFDM Systems," in *in proc. IEEE VTC Fall*, Montreal, Canada, September 2006.

[140] G. Bauch and J.S. Malik, "Differential Modulation with Cyclic Delay Diversity in OFDM," in *proc.* 9th *International OFDM Workshop*, Dresden, Germany, September 2004, pp. 123–127.

[141] G. Auer, "Channel Estimation for OFDM with Cyclic Delay Diversity," in *proc. 15th IEEE PIMRC'04*, Barcelona, Spain, 5-8 September 2004.

[142] ——, "Channel Estimation by Set Partitioning for OFDM with Cyclic Delay Diversity," in *proc. IEEE VTC Fall'04*, Los Angeles, USA, 26-29 September 2004.

[143] ——, "Analysis of Pilot-Symbol Aided Channel Estimation for OFDM Systems with Multiple Transmit Antennas," in *proc. IEEE ICC'04*, Paris, France, 20-24 June 2004.

[144] Hamid Jafarkhani, "A Quasi-Orthogonal Space-Time Block Code," *IEEE Trans. Comm.*, vol. 49, no. 1, pp. 1–4, January 2001.

[145] D. Gesbert, M. Shafi et al., "From Theory to Practice: An Overview of MIMO Space-Time Coded Wireless Systems," *IEEE JSAC*, vol. 21, no. 3, pp. 281–302, April 2003.

[146] L. Zheng and D.N.C. Tse, "Diversity and multiplexing: A fundamental tradeoff in multiple antenna channels," *IEEE Trans. Info. Theory*, vol. 49, no. 4, pp. 1073–1096, May 2003.

[147] H. Bolcskei et al., "Space-Frequency Coded MIMO-OFDM with Variable Multiplexing-Diversity Tradeoff," in *IEEE ICC*, May 2003, pp. 2837–2841.

[148] S. Barbarossa, *Multi-Antenna Wireless Communication Systems*. Artech House, Spring 2005.

[149] X. Zhuang et al., "Transmit Diversity and Spatial Multiplexing in Four-Transmit-Antenna OFDM," in *IEEE ICC*, vol. 4, May 2003, pp. 2316 – 2320.

[150] C.-B. Chae et al., "Adaptive Spatial Modulation for MIMO-OFDM," in *Proc. of WCNC*, vol. 1, March 2004, pp. 87 – 92.

[151] H. Skjevling, D. Gesbert, et al., "Combining Space-Time Codes and Multiplexing in Correlated MIMO Channels: An Antenna Assignment Strategy," in *Nordic Signal Processing Conference*, June 2003.

[152] M.H. Hairi et al., "Adaptive MIMO-OFDM Combining Space-Time Block Codes and Spatial Multiplexing," in *IEEE ISSSTA*, Sydney, Australia, August-September 2004.

[153] L. Zhao & V.K. Dubey, "Detection Schemes for Space-Time Block Code and Spatial Multiplexing Combined System," *IEEE Comm. Letters*, vol. 9, no. 1, January 2005.

[154] H. Bolcskei and A.J. Paulraj, "Space-Frequency Coded Broadband OFDM Systems," in *IEEE WCNC*, vol. 1, Chicago, USA, September 2000, pp. 1–6.

[155] A. Stamoulis, Z. Liu & G.B. Giannakis, "Space-Time Block-Coded OFDMA With Linear Precoding for Multirate Services," *IEEE Trans. on Signal Proc.*, vol. 50, no. 1, pp. 19–129, January 2002.

[156] M.I. Rahman, N. Marchetti et al., "Combining Orthogonal Space-Frequency Block Coding and Spatial Multiplexing in MIMO-OFDM System," in *proc. International OFDM Workshop, InOWo'05*, Hamburg, Germany, 31Aug-01Sep 2005.

[157] ——, "Non-Linear Detection for Joint Orthogonal Space-Frequency Block Coding and Spatial Multiplexing in OFDM-MIMO Systems," in *proc. IEEE ISWCS*, Siena, Italy, 5-7 September 2005.

[158] F.R. Farrokhi et al., "Spectral Efficiency of Wireless Systems with Multiple Transmit and Receive Antennas," in *IEEE PIMRC*, vol. 1, London, UK, September 2000, pp. 373–377.

[159] John M. Cioffi, *Course Material: Digital Communications II*. Stanford Bookstore, Spring 2005.

[160] M.I. Rahman, E. de Carvalho & R. Prasad, "Impact of MIMO Co-channel Interference," in *proc. 18th IEEE PIMRC'07*, Athens, Greece, 3-7 September 2007.

[161] Qualcomm Europe, "Description and simulations of interference management technique for OFDMA based E-UTRA downlink evaluation," 3GPP, Technical Report, TSG-RAN WG1-42, R1-050896, 2005.

© Muhammad Imadur Rahman, 2007

"Blessed are the peacemakers, for they will be called sons of God."

- Saying of Jesus (Peace be Upon Him), Matthew 5:9

Vita

Muhammad Imadur Rahman was born in Sylhet, Bangladesh on 30 January, 1976. He has obtained his B.Eng. degree in Electronics (majoring in Telecommunications) from Multimedia University, Malaysia in 2000, under a scholarship awarded by Yayasan Telekom Malaysia (Telekom Malaysia Foundation), and his MSc (Tech) degree in Radio Communications from Helsinki University of Technology, Finland in 2003. Since summer 2003, he has been working as a Research Engineer in the Wireless Networking (WING) Group of Department of Electronics Systems, Aalborg University. He has been pursuing his PhD studies from June 2004 onwards. Since June 2007, he is an Assistant Research Professor (Post-Doc Researcher) in the Radio Access Technology (RATE) section of the same department. Prior to his research work in Aalborg University, he has worked as a Research and Teaching Assistant in the Communication Laboratory, Helsinki University of Technology, Finland between February 2001 until May 2002.

His research interest includes multiple access technique, multiple antenna system, radio resource management, etc. He has been an active IEEE volunteer and has taken part in numerous IEEE activities, most notably as the General Chair of 1st AAU IEEE Student Paper Conference, AISPC'07, held in Aalborg in January 2007. He is currently the chairman of IEEE Denmark Section GOLD AG (*Graduates of the Last Decade* Affinity Group).

Permanent Address: Center for TeleInFrastruktur (CTiF)
Aalborg University
Niels Jernes Vej 12
9220 Aalborg Øst
Denmark
e-mail: *imr@es.aau.dk*

Now I've been happy lately, thinking about the good things to come
And I believe it could be, something good has begun

Oh I've been smiling lately, dreaming about the world as one
And I believe it could be, some day it's going to come

Cause out on the edge of darkness, there rides a peace train
Oh peace train take this country, come take me home again

Now I've been smiling lately, thinking about the good things to come
And I believe it could be, something good has begun

Oh peace train sounding louder, Glide on the peace train
Come on now peace train, Yes, peace train holy roller

Everyone jump upon the peace train, Come on now peace train

Get your bags together, go bring your good friends too
Cause it's getting nearer, it soon will be with you

Now come and join the living, it's not so far from you
And it's getting nearer, soon it will all be true

Now I've been crying lately, thinking about the world as it is
Why must we go on hating, why can't we live in bliss

Cause out on the edge of darkness, there rides a peace train
Oh peace train take this country, come take me home again

- Peace Train by Yusuf Islam (formerly Cat Stevens)